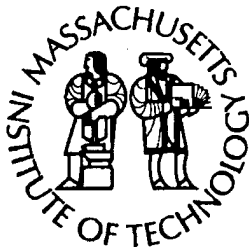
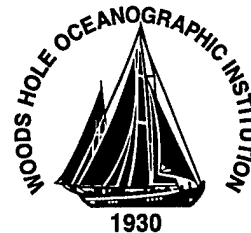


MIT/WHOI 2004-06

**Massachusetts Institute of Technology
Woods Hole Oceanographic Institution**



**Joint Program
in Oceanography/
Applied Ocean Science
and Engineering**



DISTRIBUTION STATEMENT A
Approved for Public Release
Distribution Unlimited

DOCTORAL DISSERTATION

**The Evolution of Oceanic Gabbros:
In-situ and Ancient Examples**

by

Astri Jæger Sweetman Kvassnes

June 2004

20041025 022

MIT/WHOI

2004-06

**The Evolution of Oceanic Gabbros:
In-situ and Ancient Examples**

by

Astri Jæger Sweetman Kvassnes

Massachusetts Institute of Technology
Cambridge, Massachusetts 02139

and

Woods Hole Oceanographic Institution
Woods Hole, Massachusetts 02543

June 2004

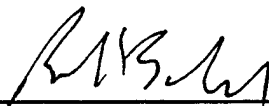
DOCTORAL DISSERTATION

Funding was provided by the Charles D. Hollister Endowed Fund, the NSF Plutonic Foundation grant #OCE-9618442 to Henry Dick, and NSF grant # OCE-9907630, Southwest Indian Ridge to Henry Dick, and by the Academic Programs Office General Fellowship Funds.

Reproduction in whole or in part is permitted for any purpose of the United States Government. This thesis should be cited as: Astri Jæger Sweetman Kvassnes, 2004. The Evolution of Oceanic Gabbros: *In-situ* and Ancient Examples. Ph.D. Thesis. MIT/WHOI, 2004-06.

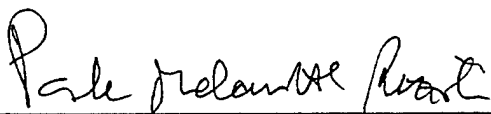
Approved for publication; distribution unlimited.

Approved for Distribution:

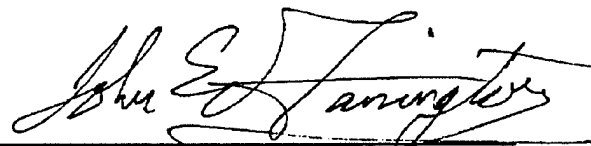


Robert S. Detrick, Chair

Department of Geology and Geophysics



Paola Malanotte-Rizzoli
MIT Director of Joint Program



John W. Farrington
WHOI Dean of Graduate Studies

The Evolution of Oceanic Gabbros: *In-situ* and Ancient Examples

By

Astri Jæger Sweetman Kvassnes

Candidatus Scientiarum, University of Bergen, 1997

Submitted in partial fulfillment of the requirements for the degree of
Doctor of Philosophy

at the

MASSACHUSETTS INSTITUTE OF TECHNOLOGY

and the

WOODS HOLE OCEANOGRAPHIC INSTITUTION

June 2004

© 2004 Astri Jæger Sweetman Kvassnes
All rights reserved.

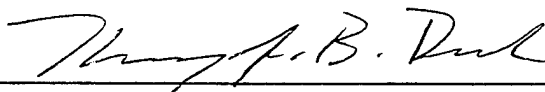
The author hereby grants to MIT and WHOI permission to reproduce paper and
electronic copies of this thesis in whole or in part and to distribute them publicly.

Signature of Author



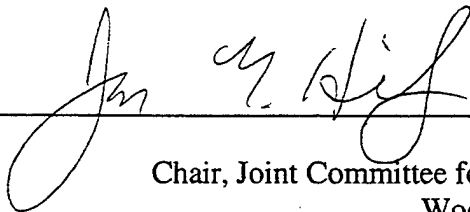
Joint Program in Oceanography/ Applied Ocean Science and Engineering
Massachusetts Institute of Technology
and Woods Hole Oceanographic Institution
April 2003

Certified by



Henry J. B. Dick
Thesis Supervisor

Accepted by



J. Gregory Hirth
Chair, Joint Committee for Marine Geology and Geophysics
Woods Hole Oceanographic Institution

The Evolution of Oceanic Gabbros: *In-situ* and Ancient Examples

by

Astri Jæger Sweetman Kvassnes

Submitted to the Department of Earth Atmosphere and Planetary Sciences
on April 30th, 2004 in Partial Fulfillment of the
Requirements for the degree of Doctor of Philosophy in
Marine Geology

Abstract

This study is a geochemical investigation into the accretion of lower oceanic crust and processes of shallow melt-rock reaction at mid-ocean ridges. Major-, trace-elements, and isotopes from whole-rocks and minerals from the Lyngen Gabbro, a 480-My old dismembered ophiolite from the Scandinavian Caledonides, indicate that this igneous complex was produced from hydrous supra-subduction zone magmas, a remnant of an incipient ocean-arc. Such ophiolites are better models for the structural evolution than the geochemical evolution of the lower oceanic crust at mid-ocean ridges.

Minerals in gabbros from Atlantis Bank, Southwest Indian Ridge, a modern, *in-situ* example of lower ocean-crust, were analyzed for major and trace-elements. The MELTS algorithm indicates that these gabbros formed by near-fractional crystallization at mid-crustal pressures. The gabbroic crust is more evolved than the lavas and represents melts fractionated 50-95% relative to a mantle-derived melt-composition, supported by trace-element models. This argues against the often-cited gabbro-glacier accretion model, where mantle-derived melts are transported to a shallow melt-lens and fractionates there before eruption. There remain >770-m of additional primitive cumulates below 1500-m deep Hole 735B or within the underlying mantle. Thus, the seismic Moho, beneath Hole 735B, could be the crust-mantle boundary, rather than an alteration front as suggested elsewhere.

The Atlantis Bank gabbros have augites that are more primitive than plagioclases and olivines with which they coexist. Melt-rock interaction, where ascending melts dissolve the pre-existing gabbroic rocks and create hybrid magma may have caused this. Dissolution-experiments for plagioclase-olivine and plagioclase-augite mineral pairs were performed at 1180°-1330°C and 20-min – 24hrs. Dissolution occurs rapidly and out of equilibrium, with the dissolution rates dependent on the ΔT above the solidus. Rocks with small grain-boundary areas (coarse grained or nearly mono-mineralic) heat internally when enclosed in hot magma, causing xenoliths or wall-rock to melt and disaggregate. The dissolution-derived magma crystallizes minerals more refractory-looking than the melts that precipitated the original gabbroic rocks. Assimilation of gabbroic rocks increases the Na content and decreases the Fe content of the melt that digests it, thus basaltic glasses formed after this hybridization will falsely reflect a lower degree and pressure of mantle melting.

Thesis Supervisor: Henry JB Dick

Title: Senior Scientist at Woods Hole Oceanographic Institution

The Evolution of Oceanic Gabbros: *In situ* and Ancient Examples

1 Acknowledgments

This research was supported by the Charles D. Hollister Endowed Fund, the NSF Plutonic Foundation Grant # OCE 9618442 to Henry Dick, and NSF grant # OCE-9907630, SW Indian Ridge to Henry Dick, and by the Academic Programs Office General Fellowship Funds. These are all gratefully acknowledged.

The Southwest Indian Ridge study materials were collected during RV James Clark Ross Leg 31 (1998), MODE 98 on RV Kairei (1999) and ABCDE on the RV Yokosuka (2000/2001). I wish to thank crews and scientific parties on the respective cruises. The samples from the Lyngen Magmatic Complex were sampled during the summers of 1994-1997, and I am grateful for the field-assistance from Dagfinn Slagstad and Harald Furnes.

I would like to thank Henry Dick my being my advisor. Few graduate-students are lucky enough to experience such a generous advisor, who takes you around the world (literally) to sample the coolest rocks, introduces you to all the important people, or better yet, make you take their classes, defend you from said people, has thought of most things at some point (it was probably in his thesis), feeds you dinner (we lost count at 50 dinner-parties), incorporates you into the family as if you were an older daughter, and lets you evolve into the best scientist you can be. I look forward to successful cooperation and continued friendship in the future.

I would like to thank my committee members Stan Hart, Nobu Shimizu, Rolf Pedersen, and Tim Grove for reading my thesis draft even if it was a draft, and for support throughout my studies. I would like to also thank Wolfgang Bach for serving as Chair. Susan Humphris and Maurice Tivey were generous generals-committee members.

I would like to thank Bob Detrick and Peter Kelemen for supporting my application into the program.

I would like to thank the exceptional Academic Programs Office staff. They seem to make it their mission that our academic experience is as amazing as possible. You guys spoil us rotten.

I would like to thank Tim Grove for serving as my advisor at MIT and for helping me become at least a little bit an experimental petrologist.

I would like to thank Neel Chatterjee and Jurek Blusztajn for technical assistance in the lab at MIT and Woods Hole Oceanographic Institution.

I would like to thank the Geochemistry/petrology group at Woods Hole Oceanographic Institution for many inspiring conversations, of which the students are welcomed as junior-scientists. In particular, Rhea Workman and Jeff Standish have provided great petrological support in this effort and help with my papers.

The Evolution of Oceanic Gabbros: *In situ* and Ancient Examples

The Joint Program is a great place to be, and has been even better due to “The Ladys who Lunch (Firn, Vanja and Bridget), the gang on the 10th and 12th floor at EAPS, the MacLean-ites and the rest of Mg&G, my 20+ house-mates during my stay in the US, and the supportive student population at Woods Hole Oceanographic Institution.

I would also like to thank my very patient and supportive newly extended family. They have made it possible for me to become a Dr. without losing sight of sustainability and reason. My husband, Andrew, has been very tolerant with me throughout the last year, hey, now it is your turn!

Dedication

I dedicate this thesis to the “Sweetnes”-Clan.

The Evolution of Oceanic Gabbros: *In situ* and Ancient Examples

Table of Contents

Chapter 1: Introduction:	15
References cited:	23
Chapter 2: The Lyngen Gabbro: The lower crust of an Ordovician Fore-Arc:	25
Introduction:	26
The Lyngen Magmatic Complex:	27
Geological Setting:	30
Sample localities:	31
Iddu:	31
Strupen:	31
Skaidevarri	32
Isskardet:	33
Ellendalen:	33
Goverdalen:	34
Veidalen:	34
Methods:	36
Whole rock analyses:	36
Mass Spectrometer analyses:	36
Mineral analyses:	37
Ion-probe analyses:	38
Mobility of elements:	38
Results:	39
Major elements:	39
Trace elements:	42
Nd-isotopes:	45
Mineral analyses: Major elements:	45
Mineral analyses: Trace elements:	48
Discussion:	48
Significance of the contrasting differentiation paths for the Eastern and Western suites:	48
Parental magma composition:	51
Temporal and spatial relations between the Western and Eastern suites	53
Plate tectonic affinity and comparison to other sites:	55
Conclusion:	57
References cited:	58
Chapter 3: Accretion of the lower crust at Atlantis Bank: The result of geochemical modeling:	101
1. Introduction:	101
2. Methods:	103
3. Results:	105
4. Discussion:	112

The Evolution of Oceanic Gabbros: *In situ* and Ancient Examples

4.1 Mode of accretion of the gabbros in Hole 735B	112
4.2 The extent of disequilibrium in the refractory gabbros:	119
4.3 What causes the high-Mg augite?	123
4.3.1 Accumulation of crystals: the solids:	123
4.3.2 Accumulation of crystals: the liquids:	127
4.3.3 Post-cumulus processes	128
5. Conclusion	135
6. References cited	136
 Chapter 4: Dissolution Kinetics of Oceanic Lower Crust	139
1. Introduction	139
2. Experimental procedures	142
2.a. Phase equilibrium experiments	144
2.b. Mineral Dissolution experiments	148
2.c. Analytical Techniques	153
2.d. Attainment of Equilibrium	158
3. Discussion	158
3.a. Experimental results	158
3.a.1. Melt compositions	170
3.b. How efficient is dissolution	172
3.c. Dissolution of gabbro in the lower ocean crust	172
Thermodynamic considerations:	176
3.d. The effect of grain-size	181
3.e. The effect of mineral density	184
3.f. Geochemical consequences of syntaxis	185
4 Conclusion	188
References cited	189
 Chapter 5: Mineral chemistry of gabbros from Atlantis Bank outside Hole 735B.	193
1. Introduction	194
2. Materials	198
3. Methods	199
4. Results	199
4.1. General mineral distribution and petrography	199
Mineral analyses	
4.1.1. Plagioclase	202
4.1.2. Clinopyroxene	206
4.1.3. Orthopyroxene	206
4.1.4. Olivine	208
4.2. Geographical variability around Atlantis Bank	208
5. Discussion	211
Conclusion	217
References cited	218

The Evolution of Oceanic Gabbros: *In situ* and Ancient Examples

Chapter 6: Trace element mineral-chemistry of gabbros from Atlantis Bank: Evidence for melt-rock interaction	239
1. Introduction	239
2. Analytical methods	240
3. Results	242
4. Discussion	242
5. Conclusion	250
References cited	250
Chapter 7: Residual melt porosities in gabbros from Atlantis Bank	253
1. Introduction	253
2. Results	255
3. Discussion	259
4. Conclusion	262
References cited	263

The Evolution of Oceanic Gabbros: *In situ* and Ancient Examples

Table of Figures

Figure 1-1: Models for Gabbro Accretion at Ocean Ridges	17
Figure 2-1: The general geology of the Lyngen Peninsula	28
Figure 2-2: A composite cross-section through the Lyngen Magmatic Complex.	35
Figure 2-3: Major element compositions of gabbroic whole-rocks from seven different areas	35
Figure 2-4: Whole-rock Mg# vs. SiO ₂ , CaO and TiO ₂ for the Western and Eastern suite	40
Figure 2-5: Whole rock Mg# (wt%) vs trace elements for the Western and Eastern suite	41
Figure 2-6: Whole rock trace-element analyses of the Lyngen Gabbro.	43
Figure 2-7: Sm-Nd element and -isotopes of the Lyngen Gabbro and associated dikes	44
Figure 2-8: An content of plagioclase vs Mg# of augite.	46
Figure 2-9: Trace element data for clinopyroxene as measured <i>in situ</i> by the ion-probe.	47
Figure 2-10: REE patterns of gabbroic augite	49
Figure 2-11: Discrimination diagram from Shervais (1982) for whole-rock analyses	52
Figure 2-12: Theoretical melt-compositions using Kd's for clinopyroxene (Arth, 1976).	54
Figure 3-1: The complete model run for SWIR PMORB with 0.05wt% H ₂ O, 1kbar, QFM.	106
Figure 3-2: Higher pressure crystallization	108
Figure 3-3: The effect of oxygen-fugacity	109
Figure 3-4: The effect of some water and batch equilibrium crystallization	110
Figure 3-5: The effect of starting composition	111
Figure 3-6: The model compared to gabbros from Hole 735D	113
Figure 3-7: Observed volume% of oxides in Hole 735B.	115
Figure 3-8: The augite coexisting with olivine of Hole 735B	118
Figure 3-9: The partition-coefficients for Fe Mg control the variation of the Mg#'s of the crystals	118
Figure 3-10: Partitioning of Fe and Mg between the minerals	121
Figure 3-11: Variation of Mg# of augite in the models with respect to temperature.	122
Figure 3-12: The solid-lines of descent for the models (Fig. 1-5) compared with Hole 735B	124
Figure 3-13: Liquid line of descent of the different SWIR melts and one MAR-melt	126
Figure 3-14: The density (g/cc) and viscosity of the melts and plagioclase (plag)	129
Figure 3-15: Diffusion distance for Ca-Na in plagioclase and Fe-Mg in olivine and augite	129
Figure 3-16: Running averages of NiO and Fo content of olivine in Hole 735B.	131
Figure 3-17: The effect of assimilation	133
Figure 4-1: Pseudoternary projection-plots of the melt compositions	143
Figure 4-2: The experimental setup.	149
Figure 4-3: Back-scatter electron images of cross-sections through dissolution experiments.	151-152
Figure 4-4: Theoretical calculation of amount of mineral dissolved based on a rate of 2µm/√s.	162
Figure 4-5: Plot of amount of mineral dissolved in microns versus the square-root of time.	163
Figure 4-6: Dissolution rates for our experiments	164
Figure 4-7: The dissolution rates for plagioclase with augite or olivine vs. ΔT°C above solidus.	165
Figure 4-8: A: Chemical profiles across the augite-melt-plagioclase interface in sample AK0024.	169
Figure 4-9: Effect of dissolution on a sample	175
Figure 4-10: The viscosities of the melts produced in our dissolution experiments	178
Figure 4-11: The fraction of olivine crystallize to equal the heat balance for dissolving rock	179
Figure 4-12: The effect of grain-sizes	180
Figure 4-13: The mechanism of dissolution of a xenolith.	183
Figure 4-14: The pseudoternary projection of the potential compositions of hybrid melts	186
Figure 4-15: A-C: The chemical effect of assimilation of lower crustal material.	187
Figure 5-1: The geology of Atlantis Bank (Dick et al., in prep).	195
Figure 5-2: Sample locations for this study.	197
Figure 5-3: Typical gabbros in this study	200-201
Figure 5-4: The mineral modes of Atlantis Bank gabbros and average Hole 735B compositions	203
Figure 5-5A: Cores and rims of clinopyroxene and plagioclase from this study.	205
Figure 5-5B: The distribution of cores and rims of plagioclase and clinopyroxene, Hole 735B	205

The Evolution of Oceanic Gabbros: *In situ* and Ancient Examples

Figure 5-6: The tetrahedral components of the pyroxenes from this study	207
Figure 5-7: Sample #JR31-12-6.	207
Figure 5-8: The composition of coexisting plagioclase and mafic minerals outside Hole 735B	209-210
Figure 5-9: Whole-rock composition of gabbros from Atlantis Bank	210
Figure 5-10: The distribution of mineral-compositions with the liquid and solid lines of descent.	213
Figure 5-11: Minor element chemistry of augites analyzed in this study	214
Figure 6-1: Spider diagrams for the augites in this study.	243
Figure 6-2: A: REE-plots for the augites in this study.	244
Figure 6-3: Crystallization models for our samples compared to the hypothetical melts	246
Figure 6-4: REE-element plots for crystallization models	247
Figure 6-5: The augite-compositions from the diabase-dike	249
Figure 7-1: The formation of trapped melts.	254
Figure 7-2: Liquid lines of descent for P_2O_5 , TiO_2 and REE for basalts from swir lavas	256
Figure 7-3: A test of the calculations for the residual melt porosity	258
Figure 7-4: Trapped melt fractions from ODP Hole 735B.	261

The Evolution of Oceanic Gabbros: *In situ* and Ancient Examples

Table of tables

Chapter 2:	
Table 1A: Whole rock analyses of the Western suite of the Lyngen Gabbro:	62-79
Table 1B: Whole rock analyses of the Eastern suite of the Lyngen Gabbro:	80-93
Table 2: Isotope chemistry for the Lyngen Gabbro	94-95
Table 3: Mineral chemistry for the Lyngen Gabbro	96-98
Table 4: Trace element chemistry and REE mineral chemistry for the Lyngen Gabbro	99
Chapter 3:	
Table 1: The starting compositions for our models	104
Table 2: Amount crystallized relative to a mantle derived melt	117
Chapter 4:	
Table 1: Theoretical starting composition, isothermal experiments	143
Table 2A: Geochemical results for "Fo73"	145
Table 2B: Geochemical results for "AK3"	146
Table 2C: Mode-results for the isothermal phase equilibrium experiments	147
Table 3: Composition of starting material in dissolution experiments	150
Table 4: Results of dissolution experiments	154
Table 5: Melts from dissolution experiments	167
Table 6: Method for calculating dissolution coefficients from diffusion coefficients	171
Table 7: Thermodynamic properties of the minerals at 1250°C	173
Table 8: Thermal re-equilibration of xenoliths	177
Chapter 5:	
Table 1: Samples analysed	220
Table 2A: Average plagioclase compositions	221
Table 2B: Average augite compositions	221
Table 2C: Average orthopyroxene compositions	221
Table 2D: Average olivine compositions	237
Chapter 6:	
Table 1: REE and trace element content of augite	241
Table 2: Partition coefficients used in this study	251
Chapter 7:	
Table 1: Residual melt porosities	260
Table 2: Example of calculation of residual melt fraction	264

Chapter 1

Introduction

The oceanic lower crust is dominated by olivine gabbro, generally composed of olivine, plagioclase and augite (Coleman (1977)). It is generally believed that this lower crust is formed by crystallization of basaltic magmas that ascend from the upper mantle. The lower crust is unfortunately difficult to study at fast-spreading ridges and ocean islands due to the 2+ km of dikes and lavas that cover it and the lack of tectonic windows. Therefore, many studies have used ophiolites as analogues for the origin and nature of the lower ocean crust. Many authors inferred that most ophiolites are the remnants of mid-oceanic crust (Nicolas, 1989, Elthon et al, 1992). However, it became apparent that the exact tectonomagmatic setting of any one ophiolite is uncertain, and it has been suggested that many ophiolites formed in *supra-subduction* settings (e.g. Miyashiro, 1975).

The extensive knowledge that rose from ophiolite studies, however, give us valuable structural, petrologic and geochemical concepts to understand and classify the origin of ophiolites and to understand crustal accretion at ocean ridges and how that might differ between tectonic settings such as mid-ocean ridges, ocean arcs and back-arc spreading centers. For example, it has been established that increasing activities of water in magma increase the An-content of plagioclase at a given Ca/Na ratio of the melt (Housh and Luhr, 1991, Arculus and Wills, 1990). In addition, the activity of augite increases with respect to olivine and plagioclase under wet conditions (Gaetani *et al.*, 1993), causing high-Ca pyroxene to crystallize before plagioclase. High-pressures (>5-kbar) have the opposite effect on the anorthite-content of plagioclase relative to melt composition (Panjasawatwong *et al.*, 1995), resulting in decreased An% content of plagioclase relative to lower pressure conditions. Variations in water content of mamgas and pressure of crystallization are likely important across the accretionary spectrum from mature ocean ridges to ocean arc environments.

Evolution of Oceanic Gabbros: In-situ and Ancient Examples

There are two main lines of thought on the geodynamic method of accretion of the lower ocean crust (Figure 1-1 A and B). One is the so-called “gabbro glacier” model, the other is the “many sills” model. The former end-member is based on observations in ophiolites (Sleep, 1975; Dewey and Kidd, 1977 and Quick and Denlinger, 1993) and developed further to account for geophysical observations at the East Pacific Rise (EPR) and other magmatically robust spreading segments (Henstock et al., 1993; Phipps Morgan and Chen, 1993). The gabbro-glacier model assumes that melt arrives directly from the upper mantle to a shallow melt sill, where the magmas fractionate and the cumulates subsequently flows downwards in a near steady-state fashion. Thus, the lower crust at such a ridge should always be more primitive than the lavas from the upper crust. The many sills model (Nisbet and Fowler, 1978; Pedersen, 1986; Bédard et al, 1988, 1991, 1993; Boudier et al., 1996; Kelemen et al., 1997b; Korenaga and Kelemen, 1997) indicates that the lower crust is accreted by the injections by individual sills that fractionate *in-situ* and eject their melt to higher levels. Thus, the lowermost crust is largely accreted there, and the composition of the gabbros becomes gradually more evolved upwards.

The truth probably lies between the gabbro glacier and the many sills model (MacLennan et al., 2004), and many models have been proposed that combine the two. Nevertheless, the extent to which the lower ocean crust interacts with subsequent ascending magmas is largely unknown. The rate of assimilation is naturally dependent on the heat available to incorporate and melt pre-existing cumulates into magma, and the residence time of the magma in the lower crust and other variables including ambient lithospheric temperature. The effect of the composition and grain-size of the assimilant, thus the compositional effects on the magma and lower crust, has not yet been established for the oceans.

The potential temperature of the melts generated in the upper mantle at mid ocean ridges could range from 1180°-1510°C (Klein and Langmuir, 1987, Kinzler and Grove, 1992), although other authors would disagree, arguing that the temperature is constant around 1250°C (e.g. Green et al, 2000; Presnall, 2002). The upper end of the temperature

Evolution of Oceanic Gabbros: In-situ and Ancient Examples

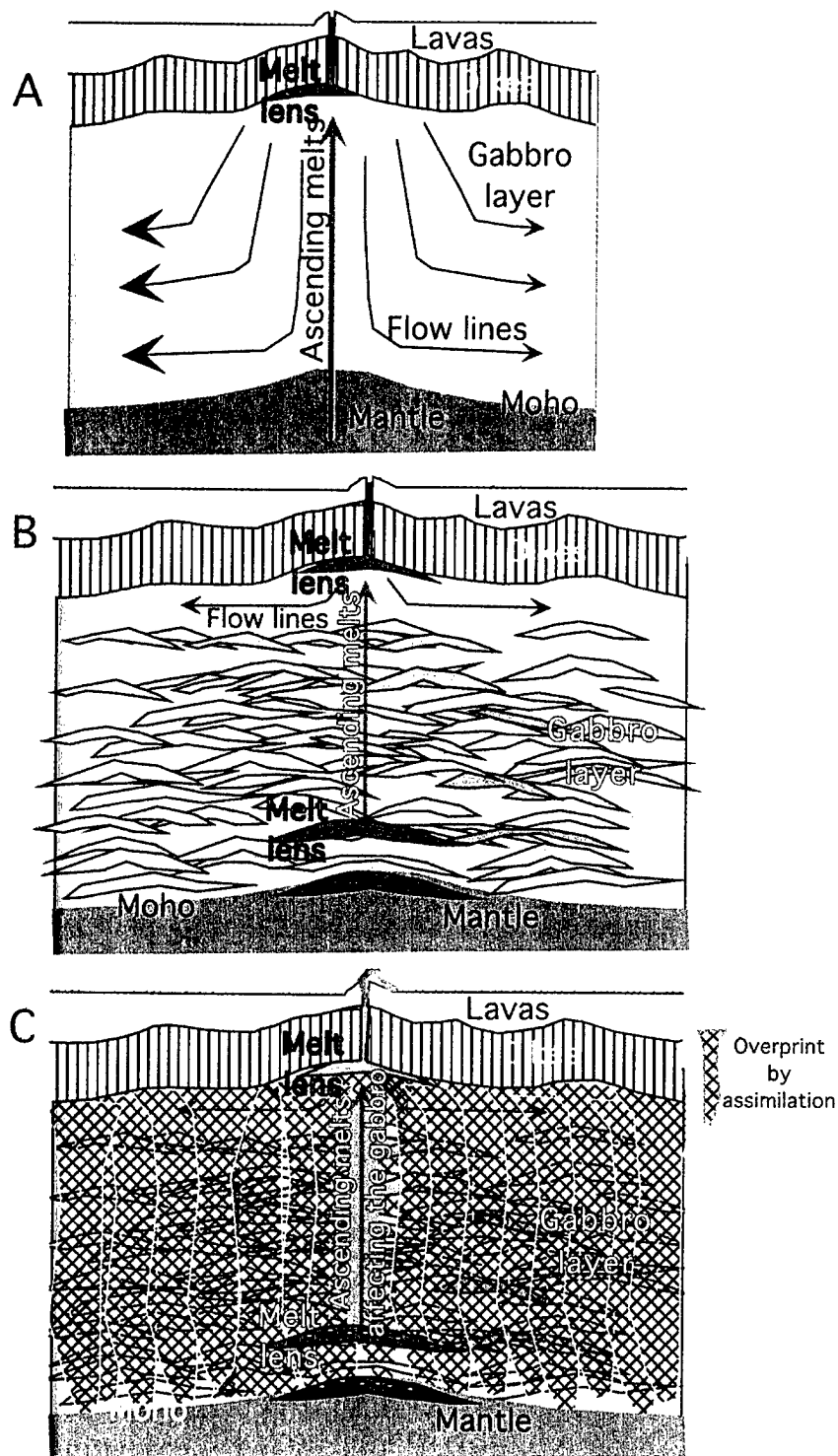


Figure 1-1: A: The Gabbro-glacier model. B: The many sills model. C: The model from this study, where the many-sills model is overprinted by melt-rock reaction, and xenoliths are being incorporated into the ascending magma.

Evolution of Oceanic Gabbros: In-situ and Ancient Examples

spectrum represents the fast spreading ridges where the EPR is the fastest and hottest. It has been documented that the EPR has a shallow axial magma chamber (AMC) (Detrick et al., 1987) that lies at low velocity zone (Harding et al., 1989; Vera et al., 1990). Dunn et al. (2000) showed the 5-8 km wide low velocity zone under the spreading center of the EPR has as much as 20 % melt fractions within it. A second melt lens has been documented near the seismic Moho transition (Crawford and Webb, 2002), and it has been argued that its stability is limited, as any crystallization in the chamber causes the surroundings to heat up and melt the surroundings in a manner that is not observed (Chen, 2001). The EPR therefore clearly has a heat-budget that is big enough to remelt the lower crustal material. At intermediate-spreading ridges, the AMC reflector is found at deeper levels in the crust (Phipps Morgan and Chen, 1993; Chen and Lin, in press). The existence of shallow steady-state magma-chambers at slower ridges is debated (Sinton and Detrick, 1992), and very deep magma chambers below the conductive boundary-layer in the mantle (Mével et al., 2002) would not be possible to detect with the seismic techniques available today (Detrick and Reeves-Sohn, pers comm. 2004). Erupted MORB show extensive differentiation and mixing that require that magma chambers exist at slow-spreading ridges, even if only ephemerally. The evidence of magma-chamber type processes happening before eruption at all ridges, suggest that there should be sites that are hot enough to dissolve preexisting crustal material even if melt bodies usually evade direct detection along the slow-spreading ocean ridges. Steady-state and ephemeral magma-chambers are likely to reside in the crust long enough for considerable interaction to occur between melts, cumulates and wallrocks.

Ocean islands are also sites of elevated magma-temperatures (Watson and McKenzie, 1991; Clague et al., 1991). In fact, there are Hawaiian picrites that record crystallization temperatures in excess of 1400°C (Natland, pers comm. 2004). Ocean - islands develop post-shield volcanism of very different compositions from the earlier shield-stage lavas. Their isotopes are more like those of mid-ocean crust, and they are frequently very alkaline in composition (Yang et al., 2003). The post-shield lavas often contain xenoliths made out of the pre-existing, tholeiitic, lower-crust that the hot-spot

Evolution of Oceanic Gabbros: In-situ and Ancient Examples

basalts had to penetrate to get to the surface (Fodor and Galar, 1997; Neumann et al., 2000). This suggests that the post-shield stage magmas, which spend more time in the lower crust than the shield-stage magmas, actually may have digested some lower crustal material on ascent.

The purpose of this study is to constrain the processes by which the lower crust at ocean ridges accretes, and to identify how the melts and cumulates interact there. The six following chapters of this thesis progressively approach these subjects.

In Chapter 2, we used geochemical techniques to investigate the tectonomagmatic origin of the Ordovician Lyngen Magmatic Complex, Northern Norway. We present 419 major and trace element analyses together with selected major- and trace element mineral analyses and $^{143}\text{Nd}/^{144}\text{Nd}$ -isotope whole-rock analyses of gabbroic to tonalitic plutonic rocks from the Ordovician Lyngen Magmatic Complex in Troms, Northern Norway. This dismembered ophiolite represents concurrent boninitic and tholeiitic magmatism in a fore-arc setting, possibly in an outer arc high. The gabbro-compositions are very different from those in silicic continental arcs. The cumulative rocks have extremely low levels of incompatible trace elements and high levels of compatible elements, reflecting melts derived from high degrees of melting in the mantle. The mineral compositions of the gabbros indicate hydrous conditions during fractionation and the transition between the boninitic and the tholeiitic cumulates is diffuse without tectonic contacts, suggesting that magmatism happened concurrently.

In Chapter 3, we utilize the large database of major-element mineral-compositions compiled for Hole 735B, at Atlantis Bank, Southwest Indian Ridge (Dick et al., 2002). We develop an extensive, quantitative and qualitative fractionation-model for the crustal section. We use a special version of the Melts program (Melts5) (Ghiorso and Sack, 1995) and in addition BASALT (1atm) (Weaver and Langmuir, 1990) and Yang et al. (1996) to evaluate the effect of melt-composition, oxygen fugacity, water, pressure, and crystallization processes that produced the lower crustal rocks at Atlantis Bank. This allows the extent of disequilibrium in the lower crustal material at Atlantis Bank to be

Evolution of Oceanic Gabbros: In-situ and Ancient Examples

quantified. We find that the best fractionation-model is fractional crystallization of a near dry melt with $\text{Na}_8 \sim 3$ and $\text{Fe}_8 \sim 9$ at crustal pressure on the quartz-fayalite-magnetite oxygen fugacity buffer. The gabbros sampled at Atlantis Bank generally represent melts that have crystallized 50-95% relative to a primary, mantle-derived magma. The basaltic glasses sampled on and around Atlantis Bank represent a melt that crystallized 30-50%. Therefore, the gabbro-glacier model is not valid for this slow-spreading ridge. Our model predicts that approximately 770 vertical meters of the lower crustal section has not been sampled and that the total crustal thickness at Atlantis Bank was more than 4.4-km. Thus, the observed seismic Moho there may indeed be the crust-mantle boundary, and not an alteration front as previously suggested by Muller et al. (1997). However, the majority of the gabbros in the lower 1000 meters of the hole have plagioclase coexisting with augite that have with Mg\# 's up to 10% higher than required by fractional crystallization of likely parental magmas in the area. Thus, we establish that interstitial melts in a mush-zone have dissolved and reprecipitated pre-existing crystals, causing the melt to become more Mg and Ca rich as plagioclase and augite dissolve rather than re-equilibrate with the melt. In the many-sills model, the gabbros become progressively more evolved upwards while accreting by fractional crystallization. Since we see that the solid-lines of descent of the gabbros indicate assimilation-processes, the many-sills model is only valid if pervasive overprints by ascending melts are incorporated (Figure 1-1C).

In Chapter 4, we demonstrate the kinetics of melting of natural mineral-pairs representative of the minerals found in lower ocean-crustal rocks, and find rapid melting rates and unusual melt-compositions. Therefore, the melts produced in the experiments allow us to assess the chemical changes that incorporating lower crustal material may cause in the ascending magmas. Our experiments were carried out using olivine - plagioclase and clinopyroxene - plagioclase mineral pairs over the temperature range of 1330 - 1220 °C at the quartz-fayalite-magnetite buffer for durations of 0.25 to 24 hours. Isothermal experiments performed over the temperature range of 1230 - 1105 °C defined the equilibrium phase relations in the system. The mechanisms of dissolution are similar

Evolution of Oceanic Gabbros: In-situ and Ancient Examples

to those found in other experimental studies that utilized end-member mineral compositions. The experimental results were used to determine to what extent cumulate igneous rocks from the oceanic lower crust would produce disequilibrium melt-compositions. We find that the efficiency of the reaction is dependent on grain-size and mineral-distribution of a rock that is reheated. Coarse-grained rocks ($>3\text{mm}$) will disintegrate internally upon reheating, whereas finer grained rocks will melt from the outside in. Mixing between the dissolution-melts and the surrounding magma is aided by the disaggregation of the xenocrysts of different densities, and the viscosities of the interstitial melts are similar to the ascending magma. The new, hybrid magma will have higher Na_8 and lower Fe_8 than the original. In addition, lower crustal assimilation of gabbro will result in the destruction of troctolites in the lower crust, and will lead to the early onset of high-Mg# olivine-gabbros.

In Chapter 5, we have analyzed the major element compositions of the magmatic minerals of 99 gabbros from on and around Atlantis Bank, covering an area of almost 660-km^2 . Tectonic windows provide the necessary exposures of the lower crust at this slow-spreading ridge (Tucholke and Lin, 1998). Samples from the northern area have the most primitive magmatic minerals, extending to ferro-gabbros with evolved mineral-compositions. Gabbros from the Western Wall and the top of the bank have intermediate compositions, whereas the southern rocks are all evolved, including layered olivine-gabbros sampled at gabbro-peridotite contacts. Despite the large variations in mineral chemistry in our samples, the primitive and evolved ends of the geochemical spectrum of ODP Hole 735B have not been found in our data. Although we have sampled the area extensively, we find that, like the gabbros from Hole 735B, the surface samples represent melts that have crystallized 50-90% relative to mantle-derived compositions. Therefore, if the lower crust was accreted by fractional crystallization, large amounts of troctolite are expected to exist somewhere in the lowermost crust or intruded into the residual mantle at depths below what is exposed on the sea-floor. However, the co-existing mineral-compositions vary in such a way as to suggest extensive reaction, dissolution and reprecipitation within the cumulate pile. A simple fractional-crystallization model, like

Evolution of Oceanic Gabbros: In-situ and Ancient Examples

that above, does not fully describe the evolution of Atlantis Bank gabbros. We propose an alternative model where primitive cumulates at higher levels may have been re-homogenized and transformed by later, interstitial melts.

In Chapter 6, we use the trace-element compositions of clinopyroxene from gabbros on and around Atlantis Bank to re-evaluate the geochemical evolution model of the gabbros and incorporated assimilation-fractionation-crystallization models (AFC) into our crustal thickness estimates. The gabbros cannot have formed by fractional crystallization alone, as the LREE/HREE ratios of the augites in the gabbros increase significantly with fractionation. We find that even though the parental melts experienced assimilation and/or *in-situ* fractionation (DePaolo, 1981; Langmuir, 1989), overall the gabbro-suite reflects melts that crystallized >50-95% relative to a parental magma in equilibrium with the mantle. This agrees well with our previous results using major-elements in Chapter 3. We therefore conclude that the estimate for the crustal thickness at Atlantis Bank of at least 4.4-km is valid, and that the melt that formed the lower ocean crust at Atlantis Bank experienced extensive melt-rock reaction during ascent. In addition, we found that the augites from a single diabase dikes indicate depleted melt compositions different from the compositions in the augites. The dike may be the result of late stage melting of the already depleted mantle.

In Chapter 7, we developed a method for calculation of trapped melt-fractions in gabbros from the Southwest Indian Ridge from whole-rock analyses. The model is calibrated with the use of *in-situ* mineral analyses mass-balanced with whole-rock compositions. We find that the trapped melt-fraction of ODP Hole 735B is ~15% on average. Eu-anomalies are inversely related to the trapped melt-fraction. This suggests that the whole-rock positive Eu-anomalies in Hole 735B, the signature of cumulate plagioclase, are masked by other REE's, as seen in diabases.

Evolution of Oceanic Gabbros: In-situ and Ancient Examples

References:

- Bédard JH, 1988: Magma chamber dynamics and recycling of crustal cumulates by the mantle: Evidence from the Bay of Islands Ophiolite (abs): *Eos* 69: 1476.
- Bédard JH, 1991: Cumulate recycling and crustal evolution on the Bay of Islands ophiolite. *Journ Geol* 99: 225-249.
- Bédard JH, 1993: Oceanic crust as a reactive filter: Synkinematic intrusion, hybridization and assimilation in an ophiolitic magma chamber, Newfoundland. *Geology* 21: 77-80.
- Boudier F. Nicholas A. Ildefonse B, 1996: Magma chambers in the Oman ophiolite: Fed from the top and the bottom. *Earth Planet Sci Lett* 144: 239-250.
- Chen YJ and Lin J in press: High sensitivity of ocean ridge thermal structure to changes in magma supply: the Galápagos Spreading Center. *Earth Planet Sci Lett*, in press.
- Chen YJ, 2001: Thermal effects of gabbro accretion from a deeper second melt lens at the fast spreading East Pacific Rise. *Journ Geophys Res.* 106 (B5): 8581-8588.
- Clague DA. Weber WB. Dixon JE, 1991: Picritic glasses from Hawaii. *Nature* 353: 553-556.
- Coleman RG, 1977. *Ophiolites*. Berlin: Springer-Verlag, 229pp.
- Crawford WC. Webb SC, 2002: Variations in the distribution of magma in the lower crust and at the Moho beneath the East Pacific Rise at 9°-10°N. *Earth Planet Sci Lett* 203: 117-130.
- Detrick RS. Buhl P. Vera E. Mutter J. Orcutt J. Madsen J. Brocher T, 1987: Multi-channel seismic imaging of a crustal magma chamber along the East Pacific Rise. *Nature* 326: 35-41.
- Dewey JF. Kidd WSF, 1977: Geometry of plate accretion. *Geol Soc Am. Bull* 88: 960-968.
- Dick HJB. Ozawa K. Meyer PS. Niu Y. Robinson PT. Constantin M. Hébert R. Natland JH. Hirth JG. Mackie SM, 2002: 10. Primary silicate mineral chemistry of a 1.5-km section of very slow spreading lower ocean crust: ODP Hole 735B, Southwest Indian Ridge. In Natland JH. Dick HJB. Miller DJ. Von Herzen RP (eds) *Proceedings of the Ocean Drilling Program, Scientific Results Volume 176*. (CD-ROM).
- Dunn RA. Toomey DR. Solomon SC, 2000: Three-dimensional seismic structure and physical properties of the crust and shallow mantle beneath the East Pacific Rise at 9°30'N. *J. Geophys Res.* 105: 23,537-23,555.
- Elthon D. Stewart M. Ross DK, 1994: Compositional trends of minerals in oceanic cumulates. *J Geophys Res* 97 (B11): 15,189-15,192.
- Fodor RV. Galar P, 1997: A View onto the Subsurface of Mauna Kea Volcano, Hawaii: Crystallization Processes Interpreted through the Petrology and Petrography of Gabbroic and Ultramafic Xenoliths. *Journ Petrol* 38 (5): 581-624.
- Gaetani GA. Grove TL. Bryan WB, 1993: The influence of water on the petrogenesis of subduction-related igneous rocks. *Nature (Lon)*, 365 (6444): 332-334.
- Ghiorso GA. Sack RO, 1995: Chemical Mass Transfer in Magmatic Processes IV: A revised and internally consistent thermodynamics model for the interpolation and extrapolation of liquid-solid equilibria in magmatic systems at elevated temperatures and pressures. *Contrib Mineral Petrol* 119: 197-212.
- Green DH. Falloon TJ. Eggins SM. Yaxley GM, 2000: Primary magmas and mantle temperatures. *Eur Journ Mineral* 13: 437-451.
- Harding AJ. Orcutt JA. Kappus ME. Vera EE. Mutter JC. Buhl P. Detrick RS. Brocher TM, 1989: Structure of young oceanic crust at 13°N on the East Pacific Rise from expanding spread profiles. *Journ Geophys Res* 94: B12,163-12,196.
- Henstock TJ. Woods AW. White RS, 1993: The accretion of oceanic crust by episodic sill intrusion. *Journ Geophys Res* 98(B4): 4,143-4,161.
- Kelemen PB. Koga K., Shimizu N, 1997b: Geochemistry of gabbro sills in the crust-mantle transition zone of the Oman ophiolite: implications for the origin of the oceanic lower crust. *Earth Planet Sci Lett* 146: 475-488.
- Kinzler RJ. and Grove TL, 1992: Primary magmas of midocean ridge basalts: 1. Experiments and Methods. *Journ Geophys Res* 97(B6): 6,885-6,906.
- Klein EM. Langmuir CH. 1987: Global correlations of ocean ridge basalt chemistry with axial depth and crustal thickness. *J. Geophys. Res.*, 92 (B8): 8,089-8,115.

Evolution of Oceanic Gabbros: In-situ and Ancient Examples

- Korenaga J. Kelemen PB, 1997: Origin of gabbro sills in the Moho transition zone of the Oman ophiolite: Implications for magma transport in the oceanic lower crust. *J. Geophys. Res.*, 102 (B12): 27,729-27,749.
- MacLennan J. Hulme T. Singh SC, 2004: Thermal models of oceanic crustal accretion: Linking geophysical, geological and petrological observations. *Geocem Geophys Geosyst* 5 (2) doi 10.1029/2003/GC000605.
- Mével C. Toplis MJ. Humpler E. Meyzen C. Ludden J, 2002: Major and Rare Earth Element Zoning of Plagioclase Phenocrysts in Basalts from the Southwest Indian Ridge (69-49°E). In: *Interridge Workshop on the Southwest Indian Ridge*, Southampton Oceanography Centre, UK, p 52.
- Miyashiro A (1975) The Troodos Ophiolite Complex was probably formed in and Island Arc, *Earth Planet Sci Lett* 19: 218-224.
- Nisbet EG. Fowler CMR, 1978: The Mid-Atlantic Ridge at 37° and 45°N: Some geophysical and petrological constraints. *Geophys J R Astron Soc* 54: 631-660.
- Neumann ER. Sørensen VB. Simonsen SL. Johnsen K, 2000: Gabbro xenoliths from La Palma, Tenerife and Lanzarote, Canary Islands: evidence for reactions between mafic alkaline Canary Islands melts and old oceanic crust. *Journ Volcanol Geotherm Res* 103: 313-342.
- Nicolas A. (1989) Structures of ophiolites and dynamics of oceanic lithosphere, Kluwer, Dordrecht, pp 367.
- Panjasawatwong Y. Danyushevsky LV. Crawford AJ. Harris KL (1995) An experimental study of the effects of melt composition on plagioclase; melt equilibria at 5 and 10 kbar; implications for the origin of magmatic high-An plagioclase, *Contrib Mineral Petrol* 118(4): 420-432.
- Pedersen RB, 1986: The nature and significance of magma chamber margins in ophiolites: examples from the Norwegian Caledonides. *Earth Planet Sci Lett* 77: 100-112.
- Phipps Morgan J. and Chen YJ, 1993: The genesis of oceanic crust, magma injection, hydrothermal circulation and crustal flow. *Journ Geophys Res* 98 (B6): 6,283-6,297.
- Presnall, DC. Gundfinnson GH. Walther MJ, 2002: Generation of mid-ocean ridge basalts at pressures from 1 to 7 GPa. *Ceochim Cosmochim Acta* 66 (12): 2,073-2,090.
- Quick JE. Denlinger RP, 1993: Ductile deformation and the origin of layered gabbro in ophiolites. *Journ Geophys Res* 98 (B14): 14,015-14,027.
- Sinton JM. Detrick RS, 1992: Mid-ocean ridge magma chambers. *J. Geophys. Res.*, 97 197-216.
- Sleep NH, 1975: Formation of oceanic crust: Some thermal constraints. *Journ Geophys Res* 80 (B4): 4,037-4,042.
- Tucholke BE. Lin J. Kleinrock MC, 1998: Megamullions and mullion structure defining metamorphic core complexes on the Mid-Atlantic Ridge. *J. Geophys Res.* 103 (B5) 9,857-9,866.
- Vera EE. Mutter JC. Buhl P. Orcutt JA. Harding AJ. Kappus ME et al., 1990: The structure of 0- to 0.2 m.y. old oceanic crust at 9°N on the East Pacific Rise from expanded spread profiles. *Journ Geophys Res* 95: B15,529-B15,556.
- Watson S. McKenzie D, 1991: Melt generation by plumes; a study of Hawaiian volcanism. *Journ Petrol* 32 (3): 501-537.
- Weaver and Langmuir CH, 1990: Calculation of phase equilibrium in mineral-melt systems. *Computers and Geosciences*, 16 (1): 1-19.
- Yang HJ. Frey FA. Clague DA, 2003: Constraints on the Source Components of Lavas Forming the Hawaiian North Arch and Honolulu Volcanics. *Journ Petrol* 44 (4): 603-627.
- Yang HJ. Kinzler RJ. Grove TL, 1996: Experiments and models of anhydrous, basaltic olivine-plagioclase-augite saturated melts from 0.001 to 10 kbar. *Contrib Mineral Petrol*, 124 (1): 1-18.

Chapter 2

The Lyngen Gabbro: The lower crust of an Ordovician Fore-Arc

Astri J. S. Kvassnes¹, Anita Hetland Strand², Heidi Moen-Eikeland³, Rolf B Pedersen⁴.

1: Woods Hole Oceanographic Institution, MS#8, Woods Hole, 02543 MA, USA,
astri@mit.edu

2: Statoil, 4035 Stavanger, Norway

3: Nipefjellet 83, 5300 Klepppestø, Norway

4: Department of Earth Science, University of Bergen, Allegt 41, 5007 Bergen, Norway

Evolution of Oceanic Gabbros: In-situ and Ancient Examples

Abstract:

We present 419 major and trace element analyses together with selected major- and trace element mineral analyses and $^{143}\text{Nd}/^{144}\text{Nd}$ -isotope whole-rock analyses of gabbroic to tonalitic plutonic rocks from the Ordovician Lyngen Magmatic Complex in Troms, Northern Norway. We find that this dismembered ophiolite represents concurrent boninitic and tholeiitic magmatism in a fore-arc setting, possibly in an outer arc high. Our geochemical data demonstrates the distribution of lower-crustal material present in such settings. The compositions are very different from silicic continental arcs. The cumulative rocks have extremely low levels of incompatible trace elements and high levels of compatible elements. Therefore, the magmas were likely the result of high degrees of melting in the mantle. The mineral compositions of the gabbros indicate hydrous conditions during fractionation. In at least one location the transition between the boninitic and the tholeiitic cumulates is diffuse without tectonic contacts, suggesting that magmatism happened concurrently.

Introduction

The lower ocean crust is generally inaccessible, and therefore its origin and nature have often been studied in ophiolites. The exact tectonomagmatic setting of any one ophiolite is, however, uncertain. Many authors have inferred that most ophiolites are the remnants of mid-oceanic crust (Nicolas, 1989, Elthon et al, 1994). Other authors have suggested that many ophiolites formed in *supra-subduction* settings (e.g. Miyashiro, 1975). The extensive knowledge that rose from this controversy gives us valuable petrologic and geochemical tools to understand and classify the origin of ophiolites. For example, it has been established that increasing activities of water in magma increase the An-content of plagioclase at a given Ca/Na ratio of the melt (Housh and Luhr, 1991, Arculus and Wills, 1990). In addition, the activity of augite increases with respect to olivine and plagioclase (Gaetani *et al.*, 1993), causing high-Ca pyroxene to crystallize before plagioclase. High-pressure (>5-kbar) crystallization also results in this reaction series, but pressure has the opposite effect on the anorthite-content of plagioclase relative to the melt composition

Evolution of Oceanic Gabbros: In-situ and Ancient Examples

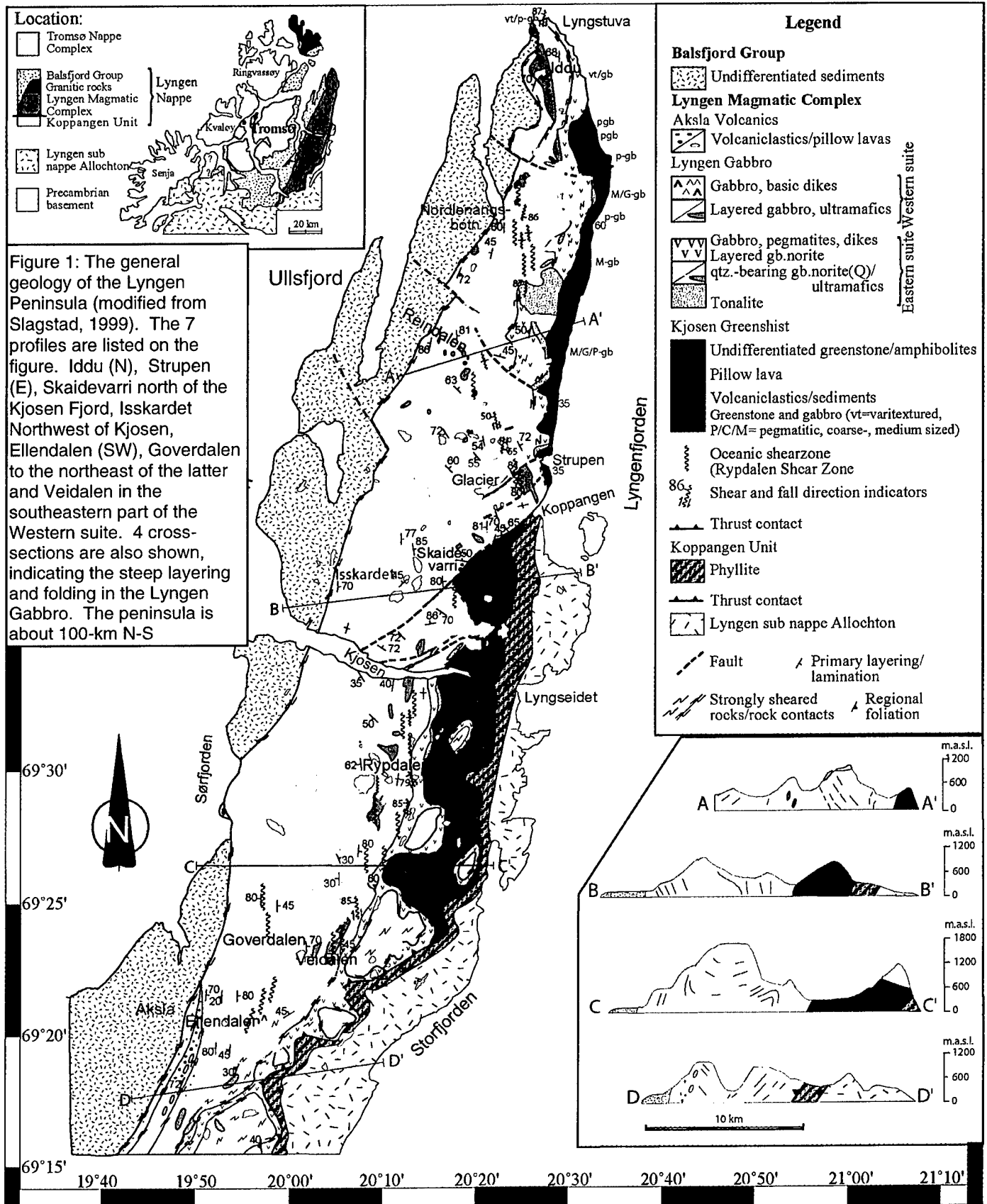
(Panjasawatwong *et al.*, 1995), resulting in decreased An% content of plagioclase relative to lower pressure conditions.

Hydrous magmatic conditions are common in arcs. Such a *supra-subduction* setting implies a tectonomagmatic environment ranging from back-arc basins, with magma sources similar to those from mid-ocean ridges re-melted with the aid of plate-derived water, through arcs and into the extremely depleted fore-arcs, often comprising boninitic magmatism. In addition, the outer-arc high represents the incipient arc made up of interspersed boninitic and tholeiitic magmatism. For instance, the Lau-Basin in the Southeast Pacific comprises a boninitic outer arc high and fore-arc, through a small arc and an actively spreading back-arc basin (Crawford *et al.*, 1981). Isotope-geochemistry and trace element geochemistry is used to support the theory that material derived from the slab is introduced into the subduction-zone mantle wedge that subsequently melt, and in addition, assimilation of existing mantle-rocks and crustal material may be assimilated into the ascending magma (e.g. AFC, DePaolo, 1981.) Consequently, dismembered magmatic complexes of oceanic origin can be put into a tectonic context using geochemistry. In this study, we used geochemical techniques to investigate the tectonomagmatic origin of the Ordovician Lyngen Magmatic Complex. We show that the Lyngen Gabbro represents the transition from MAR-like hydrous magmatism to a hydrous magma of a much more depleted source, like those in incipient arcs.

The Lyngen Magmatic Complex

The Lyngen Magmatic Complex dominates the Lyngen Peninsula and contains the largest massif of gabbroic rocks known in the Scandinavian Caledonides (Fig 2-1). It is postulated to be a dismembered ophiolite complex (Minsaas, 1981), as no mantle section or sheeted-dike complex has been identified. The Lyngen Magmatic Complex comprises the Lyngen Gabbro, the Aksla Volcanics, and the Kjosen Greenschist (Furnes and Pedersen, 1995). Its minimum age is Llanvirnian-Arenigian (469 +/- 5Ma) (Oliver and Krogh, 1995), as determined from a tonalite intrusion in the southern part of the Kjosen Greenschist. The complex has undergone Caledonian deformation, and large low-angle thrust faults dipping to the west intersect the complex. Hence, there may be some repetition of units due to tectonic events.

Evolution of Oceanic Gabbros: In-situ and Ancient Examples



Evolution of Oceanic Gabbros: In-situ and Ancient Examples

The Lyngen Gabbro is, by far, the dominant component of the Lyngen Magmatic Complex. A gravity profile has shown that the Lyngen Gabbro is wedge-shaped with the maximum thickness in the west (Chroston, 1972). The Lyngen Magmatic Complex has been subdivided into a Western and Eastern suite, both trending NNE-SSW, based on different petrological and geochemical characteristics (Furnes and Pedersen, 1995). The Lyngen Gabbro contains large shear zones originally named the Rypdalen Shear Zone. It separates the Western and Eastern suites in places and is accompanied by numerous variably sized dunite and wehrlite bodies. Later dikes with a wide range of compositions intersect the Lyngen Gabbro and Rypdalen Shear Zone, leading Slagstad (1995) to interpret the shear zone to be of oceanic origin. The ultramafic rocks and the crosscutting dikes are not the subject of this geochemical study, and will only be described as a part of the general geology. Most of the rocks of the Lyngen Gabbro have been extensively uralitized and saussuritized (Randall, 1959).

The Aksla Volcanics trend NNE-SSW along a narrow zone ~15 km long and 400 meters wide, in the Southwestern part of the Lyngen Peninsula, near Lakselvbukt (Fig. 1). The rocks are mainly deformed, greenschist-facies pillow-lavas, hyaloclastite breccias and dikes (Furnes and Pedersen, 1995) of mid-ocean ridge (MORB) to Island Arc Tholeiite (IAT) affinities (Furnes and Pedersen, 1995). An imbricated slab of gabbro, up to 600 meters wide, has a sheared, subvertical contact to the overlying sedimentary rocks in the Balsfjord Group (Minsaas and Sturt, 1985, Kvassnes, 1997). The gabbro is varitextured and cut by numerous basic dikes and these dikes are henceforth assumed to be associated with the Aksla Volcanics. The Eastern, sub-vertical contact between the Aksla Volcanics and the layered and high-level gabbros of the Lyngen Gabbro trend N-S, and is strongly sheared.

The Kjosén Greenschist outcrops from Strupen southward, defining the easternmost part of the Lyngen Magmatic Complex. It comprises pillow lavas, volcanoclastics and undifferentiated greenschists of MORB to IAT affinities (Furnes and Pedersen, 1995). The rocks of the Kjosén Greenschist are strongly sheared and deformed.

Evolution of Oceanic Gabbros: In-situ and Ancient Examples

Geological setting

The Norwegian Caledonides represent a stack of thin nappes thrust eastwards onto the Baltoscandian platform in late Silurian/early Devonian time (Dallmeyer and Andresen, 1992). The four major units are the Lower-, Middle-, Upper- and Uppermost Allocthon (Roberts and Gee, 1985). The Lower and Middle Allocthons and the lower part of the Upper Allocthon (Seve nappes) have Baltoscandian affinities. The remainder of the Upper- and especially the Uppermost Allocthon are exotic terrains thought to have been derived from spreading-ridges, rifted island arcs and marginal basins lying within the now consumed Iapetus ocean (Andresen and Stelthenpohl, 1994). These exotic magmatic complexes can be divided into two groups by U/Pb dating. Group 1 represents ophiolite complexes of Lower Ordovician (Tremadocian-Arenigian) age and comprises basaltic rocks with MOR-, IAT-, boninitic-, calc-alkaline- to alkaline affinities. Group 2 has an Upper-Ordovician (Ashgillian) age, defined by the Solund/Stavfjord Ophiolite Complex, and is predominantly N-MORB, but also contains local occurrences of basalts with E-MORB affinity (Dunning and Pedersen, 1988). The geochemical evolution of the ophiolites from the Norwegian Caledonides indicates their association with the development of island arcs (Pedersen and Furnes, 1991).

The central Troms area, northern Norway, has seven nappes. The lowermost three are the Dividal Group (autocthon) overlain by the Målselv/ Kalak Nappe Complex, all interpreted as the Baltoscandian Margin. Above these nappes are the Vaddas Nappe, the Kåfjord Nappe, the Nordmannvik Nappe, the Lyngen Nappe Complex and the Tromsø Nappe Complex, are all considered to be exotic terrains relative to Baltica (Andresen et al., 1985).

The Lyngen Nappe, a part of the Upper Allocthon has been correlated with Gratangseidet mafic complex in the Ofoten area (S-W) and the Ullsfjord nappe complex (N-E) (Andresen and Bergh, 1985). Three major lithological units can be distinguished; from the base, upwards: The Koppangen Formation, the Lyngen Magmatic Complex and the Balsfjord Group (Fig 1, insert) (Randall, 1959 and 1971(a,b), Munday, 1970 and 1974 and Binns, 1978). The Koppangen Formation is dominated by phyllites, although a strongly foliated amphibolite zone marks its contact to the Lyngen Magmatic Complex. The upper Ordovician to Silurian Balsfjord Group is interpreted to rest with a

Evolution of Oceanic Gabbros: In-situ and Ancient Examples

stratigraphic unconformity upon the very irregular paleo-topography of the Lyngen Magmatic Complex (Minsaas, 1981). The Svensby formation, a part of the Balsfjord Group, has calc-alkaline pillow-basalts (Kvassnes, 1997). In the southwest, the contacts to the Lyngen Magmatic Complex are all strongly sheared. The group is locally inverted, but is considered a coherent unit that is getting younger westwards (Andresen and Bergh, 1985).

Sample localities

Seven profiles throughout the Lyngen Gabbro have been sampled in detail. The areas north of the Kjosens Fjord are the Iddu area in the far north (81 samples, including a very detailed profile of 12 samples), Strupen in the east (128 samples), and Skaidevarri in the central part (91 samples). Isskardet is in the west, south of the Kjosens Fjord (24 samples), Ellendalen east of the contact to the volcanics (18 samples), Goverdalen is the valley to the northeast of Ellendalen (37 samples), and Veidalen is the valley in the central south (40 samples). The Norwegian Chart Service maps 1634IV, 1634V, 1633IV and 1533I in the series M711 cover the area.

Iddu

Iddu, on Lyngstuva, is the northernmost mountain of the Lyngen peninsula. The sample area is less than 1-km² and comprises gabbroic rocks and tonalites cut by basaltic dikes. Oceanic, amphibolite-grade, shear-zones and Caledonian, greenschist-grade, shear-zones crosscut the area. In addition, later, possibly Caledonian, high-angle normal faults crosscut the section.

The tonalites are classified as shear zone-related- or layered tonalites (Moen-Eikeland, 1999). The layered tonalites, interpreted to be the felsic fractionates of the original magma, are characterized by large gray-black, lens-shaped, quartz-grain-aggregates in a groundmass of quartz, plagioclase, and pyroxene. The quartz-aggregates can be up to 1.5-cm in size and their orientation follows the layering. The shear zone-related tonalites, interpreted by Slagstad (1995) to be the result of anatectic melting of amphibolized gabbro, are fine-grained and consists of plagioclase, quartz, pyroxene and amphibole.

Evolution of Oceanic Gabbros: In-situ and Ancient Examples

The gabbroic rocks are subdivided into massive and laminated gabbro, varitextured leucogabbro and gabbroic pegmatites (Moen-Eikeland, 1999). Massive and pegmatitic gabbros occur together. The massive gabbro is fine-grained with plagioclase, two pyroxenes, amphibole, and magnetite. Coarser patches often show larger grains of magnetite. The gabbroic pegmatites have plagioclase, pyroxenes, amphibole, magnetite, and quartz and the grain-sizes vary from 1- to 15-cm. The laminated gabbros are composed of plagioclase, pyroxenes, amphibole, and some quartz.

Strupen

The area consists mainly of layered, gabbroic rocks that frequently contain quartz as a cumulate mineral. Five major gabbroic rock types have been described (Hetland, 1996). Stratified layers (Type 1) grade from leuco- to melagabbro, exhibiting grain-size lamination, non-oriented cumulate clinopyroxene, and 5-10-cm long clinopyroxene-lenses oriented parallel to the layering. The oxide-rich gabbroic layers (Type 2) with plagioclase-rich horizons have unusually sharp contacts with the adjacent layers. Stratified, oxide-rich gabbroic layers (Type 3) have increasing amounts of oxide upwards. Oxide and quartz-bearing gabbroic layers (Type 4) comprise distinctive lamination defined by quartz grains oriented parallel to the layering. Tonalite (Type 5) are found as five to six-meter thick layers. The latter rock type often occurs above the oxide-rich layers, and tends to inter-finger with them. The quartz bearing gabbroic rocks are unique and characteristic features of the Eastern suite, although the volume of these rocks does not exceed 5% in the section. The profile sampled is 95-m long, and has been sampled perpendicular to the layering.

Skaidevarri

This 160-m transect is an east-west profile along the south side of Skaidevarri. The rocks range from troctolitic gabbros through olivine-gabbros, gabbros, olivine-gabbronorites, olivine-oxide-gabbros and oxide-gabbros. The rocks are mostly uniform with some fine, near-vertical layering in places. The sampling was done perpendicular to the layering. Some of the gabbros have undergone greenschist-facies metamorphism, with saussuritized plagioclase, iddingsitized olivine, and clinopyroxene partly altered to

Evolution of Oceanic Gabbros: In-situ and Ancient Examples

green amphiboles with only small amounts of relict clinopyroxene. The alteration grade ranges from 10-100%. The fresh rocks show poikilitic pink clinopyroxene, brown hornblende, and sometimes plagioclase occurs recrystallized or as inclusions in clinopyroxene. In fact, the magmatic minerals all have inclusions of the others minerals in them, suggesting a complex magmatic history.

Isskardet

The area consists of gabbro showing pronounced compositional layering that is steeply dipping and strikes N-S and perpendicular to the valley. The layering is typically of 5-10 meter scale with smaller scale (10-50 cm) layering locally superimposed. The larger scale layers can be traced laterally for 1-2 km across the valley. The rocks are generally medium to fine-grained with granulitic textures, with appearances similar to those of Skaidevarri. They range from olivine-gabbros to oxide-gabbro-norites, and no tonalites have been sampled.

Ellendalen

This valley is described in the westernmost profile in figure 2-2. An imbricated gabbro-slab west of the Aksla Volcanics is composed of high-level varitextured and massive gabbros cut by mafic dikes. The dikes trend N-S, with a 60° and 80° dip to the west. At Lakselvdalstindane, the northern wall of Ellendalen is dominated by layered gabbros folded in a large drag-synform with an N-S trending fold-axis dipping 40° to the north (Randall, 1959). The layering can be followed for at least 2200 meters along the mountain scarp and can be observed from 300 to 1400 meters above sea level. The sequence in this mountain may therefore represent 850 meters of layered gabbro. At the innermost part of Ellendalen, an up to 1-km wide, sub-vertical, N-S trending anastomosing shear zone caused a large antiformal drag-fold to form in the layered gabbros. Isotropic and varitextured gabbros have been found in the lower part of these mountain-scarps, where sampling ended. The gabbroic rocks have, in general, undergone greenschist alteration, and magmatic minerals have not been recovered except for rare cores of clinopyroxene.

Evolution of Oceanic Gabbros: In-situ and Ancient Examples

Goverdalen

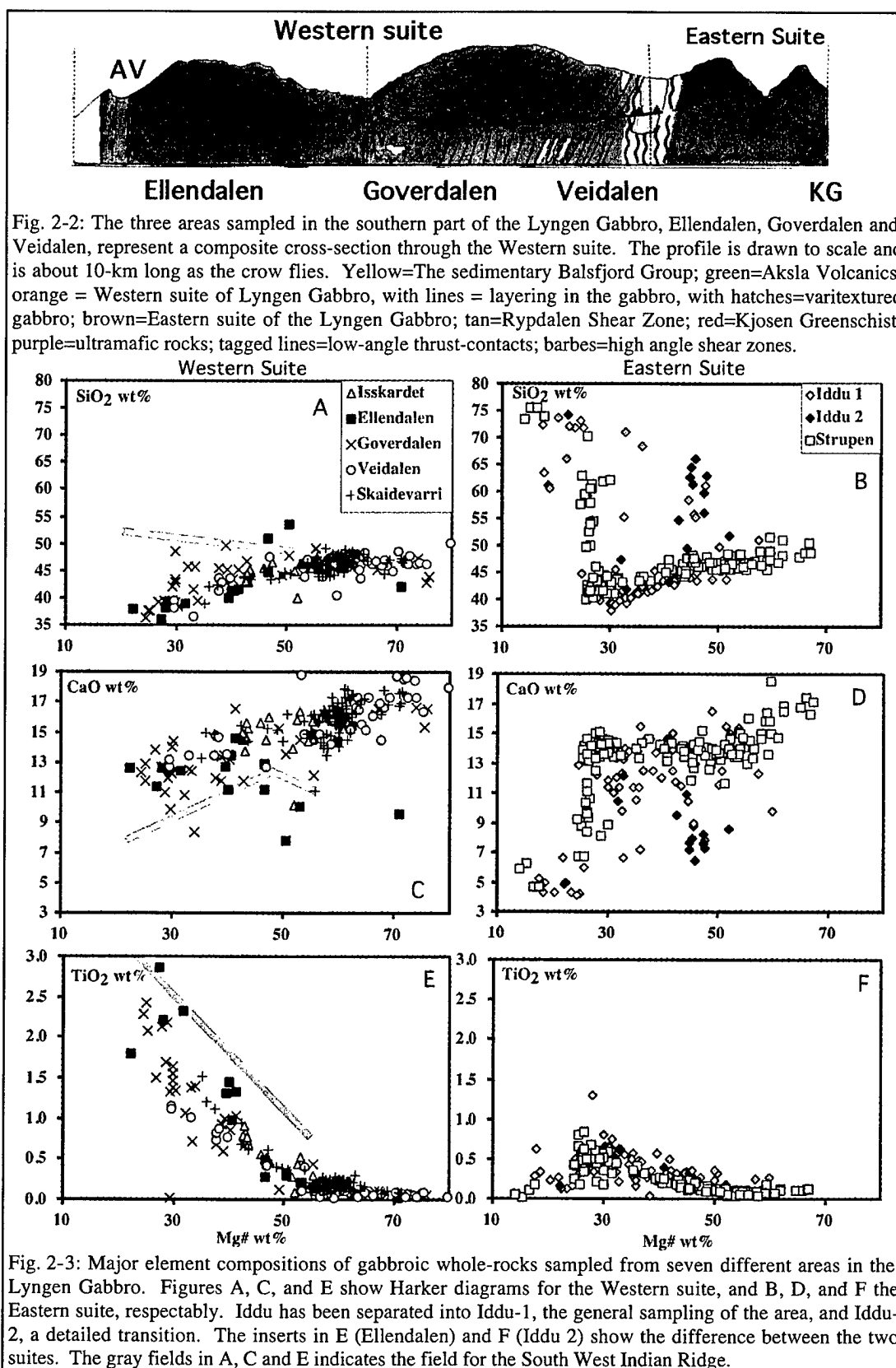
Following the shearzone northwards to Goverdalen, high-level gabbros continue into layered gabbroic rocks that can be followed eastwards through the valley and towards the Goverdalen Lake (Fig. 2-1 and 2-2). The gabbroic rocks of the Southwestern part of Mt. Nállangaisi host plagioclase-free wehrlite bodies close to the shear-zone. The steep walls of the valley display layered gabbros, and the shear-zone outcrops on the valley floor, displaying anatectic tonalites crosscut by inferred oceanic dikes (Selbekk, 1995, 1998). East of the shear-zone, layered and laminated gabbros were sampled towards the Goverdalen Lake. The rocks are generally two-pyroxene gabbros, and olivine is mostly absent. A very small outcrop of wehrlite was found. The most evolved gabbros are rich in magnetite and ilmenite. The rocks have frequently undergone greenschist alteration, and epidiosites have been found in the west of this valley.

Veidalen

East of the Goverdalen-lake, a very complicated layered sequence of wehrlites and gabbros outcrop. The layering appears to be deformed at a late magmatic stage, with multiple ductile folds, dunite pods and flame-structures. The gabbros are very fine grained, and plagioclases so dark that the rocks appear to be pyroxenites in outcrop. Some of the gabbros have high-Ca garnets and blue amphibole. The sequence looks similar to the Middle Series of the Rum layered intrusion on the Western coast of Scotland where it has been interpreted to represent the feeding zone for the intrusion (Emeleus *et al.*, 1996).

Mt. Balggesvarri, to the north of this valley, is dominated by layered gabbros, and the anastomosing shear-zone causes the layering to be folded into a synformal drag-fold. At the foot of the mountain, a large low-angle, westward dipping thrust-fault intersects the gabbro and an ultramafic body outcrops at the Eastern top. Entering Veidalen, an approximately two kilometer thick sequence of laminated meta-gabbro cut by basic and intermediate dikes can be followed towards the Rypdalen shear-zone (Selbekk, 1998). Within the shear-zone a large ultramafic body of wehrlite and dunite (2 km long and 0.5 km wide) outcrops from Sydbreen in the north to Veidalsvatnet in the south. A smaller

Evolution of Oceanic Gabbros: In-situ and Ancient Examples



Evolution of Oceanic Gabbros: In-situ and Ancient Examples

body of dunite is also seen below the small glacier in Náállancohkka south of Veidalsvatnet.

From the middle of Veidalsvatnet and eastwards into Veidalen and Gaskacóhka quartz-bearing gabbros and quartz-rich tonalites typical of the Eastern suite of the Lyngen Gabbro appear. There are no geochemical data from this part of the section. The Kjosen greenschist outcrops at the Eastern side of Mt. Njállavarre.

Methods

Whole rock analyses

Major and trace element analyses were performed at the University of Bergen. Fist size samples were crushed in a jaw crusher, and 80-100 cm³ were crushed to powder in an electrical agate mortar. The glass bead technique of Padfield and Gray (1971) was used for the major elements analyses and pressed-powder pellets for the trace elements analyses, using international basalt standards with recommended or certified values from Govindaraju (1994) for calibration. The analyses were carried out on a Phillips PW 1440 X-Ray fluorescence spectrometer. Instrumental precision for the major and trace elements for the glass-bead and pressed powder pellets have been documented by repeated analyses of representative samples. The relative standard deviations are close to 100% for low concentrations of the elements Zr, Y, Nb and P₂O₅. The whole-rock analyses are presented in Table 1.

Rare earth elements (REE), thorium, and tantalum have been analyzed at the Department of Earth Sciences, Memorial University of Newfoundland, Canada by inductively coupled plasma mass-spectrometry (ICP-MS). Analyses of international standards show that the relative uncertainties are better than 3% for Sr, Ba, Zr and the LREE, between 3 and 7% for Rb, Nb, Sc and HREE, and 10% for Ta and Th (Jenner et al., 1990). The data are presented in Table 1B.

Mass spectrometry analyses

73 samples have been measured for Sm and Nd-isotopes on a Finnegan MAT 262, 9-collector, fully automated mass spectrometer (MS) at the University of Bergen. All

Evolution of Oceanic Gabbros: In-situ and Ancient Examples

chemical processing were carried out in a clean-room environment with HEPA filtered air supply and positive pressure. The reagents were either purified in two-bottle Teflon stills or passed through ion-exchange columns. Samples were dissolved in a mixture of HF and HNO₃. REE were separated by specific extraction chromatography using the method described by Pin *et al.* (1994). Sm and Nd were subsequently separated using a low-pressure ion-exchange chromatographic set-up with HDEHP coated Teflon powder (Richard *et al.* 1976). Sm and Nd were loaded on a double filament and analyzed in multidynamic mode. Nd isotopic ratios were corrected for mass fractionation using a ¹⁴⁶Nd/¹⁴⁴Nd ratio of 0.7219. Sm and Nd concentrations were determined using a mixed ¹⁵⁰Nd/¹⁴⁹Sm spike. Repeated measurements of the JM Nd-standard yielded an average ¹⁴³Nd/¹⁴⁴Nd ratio of 0.511113 ± 15 (2 σ) (n = 62). The typical Nd blank level in the laboratory is 5pg. The results are listed in Table 2.

Mineral analyses

Major element analyses of clinopyroxene, orthopyroxene, plagioclase, and olivine have been performed using an ARL-SEMQ electron microprobe at the Nordic Volcanological Institute, Iceland. The microprobe analyses reported here are representative single-point analyses. All analyses were done with focused beam (2 μ m in diameter). The analyses were performed with a beam potential of 15 kV, sample current of ~15 nA, 4 seconds counting times for peak, and MAN (mean atomic number) corrections for background. Standards used were basaltic glasses. Chemical analyses of clinopyroxene, orthopyroxene, plagioclase, olivine and ore-minerals of 79 additional samples were carried out at the University of Bergen. These were done as standardless EDS-analyses on a scanning electron microscope (JEOL scanning microscope, JSM-6400), using the Tracor Northern energy dispersive analysing system (TN 5600), with a 20 kV beam. A final set of mineral analyses was made on an ARL-SEMQ electron microprobe at the University of Bergen. All analyses were done with a defocused beam (10 μ m in diameter). The analyses were performed with a beam potential of 15 kV, sample current of 10 nA, 40 seconds counting times for peak and 10 seconds for background (MAN (mean atomic number) background correction for Si, Ca, Al and Fe).

Evolution of Oceanic Gabbros: In-situ and Ancient Examples

Standards used were basaltic glasses, minerals, and metals. The results are listed in Table 3.

Ion-probe analyses

Three samples were selected from Goverdalen and Veidalen, representing the geochemical spectrum of plagioclase-bearing rocks in the areas. Four samples were selected from Strupen, representing four of the rock types spread out in the lower half of the profile. Unaltered cores and rims of clinopyroxene from these rocks were analyzed on the CAMECA IMS 3f ion probe at Woods Hole Oceanographic Institution using the methods of Shimizu and Hart (1982). A primary beam of O⁻ ions was focused to $\sim 20\mu\text{m}$ for REE (La, Ce, Nd, Sm, Eu, Dy, Er, Yb) and $\sim 10\mu\text{m}$ for other trace elements (Ti, V, Cr, Sr, Y, Zr). Molecular interferences were eliminated by energy filtering and a secondary voltage offset of -30 to -60V for the REE and -90 for the other trace elements. Uncertainties based on counting statistics were 5-10% (1σ) for REE and 1-5% (1σ) for the other trace elements. The data is presented in Table 4.

Mobility of elements

The rocks of the Lyngen Gabbro have been exposed to several metamorphic events, ranging from lower greenschist-facies to upper amphibolite- and possibly granulite-facies metamorphism. Several studies have investigated how elements are leached or enriched due to metamorphism of magmatic rocks. Cann (1977) and Coish (1977) investigated the mobility of different elements during sea-floor metamorphism, concluding that Ti, P, Y, Zr, Nb, Cr, and Ni are stable during greenschist-facies metamorphism. Shervais (1982) showed Ti and V to be stable under a wide range of metamorphic conditions, ranging from sea-floor metamorphism to granulite facies metamorphism. Elliot (1972) investigated gabbros that occur as isolated masses within amphibolites, and concluded that TiO_2 , FeO^1 , MgO , MnO , and Na_2O and possibly Al_2O_3 were stable during amphibolite facies metamorphism. Weaver and Tarney (1981) analyzed mafic and ultramafic dikes cutting retrograded dikes, comparing dikes exposed to varying degree of metamorphism to fresh dikes. They concluded that Nd, P, Hf, Zr, Ti and the middle to heavy REE's are immobile even during strong metamorphism with

Evolution of Oceanic Gabbros: In-situ and Ancient Examples

access to fluids. An investigation of gneisses from a mylonitic shear zone shows that SiO_2 , K_2O , Na_2O , FeO and CaO are mobile when fluid phases are present (Sinha *et al.*, 1986).

In general, it is difficult to determine whether an element is mobile or not, and whether it will be enriched or depleted during alteration and metamorphism. However, the above studies have shown that Zr, Y, P, Nb, Cr, Al, Ti, V and the REE will be relatively stable during the metamorphic conditions shown to be present along the composite cross-section. The ratios between these elements will hence be an accurate way to compare the rocks. MgO and FeO concentrations are also stable in the gabbros at higher metamorphic grades. As Sr is unstable during alteration, no Sr isotopic analyses have been attempted.

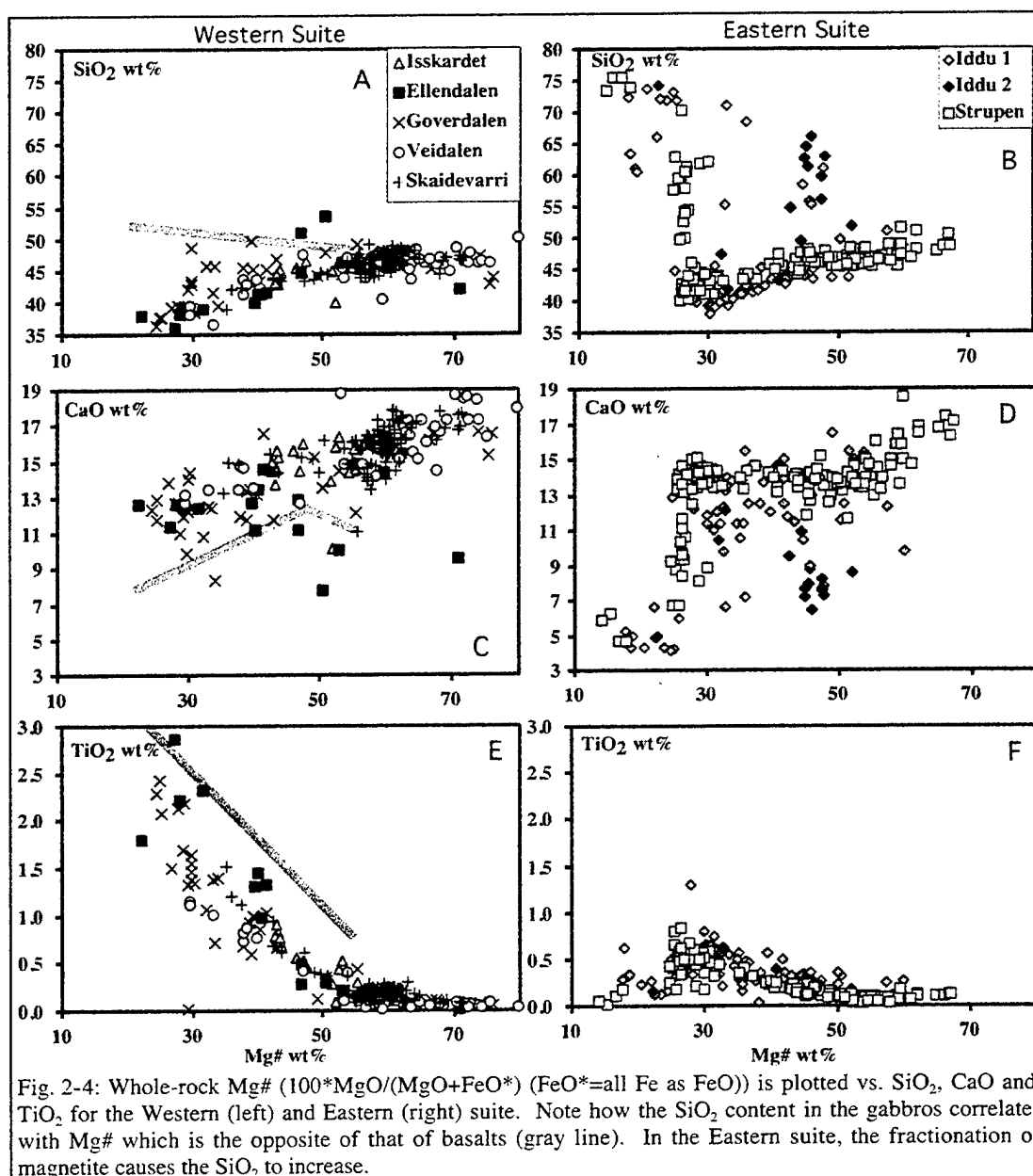
Results

Major elements

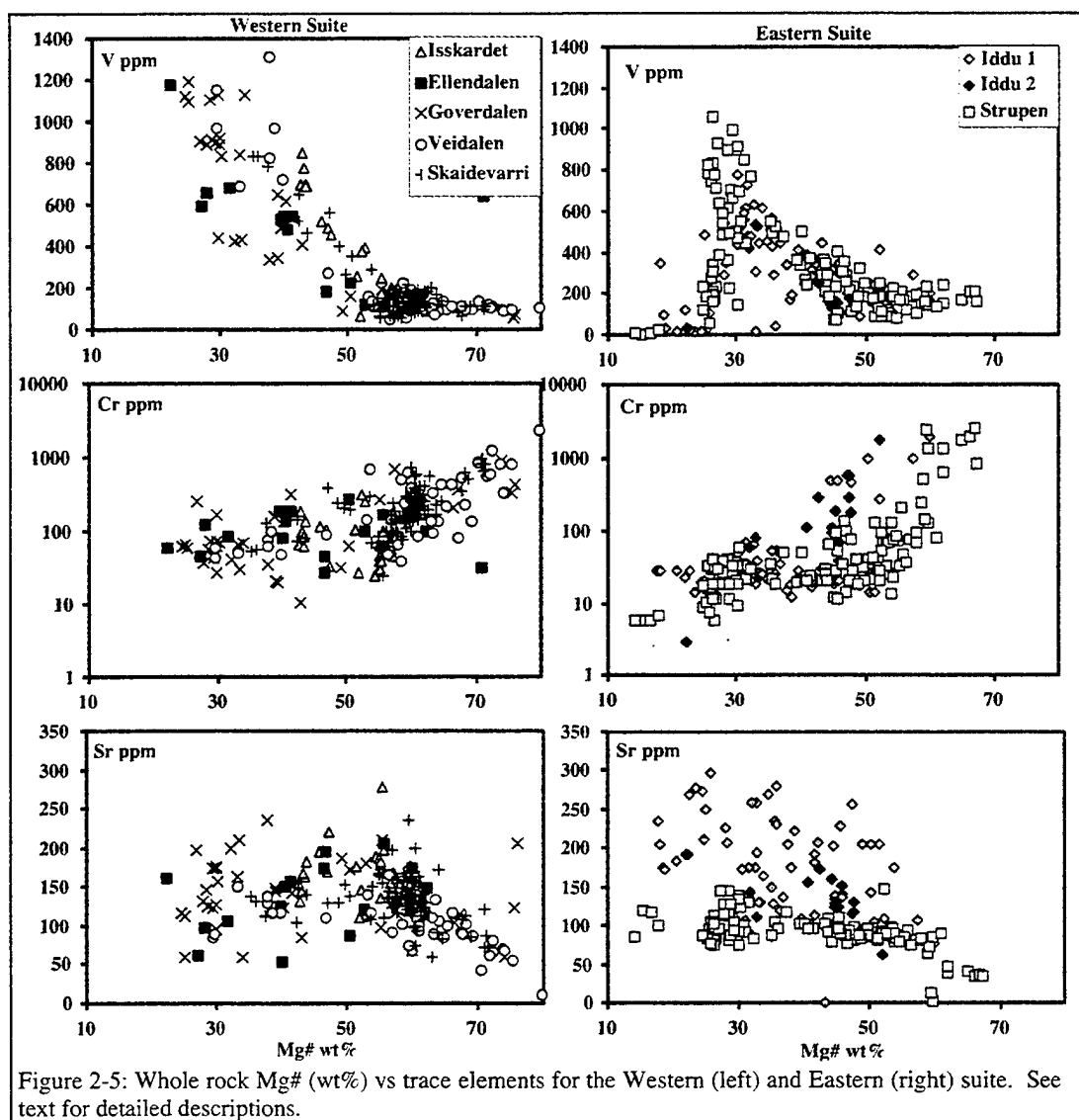
The gabbroic rocks from the Western suite of the Lyngen Gabbro are, in general, very low in silica (Fig 3) and large sections can be defined as ultrabasic ($<45\% \text{SiO}_2$). Very few samples from profiles that were analyzed from the Western suite have higher than 50-wt% SiO_2 , and the average is 45.5 wt%. The Eastern suite follows a SiO_2 enrichment trend resulting in tonalites as the most evolved rocks. However, less than 5% of the rocks of the Eastern suite are high-silica differentiates. The Al_2O_3 contents in the Eastern suite are highest for the rocks with the lowest SiO_2 contents, reflecting the importance of calcic plagioclase as a cumulate mineral. The highest Al_2O_3 contents are found in the rocks with the highest SiO_2 in the Western suite. Na_2O varies from traces to 4 wt%, but there is no clear correlation between SiO_2 and Na_2O in the Western suite, whereas the sodium-content increases with SiO_2 in the Eastern suite. K_2O and P_2O_5 are extremely low, and rarely exceed 0.1 wt%.

As the SiO_2 contents behave so differently between the suites, the degree of differentiation is explored using Mg\# 's ($100 * \text{MgO}/(\text{MgO} + \text{FeO})$) in wt-%.) The trend of decreasing SiO_2 with increased differentiation is evident in the Western suite (Fig 2-4 A and B). The rocks of the Eastern suite partly indicate this trend, even if the most evolved

Evolution of Oceanic Gabbros: In-situ and Ancient Examples



Evolution of Oceanic Gabbros: In-situ and Ancient Examples



Evolution of Oceanic Gabbros: In-situ and Ancient Examples

rocks show increased SiO_2 levels and rocks from Iddu show early SiO_2 enrichment (at Mg# 45).

The CaO (Fig 2-4C and D) contents decrease gradually during fractionation in the Western suite. However, the Eastern suite, and in particular the Strupen profile, shows near constant CaO-levels until the onset of SiO_2 enrichment.

The TiO_2 contents are dramatically different between the two suites (Fig 2-4 E and F). The Eastern suite shows few rocks with TiO_2 higher than 1 wt%, whereas the Western suite has up to 3 wt% in the most SiO_2 -poor rocks. The TiO_2 trends indicate enrichment with decreasing Mg#'s for both suites. At around Mg# 30, the TiO_2 levels drop off for the Eastern suite, whereas they increase steeply for the Western suite, indicating that the evolved, iron-rich, melts precipitated iron-titanium oxides within the cumulates.

Trace elements

The trace elements partly reflect what is observed in the major elements. It should be noted that many of the incompatible elements like Zr and Y are very close to the detection level of the XRF-method, especially in the Eastern suite.

Figure 5 demonstrates vanadium levels with similar patterns as the TiO_2 , although V indicates the presence of oxide-minerals in the Eastern suite as well as the Western suite. The V contents do, however, decrease suddenly at lower Mg#'s for the Eastern suite, possibly indicating melt-mineral segregation leaving oxide-minerals in the cumulate. In addition, the Cr concentrations are similar between the two suites but become much lower with fractionation in the Eastern suite than in the Western suite. The Sr contents show little in terms of a differentiation trend for either suite, but the concentrations are highest for the profile at Iddu.

Sm and Nd contents were measured by isotope dilution (Figure 2-6 and 2-7A). The trace elements are highest in the Western suite, where they show some correlation with Cr or Mg#. The Eastern suite has concentrations below 1ppm, and shows little correlation with either Cr or Mg#.

Evolution of Oceanic Gabbros: In-situ and Ancient Examples

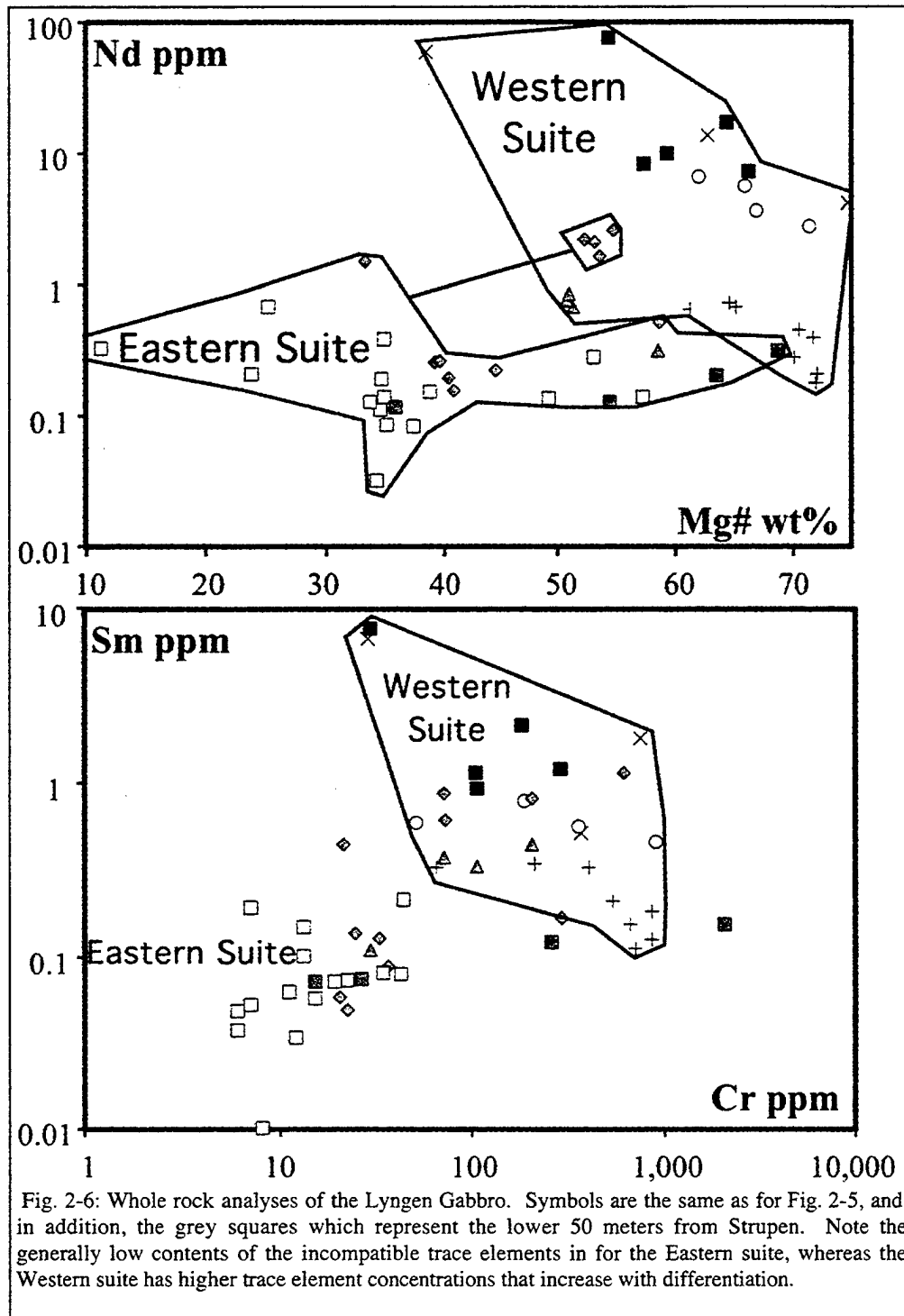
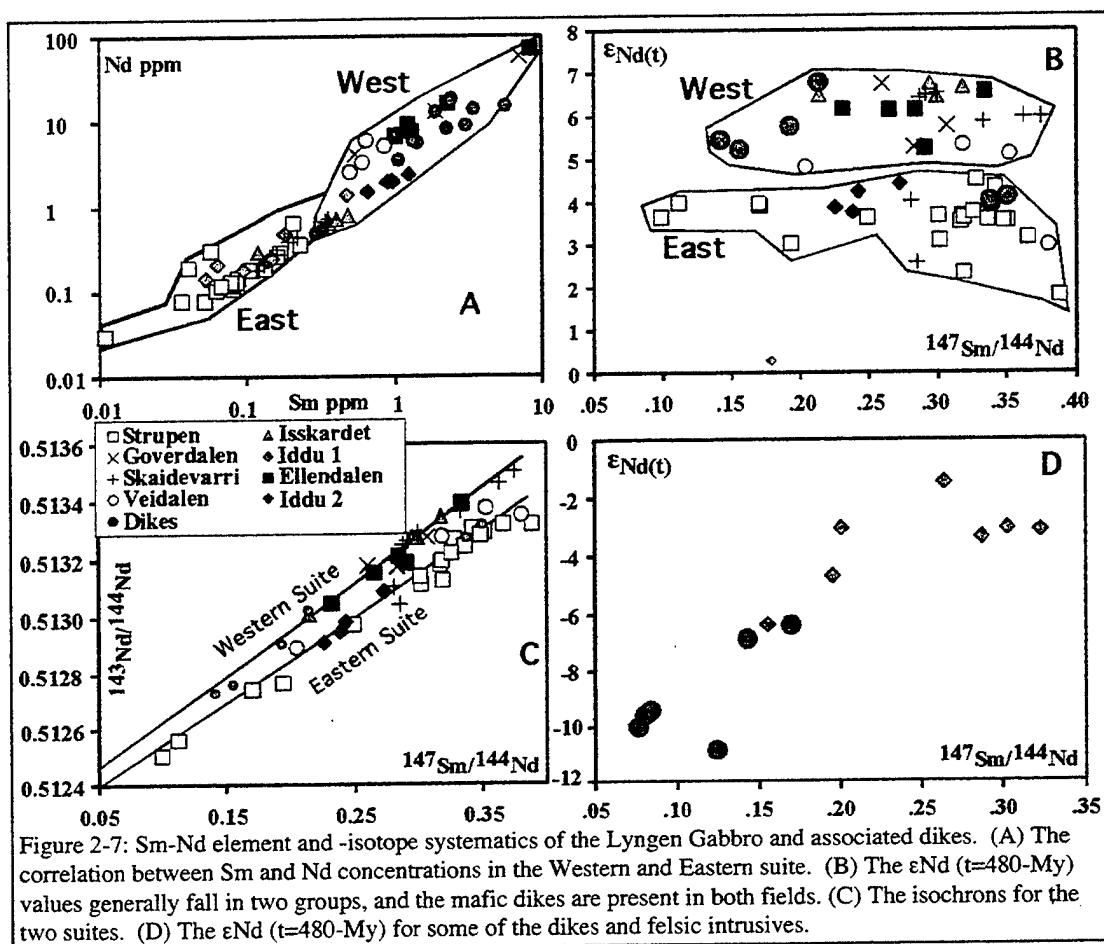


Fig. 2-6: Whole rock analyses of the Lyngen Gabbro. Symbols are the same as for Fig. 2-5, and in addition, the grey squares which represent the lower 50 meters from Strupen. Note the generally low contents of the incompatible trace elements in for the Eastern suite, whereas the Western suite has higher trace element concentrations that increase with differentiation.

Evolution of Oceanic Gabbros: In-situ and Ancient Examples



Evolution of Oceanic Gabbros: In-situ and Ancient Examples

Nd –isotopes

The $\epsilon_{\text{Nd}(t=480\text{My})}$ values for the profiles are shown in Figure 2-7. The profiles from Ellendalen, Isskardet, and Goverdalen have the highest values, around +6 (Fig. 2-7B). The Strupen samples and samples from the detailed profile at Iddu fall around +4. Veidalen samples fall in-between, whereas the Skaidevarri-profile shows values from both groups. The data plotted on an isochron-diagram indicate different initial values ($\epsilon_{\text{Nd}(t)}$ is +6.39 and +3.95 respectively) (Fig. 2-7C). The dikes that cross both suites and Rypdalen Shear Zone have ϵ_{Nd} values similar to the Western and Eastern suite. Some of the dikes and shear-zone related tonalites from Iddu have negative $\epsilon_{\text{Nd}(t)}$ values that become extremely low with differentiation (Fig. 2-7D) indicating AFC-processes (DePaolo, 1981).

Mineral analyses: major elements

Figure 8b shows a plot of Mg# of clinopyroxene vs. An% of plagioclase in all the areas of this study ($\text{Mg\#} = 100 \cdot \text{molar Mg}/(\text{Mg} + \text{Fe})$). The Easternmost profile, from Strupen, has two groups, above and below 50 meters. Plagioclase An_{90-98} coexists with Mg# 82-69 augite and Mg# 56-73 orthopyroxene. The upper half of the profile indicate the highest An contents of plagioclase found in the entire Lyngen Gabbro, and the lowest Mg#'s of clinopyroxene from the site. The lower half of the profile has clinopyroxene with Mg#'s as high as 82, but these also have An% above 90. The more An-rich trend in the upper half of the profile correlates with tonalites appearing in the layered gabbro sequence.

The next profile towards the west is Veidalen, with primitive rocks and An%'s in the higher eighties and into the 90's. The profiles in Veidalen show similar An contents to Strupen coexisting with higher Mg# augite (88 to 72). This profile is also associated with the aforementioned layered peridotites, which have augite Mg#'s up to 92 and Fo_{88} olivine. West of this geochemical transition-zone, Goverdalen gabbros have An_{87-48} plagioclase, while their augites change from Mg# 84 to 67. The olivines and orthopyroxenes follow similar trends (Fig. 2-8B and C).

The rocks of the Skaidevarre area have some plagioclase as high as An_{96} , although the majority of the plagioclases are approximately An_{85} , coexisting with Mg# 86-75

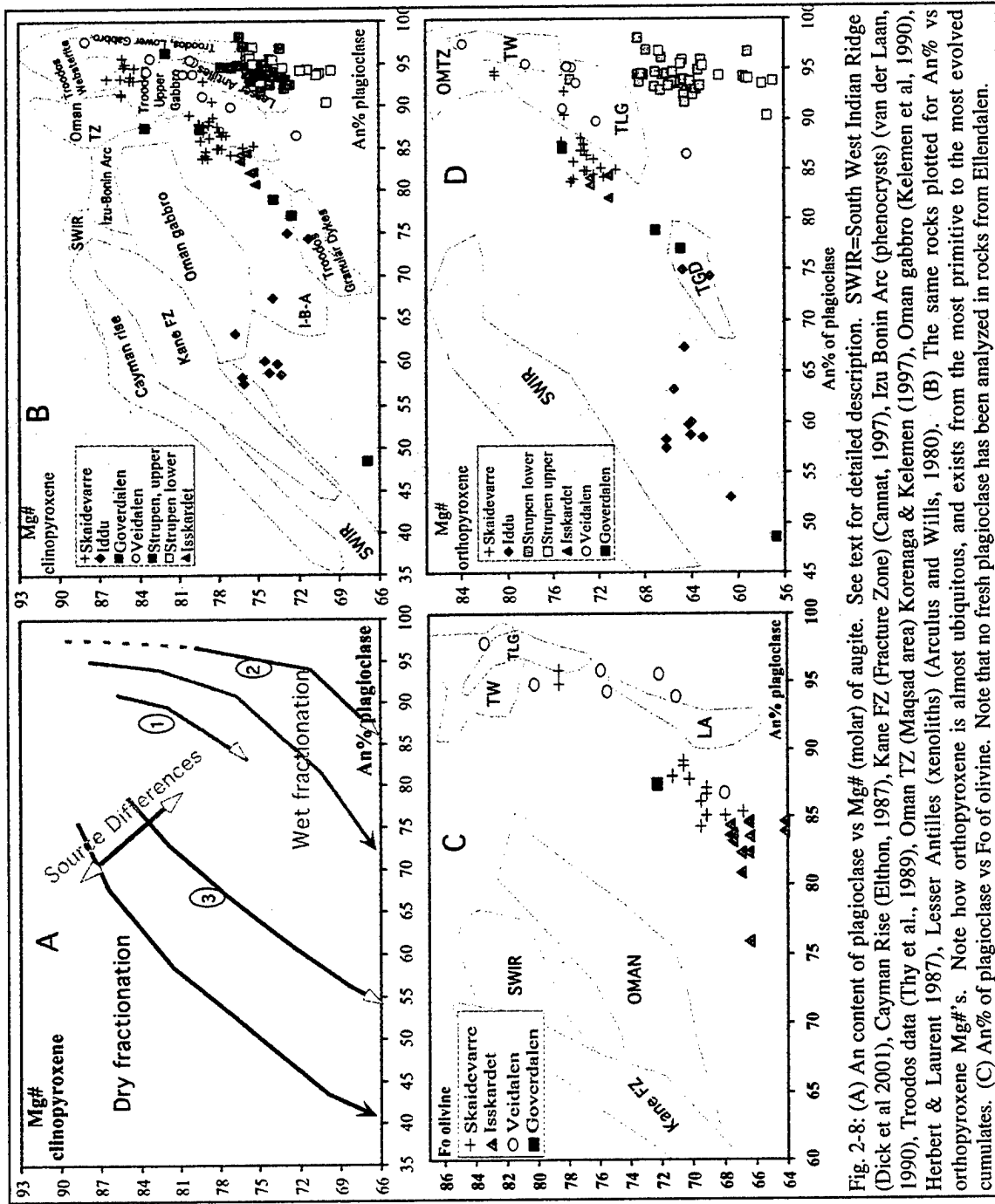
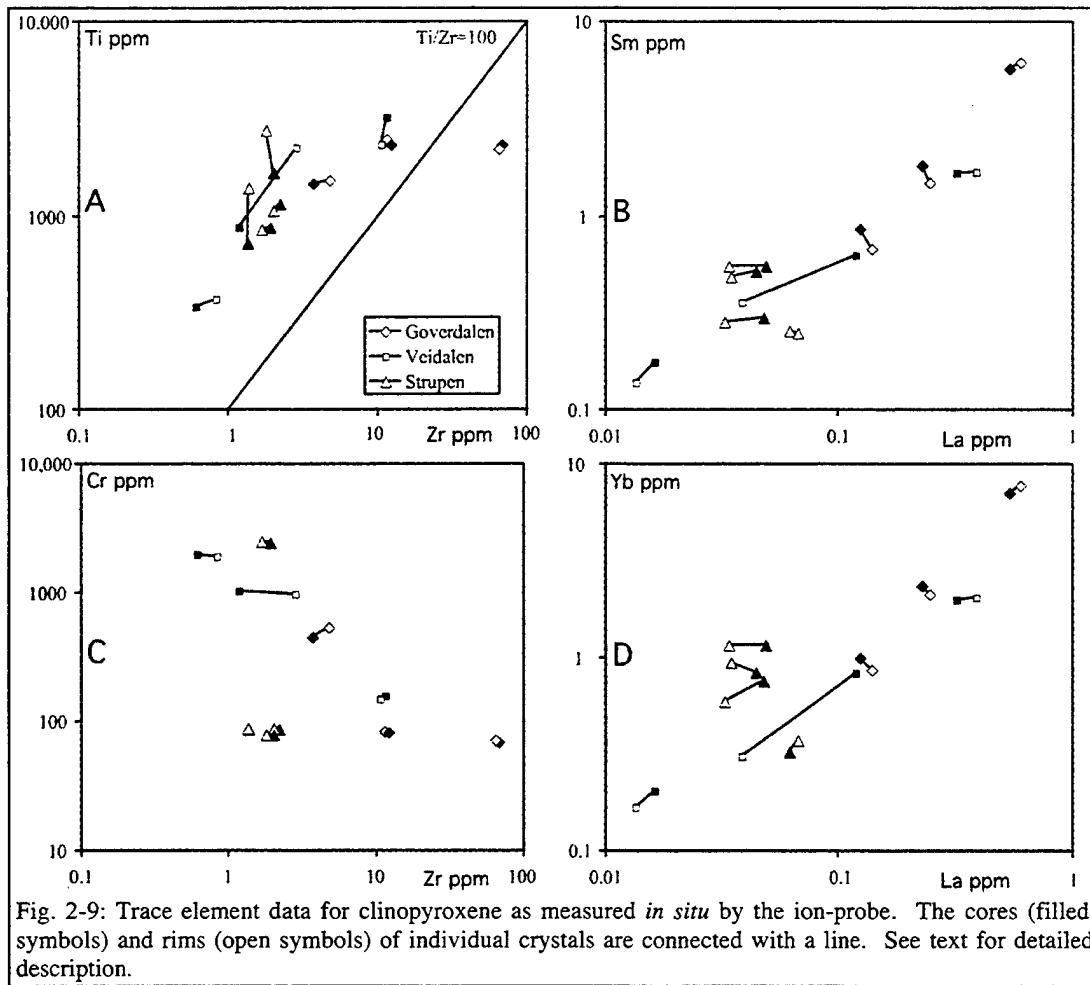


Fig. 2-8: (A) An content of plagioclase vs Mg# (molar) of augite. See text for detailed description. SWIR=South West Indian Ridge (Dick et al 2001), Cayman Rise (Elthon, 1987), Kane FZ (Fracture Zone) (Cannat, 1997), Izu Bonin Arc (phenocrysts) (van der Laan, 1990), Troodos data (Thy et al., 1989), Oman TZ (Maqad area) Korenaga & Kelemen (1997), Oman gabbro (Kelemen et al, 1990), Herbert & Laurent (1987), Lesser Antilles (xenoliths) (Arculus and Wills, 1980). (B) The same rocks plotted for An% vs orthopyroxene Mg#'s. Note how orthopyroxene is almost ubiquitous, and exists from the most primitive to the most evolved cumulates. (C) An% of plagioclase vs Fo of olivine. Note that no fresh plagioclase has been analyzed in rocks from Ellendalen.

Evolution of Oceanic Gabbros: In-situ and Ancient Examples



Evolution of Oceanic Gabbros: In-situ and Ancient Examples

augite, Mg# 68-79 orthopyroxene and Fo₆₆₋₇₈ olivine. The Easternmost rocks are the most primitive cumulates, and have plagioclase An_{>90}. The rocks westwards of these are more evolved cumulates, although they do not fall below Mg# 70 together with plagioclase of An_{~85}. Isdalen rocks have cumulates that are similar to Goverdalen and the evolved Skaidevarre.

The rocks from Iddu vary greatly with regards to the plagioclase compositions (An₅₆₋₇₅) with a near constant composition of augite and orthopyroxene, and have no olivine together with plagioclase.

Mineral analyses: trace elements

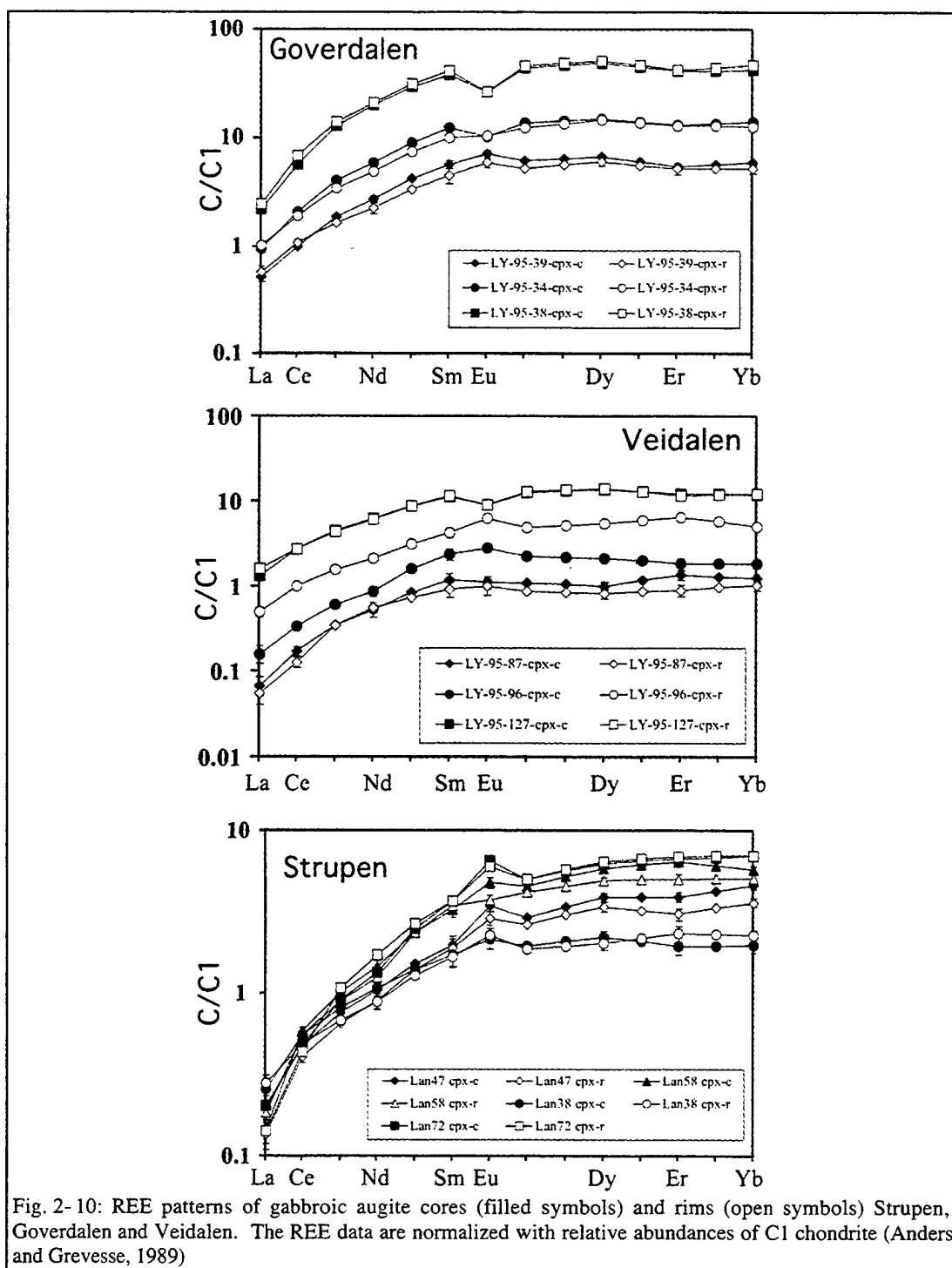
Data from three areas, Goverdalen, Veidalen and Strupen, are shown in figures 2-9 and 2-10. Fig. 2-9 indicates that the fractionation-trend for each area is different. Rocks analyzed from Goverdalen and Veidalen have a general positive correlation for the incompatible elements. Strupen appears to have a very different distribution, however. Figure 2-10, indicate that the REE become more LREE/HREE depleted as the minerals become more evolved. There are no systematics regarding core-rim analyses, in fact, reverse zoning is common. The augites from Goverdalen and Veidalen develop negative Eu anomalies with differentiation, those from Strupen does not. The anomalies are absent in the most primitive rocks but are well developed in the evolved rocks, indicating closed system fractionation of plagioclase.

Discussion

Significance of the contrasting differentiation paths for the Eastern and Western suites

It is possible that the magmas that produced the Western suite and Eastern suite of the Lyngen Gabbro had different water-contents and/or had different mantle-sources. We have explored activity of water and source-affinity using the An%(pl)-Mg#(cpx) plot which distinguish the gabbroic rocks precipitated from a hydrous magma from a dryer one by the arc of the trend (Fig. 2-8A). Dry fractionation of basaltic melt produces a convex trend whereas those for crystallization of wet melts are concave.

Evolution of Oceanic Gabbros: In-situ and Ancient Examples



Evolution of Oceanic Gabbros: In-situ and Ancient Examples

The presence of water suppresses the plagioclase-olivine cotectic relative to the plagioclase-augite cotectic (Gaetani *et al.*, 1993) and changes the reaction series to augite and even orthopyroxene crystallization before plagioclase. In addition, a melt may gain or lose water so that $Kd_{Pl/L}^{Ca/Na}$ changes, resulting in higher or lower An% plagioclase, respectively (Housh and Luhr, 1991). The effect is even more pronounced in silicic magmas (Arculus and Wills, 1990) and may cause $An_{>95}$ for more than 50% of the fractionating gabbros preceded by true ultramafic cumulates. Early fractionation of clinopyroxene before plagioclase results in a significant drop in Mg-content in the magma at a more rapid rate than if plagioclase was crystallized in concert with olivine only. Moreover, prevalent water variably depresses the liquidii and solidii of the silicic minerals, whereas there is little effect on the oxide-minerals in magmas (Gaetani *et al.*, 1993). The bend of the gabbro-trend produced by wet magma fractionation is caused by the onset of oxide fractionation. The rocks from the Western suite of the Lyngen Gabbro have this convex trend, similar to the Upper Gabbro from Troodos (Fig. 2-8B). Oxide minerals are common in primitive gabbros of both suites. The early oxide crystallization and fractionation is particularly pronounced at Iddu (Moen-Eikeland, 1999). The Iddu gabbro-compositions, however, are less systematic and range from the Izu-Bonin Arc to the field of Mid-Atlantic Ridge (MAR). The Eastern suite of the Lyngen Gabbro has rocks that have abundant quartz, coexisting with extremely An-rich plagioclase, two pyroxenes and magnetite, and the mineral-compositions are similar to the Lower Gabbros from Troodos (Fig. 2-8B). Overlapping with this trend are the Lesser Antilles lower crustal xenoliths, which Arculus and Wills (1990) demonstrated crystallized under hydrous conditions in a relatively silicic magma.

Dryer oceanic magmas, where plagioclase reaches the liquidus before clinopyroxene, experience a slower fractionation of Mg/Fe from the magma relative to Ca/Na in part because Ca is not depleted by augite-fractionation at an early stage. In addition, $Kd_{Pl/L}^{Ca/Na} \approx 1$ (Grove *et al.*, 1992), and therefore reflect the Ca/Na ratio of the melt more directly. The vertical displacement of the curve varies with the Ca/Na and Mg/Fe of the parental melt (Fig. 2-8A). For instance, Mid-Cayman Rise gabbro compositions are similar to those from the South West Indian Ridge whereas gabbros from the Kane

Evolution of Oceanic Gabbros: In-situ and Ancient Examples

Fracture Zone region of the MAR where the Ca/Na is lower and Mg/Fe is higher, have lower An% plagioclase at a given Mg# of augite (Fig. 8B).

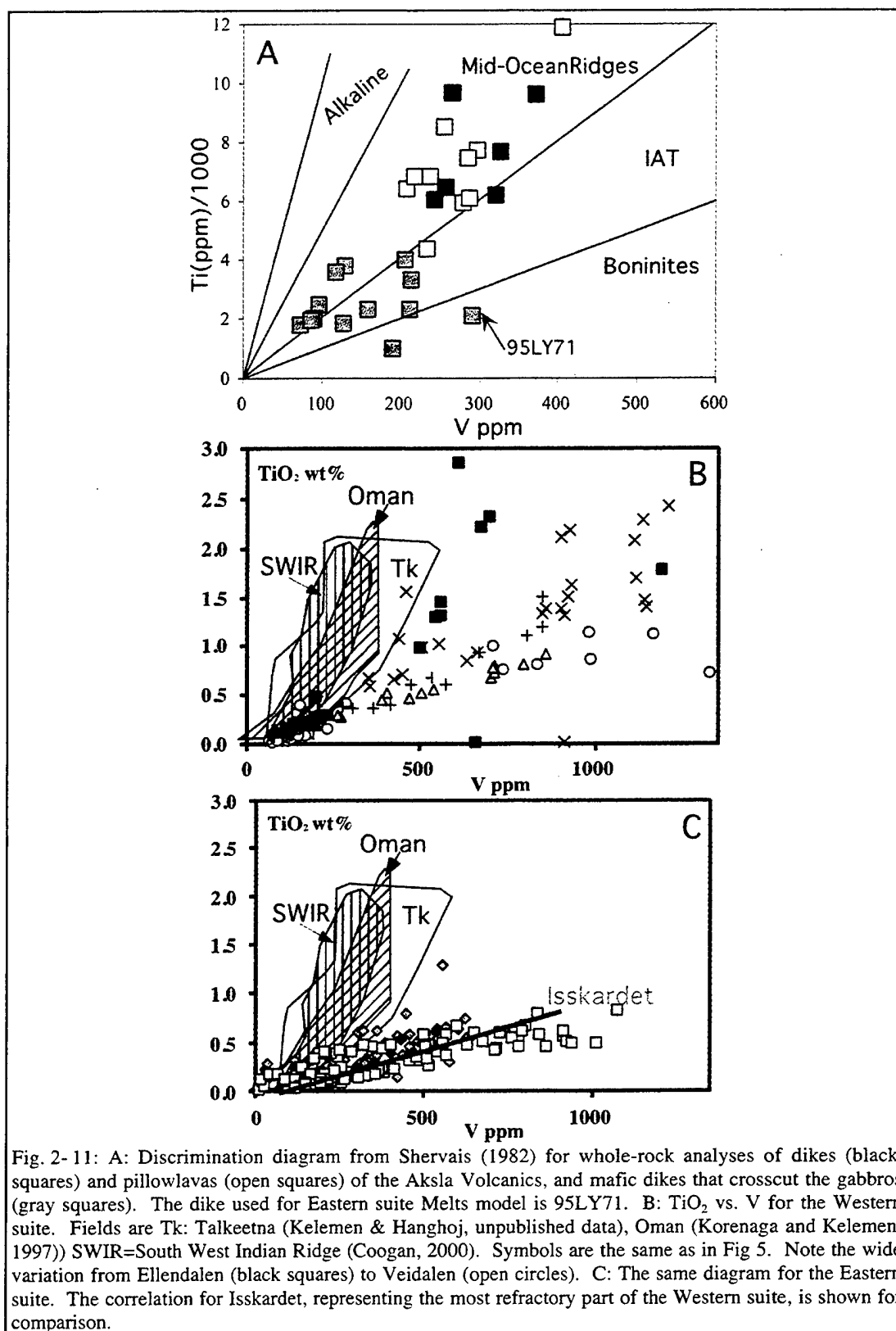
Increasing pressure lowers $Kd_{Pl/L}^{Ca/Na}$ and leads to the formation of a lower An% plagioclase (Panjasawatwong, *et al.*, 1995). In addition, the pressure depresses the plagioclase-olivine cotectic relative to the olivine-clinopyroxene cotectic, and the Ca-Tschermak-component of the clinopyroxene increases (Gaetani *et al.*, 1993). The result of fractionation at high pressures lead to ultramafic rocks with high-Al augite, followed by gabbroic cumulate with a convex trend, plagioclase starting at relatively low An-contents. Plagioclase-free wehrlites are common in the Western suite (Kvassnes, 1997), and cumulative, plagioclase-free harzburgites and lherzolites are found in the Eastern suite (Hetland, 1996). However, the high An% plagioclase and the concave fractionation-trends indicate crystallization from wet melts at relatively low pressures.

We used Melts 5 (Ghiorso and Sack, 1995) to estimate fractionation-trends for the rocks from this study (arrows 1-3 in figure 2-8A). A primitive MAR melt extracted from PetDB was used as an initial composition and partly reproduced fractionation-trends for Goverdalen and Skaidevarri by adding water to the melt at low crustal pressures (1-kbar) (arrow 1). The dry fractionation may therefore replicate some of the gabbros at Iddu. It has been argued that these calculations may be questionable for the Melts program (Yang *et al.*, 1996). On inspection, the high $Kd_{Pl/L}^{Ca/Na}$ values are comparable to those of hydrous melts (Housh and Luhr, 1991), and the partition-coefficients for the mafic minerals are reasonable. However, the addition of water to MAR-type melts or crystallization at higher pressures cannot reproduce the Strupen trend, as the Ca/Na of the melt is too low. The fractionation trend of the Stupen gabbros can, however, be reproduced by water-saturated crystallization of a dike ($\epsilon_{Nd(t=480My)}^{Nd}$ of 4.1) that cross-cuts the Western suite in Goverdalen (sample 95LY71 as shown by arrow 2 in figure 2-8A). The difference between the upper and lower half of the Strupen profile can be explained by the addition of just a little more water to the magma that produced the upper half.

Parental magma compositions

We have adapted Shervais' (1982) TiO_2 -V tectonomagmatic discrimination-diagram for basalts to accommodate our gabbroic rocks and have compared our whole-

Evolution of Oceanic Gabbros: In-situ and Ancient Examples



Evolution of Oceanic Gabbros: In-situ and Ancient Examples

rock analyses to known sites. The Ti/V-ratio provides constraints on the tectonomagmatic conditions for the primary magmas, as both TiO_2 and V follow the same magmatic processes. The source of the Eastern suite must have been derived from a more depleted mantle source than the Western suite, but the transition between the suites is gradational in the south (Fig. 2-11B and C). Most of the Aksla Volcanics dikes and pillow-lavas, however, are similar to those in oceanic ridge settings, whereas the dikes that crosscut the gabbros are more varied (Fig. 2-11A).

The REE-melt composition has been calculated using partition coefficients for the selected augite from Goverdalen, Veidalen and Strupen (Figure 2-12). The result is compared to N-MORB, IAT (Sun, 1980), the Aksla Volcanics (Furnes and Pedersen, 1995), boninites (Hickey and Frey, 1982) and Troodos lavas (Taylor and Nesbitt, 1988). The result supports that Goverdalen gabbros and Veidalen gabbros may have crystallized from magma similar to the Aksla Volcanics or an N-MORB seeing that their REE patterns are parallel. The Strupen augites, however, are very low in LREE/HREE and did not crystallize from "normal" boninitic magmas, but from ultra-depleted magmas not enriched in LREE, similar to boninitic lavas from Troodos. However, most boninitic lavas from Troodos have LREE enrichment and a U-shaped pattern (Taylor and Nesbitt, 1988). Like the Troodos magmas, the augites from Strupen indicate trends that are not parallel, suggesting source-evolution or crustal contamination (DePaolo, 1981). The patterns cross as the rocks become more evolved, suggesting that the chemical signature of the profile changes at about 50 meters above the base.

Temporal and spatial relations between the Western and Eastern suite

The gabbros in the Eastern suite uniformly have lower ϵ_{Nd} values than the Western suite and each suite follows separate, but parallel isochrons (Fig. 2-7), suggesting similar ages of the suites. Therefore, the parental magmas must have had different and relatively homogeneous compositions before emplacement. Slagstad (1995) and Selbekk (1998, 2002) suggested that the oceanic Rypdalen Shear Zone generally separates the two suites and there are several sites in the northern half of the Lyngen Peninsula that clearly supports this. However, in Skaidevarri the profile starts with low ϵ_{Nd} values and An-rich

Evolution of Oceanic Gabbros: In-situ and Ancient Examples

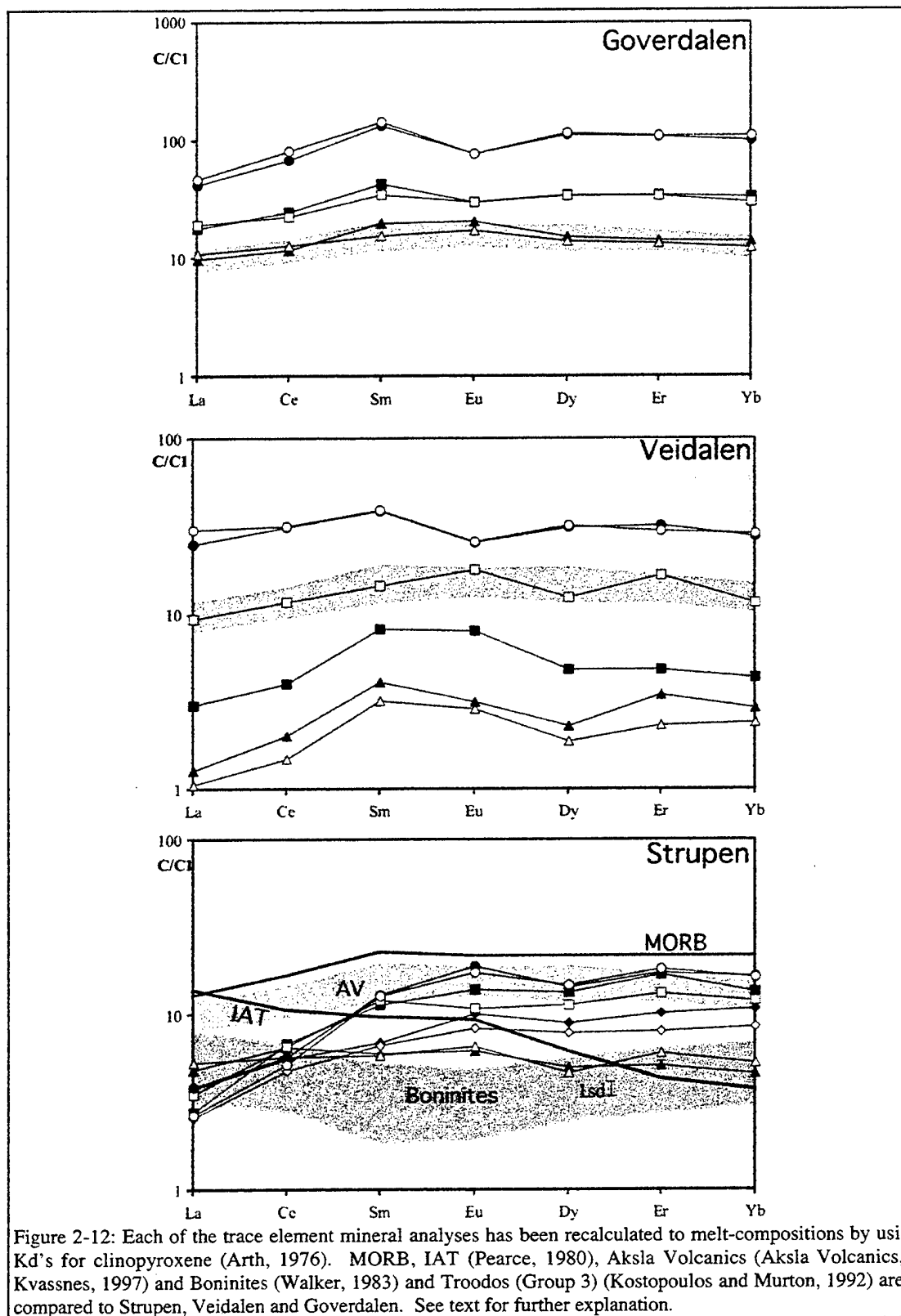


Figure 2-12: Each of the trace element mineral analyses has been recalculated to melt-compositions by using K_d 's for clinopyroxene (Arth, 1976). MORB, IAT (Pearce, 1980), Aksla Volcanics (Aksla Volcanics, Kvassnes, 1997) and Boninites (Walker, 1983) and Troodos (Group 3) (Kostopoulos and Murton, 1992) are compared to Strupen, Veidalen and Gerverdalen. See text for further explanation.

Evolution of Oceanic Gabbros: In-situ and Ancient Examples

plagioclase in the east. The trend changes over less than 10-m into higher ϵ_{Nd} values and reduced plagioclase An% contents, whereas the Mg#'s of mafic minerals remain mostly unchanged. Since the most primitive rocks are those with low ϵ_{Nd} it is not likely that the magma was contaminated by AFC-processes, and we suggest that the Skaidivarre-profile was sampled across a magmatic transition between the two suites. The layered series has no intrusive or tectonic contacts, indicating that the two magmatic systems coexisted. In Skaidivarre, the gabbros are cut by the Rypdalen Shear-Zone further to the west than the contact between the suites. It is therefore unlikely that the Rypdalen Shear-Zone caused the boninites to be emplaced together with the tholeiites, but rather that for some parts of the complex magmatism was concurrent and that the rest of the complex was produced with close proximity between the suites.

Several dikes crosscut the gabbros. On the basis of ϵ_{Nd} , the mafic dikes represent magma from both suites. However, some of the felsic dikes that crosscut the gabbros have negative values, indicating enriched material either through assimilation or by source enrichment (Fig. 2-7D). These dikes have not been dated, and it is uncertain if they were intruded at a later stage.

Plate Tectonic Affinity and comparison to other sites.

Boninites are generally believed to be derived from a peridotitic source after MORB extraction (Crawford *et al.*, 1989; Kelemen *et al.*, 1990) and frequently show a LREE enrichment causing a U-shaped pattern. However, there are several categories of boninites, Low-Ca (3 types) and High-Ca boninites and the Eastern suite represents high-Ca type boninite as seen in the extremely An-rich plagioclase. Although the augites from the Eastern-suite gabbro do not reflect the U-shaped REE-pattern often seen in boninites, the cumulates are clearly crystallized from a hydrous, ultra-depleted magma while having lower ϵ_{Nd} values than the Western suite. The Western suite gabbros were also crystallized from a hydrous magma, although the corresponding upper crustal material reflects tholeiites like those from Mid-Ocean Ridge type magmatism, making us conclude these are island arc tholeiites. In addition, the two suites were emplaced concurrently with a gradational transition between them in the south.

Evolution of Oceanic Gabbros: In-situ and Ancient Examples

It has been known for some time that a back-arc type, and arc and fore-arc (*supra-subduction zone*) type magmatic rocks occur in ophiolites. For example, Schouten and Kelemen, (2002) demonstrated that the lower (tholeiitic) and upper (boninitic) lavas in the Troodos Ophiolite are related to the Upper and Lower Gabbros, respectively, and they argue that the systems were contemporaneous. Taylor and Nesbitt (1988) showed REE-patterns that cross for the Troodos Upper Lavas, and Cameron *et al.* (1983) points out that the trace-element and isotope affinities between the Upper and Lower Lavas are so different that they must have had different magma sources.

Present-day systems, like the Izu-Bonin arc in the Southeast Pacific, comprise an outer-arc high, a boninitic fore-arc, an arc section and an actively spreading back-arc basin (Crawford *et al.*, 1981; Taylor *et al.*, 1992). It is less common to find coexisting back arc, arc, and fore-arc basin magmatism obducted in the same ophiolite (Taylor *et al.* 1992). In fact, there is no typical silicic or calc-alkaline arc-magmatism in the Lyngen Magmatic Complex, though an arc-section is present in the similar-age ophiolites in southern part of Norway (e. g. the Karmøy Ophiolite of Pedersen and Hertogen, 1990). Taylor *et al.* (1992) suggested that the tectonomagmatic conditions that produce boninites and tholeiites together is currently not active in the oceans today. It is often suggested that coexisting tholeiitic and boninitic magmatism is the result of incipient arcs, and part of the early arc of the Izu-Bonin arc is currently the outer-arc high. ODP-site 458, situated on the outer-arc high between the Mariana trench and –ridge (Hickey-Vargas, 1989) did find contemporaneously emplaced back-arc basin tholeiites and high-Ca boninite lavas. They suggest that the boninite parent-magmas were generated by high degrees of melting of a moderately depleted lithosphere residual from generating Philippine-sea MORB, and that hydrous melting at greater depth, possibly within the asthenosphere, generated the tholeiites. The close proximity to the trench make the oceanic crust more likely to be emplaced into the deeper levels on an orogenic belt, preserving them during erosion and orogenic collapse. The Svensby Formation, a part of the Balsfjord Group overlying the Lyngen Magmatic Complex, has calc-alkaline pillow-basalts dismembered from other arc rocks. It is possible that the closure of the large Iapetus Ocean may have caused several slivers of the supra-subduction zone to be

Evolution of Oceanic Gabbros: In-situ and Ancient Examples

obducted onto the continental margin, preserving only the Lyngen Magmatic Complex in this part of the Scandinavian Caledonides.

Conclusion

The Lyngen Gabbro represents the lower crustal section of an incipient arc or outer-arc high of an Ordovician oceanic *supra-subduction* zone. The Western suite was precipitated from magma that could have been derived from the same system as the associated Aksla Volcanics and Kjosén Greenschist. This primary magma was derived from a source similar to that of mid-ocean ridges, although hydrous crystal-fractionation suggests that the tectonomagmatic setting was an island-arc tholeiite produced at spreading-ridge with fluids derived from the subducted slab. The Eastern suite comprise cumulates that were crystallized from magmas similar to those of the ultra-depleted magmas of fore-arcs. Although the volcanic counterpart of the ultra-depleted Eastern suite has not been found, dikes crosscutting the gabbros may represent the magma that formed them. The oceanic Rypdalen Shear Zone generally separates the two suites, but non-tectonic transitions from boninitic to island-arc tholeiitic affinities suggest the magmatism happened concurrently.

Evolution of Oceanic Gabbros: In-situ and Ancient Examples

References:

- Anders E. Grevesse N (1989) Abundances of the elements; meteoritic and solar. *Geoch Cosm Acta*, 53 (1): 197-214.
- Andresen A. Bergh S (1985) Stratigraphy and tectonometamorphic evolution of the Ordovician-Silurian Balsfjord Group, Lyngen Nappe, North Norwegian Caledonides. In: Gee D. Sturt B (eds) *The Caledonide Orogen; Scandinavia and related areas Vol. 1*: 579-591.
- Andresen A. Fareth E. Bergh S. Kristensen SE. Krogh E. (1985) Review of Caledonian Lithotectonic units in Troms, North Norway. In: Gee D. Sturt B (eds) *The Caledonide Orogen; Scandinavia and related areas Vol. 1*: 569-577.
- Andresen A. Stelthenpohl MG (1994) Evidence of ophiolite obduction, terrain accretion and polyorogenic evolution of the north Scandinavian Caledonides. *Tectonophysics* 231: 59-70.
- Arculus RJ. Wills KJA. (1990) The petrology of the plutonic rocks and inclusions from the Lesser Antilles Island Arc. *Journal of Petrol* 21: 743-799.
- Baker PE (1973) Volcanism at destructive plate margins. *J. Earth. Sci. Leeds* 8: 183-195.
- Binns RE (1978) Caledonian Nappe correlation and orogenic history in Scandinavia north of lat 67 degrees N. *Geol Soc Am Bull* 89 (10): 1,475-1,490.
- Cameron WE. McCulloch MT, Walker DA, (1983) Boninite petrogenesis; chemical and Nd-Sr isotopic constraints. *Earth Planet. Sci. Lett.* 65(1): 75-89.
- Cann JR (1977) Rb, Sr, Y, Zr and Nb in some Ocean Floor Basaltic Rocks. *Earth Planet Sci Lett* 10: 7-11.
- Cannat M. Chatin F. Whitechurch H. Ceuleneer G (1997) Gabbroic rocks trapped in the upper mantle in the Mid-Atlantic Ridge. In: Karson JA. Cannat M. Miller DJ. Agar SM. Barling J. Casey JF. Ceuleneer G. Dilek Y. Fletcher JM. Fujibayashi N. Gaggero L. Gee JS. Hurst SD. Kelley DS. Kempton PD. Lawrence RM. Marchig V. Mutter C. Niida K. Rodway K. Ross DK. Stephens CJ. Werner C-D. Whitechurch H. Stokking L (ed) *Proceedings of the Ocean Drilling Program, Scientific Results*, 153: 243-264.
- Chroston PN (1972) A gravity profile across Lyngnehalvøya, Troms, Northern Norway. *Norsk Geologisk Tidsskrift*, 55: 295-303.
- Coish RA (1977) Ocean-floor metamorphism in the Betts cove Ophiolite, Newfoundland. *Contrib Mineral Petrol* 60: 255-270.
- Coogan LA. MacLeod CJ. Dick HJB. Edwards SJ. Kvassnes A. Natland JH. Robinson PT. Thompson G. O'Hara MJ, 2001: Whole-rock geochemistry of gabbros from the Southwest Indian Ridge: constraints on geochemical fractionations between the upper and lower oceanic crust and magma chamber processes at (very) slow-spreading ridges. *Chem Geol* 178: 1-22.
- Crawford AJ. Beccaluva L. Serri G (1981) Tectonomagmatic evolution of the West Philippine-Mariana region and the origin of boninites. *Earth Planet Sci Lett* 54: 346-356.
- Crawford AJ. Falloon TJ. Green DH (1989) Classification, petrogenesis and tectonic setting of boninites. In: Crawford AJ (ed) *Boninites and Related rocks*. Allen & Unwin, New Zealand, 2-49.
- Dallmeyer RD. Andresen A (1992) Polyphase tectonothermal evolution of exotic Caledonian nappes in Troms, Norway; evidence from $^{40}\text{Ar}/^{39}\text{Ar}$ mineral ages. *Lithos*, 29 (1-2): 19-42.
- DePaolo, DJ (1981) Trace element and isotopic effects of combined wallrock assimilation and fractional crystallization. *Earth Planet Sci Lett* 53 (2): 189-202.
- Dick HJB. Natland JH. Alt JC. Bach W. Bideau D. Gee JS. Haggas S. Hertogen JGH. Hirth JG. Holm PM. Ildefonse B. Iturrino GJ. John BE. Kelley DS. Kikawa E. Kingdon A. LeRoux PJ. Maeda J. Meyer PS. Miller DJ. Naslund HR. Niu YL. Robinson PT. Snow J. Stephen RA. Trimby PW. Worm HU. Yoshinobu A (2000) A long in situ section of the lower ocean crust; results of ODP Leg 176 drilling at the Southwest Indian Ridge. *Earth Planet Sci Lett* 179 (1): 31-51.
- Dunning GR. Pedersen RB (1988) U/Pb ages of ophiolites and arc-related plutons of the Norwegian Caledonides: implications for the development of Iapetus. *Contrib Mineral Petrol* 98: 13-23.
- Elliot RB (1972): The chemistry of gabbro/amphibolite transition in South Norway. *Contrib Mineral Petrol*, 38: 71-79.
- Elthon D (1987) Petrology of gabbroic rocks from the Mid-Cayman Rise spreading center. *J Geophys Res* 92 (B1): 658-682.
- Elthon D. Stewart M. Ross DK (1994) Compositional trends of minerals in oceanic cumulates. *J Geophys Res* 97 (B11): 15,189-15,1992.

Evolution of Oceanic Gabbros: In-situ and Ancient Examples

- Emeleus GH. Cheadle MJ. Hunter RH. Upton BGJ. Wadsworth WJ (1996) The Rum Layered Suite. In: Cawthorn, RG (ed) Layered Intrusions, Elsevier Science B. V.
- Furnes H. Pedersen RB (1995) The Lyngen Magmatic Complex: Geology and geochemistry. *Geonytt*, 22:30.
- Gaetani GA. Grove TL. Bryan WB (1993) The influence of water on the petrogenesis of subduction-related igneous rocks. *Nature (Lon)*, 365 (6444): 332-334.
- Ghiorso MS. Sack RO. (1995) Chemical Mass Transfer in Magmatic Processes, IV. A Revised and Internally Consistent Thermodynamic Model for the interpolation of Liquid-Solid Equilibria in Magmatic Systems at Elevated Temperatures and Pressures. *Contrib Mineral Petrol* 119: 197-212.
- Govindaraju K (1994) 1994 compilation of working values and sample description for 383 geostandards. *Geostandards Newsletter*, 18, special issue.
- Grove TL. Kinzler RJ. Bryan WB (1992) Fractionation of Mid-Ocean Basalt (MORB). In: Morgan JP. Blackman DK. Sinton JM (eds) *Mantle Flow and Mid Ocean Ridges*. *Geophys Monogr* 71: 281-310.
- Hetland A. (1996) Petrology and petrogenesis of high-Ca tonalites and quartz-bearing gabbros within the layered series of Lyngen Magmatic Complex (Troms, Norway). Thesis for the Cand. Scient. Degree, University of Bergen, Norway.
- Hickey-Vargas, R (1989) Boninites and tholeiites from DSDP Site 458, Mariana Forearc. In: Crawford AJ. (ed) *Boninites*. Unwin Hyman, London, UK (GBR).
- Hickey RL. Frey FA. (1982) Geochemical characteristics of boninite series volcanics: implications for their source. *Geochim Cosmochim Acta* 46: 2099-2115.
- Housh TB. Luhr JF (1991) Plagioclase-melt equilibria in hydrous systems. *Am Min* 76: 477-492.
- Jenner GA. Longerich HP. Jackson SE. Fryer BJ (1990) ICP-MS: -a powerful new tool for high-precision trace elements analysis in earth sciences: Evidence from analysis of selected USGS standards. *Chemical Geology*, 38: 323-344.
- Kelemen PB, 1990: Reaction Between Ultramafic Rock and Fractionating Basaltic Magma I: Phase relations, the origin of calc-alkaline magma-series and the formation of discordant dunite. *Jour Petrol* 31:51-98
- Korenaga J. Kelemen PB (1997) Origin of gabbro sills in the Moho transition zone of the Oman Ophiolite; implications for magma transport in the oceanic lower crust. *J Geophys Res* 102 (B12): 27,729-27,749.
- Kostopoulos DK. Murton BJ (1992) Origin and distribution of components in boninite genesis: significance of the OIB component. In: Parson LM. Murton BJ. Browning P. (eds) *Ophiolites and their Modern Oceanic Analogues*. Geological Society Special Publication No. 60: 133-154.
- Kvassnes AJ (1997) The Western suite of the Lyngen Gabbro and its Petrogenetic relations to the Volcanic and Ultramafic rocks associated with the Lyngen Magmatic Complex in Troms, Northern Norway. Thesis for the Cand. Scient. Degree, University of Bergen, Norway.
- Minsaas, O (1981) Lyngenhelvøyas geologi, med spesiell vekt på den sedimentologiske utvikling av de ordovisisk-siluriske klastiske sekvenser som overligger Lyngen Gabbrokompleks, Troms. Cand. Scient. (*The Geology of the Lyngen Peninsula, with special emphasis on the sedimentological development of the Ordovician-Silurian clastic sequences overlying Lyngen Gabbro-complex.*) Thesis, Univ. of Bergen.
- Minsaas O. Sturt BA (1985) The Ordovician-Silurian clastics sequence overlying the Lyngen Gabbro Complex, and its environmental significance. In: Gee DG. Sturt BA (eds) *The Caledonide Orogen: -Scandinavia and Related Areas*, Vol. 1: 569-577.
- Miyashiro A (1975) The Troodos Ophiolite Complex was probably formed in and Island Arc, *Earth Planet Sci Lett* 19: 218-224.
- Moen-Eikeland, H. E., 1999., Intrusive relasjoner i og petrogense av gabbroiske og tonalittiske bergarter på Lyngstuva, Troms, nord Norge. (*Intrusive relations in, and petrogenesis of gabbroic and tonalitic rocks at Lyngstuva, Troms, North Norway.*) Thesis for the Cand. Scient Degree, University of Bergen, Norway.
- Munday RJC. (1970) The Geology of the northern part of the Lyngen Peninsula, Troms, Norway. Ph. D Thesis, University of Newcastle upon Tyne.
- Munday RJC (1974) The geology of the northern half of the Lyngen Peninsula, Troms, Norway. *Norsk Geologisk Tidsskrift, Suppl.*, 54 (1): 49-62.
- Nicolas A. (1989) Structures of ophiolites and dynamics of oceanic lithosphere, Kluwer, Dordrecht, pp 367.
- Oliver GH. Krogh TE (1995) U-Pb zircon ages of 469 ± 5 Ma for a metatonalite from the Kjosén Unit of the Lyngen magmatic complex, northern Norway. *Norges Geologiske Undersøkelser*, 428: 27-33.

Evolution of Oceanic Gabbros: In-situ and Ancient Examples

- Padfield T. Gray A (1971) Major element rock analyses by X-ray fluorescence- a simple fusion method. NV Philips, Eindhoven, Analytical Equipment FS 35.
- Panjasawatwong Y. Danyushevsky LV. Crawford AJ. Harris KL (1995) An experimental study of the effects of melt composition on plagioclase; melt equilibria at 5 and 10 kbar; implications for the origin of magmatic high-An plagioclase, *Contrib Mineral Petrol* 118(4): 420-432.
- Pearce JA. (1980) Geochemical evidence for the genesis and eruptive setting of lavas from Tethyan ophiolites. In: Panayiotou, A: Ophiolites; Proceedings, International ophiolite symposium. Cyprus Minist Agric Nat Resour, Geol Surv Dep Nicosia, Cyprus (CYP).
- Pedersen RB. Furnes H (1991) Geology, magmatic affinity and geotectonic environment of some Caledonian ophiolites in Norway. *Journal of Geodyn* 13: 183-203.
- Pedersen RB. Hertogen J (1990) Magmatic Evolution of the Karmøy Ophiolite Complex, SW Norway: relationships between MORB-IAT-boninitic-Calc-alkaline and alkaline magmatism. *Contrib Mineral Petrol* 104: 227-293.
- Pin C. Briot D. Bassin C. Poitrasson F (1994) Concomitant separation of strontium and samarium neodymium for isotope analyses in silicate samples, based on extraction chromatography. *Analitica Chimica Acta*, 298: 209-217.
- Randall BAO (1959) A preliminary account of the geology of the southern portion of Lyngen, Troms, north Norway. Ph. D thesis, Univ. of Durham.
- Randall BAO (1971) An outline of the geology of the Lyngen Peninsula, Troms, Norway. In: The Caledonian geology of northern Norway. Bulletin - Norges Geologiske Undersøkelse. 269: 68-71.
- Randall BAO (1971) The igneous rocks of the Lyngen Peninsula, Troms, Norway. In: The Caledonian geology of northern Norway. Bulletin - Norges Geologiske Undersøkelse 269: 143-146.
- Richard P. Shimizu N. Allégre CJ (1976) $^{143}\text{Nd}/^{144}\text{Nd}$, a natural tracer: An application to oceanic basalts. *Earth Planet Sci Lett* 60: 93-104.
- Roberts D. Gee DG (1985) An introduction to the structure of the Scandinavian Caledonides In: Gee DG. Sturt BA (eds) *The Caledonide Orogen: -Scandinavia and Related Areas*, Vol 1: 55-68.
- Ross DK. Elthon D (1997) Cumulus and postcumulus crystallization in the oceanic crust; major and trace-element geochemistry of Leg 153 gabbroic rocks. In: Karson JA. Cannat M. Miller DJ. Agar SM. Barling J. Casey JF. Ceuleneer G. Dilek Y. Fletcher JM. Fujibayashi N. Gaggero L. Gee JS. Hurst SD. Kelley DS. Kempton PD. Lawrence RM. Marchig V. Mutter C. Niida K. Rodway K. Ross DK. Stephens CJ. Werner C-D. Whitechurch H. Stokking L (ed) *Proceedings of the Ocean Drilling Program. Scientific Results*, 153: 277-284.
- Schouten H. Kelemen PB (2002) Melt viscosity, temperature and transport processes, Troodos Ophiolite, Cyprus. *Earth Planet Sci Lett* 201 (2): 337-352.
- Selbekk RS. Bray CJ. Spooner ETC (2002) Formation of tonalite in island arcs by seawater-induced anatexis of mafic rocks; evidence from the Lyngen Magmatic Complex, North Norwegian Caledonides. *Chemical Geology*, 182: 69-84.
- Selbekk RS. Furnes H. Pedersen RB. Skjerlie KP. (1998) Contrasting tonalite genesis in the Lyngen magmatic complex, North Norwegian Caledonides. *Lithos*, 42 (3-4): 241-268.
- Selbekk RS (1995) Tonalitt genese i Lyngen Magmatiske kompleks, Troms. (*Tonalite genesis in the Lyngen Magmatic Complex, Troms.*) Thesis for the Cand. Scient. Degree, University of Bergen, Norway.
- Shervais JW (1982) Ti-V plots and the petrogenesis of modern and ophiolite lavas. *Earth Planet. Sci. Lett.* 59: 101-118.
- Shimizu N. Hart SR, 1982: Applications of the ion microprobe to geochemistry and cosmochemistry. *Ann Rev Earth Planet Sci* 10: 483-526.
- Sinha AK. Hewitt DA (1986) Fluid interaction and element mobility in the development of ultramylonites. *Geology*, 14: 883-886.
- Slagstad D (1995) Rypdalen skjærsone, en oceansk skjærsone i Lyngen Magmatiske Kompleks. (*Rypdalen Shear Zone, an Oceanic Shearzone in the Lyngen Magmatic Complex.*) Thesis for the Cand. Scient. Degree University of Bergen, Norway.
- Sun S-S (1980) Lead isotopic study of young volcanic rocks from mid-ocean ridges, ocean islands and island arcs. *Phil. Trans. R. Soc. Lond.*, A297: 409-45.
- Taylor RN. Nesbitt RW. (1988) Light rare-earth enrichment of supra subduction-zone mantle: Evidence from the Troodos ophiolite, Cyprus. *Geology*, 16: 448-451.

Evolution of Oceanic Gabbros: In-situ and Ancient Examples

- Taylor RN. Bramley JM. Nesbitt RW. (1992) Chemical transects across intra-oceanic arcs: implications for the tectonic setting of ophiolites. In: Parson LM. Murton BJ. Browning P (eds) *Ophiolites and their Modern Oceanic Analogues*. Geological Society Special Publication No. 60: 117-132.
- Thy P. Schiffman P. Moores EM (1989) Igneous Mineral Stratigraphy and Chemistry of the Cyprus Crustal Study Project Drill Core in the Plutonic Sequences of the Troodos Ophiolite. In: Gibson IL. Malpas J. Robinson PT. Xenophontos C (eds), *Cyprus Crustal Study Project: Initial Report, Hole CY-4*, pp 147-185.
- Walker DA. Cameron WE. (1983) Boninite primary magmas; evidence from the Cape Vogel Peninsula, PNG. *Contrib Mineral Petrol*, 83 (1-2): 150-18.
- Weaver BL. Tarney J (1981) Chemical changes during dyke metamorphism in high-grade basement terranes. *Nature*, 289: 47-49.
- Yang HJ. Kinzler RJ. Grove TL (1996) Experiments and models of anhydrous, basaltic olivine-plagioclase-augite saturated melts from 0.001 to 10 kbar. *Contrib Mineral Petrol*, 124 (1): 1-18.

Evolution of Oceanic Gabbros: In-situ and Ancient Examples

Table 1: A: Whole-rock analyses of the Western suite of the Lyngen Gabbro. Fe2O3* is all Fe measured as Fe2O3. Mg# is 100*MgO/(MgO+0.899*Fe2O3*). FeO and Fe2O3 was determined for some samples by wet chemistry. Abbreviations: gb=gabbro, tex=textured, pegm=pegmatite, ol=olivine, ox=magnetite and/or ilmenite, diss=disseminated, troct=troctolite, hbl=hornblende, qz=quartz, pyxite=pyroxenite. "Place in profile" indicates the relative distance from east for each of the profiles. Strupen and Skaidevarri are individual profiles, Ellendalen, Goverdalen and Veidalen has a common profile.

Location	Isskardet	Isskardet	Isskardet	Isskardet	Isskardet	Isskardet	Isskardet	Isskardet	Isskardet	Isskardet	Isskardet	Isskardet	Isskardet
Sample#	LY-IS-1	LY-IS-2	LY-IS-3	LY-IS-4	LY-IS-6	LY-IS-7	LY-IS-9	LY-IS-10	LY-IS-11	LY-IS-12	LY-IS-13	LY-IS-16	
Description													
Place in profile													
W<=E													
Major elements (XRF)													
SiO ₂	47.2	47.5	47.4	46.1	45.7	46.8	40.2	46.7	45.0	45.3	45.0	43.2	
TiO ₂	.18	.23	.24	.20	.15	.54	.10	.21	.70	.29	.54	.83	
Al ₂ O ₃	21.4	17.7	17.9	19.5	21.3	12.3	16.8	21.5	19.7	21.0	20.7	18.1	
Fe ₂ O ₃ *	7.9	7.7	7.7	8.7	8.3	11.3	14.3	7.0	10.8	9.6	10.4	13.7	
MnO	0.14	0.16	0.15	0.15	0.14	0.19	0.19	0.13	0.14	0.14	0.14	0.16	
MgO	8.6	9.3	9.1	9.6	8.9	11.3	13.8	7.8	7.5	9.1	8.2	9.2	
CaO	14.6	16.1	16.2	14.7	14.5	16.4	10.3	15.8	15.3	14.0	14.6	13.8	
Na ₂ O	.93	.79	.84	.86	.91	.53	.56	.97	.91	.86	.87	.70	
K ₂ O	0	0	0	0	0	0	0	0	0	0	0	0	
P ₂ O ₅	.03	.01	.02	.02	.01	.02	.00	.01	.01	.00	.02	.00	
LOI	0.8	1.4	0.6	0.9	0.4	0.8	1.3	0.9	1.2	1.0	0.4	0.8	
Sum	101.8	100.8	100.1	100.6	100.2	100.2	97.6	101.0	101.2	101.2	100.8	100.5	
Trace elements (XRF)													
V	136	194	209	151	122	401	72	190	697	265	498	787	
Cr	33	47	58	32	26	266	29	108	144	111	113	105	
Co	37	43	37	45	40	57	82	35	55	49	42	61	
Ni	36	35	35	48	54	62	111	35	41	63	34	48	
Cu	13	16	28	22	17	70	39	24	131	28	8	13	
Zn	37	36	35	39	38	47	63	32	33	37	38	41	
Rb	0	1	0	0	0	1	1	0	1	0	0	2	
Sr	181	170	170	172	190	115	113	199	185	179	171	146	
Y	5	7	6	6	4	10	4	6	6	6	4	6	
Zr	15	13	15	14	12	18	13	13	14	12	14	13	
Nb	3	2	3	2	2	2	2	2	2	3	2	2	
Ba	0	0	0	1	1	1	0	3	6	0	4	0	
La	0	0	0	0	0	0	0	0	0	0	0	0	
S	10	14	18	8	8	20	3	11	15	12	9	12	
Ce	9	7	7	6	1	3	3	6	10	6	5	4	
Nd	68.7	70.5	70.2	68.8	68.1	66.6	65.8	69.1	57.9	65.4	61.1	57.4	
Mg#	5.6	5.3	5.2	6.1	6.0	7.2	10.0	4.9	2.9	8.1	6.5	8.1	
FeO	1.8	2.0	2.0	1.9	1.7	3.3	3.3	1.6	7.6	0.0	3.3	4.8	
Fe ₂ O ₃													

Evolution of Oceanic Gabbros: In-situ and Ancient Examples

Table 1A: Continued.

Location	Isskardet	Isskardet	Isskardet	Isskardet	Isskardet	Isskardet	Isskardet	Isskardet	Isskardet	Isskardet	Isskardet	Isskardet
Sample#	LY-IS-17	LY-IS-19	LY-IS-20	LY-IS-23	LY-IS-25	LY-IS-26	LY-IS-28	LY-IS-29	LY-IS-29a	LY-IS-30	LY-IS-31	LY-IS-33
Description												
Place in profile												
W<=E												
Major elements												
SiO ₂	46.6	47.1	46.6	45.6	43.5	44.3	46.8	46.8	46.8	45.4	44.7	47.5
TiO ₂	.32	.24	.46	.58	.81	.75	.19	.48	.20	.79	.93	.13
Al ₂ O ₃	16.3	17.1	16.2	21.2	18.4	19.2	20.3	22.8	19.6	18.2	15.3	31.6
Fe ₂ O ₃ *	9.1	8.4	10.0	9.1	12.3	12.0	8.1	7.6	8.3	11.1	14.3	3.4
MnO	0.16	0.16	0.17	0.13	0.15	0.15	0.14	0.12	0.15	0.14	0.17	0.06
MgO	10.0	9.8	9.8	6.8	8.1	8.2	8.9	6.1	9.2	7.6	9.5	3.8
CaO	15.8	16.1	15.9	15.7	14.5	14.7	15.0	16.1	15.0	15.7	15.1	15.0
Na ₂ O	.73	.74	.73	1.10	.79	.84	.99	1.05	.92	.83	.66	2.24
K ₂ O	0	0	0	0	0	0	0	0	0	0	0	0
P ₂ O ₅	.00	.02	.02	.03	.02	.02	.03	.02	.01	.02	.00	.01
LOI	1.2	0.5	0.1	0.2	0.8	0.1	0.4	0.3	0.5	0.2	0.0	2.8
Sum	100.2	100.0	99.9	100.5	99.3	100.2	100.8	101.3	100.6	99.9	100.5	106.5
Trace elements												
V	254	202	386	531	704	705	163	462	181	700	853	131
Cr	70	76	329	122	70	67	47	36	41	92	201	41
Co	45	44	46	37	53	49	43	31	44	46	64	23
Ni	45	59	34	45	17	17	31	12	33	98	58	12
Cu	20	204	22	15	13	14	13	14	17	449	221	11
Zn	38	34	37	30	33	38	36	26	35	36	47	20
Rb	0	0	1	0	0	0	0	0	0	0	0	0
Sr	138	157	148	198	157	166	189	222	184	169	133	281
Y	7	7	7	6	5	5	5	6	5	7	8	4
Zr	15	15	16	12	15	13	12	11	12	14	14	7
Nb	3	2	1	2	3	2	2	2	2	3	2	2
Ba	5	0	6	1	1	0	0	0	11	0	0	1
La												
S												
Ce	14	13	17	15	9	15	13	15	13	13	20	7
Nd	6	4	3	3	7	7	12	7	10	9	5	4
Mg#	68.8	70.1	66.2	60.0	56.7	57.7	68.6	61.5	68.8	57.6	57.0	69.0
FeO	5.9	11.8	6.4	6.0	6.8	7.0	5.7	4.6	6.1	6.3	8.5	2.1
Fe ₂ O ₃	2.5	-4.6	3.0	2.5	4.8	4.2	1.8	2.6	1.6	4.2	4.9	0.9

Evolution of Oceanic Gabbros: In-situ and Ancient Examples

Table 1A: Continued.

Location	Ellendalen Ellendalen Ellendalen Ellendalen Ellendalen Ellendalen Ellendalen Ellendalen Ellendalen Ellendalen Ellendalen Ellendalen Ellendalen Ellendalen Ellendalen													
Sample#	92LY93	92LY119	93LY20	93LY20	93LY19	94LY20	94LY20	94LY21	94LY23	94LY25	94LY26	94LY24	94LY39	94LY29
Description	metagb	metagb	metagb	metagb	massiv gb	gabbro	gabbro	gabbro	gabbro	varitex gb	varitex gb	gabbro	gabbro	gabbro
Place in profile														
W<=E	9350	9350	8600	8600	8500	7450	7450	7400	7150	7000	6950	6800	6450	5400
Major elements														
SiO ₂	54.0	51.3	48.4	47.9	47.7	45.5	42.4	36.2	38.4	47.1	46.6	38.2		
TiO ₂	.31	.50	.09	.13	.25	.17	.03	2.88	2.24	.24	.22	1.81		
Al ₂ O ₃	12.8	15.1	20.2	20.3	15.3	20.3	3.8	8.2	10.6	14.8	19.6	16.1		
Fe ₂ O ₃ *	10.4	10.1	5.2	5.4	7.5	7.0	13.0	27.7	24.1	8.0	10.3	20.8		
MnO	.17	.19	.10	.10	.16	.14	.19	.24	.20	.16	.15	.18		
MgO	9.4	7.9	7.7	7.3	9.9	7.9	28.2	9.2	8.4	10.5	10.3	5.3		
CaO	7.9	11.2	15.5	16.4	14.5	15.0	9.7	11.4	12.7	16.0	10.1	12.7		
Na ₂ O	3.95	2.78	1.11	1.20	1.00	1.17	0.00	1.44	1.13	0.39	2.33	0.68		
K ₂ O	.00	.16	.58	.00	.00	.00	.00	.03	.04	.00	.00	.02		
P ₂ O ₅	.01	.08	.00	.01	.00	.02	.01	.02	.00	.01	.01	.01		
LOI	2.2	2.1	2.3	2.5	2.5	2.9	1.5	1.8	2.5	1.5	1.1	2.6		
Sum	101.0	101.3	101.2	101.1	98.8	99.9	98.6	98.7	100.3	98.6	100.6	98.4		
Trace elements (
V	229	191	96	110	144	124	648	600	667	165	128	1182		
Cr	281	29	104	179	180	181	33	49	130	193	103	63		
Co	32	43	34	37	48	47	47	68	78	57	45	64		
Ni	128	37	44	47	49	51	11	25	64	71	65	77		
Cu	5	41	29	17	9	7	25	120	164	55	91	229		
Zn	75	58	37	32	79	48	83	118	98	72	65	88		
Rb	0	1	18	1	0	0	0	0	2	0	0	0		
Sr	89	198	150	177	137	207	435	64	100	120	122	164		
Y	9	25	5	6	7	6	6	17	11	7	2	8		
Zr	8	39	10	11	11	11	15	18	13	9	7	9		
Nb	3	5	1	2	2	0	2	3	3	2	2	4		
Ba	63	86	188	24	24	66	71	0	32	0	34	74		
La	2	5		10	6	6	0	0	8	9	13	13		
S					0.02	0.02	0.07			0.04	0.03	0.26		
Ce	13	19	17	21	8	18	12	14	18	11	11	0		
Nd	0	4	11	14	7	10	8	10	10	7	8	4		
Mg#	64.4	60.9	74.7	72.8	72.6	69.2	81.2	39.8	40.9	72.4	66.6	33.7		
FeO														
Fe ₂ O ₃														

Evolution of Oceanic Gabbros: In-situ and Ancient Examples

Table 1A: Continued.

Location	Ellendalen						Goverdalen					
Sample#	94LY38	94LY37	94LY36	94LY35	94LY34	94LY33	95LY1	95LY2	95LY3	95LY5	95LY24	95LY23
Description	melagb	melagb	gabbro	gabbro	gabbro	leucogb	massiv gb	massiv gb	gabbro	microgb	melagb	leucogb
Place in profile												
W<=E	5250	5220	5190	5160	5130	5000	4550	4550	4550	4550	3849	3839
Major elements												
SiO ₂	41.7	39.2	40.2	41.9	41.7	44.9	44.1	43.0	47.7	39.6	36.7	48.0
TiO ₂	1.47	2.34	1.32	1.34	1.00	.29	.07	.06	.08	2.14	2.31	.36
Al ₂ O ₃	9.0	9.8	13.3	16.6	15.9	23.3	16.1	15.1	15.6	13.6	13.3	19.3
Fe ₂ O ₃ *	22.9	22.9	17.7	14.4	14.0	6.1	5.0	5.9	4.1	21.2	23.5	8.3
MnO	.23	.23	.18	.18	.18	.10	.08	.11	.08	.21	.18	.16
MgO	13.6	9.4	10.3	9.0	8.5	4.7	13.9	16.0	10.5	7.3	6.8	7.5
CaO	11.3	12.5	12.8	14.6	13.5	13.0	16.7	15.5	16.7	12.8	12.4	13.7
Na ₂ O	0.96	0.97	1.06	1.12	1.66	2.94	0.39	0.28	1.19	0.43	0.64	1.80
K ₂ O	.03	.05	.02	.00	.00	.01	.00	.00	.01	.00	.01	.00
P ₂ O ₅	.02	.03	.00	.02	.01	.03	.01	.00	.01	.01	.02	.01
LOI	3.5	2.6	3.2	2.7	2.9	2.9	2.9	3.6	1.8	2.6	3.1	2.8
Sum	101.9	99.9	100.2	102.0	99.3	98.2	99.2	99.4	100.6	99.9	98.9	98.3
Trace elements (ppm)												
V	550	691	536	553	492	194	80	63	101	895	1126	172
Cr	84	92	194	200	145	48	450	359	971	40	65	65
Co	70	73	67	69	63	33	44	46	32	73	62	44
Ni	47	88	23	22	33	18	207	258	81	32	45	25
Cu	6	306	14	55	11	15	13	5	8	147	174	14
Zn	101	89	77	63	70	50	24	33	22	99	106	47
Rb	0	2	0	0	0	2	0	0	0	0	0	0
Sr	56	108	127	160	153	177	208	126	61	133	119	173
Y	9	10	7	7	7	4	0	2	4	9	8	6
Zr	12	14	13	14	12	12	10	9	7	11	12	11
Nb	2	4	0	2	3	0	6	4	5	6	5	5
Ba	0	71	5	85	0	69	69	57	0	55	42	66
La	5	8	13	0	5	0	0	0	0	0	0	0
S							0.03	0.03	0.02	0.29	0.18	0.02
Ce	12	14	8	19	18	26	18	10	18	16	7	3
Nd	8	6	0	8	11	8	12	5	4	6	6	0
Mg#	54.2	45.0	53.8	55.5	54.7	60.8	84.8	84.5	83.5	40.7	36.5	64.5
FeO												
Fe ₂ O ₃												

Evolution of Oceanic Gabbros: In-situ and Ancient Examples

Table 1A: Continued.

Location	Goverdalen Goverdalen Goverdalen Goverdalen Goverdalen Goverdalen Goverdalen Goverdalen Goverdalen Goverdalen											
Sample#	95LY22	95LY21	95LY19	95LY18	95LY17	95LY16	95LY14	95LY13	95LY12	95LY11	95LY10	95LY9
Description	melagb	melagb	melagb	melagb	leucogb	melagb	leucogb	melagb	melagb	melagb	leucogb	melagb
Place in profile												
WV<=E	3834	3815	3803	3791	3784	3779	3770	3762	3756	3732	3724	3714
Major elements												
SiO ₂	39.3	39.4	45.4	39.4	49.3	37.9	49.8	42.3	41.7	45.4	44.8	37.8
TiO ₂	1.40	1.52	1.01	1.71	.45	2.10	.61	1.34	1.40	1.04	.19	2.44
Al ₂ O ₃	17.5	18.1	13.6	14.6	11.4	12.5	19.4	18.2	14.2	13.6	22.2	9.1
Fe ₂ O ₃ *	16.7	16.8	13.4	20.0	10.4	23.1	8.5	15.8	17.6	13.4	7.4	26.5
MnO	.15	.14	.16	.18	.23	.19	.12	.17	.20	.18	.12	.19
MgO	6.3	5.5	7.7	7.1	11.5	6.9	4.8	5.8	7.8	8.4	7.4	7.9
CaO	14.1	14.0	13.6	12.8	14.7	13.0	11.8	12.1	12.6	16.7	14.6	11.9
Na ₂ O	0.75	0.13	1.32	0.20	0.33	0.51	2.72	1.36	0.51	0.23	1.31	0.64
K ₂ O	.00	.00	.01	.00	.00	.01	.00	.00	.01	.00	.00	.01
P ₂ O ₅	.01	.01	.01	.01	.02	.01	.01	.00	.00	.01	.01	.00
LOI	3.4	3.8	3.5	3.4	1.9	2.7	2.2	3.1	3.1	2.9	2.8	1.8
Sum	99.7	98.3	99.5	99.3	100.3	98.8	99.9	100.2	99.2	101.9	100.8	98.3
Trace elements												
V	899	915	499	1110	199	1106	349	908	852	548	117	1202
Cr	177	273	21	60	284	64	22	51	71	327	106	68
Co	65	62	67	66	60	68	39	57	64	79	49	71
Ni	65	68	34	183	45	51	16	29	36	98	48	69
Cu	75	167	72	307	15	222	46	51	190	363	9	131
Zn	69	72	45	80	63	101	43	83	92	63	44	103
Rb	0	0	0	0	0	0	0	0	0	0	0	0
Sr	177	200	127	149	100	115	146	177	166	144	182	62
Y	6	4	14	7	10	8	5	6	7	9	4	10
Zr	10	11	13	11	11	12	10	11	11	10	10	11
Nb	4	5	7	6	4	5	5	4	5	6	5	6
Ba	84	53	37	21	22	72	0	93	50	52	49	86
La	7	0	4	0	0	0	0	5	0	0	0	0
S	0.10	0.14	0.02	0.78	0.03	0.22	0.03	0.03	0.02	0.12	0.03	0.15
Ce	11	13	15	6	15	9	19	16	11	14	18	8
Nd	6	6	7	7	4	6	0	4	4	5	5	3
Mg#	43.0	39.4	53.6	41.4	68.8	37.3	53.1	42.4	46.8	55.6	66.7	37.3
FeO												
Fe ₂ O ₃												

Evolution of Oceanic Gabbros: In-situ and Ancient Examples

Table 1A: Continued.

Location		Goverdalen Goverdalen Goverdalen Goverdalen Goverdalen Goverdalen Goverdalen Goverdalen											
Sample#		95LY8	95LY6	94LY67	94LY68	95LY43	95LY42	95LY41	95LY29	95LY30	95LY31	95LY32	95LY33
Description		leucogb	melagb	gabbro	gabbro	gabbro	melagb	gabbro	gabbro	gabbro	leucogb	melagb	pegmatite
Place in profile		3705	3701	3500	3500	3100	3100	3000	2880	2740	2560	2550	2547
Major elements													
SiO ₂		44.4	38.7	47.1	46.0	45.7	39.8	47.0	39.6	39.8	43.3	43.7	47.1
TiO ₂		.14	1.36	.25	.13	.69	2.20	.17	.04	1.42	.95	.87	.68
Al ₂ O ₃		26.9	15.7	16.2	14.6	23.9	13.0	17.2	12.6	14.0	16.5	13.0	10.1
Fe ₂ O ₃ *		5.8	18.1	7.5	9.0	9.3	22.2	9.0	20.9	22.1	14.2	15.7	16.8
MnO		.09	.16	.15	.15	.13	.23	.16	.22	.20	.19	.20	.23
MgO		5.0	7.0	9.1	12.0	5.0	8.0	10.0	7.7	10.1	8.0	9.4	11.3
CaO		15.4	14.5	16.3	15.7	12.1	11.1	12.2	12.5	8.4	13.5	13.2	11.8
Na ₂ O		1.43	0.55	0.68	0.22	2.02	0.94	1.02	0.68	0.81	0.91	0.51	1.30
K ₂ O		.00	.00	.00	.00	.00	.06	.00	.06	.04	.03	.02	.07
P ₂ O ₅		.01	.01	.01	.01	.03	.01	.02	.00	.01	.01	.01	.01
LOI		3.1	3.2	1.8	2.5	2.8	1.7	3.1	2.2	3.3	2.7	2.6	1.0
Sum		102.2	99.2	99.0	100.2	101.5	99.2	100.0	98.6	100.2	100.3	99.2	100.3
Trace elements (
V		93	844	148	172	343	923	130	905	1137	657	626	417
Cr		33	74	741	402	37	76	67	46	73	170	141	11
Co		41	68	62	61	43	55	45	67	41	62	67	64
Ni		30	38	70	96	26	49	40	34	76	88	79	51
Cu		9	56	62	184	56	159	29	139	86	123	170	13
Zn		37	79	85	43	62	118	67	108	98	78	79	70
Rb		0	0	0	0	0	2	0	0	0	0	0	0
Sr		189	160	119	70	238	128	213	125	61	150	126	88
Y		3	5	4	0	7	10	6	9	14	5	9	43
Zr		11	10	8	5	14	14	13	11	14	9	10	47
Nb		3	6	4	5	5	5	4	5	6	6	5	7
Ba		31	54	28	61	81	81	54	58	93	30	36	53
La		0	5	4	0	0	9	0	0	0	0	0	0
S		0.02	0.11	0.02	0.03	0.14	0.37	0.02	0.23	0.09	0.16	0.36	0.02
Ce		8	16	19	11	13	6	12	7	15	12	14	9
Nd		8	7	7	6	8	5	7	4	5	3	0	6
Mg#		63.3	43.5	70.7	72.7	51.9	41.7	68.9	42.4	47.7	53.0	54.5	57.2
FeO													
Fe ₂ O ₃													

Evolution of Oceanic Gabbros: In-situ and Ancient Examples

Table 1A: Continued.

Location	Goverdalen Goverdalen Goverdalen Goverdalen Goverdalen Goverdalen										Veidalen	Veidalen	Veidalen	Veidalen	Veidalen
Sample#	95LY34	95LY35	95LY36	95LY37	95LY38	95LY39	95LY40	95LY127	95LY126	95LY125	95LY124	95LY122			
Description	melagb	melagb	gabbro	gb pegm	gabbro	melagb	gabbro	gabbro	gabbro	metagb	gabbro	metagb			
Place in profile	2535	2420	2290	2290	2280	2215	2190	2080	2050	2030	2000	1900			
W<=E	2535	2420	2290	2290	2280	2215	2190	2080	2050	2030	2000	1900			
Major elements															
SiO ₂	43.2	43.5	46.1	46.1	48.8	45.6	47.1	46.40	46.37	47.75	43.82	47.38			
TiO ₂	1.49	1.65	1.09	.73	1.57	.13	.13	0.1	0.17	0.44	0.78	0.15			
Al ₂ O ₃	11.4	13.7	17.3	19.7	15.0	16.2	17.5	16.13	17.69	14.78	15.65	15.47			
Fe ₂ O ₃ *	22.9	20.9	14.7	13.0	16.0	6.9	5.5	7.75	8.26	13.49	14.42	7.35			
MnO	.22	.22	.22	.18	.22	.12	.11	0.13	0.15	0.24	0.19	0.15			
MgO	8.6	7.9	6.2	5.8	6.1	12.2	10.1	11.26	10.19	10.58	8.45	10.28			
CaO	12.4	12.4	11.0	12.5	10.0	16.3	16.6	15.24	15.97	12.75	13.59	15.73			
Na ₂ O	0.76	0.86	1.82	1.79	2.87	0.69	0.70	0.56	0.48	0.52	0.8	0.52			
K ₂ O	.00	.00	.00	.02	.01	.00	.02	0.02	0	0	0.08	0			
P ₂ O ₅	.00	.02	.02	.00	.10	.01	.01	0.01	0.01	0.01	0	0.01			
LOI	0.9	0.9	2.1	2.0	0.4	1.4	2.2	2.34	1.22	0.27	1.95	2.25			
Sum	101.8	102.0	100.5	101.6	100.9	99.5	100.0	99.95	100.51	100.82	99.73	99.75			
Trace elements															
V	1134	927	433	442	452	106	114	101	140	280	731	154			
Cr	77	65	44	32	28	216	395	185	71	94	50	88			
Co	71	65	51	48	47	49	43	52	55	56	57	48			
Ni	77	26	27	22	15	101	126	73	38	38	24	44			
Cu	242	150	104	132	64	178	192	135	78	107	148	33			
Zn	60	77	83	79	81	33	29	33	46	80	70	49			
Rb	0	0	0	0	0	0	2	0	0	0	7	0			
Sr	97	130	202	212	178	107	116	119	125	112	118	101			
Y	11	13	12	4	23	6	3	3	6	8	6	6			
Zr	11	11	14	10	22	7	8	8	9	8	9	10			
Nb	7	6	6	4	6	4	5	4	3	6	5	3			
Ba	47	31	24	92	109	36	0	53	83	65	82	46			
La	0	4	5	5	5	0	0	0	7	6	0	10			
S	0.79	0.46	0.39	0.51	0.20	0.24	0.10	0.19	0.16	0.22	0.33	0.03			
Ce	14	18	8	6	8	15	8	12	13	9	13	15			
Nd	5	5	6	6	10	5	6	10	11	3	0	7			
Mg#	42.9	43.0	45.8	47.1	43.0	77.9	78.4	74.3	71.1	61.0	53.9	73.6			
FeO															
Fe ₂ O ₃															

Evolution of Oceanic Gabbros: In-situ and Ancient Examples

Table 1A: Continued.

Location	Veidalen	Veidalen	Veidalen	Veidalen	Veidalen	Veidalen	Veidalen	Veidalen	Veidalen	Veidalen	Veidalen	Veidalen	Veidalen	Veidalen	Veidalen	Veidalen	Veidalen
Sample#	95LY123	95LY110	95LY109	95LY108	95LY107	95LY106	95LY105	95LY104	95LY102	95LY99	95LY97	95LY96					
Description	melagabbro	metagb	metagb	metagb	gabbro	gabbro	metagb	gabbro	metagb	metagb	metagb	gabbro					
Place in profile	W<=E																
Major elements																	
SiO ₂	39.81	46.40	48.14	46.85	45.32	48.79	46.90	46.62	46.60	46.16	46.19	46.52					
TiO ₂	1.16	0.07	0.09	0.09	0.07	0.1	0.06	0.1	0.06	0.07	0.08	0.07					
Al ₂ O ₃	11.9	15.39	14.12	14.42	17.72	10.74	15.42	12.49	15.7	16.88	15.95	17.38					
Fe ₂ O ₃ *	22.7	4.81	5.25	5.3	5.8	6.79	5.16	5.62	4.85	5.89	6.3	6.66					
MnO	0.17	0.1	0.09	0.11	0.11	0.14	0.1	0.1	0.09	0.11	0.13	0.12					
MgO	8.44	12	12.17	11.94	11.61	14.32	13.06	15.21	11.17	11.25	11.57	11.2					
CaO	12.79	18.49	17.41	18.62	17.38	18.79	17.41	16.47	18.74	16.71	17.05	17.4					
Na ₂ O	0.57	0.23	0.3	0.26	0.38	0.15	0.3	0.14	0.23	0.24	0.2	0.36					
K ₂ O	0.11	0	0	0	0	0	0	0	0	0	0	0					
P ₂ O ₅	0.02	0.01	0.01	0.01	0.01	0.02	0	0	0.01	0.02	0.01	0.01					
LOI	2.25	2.22	1.78	1.95	1.432	0.42	1.51	2.91	2	2.71	2.483	1.501					
Sum	99.9	99.7	99.35	99.55	99.83	100.24	99.93	99.65	99.46	100.03	99.94	101.22					
Trace elements (ppm)																	
V	976	105	124	129	108	146	100	104	112	107	114	105					
Cr	46	861	1317	597	143	890	345	839	616	248	84	226					
Co	78	41	42	44	43	51	42	44	41	45	48	49					
Ni	12	103	87	72	54	57	56	204	121	86	41	113					
Cu	66	77	73	98	159	49	80	211	137	52	135	173					
Zn	78	21	14	21	16	18	25	17	15	29	25	21					
Rb	0	0	0	0	0	0	0	0	0	0	0	0					
Sr	87	72	68	63	89	45	69	57	83	104	94	101					
Y	11	0	2	3	0	0	0	2	0	0	3	0					
Zr	9	5	6	6	6	6	5	6	6	8	8	7					
Nb	4	4	5	3	5	4	3	3	4	5	4	5					
Ba	72	45	35	27	45	35	51	67	48	31	53	44					
La	0	8	0	15	0	0	7	0	9	0	8	0					
S	0.03	0.03	0.02	0.03	0.04	0.03	0.03	0.08	0.03	0.03	0.04	0.07					
Ce	7	13	17	19	13	13	21	20	18	14	17	13					
Nd	6	6	3	5	0	6	7	8	0	0	5	8					
Mg#	42.6	83.3	82.2	81.8	80.0	80.8	83.5	84.4	82.1	79.2	78.6	77.0					
Fe#																	
Fe ₂ O ₃ *																	

Evolution of Oceanic Gabbros: In-situ and Ancient Examples

Table 1A: Continued.

Location	Veidalen	Veidalen	Veidalen	Veidalen	Veidalen	Veidalen	Veidalen	Veidalen	Veidalen	Veidalen	Veidalen	Veidalen	Veidalen	Veidalen
Sample#	95LY95	95LY94	95LY93	95LY91	95LY90	95LY88	95LY87	95LY81	95LY79	95LY76	95LY75	95LY73	95LY73	95LY73
Description	gabbro	gabbro	gabbro	metagb	gabbro	metagb	gabbro	ferrogabbro	gabbro	ferrogabbro	leucogb	metagb	metagb	metagb
Place in profile														
W<=E	1480	1468	1460	1452	1448	1432	1429	1370	1370	1350	1350	1350	1340	1340
Major elements														
SiO ₂	48.50	46.15	45.39	43.84	45.90	44.19	50.43	38.50	44.00	41.67	44.05	47.41	47.41	47.41
TiO ₂	0.07	0.09	0.07	0.75	0.12	0.12	0.05	1.14	0.06	0.83	0.06	0.09	0.09	0.09
Al ₂ O ₃	19.19	14.65	18.9	15.46	14.83	21.26	4.81	14	21.77	15.72	25.08	17.22	17.22	17.22
Fe ₂ O ₃ *	6.38	7.96	6.78	16.07	8.59	6.88	5.92	21.38	6.03	15.42	5.73	6.11	6.11	6.11
MnO	0.13	0.16	0.13	0.2	0.15	0.11	0.11	0.16	0.1	0.16	0.1	0.12	0.12	0.12
MgO	10.15	12.24	10.32	8.63	12.03	6.97	20.73	7.96	9.35	8.32	6.64	11.41	11.41	11.41
CaO	15.58	17.38	16.77	13.54	16.12	18.87	18.04	13.26	16.51	14.83	14.96	14.59	14.59	14.59
Na ₂ O	0.34	0.39	0.26	1	0.25	0.28	0.12	0.6	0.68	0.39	1.01	0.54	0.54	0.54
K ₂ O	0	0.01	0	0.12	0	0.02	0.01	0.15	0.04	0.05	0	0.59	0.59	0.59
P ₂ O ₅	0.01	0.02	0.02	0	0	0.01	0	0.01	0.02	0	0.01	0.01	0.01	0.01
LOI	0.345	1.72	1.16	1.296	2.178	2.14	0.627	1.73	2.997	2.631	3.311	2.55	2.55	2.55
Sum	100.68	100.77	99.78	100.9	100.16	100.86	100.85	98.88	101.56	100	100.094	100.65	100.65	100.65
Trace elements (
V	98	140	111	1321	136	169	111	1159	82	829	57	121	121	121
Cr	143	350	142	81	259	156	2496	61	100	66	50	565	565	565
Co	41	57	50	72	59	49	52	72	45	69	40	41	41	41
Ni	57	80	77	38	103	40	260	39	63	44	28	102	102	102
Cu	155	229	134	692	111	84	12	590	6	246	12	35	35	35
Zn	26	41	35	59	38	18	20	43	30	45	26	33	33	33
Rb	0	3	0	7	5	0	0	0	0	0	0	45	45	45
Sr	108	91	112	132	95	143	13	92	136	140	168	91	91	91
Y	2	3	3	3	3	3	0	0	0	4	2	4	4	4
Zr	7	6	6	8	7	8	5	7	8	9	10	7	7	7
Nb	5	5	4	4	4	4	4	6	3	7	4	5	5	5
Ba	59	40	53	120	51	37	27	75	59	48	32	169	169	169
La	0	5	4	0	5	0	6	0	5	9	5	0	0	0
S	0.07	0.08	0.12	0.25	0.09	0.02	0.03	0.56	0.02	0.41	0.02	0.03	0.03	0.03
Ce	21	16	21	14	15	17	18	10	21	7	12	10	10	10
Nd	9	6	11	5	4	7	5	4	4	6	4	0	0	0
Mg#	76.0	75.4	75.2	51.7	73.6	66.9	87.5	42.6	75.6	51.8	69.8	78.8	78.8	78.8
FeO														
Fe ₂ O ₃ *														

Evolution of Oceanic Gabbros: In-situ and Ancient Examples

Table 1A: Continued.

Location	Veidalen	Veidalen	Veidalen	Veidalen	Veidalen	Veidalen	Veidalen	Veidalen	Veidalen	Veidalen	Veidalen	Skatidevarri
Sample#	95LY70	95LY68	95LY67	95LY65	95LY64	95LY63	95LY61	95LY60	95LY59	95LY58	95LY57	90LY141
Description	metagb	metagb	metagb	metagb	metagb	metagb	metagb	metagb	metagb	metagb	metagb	Olgbonrite
Place in profile	990	960	910	860	810	770	720	620	570	550	500	10.5
W<=E												
Major elements												
SiO ₂	45.75	45.98	47.33	47.91	46.20	43.03	48.01	47.16	46.92	40.66	36.90	46.72
TiO ₂	0.12	0.13	0.41	0.11	0.08	0.89	0.17	0.1	0.07	0.04	1.03	0.17
Al ₂ O ₃	15.38	14.56	11.83	12.28	22.31	16.3	13.83	15.51	16.03	22.79	19.51	18.74
Fe ₂ O ₃ *	9.11	8.98	11.16	9.11	6.35	15.25	8.74	7	6.82	7.33	16.7	7.19
MnO	0.16	0.15	0.27	0.19	0.13	0.15	0.18	0.14	0.14	0.11	0.19	0.12
MgO	10.8	12.01	11.54	11.93	7.97	8.45	11.07	11.47	11.86	9.45	7.33	9.65
CaO	16.07	15.68	14.92	15.98	14.28	14.73	15.76	15.25	16.17	15.91	13.55	15.4
Na ₂ O	0.21	0.22	0.31	0.35	0.5	0.22	0.42	0.46	0.29	0.57	0.49	0.82
K ₂ O	0.02	0	0	0.03	0.34	0.03	0.04	0.17	0.11	0.09	0.09	0
P ₂ O ₅	0.01	0.01	0.01	0	0	0.01	0	0.01	0.01	0	0.01	0
LOI	2.3	2.49	2.2	1.46	3.31	2.57	1.621	2.595	1.98	3.05	3.592	1.78
Sum	99.93	100.2	99.98	99.34	101.55	101.63	99.84	99.88	100.39	100	99.39	100.6
Trace elements												
V	174	172	148	163	111	980	229	141	123	68	698	105
Cr	151	402	741	672	42	108	533	449	449	260	53	207
Co	60	61	62	57	39	69	56	45	46	47	62	45
Ni	58	96	70	69	33	34	82	76	108	57	21	84
Cu	44	184	62	20	37	168	24	94	48	9	103	118
Zn	45	43	85	76	41	47	64	36	28	36	74	22
Rb	0	0	0	0	30	0	0	13	7	6	11	2
Sr	93	70	119	77	123	118	105	86	119	133	153	148
Y	0	0	4	5	0	0	4	2	2	0	0	6
Zr	8	5	8	6	8	7	7	7	7	7	9	11
Nb	4	5	4	4	4	4	4	5	4	4	5	0
Ba	0	61	28	37	138	29	52	39	40	46	74	32
La	0	0	4	0	0	7	0	0	5	0	0	0
S	0.03	0.03	0.02	0.02	0.03	0.33	0.02	0.03	0.03	0.02	0.07	18
Ce	9	11	19	14	6	10	17	16	13	10	12	18
Nd	0	6	7	10	0	3	7	7	6	5	3	18
Mg#	70.3	72.7	67.3	72.3	71.5	52.5	71.6	76.6	77.6	72.0	46.7	72.81
FeO												3.57
Fe ₂ O ₃												3.26

Evolution of Oceanic Gabbros: In-situ and Ancient Examples

Table 1A: Continued.

Location	Skaidevarri	Skaidevarri	Skaidevarri	Skaidevarri	Skaidevarri	Skaidevarri	Skaidevarri	Skaidevarri	Skaidevarri	Skaidevarri	Skaidevarri	Skaidevarri	Skaidevarri
Sample#	90LY142	90LY143	90LY144	90LY145	90LY146	90LY147	90LY148	90LY149	90LY150	90LY151	90LY152		
Description	Olgnorite	Olgnorite	Olgb	gbnorite	Altered	Gabbro	Gabbro	Gabbro	Gabbro	Gabbro	Gabbro		
Place in profile	W<=E	12	13.5	15	16.5	18	19.5	22	23.5	25	26.5	28	
Major elements													
SiO ₂	47.26	47.16	47.67	45.57	48.69	46.29	47.14	46.51	48.33	46.97	47.26		
TiO ₂	0.18	0.18	0.19	0.14	0.24	0.15	0.15	0.17	0.31	0.17	0.17		
Al ₂ O ₃	19.41	16.53	17.15	18.15	14.16	18.49	21.19	18.59	8.48	18.98	19.41		
Fe ₂ O ₃ *	7.21	8.1	7.81	8.81	7.08	6.91	5.05	6.87	9	6.08	5.1		
MnO	0.13	0.13	0.13	0.14	0.15	0.12	0.11	0.13	0.17	0.12	0.11		
MgO	9.31	10.85	10.33	10.51	10.04	9.64	7.15	9.95	13.65	8.33	7.12		
CaO	15.62	15.73	15.79	14.24	17.86	15.51	16.82	15.04	16.34	16.61	17.95		
Na ₂ O	0.83	0.5	0.56	0.62	0.78	0.66	0.83	0.85	0.33	0.97	0.91		
K ₂ O	0	0	0	0.01	0	0.01	0.01	0.04	0	0.02	0		
P ₂ O ₅	0.01	0.02	0.02	0.02	0	0.01	0	0.01	0	0.01	0		
LOI	1.25	1.77	1.58	2.8	1.84	2.46	2.55	2.94	4.64	2.35	2.33		
Sum	101.2	100.97	101.25	101.01	100.85	100.26	100.99	101.1	101.24	100.62	100.36		
Trace elements (ppm)													
V	104	132	134	86	176	100	131	131	207	129	158		
Cr	138	302	209	101	205	163	231	235	580	250	245		
Co	46	52	51	52	46	43	34	47	58	42	36		
Ni	81	89	106	48	102	78	56	92	104	81	52		
Cu	115	197	140	44	195	47	173	114	201	156	155		
Zn	26	22	27	28	26	20	27	33	31	17	12		
Rb	0	0	0	0	0	2	0	3	2	0	0		
Sr	147	115	118	127	115	132	157	143	61	143	166		
Y	7	7	8	7	9	7	6	8	11	8	8		
Zr	12	9	11	10	12	11	12	12	11	11	11		
Nb	2	3	0	0	0	0	0	0	0	0	2		
Ba	34	0	28	54	29	20	56	36	77	34	0		
La													
S													
Ce													
Nd	12	18	14	24	26	18	24	27	22	14	16		
Geochemical indices													
Mg#	72.03	72.77	72.52	70.41	73.88	73.56	73.85	74.29	75.16	73.21	73.58		
FeO	4.15	4.76	4.28	5.92	4.32	4.56	3.20	4.45	5.81	3.81	3.16		
Fe ₂ O ₃	2.65	2.86	3.10	2.30	2.33	1.89	1.53	1.98	2.61	1.89	1.62		

Evolution of Oceanic Gabbros: In-situ and Ancient Examples

Table 1A: Continued.

Location	Skaidevarri	Skaidevarri	Skaidevarri	Skaidevarri	Skaidevarri	Skaidevarri	Skaidevarri	Skaidevarri	Skaidevarri	Skaidevarri	Skaidevarri	Skaidevarri
Sample#	90LY153	90LY154	90LY155	90LY156	90LY157	90LY158	90LY159	90LY160	90LY161	90LY162	90LY163	
Description	Gabbro	Gabbro	Gabbro	Gabbro	Gabbro	Olgabnorite	gbnorite	gbnorite	Olgabnorite	Olgabnorite	Diss oxol g b	
Place in profile W<=E	29.5	31	32	33.5	35	36.5	38	39.5	41	42.5	44	
Major elements												
SiO ₂	48.15	46.78	48.88	46.52	48.32	49.18	47.39	46.07	48.17	47.15	48.09	
TiO ₂	0.22	0.17	0.24	0.15	0.22	0.26	0.22	0.13	0.26	0.17	0.21	
Al ₂ O ₃	14.79	17.18	13.84	16.93	17.23	11.16	14.91	16.53	12.79	18.36	14.77	
Fe ₂ O ₃ *	7.19	6.99	7.16	7.21	5.81	9.58	7.06	7.37	7.9	7.2	7.71	
MnO	0.14	0.14	0.17	0.14	0.13	0.19	0.14	0.13	0.15	0.12	0.15	
MgO	10.37	9.84	10.38	10.56	8.52	13.09	9.99	10.79	10.99	9.47	10.9	
CaO	17.27	16.38	17.18	16.08	17.47	15.52	16.66	16.31	17.42	15.6	15.97	
Na ₂ O	0.45	0.67	0.98	1.04	1.22	0.42	0.77	0.48	0.51	0.61	0.55	
K ₂ O	0	0.02	0.02	0.05	0.02	0	0.01	0	0	0	0	
P ₂ O ₅	0	0	0	0	0	0	0	0	0	0	0	
LOI	1.94	2.35	1.8	2.74	1.92	1.11	1.4	2.68	1.01	1.81	1.72	
Sum	100.52	100.52	100.65	101.44	100.86	100.5	98.54	100.51	99.21	100.49	100.08	
Trace elements (ppm)												
V	173	136	193	123	183	193	173	112	199	119	147	
Cr	275	265	334	266	439	607	340	175	617	293	428	
Co	50	47	46	50	40	55	48	51	51	49	50	
Ni	72	79	46	75	63	83	55	77	55	82	92	
Cu	107	44	13	120	66	103	80	52	23	130	101	
Zn	28	25	27	24	13	35	21	26	21	24	30	
Rb	0	0	0	3	0	2	0	0	0	0	0	
Sr	111	140	121	126	131	76	121	120	96	128	129	
Y	10	7	10	7	11	9	8	7	10	7	9	
Zr	10	10	11	10	12	9	10	10	9	9	11	
Nb	3	2	2	2	3	4	3	0	3	2	0	
Ba	0	62	41	77	30	93	0	58	30	30	52	
La												
S												
Ce	24	15	23	21	28	19	21	24	16	16	22	
Nd												
Mg#	74.21	73.74	74.31	74.50	74.52	73.16	73.84	74.49	73.51	72.40	73.82	
FeO	4.76	4.52	4.62	4.62	3.67	5.71	4.62	4.93	4.76	4.39	4.69	
Fe ₂ O ₃	1.95	2.02	2.08	2.13	1.77	3.30	1.98	1.95	2.66	2.37	2.55	

Evolution of Oceanic Gabbros: In-situ and Ancient Examples

Table 1A: Continued.

Location	Skaidevarri	Skaidevarri	Skaidevarri	Skaidevarri	Skaidevarri	Skaidevarri	Skaidevarri	Skaidevarri	Skaidevarri	Skaidevarri	Skaidevarri	Skaidevarri	Skaidevarri	Skaidevarri	Skaidevarri	Skaidevarri	Skaidevarri	Skaidevarri	Skaidevarri	Skaidevarri
Sample#	90LY164	90LY165	90LY166	90LY167	90LY168	90LY169	90LY170	90LY171	90LY172	90LY173	90LY174									
Description	Gabbro	Olgbnorite	Olgbnorite	Altered	Olivinegb	Olgbnorite	Altered	Altered	Altered	Altered	Altered									
Place in profile	W<=E	47	48.5	50	51.5	53	54.5	56	57.5	59.5	61									
Major elements																				
SiO ₂	47.13	47.56	47.09	47.78	45.49	47.4	47.98	47.17	47.33	44.58	47.04									
TiO ₂	0.18	0.24	0.24	0.21	0.16	0.2	0.22	0.13	0.16	0.13	0.14									
Al ₂ O ₃	14.38	13.19	15.27	19.39	16.45	17.82	18.33	19.52	20.63	19.05	21.21									
Fe ₂ O ₃ *	7.14	8.27	8.27	5.95	9.74	7.04	6.23	5.35	5.89	8.26	5.92									
MnO	0.14	0.16	0.16	0.12	0.15	0.13	0.13	0.1	0.1	0.13	0.11									
MgO	11.64	11.31	9.88	7.55	12.04	9.19	8.25	8.47	7.69	9.83	7.92									
CaO	17.3	16.68	16.53	16.85	14.04	15.99	17.06	17.21	16.08	14.03	14.14									
Na ₂ O	0.4	0.46	0.69	1.15	0.49	0.72	0.8	0.86	0.88	0.59	0.85									
K ₂ O	0	0	0.01	0.03	0	0.02	0.03	0.03	0.02	0.02	0.02									
P ₂ O ₅	0.03	0.02	0	0	0.01	0	0	0.01	0.02	0.01	0									
LOI	2.56	1.88	1.38	1.92	2.14	2.03	1.93	2.52	1.84	2.93	3.14									
Sum	100.9	99.77	99.52	100.95	100.7	100.55	100.96	101.38	100.64	98.56	100.48									
Trace elements																				
V	147	169	160	145	94	132	171	128	112	68	96									
Cr	271	421	256	83	98	153	158	174	149	137	108									
Co	51	53	52	39	58	46	43	37	39	49	34									
Ni	84	83	90	47	85	71	40	44	41	80	25									
Cu	118	116	96	109	112	95	31	25	17	85	9									
Zn	21	27	24	18	32	22	15	13	15	26	22									
Rb	2	0	3	3	0	3	3	2	0	2	0									
Sr	85	102	130	160	131	142	179	174	150	132	161									
Y	7	8	9	8	6	7	9	5	5	6	6									
Zr	10	10	11	12	9	12	13	12	11	12	11									
Nb	2	2	0	3	0	0	2	0	0	0	0									
Ba	43	34	0	21	73	0	0	79	0	66	38									
La																				
S																				
Ce	21	13	23	9	8	32	25	22	14	18	17									
Nd																				
Mg#	76.48	73.18	70.44	71.68	71.15	72.25	72.54	75.95	72.26	70.36	72.74									
FeO	4.42	5.17	4.76	3.81	6.02	4.28	4.42	3.50	3.88	5.20	3.88									
Fe ₂ O ₃	2.28	2.58	3.03	1.76	3.12	2.33	1.37	1.50	1.62	2.54	1.65									

Table 1A: Continued.

Location	Skaidevarri	Skaidevarri	Skaidevarri	Skaidevarri	Skaidevarri	Skaidevarri	Skaidevarri	Skaidevarri	Skaidevarri	Skaidevarri	Skaidevarri	Skaidevarri
Sample#	90LY175	90LY176	90LY177	90LY178	90LY179	90LY180	90LY181	90LY182	90LY183	90LY184	90LY185	
Description	Altered	Altered	Altered	Altered	Altered	Altered	Altered	Altered	Altered	Altered	Altered	Altered
Place in profile	W<-E	65	67	69	71	73	75	77	79	81	83	
Major elements	62.5											
SiO ₂	44.52	45.98	48.34	46.13	48.33	44.5	48.09	47.29	45.63	47.53	45.78	
TiO ₂	0.11	0.14	0.2	0.18	0.26	0.18	0.24	0.24	0.15	0.24	0.17	
Al ₂ O ₃	21.59	20.49	13.03	17.41	16.38	15.62	15.93	14.87	20.62	17.8	18.47	
Fe ₂ O ₃ *	6.68	6.42	7.52	7.37	7.09	10.33	7.35	8.76	6	6.4	7.3	
MnO	0.11	0.12	0.15	0.13	0.15	0.16	0.14	0.14	0.11	0.12	0.12	
MgO	8.41	8.66	11.87	10.32	8.83	12.59	9.47	10.57	7.75	8.78	9.74	
CaO	14.83	16.16	16.93	15.9	16.59	13.53	16.48	16.2	16.58	17.01	15.07	
Na ₂ O	0.69	0.84	0.55	0.65	0.77	0.35	0.78	0.62	1.07	0.55	0.79	
K ₂ O	0.03	0	0.01	0.02	0.01	0	0	0.02	0	0	0	
P ₂ O ₅	0.02	0	0.02	0.01	0	0	0.01	0.02	0	0	0.01	
LOI	3.53	2.74	2.18	2.54	1.92	3.6	2.06	1.74	2.42	2.15	2.99	
Sum	100.51	101.54	100.8	100.66	100.32	100.86	100.57	100.47	100.33	100.58	100.45	
Trace elements (ppm)												
V	67	104	175	125	195	93	181	168	108	166	133	
Cr	89	313	247	154	165	101	162	197	152	183	194	
Co	44	44	55	50	48	59	50	56	42	43	49	
Ni	61	67	75	81	54	82	66	58	67	42	58	
Cu	26	38	143	46	99	83	117	92	48	61	18	
Zn	27	32	25	25	22	41	20	18	21	19	26	
Rb	0	0	0	0	0	0	0	0	0	0	0	
Sr	150	156	94	152	135	118	128	144	166	141	131	
Y	5	6	8	7	9	7	9	10	7	9	7	
Zr	12	12	10	11	11	7	12	10	11	12	10	
Nb	0	2	2	0	0	0	0	0	0	0	1	
Ba	74	43	32	0	35	0	31	29	41	0	13	
La												
S												
Ce												
Nd	24	19	14	21	24	20	17	19	16	23	13	
Mg#	71.52	72.91	75.90	73.64	71.30	70.86	71.99	70.65	72.04	73.24	72.69	
Fe#	4.18	3.91	4.73	4.66	4.45	6.56	4.56	5.61	3.74	3.98	4.45	
Fe ₂ O ₃	2.08	2.12	2.32	2.24	2.20	3.11	2.33	2.59	1.89	2.02	2.41	

Evolution of Oceanic Gabbros: In-situ and Ancient Examples

Table 1A: Continued.

Location	Skaidevarri	Skaidevarri	Skaidevarri	Skaidevarri	Skaidevarri	Skaidevarri	Skaidevarri	Skaidevarri	Skaidevarri	Skaidevarri	Skaidevarri	Skaidevarri	Skaidevarri	Skaidevarri
Sample#	90LY186	90LY187	90LY188	90LY189	90LY190	90LY191	90LY192	90LY193	90LY194	90LY195	90LY196			
Description	Altered	Altered	Altered	Altered	Gabbro	gbnorite	Oxgnorite	Altered	Altered	Altered	Altered			
Place in profile														
W<=E	85	87	89	91	93	94.5	96	98	100	102	104			
Major elements														
SiO ₂	48.39	44.27	44.05	43.89	46.9	49.28	44.1	44.2	46.51	46.94	45.86			
TiO ₂	0.22	0.09	0.16	0.41	0.38	0.25	0.96	0.13	0.22	0.19	0.1			
Al ₂ O ₃	17.43	23.21	15.79	17.85	13.79	16.45	14.84	19.59	17.74	18.01	24.23			
Fe ₂ O ₃ *	5.8	5.36	11.34	10.53	9.95	7.68	14.72	8.39	7.82	7.17	4.64			
MnO	0.12	0.09	0.17	0.13	0.15	0.14	0.16	0.14	0.14	0.13	0.09			
MgO	8.65	6.57	12.71	8.94	10.29	9.14	9.59	9.77	8.98	8.76	5.06			
CaO	17.62	15.77	11.22	15.24	15.84	16.3	14.56	14.36	15.75	16.01	16.18			
Na ₂ O	0.49	1.21	0.53	0.69	0.63	0.78	0.67	0.72	0.95	1.07	1.66			
K ₂ O	0.01	0	0	0.02	0.02	0.01	0.02	0.03	0.02	0.02	0			
P ₂ O ₅	0.02	0	0	0.01	0.01	0.01	0	0	0.01	0	0.01			
LOI	1.85	3.22	4.1	2.85	1.9	0.7	1.15	3.19	2.34	2.07	2.59			
Sum	100.6	99.78	100.07	100.57	99.87	100.74	100.79	100.53	100.48	100.37	100.42			
Trace elements (ppm)														
V	191	73	112	407	300	180	659	74	152	139	66			
Cr	210	105	26	255	311	140	150	74	106	135	91			
Co	41	39	53	59	62	48	65	51	51	48	28			
Ni	31	41	71	86	67	87	67	69	65	81	42			
Cu	25	9	119	180	205	215	187	17	113	59	38			
Zn	11	19	47	40	32	19	29	40	19	16	7			
Rb	1	1	0	1	4	1	3	3	2	1	1			
Sr	119	162	112	132	111	125	107	146	138	156	167			
Y	9	4	4	6	11	8	8	7	8	8	6			
Zr	11	10	8	10	10	11	9	12	12	12	11			
Nb	1	2	2	0	1	3	1	1	3	2	1			
Ba	37	18	53	52	109	23	125	36	37	13	66			
La														
S														
Ce	19	18	16	16	20	17	24	20	25	22	12			
Nd														
Mg#	74.84	70.97	69.10	62.87	67.35	70.36	56.51	69.91	69.61	70.91	68.51			
FeO	3.47	3.23	7.68	5.95	5.37	4.73	7.38	5.17	4.90	4.69	2.58			
Fe ₂ O ₃	1.98	1.81	2.89	3.99	4.04	2.48	6.60	2.70	2.43	2.01	1.80			

Evolution of Oceanic Gabbros: In-situ and Ancient Examples

Table 1A: Continued.

Location	Skaidevarri	Skaidevarri	Skaidevarri	Skaidevarri	Skaidevarri	Skaidevarri	Skaidevarri	Skaidevarri	Skaidevarri	Skaidevarri	Skaidevarri	Skaidevarri
Sample#	90LY197	90LY198	90LY199	90LY200	90LY201	90LY202	90LY203	90LY204	90LY205	90LY206	90LY207	
Description	Altered	Altered	Altered	Altered	Altered	Altered	Altered	Altered	Altered	Altered	Olivinegb	
Place in profile	W<=E	106	109	111	113	115	116.5	117.5	119.5	121.5	123.5	125
Major elements												
SiO ₂	48.18	44.97	46.02	48.45	45.21	47.62	44.59	44.84	47.05	46.18	43.73	
TiO ₂	0.24	0.14	0.18	0.3	0.16	0.17	0.38	0.14	0.26	0.23	0.62	
Al ₂ O ₃	16.42	18.87	18.94	14.9	19.49	21.83	16.81	20.11	18.38	17.14	15.31	
Fe ₂ O ₃ *	6.94	7.19	6.95	7.67	7.4	4.68	10.28	7.43	6.69	8.24	12.24	
MnO	0.15	0.12	0.11	0.14	0.13	0.1	0.15	0.12	0.13	0.14	0.15	
MgO	9.19	9.8	9.3	9.98	9.67	5.93	9.4	8.83	8.1	9.54	9.72	
CaO	15.82	16.04	15.57	16.45	15.55	17.42	16.29	14.8	16.5	15.82	15.37	
Na ₂ O	0.85	0.69	0.83	0.6	0.68	1.34	0.32	1.15	0.94	0.54	0.75	
K ₂ O	0.01	0.01	0.01	0.01	0	0	0.01	0	0.01	0	0.01	
P ₂ O ₅	0.01	0	0.01	0.01	0.01	0.01	0.01	0.01	0.01	0.01	0.02	
LOI	2.05	2.72	2.71	1.75	2.93	1.83	2.52	2.87	2.15	2.53	2.53	
Sum	99.84	100.55	100.64	100.24	101.22	100.57	100.76	100.3	100.21	100.36	100.44	
Trace elements (ppm)												
V	177	92	116	223	100	146	359	97	200	155	569	
Cr	142	143	183	318	120	82	212	96	151	77	407	
Co	44	50	46	49	49	32	61	45	45	52	67	
Ni	53	79	60	46	53	28	86	56	45	62	104	
Cu	130	36	21	65	35	21	175	22	82	120	140	
Zn	22	26	18	21	24	9	42	26	22	30	35	
Rb	1	0	1	0	0	1	0	0	0	0	1	
Sr	122	159	129	124	137	169	140	199	144	138	132	
Y	8	5	7	8	7	6	7	6	9	9	7	
Zr	10	11	10	11	11	10	8	11	12	10	11	
Nb	1	3	2	2	1	1	1	1	2	1	1	
Ba	60	42	65	15	50	51	59	20	23	30	60	
La												
S												
Ce	18	23	15	14	17	23	17	10	21	16	24	
Nd												
Geochemical indices												
Mg#	72.54	73.11	72.75	72.19	72.27	71.65	64.59	70.33	70.72	69.78	61.30	
FeO	4.52	4.52	4.35	4.90	4.62	3.03	5.92	4.62	4.15	4.96	0.15	
Fe ₂ O ₃	1.97	2.22	2.17	2.28	2.32	1.35	3.77	2.35	2.13	2.78	4.61	

Evolution of Oceanic Gabbros: In-situ and Ancient Examples

Table 1A: Continued.

Location	Skaidevarri	Skaidevarri	Skaidevarri	Skaidevarri	Skaidevarri	Skaidevarri	Skaidevarri	Skaidevarri	Skaidevarri	Skaidevarri	Skaidevarri	Skaidevarri	Skaidevarri
Sample#	90LY208	90LY209	90LY210	90LY211	90LY212	90LY213	90LY214	90LY215	90LY216	90LY217	90LY218	Olox	Troct gb
Description	Olgnorite	Gabbro	Olgnorite	Altered	Altered	Gabbro	Gabbro	Gabbro	Gabbro	Oloxb	gbnorite	Olox	Troct gb
Place in profile	WV<=E	126.5	128	130	135	137	139	141	143	145.5	147	147	149
Major elements													
SiO ₂	45.89	47.36	46.92	46.02	46.24	45.62	46.99	47.48	42.36	44.96	46.49		
TiO ₂	0.21	0.25	0.29	0.25	0.22	0.26	0.25	0.27	1.22	0.4	0.15		
Al ₂ O ₃	17.99	18.88	15.61	14.16	16.37	13.39	17.72	17.09	17.62	19.24	21.12		
Fe ₂ O ₃ *	8.47	6.16	8.64	9.04	7.86	9.72	6.66	7.05	14.98	10.37	7.96		
MnO	0.14	0.12	0.15	0.16	0.13	0.15	0.12	0.14	0.14	0.15	0.14		
MgO	10.36	8.08	10.24	12.91	10.92	13.12	9.14	9.34	7.49	9.17	8.68		
CaO	15	15.49	16.21	14.61	15.97	15.39	15.75	16.71	15.04	14.45	15.12		
Na ₂ O	0.69	1.26	0.72	0.74	0.58	0.5	1.08	0.72	0.71	0.74	0.86		
K ₂ O	0.01	0.06	0	0.01	0.01	0.03	0.09	0.01	0	0	0		
P ₂ O ₅	0.01	0.01	0	0	0.01	0	0.01	0.01	0.01	0.01	0.02		
LOI	1.72	2.65	0.97	2.47	2.51	2.82	2.54	1.87	1.07	0.94	0.46		
Sum	100.47	100.31	99.75	100.37	100.82	101.02	100.36	100.71	100.64	100.42	101		
Trace elements													
V	117	185	186	157	144	169	184	160	841	273	71		
Cr	145	170	180	289	396	778	349	195	58	218	63		
Co	52	41	55	56	50	63	44	43	66	54	47		
Ni	77	45	83	85	75	146	65	51	45	53	36		
Cu	49	31	109	36	67	118	92	35	140	46	14		
Zn	27	17	27	38	22	23	37	19	27	30	26		
Rb	0	5	0	2	1	3	8	2	1	0	0		
Sr	141	237	131	133	125	100	202	164	134	155	169		
Y	7	8	9	8	7	9	7	8	7	6	7		
Zr	11	12	11	10	10	9	12	13	11	13	11		
Nb	3	1	2	2	1	3	1	0	2	1	0		
Ba	30	105	14	38	41	49	80	14	39	57	17		
La													
S													
Ce	16	16	26	16	17	22	23	19	21	20	15		
Nd													
Mg#	70.93	72.35	70.27	74.02	73.48	72.92	73.24	72.55	49.93	63.82	68.51		
FeO	5.10	4.15	5.47	6.09	4.79	5.41	4.25	4.49	6.43	5.00	4.22		
Fe ₂ O ₃	2.86	1.60	2.62	2.34	2.59	3.77	1.99	2.11	7.91	4.87	3.32		

Evolution of Oceanic Gabbros: In-situ and Ancient Examples

Table 1A: Continued.

Location	Skaidevarri	Skaidevarri	Skaidevarri	Skaidevarri	Skaidevarri	Skaidevarri	Skaidevarri
Sample#	90LY219	90LY220	90LY221	90LY222	90LY223	90LY224	90LY224
Description	Oloxbg	Oloxbg	Oloxbg	Oloxbg	Oloxbg	Oloxbg	Oloxbg
Place in profile	151	153	155	157	159	160.5	160.5
Major elements							
SiO ₂	47.8	39.25	43.68	42.59	45.9	43.87	43.87
TiO ₂	0.21	1.53	0.63	1.13	0.22	0.69	0.69
Al ₂ O ₃	20.46	13.71	19.25	15.81	19.68	18.69	18.69
Fe ₂ O ₃ *	7.23	19.84	11.88	16.16	8.61	11.17	11.17
MnO	0.14	0.19	0.16	0.16	0.15	0.14	0.14
MgO	8.04	9.59	8.21	8.63	9.05	7.31	7.31
CaO	16.31	13.34	14.48	14.95	15	15.49	15.49
Na ₂ O	0.84	0.35	0.7	0.6	0.62	1.07	1.07
K ₂ O	0	0.01	0.01	0	0.01	0.03	0.03
P ₂ O ₅	0.01	0	0	0.01	0.02	0.01	0.01
LOI	0.003	3.09	1.82	0.64	1.78	2.13	2.13
Sum	101.05	100.9	100.81	100.66	101.03	100.59	100.59
Trace elements							
V	130	842	470	796	127	529	529
Cr	64	55	84	138	72	76	76
Co	45	74	60	68	51	56	56
Ni	28	46	45	65	50	39	39
Cu	72	233	88	200	27	152	152
Zn	17	52	26	26	25	29	29
Rb	1	2	1	2	1	3	3
Sr	156	141	142	114	152	151	151
Y	6	6	6	9	7	8	8
Zr	11	9	11	10	10	9	9
Nb	2	2	1	3	3	2	2
Ba	4	60	70	54	6	50	50
La							
S							
Ce	16	11	25	25	20	7	7
Nd							
Mg#	68.93	49.09	57.96	51.58	67.71	56.62	56.62
FeO	4.28	10.81	5.78	6.87	4.52	6.19	6.19
Fe ₂ O ₃	2.52	7.95	5.52	8.60	3.64	4.36	4.36

Evolution of Oceanic Gabbros: In-situ and Ancient Examples

Table 1B: The Eastern suite of the Lyngen Gabbro. The data are similar to those in Table 1A.

Location Sample#	Skaidevarri 90-LY-134	Skaidevarri 90-LY-135	Skaidevarri 90-LY-136	Skaidevarri 90-LY-137	Skaidevarri 90-LY-138	Skaidevarri 90-LY-139	Skaidevarri 90-LY-140	Iddu HLY-9-93	Iddu HLY-10-93	Iddu HLY-12-93	Iddu HLY-14-93	Iddu HLY-16-93
Description	Gbnorite	Gbnorite	Oxgabbro	Gabbro	Altered	Olgbnorite	Olgabbro	qz-gabbro	tonalite-	gb pegm	pyxite	gb pegm
Place in profile W<E (m)	0	1.5	3	4.5	6	7.5	9					
Major elements (XRF)												
SiO ₂	47.3	47.0	47.4	46.7	44.7	46.9	47.3	45.8	61.3	45.6	51.3	49.0
TiO ₂	.13	.11	.11	.11	.08	.08	.10	.67	.12	.34	.26	.29
Al ₂ O ₃	15.4	14.7	15.4	17.8	19.7	16.6	14.8	14.0	11.5	19.0	8.5	9.0
Fe ₂ O ₃ *	6.2	5.9	5.6	5.3	5.9	5.5	5.7	18.3	9.9	13.3	11.7	12.6
MnO	.11	.11	.10	.10	.09	.10	.10	.34	.19	.18	.19	.20
MgO	12.3	12.8	12.1	10.1	11.0	12.0	12.5	7.4	8.1	9.0	14.0	16.8
CaO	17.0	16.8	17.7	17.9	16.2	17.1	17.8	11.1	7.9	11.6	12.4	9.9
Na ₂ O	.35	.28	.41	.49	.27	.26	.19	1.33	1.50	1.12	1.00	1.08
K ₂ O	.03	.00	.05	.02	.00	.01	.00	.14	.00	.25	.32	.22
P ₂ O ₅	.00	.00	.00	.00	.00	.02	.00	.01	.02	.01	.03	.06
LOI	2.5	2.9	2.6	2.6	2.2	2.9	2.5	1.4	0.6	1.4	1.3	1.5
Sum	101.4	100.7	101.5	101.0	100.1	101.5	101.0	100.5	101.2	101.8	101.0	100.6
Trace elements (XRF)												
V	118	118	118	120	71	101	123	563	180	453	299	208
Cr	534	853	991	660	372	703	849	31	499	32	1028	1994
Co	46	43	43	39	45	42	42	58	33	56	58	55
Ni	143	121	138	82	78	139	141	10	92	8	243	429
Cu	217	69	195	66	49	179	170	75	13	63	162	39
Zn	17	26	15	11	14	23	8	141	90	71	76	75
Rb	3	2	4	0	0	0	0	6	2	182	12	5
Sr	87	74	122	115	111	89	74	109	119	3	108	78
Y	6	5	6	5	6	3	4	15	12	13	8	10
Zr	9	9	10	10	10	8	9	15	13	1	25	36
Nb	0	0	0	0	2	3	0	2	1	71	1	2
Ba	33	0	47	76	24	0	58	145	0	13	49	52
La								10	4	0.155	8	13
S								0.31	0.03	0.04	0.05	0.03
Ce	21	12	21	21	18	16	19	32	0	2	40	5
Nd								8	0		3	4
Mg#	66.3	68.4	68.4	65.6	65.1	68.6	68.9	28.6	44.7	40.5	54.5	57.1
FeO	3.6	3.2	3.1	3.1	3.3	3.0	3.0					
Fe ₂ O ₃	2.3	2.5	2.1	1.8	2.3	2.2	2.3					

Evolution of Oceanic Gabbros: In-situ and Ancient Examples

Table 1B: Continued

Location Sample#	Iddu HL Y-18-93	Iddu HL Y-19-93	Iddu HL Y-20-93	Iddu HL Y-22b-93	Iddu HL Y-23-93	Iddu HL Y-24-93	Iddu HL Y-25-93	Iddu HL Y-26-93	Iddu HL Y-27-93	Iddu HL Y-31-93	Iddu HL Y-35-93	Iddu HL Y-38-93	Iddu HL Y-39-93	Iddu HL Y-40-93	Iddu HL Y-41-93
Description	tonalite- gb pegm	tonalite- qz-granit.	gb pegm	melagb	gb pegm	gb pegm	tonalite- qz-granit.	tonalite- qz-granit.	tonalite- qz-granit.	tonalite- qz-granit.	gb pegm	melagb	gb pegm	tonalite- qz-granit.	tonalite- qz-granit.
Place in profile	W<=E (m)														
Major elements															
SiO ₂	42.2	74.1	38.3	41.3	41.3	47.0	71.3	68.8	61.4	41.5	40.3	41.0	66.3	72.7	41.3
TiO ₂	.31	.24	.67	.63	.59	.16	.23	.17	.34	.46	.60	.76	.29	.30	.61
Al ₂ O ₃	16.9	14.6	17.6	14.7	14.7	18.3	13.7	14.8	10.9	15.2	17.3	16.2	14.8	13.2	20.1
Fe ₂ O ₃ *	16.7	4.6	18.1	20.2	20.9	9.8	5.6	5.7	4.4	21.0	18.4	2.4	6.7	4.9	15.7
MnO	.13	.04	.14	.17	.20	.13	.10	.11	.18	.16	.15	.17	.13	.10	.24
MgO	8.2	1.0	7.0	8.4	10.1	9.5	2.4	2.8	0.9	9.0	8.2	8.4	1.7	0.9	5.5
CaO	13.9	4.4	11.9	13.4	10.6	15.1	6.7	7.3	4.4	12.4	13.7	12.2	6.7	5.3	14.0
Na ₂ O	1.13	2.40	.99	.80	.64	1.19	1.90	2.42	3.15	1.19	.70	1.11	2.03	2.55	.74
K ₂ O	.02	.00	.18	.00	.00	.07	.11	.13	.00	.02	.00	.18	.03	.05	.04
P ₂ O ₅	.01	.10	.01	.02	.01	.02	.12	.10	.06	.00	.01	.02	.05	.08	.17
LOI	2.7	1.5	2.4	2.0	3.1	0.9	0.7	0.7	1.0	1.4	2.3	1.5	2.0	1.7	3.2
Sum	102.2	103.0	97.2	101.7	102.2	102.1	103.0	102.9	86.7	102.3	101.7	101.8	100.7	101.8	101.5
Trace elements															
V	574	26	789	734	515	420	27	51	109		456	621	128	33	302
Cr	55	30	36	36	28	286	22	26	16		28	72	24	30	29
Co	65	11	66	75	53	59	20	22	12		69	70	21	13	57
Ni	21	7	27	10	9	40	7	8	6		10	27	5	7	8
Cu	86	12	105	165	73	139	14	23	8		91	163	21	12	34
Zn	55	24	83	64	104	30	32	38	70		77	72	85	56	101
Rb	3	2	13	3	3	2	2	4	2		2	9	4	4	1
Sr	130	186	136	94	88	112	261	282	177		133	139	194	237	229
Y	4	10	2	2	3	3	36	29	8		3	4	8	4	10
Zr	11	96	11	10	9	11	94	82	11		11	12	17	12	14
Nb	0	2	2	0	2	1	5	6	0		1	2	1	0	3
Ba	5	66	68	47	35	0	55	87	44		80	62	13	60	1
La	5	13	12	10	7	10	6	11	7		10	8	8	0	10
S	0.22	0.03	0.19	0.38	0.20	0.13	0.03	0.03	0.03		0.50	0.46	0.03	0.03	0.08
Ce	8	24	0	0	0	3	22	24	0		19	14	17	12	15
Nd	6	9	2	4	5	0	15	17	2		7	9	8	8	12
Mg#	32.8	18.6	27.8	29.3	32.7	49.3	30.3	33.3	16.7	30.1	30.9	77.7	19.9	15.8	25.8
FeO															
Fe ₂ O ₃															

Evolution of Oceanic Gabbros: In-situ and Ancient Examples

Table 1B: Continued

Location Sample#	Iddu HL Y-42-93	Iddu HL Y-43-93	Iddu HL Y-45-93	Iddu HL Y-46-93	Iddu HL Y-48-93	Iddu HL Y-1.1	Iddu HL Y-2.1	Iddu HL Y-3.1	Iddu HL Y-4.1	Iddu HL Y-1.2	Iddu HL Y-2.2	Iddu HL Y-3.2	Iddu HL Y-4.2	Iddu HL Y-5.2	Iddu HL Y-6.2
Description	gb pegm	qz-granit.	gb pegm	qz-granit.	gb pegm	qz-granit.	qz-granit.	qz-granit.	qz-granit.	qz-granit.	qz-granit.	qz-granit.	qz-granit.	qz-granit.	qz-granit.
Place in profile	W<E	W<E	W<E	W<E	W<E	W<E	W<E	W<E	W<E	W<E	W<E	W<E	W<E	W<E	W<E
W<E (m)	W<E	W<E	W<E	W<E	W<E	W<E	W<E	W<E	W<E	W<E	W<E	W<E	W<E	W<E	W<E
Major elements	Major elements	Major elements	Major elements	Major elements	Major elements	Major elements	Major elements	Major elements	Major elements	Major elements	Major elements	Major elements	Major elements	Major elements	Major elements
SiO ₂	39.5	58.6	45.6	60.8	55.6	43.7	45.5	45.5	46.1	40.0	44.3	43.8	45.6	44.2	44.0
TiO ₂	.82	.33	.05	.36	.59	.30	.24	.35	.13	1.31	.52	.58	.33	.33	.14
Al ₂ O ₃	14.7	13.8	10.1	12.4	18.0	20.1	19.5	18.3	25.8	15.6	16.0	15.6	15.3	18.4	25.7
Fe ₂ O ₃ *	22.8	8.4	14.1	4.8	10.7	11.7	10.8	12.8	6.0	22.3	15.3	16.8	13.3	11.8	5.6
MnO	.19	.16	.27	.09	.11	.15	.17	.19	.11	.18	.21	.22	.20	.16	.09
MgO	8.7	6.0	7.8	1.0	4.6	8.9	9.7	9.3	6.3	7.8	9.9	9.8	12.2	8.5	5.3
CaO	11.5	10.5	12.6	5.1	9.9	13.9	14.0	13.6	15.5	12.3	12.6	12.1	12.6	14.3	15.6
Na ₂ O	1.10	1.19	.64	2.24	1.43	.83	.85	.00	1.02	.24	.43	.76	1.09	.32	1.16
K ₂ O	.03	.08	.00	.36	.00	.05	.06	.15	.13	.33	.39	.39	.35	.39	.30
P ₂ O ₅	.02	.06	.03	.10	.14	.00	.01	.01	.00	.02	.00	.01	.02	.01	.01
LOI	2.5	2.6	0.1	1.8	0.0	0.8	1.0	0.4	1.0	0.8	0.8	1.0	1.2	1.3	1.1
Sum	101.8	101.8	101.7	89.0	101.0	100.5	101.8	100.5	102.0	100.9	100.5	101.0	102.0	99.7	99.1
Trace elements	Trace elements	Trace elements	Trace elements	Trace elements	Trace elements	Trace elements	Trace elements	Trace elements	Trace elements	Trace elements	Trace elements	Trace elements	Trace elements	Trace elements	Trace elements
V	444	156	178	44	638	309	249	327	123	553	384	419	262	325	156
Cr	49	529	18	13	70	41	29	19	26	38	23	29	15	21	15
Co	61	36	50	16	68	60	61	66	39	75	68	70	67	64	40
Ni	44	92	6	5	36	6	17	14	17	22	16	18	16	10	8
Cu	89	25	9	10	134	179	198	150	133	143	105	110	146	111	133
Zn	94	77	101	50	71	52	69	69	52	105	98	128	113	58	47
Rb	2	3	1	13	8	4	7	7	9	9	12	8	10	14	16
Sr	94	205	178	174	178	142	146	137	177	118	115	110	106	141	206
Y	2	15	4	11	4	2	3	2	2	5	2	0	3	4	0
Zr	11	48	11	24	12	9	9	10	11	11	11	11	10	10	11
Nb	1	4	1	4	1	0	0	0	0	3	0	0	0	0	0
Ba	37	21	27	207	50	40	21	29	24	58	54	114	85	102	43
La	17	9	12	7	7	7	0	7	5	5	7	6	6	7	0
S	0.15	0.04	0.04	0.03	0.18										
Ce	16	18	6	14	22	24	13	20	19	13	21	16	18	33	22
Nd	3	14	4	7	5	10	6	8	5	6	17	5	10	11	10
Mg#	27.7	41.7	35.6	17.0	30.1	43.1	47.3	42.1	51.0	25.8	39.1	36.9	47.8	42.0	48.5
FeO															
Fe ₂ O ₃															

Evolution of Oceanic Gabbros: In-situ and Ancient Examples

Table 1B: Continued

Location Sample#	Iddu HLY1.3	Iddu HLY2.3	Iddu HLY3.3	Iddu HLY1.4	Iddu HLY2.4	Iddu HLY3.4	Iddu HLY1.5	Iddu HLY3.5	Iddu HLY4.5	Iddu HLY5.5	Iddu HLY6.5	Iddu HLY1.6	Iddu HLY2.6	Iddu HLY3.6	Iddu HLY4.6
Description	gb pegm	qz-gabbro	qz-gabbro	tonalite- qz-granit.	melagb	gb pegm	qz-gabbro	melagb	melagb	melagb	melagb	tonalite- qz-granit.	tonalite- qz-granit.	tonalite- qz-granit.	tonalite- qz-granit.
Place in profile															
W<=E (m)															
Major elements															
SiO ₂	60.1	56.0	55.5	40.1	41.2	44.0	50.0	43.4	41.3	41.6	43.6	59.5	72.1	63.8	72.1
TiO ₂	.29	.33	.35	.53	.35	.11	.37	.37	.45	.38	.30	.34	.21	.64	.15
Al ₂ O ₃	13.5	14.4	14.3	20.7	26.0	24.5	14.2	18.7	21.2	22.7	20.5	18.6	14.2	14.8	14.4
Fe ₂ O ₃ *	8.4	9.3	9.5	15.3	12.0	5.3	12.2	13.0	13.1	12.0	10.9	5.8	3.2	9.4	2.5
MnO	.15	.18	.18	.13	.09	.09	.19	.14	.12	.12	.13	.05	.03	.05	.02
MgO	6.7	6.9	7.1	6.3	4.2	4.5	11.0	8.5	6.2	5.9	7.0	1.8	1.0	1.8	0.7
CaO	7.7	8.8	9.0	14.2	14.5	16.6	11.6	11.9	11.4	11.5	13.9	6.1	4.3	4.9	4.4
Na ₂ O	1.61	1.60	1.27	.02	.15	.20	.59	.16	.03	.04	.27	2.45	2.30	1.61	2.50
K ₂ O	.74	.75	.84	.23	.32	.40	.35	1.43	2.06	1.75	.66	1.39	.64	.80	.47
P ₂ O ₅	.07	.07	.08	.00	.02	.01	.06	.00	.01	.02	.01	.05	.09	.04	.07
LOI	1.0	1.2	1.4	1.9	1.4	2.1	1.1	2.0	2.3	2.4	1.9	1.4	0.8	1.0	0.7
Sum	100.2	99.6	99.5	99.5	100.3	97.8	101.6	99.5	98.2	98.4	99.2	97.4	98.7	98.9	98.0
Trace elements															
V	121	164	161	483	353	95	215	348	458	434	321	114	35	357	24
Cr	614	518	525	26	19	18	1035	24	23	20	17	18	16	30	15
Co	32	39	37	63	57	34	52	55	50	50	56	19	9	21	6
Ni	119	99	100	7	6	6	148	6	7	5	6	10	6	12	6
Cu	30	32	33	69	112	99	24	111	62	53	111	28	13	27	15
Zn	74	76	74	66	46	237	83	57	57	56	57	50	26	50	25
Rb	24	21	23	13	17	23	9	65	92	81	30	60	28	32	20
Sr	258	230	230	177	210	208	207	210	272	236	184	298	252	208	279
Y	19	16	16	3	2	2	10	2	1	2	2	6	7	5	7
Zr	61	35	40	10	12	11	39	12	12	13	11	62	99	79	89
Nb	6	5	5	2	1	1	3	1	1	2	1	11	5	4	3
Ba	226	156	284	41	23	142	66	411	1073	742	231	804	361	391	289
La	10	14	16	13	6	6	14	6	10	3	6	18	21	18	22
S															
Ce	35	28	35	9	18	12	33	17	14	1	18	38	46	27	50
Nd	18	14	18	10	8	10	17	9	10	7	6	14	19	9	18
Mg#	44.5	42.7	42.8	29.2	26.0	46.0	47.3	39.4	32.1	33.0	39.1	23.6	22.9	16.2	21.4
FeO															
Fe ₂ O ₃															

Evolution of Oceanic Gabbros: In-situ and Ancient Examples

Table 1B: Continued

Location Sample#	Iddu HLY5.6	Iddu HLY6.6	Iddu HLY1.7	Iddu HLY2.7	Iddu HLY3.7	Iddu HLY4.7	Iddu HLY1.8	Iddu HLY2.8	Iddu HLY1.9	Iddu HLY2.9	Iddu HLY20-94	Iddu HLY21-94	Iddu HLY22-94	Iddu HLY24-94	Iddu HLY25-94
Description Place in profile W<=E (m)	tonalite- qz-granit.	tonalite- qz-granit.	melagb	melagb	melagb	melagb	melagb	melagb	melagb	melagb	melagb	melagb	gb pegm	melagb	melagb
Major elements															
SiO ₂	73.5	72.3	39.4	41.7	41.8	42.9	39.6	42.6	40.7	42.7	40.5	41.2	45.1	41.8	39.2
TiO ₂	.17	.14	.64	.48	.28	.22	.66	.25	.64	.38	.57	.52	.38	.36	.66
Al ₂ O ₃	14.3	15.1	17.0	17.8	24.4	24.7	18.5	26.1	20.6	23.7	17.8	18.7	15.2	24.6	17.6
Fe ₂ O ₃ *	2.6	2.4	19.0	15.2	9.5	8.0	18.4	7.8	15.2	10.3	17.5	16.0	13.2	10.9	19.0
MnO	.02	.02	.16	.15	.10	.09	.14	.10	.16	.14	.16	.14	.19	.11	.16
MgO	0.7	0.6	8.4	7.9	5.1	5.1	7.2	3.9	6.6	5.8	8.0	7.7	10.0	4.6	7.6
CaO	4.2	5.1	14.1	14.7	14.8	15.1	14.2	15.5	13.3	13.8	13.9	13.9	13.1	11.5	14.0
Na ₂ O	2.69	2.27	.00	.00	.11	.13	.00	.19	.36	.15	.00	.00	.23	.24	.00
K ₂ O	.62	.47	.13	.14	.24	.22	.07	.26	.43	.48	.23	.25	.38	1.91	.10
P ₂ O ₅	.07	.07	.02	.01	.01	.01	.02	.02	.03	.16	.01	.01	.04	.01	.01
LOI	0.4	0.9	1.5	1.8	1.6	1.7	1.9	1.2	1.4	1.1	2.2	2.0	1.9	2.5	2.4
Sum	99.3	99.4	100.2	100.0	97.9	98.0	100.7	98.0	99.4	98.7	100.8	100.1	99.7	98.5	100.6
Trace elements															
V	22	32	538	456	352	291	536	301	316	202	622	559	360	486	596
Cr	20	30	40	37	16	20	32	20	19	13	26	21	21	22	24
Co	7	9	76	70	51	46	73	43	63	49	72	68	61	43	72
Ni	6	5	9	8	6	5	8	7	6	4	9	8	7	7	6
Cu	12	17	75	100	33	41	91	31	64	38	96	99	87	17	103
Zn	21	24	67	55	51	51	52	46	69	64	65	69	70	48	72
Rb	26	18	7	9	14	13	4	14	21	22	11	14	16	97	6
Sr	276	272	132	138	207	194	174	232	196	224	167	151	138	261	139
Y	6	6	2	2	2	2	1	1	2	2	1	0	3	1	1
Zr	96	80	9	9	11	10	10	11	14	14.5	20	18	22	21	19
Nb	5	5	2	1	1	1	2	1	2	1	4	4	4	4	3
Ba	368	256	48	7	101	25	84	105	124	66	90	93	102	884	118
La	15	19	11	10	1	1	10	8	14	10	0	0	0	0	0
S															
Ce	45	50	11	10	16	14	15	14	15	13	8	15	14	3	9
Nd	19	17	15	2	9	2	7	6	11	9	0	0	3	4	3
Mg#	22.4	20.5	30.6	34.3	35.1	39.0	28.1	33.3	30.4	36.0	31.3	32.6	43.0	29.7	28.6
FeO															
Fe ₂ O ₃															

Evolution of Oceanic Gabbros: In-situ and Ancient Examples

Table 1B: Continued

Location Sample#	Iddu HLY-26-94	Iddu HLY-1Pa	Iddu HLY-2Pa	Iddu HLY-3Pa	Iddu HLY-4Pa	Iddu HLY-5Pa	Iddu HLY-6Pa	Iddu HLY-7Pa	Iddu HLY-9PB	Iddu HLY-10Pa	Iddu HLY-11PB	Iddu HLY-12PB	Iddu HLY-16PB	Iddu HLY-19PB	Iddu HLY-21PB
Description	melagb	qz-granit.	tonalite-	tonalite-	melagb	qz-granit.	tonalite-	melagb	melagb	qz-granit.	melagb	qz-granit.	tonalite-	tonalite-	tonalite-
Place in profile W<=E (m)															
Major elements															
SiO ₂	45.0	66.4	62.9	56.3	52.2	61.6	64.8	49.6	47.6	74.4	43.4	42.0	55.1	63.3	59.9
TiO ₂	.51	.21	.15	.20	.19	.15	.14	.19	.54	.18	.41	.64	.25	.12	.14
Al ₂ O ₃	22.1	12.9	13.1	10.8	8.5	13.4	12.7	17.0	16.7	13.8	16.9	18.2	14.1	12.2	12.2
Fe ₂ O ₃ *	11.5	7.5	8.7	12.6	15.0	8.9	7.8	11.8	15.3	3.6	13.1	16.4	11.7	8.6	9.6
MnO	.10	.14	.16	.23	.33	.15	.14	.21	.25	.06	.24	.23	.20	.15	.17
MgO	3.4	5.6	6.3	10.1	14.5	6.6	5.7	8.4	6.4	0.9	8.1	7.2	7.8	7.0	7.7
CaO	13.0	6.5	7.8	8.3	8.7	8.0	7.3	11.0	10.5	4.9	14.7	12.2	9.6	7.4	7.7
Na ₂ O	.97	1.53	1.53	1.13	.80	1.43	1.41	1.19	1.17	2.54	.34	.37	.90	1.27	1.24
K ₂ O	.68	.00	.00	.00	.00	.00	.00	.01	.06	.05	.02	.12	.04	.05	.02
P ₂ O ₅	.26	.04	.03	.01	.01	.02	.02	.00	.00	.01	.00	.00	.01	.01	.01
LOI	1.2	0.4	0.3	0.7	0.4	0.4	0.7	0.8	1.3	0.7	1.5	2.0	0.9	0.7	1.1
Sum	98.7	101.2	101.1	100.3	100.7	100.6	100.6	100.2	99.9	101.2	98.8	99.4	100.5	100.8	99.7
Trace elements (
V	495	111	134	209	172	168	152	173	429	42	399	539	261	136	187
Cr	21	71	118	604	1858	201	99	70	62	3	116	84	310	184	299
Co	53	23	33	41	42	34	31	50	47	10	59	48	44	30	36
Ni	19	44	47	80	194	47	43	55	15	7	29	14	60	52	66
Cu	157	23	15	15	19	12	21	135	90	18	160	113	82	18	20
Zn	56	84	74	105	147	75	71	97	116	34	76	112	93	76	88
Rb	33	3	4	1	1	1	3	2	3	3	2	8	5	5	5
Sr	214	153	125	95	63	126	131	162	145	194	158	114	176	133	117
Y	4	13	15	19	24	13	14	16	21	8	8	7	13	11	14
Zr	23	17	20	19	20	18	19	20	26	19	14	14	20	19	18
Nb	4	2	3	4	4	2	1	3	4	2	0	2	3	1	3
Ba	163	8	8	6	47	96	29	97	29	52	0	81	134	42	56
La	0	7	6	9	10	8	9	8	12	8	7	5	7	8	8
S		0.03	0.03	0.03	0.03	0.02	0.03	0.08	0.08	0.03	0.12	0.12	0.05	0.03	0.02
Ce	9	5	9	6	8	0	0	5	20	0	4	0	0	0	0
Nd	8	0	5	0	12	4	0	0	3	0	0	0	0	0	0
Mg#	22.7	43.0	42.0	44.4	49.1	42.5	42.1	41.4	29.5	20.1	38.1	30.4	39.9	44.9	44.6
FeO															
Fe ₂ O ₃															

Evolution of Oceanic Gabbros: In-situ and Ancient Examples

Table 1B: Continued

Location Sample#	Strupen Lan-1	Strupen Lan-2	Strupen Lan-3	Strupen Lan-4	Strupen Lan-5	Strupen Lan-6	Strupen Lan-7	Strupen Lan-8	Strupen Lan-9	Strupen Lan-10	Strupen Lan-11	Strupen Lan-12	Strupen Lan-13	Strupen Lan-14	Strupen Lan-15	Strupen Lan-16	Strupen Lan-17
Description																	
Place in profile W<E (m)	1.25	2.5	3.25	3.6	4.25	4.9	5.5	6.25	6.6	7.25	8.25	9.1	9.75	10.25	11	11.25	11.5
Major elements																	
SiO ₂	46.6	47.3	46.8	41.8	41.4	42.9	47.3	47.3	47.3	46.8	48.1	48.2	46.4	46.6	45.8	42.9	44.5
TiO ₂	.09	.13	.10	.46	.60	.49	.10	.08	.10	.12	.07	.15	.20	.13	.22	.56	.17
Al ₂ O ₃	16.5	13.5	17.5	18.9	17.2	19.1	17.7	16.9	17.6	18.6	18.4	17.6	16.5	18.7	18.1	18.2	19.4
Fe ₂ O ₃ *	7.6	8.9	9.8	15.0	16.9	16.3	9.4	9.8	10.1	10.0	9.1	10.9	11.6	10.8	12.7	18.8	10.3
MnO	.16	.17	.18	.17	.21	.20	.19	.20	.19	.17	.18	.20	.20	.19	.19	.17	.19
MgO	9.6	11.3	9.9	5.5	6.7	5.8	9.3	10.1	10.2	9.5	9.3	9.0	9.2	8.7	8.0	5.8	7.2
CaO	16.0	16.5	13.7	14.8	14.5	13.6	14.9	14.5	13.8	13.8	13.9	14.2	15.3	14.2	14.4	14.3	14.0
Na ₂ O	.16	.22	.23	.24	.26	.41	.33	.27	.26	.25	.09	.14	.25	.28	.31	.27	.21
K ₂ O	.01	.01	.00	.02	.01	.01	.00	.00	.00	.00	.00	.00	.00	.00	.00	.00	.01
P ₂ O ₅	.01	.00	.02	.01	.01	.02	.01	.00	.01	.00	.02	.01	.01	.01	.01	.00	.01
LOI	2.3	1.4	0.1	1.8	1.8	2.2	0.2	0.2	0.0	0.3	0.3	0.0	0.3	0.4	0.2	0.4	2.4
Sum	98.9	99.3	98.3	98.7	99.5	101.0	99.4	99.4	99.5	99.6	99.4	100.4	99.8	99.9	99.9	101.4	98.4
Trace elements																	
V	153	207	187	709	562	624	162	133	217	241	121	242	303	227	380	776	222
Cr	254	552	74	41	36	27	76	71	72	33	27	29	105	22	25	31	32
Co	46	53	51	65	69	66	57	51	58	58	52	60	65	56	57	63	56
Ni	71	79	57	20	13	9	50	51	54	49	36	39	34	33	24	10	25
Cu	114	74	59	203	123	163	98	107	101	196	135	150	120	110	176	219	110
Zn	48	50	57	58	85	90	62	57	62	58	62	61	61	57	53	50	73
Rb	2	0	0	4	2	0	0	0	0	0	2	2	1	0	0	0	2
Sr	83	67	95	111	102	117	93	88	89	94	101	97	87	101	98	98	111
Y	2	3	3	2	2	1	2	3	1	1	2	2	1	1	2	1	2
Zr	17	19	17	19	19	18	18	18	16	17	22	19	16	17	16	15	20
Nb	4	2	5	3	3	4	4	4	5	4	2	2	4	4	4	5	2
Ba	6	3	10	2	2	5	2	4	8	2	3	5	4	6	3	3	7
La	20	10	17	6	5	3	22	10	8	13	13	14	8	15	14	13	18
S	0.05	0.03	0.04	0.34	0.42	0.38	0.13	0.06	0.05	0.05	0.05	0.09	0.09	0.09	0.23	0.35	0.19
Ce	53	48	31	2	47	64	63	42	49	23	11	37	52	66	55	59	25
Nd	6	2	2	2	2	7	7	8	5	7	2	2	2	2	2	10	2
Mg#	55.8	56.1	50.3	26.7	28.3	26.3	49.7	50.6	50.2	48.6	50.5	45.1	44.2	44.7	38.7	23.7	40.9
FeO	5.03	5.81	6.02	8.06	9.04	8.23	6.87	5.54	4.96	6.94	7.48	7.89	7.38	6.29	5.81	6.77	7.00
Fe ₂ O ₃	2.05	2.48	3.19	6.15	6.91	7.23	1.85	3.74	4.65	2.40	0.89	2.22	3.47	3.86	6.32	11.32	2.63

Evolution of Oceanic Gabbros: In-situ and Ancient Examples

Table 1B: Continued

Location Sample#	Strupen Lan-18	Strupen Lan-19	Strupen Lan-20	Strupen Lan-21	Strupen Lan-22	Strupen Lan-23	Strupen Lan-24	Strupen Lan-25	Strupen Lan-26	Strupen Lan-27	Strupen Lan-28	Strupen Lan-29	Strupen Lan-30	Strupen Lan-31	Strupen Lan-32	Strupen Lan-33	Strupen Lan-34	Strupen Lan-35	
Description																			
Place in profile W<E (m)	11.9	12.1	13	13.4	14	14.1	14.5	14.75	15	15.3	16.25	17	17.5	17.9	18.1	18.25	18.4		
Major elements																			
SiO ₂	42.2	44.1	47.3	47.1	40.8	47.4	48.3	41.2	46.6	47.2	47.4	49.1	51.3	47.7	43.7	45.8	49.1		
TiO ₂	.56	.34	.08	.11	.62	.10	.07	.53	.25	.09	.10	.10	.15	.08	.33	.05	.17		
Al ₂ O ₃	18.3	22.6	16.8	18.2	17.6	14.8	16.7	19.8	16.8	17.3	16.5	16.3	9.9	16.6	19.3	27.1	2.8		
Fe ₂ O ₃ *	17.5	12.7	10.4	10.6	17.4	11.4	9.9	15.4	12.1	9.6	9.6	8.3	9.2	8.4	13.1	5.6	11.9		
MnO	.17	.16	.20	.19	.18	.27	.21	.14	.19	.18	.18	.16	.18	.16	.18	.11	.26		
MgO	5.4	5.2	10.4	9.6	5.8	10.7	10.1	5.7	9.0	10.4	11.1	10.1	13.3	11.0	7.0	5.5	15.6		
CaO	14.3	14.5	13.5	13.4	14.4	14.1	13.5	14.4	14.3	14.1	14.1	15.1	17.0	15.1	14.7	14.7	18.6		
Na ₂ O	.41	.37	.26	.28	.35	.28	.11	.21	.13	.24	.23	.07	.03	.24	.29	.59	.06		
K ₂ O	.01	.00	.00	.00	.02	.00	.00	.00	.00	.00	.00	.00	.00	.00	.03	.01	.00		
P ₂ O ₅	.00	.02	.01	.00	.01	.01	.00	.02	.01	.01	.01	.00	.00	.01	.00	.01	.01		
LOI	2.3	1.0	0.1	0.0	2.1	0.5	0.4	0.7	0.2	0.0	0.1	0.3	0.6	0.0	2.2	1.7	0.0		
Sum	101.2	101.0	99.1	99.4	99.2	99.5	99.3	98.2	99.7	99.1	99.3	99.6	101.6	99.3	100.8	101.2	98.5		
Trace elements																			
V	755	457	130	198	646	97	113	669	409	196	195	203	250	158	487	96	155		
Cr	34	23	34	36	26	134	74	28	56	75	81	101	670	140	53	98	1443		
Co	64	54	58	52	78	59	60	63	69	56	56	58	60	54	62	36	72		
Ni	7	12	53	39	7	37	51	12	51	54	61	75	88	68	25	19	109		
Cu	230	104	22	74	293	52	73	259	200	46	153	98	54	23	242	11	24		
Zn	68	50	71	57	80	80	69	47	67	57	55	51	47	51	62	48	67		
Rb	0	0	1	0	3	0	2	3	3	0	0	2	2	0	2	0	0		
Sr	107	132	93	98	105	84	98	107	91	89	83	83	41	87	119	149	5		
Y	2	1	4	1	2	2	2	2	2	3	1	2	3	3	2	0	9		
Zr	18	18	18	17	18	17	17	18	18	18	17	18	17	18	18	19	17		
Nb	6	4	5	4	5	5	2	2	2	4	4	4	2	4	5	4	4		
Ba	5	10	8	6	2	9	8	4	3	4	7	5	6	5	2	4	7		
La	17	12	8	16	8	13	17	11	10	21	15	24	22	19	10	13	23		
S	0.49	0.16	0.03	0.07	0.49	0.09	0.08	0.27	0.19	0.03	0.04	0.03	0.03	0.03	0.26	0.03	0.03		
Ce	58	69	43	9	23	59	4	2	45	16	58	2	9	39	80	38	26		
Nd	2	5	2	8	6	2	2	2	2	2	2	2	2	2	5	2	8		
Mg#	23.7	29.1	50.1	47.5	25.0	48.4	50.5	27.1	42.7	52.0	53.8	54.9	59.1	56.8	34.7	49.4	56.7		
FeO	8.43	3.81	7.14	4.32	9.18	7.96	7.68	8.26	8.50	3.64	1.87	6.15	6.86	5.54	9.69	4.52	8.33		
Fe ₂ O ₃	8.21	8.48	2.52	5.85	7.31	2.65	1.41	6.34	2.77	5.56	7.49	1.56	1.65	2.26	2.41	0.64	2.75		

Evolution of Oceanic Gabbros: In-situ and Ancient Examples

Table 1B: Continued

Location Sample#	Strupen Lan-36	Strupen Lan-37	Strupen Lan-38	Strupen Lan-39	Strupen Lan-40	Strupen Lan-41	Strupen Lan-42	Strupen Lan-43	Strupen Lan-44	Strupen Lan-45	Strupen Lan-46	Strupen Lan-47	Strupen Lan-48	Strupen Lan-49	Strupen Lan-50	Strupen Lan-51	Strupen Lan-52
Description																	
Place in profile W<=E (m)	18.5	18.9	19.75	20.25	20.75	21.4	22	22.75	23.5	24.25	25.4	26.1	27	27.5	28.5	29	29.05
Major elements																	
SiO ₂	48.3	48.1	49.1	51.8	50.8	48.8	42.8	42.8	46.8	46.7	46.7	46.6	40.2	40.5	41.8	44.2	46.9
TiO ₂	.12	.13	.13	.19	.14	.14	.44	.50	.13	.11	.24	.17	.68	.62	.60	.46	.17
Al ₂ O ₃	9.8	8.9	8.4	5.2	8.4	8.1	19.6	21.1	17.4	17.6	18.3	18.0	16.8	18.8	21.8	23.8	13.8
Fe ₂ O ₃ *	9.6	8.8	8.1	12.1	8.1	8.4	15.4	14.0	10.3	10.5	11.9	11.8	19.7	17.9	15.3	12.9	13.6
MnO	.20	.18	.17	.25	.16	.17	.17	.16	.20	.19	.20	.20	.19	.19	.19	.17	.35
MgO	13.9	14.4	14.1	15.8	14.6	15.2	5.9	5.3	9.6	10.1	8.2	9.3	6.0	5.8	5.2	4.6	11.0
CaO	16.5	16.9	17.5	15.9	16.4	17.2	14.0	14.6	14.3	13.7	14.3	13.9	14.0	14.6	15.1	15.2	13.6
Na ₂ O	.27	.23	.05	.00	.06	.17	.53	.33	.37	.32	.09	.26	.14	.16	.21	.36	.25
K ₂ O	.00	.00	.01	.01	.02	.00	.02	.04	.00	.00	.00	.00	.00	.00	.00	.00	.00
P ₂ O ₅	.02	.01	.01	.00	.00	.01	.01	.02	.02	.00	.01	.01	.00	.02	.00	.00	.02
LOI	0.2	1.0	1.0	0.2	1.6	0.0	2.3	2.9	0.7	0.2	0.2	0.0	0.4	0.5	0.6	0.3	0.0
Sum	99.0	98.6	98.5	101.5	100.2	98.2	101.3	101.8	99.8	99.5	100.0	100.0	98.1	99.0	100.8	102.0	99.7
Trace elements																	
V	159	181	215	246	219	169	708	512	182	195	373	271	796	720	497	375	120
Cr	1388	1851	2035	2592	2721	865	63	22	23	30	21	15	34	32	21	19	82
Co	57	58	55	73	58	53	62	61	56	58	67	61	71	74	60	48	61
Ni	103	128	129	145	166	141	25	9	39	50	34	33	8	7	6	12	33
Cu	33	44	28	74	39	12	120	229	118	149	216	126	254	142	75	57	33
Zn	59	54	41	67	46	42	82	52	58	63	63	64	49	62	53	49	95
Rb	0	0	2	2	2	0	0	0	1	0	2	0	2	2	2	2	0
Sr	49	43	36	15	39	36	126	140	94	94	103	97	98	105	131	147	83
Y	6	4	2	2	2	4	2	3	1	3	2	2	2	2	2	2	5
Zr	17	17	19	18	18	17	19	19	16	18	18	17	17	19	19	17	18
Nb	4	4	2	4	3	4	4	5	4	4	3	5	5	3	2	3	4
Ba	3	6	5	5	5	6	3	8	7	2	2	11	2	7	2	8	6
La	23	16	18	10	13	14	10	11	16	13	8	20	4	16	8	15	4
S	0.04	0.04	0.03	0.06	0.03	0.03	0.26	0.32	0.12	0.09	0.10	0.08	0.65	0.49	0.30	0.11	0.08
Ce	69	29	2	2	10	60	106	74	74	59	2	57	86	16	2	2	69
Nd	5	2	2	2	3	6	2	2	4	2	3	3	2	8	2	2	2
Mg#	59.1	62.1	63.4	56.6	64.2	64.5	27.9	27.6	48.2	49.1	40.7	44.0	23.3	24.5	25.4	26.2	44.8
Fe#	6.94	6.73	5.91	8.23	5.89	5.78	8.26	8.26	6.32	3.67	7.75	2.38	10.00	9.08	7.82	6.26	5.71
Fe ₂ O ₃	2.00	1.37	1.62	3.09	1.63	2.00	6.29	4.88	3.35	6.44	3.35	9.14	8.73	7.91	6.68	6.05	7.31

Evolution of Oceanic Gabbros: In-situ and Ancient Examples

Table 1B: Continued

Location Sample#	Strupen Lan-53	Strupen Lan-54	Strupen Lan-55	Strupen Lan-56	Strupen Lan-57	Strupen Lan-58	Strupen Lan-59	Strupen Lan-60	Strupen Lan-61	Strupen Lan-62	Strupen Lan-63	Strupen Lan-64	Strupen Lan-65	Strupen Lan-66	Strupen Lan-67	Strupen Lan-68	Strupen Lan-69	
Description																		
Place in profile W<=E (m)	29.5	31	31.75	32.5	33.5	34.75	35	35.4	35.6	36.25	36.6	37.75	38.5	39.5	39.75	39.85	42	
Major elements																		
SiO ₂	48.8	43.8	41.7	46.1	46.0	46.2	41.7	44.4	47.9	46.7	48.4	48.7	47.1	46.6	45.2	46.2	46.2	
TiO ₂	.09	.58	.63	.24	.27	.22	.60	.37	.19	.12	.12	.12	.10	.16	.28	.23	.21	
Al ₂ O ₃	16.6	16.0	15.6	18.7	18.3	19.1	18.4	23.7	14.7	18.0	17.0	17.7	19.9	20.4	20.4	15.0	17.8	
Fe ₂ O ₃ *	10.3	19.2	19.2	13.0	13.2	12.9	17.5	12.6	13.4	8.4	9.1	8.8	8.5	10.5	12.7	13.2	12.2	
MnO	.22	.21	.21	.21	.21	.22	.17	.15	.28	.16	.17	.16	.16	.18	.18	.22	.20	
MgO	9.9	7.3	6.8	7.7	7.7	7.9	5.5	4.8	9.5	9.4	9.5	9.2	9.6	7.7	7.6	10.3	9.4	
CaO	13.8	14.0	14.1	14.2	14.4	13.6	14.7	14.5	13.6	16.1	15.2	15.1	14.6	13.6	14.1	14.5	14.0	
Na ₂ O	.09	.31	.11	.35	.37	.39	.17	.45	.14	.22	.05	.08	.20	.06	.22	.21	.25	
K ₂ O	.00	.00	.00	.00	.00	.00	.00	.00	.00	.00	.00	.00	.00	.00	.00	.00	.00	
P ₂ O ₅	.01	.01	.02	.01	.01	.00	.02	.01	.02	.01	.00	.00	.00	.02	.01	.00	.00	
LOI	0.1	0.2	0.0	0.0	0.0	0.2	0.1	0.6	<0.01	1.1	0.1	0.1	0.3	0.1	0.0	0.0	0.0	
Sum	99.9	101.5	98.5	100.5	100.4	100.6	98.8	101.4	99.7	100.1	99.6	99.9	100.4	99.2	100.6	99.8	100.3	
Trace elements (
V	138	910	908	349	371	273	839	476	198	215	197	231	178	241	513	365	317	
Cr	45	39	43	22	20	22	31	19	68	222	140	80	51	30	52	143	37	
Co	58	78	71	62	65	57	77	60	65	53	51	58	52	56	61	67	61	
Ni	52	27	22	21	19	21	11	8	15	54	44	55	49	22	31	50	41	
Cu	60	220	193	126	136	109	196	131	78	38	34	137	169	125	230	185	75	
Zn	71	69	55	64	67	70	57	56	78	49	44	54	51	57	58	66	69	
Rb	2	0	2	0	0	0	2	1	2	0	2	2	0	2	0	1	1	
Sr	94	87	83	104	105	103	103	136	81	86	82	88	97	114	104	78	90	
Y	3	2	2	2	2	2	2	1	2	1	2	2	3	2	2	4	2	
Zr	19	17	18	18	17	16	18	17	19	16	19	17	17	18	16	17	16	
Nb	2	5	4	4	4	4	3	4	2	4	2	4	5	2	3	5	4	
Ba	3	5	2	6	7	3	5	4	5	5	5	5	9	4	4	6	7	
La	10	22	2	15	16	8	3	9	5	13	21	14	19	9	15	14	14	
S	0.07	0.40	0.32	0.17	0.19	0.18	0.36	0.21	0.12	0.04	0.03	0.04	0.04	0.09	0.12	0.09	0.05	
Ce	2	52	2	45	31	41	47	16	5	46	13	2	52	84	49	56	61	
Nd	2	6	2	2	3	7	2	7	6	6	2	2	3	2	5	10	4	
Mg#	48.9	27.5	26.2	37.2	36.8	38.0	23.9	27.6	41.5	52.7	51.0	51.2	52.9	42.5	37.5	43.8	43.5	
FeO	8.33	11.02	10.74	8.84	3.91	3.50	8.94	2.89	9.72	2.24	6.80	6.73	6.05	7.34	5.64	3.03	4.79	
Fe ₂ O ₃	1.14	7.12	7.43	3.24	8.92	9.01	7.65	9.42	2.69	5.96	1.64	1.36	1.87	2.40	6.49	9.82	6.93	

Evolution of Oceanic Gabbros: In-situ and Ancient Examples

Table 1B: Continued

Location Sample#	Strupen Lan-70	Strupen Lan-71	Strupen Lan-72	Strupen Lan-73	Strupen Lan-74	Strupen Lan-75	Strupen Lan-76	Strupen Lan-77	Strupen Lan-78	Strupen Lan-79	Strupen Lan-80	Strupen Lan-81	Strupen Lan-82	Strupen Lan-83	Strupen Lan-84	Strupen Lan-85	Strupen Lan-86
Description																	
Place in profile																	
W<=E (m)	42.25	42.75	43.25	43.35	43.6	44.6	45.76	46.25	46.5	47.5	48	49.5	50	50.5	51.25	52	52.5
Major elements																	
SiO ₂	44.6	50.4	60.8	61.6	47.6	46.0	45.9	45.9	45.4	44.7	54.8	45.6	49.9	44.1	43.5	44.4	45.8
TiO ₂	.36	.47	.40	.38	.27	.10	.11	.06	.20	.47	.37	.69	.81	.48	.53	.43	.18
Al ₂ O ₃	18.7	18.3	14.9	15.1	17.1	17.6	18.2	17.9	19.2	22.2	17.5	15.9	15.3	16.1	17.8	17.8	17.3
Fe ₂ O ₃ *	15.1	12.6	9.6	9.1	13.5	10.2	10.4	9.6	12.1	14.6	10.2	17.4	22.7	18.6	18.6	15.5	11.9
MnO	.23	.17	.13	.12	.27	.19	.18	.19	.20	.18	.12	.22	.23	.19	.18	.22	.19
MgO	7.5	4.0	3.1	2.9	8.3	10.7	10.1	10.0	8.2	5.3	3.3	6.0	6.9	7.5	7.1	7.8	10.1
CaO	13.4	11.8	9.4	9.4	13.2	14.0	13.9	13.7	14.1	14.3	10.8	12.6	13.5	13.5	13.8	14.5	14.1
Na ₂ O	.11	.39	.21	.11	.14	.33	.36	.35	.43	.46	.39	.38	.46	.44	.37	.34	.35
K ₂ O	.00	.00	.00	.00	.00	.00	.00	.00	.00	.00	.00	.00	.00	.00	.00	.00	.00
P ₂ O ₅	.01	.00	.00	.01	.01	.01	.00	.01	.01	.02	.01	.01	.00	.01	.00	.01	.01
LOI	<0.01	0.8	0.1	0.1	0.0	0.4	0.5	1.5	0.7	0.2	0.1	1.5	0.2	0.0	0.6	0.6	0.0
Sum	100.0	98.9	98.7	98.9	100.4	99.5	99.8	99.3	100.6	102.4	97.6	100.4	103.0	101.0	102.4	101.5	99.9
Trace elements																	
V	504	345	186	238	250	194	249	101	296	500	241	595	831	861	923	538	328
Cr	23	17	6	13	21	24	21	14	21	19	12	41	34	34	34	19	22
Co	69	48	32	33	66	57	59	55	58	64	34	54	73	69	77	68	64
Ni	18	7	6	6	33	46	44	43	25	9	7	14	7	24	38	19	38
Cu	165	90	55	70	98	239	180	116	146	96	50	95	163	173	205	136	92
Zn	71	82	51	45	92	57	65	67	63	63	40	88	79	57	61	64	62
Rb	2	0	0	2	2	0	0	0	0	0	0	0	1	0	0	0	0
Sr	107	116	100	94	99	86	91	92	105	130	106	102	89	93	94	98	91
Y	2	2	2	2	2	1	1	2	1	0	0	2	3	3	2	2	3
Zr	16	18	17	16	18	6	5	7	8	5	7	7	5	6	7	7	7
Nb	4	4	4	3	4	5	5	5	4	5	4	5	6	4	6	4	4
Ba	2	5	4	2	69	2	7	5	7	5	8	3	6	4	7	2	3
La	2	17	23	3	3	16	17	14	20	12	11	7	9	22	17	8	17
S	0.18	0.14	0.09	0.08	0.07	0.07	0.06	0.08	0.17	0.24	0.10	0.31	0.67	0.40	0.38	0.26	0.08
Ce	2	85	31	75	2	41	39	31	44	44	38	48	65	57	57	61	55
Nd	4	4	2	2	2	0	4	5	0	4	0	0	0	4	6	5	2
Mg#	33.0	24.0	24.3	24.2	38.1	51.2	49.3	51.0	40.5	26.4	24.6	25.5	23.4	28.7	27.7	33.5	46.0
FeO	8.87	5.51	5.88	4.93	9.76	5.26	6.12	6.48	6.08	4.50	4.36	8.10	3.02	3.31	12.64	10.87	7.99
Fe ₂ O ₃	5.38	6.54	3.17	3.68	2.80	4.36	3.69	2.49	5.42	9.65	5.44	8.53	19.33	15.00	4.69	3.55	3.06

Evolution of Oceanic Gabbros: In-situ and Ancient Examples

Table 1B: Continued

Location Sample#	Strupen Lan-87	Strupen Lan-88	Strupen Lan-89	Strupen Lan-90	Strupen Lan-91	Strupen Lan-92	Strupen Lan-93	Strupen Lan-94	Strupen Lan-95	Strupen Lan-96	Strupen Lan-97	Strupen Lan-98	Strupen Lan-100	Strupen Lan-101	Strupen Lan-102	Strupen Lan-103
Description																
Place in profile																
W<=E (m)	53	55.3	55.8	57	58.8	60.25	61	61.8	62	62.5	62.8	63.2	64	65	66	68.3
Major elements																
SiO ₂	45.8	45.9	45.7	43.4	46.4	45.8	43.7	46.4	54.6	75.9	75.9	63.2	46.7	45.7	45.9	44.9
TiO ₂	.14	.10	.15	.47	.07	.09	.38	.50	.41	.03	.13	.26	.07	.14	.13	.16
Al ₂ O ₃	17.7	17.0	18.5	16.0	15.9	14.9	17.0	19.4	16.1	13.0	13.1	15.7	16.9	16.9	17.6	19.0
Fe ₂ O ₃ *	11.2	10.6	11.4	18.7	10.6	10.1	16.6	13.6	10.4	0.9	1.9	7.3	10.7	11.4	11.5	11.4
MnO	.19	.19	.19	.19	.24	.18	.19	.19	.14	.02	.04	.12	.22	.21	.21	.18
MgO	10.8	11.6	10.1	7.9	11.3	13.0	8.1	4.5	3.3	0.1	0.3	2.1	10.5	10.3	10.0	8.0
CaO	14.1	13.0	13.7	13.6	14.8	13.7	14.1	13.5	9.8	6.4	4.8	6.8	13.7	13.8	14.0	13.9
Na ₂ O	.34	.35	.34	.35	.33	.34	.37	.78	.56	1.08	2.15	1.46	.55	.36	.40	.36
K ₂ O	.00	.00	.00	.00	.00	.00	.00	.00	.00	.01	.00	.00	.00	.00	.00	.00
P ₂ O ₅	.00	.01	.00	.00	.01	.02	.01	.01	.00	.02	.03	.02	.01	.03	.01	.01
LOI	0.0	0.7	0.1	0.1	0.0	0.8	1.9	2.0	2.5	1.1	0.8	0.4	0.0	0.7	0.4	2.3
Sum	100.2	99.4	100.2	100.7	99.6	98.8	101.3	100.7	97.6	98.5	99.2	97.2	99.3	99.4	100.0	100.3
Trace elements (
V	255	181	259	778	93	166	561	397	220	7	13	132	121	212	191	302
Cr	22	34	22	32	92	152	37	19	13	6	6	9	55	42	33	27
Co	59	54	59	70	55	56	63	50	30	0	4	17	56	57	56	60
Ni	38	45	30	19	54	76	27	10	6	5	5	17	54	48	35	24
Cu	144	248	174	232	26	38	217	62	42	8	8	59	70	139	138	133
Zn	57	56	56	55	73	62	65	93	58	2	13	87	78	65	62	74
Rb	0	0	0	0	0	0	0	0	0	0	0	72	0	0	0	0
Sr	91	87	98	85	82	74	90	148	107	122	119	679	91	87	89	93
Y	0	1	0	2	3	2	1	10	6	3	3	22	3	2	2	2
Zr	5	6	6	6	7	7	6	9	8	14	14	243	7	6	6	7
Nb	4	4	4	5	4	5	4	5	5	3	3	14	6	4	4	3
Ba	7	4	8	7	7	11	6	10	0	1	1	30	5	3	1	8
La	11	11	13	9	21	17	13	17	5	7	0	54	16	22	5	16
S	0.07	0.07	0.13	0.34	0.04	0.03	0.29	0.15	0.09	0.02	0.03	0.04	0.06	0.07	0.08	0.14
Ce	38	58	72	70	59	31	32	40	91	27	54	1169	67	52	85	29
Nd	0	6	4	8	0	2	2	0	1	0	0	36	0	5	0	0
Mg#	49.1	52.3	46.9	29.8	51.8	56.3	32.7	25.1	24.1	13.7	14.9	22.5	49.6	47.4	46.7	41.1
FeO	6.77	7.49	8.71	10.51	5.98	6.19	7.78	6.88	5.26	0.54	1.01	3.06	6.62	3.60	5.26	8.50
Fe ₂ O ₃	3.76	2.32	1.82	7.11	3.98	3.26	8.06	6.01	4.56	0.29	0.83	3.88	3.40	7.42	5.67	2.08

Evolution of Oceanic Gabbros: In-situ and Ancient Examples

Table 1B: Continued

Location Sample#	Strupen Lan-104	Strupen Lan-105	Strupen Lan-106	Strupen Lan-107	Strupen Lan-108	Strupen Lan-109	Strupen Lan-110	Strupen Lan-111	Strupen Lan-112	Strupen Lan-113	Strupen Lan-114	Strupen Lan-116	Strupen Lan-117	Strupen Lan-118	Strupen Lan-119	Strupen Lan-120	Strupen Lan-121
Description																	
Place in profile W<=E (m)	69	70.5	71.6	72.5	74	74.2	74.8	75.2	77.8	77.8	75.7	79.5	80.3	81	81.9	83	83.8
Major elements																	
SiO ₂	42.6	43.7	52.8	58.1	73.6	75.3	74.2	41.7	59.8	54.1	48.4	47.2	47.0	44.6	44.3	44.3	62.5
TiO ₂	.64	.52	.43	.40	.07	.14	.20	.85	.23	.42	.49	.12	.14	.52	.52	.52	.19
Al ₂ O ₃	16.1	19.9	15.6	14.0	12.2	12.3	12.9	14.4	14.5	13.8	16.3	15.2	15.4	18.6	18.6	18.6	15.7
Fe ₂ O ₃ *	20.9	16.0	11.5	10.1	1.7	1.9	3.3	23.4	8.4	9.8	12.8	13.7	12.8	18.5	18.4	18.4	7.4
MnO	.21	.20	.14	.14	.03	.03	.05	.23	.10	.12	.14	.35	.28	.25	.17	.16	.08
MgO	6.7	5.5	3.6	3.2	0.2	0.1	0.6	7.5	3.0	3.0	4.0	10.0	9.6	6.9	6.0	6.0	2.8
CaO	13.2	13.4	10.5	9.7	6.0	4.5	4.8	13.7	8.3	8.8	11.2	11.9	12.8	13.1	13.7	14.2	8.9
Na ₂ O	.38	.64	.37	.47	1.46	2.89	2.30	.44	.54	.34	.50	.53	.42	.32	.42	.42	.25
K ₂ O	.00	.00	.00	.00	.02	.00	.00	.00	.00	.00	.00	.00	.00	.00	.00	.00	.00
P ₂ O ₅	.01	.01	.02	.01	.02	.02	.02	.01	.00	.01	.02	.02	.01	.00	.00	.03	.01
LOI	1.6	2.1	2.2	1.9	1.0	1.0	0.9	1.6	0.9	0.9	0.0	0.0	0.2	0.0	0.2	1.1	0.3
Sum	102.3	101.9	97.0	98.0	96.2	98.2	99.3	103.8	97.7	97.0	99.5	100.2	98.7	100.9	103.6	103.7	98.2
Trace elements (
V	787	552	280	202	18	10	34	1070	232	197	319	77	114	191	1006	937	156
Cr	33	28	15	19	6	7	7	43	12	11	13	13	12	19	34	31	10
Co	68	58	37	26	3	3	7	69	25	25	37	47	52	56	70	73	24
Ni	12	13	7	7	5	5	5	25	7	7	7	26	34	32	14	12	7
Cu	135	75	60	44	9	7	9	222	37	37	68	34	83	75	347	220	57
Zn	73	115	70	52	6	6	13	109	36	50	43	98	91	73	51	60	25
Rb	0	0	0	0	0	0	0	0	0	1	0	0	0	0	0	0	0
Sr	85	118	99	84	88	137	103	77	89	85	100	93	92	85	96	99	76
Y	1	1	2	1	0	3	3	6	1	1	2	3	2	1	2	1	0
Zr	6	8	7	7	7	15	10	9	9	7	6	6	6	6	6	7	5
Nb	5	5	5	5	1	2	2	5	4	4	5	5	4	5	4	6	4
Ba	7	3	6	4	3	2	1	4	1	3	4	6	4	8	4	5	0
La	14	10	7	4	2	2	4	10	0	9	11	12	7	15	4	15	6
S	0.45	0.29	0.17	0.10	0.02	0.02	0.03	0.60	0.06	0.09	0.24	0.09	0.40	0.10	0.40	0.39	0.07
Ce	57	68	32	63	48	44	48	97	10	55	88	35	37	33	37	42	60
Nd	0	0	0	0	0	0	0	4	3	0	3	0	7	9	7	1	0
Mg#	24.2	25.4	23.9	24.1	12.7	6.0	16.0	24.1	26.4	23.1	24.0	42.3	42.8	45.9	27.0	24.7	27.7
Fe#	9.50	8.35	5.54	5.11	0.72	0.43	1.55	10.51	3.96	4.64	5.33	6.44	6.08	6.55	7.45	6.30	3.24
Fe ₂ O ₃	10.45	6.79	5.37	4.48	0.86	1.40	1.61	11.85	4.01	4.73	6.89	6.59	6.10	5.54	10.35	11.43	3.87

Evolution of Oceanic Gabbros: In-situ and Ancient Examples

Table 1B: Continued

Location Sample#	Strupen Lan-123	Strupen Lan-124	Strupen Lan-125	Strupen Lan-126	Strupen Lan-127	Strupen Lan-128	Strupen Lan-129	Strupen Lan-130	Strupen Lan-131
Description									
Place in profile									
W<=E (m)	84.8	86	87.3	89	90.5	91	91.5	92.3	93
Major elements									
SiO ₂	47.1	46.9	46.6	47.1	46.0	57.8	60.9	70.5	48.0
TiO ₂	.10	.07	.06	.08	.11	.45	.36	.19	.15
Al ₂ O ₃	17.5	16.0	16.5	19.2	16.0	14.0	14.3	13.1	15.2
Fe ₂ O ₃ *	12.2	10.5	9.3	7.6	12.7	11.1	9.1	5.4	13.3
MnO	.25	.20	.19	.14	.23	.13	.12	.08	.35
MgO	10.3	12.0	11.4	10.6	11.9	3.2	2.9	1.7	9.9
CaO	12.7	13.4	14.7	14.8	11.7	9.3	8.5	6.8	13.1
Na ₂ O	.31	.27	.31	.42	.29	.43	.43	.31	.13
K ₂ O	.00	.00	.00	.00	.00	.00	.00	.00	.00
P ₂ O ₅	.02	.01	.01	.02	.02	.00	.00	.01	.01
LOI	0.4	1.1	1.6	1.1	1.7	1.6	1.4	0.5	0.0
Sum	100.8	100.4	100.7	101.1	100.7	98.1	97.9	98.5	100.2
Trace elements									
V	145	129	115	142	189	244	168	63	84
Cr	43	39	74	85	46	18	12	8	101
Co	56	53	52	49	52	29	26	12	59
Ni	47	55	59	82	53	7	6	5	25
Cu	75	207	75	72	168	80	43	13	37
Zn	80	59	69	52	81	58	62	27	112
Rb	0	0	0	0	0	1	0	0	0
Sr	90	76	86	92	85	90	105	79	99
Y	1	1	2	1	1	2	1	1	4
Zr	7	6	7	6	6	7	8	7	6
Nb	5	5	5	5	4	4	6	3	4
Ba	4	10	8	7	6	5	7	4	2
La	17	18	14	19	16	9	8	6	12
S	0.08	0.06	0.05	0.03	0.15	0.13	0.09	0.03	0.05
Ce	46	66	39	53	59	68	54	44	30
Nd	0	2	2	0	0	0	5	0	3
Mg#	45.6	53.3	55.0	58.1	48.3	22.4	24.1	23.5	42.6
FeO	6.88	5.36	6.01	4.93	6.59	5.51	4.72	2.81	7.52
Fe ₂ O ₃	4.67	4.60	2.69	2.21	5.48	5.03	3.87	2.27	5.06

Evolution of Oceanic Gabbros: In-situ and Ancient Examples

Table 2: Isotope chemistry for the Lyngen Gabbro. In addition to data from each area, dikes crosscutting the gabbros in Goverdalen and at Iddu are included for comparison.

Sample	Sm (ppm)	Nd(ppm)	$^{147}\text{Sm}/^{144}\text{Nd}$	$^{143}\text{Nd}/^{144}\text{Nd}$	$^{143}\text{Nd}/^{144}\text{Nd}$ CHUR	Initial $^{143}\text{Nd}/^{144}\text{Nd}$	E_CHUR	$\epsilon_{\text{Nd}}(480\text{My})$ CHUR
Skaidevarri								
90-LY-134	0.21	0.46	0.284	0.513055	0.51203	0.512162	7.962	2.60
90-LY-135	0.19	0.40	0.280	0.513117	0.51203	0.512236	9.162	4.05
90-LY-137	0.16	0.28	0.332	0.513374	0.51203	0.512330	14.178	5.89
90-LY-139	0.11	0.18	0.374	0.513511	0.51203	0.512335	16.862	5.99
90-LY-140	0.13	0.21	0.362	0.513472	0.51203	0.512335	16.096	5.99
90-LY-141	0.35	0.74	0.286	0.513259	0.51203	0.512359	11.941	6.44
90-LY-212	0.33	0.69	0.290	0.513276	0.51203	0.512362	12.261	6.52
90-LY-219	0.33	0.67	0.299	0.513303	0.51203	0.512364	12.792	6.55
Strupen								
Lan-1	0.12	0.21	0.363	0.513336	0.51203	0.512195	13.446	3.24
Lan-23	0.08	0.12	0.386	0.513337	0.51203	0.512125	13.467	1.88
Lan-38	0.16	0.32	0.299	0.513131	0.51203	0.512191	9.446	3.18
Lan-47	0.07	0.13	0.340	0.513323	0.51203	0.512255	13.181	4.42
Lan-58	0.07	0.14	0.326	0.513288	0.51203	0.512264	12.502	4.60
Lan-72	0.05	0.09	0.349	0.513311	0.51203	0.512215	12.946	3.64
Lan-84	0.08	0.16	0.316	0.513147	0.51203	0.512153	9.758	2.42
Lan-97	0.04	0.21	0.110	0.512582	0.51203	0.512237	-1.274	4.08
Lan-100	0.08	0.14	0.345	0.513302	0.51203	0.512216	12.768	3.65
Lan-106	0.059	0.113	0.315100	0.513211	0.51203	0.512221	11.007	3.75
Lan-107	0.073	0.141	0.3139	0.513201	0.51203	0.512214	10.806	3.62
Lan-109	0.054	0.336	0.0970	0.512525	0.51203	0.512220	-2.389	3.73
Lan-110	0.195	0.703	0.1680	0.512762	0.51203	0.512234	2.240	4.01
Lan-110	0.20	0.70	0.167	0.512762	0.51203	0.512235	2.241	4.04
Lan-111	0.217	0.394	0.3337	0.513265	0.51203	0.512216	12.063	3.66
Lan-112	0.035	0.085	0.2464	0.512993	0.51203	0.512219	6.758	3.72
Lan-113	0.064	0.129	0.2983	0.513159	0.51203	0.512221	9.987	3.76
Lan-114	0.103	0.197	0.3160	0.513213	0.51203	0.512219	11.032	3.72
Lan-116	0.152	0.284	0.3229	0.513240	0.51203	0.512225	11.570	3.84
Lan-130	0.01	0.03	0.191	0.512788	0.51203	0.512188	2.745	3.11
Isskardet								
LY-IS-9	0.11	0.32	0.211	0.513030	0.51203	0.512366	7.478	6.58
LY-IS-16	0.34	0.70	0.292	0.513296	0.51203	0.512379	12.653	6.84
LY-IS-25	0.38	0.78	0.297	0.513295	0.51203	0.512363	12.643	6.53
LY-IS-31	0.46	0.87	0.315	0.513365	0.51203	0.512374	14.007	6.75
Ellendalen								
92LY119	7.92	78.15	0.2289	0.513068	0.51203	0.512348	8.212	6.24
92LY93	1.24	8.47	0.3314	0.513411	0.51203	0.512369	14.903	6.65
93LY20	0.95	7.42	0.2882	0.513208	0.51203	0.512302	10.943	5.34
94LY24	2.18	17.55	0.281	0.513231	0.51203	0.512347	11.392	6.23
94LY39	1.17	10.07	0.2625	0.513173	0.51203	0.512348	10.260	6.23
Goverdalen								
95LY2	0.53	4.24	0.2818	0.513187	0.51203	0.512301	10.534	5.32
94LY67	1.87	13.79	0.3057	0.513287	0.51203	0.512326	12.484	5.81
95LY38	6.92	60.35	0.2589	0.513190	0.51203	0.512376	10.592	6.79
Veidalen								
95LY127	0.80	5.72	0.3156	0.513298	0.51203	0.512306	12.699	5.41
95LY106	0.47	2.81	0.3775	0.513373	0.51203	0.512186	14.162	3.08
95LY94	0.57	3.70	0.3497	0.513394	0.51203	0.512294	14.571	5.19

Evolution of Oceanic Gabbros: In-situ and Ancient Examples

Table 2: Continued

Sample	Sm (ppm)	Nd(ppm)	$^{147}\text{Sm}/^{144}\text{Nd}$	$^{143}\text{Nd}/^{144}\text{Nd}$	$^{143}\text{Nd}/^{144}\text{Nd}$ CHUR	Initial $^{143}\text{Nd}/^{144}\text{Nd}$	E_CHUR	$\epsilon_{\text{Nd}}(480\text{My})$ CHUR
95LY75	0.60	6.73	0.2016	0.512914	0.51203	0.512280	5.208	4.91
Iddu 1								
Hly 2.8	0.06	0.23	0.154	0.512193	0.51203	0.511709	-8.856	-6.24
Hly 24-93	0.17	0.53	0.194	0.512404	0.51203	0.511794	-4.740	-4.58
Hly 24-94	0.05	0.16	0.199	0.512505	0.51203	0.511879	-2.770	-2.91
Hly 26-94	0.45	1.53	0.178	0.512604	0.51203	0.512044	-0.839	0.31
Hly 22b-93	0.09	0.2	0.285	0.512759	0.51203	0.511863	2.185	-3.23
Hly 11-94	0.92	2.13	0.262	0.512783	0.51203	0.511959	2.653	-1.35
Hly 1.8	0.13	0.26	0.301	0.512826	0.51203	0.511880	3.492	-2.91
Hly 25-94	0.14	0.27	0.321	0.512885	0.51203	0.511876	4.643	-2.98
Iddu 2								
Hly 5 PA	0.84	2.15	0.236	0.512967	0.51203	0.512225	6.242	3.84
Hly 1PA	0.62	1.67	0.223	0.512932	0.51203	0.512231	5.559	3.95
Hly 3PA	1.18	2.65	0.27	0.513108	0.51203	0.512259	8.993	4.50
Hly 7 PA	0.9	2.27	0.24	0.513005	0.51203	0.512250	6.983	4.33
Dikes, Goverdalen								
93LY30	2.976	9.469	0.1900	0.512925	0.51203	0.512328	5.423	5.84
95LY72	1.400	6.006	0.1409	0.512121	0.51203	0.511678	-10.254	-6.84
95LY72	1.396	5.995	0.1408	0.512125	0.51203	0.511683	-10.176	-6.75
95LY71	0.314	0.566	0.3357	0.513290	0.51203	0.512235	12.544	4.02
95LY71	0.284	0.494	0.3475	0.513336	0.51203	0.512244	13.441	4.20
95LY71	0.289	0.522	0.3347	0.513292	0.51203	0.512240	12.581	4.12
Dikes, Iddu								
HLY 2993	2.23	8.8	0.153	0.512781	0.51203	0.512300	2.614	5.30
Hly 33-93	3.38	14.73	0.139	0.512749	0.51203	0.512312	1.990	5.54
Hly 28-93	5.54	15.86	0.211	0.513043	0.51203	0.512380	7.725	6.86
Hly 4.6	2.4	19.49	0.074	0.511753	0.51203	0.511520	-17.439	-9.93
Hly 6.5	2.36	18.28	0.078	0.511789	0.51203	0.511544	-16.737	-9.47
Hly 27-93	1	7.53	0.081	0.511805	0.51203	0.511550	-16.425	-9.34
Hly 5.6	1.84	13.61	0.082	0.511810	0.51203	0.511552	-16.327	-9.30
Hly 36-93	1.29	6.39	0.122	0.511862	0.51203	0.511478	-15.313	-10.74
HLY 22a-93	1.04	3.76	0.168	0.512235	0.51203	0.511707	-8.037	-6.28

Evolution of Oceanic Gabbros: In-situ and Ancient Examples

Table 3: Mineral chemistry of the Lyngen Gabbro. All areas are represented, except for Ellendalen. Abbreviations: pl = plagioclase, c = core, r=rim, cpx = augite, opx= orthopyroxene, Fo=forsterite% of olivine. The minerals are listed so cores are aligned with cores, rims with rims. There is therefore some repetition in the table so that the representative mineral-pairings are obvious. Orthopyroxene and olivine show internal variation, and the 1 sigma is therefore equal to the analytical error.

Sample#	An %	1 σ	Sample#	Mg# cpx	1 σ	Sample#	Mg# opx	Sample#	Fo
Skaidevarri									
90LY134 plc (5)	93.0	0.71	90LY134 cpxc (5)	84.5	0.20				
90LY134 plrtocpx (5)	93.5	1.03	90LY134 cpxrtopl (5)	84.7	0.70				
90LY134 plc (5)	93.0	0.71	90LY134 cpx2- (6)	84.7	0.30				
90LY136-1-plrtocpx (4)	93.2	0.28	90LY136-1 cpxc (3)	85.4	0.24				
90LY136-1-plrtocpx (4)	93.2	0.28	90LY136-1 cpxrtopl (5)	86.4	1.11				
90LY136-2-plc (3)	91.3	0.28	90LY136-2 cpxc (4)	85.3	0.68				
90LY136-2-plrtocpx (5)	91.5	1.62	90LY136-2 cpxc (4)	85.3	0.68				
90LY138-1-pl (7)	94.7	0.85	90LY138-1 cpxc (5)	85.1	0.63			90LY138-1-ol (6)	78.7
90LY138-1-plrtocpx (2)	95.7	3.82	90LY138-1 cpxr (5)	85.3	0.74			90LY138-1-ol (6)	78.7
90LY138-2-plc (5)	94.6	0.67	90LY138-2 cpxc (5)	84.4	0.28	90LY138-2 opx (6)	81.1		
90LY138-2-plr (5)	95.0	1.19	90LY138-2 cpxrtopl (5)	85.0	0.64	90LY138-2 opx (6)	81.1		
90LY141-1-plr (5)	84.1	0.98	90LY141-1 cpxc (5)	79.0	0.42	90LY141-1 opx (6)	74.2	90LY141-1-ol (6)	69.6
90LY141-1-plrtocpx (5)	85.9	1.97	90LY141-1 cpxr (5)	79.4	1.23	90LY141-1 opx (6)	74.2	90LY141-1-ol (6)	69.6
90LY141-2-plc (5)	83.9	0.42	90LY141-2 cpxc (5)	78.8	0.33	90LY141-2 opx (6)	74.5		
90LY141-2-plr (5)	83.8	0.64	90LY141-2 cpxrtopl (6)	79.2	1.08	90LY141-2 opx (6)	74.5		
90LY142-2 plc (5)	85.0	0.67	90LY142-1cpx (5)	78.0	0.79	90LY142-1 opx (6)	73.0	90LY142-2ol (6)	69.2
90LY142-2 plrtocpx (5)	86.5	1.10	90LY142-1cpx (5)	77.7	0.63	90LY142-1 opx (6)	73.0	90LY142-2ol (6)	69.2
90LY142-2 plc (5)	85.0	0.67	90LY142-2cpxc (5)	77.7	0.93				
90LY142-2 plrtocpx (5)	86.5	1.10	90LY142-2cpxrtopl (5)	77.4	0.66				
90LY143-1-plc (5)	87.8	0.81	90LY143-1 cpxc (5)	78.7	0.73	90LY143-1 opx (6)	75.3	90LY143-1-ol (6)	71.3
90LY143-1-plrtocpx (5)	87.9	0.88	90LY143-1 cpxrtopl (5)	79.5	0.16	90LY143-1 opx (6)	75.3	90LY143-1-ol (6)	71.3
90LY143-2-plc (3)	88.6	1.38	90LY143-2 cpxc (5)	78.4	1.81			90LY143-2-ol (6)	70.6
90LY143-2-plrtocpx (4)	88.9	0.66	90LY143-2 cpxrtopl (5)	80.2	0.49			90LY143-2-ol (6)	70.6
90LY144-1-plc (5)	87.0	0.62	90LY144-1 cpxc (5)	79.2	0.63	90LY144-1 opx (5)	73.6		
90LY144-1-plrtocpx (5)	88.3	1.04	90LY144-1 cpxrtocpx (5)	78.6	1.25	90LY144-1 opx (5)	73.6		
90LY144-2-plc (5)	90.6	1.45	90LY144-2 cpxc (5)	78.5	1.19	90LY144-2 opx (6)	75.0		
90LY144-2-plrtocpx (5)	92.9	1.41	90LY144-2 cpxrtopl (5)	79.1	0.92	90LY144-2 opx (6)	75.0		
90LY166 plag (7)	87.6	0.67	90LY166 cpxc (4)	79.1	1.64	90LY166 opx (10)	73.4	90LY166-ol (11)	70.3
90LY166 plag (7)	87.6	0.67	90LY166 cpxrtopl (4)	78.0	0.68	90LY166 opx (10)	73.4	90LY166-ol (11)	70.3
90LY168-2 plc (5)	85.0	0.28	90LY168-1 cpxc (4)	78.1	0.52			90LY168-1ol (6)	69.2
90LY168-2 plrtocpx (5)	87.0	0.89	90LY168-1 cpxrtopl (5)	77.9	0.76			90LY168-1ol (6)	69.2
90LY168-2 plc (5)	85.0	0.28	90LY168-2 cpxc (4)	78.0	0.84	90LY168-2 opx (4)	73.3		
90LY168-2 plrtocpx (5)	87.0	0.89	90LY168-2 cpxrtopl (4)	77.6	0.39	90LY168-2 opx (4)	73.3		
90LY169-1 plc (5)	84.6	0.46	90LY169-1 cpxc (5)	78.9	0.67	90LY169-1 opx (6)	72.5		
90LY169-1 plrtocpx (5)	86.2	0.68	90LY169-1 cpxrtopl (5)	78.7	0.89	90LY169-1 opx (6)	72.5		
90LY169-2 pl (6)	84.9	0.49						90LY169-2ol (6)	68.1
90ly 192 pl (6)	85.1	1.00	90ly 192 cpx rage(6)	76.1	1.93	90ly192 opx (6)	70.5		
90ly-216 plag (6)	84.3	0.95	90ly-216 cpx (6)	77.1	1.20	90ly-216 opx (6)	71.6		
90ly221 plag (5)	85.3	0.55	90ly221 cpx (5)	75.3	1.26	90ly221 opx (5)	71.8	90ly221-ol (6)	66.9
Iddu									
1pa-plag	52.6	2.03				1pa-opx	60.7		
2pa-plag	59.8	2.57	2pa-cpx	73.5	0.89	2pa-opx	64.3		
3pa-plag	60.2	1.70	3pa-cpx	74.5	0.84	3pa-opx	64.0		
4pa-plag	58.4	1.90	4pa-cpx	76.1	1.06	4pa-opx	66.1		
5pa-plag	58.9	0.59	5pa-cpx	74.2	1.09	5pa-opx	64.1		
6pa-plag	58.6	1.19	6pa-cpx	73.3	1.26	6pa-opx	63.0		
7pa-plag	74.4	2.28	7pa-cpx	71.2	1.89	7pa-opx	62.4		
11pb			11pb-cpx	72.6	1.69				
pb16-plag	75.0	1.16	16pb-cpx	72.8	1.26	16pb-opx	64.8		
pb18-plag	67.4	1.24	18pb-cpx	73.9	1.26	18pb-opx	64.6		
pb19-plag	57.6	1.19	19pb-cpx	76.0	1.15	19pb-opx	66.1		
pb21-plag	63.4	2.20	Pb21-cpx	76.7	0.89	Pb21-opx	65.4		

Evolution of Oceanic Gabbros: In-situ and Ancient Examples

Table 3: Continued

Sample#	An%	1 σ	Sample#	Mg# cpx	1 σ	Sample#	Mg# opx	Sample#	Fo
Strupen									
Lan-1			Lan-1	76.9		Lan-1	67.8		
Lan-2	97.1		Lan-2	76.1		Lan-2	68.6		
Lan-3	94.6		Lan-3	75.6		Lan-3	66.4		
Lan-4			Lan-4	73.1		Lan-4	59.3		
Lan-5	96.9		Lan-5	73.4		Lan-5	63.6		
Lan-7	93.1		Lan-7	72.9		Lan-7	64.1		
Lan-8	93.7		Lan-8	75.2		Lan-8	64.9		
Lan-9	94.1		Lan-9	75.3		Lan-9	66.5		
Lan-10	94.6		Lan-10	75.7		Lan-10	67.1		
Lan-11	93.4		Lan-11	75.5		Lan-11	66.6		
Lan-12	93.0		Lan-12	75.5		Lan-12	65.0		
Lan-13	93.7		Lan-13	73.9		Lan-13	65.6		
Lan-14	93.7		Lan-14	74.7		Lan-14	65.2		
Lan-15	93.9		Lan-15	73.3		Lan-15	64.2		
Lan-16	94.0		Lan-16	74.3		Lan-16	64.8		
Lan-17			Lan-17			Lan-17	63.2		
Lan-18	95.5		Lan-18	74.1		Lan-18			
Lan-19	92.2		Lan-19	73.0		Lan-19	63.9		
Lan-20	92.6		Lan-20	72.6		Lan-20	63.7		
Lan-21	93.2		Lan-21	75.5		Lan-21	64.6		
Lan-22	92.6		Lan-22	74.0		Lan-22	65.7		
Lan-23	93.9		Lan-23	73.3		Lan-23	63.3		
Lan-24	93.5		Lan-24	73.3		Lan-24	64.6		
Lan-25	91.9		Lan-25	74.8		Lan-25	65.9		
Lan-26	93.5		Lan-26	75.3		Lan-26	67.0		
Lan-27	94.8		Lan-27	76.5		Lan-27	66.0		
Lan-28	94.7		Lan-28	77.8		Lan-28	68.4		
Lan-29	93.9		Lan-29	75.7		Lan-29	68.1		
Lan-30	94.6		Lan-30	77.0		Lan-30	68.6		
Lan-31	98.2		Lan-31	76.3		Lan-31	68.3		
Lan-32	94.7		Lan-32	77.0		Lan-32	68.7		
Lan-33			Lan-33	74.6		Lan-33	66.5		
Lan-38	96.3		Lan-38	82.0		Lan-38	74.5		
Lan-44	94.1		Lan-44	74.8		Lan-44	64.6		
Lan-45	94.2		Lan-45	73.9		Lan-45	65.5		
Lan-47	94.9		Lan-47	74.6		Lan-47	64.1		
Lan-48	93.9		Lan-48	74.5		Lan-48	63.4		
Lan-49	95.1		Lan-49			Lan-49			
Lan-50	94.3		Lan-50	74.3		Lan-50	62.8		
Lan-51	95.0		Lan-51			Lan-51			
Lan-52	94.5		Lan-52	73.1		Lan-52	61.7		
Lan-54	95.6		Lan-54			Lan-54			
Lan-56	95.6		Lan-56			Lan-56			
Lan-58	94.4		Lan-58	71.3		Lan-58	59.6		
Lan-60	95.6		Lan-60			Lan-60			
Lan-61	94.2		Lan-61	71.8		Lan-61	59.4		
Lan-62			Lan-62			Lan-62	65.9		
Lan-64	96.9		Lan-64	75.4		Lan-64	66.7		
Lan-65			Lan-65	75.0		Lan-65	67.4		
Lan-66			Lan-66	76.4		Lan-66	66.4		
Lan-67	96.0		Lan-67	75.9		Lan-67	63.2		
Lan-68	96.1		Lan-68	75.6		Lan-68	64.8		
Lan-69	95.7		Lan-69	75.6		Lan-69	64.9		
Lan-70	95.5		Lan-70	73.9		Lan-70	63.0		
Lan-71	94.2		Lan-71	69.6		Lan-71	59.1		
Lan-72	93.9		Lan-72	70.4		Lan-72	57.0		
Lan-73	90.5		Lan-73	69.9		Lan-73	57.5		
Lan-74	93.7		Lan-74	70.6		Lan-74	58.0		
Lan-76	95.0		Lan-76	75.3		Lan-76			

Evolution of Oceanic Gabbros: In-situ and Ancient Examples

Table 3: Continued

Sample#	An%	1 σ	Sample#	Mg# cpx	1 σ	Sample#	Mg# opx	Sample#	Fo
Goverdalen									
95ly34	77.2		95LY34	72.5		95LY34	64.9		
95ly35	79.0		95ly35	73.8		95ly35	67.0		
95ly38	48.6		95ly38	66.9		95ly38	56.8		
95ly39	87.2		95ly39	79.4		95ly39	75.2	95ly39	72.3
95ly40	87.6		95ly40	83.6					
Veidalen									
95ly127	86.6		95ly127	72.1		95ly127	64.4	95LY126	68.1
95LY126	89.9		95LY126	77.0		95LY126	72.3		
95ly107	94.2		95ly107	83.4				95ly107	75.5
95ly106	95.7		95ly106	83.2		95ly106	78.4	95ly106	75.9
95LY105	94.7							95LY105	80.3
95LY90	91.2		95LY90	79.2		95LY90	75.2		
95LY93	93.8		95LY93	80.7					
95LY94	95.3		95LY94	79.9		95LY94	74.3		
95LY95	93.8		95LY95	79.9		95LY95	74.0	95LY95	71.1
95LY96	95.4		95LY96	80.2		95LY96	74.8	95LY96	72.2
95LY87	97.7		95LY87	88.0		95LY87	83.8	95LY87	83.5
Isskardet									
IS-2 plagc (5)	83.8	0.69	IS-2 cpxc (5)	75.9	0.61			IS-2ol (6)	64.2
IS-2 plagr (5)	84.5	1.94	IS-2 cpxr (5)	75.8	0.70			IS-2ol (6)	64.2
IS-6 plagc (5)	75.7	7.29	IS-6 cpxc (5)	75.7	0.18			IS-6ol (6)	66.5
IS-6 plagr (5)	83.4	1.25	IS-6 cpxr (5)	76.4	0.25			IS-6ol (6)	66.5
IS-9 plagc (5)	83.0	0.92						IS-9ol (6)	67.6
IS-9 plagr (5)	83.6	0.63						IS-9ol (6)	67.6
IS-16 plagc (5)	84.2	0.96	IS-16 cpxc (5)	76.3	1.02	IS-16 opx (6)	72.7	IS-16ol (6)	67.8
IS-16 plagr (5)	83.5	1.45	IS-16 cpxr (5)	76.3	0.42	IS-16 opx (6)	72.7	IS-16ol (6)	67.8
IS-20 plag1-c (5)	82.2	0.59	IS-20 cpxc (5)	75.5	0.71	IS-20 opx (6)	71.2	IS-20ol (6)	66.6
IS-20 plag1-r (5)	84.5	1.12	IS-20 cpxr (5)	75.8	0.46	IS-20 opx (6)	71.2	IS-20ol (6)	66.6
IS-20 plag2- (4)	84.4	0.92	IS-20 cpxr (5)	75.8	0.46	IS-20 opx (6)	71.2	IS-20ol (6)	66.6
IS-26 plagc (5)	80.8	1.65	IS-26 cpxc (5)	75.2	0.43			IS-26ol (6)	67.1
IS-26 plagr (5)	82.2	2.55	IS-26 cpxr (5)	75.3	0.20			IS-26ol (6)	67.1

Evolution of Oceanic Gabbros: In-situ and Ancient Examples

Table 4: Trace-element and REE- mineral chemistry for ten samples from the Lyngen Gabbro. All the analyses are listed as ppm. Cpx=augite, c=core, r=rims. The errors are less than 10% for the REE, and less than 5% for the trace elements.

Sample	La ppm	Ce ppm	Nd ppm	Sm ppm	Eu ppm	Dy ppm	Er ppm	Yb ppm	Ti ppm	V ppm	Cr ppm	Sr ppm	Y ppm	Zr ppm
Goverdalen														
LY-95-39-cpx-c	0.12	0.62	1.25	0.86	0.41	1.67	0.89	0.99	1486	260	449	8.7	8.7	3.7
LY-95-39-cpx-r	0.14	0.67	1.03	0.68	0.34	1.51	0.84	0.87	1537	262	541	7.8	8.9	4.7
LY-95-34-cpx-c	0.23	1.29	2.76	1.85	0.59	3.75	2.14	2.34	2508	437	85	10.0	22.6	11.3
LY-95-34-cpx-r	0.24	1.17	2.28	1.50	0.60	3.65	2.11	2.12	2338	413	83	9.3	23.5	12.0
LY-95-38-cpx-c	0.54	3.53	9.32	5.76	1.52	12.18	6.64	7.04	2352	265	70	11.6	67.5	67.3
LY-95-38-cpx-r	0.60	4.21	9.75	6.20	1.52	12.62	6.82	7.72	2221	258	72	11.2	74.2	64.2
Veidalen														
LY-95-87-cpx-c	0.02	0.11	0.24	0.18	0.06	0.25	0.22	0.21	339	236	1994	8.6	1.4	0.6
LY-95-87-cpx-r	0.01	0.08	0.26	0.14	0.06	0.20	0.14	0.17	371	255	1924	6.1	1.6	0.8
LY-95-96-cpx-c	0.04	0.21	0.40	0.35	0.16	0.52	0.30	0.31	872	299	1036	8.1	4.1	1.2
LY-95-96-cpx-r	0.12	0.62	0.96	0.63	0.36	1.36	1.05	0.83	2244	401	965	28.5	15.2	2.8
LY-95-127-cpx-c	0.32	1.65	2.86	1.69	0.51	3.41	1.99	1.98	3219	441	160	9.5	22.4	11.4
LY-95-127-cpx-r	0.39	1.66	2.81	1.71	0.51	3.50	1.85	2.04	2343	357	151	9.8	20.7	10.5
Strupen														
Lan38 cpx-c	0.06	0.34	0.49	0.26	0.12	0.54	0.32	0.32	869	310	2437	6.5	3.5	1.9
Lan38 cpx-r	0.07	0.30	0.40	0.25	0.13	0.50	0.37	0.37	857	312	2486	6.7	3.5	1.7
Lan47 cpx-c	0.05	0.29	0.48	0.30	0.20	0.95	0.63	0.76	1411	380	88	6.5	6.4	1.4
Lan47 cpx-r	0.03	0.25	0.41	0.28	0.16	0.84	0.49	0.60	723	248	90	5.5	3.3	1.3
Lan58 cpx-c	0.03	0.35	0.67	0.48	0.27	1.44	1.04	0.95	1158	280	88	6.0	7.2	2.2
Lan58 cpx-r	0.04	0.34	0.57	0.51	0.21	1.21	0.81	0.84	1067	283	89	6.6	6.1	2.0
Lan72 cpx-c	0.05	0.29	0.61	0.55	0.37	1.55	1.07	1.16	1675	202	80	8.6	11.2	2.0
Lan72 cpx-r	0.03	0.27	0.78	0.55	0.34	1.57	1.11	1.15	2779	198	80	8.1	10.8	1.8

Evolution of Oceanic Gabbros: In-situ and Ancient Examples

Chapter 3

Accretion of the lower crust at Atlantis Bank: The results of geochemical modeling

Abstract

We have developed a quantitative and qualitative model for the accretion of the lower crustal rocks at Atlantis Bank, Southwest Indian Ridge. We use the Melts-program to establish the mode of accretion and extent of reaction for gabbros sampled in Hole 735B, and find that fractional crystallization of a near dry melt with $\text{Na}_8 \sim 3$ and $\text{Fe}_8 \sim 9$ at crustal pressure on the quartz-fayalite-magnetite oxygen fugacity buffer fits the general evolution of the solid- and liquid-line of descent at Atlantis Bank. Our model predicts that approximately 770 vertical meters of the lower crustal section has not been sampled and that the total crustal thickness at Atlantis Bank was more than 4.4-km. Thus, the observed seismic Moho may indeed be the crust-mantle boundary, and not an alteration front as previously suggested.

Slow-spreading ocean ridges typically have gabbros with unusually high Mg-augites. We use our models and the degree of disequilibrium between the minerals to establish how far off the fractionation-trend the rocks plot. The majority of the gabbros in the lower 1000 meters of the hole have augite with elevated Mg#'s, up to 10 mol% higher than what is required by fractional crystallization. Thus, we propose that interstitial melts in a mush-zone have dissolved pre-existing minerals, causing the melt to become more Mg and Ca rich. Plagioclase and augite do not re-equilibrate with the melt, as solid-state diffusion is very slow. Thus, when the hybrid melt crystallizes, this will result in higher Mg# augites and higher anorthite plagioclase.

1 Introduction

Coexisting phases in Atlantis Bank gabbros, and in other gabbros produced from elevated Na_8 basalts, are often out of equilibrium with each other, i.e. they could not have been crystallized directly from mid-ocean ridge basalts at crustal pressures (Bloomer et

Evolution of Oceanic Gabbros: In-situ and Ancient Examples

al., 1989, 1991; Meyer et al., 1989; Elthon et al., 1987, 1992, Michael and Cornell, 1998, Dick et al., 2002). High Mg# augite is easily identifiable in the lower crust at these slow-spreading. Bloomer et al. (1989) showed that most gabbros from Indian Ocean fracture zones crystallized from more fractionated liquids than spatially associated erupted pillow basalts. It has been suggested that the primitive magmas are emplaced towards the center of each ridge-segment, which is why we do not see primitive gabbros in the fracture zones (Whitehead et al., 1984; Dick 1989; Magde, et al., 1997). Bloomer et al. (1989) also found that augite coexisting with plagioclase was more magnesian than expected for plagioclase anorthite content, and that augite starts crystallizing earlier relative to plagioclase than in 1-atm experiments. Bloomer et al. (op. cit.) suggested that they formed by in-situ crystallization (as parameterized by Langmuir, 1989) along the edges of small magma-bodies while higher-T magmas were repeatedly injected along them. These observations effectively require that there must be olivine-rich cumulates representing higher-T melts somewhere in the crust or shallow mantle. Elthon et al. (1987, 1992) observed the same early-onset crystallization of primitive-looking clinopyroxene along the Mid-Cayman rise, and suggested that they formed by high-pressure (3-10 kbar) crystallization, whereas Meyer et al. (1989) also found early onset of high-Mg pyroxene in dredged gabbros between the Shaka- and Islas Orcadas Fracture Zones, Southwest Indian Ridge. They argued that the high-Mg augites in the gabbros are due to small amounts of trapped liquid. Solid-state Fe/Mg diffusion is fast in olivine, therefore the interstitial melt gains Mg and loses Fe to the olivine as the melt evolves. As a result, the Mg# of the augite subsequently precipitated from this melt has constant Mg#'s, but very varied incompatible element levels. Bédard et al., (2000 and references therein) concurred, but argued that syntexis (the processes, mechanical and chemical, by which magmas react with and assimilate their host rocks) causes the shift to high Mg augite relative to the anorthite content of the coexisting plagioclase. In this view, the chemical evolution of primary MORB are as dependent on assimilation and reaction with older cumulates as on fractional crystallization, as the crust acts as a reactive filter during melt transport.

Evolution of Oceanic Gabbros: In-situ and Ancient Examples

ODP Hole 735B was drilled at the center of a ridge-segment immediately to the east of Atlantis II Fracture Zone at 700-m water depth on top of Atlantis Bank, Southwest Indian Ridge (Shipboard Scientific Party, 1989; Dick et al., 1991a). The relatively shallow drill site is an uplifted oceanic core complex, and flexural uplift from the detachment and transform-parallel faults partly explains the shallow bathymetry (Baines et al., 2003). The seismic crustal thickness at the bank is 5 ± 1 km thick (Muller et al., 1997). Two ODP Legs, 118 and 176, drilled a total of ~1500-m mostly gabbroic rocks with unusually high recovery (87%). In addition, another site, 158-m deep Hole 1105A was drilled 1-km to the north of Hole 735B (Shipboard Scientific Party, 1999) in very similar rocks.

There is a very large major-element mineral-, and major-element-, trace-element-, and isotope- whole-rock database for the entire core, as compiled by Dick et al. (2002) and Natland and Dick (2002). An extensive, quantitative and qualitative fractionation-model has not been demonstrated for the entire crustal section, although attempts have been made for Hole 1105A (Thy, 2003). In this chapter, we use a special version of the Melts program (Melts5) (Ghiorso and Sack, 1995) to evaluate the solid-lines of descent for the lower crustal rocks at Atlantis Bank to quantify the extent of disequilibrium. The effect of melt-composition, oxygen fugacity, water, pressure, and crystallization processes are evaluated. In addition, BASALT (1atm) (Weaver and Langmuir, 1990) and Yang et al. (1996) was used to assess the accuracy of the Melts algorithm in this system.

2 Methods

Melts5 (Ghiorso and Sack, 1995; Asimow and Ghiorso, 1998; Asimow pers comm. 2002) provides oxide-compositions, components, and thermodynamic properties of the silicate-, spinel (including ulvöspinel) and some accessory minerals, together with the properties of the evolving melt. This offers an opportunity to directly compare electron-microprobe mineral-analyses of the Atlantis Bank gabbros to model-minerals produced from several starting-compositions (Table 3-1) under different starting conditions. We varied the water-content from dry to 0.5 wt%, the oxygen fugacity from QFM+1 to QFM-1 and the pressure from 1kbar (0.1GPa) to 3kbar (0.3GPa). The original

Evolution of Oceanic Gabbros: In-situ and Ancient Examples

Table 1: The starting compositions of the melts used for our models
Cp10 had 6% olivine removed and 10% gabbro added (See chapter 3).

	SWIR PMORB	Site 3 5/2 SWIR	Ridge glass RC27-9-44-14	Cp10, assimilated 10% gabbro	AII107-D20 MAR PMORB
SiO ₂	50.3	50.3	49.9	51.1	49.6
TiO ₂	0.91	1.94	1.67	0.96	0.63
Al ₂ O ₃	16.4	15.3	15.9	17.6	17.5
Fe ₂ O ₃		1.2	1.6	1.1	1.3
FeO		9.0	8.4	5.3	6.3
FeO*	7.45	10.0	9.9	6.3	7.5
MnO	N.d.	0.2	0.2	0.01	N.d.
MgO	10.9	7.6	8.2	8.7	9.9
CaO	11.4	10.6	10.9	12.6	13.0
Na ₂ O	2.52	3.35	2.92	2.62	1.65
K ₂ O	0.07	0.2	0.11	0.01	0.02
P ₂ O ₅	0.12	0.2	0.19	0.2	0.12
H ₂ O	Variable	0.3	0.05	0.0	0.0
Mg#	72.3	57.4	59.8	71.2	70.4
Ca#	71.4	63.5	67.3	72.7	81.3
Reference	Dick et al, 2000	Robinson, 2000	Johnson and Dick, 1992	Modified from Kinzler and Grove, example 6 (1992)	PetDB, sample location is near Tristan da Cunha Fracture Zone

Evolution of Oceanic Gabbros: In-situ and Ancient Examples

compositions were evolved by fractionation of solids in 1°C intervals. Thus, the models represent an approximation to fractional crystallization, with large jumps produced where the model meets phase-boundary reaction-points. We performed batch equilibrium crystallization in only one model-run. We tested our results by using BASALT (Weaver and Langmuir, 1990, "W&L") and the algorithms from Yang et al., (1996), and compared the modeled mineral-compositions to the available data from Hole 735B. Each model run is evaluated using coexisting mafic minerals with plagioclase, together with the composition of the evolving melt.

3 Results

Dick et al. (2000) selected a primary melt composition ("SWIR PMORB", Table 3-1) from Kinzler and Grove (1992) as best fitting the bulk composition of Hole 735B. SWIR PMORB has $\text{Na}_8 = 2.95$ and a $\text{Fe}_8 = 9.2$ (using the algorithms from Klein and Langmuir, 1987), similar to published glass compositions from the Atlantis II Fracture Zone (Johnson and Dick, 1992). We test whether this is a valid starting composition by theoretically fractionating it at 1kbar, which represent mid- to lower crustal levels at Atlantis Bank. The liquid-line of descent and solid-lines of descent are shown in Figure 3-1. Our starting-composition has no Cr_2O_3 , so chrome-spinel is not produced. The primary melt has olivine on its liquidus at 1253°C (1259°C, W&L) and starts precipitating plagioclase after only 6% fractionation at 1220°C (1224°C, 4% W&L). This troctolitic assemblage is precipitated until 26% crystallization (1207°C) (1186°C, 32% W&L), where augite falls on the liquidus. The olivine-plagioclase-augite assemblage is crystallized together to ~1183°C (49% fractionated) (1000°C, 90% W&L), where olivine is replaced by low-Ca pyroxene. BASALT was run at 1atm, and does not crystallize a spinel-phase ("spinel" is ulvöspinel), accounting for this calculated discrepancy at low temperatures. The magnetite/ilmenite boundary is found at 1108°C (78% crystallized), late-stage olivine appears at 1034°C (90% crystallized), and apatite starts precipitating late, at 950°C (97.5% crystallized). The algorithm developed by Yang et al. (1996), indicates temperatures ~50°C lower than Melts5 (Fig. 3-11B), and we will include this

Evolution of Oceanic Gabbros: In-situ and Ancient Examples

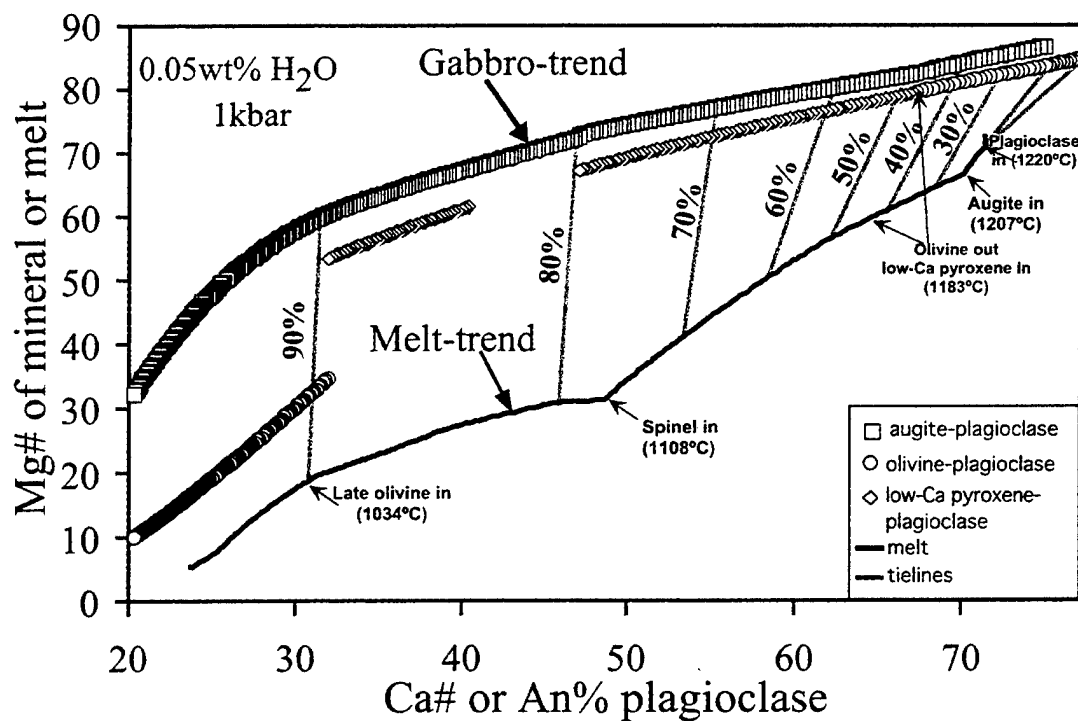


Figure 3-1: The complete model run for SWIR PMORB with 0.05wt% H₂O at 1kbar and QFM. The symbols represent the An% ($=100 \cdot \text{Ca}/(\text{Ca}+\text{Na})$, K is near absent from the system) of plagioclase co-precipitated with augite (squares), olivine (circles) and pigeonite (diamonds) as represented by their Mg#'s ($100 \cdot \text{Mg}/(\text{Mg}+\text{Fe})$). The black line represents the Mg# and Ca# of the evolving melt, and the gray lines connect the melt and mineral-pairs at 10% crystallization intervals relative to the original melt.

Evolution of Oceanic Gabbros: In-situ and Ancient Examples

discrepancy in the later evaluation, but will continue to use the 1kbar-model as a baseline-model.

Crystallization of the SWIR PMORB (damp and dry) at 3kbar and QFM (Fig. 3-2) has subtle differences between them. Three kbar at Atlantis Bank represents depths equal to crystallization within the mantle (e.g. 9-km). In the dry model (Fig. 3-2A), olivine is on the liquidus early (1270°C), but ceases to crystallize (1241°C) before plagioclase starts and is replaced by high and low-Ca pyroxene. Thus, the primitive, plagioclase-bearing cumulates are gabbro-noritic in composition and olivine does not show in the plot. Olivine comes back on the solidus early (1176°C, after ~70% crystallization) and the ulvöspinel-phase starts crystallizing at 1119°C (85%). The damp melt (Fig. 3-2B) has two main differences from the dry melt: 1) Late-stage olivine comes back on the liquidus at 40°C below that of the dry melt. 2) The plagioclase has higher An% at any given mafic mineral Mg# and melt Ca#, as is clear from the right-slanted tilt in the gray lines that joins the crystallization steps of melt and the cumulates.

The basaltic carapace that once overlay Atlantis Bank is exposed on a lithospheric flow-line in the rift mountains ~55-km north of the ridge. Robinson et al. (2001) analyzed pillow-basalt glasses from this reciprocal basaltic carapace, and we have used one of these samples for a test of the models of the sensitivity to the oxygen fugacity (Table 3-1). It should be noted that since there are no Cr in these analyses, chrome-spinel is not a part of these calculations. The glasses contained some water (0.27 wt%), which we use in the model shown in Figure 3-3. At QFM+1 (more oxidized) the model gives very high forsterite-contents for olivine relative to augite, and augite crystallizes early (Fig. 3-3A). This occurs as the olivine only takes up Fe²⁺ ions, making the effective Mg# higher than at lower oxygen fugacities. The high oxygen-fugacity model fails to lower the Mg# of the solids and liquids as the melt evolves, as a large fraction of the ulvöspinel-phase crystallizes (it uses 5 wt% of the original liquid to crystallize), keeping the Fe low in the melt. Thus, there is no late-stage olivine. The reduced case (QFM-1) sees the opposite effect (Fig. 3-3B). The spinel-phase is nearly suppressed, with lower melt and solid Mg#'s. relative to plagioclase. Augite crystallizes after 30% fractionation.

Evolution of Oceanic Gabbros: In-situ and Ancient Examples

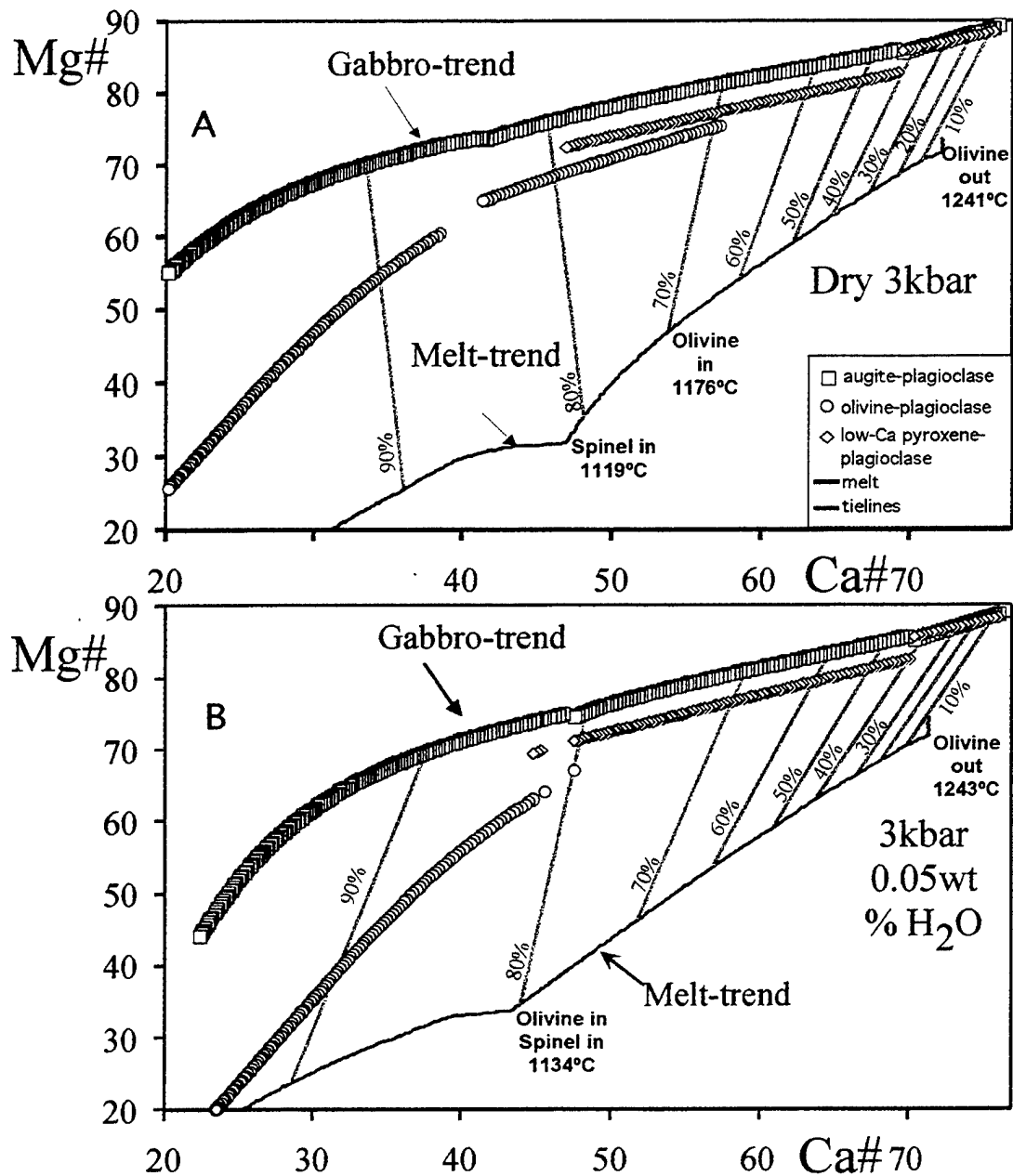


Figure 3-2: Higher pressure crystallization. The symbols are the same as in Figure 1. **A:** The crystallization sequence of SWIR PMORB at dry conditions and 3kbar pressure. **B:** The same melt crystallized with 0.05wt% H₂O in the starting composition.

Evolution of Oceanic Gabbros: In-situ and Ancient Examples

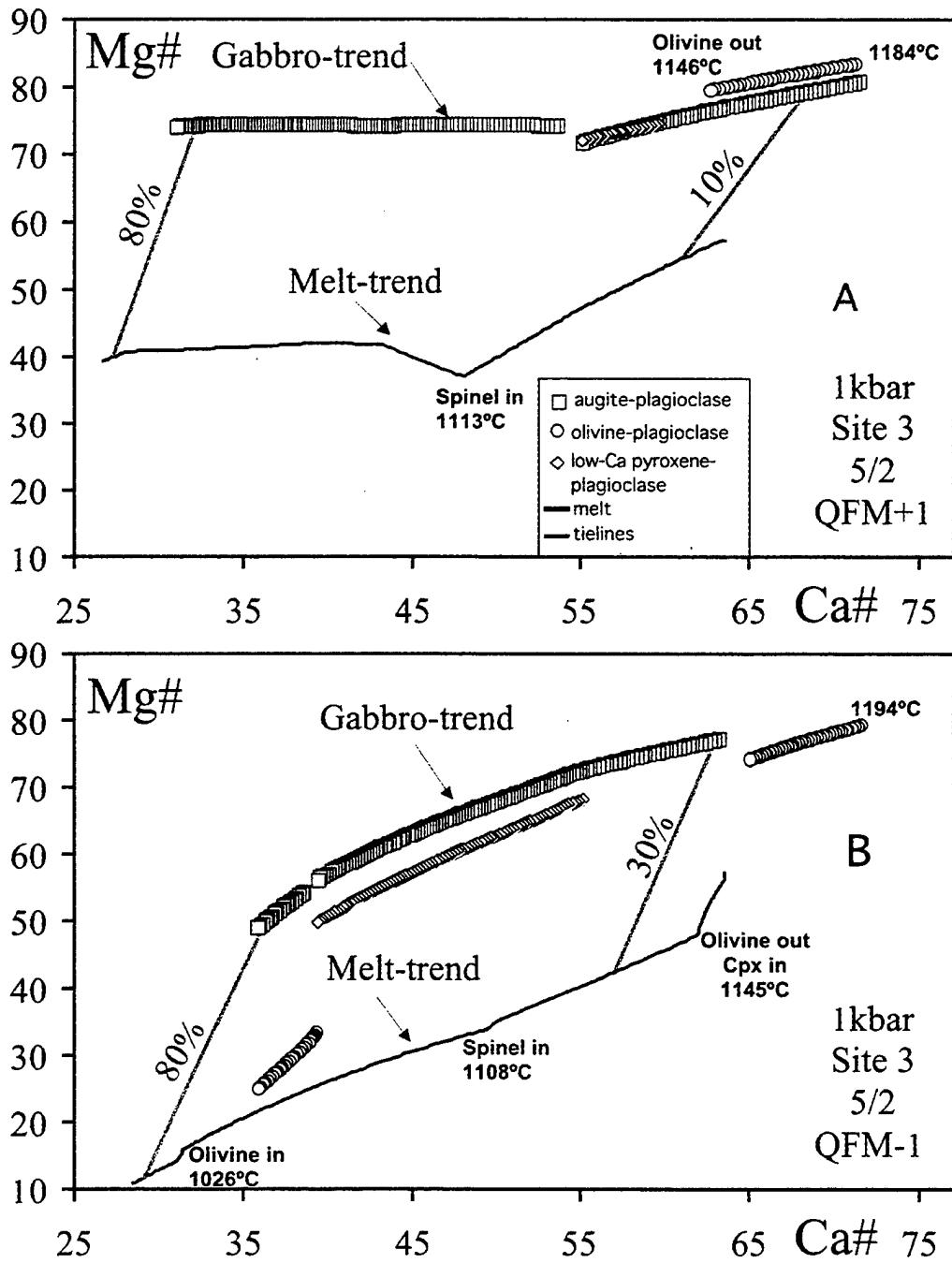


Figure 3-3: Crystallization of a glass from north of the ridge segment, at the upper crust produced reciprocally to Atlantis Bank, Sample Site3-5-2 (Robinson et al., 2001, Table 3-1). **A:** 1kbar, at QFM+1 log-unit. Only the tie-line at 10% crystallized and 80% crystallized are shown. At QFM+1 the melt is near saturated in plagioclase-augite-olivine. **B:** The same melt crystallized at QFM-1. Augite is suppressed until 34% crystallized.

Evolution of Oceanic Gabbros: In-situ and Ancient Examples

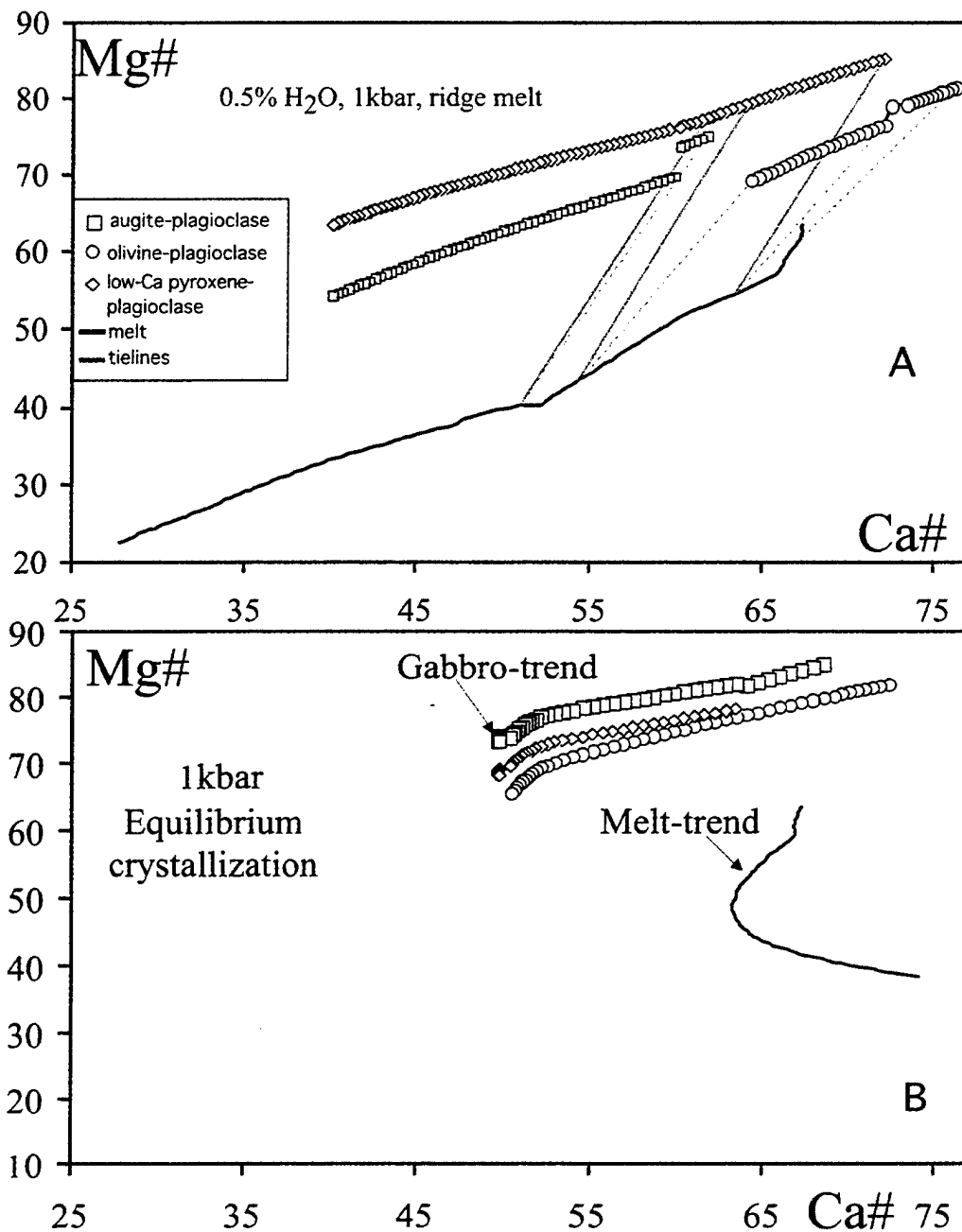


Figure 3-4: **A:** Crystallization of RC27-9-44-14 with 0.5 wt% H₂O at 1kbar and QFM. **B:** Bulk crystallization of the same melt, where the solid is not separated from the liquid. Note how the melt compositions turns around and becomes higher in Ca# with crystallization.

Evolution of Oceanic Gabbros: In-situ and Ancient Examples

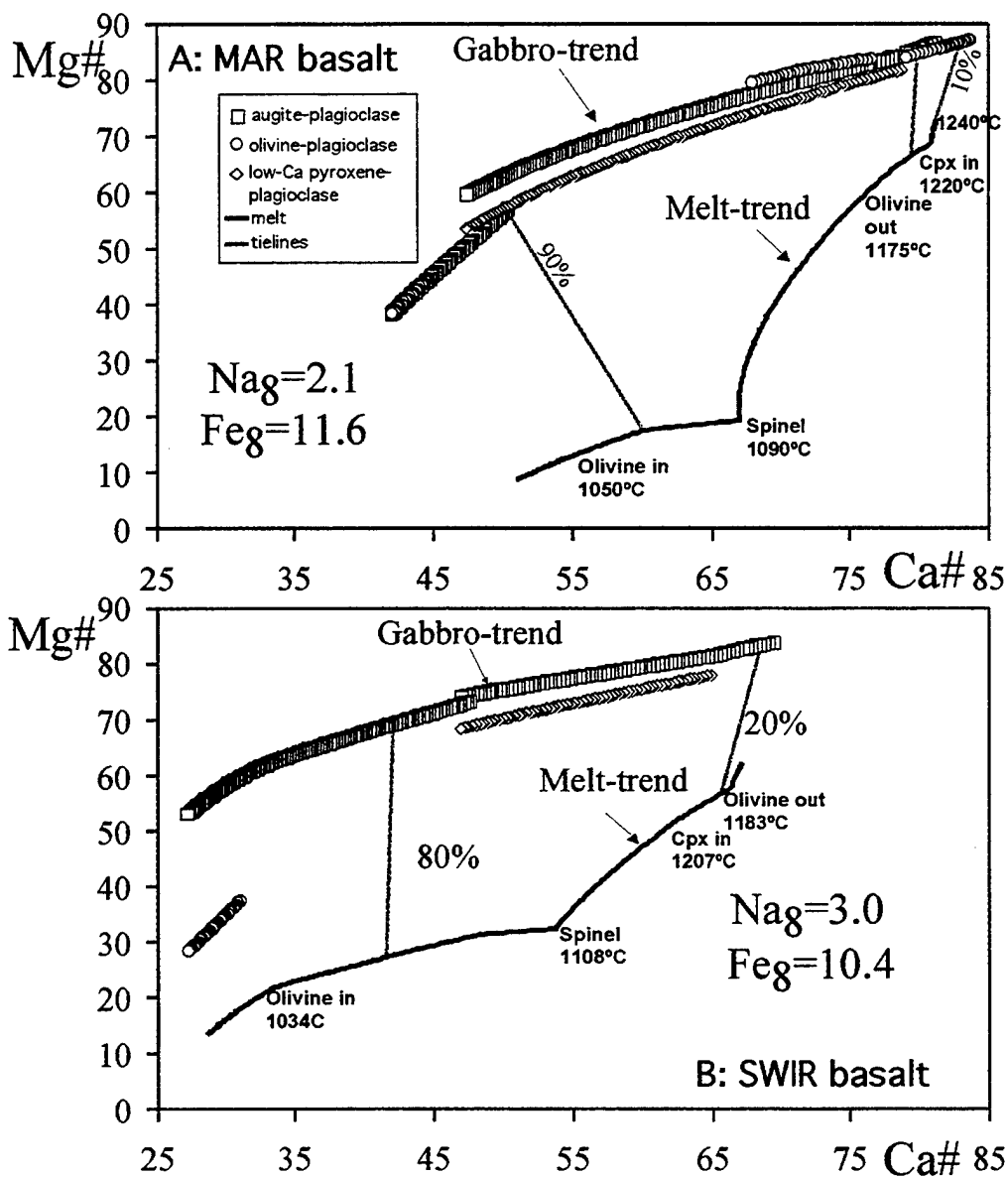


Figure 3-5: Note that the axes are slightly different from Figure 1-4. **A:** Crystallization of AII107-D20 at QFM and 1kbar. Tie-lines for 10 and 90% crystallized are shown, together with augite-in (23% crystallized). **B:** Crystallization of dry RC27-9-44-14 at 1kbar. Tie-lines for 20 and 80% crystallized (with respect to the starting-composition) are shown.

Evolution of Oceanic Gabbros: In-situ and Ancient Examples

Water has a strong effect on the solid-line of descent. Figure 3-4A shows the fractionation of glass RC27-9-44-14 collected from Atlantis II Fracture Zone at 1kbar and QFM with 0.5% of water added (Table 3-1). Compared to the previous models, it has elevated plagioclase anorthite and no late-stage olivine as Ca partitions more strongly into the plagioclase than the melt at such hydrous conditions (Housh and Luhr, 1991). Nonetheless, the Mg# of the augite is still high, while the Fo-content of olivine is low relative to drier model runs.

Batch equilibrium crystallization, where the solid and the liquid stay in equilibrium throughout solidification, is very different from the previous models (Fig. 3-4B). The model terminates for plagioclase around An_{50} and no mafic mineral has Mg#'s below 65.

The composition of the original melt strongly influences how the composition of the solid will evolve. Figure 3-5A shows a dry fractionation of a southern Mid-Atlantic ridge basalt glass from near Tristan De Cunha (PetDB) compared to that for the Atlantis II Fracture Zone glass above (Fig. 3-5B). Note that the abscissa is wider in this figure than in the others. The Atlantic basalt is more depleted than the Southwest Indian Ridge basalt, with much lower Na_8 and higher Fe_8 . This produces a model result with composition of the solid having higher plagioclase anorthite contents at the same Mg# of the solids, and little plagioclase forming below An_{50} . In the Southwest Indian Ridge-sample, however, the plagioclase has much lower An-contents, and 1/3 of the plagioclase crystallizes below An_{50} .

4 Discussion

4.1 Mode of accretion of the gabbros in Hole 735B

We now compare our models to the existing data from Hole 735B (Dick et al., 2002) (Fig. 3-6) using co-existing minerals in the gabbros. Many authors have described the compositional variations in the minerals in Hole 735B (Bloomer et al., 1991; Dick et al., 1991a; Natland et al., 1991; Ozawa et al., 1991; Hébert et al., 1991; Dick et al., 1992; Dick et al., 2000; Natland and Dick, 2001; Thy and Dilek, 2000). Hole 735B has 953

Evolution of Oceanic Gabbros: In-situ and Ancient Examples

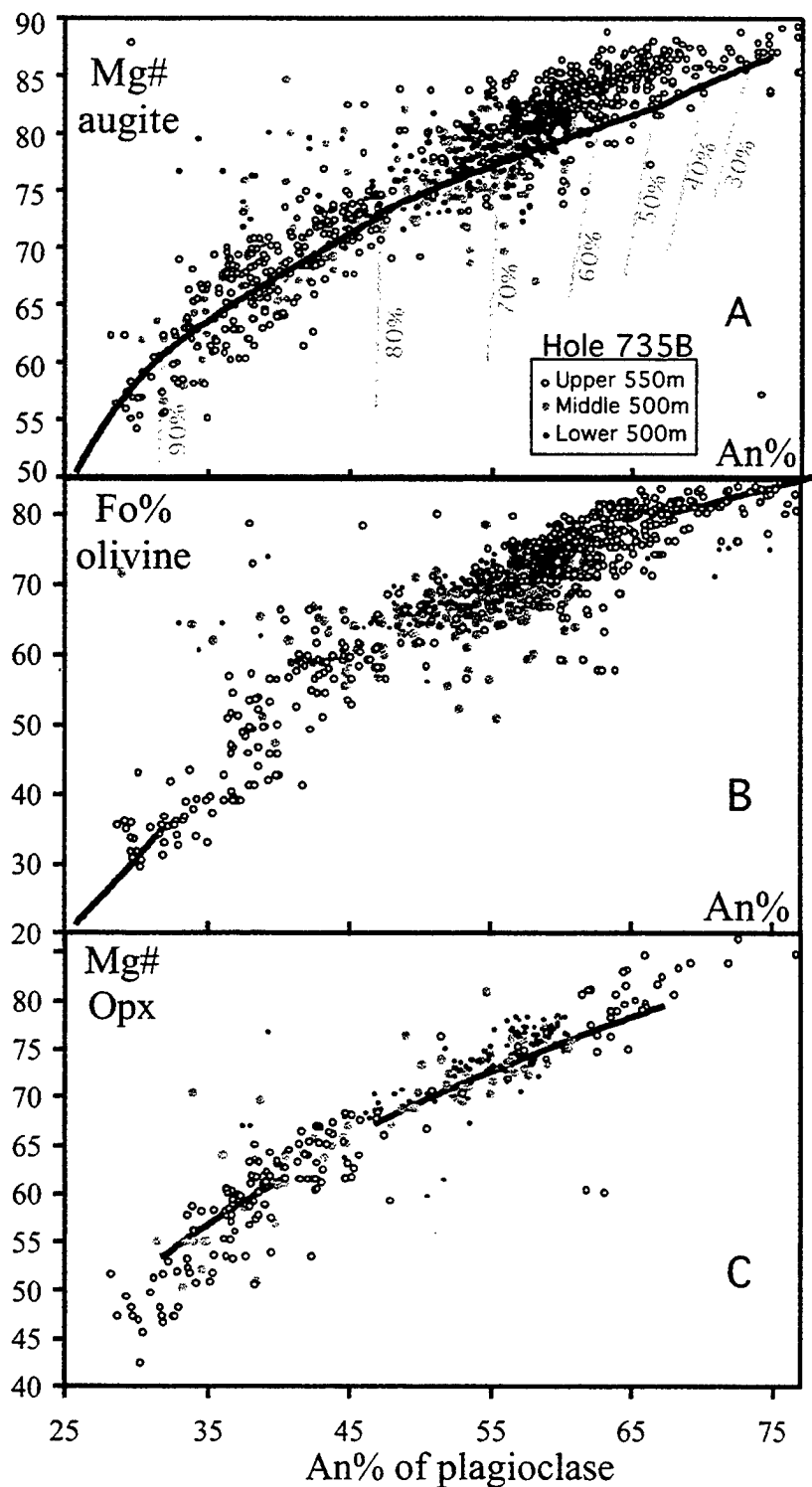


Figure 3-6: Average compositions of coexisting minerals from Hole 735B compared to the model (black model-line and gray tie-lines to the melts) in Figure 1. Open symbols are the top 550 meters, gray symbols are the middle 500 meters and the black symbols are the bottom 500 meters of Hole 735B. **A:** The Mg#'s augite with the An% of coexisting plagioclase. If made possible by the dataset (Dick et al., 2000), cores are plotted with cores, and rims with rims. **B:** The forsterite content of olivine with the An% of the coexisting plagioclase. Note how the model calls for a break in olivine crystallization, whereas olivine is near ubiquitous in the core. **C:** The Mg# of low-Ca pyroxene in the core compared to the coexisting An% of plagioclase.

Evolution of Oceanic Gabbros: In-situ and Ancient Examples

discrete described igneous intervals, with additional subdivision possible on centimeter scales (Dick et al., 2000). Plagioclase and clinopyroxene are ubiquitous, and the gabbro-types are distinguished largely by variations in grain size and amount of olivine, oxides (magmatic ilmenite and titanomagnetite) and orthopyroxene. The average grain-size varies from 5-15 mm to 15-30 mm (the definition of very coarse grain-size is >30 mm) and crystals in excess of 10-cm have been found. Only a small fraction of the lithologic contacts are simple faults rather than involving a magmatic origin. The igneous stratigraphy is divided into 12 polygenetic units, but are separated into three major associations: 1) the dominant, oxide poor, olivine-bearing gabbros (and coarse-grained troctolites), 2) cross-cutting microgabbros and fine- to medium-grained troctolite, and 3) ferrogabbros often highly deformed relative to the olivine gabbro that encompass oxide-bearing gabbros and gabbro-norites. The nature, origin and number of geochemical units are much debated. Of the studies that involve the entire core, Dick et al (2000) demonstrate five major olivine-gabbro units from 200 to 600m thick, crosscut by many ferrogabbro units that diminish in size and number down-hole. The ferrogabbros were interpreted to represent the intrusion of late interstitial melts that migrated from the cumulate into shear-zones during the detachment faulting that exposed the core-complex. The fraction of oxides down-hole is shown in Figure 3-7. Natland and Dick (2001) identified 97 separate olivine gabbro sequences, arguing that each represent an individual injection of magma forming two principal bodies of olivine gabbro. Thy and Dilek (2000) suggested the core represents four individual blocks of gabbro.

For the purpose of this study, the mineral-data is separated into the upper 550-m, the middle 450-m and the bottom 500-m, and is compared to the 1-kbar SWIR-PMORB model (Fig. 3-6). The upper 1000 meters of Hole 735B have a range of compositions best described by fractional crystallization, whereas the lower 500 meters terminate at the plagioclase anorthite contents similar to the batch-equilibrium crystallization-model (Fig. 3-4B) making it difficult to distinguish these processes there based on major elements alone. The more than 1500 plagioclase and clinopyroxene-averages have been meticulously sorted, so that cores are plotted with cores and rims with rims. This, and as

Evolution of Oceanic Gabbros: In-situ and Ancient Examples

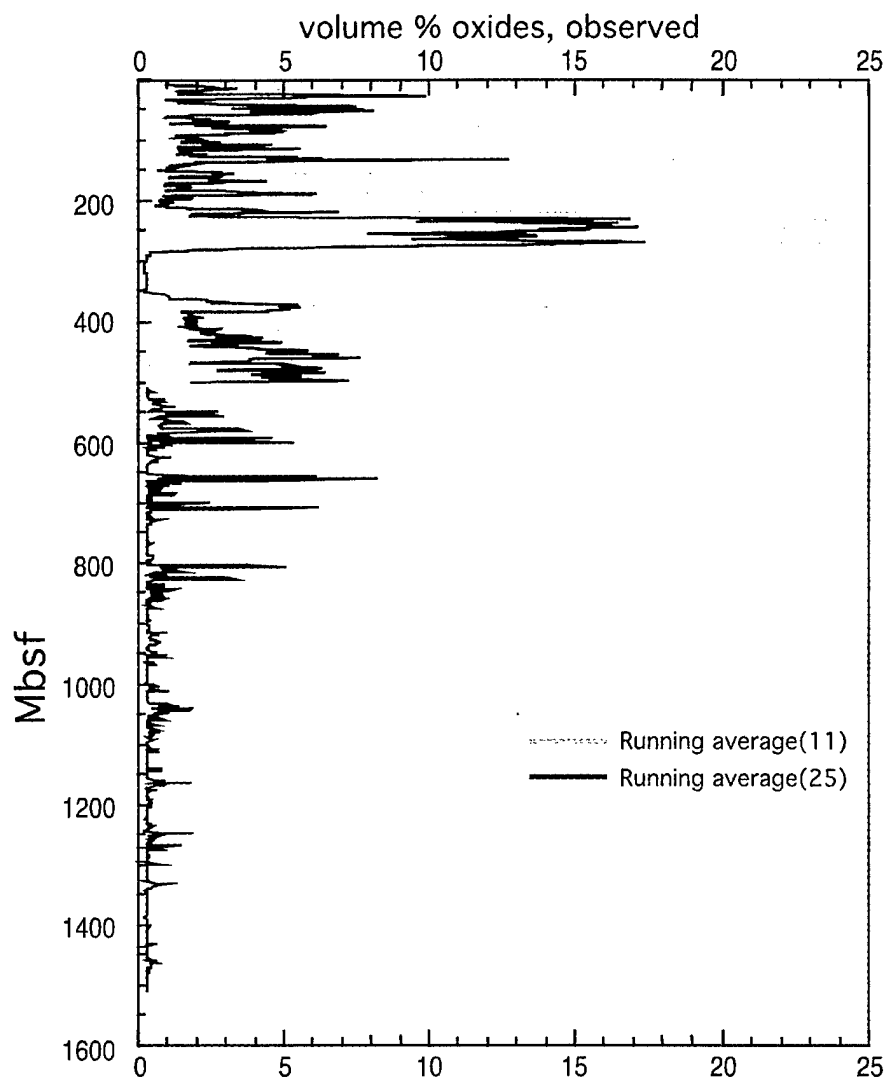


Figure 3-7: Observed volume% of oxides in Hole 735B. The lower 1000 meters are from Dick et al. (2000), whereas the upper 500 meters were logged by inspection with a hand-lens at TAMU. Variations in the volume of oxides were logged so that a total of ~1500 observations were made. The gray lines represent running averages of 11 observations, the black lines represent running averages of 25. As much as 50% oxides were observed in the core.

Evolution of Oceanic Gabbros: In-situ and Ancient Examples

errors in the analyses are small (± 0.5 mol % An, Fo or Mg#), the scatter seen in the plot is not due to errors in the large data-set. A bimodal mineral-composition distribution is obvious in the upper third of the hole, as described by Bloomer et al (1991) and the many others mentioned above. The lower ~1000 meters do not have this bimodality, with plagioclase < An₄₅ rare, and the sections become progressively more homogeneous downwards. In the upper 550-m, the cross-cutting fine to medium-grained troctolites represent 25-45% crystallization, the olivine gabbros 45-70% crystallization, and the ferrogabbros represent 80-90% crystallization (by volume or weight) relative to the modeled primary melt composition (SWIR PMORB). The cross-cutting troctolites are the most primitive rocks in Hole 735B and differ significantly from the coarser, conformable troctolites deeper in the Hole. The olivine gabbros from the lower 1000-m were produced from melts fractionated > 60% elsewhere, and crystallized more than 80%. Thus, if mantle-derived melts do form these gabbros, and crystallization shielded from mantle olivine has not occurred in the mantle, there are at least 700 vertical meters of primitive crust somewhere else in the section not yet drilled (Table 3-2). Crystallization of melts in the presence of mantle olivine would, like Meyer et al. (1989) suggested, keep a constant Mg# of the magma while the Ca# of the melt evolves. The 3 % troctolites in the upper 550-m make up far less volume than the 20% expected from the model, suggesting ~70 meters of missing troctolites, making the total missing cumulates 770 vertical meters. If the gabbro complex becomes more differentiated towards the ends of the paleo-ridge segment, which is likely, then the undrilled cumulate-section would become even longer. In addition, escape of differentiated melts from the cumulate-pile, similar to erupted MORB's in the region would also increase the estimated thickness of the undrilled -section proportionally.

Evolution of Oceanic Gabbros: In-situ and Ancient Examples

Table 3-2: Amount crystallized relative to a mantle derived melt for Hole 735B and the calculated undrilled section on the basis of the fractional crystallization model.				
Unit:	Troctolite	Olivine gabbro	Ferro gabbro	Undrilled section
Upper 550m	25-40%	40-80%	80-90% (+)	137m + 12% (troct) (=66m) ~200m
Lower 950m		60-80% (+)		570m
Total undrilled section				770m

As is described in Chapter 4, augite is texturally younger than the coexisting plagioclase in the rocks. Mineral-pairs that plot below the solid line of descent, towards more refractory plagioclase or less refractory augite, are consistent with this textural observation and the simple progressive crystallization model. Major parts of Hole 735B plot above the model solid-line of descent, however, and thus late crystallization of more evolved interstitial melts cannot explain them. The model also predicts a pause in olivine crystallization, but olivine is close to ubiquitous in the core, and there is no compositional discontinuity in forsterite content. It is important to note that the olivine – plagioclase pairs in the evolved oxide-gabbros generally do follow the same path as the model, indicating that the ferrogabbros have internal equilibrium (Fig. 3-6b). Low-Ca interstitial pyroxene (orthopyroxene) is also common throughout the core, at both the evolved and primitive end of the spectrum with a much wider range than the model predicts. It is therefore possible that there are reactions between pyroxene, olivine and silica over- and undersaturated interstitial melt, due to the peritectic reaction between olivine and melt that produce pyroxene and vice versa.

The primitive end of the model indicates that olivine is fairly close to equilibrium with plagioclase. However, if the system is in equilibrium, the coexisting mafic minerals also should be in equilibrium. Figure 3-8 compares Hole 735B data to the solid line of descent for SWIR PMORB. Again, if the system is well described by a fractional crystallization model, there should be no points plotting significantly above these lines whereas most of the refractory gabbros do. The extremely evolved oxide-olivine gabbros, however, follow the trend beautifully, and the iron-rich late-stage olivine defines the QFM-buffer with coprecipitating fayalite and magnetite. According to our model calculations, these late-stage rocks must be crystallized from melts that have fractionated

Evolution of Oceanic Gabbros: In-situ and Ancient Examples

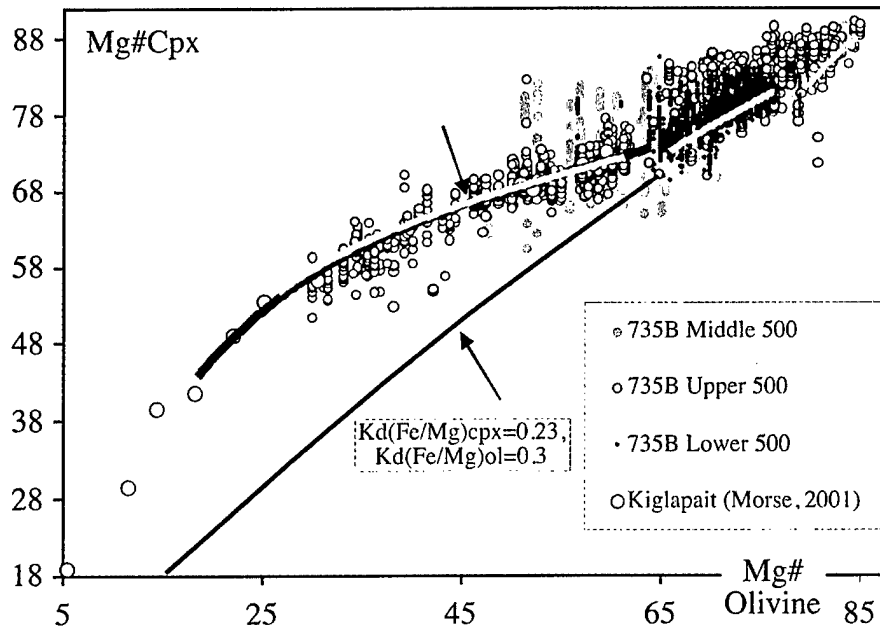


Figure 3-8: The augite coexisting with olivine of Hole 735B, as represented by their respective Mg#'s and Fo%. The augite-analyses represent all the analyses for each crystal, the olivines are averages. The thin black line represent a hypothetical olivine-augite pair in equilibrium with a melt as calculated by often-used partition-coefficients (as indicated). The thick gray line to the upper right represent the 1kbar model, the two to the left represent the 3kbar dry model, whereas the thick black curve represents the damp 3kbar model. Also included are data from the layered intrusion in Kiglapait (Morse, 2001), demonstrating how the ferrogabbros from Hole 735B are similar to the sandwich-horizons in layered intrusions.

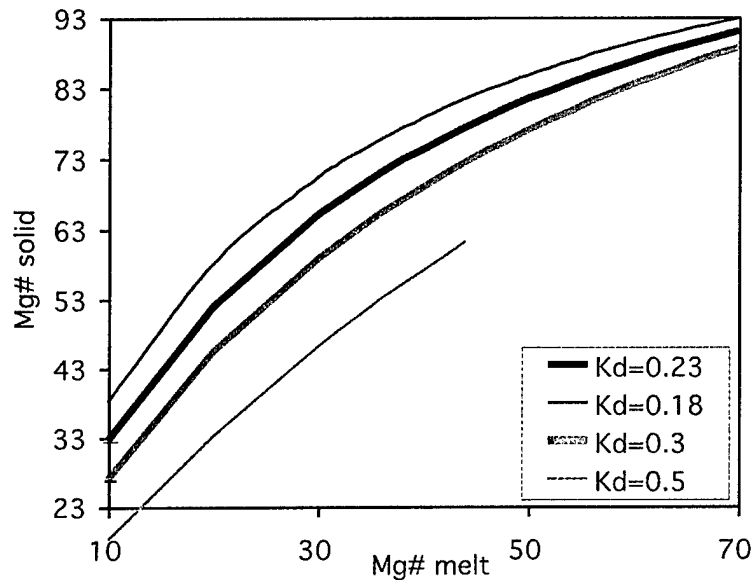


Figure 3-9: This figure demonstrates how the partition-coefficients for iron and magnesium between the crystals and melt control the variation of the Mg#'s of the crystals. Higher magma-temperatures makes the Mg#'s more similar (thick lines), whereas lower temperatures make them diverge (thin lines).

Evolution of Oceanic Gabbros: In-situ and Ancient Examples

more than 90% relative to SWIR PMORB. Thus the liquid-line of descent must have been controlled by near fractional crystallization at crustal pressures on the QFM-buffer.

4.2 The extent of disequilibrium in the refractory gabbros

The partition-coefficient dependency between the minerals and melts can be described by:

$$K_{\text{Fe/Mg}}^{\text{xtl/melt}} = \frac{X_{\text{FeO}}^{\text{xtl}}}{X_{\text{FeO}}^{\text{liq}}} * \frac{X_{\text{MgO}}^{\text{liq}}}{X_{\text{MgO}}^{\text{xtl}}}; \quad (1) \text{ so:}$$

$$K_{\text{Fe/Mg}}^{\text{xtl/melt}} = \frac{\text{Mg\#}_{\text{melt}} - \text{Mg\#}_{\text{melt}} * X_{\text{Mg}}}{X_{\text{Mg}} - X_{\text{Mg}} * \text{Mg\#}_{\text{melt}}}, \quad (2a), \text{ therefore}$$

$$X_{\text{Mg}} = \frac{\text{Mg\#}_{\text{melt}}}{K_{\text{Fe/Mg}}^{\text{xtl/melt}} - \text{Mg\#}_{\text{melt}} * K_{\text{Fe/Mg}}^{\text{xtl/melt}} + \text{Mg\#}_{\text{melt}}}, \quad (2b)$$

$$\text{Mg\#}_{\text{melt}} = \frac{X_{\text{Mg}} * K_{\text{Fe/Mg}}^{\text{xtl/melt}}}{1 - X_{\text{Mg}} + X_{\text{Mg}} * K_{\text{Fe/Mg}}^{\text{xtl/melt}}}, \quad (2c), \text{ and}$$

$$K_{\text{Fe/Mg}}^{\text{xtl1/xtl2}} = \frac{X_{\text{Mg}}^{\text{xtl1}} - X_{\text{Mg}}^{\text{xtl1}} * X_{\text{Mg}}^{\text{xtl2}}}{X_{\text{Mg}}^{\text{xtl2}} - X_{\text{Mg}}^{\text{xtl1}} * X_{\text{Mg}}^{\text{xtl2}}}, \quad (2d).$$

(Roeder and Emslie, 1970; Wood and Blundy, 1997) where $X_{\text{Mg}}^{\text{phase}}$ is the Mg# (molar Mg/(Mg+Fe) for these formulas only, 100* Mg/(Mg+Fe) for the rest of this chapter) of a phase (usually the solid unless mentioned), and $K_{\text{xtl/melt}}^{\text{Fe/Mg}}$ are the partition coefficients between a solid and a liquid. Equation 2d describes the partitioning of Fe/Mg between two minerals. It is known that $K_{\text{augite/melt}}^{\text{Fe/Mg}}$ evolves with fractionation from 0.23 towards 0.17 (all Fe as FeO) (Grove and Bence, 1977). $K_{\text{xtl/melt}}^{\text{Fe/Mg}}$ is generally 0.3±0.03 for melts that have Mg# > 45 (Roeder and Emslie, 1970). The primitive end of the fractionation-trend is not very sensitive to the partition-coefficients (Figure 3-9), in fact the entire spectrum of $K_{\text{augite/melt}}^{\text{Fe/Mg}}$, 0.23-0.17 (Grove and Bence, 1977), only increases the Mg# by ~2.5 mol%. Toplis and Carroll (1995) described $K_{\text{ol/melt}}^{\text{Fe/Mg}}$ as high as 0.5 in ferro-basalts. Therefore, the evolved melts are far more sensitive to partition-changes, as $K_{\text{augite/melt}}^{\text{Fe/Mg}}$ is much lower and $K_{\text{olivine/melt}}^{\text{Fe/Mg}}$ much higher.

Evolution of Oceanic Gabbros: In-situ and Ancient Examples

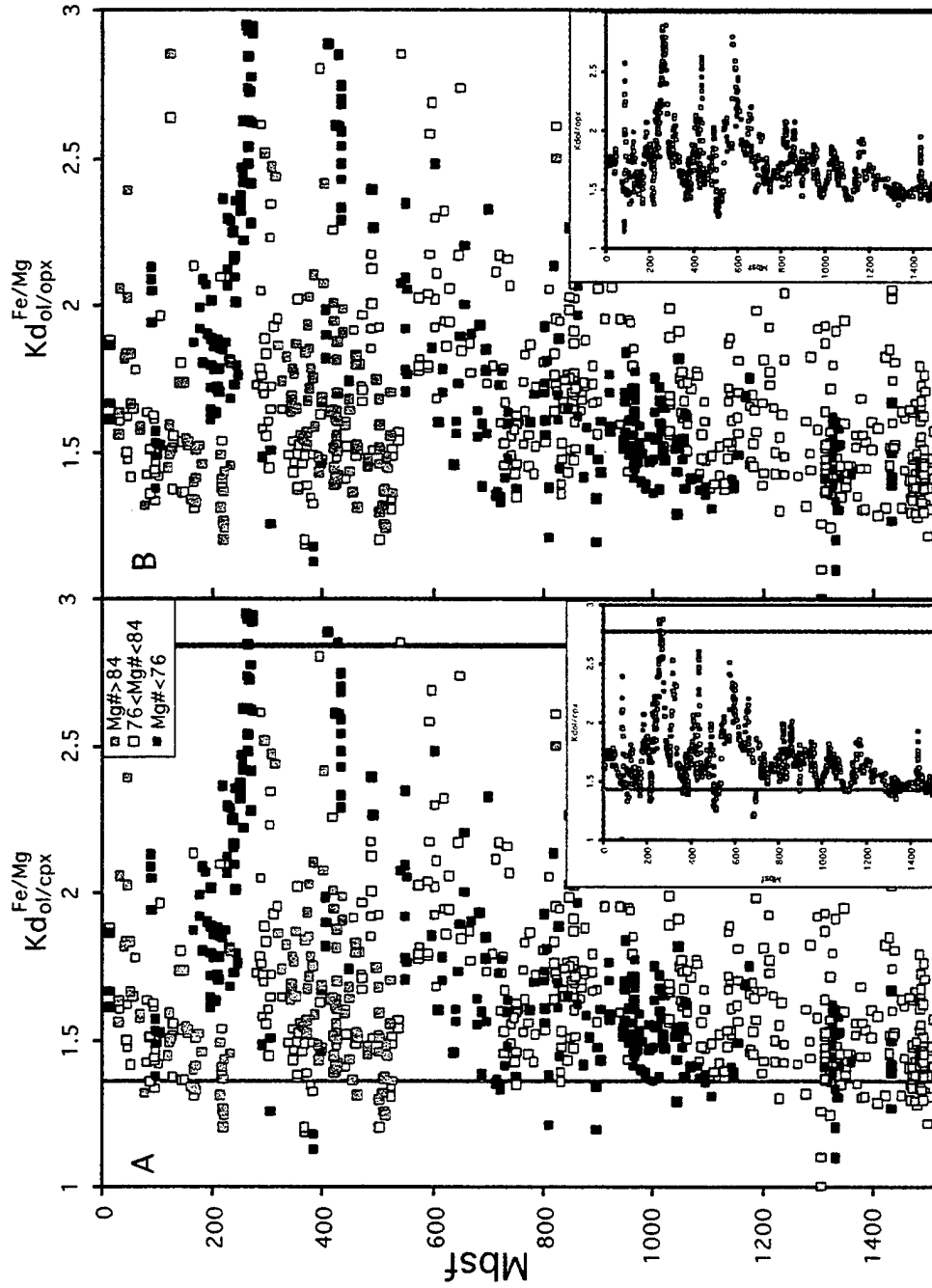
Both $Kd_{\text{olivine/ augite}}^{\text{Fe/Mg}}$ and $Kd_{\text{olivine/ opx}}^{\text{Fe/Mg}}$ vary inversely with temperature (Loucks, 1996; Braun, pers. comm. 2004) and is used to subtract the effect of temperature of crystallization from the actual geochemical offset provided by the post-cumulus processes and quantify the disequilibrium with depth in Hole 735B relative to the Melts-model. Figure 3-10 shows the partitioning between coexisting olivine-augite and olivine-orthopyroxene, so they can be compared to the equilibrium-lines for the primitive and evolved gabbros. For $Kd_{\text{olivine/ augite}}^{\text{Fe/Mg}}$ (Fig. 3-10A) the gray line to the left indicates a $Kd_{\text{olivine/ augite}}^{\text{Fe/Mg}}$ of ~1.4 produced by $Kd_{\text{augite/ melt}}^{\text{Fe/Mg}} = 0.23$ and $Kd_{\text{ol/ melt}}^{\text{Fe/Mg}} = 0.33$, the right line represents a $Kd_{\text{olivine/ augite}}^{\text{Fe/Mg}}$ of ~2.8 calculated from $Kd_{\text{augite/ melt}}^{\text{Fe/Mg}} = 0.18$ and $Kd_{\text{ol/ melt}}^{\text{Fe/Mg}} = 0.5$, respectively (op. cit.). The geothermometer of Loucks (1996) provide $Kd_{\text{olivine/ augite}}^{\text{Fe/Mg}}$'s that plot non-linearly with temperature.

The expected decrease in crystallization temperature for Mg# 89-84 augite increases in $Kd_{\text{olivine/ augite}}^{\text{Fe/Mg}}$ by 0.15. We used the baseline-model of PMORB SWIR as a reference for augite Mg#'s (Fig. 3-11) and recalculated the crystallization-temperatures of the melts using the algorithm from Yang et al. (1996) as Melts appears to give crystallization-temperatures ~50°C too high.

Similarly, over the compositional range of the intermediate gabbros (white squares in Fig. 3-10) (Mg#84-76) the $Kd_{\text{olivine/ augite}}^{\text{Fe/Mg}}$ can increase by 0.51. Examination of Figure 3-10 shows that many olivine-gabbros with augite > Mg# 84 plot far to the right of the 0.15 shift permitted by equilibrium, and many of the intermediate gabbros plot to the right of the maximum 0.51 shift. The oxide-gabbros (black squares in Fig. 3-10), however, should and do extend to the far right side of the diagram, representing crystallization of extremely evolved ferro-basalts. If we assume that the lowest value for $Kd_{\text{olivine/ augite}}^{\text{Fe/Mg}} = 1.35$ is correct for the most primitive gabbros and troctolites the temperature-dependence will only increase the Mg# of augite by 1.5 mol% for Fo₈₀ or 6 mol% for Fo₇₀. Thus, the olivine-augite system is out of equilibrium in the gabbros: more than 5 mol% Mg# for the troctolites and 10 mol% Mg# for the olivine gabbros, leaving ~3.5 and ~4 mol% Mg# unaccounted for, respectively. It could be suggested that some

Evolution of Oceanic Gabbros: In-situ and Ancient Examples

Figure 3-10: Partitioning of Fe and Mg between olivine and augite (A), and olivine and low-Ca pyroxene (B). The gray symbols indicate augites with Mg# > 84, the black symbols have Mg# < 76 and the white squares are intermediate compositions. The insert represents a running average of 9 analyses. The gray lines represent refractory (left) and evolved (right) partition coefficients, as described in the text.



Evolution of Oceanic Gabbros: In-situ and Ancient Examples

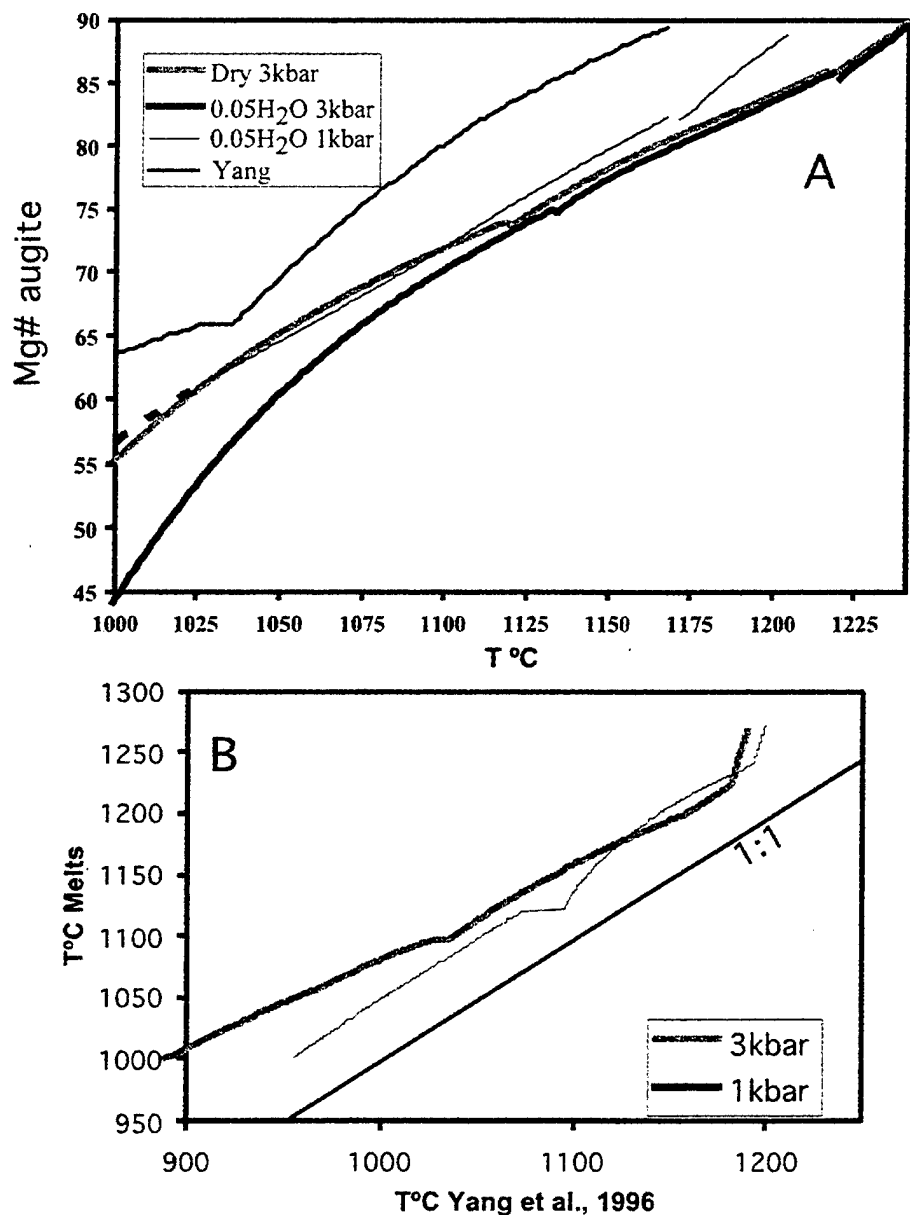


Figure 3-11: A: The variation of Mg# of augite in the models with respect to temperature. The line for Yang et al. (1996) is calculated on the 1kbar model melts using a Fe/Mg partition coefficient for augite/melt of 0.23. B: Comparison of the temperatures resolved using Melts5 and Yang et al (1996), indicating that there is a discrepancy of ~50°C between the models.

Evolution of Oceanic Gabbros: In-situ and Ancient Examples

of these effects were due to closure temperature effects, however the extent of disequilibrium of augite with respect to plagioclase in a rock is unaffected by the presence or absence of olivine. Likewise, the analyses of the augite have purposefully included exsolution-lamellae of orthopyroxene within the clinopyroxene in order to approximate the igneous composition.

Therefore, factors other than fractional crystallization at 1kbar must have affected the rocks. Note that some of the temperature-dependence discussed above is incorporated into the Melts algorithm, as will become apparent when the model is compared to those by other authors' models.

4.3 What caused the high-Mg augite?

Consistently, then, augites of the Hole 735B olivine-gabbros are more Mg-rich than predicted from the composition of the coexisting olivine and plagioclase. The formation of cumulus rocks, however, invokes two separate processes: accumulation of crystals; and postcumulus solidification and consolidation of the crystal pile (Wager et al., 1960; Hess, 1960). Although these processes may be related, they have different effects on the resulting rocks and should be treated separately, particularly for potentially open magmatic systems.

4.3.1 Accumulation of crystals, the solids:

The conditions that potentially can affect the composition of the accumulating crystals during crystallization are shown in Figure 3-12. This figure compares solid lines of descent calculated from fractionation-models for different conditions and melt compositions with the coexisting plagioclase and augite of Hole 735B. We have also included a model derived from the work in Chapter 3, where 10 wt% of gabbro is assimilated into a primitive melt before emplacement. Near-fractional crystallization at 3kbar creates a higher Mg# of augite relative to the field for Hole 735B, while the 1kbar model for the SWIR PMORB composition best fits the observed gabbro-compositions overall. The damp melt, containing 0.05% H₂O, clearly fits the evolved end of the spectrum better than the dry melt. However, if Southwest Indian Ridge-type magma

Evolution of Oceanic Gabbros: In-situ and Ancient Examples

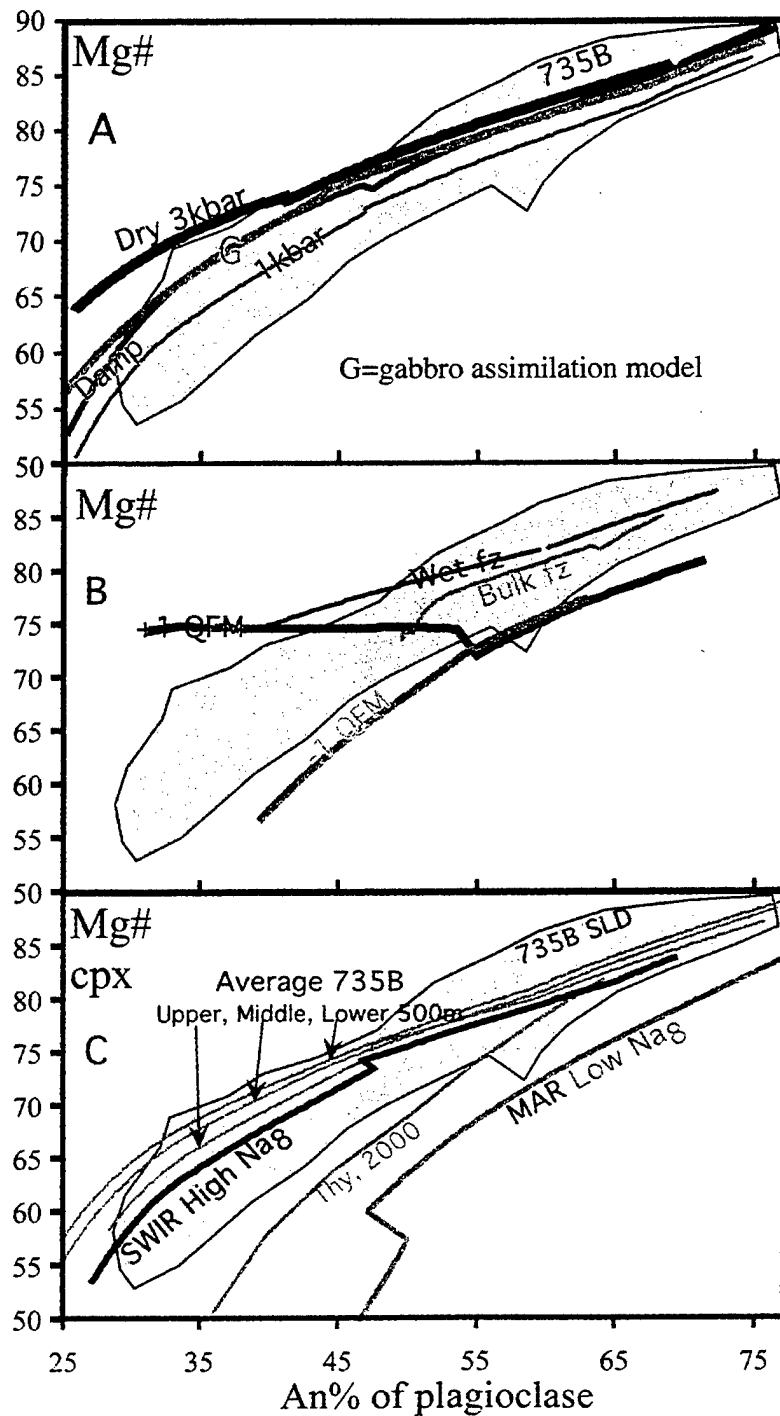


Figure 3-12: The solid-lines of descent for the models described in Figures 1-5, compared to the Mg# of augite and An% of plagioclase occurring together as in Hole 735B (outlined by the gray enclosed field). A: "1kbar"=the model from Figure 1. This figure includes a model run for a melt that has assimilated 10% gabbro (gray lines, "G", e.g. Chapter 3). The 3kbar models (Damp=0.05 wt% H₂O; Dry) demonstrated in Figure 2 resemble the 1kbar fractionated melt that assimilated gabbros before emplacement. See text for details. B: The lines represent the models as indicated. +/-1 QFM= Site 3 glass 5/2 at QFM +/-1 (Fig. 3 A, B); Bulk fz= Batch equilibrium crystallization, the solid is not separated from the liquid; Wet fz: RC27-9-44-14 with 0.5 wt% H₂O at 1kbar and QFM; C: High Na₈= Dry RC27-9-44-14 1kbar and QFM,

low Na₈= AII107-D20 at QFM and 1kbar. Thy (2003) (thin gray line). Also shown are solid lines of descent for the upper, middle and lower 500-m buld compositions for Hole 735B.

Evolution of Oceanic Gabbros: In-situ and Ancient Examples

assimilated only 10% gabbroic material on ascent and subsequently crystallized at 1kbar, the solid-line of descent is similar to the one produced by the uncontaminated 3-kbar model (Fig. 3-12a). Troctolite-assimilation follows the same trend, although augite is suppressed until 27% crystallization, compared to 18% for gabbro assimilation.

The effect of bulk-composition is illustrated in the Figure 3-12C, where the AIIFZ-glass ("High Na_8 ") plots within the field for Hole 735B, while the solid line of descent for a MAR-glass (Low Na_8) plots below it. The model of Thy (2000), where the author used a glass from AIIFZ at constant K_d 's and 1atm crystallization, fits the data poorly, as it does not account for temperature-dependence. Thy used another starting-composition with extremely high Na_8 (~ 3.7), a basalt-glass from west of the Rodrigues Triple Junction ("Type 3 basalt", Natland, 1991b). This model (not shown) fits the data much better, and plots higher than the AIIFZ glass, but the lava is very uncharacteristic of magmas found west of the Melville FZ (Mével et al., 2003) and is an unrealistic parental magma. We also modeled the solid-lines of descent for the bulk-composition of the lower, middle and upper 500-m of Hole 735B. The Na_8 of the bulk becomes higher while Fe_8 decreases deeper in the Hole (3.1, 3.3, 3.3 and 10.3, 9.3, 8.4 respectively), resulting in fractional crystallization models that have higher Mg# augites at plagioclase with the same anorthite content. However, the Mg#'s are not as high as those in Hole 735B. In fact, only the average upper 500-m of Hole 735B falls on the fractionation-trend of the basalts in the area.

The wet melt (0.5% H_2O) model fits the primitive end of the gabbro-field, but overestimates the Mg#'s of augite in towards the evolved cumulates. Varying oxygen-fugacities using Site 3 lavas demonstrates that higher oxygen fugacities stabilize augite earlier on the liquidus relative to more reducing conditions (Fig. 3-12B), and when ulvöspinel becomes stable, the Mg#'s of augite become near constant with further crystallization. Thus, very locally, increasing oxygen fugacity due to crystallization could produce the Hole 735B gabbros plotting above the solid-line of descent at the evolved fractionation-trend.

Evolution of Oceanic Gabbros: In-situ and Ancient Examples

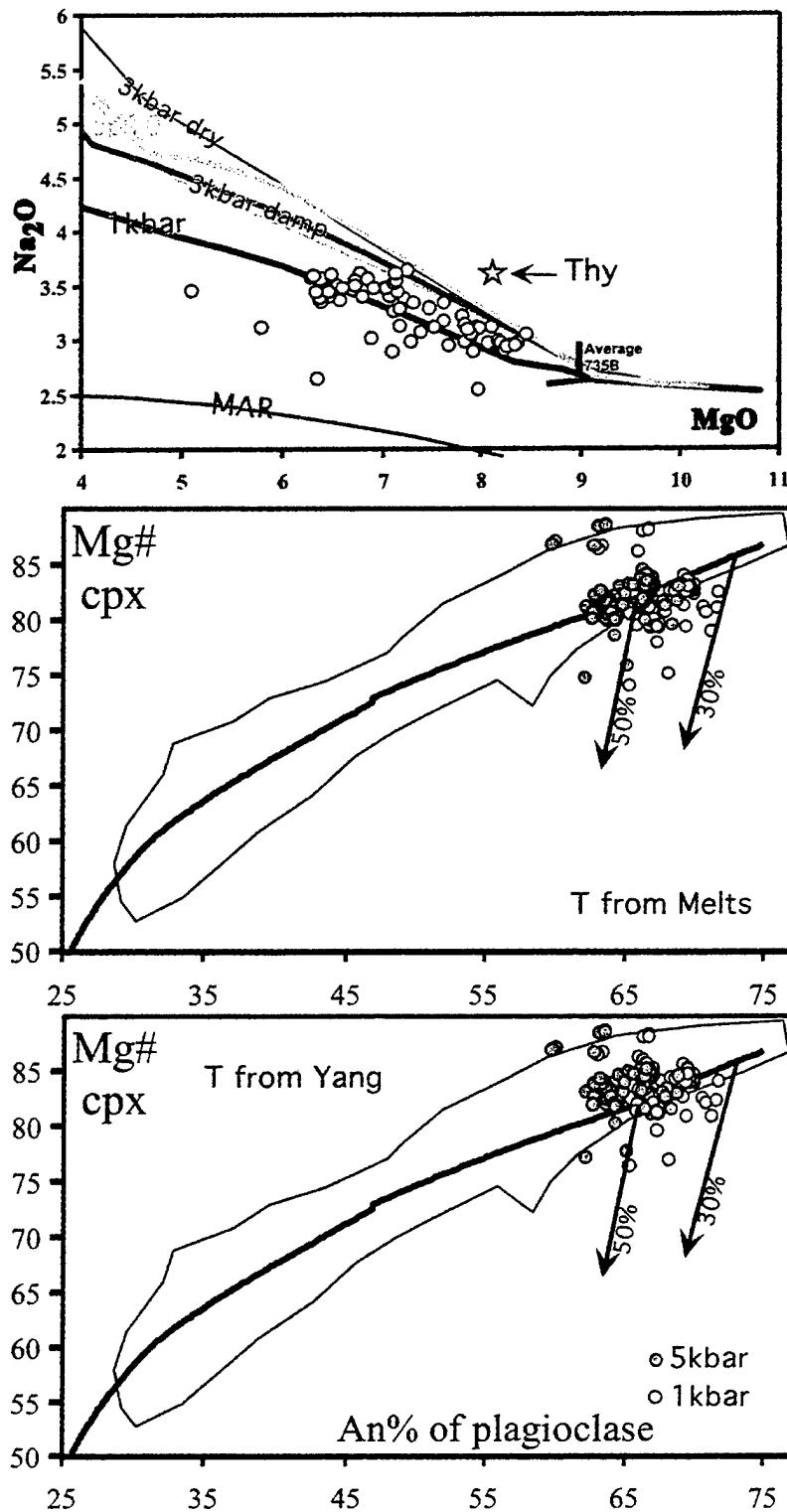


Figure 3-13: Liquid line of descent of the different Southwest Indian Ridge melts and one MAR-melt, and their relation to the solids. **A:** A suite of glasses from the ridge (open symbols, Johnson et al., 1990), compared to the starting composition from near the Rodrigues Triple Junction (star; Thy, 2003), and some of the models: "MAR"= AII107-D20 at QFM and 1kbar; "1kbar"=SWIR PMORB at 0.05wt% H_2O , QFM and 1kbar fractionation; "3kbar dry"=same melt crystallized at 3kbar, "3kbar damp" = SWIR PMORB with 0.05wt% H_2O ; "cp10" (thick gray line)=the melt that assimilated 10 wt% gabbro, thin gray line= Site 3 5/2 at QFM+1. **B:** Comparison of the field for Hole 735B gabbros and the 1kbar model to the calculated minerals that will be in equilibrium with the glasses at the ridge at 1kbar (white circles) or 5kbar (gray circles). The temperatures and melt-compositions from Melts5 were used to calculate the partition coefficients using Grove et al. (1992) for plagioclase and Putirka (1999) for augite. The tie-lines at 30 and 50% crystallized are indicated on the model. **C:** the same calculations using temperatures from Yang et al. (1996).

4.3.2 Accumulation of crystals: the liquids:

Even if a crystallization model fits the solids, it may not fit the liquids erupted along the ridge as we suggested for the high Na_8 model of Thy (2003). Figure 3-13 shows some of the models compared to a glass-suite from AIIFZ. The most efficient liquid line of descent-modifier is clearly the composition of the original magma (Fig. 3-13A). The MAR-melt clearly underestimates the Na-content in the melts, whereas Thy (2003)'s starting composition (star) is too high in Na_2O . The 1kbar model fits the data best, although the higher pressure-crystallization model, and the Melts-model with assimilated gabbro lie close to the distribution as well. We have calculated augite and plagioclase compositions in equilibrium with the ridge-glass compositions in order to directly compare them to those in the gabbroic rocks. The partition coefficients (Grove et al., 1992; Putirka, 1999) depend on melt composition and temperature, thus we have used both the temperatures of Yang et al. (1996) and those of Melts5 (Fig. 3-13 B,C). The ridge glasses recalculated at 1kbar represent melts crystallized ~30-50% respective to the SWIR PMORB melt, and most of the Hole 735B gabbros have more evolved compositions than these (as was pointed out by Bloomer et al. (1991) and Dick et al. (1991)). Based on fluid inclusions, Vanko and Stakes (1991) found that Unit V of Hole 735B formed 2 km below the seafloor, indicating that the upper crust was at least 1.65 km thick before the detachment exposed the lower crust. Since the upper crust in the area is shown to have crystallized 30% before emplacement, this adds another ~500 meters to the lower crustal budget. Increasing the pressure to 5-kbar elevates the augite Mg\# 's as much as the Melts model does at 3-kbar (at 5-kbar plagioclase starts being suppressed with respect to augite in the Melts-model) and therefore, simply increasing the pressure more does not produce the high-Mg olivine-gabbros either.

The observed variation in the Hole 735B gabbros, then, may not be attributed to simple accumulation of crystals during fractional crystallization or batch equilibrium crystallization. The most evolved rocks are also difficult to model except by using a locally appropriate melt compositions. This also requires relatively low pressures, low water-contents at the fayalite-quartz-magnetite oxygen buffer to accrete these gabbros,

Evolution of Oceanic Gabbros: In-situ and Ancient Examples

whereas the elevated Mg#s require post-cumulus processes as discussed in the next section. However, the damp SWIR-PMORB fractional crystallization model at 1-kbar explain the overall solid-line of descent of the data.

4.3.3 Post-cumulus processes

Meyer et al. (1989), Dick et al. (2000, 2002) and Coogan et al. (2001) cited processes within the crystal mush as the cause for the enormous variability of Southwest Indian Ridge augite compositions at constant forsterite or anorthite in primitive olivine-gabbros. Meyer et al. (op. cit.) described the unusually TiO₂-enriched high-Mg# augite common in the primitive Southwest Indian Ridge gabbros as buffered by the olivine in mush while plagioclase and augite are slow to react with the melt, allowing the melts to evolve with respect to incompatible elements but not Mg, Fe and Ni.

Coogan et al. (2001) took a more radical approach, and suggested that the entire section of gabbros were made up from 50/50 melt and crystals. Moreover, as elements with different partition-coefficients indicate different amounts of trapped melt, they argue that the trapped melt moves within the mush and later returns to the eruptible magma reservoir, even *after* fractionation of a spinel-phase. We find that the melts evolved in our models have ~50 wt% SiO₂ until ~80% fractionation (when ulvöspinel is produced), as the silicates have SiO₂ contents similar to the melt. The melts become denser and retain a low viscosity (Fig. 3-14) due to increasing Na₂O and FeO, and the viscosity increases abruptly after 80% crystallization. Plagioclase is also lighter than most of these melts. The evolved, oxide-rich, cumulates at Atlantis Bank are indeed abundant, and more than 200 felsic veins were described in the lower 1000-m of the section (Dick et al., 2000) suggesting that fractional crystallization went to completion. Although the evolved melts escaped into veins and shear-zones and crystallized there, we find it unlikely that the highly evolved, interstitial melts would return from the mush into the main magma-chamber, due to the abundance of oxide-minerals in Hole 735B suggesting that the last melt had high viscosities.

Evolution of Oceanic Gabbros: In-situ and Ancient Examples

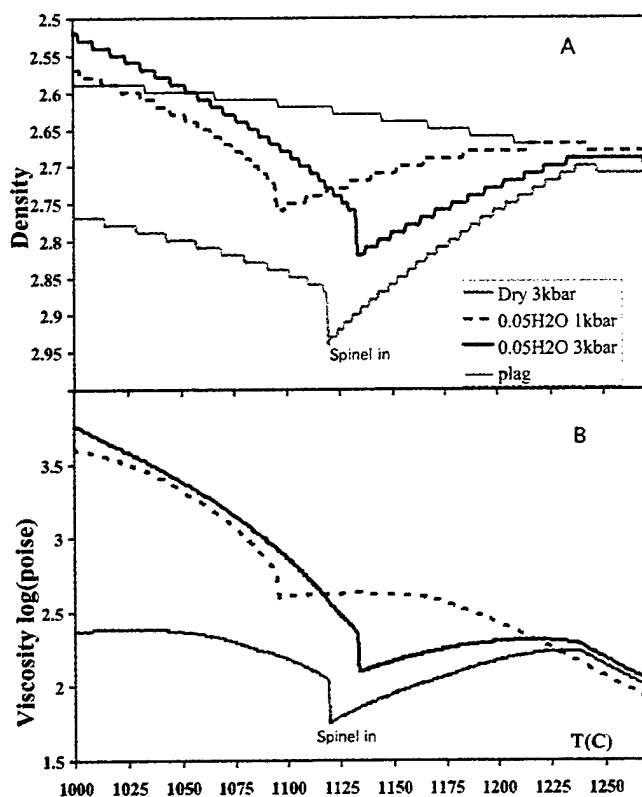


Figure 3-14: A: The density (g/cc) of the melts and plagioclase (plag) as determined by Melts. The models are as indicated in previous figures. B: The viscosity of the melts with fractionation as determined by melts for the same models.

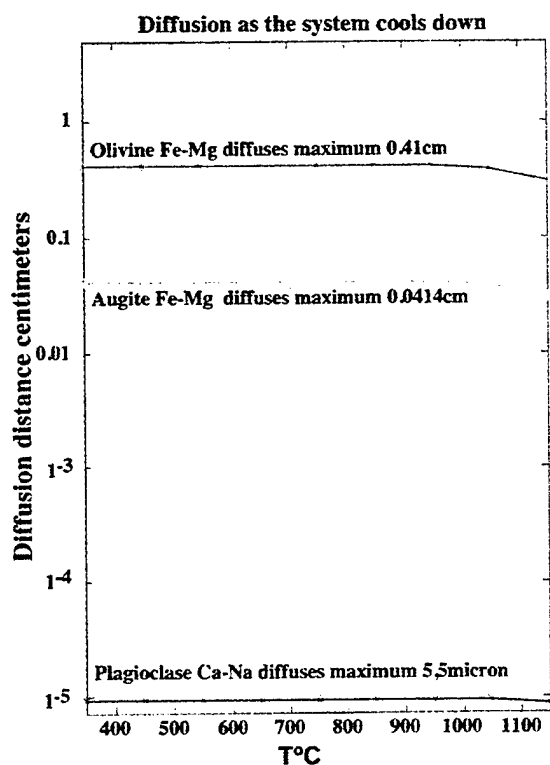


Figure 3-15: The longest diffusion distance for Ca-Na in plagioclase and Fe-Mg in olivine and augite that possible during cooling of Atlantis Bank, as determined by the cooling model of John et al (in press). Two scenarios, starting at 1350 $^{\circ}\text{C}$ and 1150 $^{\circ}\text{C}$, respectively, demonstrate the temperature dependency on the diffusion. Thus, the lower temperatures ("postmagmatic") are the most applicable to this study. The rates are from Gaetani and Watson (2000) (Fe-Mg olivine), Gaetani (pers. comm. 2000; Fe-Mg augite) and Grove et al. (1984) (Ca-Na plagioclase).

Evolution of Oceanic Gabbros: In-situ and Ancient Examples

Dick et al. (2000) investigated the contacts between lithologic units in Hole 735B and found mineral-composition discontinuities that are inconsistent with fractional crystallization. They suggested that these were the result of more evolved late-magmatic liquids migrating upwards in the section across the contacts. Angeloni and Dick (1990) showed that cross-cutting fine-grained troctolites consistently have reversely-zoned plagioclase, indicating melt percolation and overgrowth on plagioclase by later, more *primitive* melts, but that the coexisting augites have higher levels of incompatible elements than would be expected at their Mg#’s. Bloomer et al. (1991) described Unit V of ODP Hole 735B to be typified by reversely zoned plagioclase chadacrysts surrounded by high-Mg augite oikocrysts, whereas the shallower gabbros have normal zoning. This observation is unfortunately not documented by published mineral analyses. Unit V (274-382mbsl), a massive, almost undeformed and oxide-free (e.g. Fig. 3-7) olivine-gabbro section, underlies the most massive oxide-gabbro sequence of the Hole. Natland and Dick (2002) describe the Unit IV-V contact as cross-cut by a hydrothermally altered dioritic intrusive breccia. Their description is similar to that of the migmatized aureole around gabbro-bodies that are found at Fuerteventura, Canary Islands (Hobson et al., 1998) suggesting that this contact is indeed intrusive. The intrusive boundary-theory is supported by John et al. (in press), who found evidence for re-heating events at 8.5-9-Ma related to off-axis magmatism.

In order to evaluate the many views of the post-cumulus evolution of the Hole 735B section, it is necessary to know the elemental diffusion-distances for each of the minerals in the gabbros (as shown in Figure 3-15), i.e. which minerals will be affected by major-element solid-state diffusion with melts percolating through a crystal mush. In addition, solid-state diffusion also shows the likelihood of disequilibrium augite crystallization. We use cooling rates determined for Atlantis Bank from the data from John et al. (in press) to estimate the potential diffusion-distances. The highest temperatures indicate the earliest magmatic stage for each mineral, with a diffusion-distance for the given time at this temperature. As the mineral cools, the accumulative diffusion-distance grows, and the resulting distance at the lowest temperature is the

Evolution of Oceanic Gabbros: In-situ and Ancient Examples

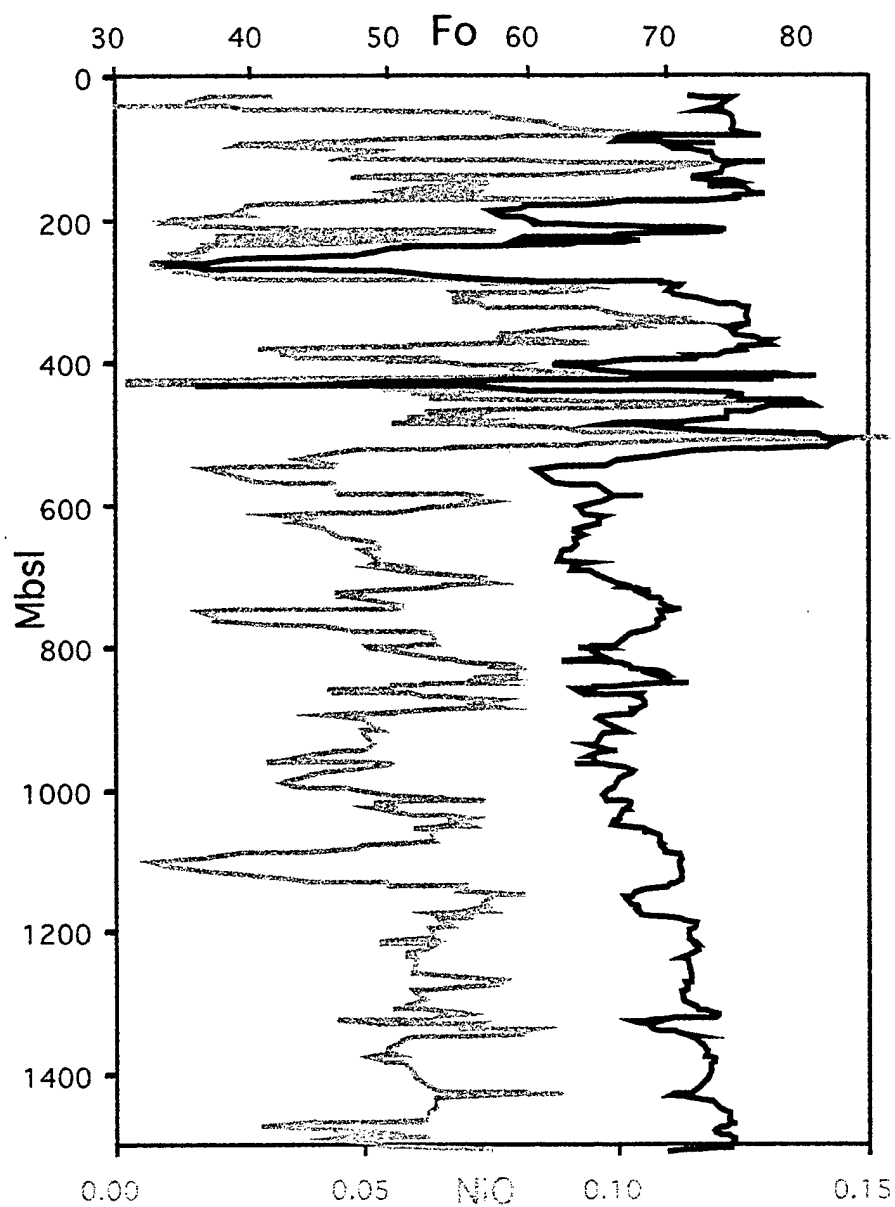


Figure 3-16: Running averages (of 9) of the NiO (wt%, gray) and Fo (black) content of olivine in Hole 735B.

Evolution of Oceanic Gabbros: In-situ and Ancient Examples

largest possible diffusion distance for a given mineral if diffusion started at the highest temperature. The Ca/Na of plagioclase, once crystallized, will not re-equilibrate with a melt in its solid state, the Fe/Mg of augite may equilibrate somewhat, whereas the Fe/Mg of olivine is easily re-equilibrated. Meyer et al. (1989), who studied very primitive cumulates from 7°E on the Southwest Indian Ridge, assumed that the olivines re-equilibrated with the interstitial melts to form the high-Mg# augites with elevated incompatible elements. If crustal accretion is assumed to occur by fractional crystallization, no olivines are formed at the intermediate temperatures in the model where the olivine-gabbros actually occur in Hole 735B, and there should be no olivine to react with. On the other hand, the magma could crystallize dunitic and troctolitic assemblages at the crust-mantle boundary and intrude as a mush (with the residues) into the crust. In such a mush, synneusis (the tendency of plagioclase crystals to cluster together due to surface-tension effects) will cause glomerophyric (or cumulophyric) clusters of plagioclase-phenocrysts, and these plagioclase-chains can create a semi-rigid network (Philpotts et al., 1998). If olivine settles out as the chains form, plagioclase will rise towards the ceiling of the magma-chamber. When there are 25% crystals present as chains, a semi-rigid framework may be completed, in which cumulates can mature. As major-element solid-state diffusion is slow in plagioclase and augite, they may only interact with the interstitial magma by dissolution, and once a plagioclase-plagioclase grain-boundary is formed, it is nearly impossible to disintegrate by dissolution (e.g. Chapter 4). Olivines, however, are free to exchange Fe and Mg with the melt. Refractory melts that intrude from below will be less dense than the melts in the network, and should therefore be able to infiltrate the mush.

Figure 3-16 shows running averages of NiO and forsterite content of olivines down-hole. Although the scatter is misleading, the lower 1000 meters of the hole has more NiO in olivine (average 0.057 wt% NiO with average Fo of 69.1) compared to the upper 550 meters (average 0.0515 wt% with average Fo of 68.7). If only the olivine-gabbros are taken into account, however, the numbers are 0.057 wt% NiO and average Fo_{69.6}, and 0.074 wt% NiO and average Fo_{75.3}. The Melts model indicates that 8%

Evolution of Oceanic Gabbros: In-situ and Ancient Examples

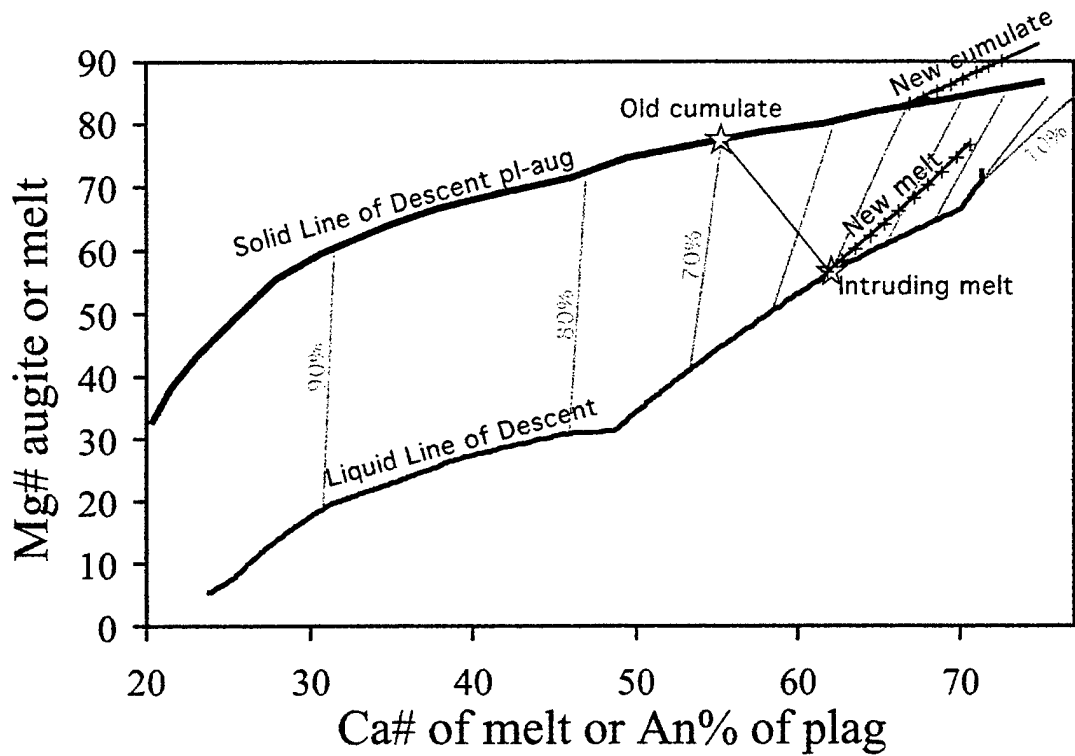


Figure 3-17: Compare to Figure 1: The upper black line represents coexisting augite and plagioclase, the lower black line is the Mg# and Ca# of the evolving melt, and the gray lines are the 10% incremental crystallization-tielines. The consequence of assimilating a cumulate representing 70% fractionated (upper star, 1140°C) into a 50% crystallized melt (lower star, 1180°C) is to increase the Mg# and Ca# of the melt (along the lower line where 10% increments are indicated with crosses), resulting in new cumulates following the upper respective line. Thus, the new cumulate will have higher Mg# augite and more anorthitic plagioclase than the original melt.

Evolution of Oceanic Gabbros: In-situ and Ancient Examples

fractionation (of plagioclase, clinopyroxene and orthopyroxene) is required to reduce the Mg# of the melt sufficiently from the average equilibrium liquids of the upper 550-m-s to those of the lower 1000-m. We can therefore contrast this amount of crystallization to what is required to reduce NiO from 0.074 to 0.057 wt%. The partitioning of Ni in olivine is dependent on the MgO of the melt (Hart and Davis, 1978), and we find $D^{Ni} \sim 21$ (we used the MgO of the liquids in the 1kbar-model at the correct Mg#'s relative to the forsterite content of the average sections). Thus, a melt in equilibrium with the olivines in the upper 550 meters will have to fractionate 5.5 wt% olivine (plus other minerals) in order to reduce the NiO to that of the lower 1000 meters. If the parental melts of the upper and lower part of Hole 735B were similar, it is not fair to assume that the olivines we analyze today have the same composition as the olivines that initially crystallized and injected with the mush.

If we assume that early olivine are dispersed in a plagioclase mush-network, and that there is melt-flow through this mush, the olivines will re-equilibrate quickly with the interstitial melt. The interstitial olivines are sources of Mg and sinks for Fe for the evolving interstitial melt as Meyer et al (1989) suggested. Moreover, any melt that dissolves a pre-existing cumulate (i.e. the melt has a higher temperature than the solidus of what is melted) will produce a hybrid melt that has higher Mg# (and lower TiO_2) (see Chapter 4). This is illustrated in Figure 3-17, where each tie-line connects a cumulate to its equilibrium melt. Therefore, a melt at slightly higher Mg# and Ca# will be able to dissolve rocks lower on the reaction-series (See Chapter 4 for details). The mixing-line between the cumulate-composition and the melt composition is indicated on the figure. Note that augite is Ca-rich (up to 22 wt% CaO), so the Ca# also increases. The hybrid melt initially crystallizes higher anorthite-content plagioclase and Mg# augite. This creates reverse zoning in plagioclase and augite, like Bloomer et al. (1991) observed in Unit V and the cross-cutting troctolites. It may also additionally create high-Mg augite with high levels of incompatible elements in them, as Meyer et al. (1989) found. As the hybrid melt crystallizes, it will produce gradually more evolved cumulates, just like the Melts-models outline.

5 Conclusion

The rocks sampled in Hole 735B represent 25-90% crystallization of a primary mantle-derived melt with $\text{Na}_8 \sim 3$ and $\text{Fe}_8 \sim 9$ at crustal pressure on the quartz-fayalite-magnetite oxygen fugacity buffer. The majority of the gabbros in the lower 1000 meters of the Hole represent 60-80% crystallization. The upper 550 meters have a very bimodal distribution with cross-cutting troctolites and massive olivine gabbros representing 25-45% and 45-70% crystallization respectively, whereas the ferrogabbros represent 80-90% crystallization. The glasses sampled along the ridge, on the other hand, represent 30-50% crystallized relative to the same mantle-derived melt, and most of the crustal section is far more evolved than the upper crust. If we assume a traditional view of the accretion of the lower ocean crust, ~1200 meters of the lower crustal section has not been drilled. With the missing upper crust, this brings the minimum total crustal thickness to ~4.4 km, suggesting that the observed seismic Moho at Atlantis Bank is indeed the crust-mantle boundary rather than an alteration-front as suggested by Muller et al. (1997). We find that the olivine-gabbros have augites in disequilibrium with the coexisting plagioclase relative to crystallization at crustal pressures, and that this 10 mol% discrepancy may be accounted for by dissolution and reprecipitation within a crustal mush-zone due to the intrusions of melt from below.

Evolution of Oceanic Gabbros: In-situ and Ancient Examples

6 References

- Angeloni LM. Dick HJB, 1990: Troctolitic Gabbros from Hole 735B, Atlantis II Fracture Zone, Southwest Indian Ridge. *EOS* 71(43): 1704.
- Asimow PD. Ghiorso MS, 1998: Algorithmic Modifications Extending MELTS to Calculate Subsolidus Phase Relations. *Amer Mineral* 83: 1127-1131.
- Baines AG. Cheadle MJ. Dick HJB. Scheirer AH. John BE. Kuznir NJ. Matsumoto T, 2003: Mechanism for generating the anomalous uplift of oceanic core complexes: Atlantis Bank, Southwest Indian Ridge. *Geology* 31 (12): 1105-1108.
- Bédard JH, 2000: Syntesis and the genesis of lower ocean crust. In Dilek Y. Moores EM> Elthon D> Nicholas A (eds), *Ophiolites and Oceanic Crust: New insights from Field Studies and the Ocean Drilling Program: Boulder Colorado, Geological Soc America Spec Paper* 349: 105-119.
- Bloomer SH. Meyer PS. Dick HJB. Ozawa K. Natland JH, 1991: Texture and mineralogic variations in gabbroic rocks from Hole 735B. In: *Proceeding of the Ocean Drilling Program, Scientific Results*, 118: 21-39.
- Bloomer SH. Natland JH. Fisher RL, 1989: Mineral relationships in gabbroic rocks from fracture zones of Indian Ocean ridges: evidence for extensive fractionation, parental diversity and boundary-layer recrystallization. In: Saunders AD. Norry MJ, (eds) *Magmatism in the Ocean Basins*, *Geol Soc Spec Publ* 42: 107-124.
- Coogan LA. MacLeod CJ. Dick HJB. Edwards SJ. Kvassnes A. Natland JH. Robinson PT. Thompson G. O'Hara MJ, 2001: Whole-rock geochemistry of gabbros from the Southwest Indian Ridge: constraint on geochemical fractionations between the upper and lower oceanic crust and magma chamber processes at (very) slow-spreading ridges. *Chem Geol* 178:1-22.
- Dick HJB, 1989: Abyssal peridotites, very slow spreading ridges and ocean ridge magmatism. In: Saunders AD. Norry MJ, (eds): *Magmatism in the ocean basins*, *Geol Soc Spec Publ* 42: 71-105.
- Dick HJB. Meyer PS. Bloomer S. Kirby S. Stakes D. Mawer C, 1991a: Lithostratigraphic evolution of an in-situ section of oceanic layer 3. In: Von Herzen RP. Robinson PT. et al., *Proc ODP, Sci Res* 118: College Station, TX (Ocean Drilling Program): 439-538.
- Dick HJB. Natland JH. Alt JC. Bach W. Bideau D. Gee JS. Haggas S. Hertogen JGH. Hirth JG. Holm PM. Ildefonse B. Iturrino GJ. John BE. Kelley DS. Kikawa E. Kingdon A. LeRoux PJ. Maeda J. Meyer PS. Miller DJ. Naslund HR. Niu YL. Robinson PT. Snow J. Stephen RA. Trimby PW. Worm HU. Yoshinobu A, 2000: A long in situ section of the lower ocean crust; results of ODP Leg 176 drilling at the Southwest Indian Ridge. *Earth Planet Sci Lett* 179 (1): 31-51.
- Dick HJB. Ozawa K. Meyer PS. Niu Y. Robinson PT. Constantin M. Hébert R. Natland JH. Hirth JG. Mackie SM, 2002: 10. Primary silicate mineral chemistry of a 1.5-km section of very slow spreading lower ocean crust: ODP Hole 735B, Southwest Indian Ridge. In Natland JH. Dick HJB. Miller DJ. Von Herzen RP (eds) *Proceedings of the Ocean Drilling Program, Scientific Results Volume* 176. (CD-ROM).
- Dick HJB. Robinson PT. Meyer PS, 1992: The plutonic foundation of a slow-spreading ridge. In: *Synthesis of Results from Scientific Drilling in the Indian Ocean*. *Geophys Monogr* 70: 1-39
- Dick HJB. Schouten H. Meyer PS. Gallo DG. Bergh H. Tyce R. Patriat P. Johnson KTM. Snow J. Fisher A, 1991b: Tectonic evolution of the Atlantis II Fracture Zone. In: Von Herzen RP. Robinson PT. et al., *Proc ODP, Sci Res* 118: College Station, TX (Ocean Drilling Program): 359-398.
- Elthon D. Stewart M. Ross K, 1992: Compositional trends of minerals in oceanic cumulates. *Journ Geophys Res* 97 (B11): 15,189-15,199.
- Elthon D, 1987: Mineral chemistry of gabbroic rocks from the Mid-Cayman Rise spreading center. *Journ Geophys Res* 92:658-682
- Gaetani GA. Watson EB, 2000: Open system behavior of olivine-hosted melt inclusions. *Earth Planet Sci Lett* 183: 27-41.
- Ghiorso GA. Sack RO, 1995: Chemical Mass Transfer in Magmatic Processes IV: A revised and internally consistent thermodynamics model for the interpolation and extrapolation of liquid-solid equilibria in magmatic systems at elevated temperatures and pressures. *Contrib Mineral Petrol* 119: 197-212.

Evolution of Oceanic Gabbros: In-situ and Ancient Examples

- Grove TL, Baker MB, Kinzler RJ, 1984: Coupled CaAl-NaSi diffusion in plag feldspar: Experiments and applications to cooling rate speedometry. *Geochim Cosmochim Acta* 48: 2113-2121.
- Grove TL, Bence AE, 1977: Experimental study of pyroxene-liquid interaction in quartz-normative basalt 15597. *Proc Lunar Sci Conf 8th*: 1549-1579.
- Grove TL, Kinzler RJ, Bryan WB, 1992: Fractionation of mid-ocean ridge basalts. In: *Mantle flow and melt generation at mid-ocean ridges*, *Geophys monogr* 71: 281-310.
- Hart SR, Davis KE, 1978: Nickel partitioning between olivine and silicate melt. *Earth Planet Sci Lett* 40: 203-219.
- Hébert R, Constantin M, Robinson PT, 1991: Primary mineralogy of Leg 118 gabbroic rocks and their place in the spectrum of oceanic mafic igneous rocks. In: Von Herzen RP, Robinson PT et al., *Proc ODP, Sci Res, 118: College station, TX (Ocean Drilling Program)*: 3-20.
- Hess, HH, 1960: Stillwater igneous complex, Montana, a quantitative mineralogical study. *Geol Soc Am Mem* 80.
- Hobson A, Bussy F, Hernandez J, 1998: Shallow-Level Migmatization of Gabbros in a Metamorphic Contact Aureole, Fuerteventura Basal complex, Canary Islands. *Journ Petrol* 39 (5): 1025-1037.
- Housh TB, Luhr JF (1991) Plagioclase-melt equilibria in hydrous systems. *Am Min* 76: 477-492.
- John BE, Foster DA, Murphy JM, Cheadle MJ, Baines G, Fanning CM, Copeland P, in press: Determining the cooling history of in situ lower oceanic crust-Atlantis Bank, SW Indian Ridge.
- Kinzler RJ, and Grove TL, 1992: Primary magmas of midocean ridge basalts: 1. Experiments and Methods. *Journ Geophys Res* 97: B6,885-6,906.
- Klein EM, Langmuir CH, 1987: Global correlations of ocean ridge basalt chemistry with axial depth and crustal thickness. *J. Geophys. Res.*, 92 (B8) 8089-8115.
- Kvassnes, AJ, Dick HJB, Grove TL, 2003: The Atlantis Bank gabbro-suite was not a "normal" magma-chamber that produced basalts. *Geophysical Research Abstracts*, Vol. 5, 12,203. European Geophysical Society.
- Langmuir, CH, 1989: Geochemical consequences of in situ differentiation. *Nature*, 340, 199-205.
- Loucks, RR, 1996: A precise olivine-augite Mg-Fe exchange geothermometer. *Contrib Mineral Petrol* 125 (2-3): 140-150.
- Magde LS, Sparks DW, 1997: Three-dimensional mantle upwelling, melt generation, and melt migration beneath segment slow spreading ridges. *Journ Geophys Res* 102 (B9) 20,571-20,583.
- Meyer PS, Dick HJB, Thompson G, 1989: Cumulate gabbros from the Southwest Indian Ridge, 54°S-7°16'E: implications for magmatic processes at a slow ridge. *Contrib Mineral Petrol* 103: 44-63.
- Meyzen CM, Toplis MJ, Humler E, Ludden JN, Mével C: A discontinuity in mantle composition beneath the Southwest Indian Ridge. *Nature* 421 (6924): 731-733.
- Michael PJ, Cornell WC, 1998: Influence of spreading rate and magma supply on crystallization and assimilation beneath mid-ocean ridges: Evidence from chlorine and major element chemistry of mid-ocean ridge basalts. *Journ Geophys Res* 103 (B8): 18,325-18,356.
- Muller MR, Robinson CJ, Minshull TA, White RS, Bickle MJ, 1997: Thin crust beneath Ocean Drilling Program Borehole 735B at the Southwest Indian Ridge? *Earth Planet Sci Lett* 148 (1-2): 93-107.
- Natland JH, 1991b: Indian Ocean Crust. In Floyd PA (ed): *Oceanic Basalts*: Glasgow (Blackie): 288-310.
- Natland JH, Dick HJB, 2001: Formation of the lower ocean crust and the crystallization of gabbroic cumulates at a very slowly spreading ridge. *Journ Volc Geotherm Res* 110: 191-233.
- Natland JH, Dick HJB, 2002: Stratigraphy and Composition of Gabbros Drilled in Ocean Drilling Program Hole 735B, Southwest Indian Ridge: A synthesis of Geochemical Data. In Natland JH, Dick HJB, Miller DJ, Von Herzen RP (eds) *Proceedings of the Ocean Drilling Program, Scientific Results Volume 176*. 1-69 (CD-ROM).
- Natland JH, Meyer PS, Dick HJB, Bloomer SH, 1991a: Magmatic oxides and sulfides in gabbroic rocks from Hole 735B and the later development of the liquid line of descent. In: Von Herzen RP, Robinson PT et al., *Proc ODP, Sci Res, 118: College station, TX (Ocean Drilling Program)*: 75-111.
- Ozawa K, Meyer PS, Bloomer SH, 1991: Mineralogy and textures of iron-titanium oxide gabbros and associated olivine gabbros from Hole 735B. In: Von Herzen RP, Robinson PT et al., *Proc ODP, Sci Res, 118: College station, TX (Ocean Drilling Program)*: 41-73.
- Philpotts AR, Shi J, Brustmann C, 1998: Role of plagioclase crystal chains in the differentiation of partly crystallized magma. *Nature* 395 (24): 343-346.
- Putirka K, 1999: Clinopyroxene+liquid equilibria to 100kbar and 2450K. *Cont Min Petr* 29:275-289.

Evolution of Oceanic Gabbros: In-situ and Ancient Examples

- Robinson CJ, Bickle MJ, Minshull TA, White RS, Nichols ARL, 2001: Low degree melting under the Southwest Indian Ridge: the roles of mantle temperature, conductive cooling and wet melting. *Eart Planet Sci Lett* 188:383-398.
- Roeder PL, Emslie RF, 1970. Olivine-liquid equilibrium. *Contrib Mineral Petrol* 29:275-289.
- Shipboard Scientific Party, 1989: Site 735. In: Robinson PT, Von Herzen R. et al.: *Proc ODP, Init Repts*, 118: College Station, TX (Ocean Drilling Program): 89-222.
- Shipboard Scientific Party, 1999: Hammer Drill Sotes (1104 and 1106) and Site 1105. In: Pettigrew T, Casey J, Miller DJ. et al., *Proc ODP, Init Repts*, 179: College Station, TX (Ocean Drilling Program) CD Rom.
- Thy P, 2003: 2. Igneous Petrology of Gabbros from Hole 1105A: Oceanic Magma Chamber Processes. In: Casey JF, Miller DJ (eds): *Proceeding of the Ocean Drilling Program, Scientific Results*, Vol 179. Web publication.
- Thy P, Dilek Y, 2000: Magmatic and tectonic controls on the evolution of oceanic magma chambers at slow-spreading ridges: Perspectives from ophiolitic and continetal layered intrusions. In: Dilek Y, Moores EM, Elthon D, Nicholas A (eds) *Ophiolites and Oceanic Crust: New insights from Field Studies and the Ocean Drilling Program*: Boulder Colorado. *Geol Soc Spec Paper* 349: 87-104.
- Toplis MJ, Carrol MR, 1995: An Experimental Study of the Infuence of Oxygen Fugacity on Fe-Ti Oxide Stability, Phase Relations and Mineral-Melt Equilibria in Ferro-Basaltic Systems. *Journ Petrol* 36 (5): 1137-1179.
- Vanko DA, Stakes DS, 1991: Fluids in oceanic layer 3: Evidence from veined rocks, Hole 735B, Southwest Indian Ridge. *Proc Ocean Drill Prog Sci Res* 118: 181-215..
- Wager LR, Brown GM, Wadsworth WJ, 1960: Types of igneous cumulates. *Journ Petrol* 1: 73-85.
- Weaver and Langmuir CH, 1990: Calculation of phase equilibrium in mineral-melt systems. *Computers and Geosciences*, 16 (1): 1-19.
- Whitehead JM, Dick HJB, Schouten H, 1984: A mechanism for magmatic accretion under spreading centers. *Nature* 312: 146-148.
- Yang HJ, Kinzler RJ, Grove TL (1996) Experiments and models of anhydrous, basaltic olivine-plagioclase-augite saturated melts from 0.001 to 10 kbar. *Contrib Mineral Petrol*, 124 (1): 1-18.

Chapter 4

Dissolution Kinetics of Oceanic Lower Crust

Abstract

We have carried out dissolution experiments using natural olivine, plagioclase and clinopyroxene, and equilibrium melting experiments on synthetic cumulate gabbro compositions to quantify the melting kinetics of oceanic gabbros. Dissolution experiments were carried out using olivine – plagioclase and clinopyroxene - plagioclase mineral pairs over the temperature range of 1330 - 1220 °C at the quartz-fayalite-magnetite buffer for durations of 0.25 to 24 hours. Isothermal experiments performed over the temperature range of 1230 – 1105 °C defined the equilibrium phase relations in the system. Dissolution mechanisms are similar to those found in other experimental studies that utilized end-member mineral compositions. The experimental results are used to assess the extent to which dissolution of cumulate igneous rocks from the oceanic lower crust will produce disequilibrium melts compositions. The efficiency of the reaction is dependent on the area of grain-boundaries between different minerals in a rock that is reheated. Coarse-grained rocks (>3mm) will disintegrate internally upon reheating, whereas finer grained rocks will melt from the outside in. If these disequilibrium melts are allowed to mix into the ascending magma, the new magma will have higher Na_8 and lower Fe_8 than the original. Lower crustal assimilation of gabbro will result in the destruction of troctolites in the lower crust, and will lead to the early onset of high-Mg# olivine-gabbros.

1. Introduction

The oceanic lower crust is dominated by olivine gabbro, generally composed of olivine, plagioclase and augite (Coleman, 1977). It is commonly accepted that this lower crust is formed by crystallization of basaltic magmas that ascend from the upper mantle. However, there are two main lines of thought on the geodynamic method of accretion of

Evolution of Oceanic Gabbros: In-situ and Ancient Examples

the lower ocean crust. One is the so-called "gabbro glacier" model, whereas the other is the "many sills" model. The former end-member is based on observations in ophiolites (Sleep, 1975; Dewey and Kidd, 1977 and Quick and Denlinger, 1993), and developed further to account for geophysical observations at the East Pacific Rise (EPR) and other magmatically robust spreading segments (Henstock et al., 1993; Phipps Morgan and Chen, 1993). The gabbro-glacier model assumes that melt arrives directly from the upper mantle to a shallow melt sill, where it crystallizes gabbro cumulates that subsequently flows downwards in a near steady-state fashion. The many sills model (Pedersen, 1986; Bédard et al, 1988, 1991, 1993; Boudier et al., 1996; Kelemen et al., 1997b; Korenaga and Kelemen, 1997) postulates that the lower crust is accreted by the injections of individual sills that fractionate in-situ and eject their melt to higher levels. Thus, particularly for the fast-spreading ridges, the lower crust is accreted within the lower crust. Modifications of this latter model are generally favored for slow-spreading ridges.

In general, truth probably lies between the gabbro glacier and the many sills model (MacLennan et al., 2004). In either case, the extent to which the lower ocean crust interacts with subsequent ascending magmas is largely unknown. The rate of assimilation is naturally dependent on the heat available to incorporate and melt pre-existing cumulates into magma, and the residence time of the magma in the lower crust. The effect of the composition and grain-size of the assimilant, thus the compositional effects on the magma and lower crust, has not yet been established for the oceans.

The potential temperature of the melts generated in the upper mantle at mid ocean ridges could range from 1180°-1510°C (Klein and Langmuir, 1987; Kinzler and Grove, 1992), although other authors would disagree, arguing that the temperature is constant around 1250°C (e.g. Green et al, 2000; Presnall, 2002). The upper end of the temperature spectrum represents the fast spreading EPR. It has been documented that the EPR has a shallow axial magma chamber (AMC) (Detrick et al., 1987) that lies on a low velocity zone (Harding et al., 1989; Vera et al., 1990). Dunn et al. (2000) showed a 5-8 km wide low velocity zone under the spreading center of the EPR has as much as 20 % melt fractions within it. A second melt lens has been documented near the seismic Moho

Evolution of Oceanic Gabbros: In-situ and Ancient Examples

transition (Crawford and Webb, 2002); it has been argued that its stability is limited, as any crystallization in the chamber causes the surroundings to heat up and melt the surroundings in a manner that is not observed (Chen, 2001). The EPR therefore clearly has a heat-budget that is large enough to remelt lower crustal material. At intermediate-spreading ridges, the AMC reflector is found at deeper levels in the crust (Phipps Morgan and Chen, 1993b; Chen and Lin, in press). The existence of shallow steady-state magma-chambers at slower ridges is indeed debated (Sinton and Detrick, 1992), and very deep magma chambers below the conductive boundary-layer in the mantle (Mével et al., 2002) would not be possible to detect with the seismic techniques available today (Detrick and Reeves-Sohn, pers comm. 2004). Erupted MORB show extensive differentiation and mixing that require that magma chambers exist, even if only ephemerally. The evidence of magma-chamber type processes happening before eruption at all ridges, suggest that there should be sites that are hot enough to dissolve preexisting crustal material even if the magma-lenses evade us along the slower ocean ridges. Therefore, the magmas likely reside for long enough to interact with their surroundings in either steady state- or ephemeral magma chambers.

Ocean islands are also sites of elevated magma-temperatures (Watson and McKenzie, 1991). In fact, there are Hawaiian picrites that record crystallization temperatures in excess of 1400°C (Natland, pers comm. 2004). In Hawaii post-shield volcanism of very different composition develops after the earlier shield-stage lavas. Their isotopes are more like those of mid-ocean crust, and they are frequently very alkaline in composition (Yang et al., 2003). The post-shield lavas often contain xenoliths made out of the pre-existing, tholeiitic, lower-crust that had to be penetrated to get to the surface (Fodor and Galar, 1997; Neumann et al., 2000). This suggests that the post-shield stage magmas, which spend more time in the lower crust than the shield-stage magmas, may have digested some lower crustal material on ascent.

The lower crust is generally difficult to study at fast-spreading ridges and ocean islands due to the 2+ km of dikes and lavas that cover it and the lack of tectonic windows. However, the lower crust is often exposed in tectonic windows at slow-spreading ridges

Evolution of Oceanic Gabbros: In-situ and Ancient Examples

(Tucholke and Lin, 1998). The gabbroic outcrops on Atlantis Bank at the slow Southwest Indian Ridge have been studied extensively (Dick et al., 2000; Natland and Dick, 2000, and references therein). Even the most primitive, ophitic, gabbros sampled in the bank have high-Mg augite oikocrysts surrounding more evolved plagioclase chadacrysts with which they are not in equilibrium at magmatic temperatures (Chapter 3, this thesis). Nearly all these rocks have petrologic characteristics that provide strong evidence for complex magmatic histories that may involve several magmas and potential remelting.

The purpose of this study is to constrain on the processes of magma – cumulate interaction that occurs within the oceanic crust. We have therefore investigated the kinetics of melting between natural mineral-pairs representative of the those found in lower ocean-crustal rocks; finding rapid melting rates and unusual melt-compositions. Unlike previous dissolution-experiments, our mineral compositions are similar to those at mid-ocean ridges. Therefore, the melts produced in the experiments allow us to assess the chemical changes that incorporation of lower crustal material may cause in the ascending magmas.

2. Experimental Procedures

During the course of this study, we performed two types of experiments. The first type was dissolution-experiments on olivine-plagioclase and augite-plagioclase mineral pairs designed to provide information on the mineral melting kinetics in ocean gabbro cumulates. Second, in order to quantify the kinetic controls on melting, we also determined the solidus to near-liquidus phase relations of two synthetic CMASNF (CaO – MgO – Al₂O₃ – SiO₂ – Na₂O – FeO) olivine – plagioclase – clinopyroxene cumulate-compositions that represented bulk compositions applicable to the mineral pairs used in the dissolution experiments.

Evolution of Oceanic Gabbros: In-situ and Ancient Examples

Table 1: Theoretical starting composition isothermal experiment, in weight %		
Label	Melt Fo	Melt AK3
SiO ₂	53.1	50.6
Al ₂ O ₃	17.7	14.7
FeO	3.2	6.7
MgO	7.0	12.0
CaO	16.1	13.4
Na ₂ O	2.9	2.4
Total	100	100
Mg#	79.7	76.1
Ca#	75.5	75.5

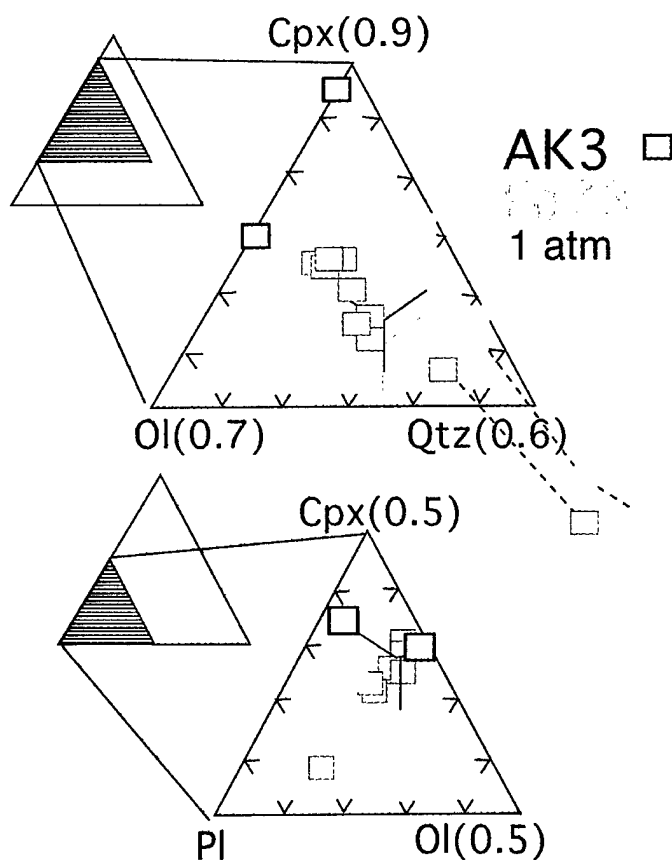


Figure 4-1: Pseudoternary projection-plots of the melt compositions of the isothermal phase-equilibrium experiments (projection from Grove et al., 1992). Cpx=augite, ol=olivine, qtz=quartz, pl=plagioclase. Open squares represent AK3, closed gray squares are Fo73. The inferred phase-saturation boundaries are indicated on the figures for reference. The Cpx-ol-qtz projection shows how the low-temperature experiments plot below the olivine-plagioclase-clinopyroxene-melt saturation-boundary for the basaltic system, towards more silicic compositions. Fo73 has a very small olivine component, whereas AK3 generally follows the trends for basalts.

2.a. Phase equilibrium experiments

Starting material - Phase equilibrium experiments were performed on two model olivine-gabbro compositions, "AK3" and "Fo73" (Table 4-1) where the former has the larger olivine component. Mechanical mixtures of each composition were prepared from high-purity oxides and silicates ground in an agate mortar under ethanol for 6 hours. Pressed pellets of AK3 or Fo73 powdered mix were sintered onto a 0.8 mm diameter Pt_{91.93}-Fe_{7.9} loop that was chosen to minimize Fe exchange with the pellet. The loop and pellet were suspended in the hotspot of a Deltech DT31VT vertical gas-mixing furnace. We controlled the oxygen fugacity by mixing CO₂ and H₂ gases and f_{O_2} was monitored using a solid ZrO₂-CaO electrolyte O sensor calibrated against the Fe-FeO, Ni-NiO, and Cu-Cu₂O buffers. Temperature was measured using a Pt-Pt₉₀Rh₁₀ thermocouple calibrated against the melting points of NaCl, Au and Pd on the IPTS 1968 temperature scale. The thermocouple junction was placed immediately adjacent to the experimental charge, and temperatures are believed to be accurate within $\pm 2^\circ\text{C}$. The experiments were carried out at 0.1MPa, with oxygen fugacity buffered at quartz – fayalite – magnetite (QFM) from near-solidus- to near-liquidus temperature. Experiments were run at constant temperature for 5 to 119 hrs, and were terminated by drop-quenching into a water bath. The results are listed in Table 4-2 (a, b and c).

Volatilization of sodium from the experimental charge, and mass transfer of iron between the experimental charge and wire loop can be significant in 0.1MPa experiments. We attempted to minimize the iron exchange by using a loop containing ~8 wt% iron, making it in equilibrium with tholeiite at QFM over the temperature interval of 1100°C to 1400°C (Grove, 1981). Sodium volatilization is related to sample size, gas flow rate, oxygen fugacity, experimental duration and experimental temperature (Tormey et al., 1987). As a result, we used larger sample sizes (100mg) and lower gas-flow rates (0.1ml/s) to reduce sodium volatilization.

Table 2A: Results of isothermal Fo73 experiments.

Temperature°C	1190	1175	1165	1150	1135	1120	1105					
Glass												
SiO ₂	56.6	.15	59.8	.49	59.5	.41	60.4	.49	66.9	1.11	71.1	.73
Al ₂ O ₃	15.1	.09	14.1	.12	14.7	.33	13.8	.10	13.9	1.02	11.9	.44
FeO	4.6	.15	5.6	.23	5.8	.34	6.7	.27	4.0	.30	2.5	.44
MgO	6.9	.06	4.7	.18	5.4	.16	4.5	.08	3.1	.46	1.4	.40
CaO	14.4	.11	11.0	.15	11.4	.27	10.9	.08	8.2	.92	6.1	.79
Na ₂ O	2.1	.10	2.8	.12	2.7	.08	2.6	.07	2.1	.40	2.2	.21
Total	99.7	98.2	99.4	98.9	98.2	95.1						
Mg#	73.0	59.8	62.2	54.5	58.0	49.5						
Ca#	79.1	68.7	70.1	69.9	67.9	60.8						
Augite												
3 px (15)	54.4	.94	54.2	.95	55.0	1.14	53.9	.94	53.5	.98	56.3	1.34
1 px (10)	2.1	1.17	2.3	.85	2.5	1.37	1.8	.48	2.6	2.01	3.4	2.73
Al ₂ O ₃	2.7	.20	3.6	.68	3.9	.34	5.0	.62	4.5	.61	4.5	3.0
FeO	17.5	.64	16.4	.64	17.2	1.00	16.0	.52	15.3	1.05	13.3	6.5
MgO	23.6	.53	22.4	1.25	21.6	1.30	22.8	1.16	22.4	1.26	21.9	13.6
CaO	0.1	.04	0.3	.14	0.3	.24	0.2	.06	0.4	.23	0.5	23.5
Na ₂ O	100.4	99.2	99.2	100.4	100.4	99.7	99.7	98.7	98.7	99.8	101.2	0.5
Total	92.0	89.1	88.6	85.0	85.7	84.1						78.8
Mg#	92.0	89.1	88.6	85.0	85.7	84.1						
Plagioclase												
3 pl (12)	49.5	1.55	51.2	1.61	53.4	.96	53.9	.98	53.7	3.88	56.3	56.1
1 pl (9)	31.3	1.65	29.6	2.04	29.0	.92	28.5	.90	26.7	3.98	27.0	27.5
Al ₂ O ₃	0.6	.27	0.8	.34	0.5	.13	0.5	.13	1.1	.46	0.3	0.3
FeO	0.9	.49	0.8	.46	0.6	.12	0.4	.16	1.8	1.35	0.3	0.2
MgO	16.1	.81	14.5	.76	13.1	.47	13.0	.67	14.5	1.55	11.3	11.5
CaO	2.0	.49	2.8	.40	3.6	.19	3.6	.23	2.5	.54	4.3	4.4
Na ₂ O	100.5	99.7	99.7	100.2	100.2	99.8	99.8	100.4	100.4	99.4	99.9	99.9
Total	81.4	74.1	66.7	66.7	76.6	59.2						59.0
Ca#	81.4	74.1	66.7	66.7	76.6	59.2						

Notes: gl=glass, px=augite, pl=plagioclase, ol=olivine, pig=pigeonite

Notes: gl=glass, px=augite, pl=plagioclase, ol=olivine, pig=pigeonite

Evolution of Oceanic Gabbros: In-situ and Ancient Examples

Table 2B: Results of isothermal AK3 experiments

Table 2B: Results of isothermal AK3 experiments																						
Temperature°C	1230	1210	1197	1190	1190	1190	1170	1170	1150	1130	1110											
Glass	4 gl (10)	σ	2 gl (10)	σ	7 gl (13)	σ	1 gl (13)	σ	1 gl (11)	σ	3 gl (10)	σ	5 gl (8)	σ	10 gl (11)	σ	8 gl (8)	σ	6 gl (6)	σ	9 gl (6)	σ
SiO ₂	52.23	0.27	51.95	0.38	52.86	0.24	53.26	0.47	53.11	0.33	52.46	0.40	54.50	0.40	54.55	0.21	55.62	0.62	57.75	1.28	70.32	0.60
Al ₂ O ₃	15.12	0.14	15.52	0.13	15.07	0.29	14.72	0.15	14.38	0.13	14.53	0.17	14.27	0.14	14.36	0.10	14.69	1.22	14.50	3.46	13.54	0.72
FeO	6.30	0.23	6.45	0.30	6.97	0.24	7.27	0.33	8.17	0.32	7.92	0.23	8.08	0.22	9.21	0.19	9.31	0.40	8.08	1.55	5.00	0.39
MgO	10.82	0.07	10.16	0.16	9.61	0.17	8.41	0.24	8.56	0.19	9.16	0.19	7.73	0.13	7.88	0.10	6.43	1.13	5.49	1.85	3.14	0.88
CaO	14.01	0.20	14.20	0.15	14.24	0.25	12.16	0.48	12.95	0.19	13.55	0.23	11.63	0.16	11.84	0.07	10.30	0.36	10.89	0.88	6.16	0.34
Na ₂ O	1.74	0.15	1.57	0.11	1.64	0.09	1.84	0.13	1.81	0.19	1.95	0.07	2.32	0.16	1.85	0.07	3.24	0.25	2.08	0.36	3.03	0.79
Total	100.2		99.8		100.4		97.7		99.0		99.6		98.5		99.7		99.6		98.8		101.2	
Mg#	75.4		73.7		71.1		67.4		65.1		67.3		63.0		60.4		55.2		54.8		52.9	
Ca#	81.6		83.4		82.7		78.5		79.8		79.4		73.5		71.9		63.7		74.3		52.9	
Augite	7 px (10)	σ	1 px (14)	σ	1 px (10)	σ	1 px (10)	σ	1px (10)	σ	3px (10)	σ	5px (10)	σ	10 px (9)	σ	8 px (8)	σ	6 px (5)	σ	9 px (3)	σ
SiO ₂	55.1	0.48	51.9	0.77	53.7	0.01	53.6	1.01	53.6	0.88	54.5	0.55	54.4	0.64	54.7	0.31	55.1	0.21				
Al ₂ O ₃	2.0	0.56	4.1	0.85	3.4	0.05	4.3	1.56	3.4	0.72	3.4	0.58	2.2	0.44	1.6	0.33	3.2	1.71				
FeO	3.6	0.10	4.8	0.39	4.7	0.01	4.5	0.84	4.6	0.70	5.9	0.85	6.9	0.44	7.6	0.96	7.2	1.44				
MgO	20.2	0.59	18.1	1.09	19.4	0.18	18.3	1.07	18.5	1.11	16.8	0.60	18.1	0.52	17.9	0.85	16.2	2.64				
CaO	20.0	0.61	20.7	1.43	19.5	0.97	21.2	1.26	20.1	1.94	20.4	0.80	19.1	0.99	18.8	1.76	20.1	2.41				
Na ₂ O	0.2	0.04	0.1	0.07	0.2	1.70	0.2	0.12	0.2	0.15	0.4	0.07	0.3	0.05	0.2	0.06	0.7	0.34				
Total	101.1		100.9		100.9		100.3		100.5		101.4		100.9		100.7		102.5					
Mg#	90.8		87.1		88.0		87.8		87.8		83.4		82.5		80.7		80.1					
Plagioclase	2pl (10)	σ	7 pl (10)	σ	1 pl (13)	σ	1pl (10)	σ	3pl (10)	σ	5pl (7)	σ	10 pl (9)	σ	8 pl (7)	σ	6 pl (3)	σ	9 pl (2)	σ		
SiO ₂	47.0	0.48	47.8	0.79	47.5	1.56	48.2	1.23	47.0	0.75	49.0	0.65	47.9	1.19	54.5	0.86	52.6	2.29				
Al ₂ O ₃	33.5	0.14	31.8	0.19	31.3	0.29	30.6	0.57	31.1	0.25	30.6	0.17	31.0	0.56	27.4	0.20	26.1	1.45	24.5	0.11		
FeO	0.7	0.19	0.9	0.29	1.3	0.39	1.4	0.67	1.7	0.64	0.9	0.51	1.6	0.77	1.0	0.52	2.4	0.38	1.0	2.58		
MgO	0.5	0.00	1.0	0.02	1.4	0.02	1.3	1.2	0.00	1.0	0.00	1.5	0.00	1.1	0.03	2.5	0.02	2.6	0.02			
CaO	16.9	0.46	16.7	0.56	16.2	0.47	16.2	0.47	16.5	0.84	15.0	0.66	16.2	0.38	12.1	0.66	12.8	0.46	10.5	0.64		
Na ₂ O	1.7	0.02	1.7	0.03	1.7	0.03	1.9	0.01	1.7	0.03	2.6	0.03	1.6	0.05	4.8	0.03	2.8	0.05	5.5	0.06		
Total	100.5		99.9		99.3		99.5		99.2		99.1		99.8		100.9		99.3		101.5			
Mg#	84.6		84.5		84.4		82.8		84.1		76.2		83.8		58.4		71.7		51.2			
Olivine	4ol (10)	σ	2ol (10)	σ	7 ol (10)	σ	1 ol (15)	σ	3ol (10)	σ	5ol (11)	σ	10 ol (10)	σ	8 ol (8)	σ	9 plg (1)	σ				
SiO ₂	40.9	0.31	40.6	0.28	40.2	0.17	39.7	0.24	40.3	0.45	39.7	0.35	39.4	0.44	39.7	0.32	54.7	2.29				
Al ₂ O ₃	0.1	0.01	0.1	0.16	0.1	0.02	0.1	0.08	0.1	0.15	0.1	0.11	0.15	0.1	0.05	0.5	0.27	0.9				
FeO	7.3	0.53	8.4	0.43	9.8	0.24	11.4	0.41	12.0	0.29	10.0	0.30	13.3	0.38	15.5	0.22	20.0	0.47				
MgO	51.2	0.58	50.2	0.76	49.6	0.31	47.9	0.31	47.1	0.36	48.7	0.56	45.5	0.43	44.6	0.30	40.5	0.57				
CaO	0.4	0.03	0.5	0.18	0.5	0.03	0.5	0.05	0.4	0.11	0.6	0.25	0.4	0.03	0.6	0.18	0.1	0.1				
Na ₂ O																						
Total	100.0		99.8		100.2		99.6		99.6		99.2		100.0		101.3		100.9					
Mg#	92.6		91.4		90.0		88.2		87.5		85.9		83.7		78.3		75.9					

Notes: ol=olivine, pl=plagioclase, ol=olivine, plg=nepheline

Notes: gl=glass, px=augite, pl=plagioclase, ol=olivine, plg=pigeonite

Evolution of Oceanic Gabbros: In-situ and Ancient Examples

Table 2C: Results of isothermal phase-equilibrium experiments.

Experiment#	Temperature °C	Duration (hr)	Pressure (kbar)	Sum R ²	Minerals	Mineral	Kd ^{Fe/Mg} cpx	Kd ^{Ca/Na} pl	Kd ^{Fe/Mg} ol	Kd ^{Fe/Mg} pig	Mg# gl	Ca# gl	Mg# cpx	Fo ol	An pl
AK3-4	1230	5.5	0.1	0.75	gl(94.9)pl(3.2)				0.25		75.4	81.7		92.6	
AK3-2	1210	6	0.1	0.67	gl(93.3)pl(0.5)pl(5)			1.10	0.26		73.7	83.4		91.4	84.6
AK3-7	1196	6	0.1	0.50	gl(83.1)cpx(0.9)pl(6.9)pl(7.5)		0.25	1.14	0.27		71.1	82.8	90.8	90.0	84.5
AK3-1	1190	14	0.1	0.50	gl(57.4)cpx(13.4)pl(19.7)ol(8.9)		0.25	1.21	0.27		65.1	79.9	88.0	87.5	82.8
AK3-3	1190	6.25	0.1	0.50	gl(70.2)cpx(7.9)pl(13.6)ol(8.1)		0.29	1.38	0.24		67.3	79.4	87.8	89.7	84.2
AK3-5	1170	16.5	0.1	0.50	gl(43.9)cpx(19.7)pl(25.1)ol(10.3)		0.24	1.16	0.28		63.0	73.5	87.8	85.9	76.3
AK3-8	1150	15	0.1	0.50	gl(4)cpx(33)pl(47)ol(13)		0.26	0.80	0.34		55.2	63.7	82.5	78.3	58.4
AK3-6	1130	6	0.1	0.65	gl(3)cpx(46)pl(46.4)		0.29	0.88			54.8	74.3	80.7		71.8
AK3-9	1110	20	0.1	0.49	gl(-30)cpx(25)pl(71)pl(31)		0.28	0.93		0.36	52.9	52.9	80.1		51.2

Experiment#	Temperature° C	Duration (hr)	P (kbar)	Sum R ²	Minerals	Kd ^{Fe/Mg} cpx	Kd ^{Ca/Na} pl	Mg# gl	Ca# gl	Mg# cpx	An pl
Fo73-3	1190	70.5	0.1	1.45 (0.11)	gl(53.3)cpx(15.5)pl(29.5) gl(51.5)cp	0.24	1.16	73.0	79.1	92.0	81.4
Fo73-1	1175	95	0.1	1.44 (0.57)	gl(19.9)cpx(31.9)pl(47.1) gl(19.1)cp	0.18	1.30	59.8	68.7	89.1	74.1
Fo73-2	1165	69	0.1	1.58 (0.47)	gl(8.9)cpx(36.1)pl(52.8) gl(3.5)cpx(3	0.21	0.85	62.2	70.1	88.6	66.7
Fo73-4	1150	71	0.1	1.38	gl(5.3)cpx(37)pl(56)	0.21	0.86	54.5	69.9	85.0	66.7
Fo73-5	1135	119	0.1	2.74 (1.3)	gl(5.5)cpx(33.3)pl(59) gl(5.4)cpx(33	0.23	1.54	58.0	67.9	85.7	76.6
Fo73-6	1120	45	0.1	2.57(1.06)	gl(-13.1)cpx(46.9)pl(64.1) gl(-13.2)c	0.19	0.94	50.6	60.8	84.1	59.2
Fo73-7	1105	72	0.1	3.09	cpx(40.5)pl(56.6)					78.8	59.0

Notes: gl=glass, ol=olivine, cpx=augite, pl=plagioclase, pig=pigeonite. All analyses done using natural mineral standards at the MIT electron microprobe, as mentioned in the text.

2.b. Mineral Dissolution Experiments

Two sets of mineral pairs were used in these experiments (Table 4-3). The first consisted of clinopyroxene (Mg# 82-84), and plagioclase (An₆₀ and An₅₄). The second set of experiments used An₆₀ plagioclase and Fo₇₃ olivine; or An₅₄ plagioclase with Fo₈₂ olivine. The experiments were carried out over a the temperature range of 1240-1330 °C for the olivine – plagioclase pairs and 1180-1300 °C for the plagioclase – clinopyroxene pairs. The duration of the experiments varied from 15 minutes to 24 hours (Table 4-4).

The An₆₂ plagioclase, the Fo₇₃ olivine and the augite were sampled from olivine gabbros of homogeneous compositions from Atlantis Bank, Southwest Indian Ridge, ODP Hole 735B, at ~1400 m depth (Natland and Dick, 2002). Due to the limited availability and grain-size of the material from the Southwest Indian Ridge, we selected alternative sources of plagioclase and olivine, in order to run longer experiments. The An₅₄ plagioclase was sampled from a single crystal from the layered Bjerkreim-Sokndal intrusion in Southwestern Norway. The Fo₈₂ olivine is from a granular dunite from the Balmuccia lherzolite massif, Italy (Rivalenti, 1980). Although the An₅₄ plagioclase and the Fo₈₂ olivine are not exactly the compositions expected from a gabbro from the ocean crust, they are desirable as they are natural materials with more appropriate compositions compared to synthetic endmembers of the solid solution series.

Sample preparation and experimental procedures Each mineral was cut with a diamond wafering-saw into parallelepipeds of roughly the same width. No attempt was made to select a specific crystallographic orientation for any of the minerals. One side of each piece were polished with Al₂O₃-paper and diamond pastes to 5 μ m grit. The thickness of each mineral-piece was measured with a micrometer to a precision of ~10 μ m perpendicular to the polished surface. The mineral pairs were placed together with the polished surfaces in contact, and tied with a 0.8mm diameter Pt wire. Each experiment was held at a constant temperature at the QFM buffer for a specified time in the hotspot of a Deltech DT31VT vertical gas-mixing furnace. Each experimental assembly achieved thermal equilibrium within 5 minutes or less after being positioned in the hotspot. The beginning of dissolution was measured from that point on until the

Evolution of Oceanic Gabbros: In-situ and Ancient Examples

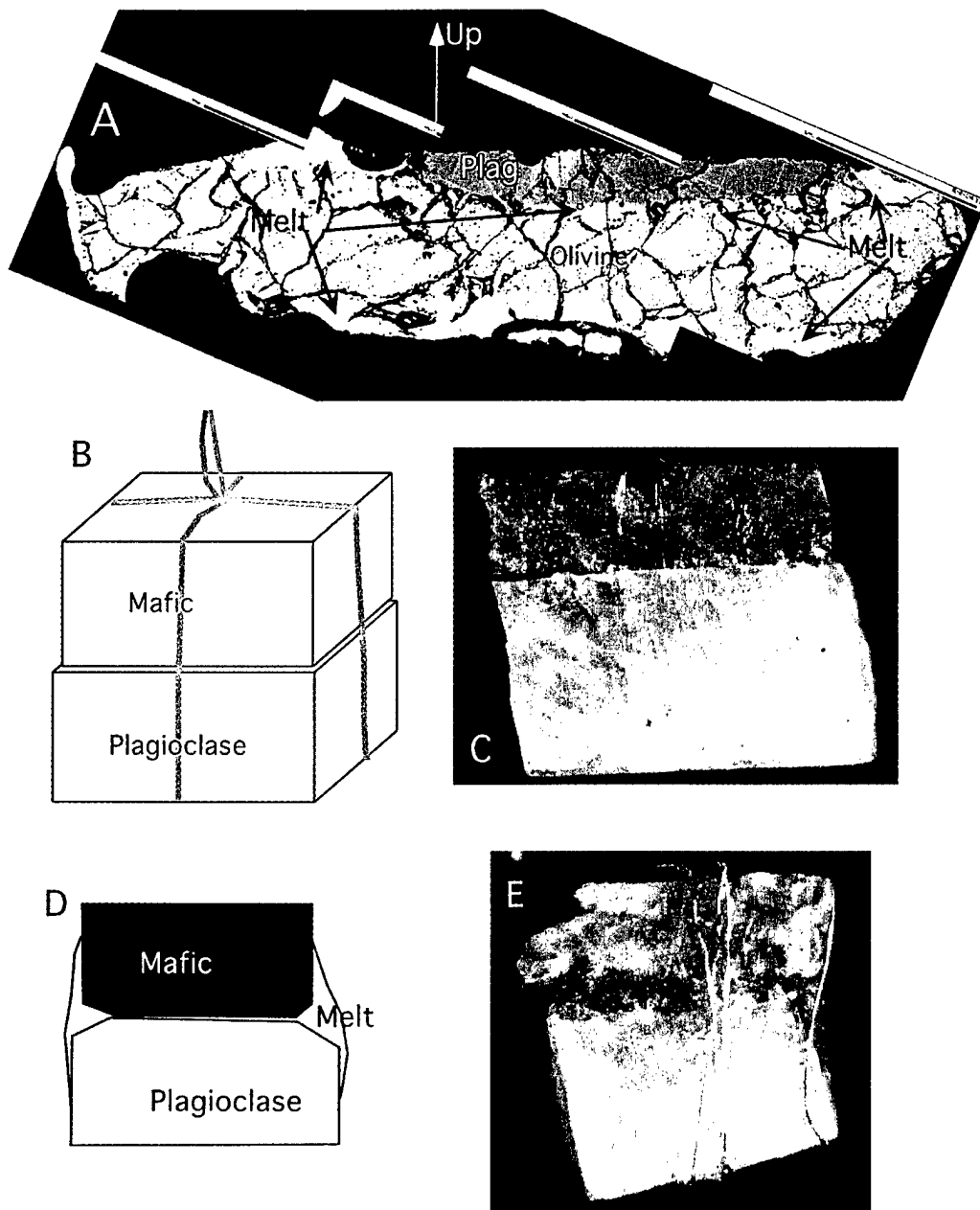


Figure 4-2: The experimental setup. A: Composite back-scatter electron image an early plagioclase-olivine experiment. Early experiments were performed with the plagioclase on top of olivine, causing the interfacial melt to become thicker due to plagioclase floatation. The melt produced is pressed to the sides of the interface and wraps the crystals. B: A latter experiment performed with the mafic mineral on top of plagioclase, wrapped with a platinum quenching wire. C: The appearance of an experiment before melting. D: Schematic cross-section of the experiments after melting. The melt is produced at the interface between the minerals and at the immediate corners, and is pressed out to the sides. E: The appearance of an experiment after melting. The melt clearly wraps the outside of the mineral.

Evolution of Oceanic Gabbros: In-situ and Ancient Examples

Table 3: The composition of the starting material for the dissolution experiments.

Element	Whole-rock analysis, sample 1		Plag1a	Plag1b	Plag 2	Augite 1a	Augite 1b	Augite 2	Olivine 1a	Olivine 1b	Olivine 2
SiO ₂	52.1	SiO ₂	53.5	53.3	55.2	52.3	52.1	52.7	38.5	38.1	41.0
TiO ₂	0.4	TiO ₂				.57	.56	1.20			
Al ₂ O ₃	15.4	Al ₂ O ₃	29.4	30.0	28.9	2.88	3.28	2.70	.02	.01	.19
FeO(tit)	4.0	Cr ₂ O ₃				.065	.304	.181	.004	.002	.078
Fe ₂ O ₃	0.8										
FeO*	4.7	FeO	.33	.34	.19	6.5	6.5	5.5	24.0	23.7	15.7
MnO	0.1	MnO				.20	.16	.18	.37	.36	.20
MgO	9.5	MgO	.04	.02	.01	17.13	16.80	16.28	38.11	38.32	44.06
CaO	15.4	CaO	12.1	12.6	10.8	19.9	20.1	22.3	.07	.05	.12
Na ₂ O	2.3	Na ₂ O	4.82	4.57	4.93	.35	.37	.36			
K ₂ O	0.0	K ₂ O	.06	.06	.33			.01			
P ₂ O ₅	0.0	NiO						.04	.03	.03	
Total	100.0	Total	100.2	100.8	100.2	99.9	100.1	101.5	101.0	100.6	101.4
V (ppm)	220	An%	57.9	60.1	54.7						
Cr (ppm)	272	Mg#				82.4	82.2	84.1	73.9	74.2	83.3
Ni (ppm)	81	Wo				42	42	46			
Cu (ppm)	50	En				50	49	47			
Zn (ppm)	31	Fs				8	9	7			
Rb (ppm)	1	Notes: Plag=plagioclase. All minerals used are natural mineral separates cut from Hole 735B and other sites as mentioned in the text. The mineral compositions were determined on the MIT electron microprobe Minerals 1a, 1b and 2 refers to those used in the AK00- AK01- and AK3K- experiments. An is Anorthite % of plagioclase, calculated from the molar Ca/(Ca+Na). Mg# is the molar Mg/(Mg+Fe) of clinopyroxene. Fo is forsterite content of olivine, and is calculated as Mg#.									
Sr (ppm)	150										
Y (ppm)	14										
Zr (ppm)	26										
Nb (ppm)	1.0										

Mg# is the molar Mg/(Mg+Fe) of clinopyroxene. Fo is forsterite content of olivine, and is calculated as Mg#.

All values are in wt% unless otherwise noted. The whole-rock analysis is from Coogan et al, 2000.

Evolution of Oceanic Gabbros: In-situ and Ancient Examples

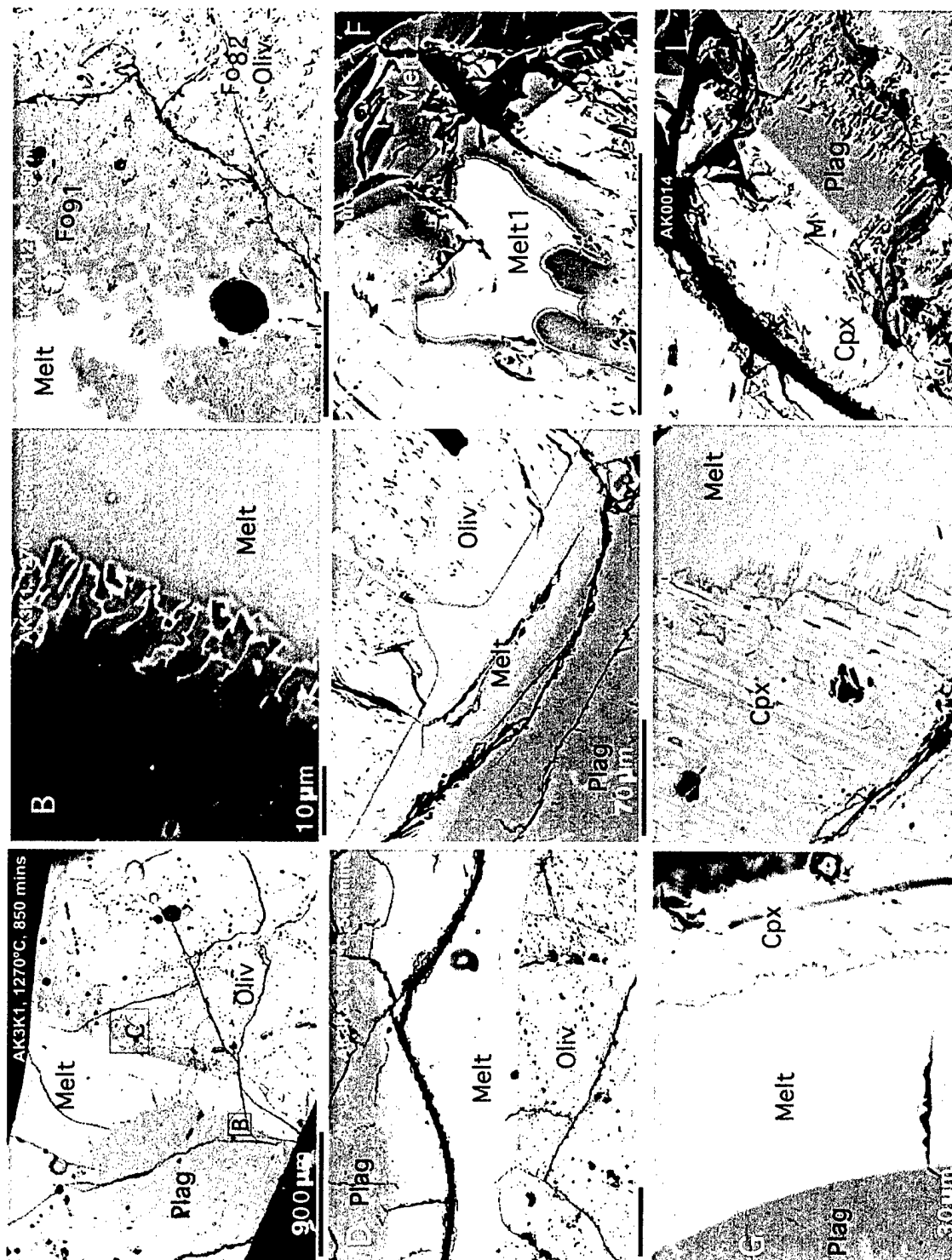


Figure 4-3: Back-scatter electron images of cross-sections through dissolution experiments. A: A1/4 cross-section through the experiment shown in 2E. The bottom edge is the center. The interface between the minerals is smooth, and the corners of the minerals are melted. Impurities inside the natural olivine have caused some melting in the olivine (light color), but this does not effect the general dissolution rate. B: Inset in A; the reaction surface between plagioclase and melt is very narrow, although jagged. C: inset in A; there is some recrystallized olivine at its corner, and this olivine has a very high forsterite content. D: The general appearance of the plagioclase-melt-olivine interface. Note the weakly undulating surfaces and the lack of Fe-Mg diffusion in the olivine indicated by a lack of significant color variations. E: Preferential dissolution occurs at an olivine grain boundary, though this does not affect the overall dissolution rate. F: Color variations adjacent to a melt pocket (Melt 1) inside olivine shows strong re-equilibration with the host, although the adjacent melt disk (Melt 2) is less than 2 μ m away and in complete disequilibrium with the olivine. G: The interface melts between plagioclase and augite (cpx). The orthopyroxene exsolution lamellae in augite do not appear to affect the general dissolution at the interface. Note also how smooth the surface of plagioclase is, possibly because of the high Ca# of the melt. H: Higher temperature experiments see some melting inside the augite, although this does not affect the general interface. The perpendicular crystals are from quenching. I: The smooth interface to the melt-disk between plagioclase and augite is clear even when the lamellae are almost perpendicular to the surface.

Evolution of Oceanic Gabbros: In-situ and Ancient Examples

experiment was terminated. The experiments were quenched in air, as it was discovered that very little quench-growth was produced compared to the experiments that were quenched in a water-bath. The sample assembly was cast in epoxy and cut perpendicular to the mineral-melt interface. The thickness of each mineral was measured using a microscope and the same micrometer as before in the center of each experiment after 5 μ m grit polishing. Finer polishing caused the plagioclase and glass to become almost indistinguishable in reflected light. In addition, the thickness of each mineral was measured in the electron microprobe using backscatter-electron imaging. Both measurement techniques produced similar results. The measurements of mineral thickness after each experiment probably have the largest errors, because the shapes of the partly dissolved minerals were not always uniform. Thus, we estimate the error in thickness and measurements of each side of the experimental charge based on repeated measurements to be ~5% relative. The absolute errors are smaller for the experiments that melted less, as the interfaces were smoother and the geometry simpler. No attempt was made to account for dissolution during heating or quenching, as this effect is small compared to the precision of the thickness measurements.

2.c. Analytical techniques

Phase compositions were analyzed with the MIT 4 and 5-spectrometer JEOL 733 Superprobes, using 15kV accelerating voltage and 10nA beam current. Beam-size is 10 μ m for glass analyses, except for some of the lower temperature experiments where only small glass-pockets were available, and 1 μ m for crystalline phases. In addition, the large mineral grains used in the dissolution experiments were analyzed with a 10 μ m beam. Counting times were 10-40 s depending on the elements. Data were reduced with the CITZAF correction package using the atomic number correction of Duncumb and Reed, the absorption coefficients of Heinrich and the fluorescence correction of Reed (Armstrong, 1995).

Evolution of Oceanic Gabbros: In-situ and Ancient Examples

Table 4: Results of dissolution experiment

Table 4: Results of dissolution experiment													
Run #	Plag #	Oliv #	T (°C)	t (min)	Plagioclase thickness			Error (5%)	Olivine thickness			Total melt (μm)	
					Before (μm)	After (μm)	Melt (μm)		Before (μm)	After (μm)	Melt (μm)		
AK0019	1a	1a	1270	24	940	851	89	4	965	930	35	2	124
AK0020	1a	1a	1270	60	2314	1899	415	21	2113	1824	290	14	705
AK0021	1a	1a	1270	60	1067	684	383	19	1245	950	295	15	677
AK0025	1a	1a	1272	240	1615	1161	454	23	864	679	184	9	639
AK0104	1b	1b	1300	30	2362	528	1834	92	1242	1001	241	12	2075
AK0105	1b	1b	1300	240	2197	0	2197	110	841	508	333	17	2530
AK0106	1b	1b	1300	60	2337	818	1519	76	1144	557	587	29	2690
AK0106	1b	1b	1300	60	2337	234	2103	105	1144	557	587	29	2690
AK3K1	2	2	1270	850	4216	3011	1205	60	2088	1804	284	14	1489
AK3K2	2	2	1270	175	4191	4026	165	8	2129	2129			165
AK3K3	2	2	1270	565	2695	2225	470	23	2134	1905	229	11	699
AK3K4	2	2	1270	1320	3533	1975	1558	78	2306	2027	279	14	1837
AK3K6	2	2	1247	1080	2631	2631			2383	2383			
AK3K7	2	2	1255	1451	2631	2032	599	30	2383	1617	766	38	1365
AK3K8	2	2	1255	1118	2113	1473	640	32	2136	1588	549	27	1189
AK3K10	2	2	1330	183	4012	1629	2383	119	2357	2066	291	15	2674
AK3K11	2	2	1330	69	2431	1575	856	43	2418	2240	178	9	1034
AK3K12	2	2	1330	30	2273	1778	495	25	2413	2151	262	13	758
AK3K18	2	2	1290	91	2332	1725	607	30	2421	2210	211	11	818
AK3K5	2	2	1290	60	3782	2455	1327	66	2395	1659	736	37	2062

Notes: The errors are based on the errors in replicability of the measurements.

Plag=plagioclase, oliv=olivine, cpx=augite, t(min) =duration of the run in minutes.

Notes: The errors are based on the errors in replicability of the measurements.

Plag=plagioclase, oliv=olivine, cpx=augite. t(min) =duration of the run in minutes

Evolution of Oceanic Gabbros: In-situ and Ancient Examples

Table 4, continued: Results of dissolution experiment

Run #	Plag #	Cpx #	T (°C)	t (min)	Plagioclase thickness			Clinopyroxene thickness			Total melt (μm)
					Before (μm)	After (μm)	Error (5%)	Before (μm)	After (μm)	Melt (μm)	
AK0018	1a	1a	1270	20	1676	1494	182	940	834	106	288
AK0024	1a	1a	1271	235	1476	825	651	1697	0	1697	2348
AK0101	1b	1b	1240	60	597	448	149	991	802	189	338
AK0102	1b	1b	1240	120	643	494	149	978	738	240	389
AK0103	1b	1b	1240	840	1168	727	441	1168	426	742	1184
AK3K14	2	2	1290	104	4493	3556	937	3005	508	2497	3434
AK3K15	2	2	1280	30	2263	1956	307	2830	1778	1052	1359
AK3K16	2	2	1260	60	2294	1981	312	2916	2769	147	460
AK3K17	2	2	1260	180	2314	1880	434	2992	2362	630	1064
AK3K19	2	2	1210	670	4478	4069	409	2916	2819	97	505
AK3K21	2	2	1300	45	4036	3086	950	2974	0	2974	3924
AK3K22	2	2	1300	15	3965	3429	536	2967	2253	714	1250
AK3K23	2	2	1290	33	4018	3772	246	2817	0	2817	3063
AK3K24	2	2	1240	293	3952	3193	759	2906	2187	719	1478
AK3K26	2	2	1220	776	3828	2868	960	2819	1908	912	1872
AK3K27	2	2	1220	420	3642	3183	460	2822	2517	305	765

Notes: The errors are based on the errors in replicability of the measurements.

Plag=plagioclase, oliv=olivine, cpx=augite. t(min) =duration of the run in minutes

Evolution of Oceanic Gabbros: In-situ and Ancient Examples

Table 4 Cont: Results of dissolution experiment									
Dissolution rates (mm/s)				Errors		Dissolution rates mm ³ /s			
Run #	Plag	Olivine	Total	Plag	Oliv	Total	Plagio clase	Olivine	Total
AK0019	6.2E-6	2.4E-6	8.6E-6	3.1E-7	2.4E-6	4.3E-7	2.3E-4	9.3E-5	3.3E-4
AK0020	1.2E-5	8.0E-6	2.0E-5	5.8E-7	8.0E-6	9.8E-7	6.9E-4	4.8E-4	1.2E-3
AK0021	1.1E-5	8.2E-6	1.9E-5	5.3E-7	8.2E-6	9.4E-7	6.4E-4	4.9E-4	1.1E-3
AK0025	3.2E-6	1.3E-6	4.4E-6	1.6E-7	1.3E-6	2.2E-7	3.8E-4	1.5E-4	5.3E-4
AK0104	1.0E-4	1.3E-5	1.2E-4	5.1E-6	1.3E-5	5.8E-6	4.3E-3	5.7E-4	4.9E-3
AK0105	1.5E-5	2.3E-6	1.8E-5	7.6E-7	2.3E-6	8.8E-7	1.8E-3	2.8E-4	2.1E-3
AK0106	4.2E-5	1.6E-5	7.5E-5	2.1E-6	1.6E-5	2.9E-6	2.5E-3	9.8E-4	4.5E-3
AK0106	5.8E-5	1.6E-5	7.5E-5	2.9E-6	1.6E-5	3.7E-6	3.5E-3	9.8E-4	4.5E-3
AK3K1	2.4E-6	5.6E-7	2.9E-6	1.2E-7	5.6E-7	1.5E-7	5.3E-4	1.3E-4	6.6E-4
AK3K2	1.6E-6		1.6E-6	7.9E-8		7.9E-8	1.6E-4		1.6E-4
AK3K3	1.4E-6	6.7E-7	2.1E-6	6.9E-8	6.7E-7	1.0E-7	2.6E-4	1.2E-4	3.8E-4
AK3K4	2.0E-6	3.5E-7	2.3E-6	9.8E-8	3.5E-7	1.2E-7	5.5E-4	9.9E-5	6.5E-4
AK3K6									
AK3K7	6.9E-7	8.8E-7	1.6E-6	3.4E-8	8.8E-7	7.8E-8	2.0E-4	2.6E-4	4.6E-4
AK3K8	9.5E-7	8.2E-7	1.8E-6	4.8E-8	8.2E-7	8.9E-8	2.5E-4	2.1E-4	4.6E-4
AK3K10	2.2E-5	2.7E-6	2.4E-5	1.1E-6	2.7E-6	1.2E-6	2.3E-3	2.8E-4	2.6E-3
AK3K11	2.1E-5	4.3E-6	2.5E-5	1.0E-6	4.3E-6	1.2E-6	1.3E-3	2.8E-4	1.6E-3
AK3K12	2.8E-5	1.5E-5	4.2E-5	1.4E-6	1.5E-5	2.1E-6	1.2E-3	6.2E-4	1.8E-3
AK3K18	1.1E-5	3.9E-6	1.5E-5	5.6E-7	3.9E-6	7.5E-7	8.2E-4	2.9E-4	1.1E-3
AK3K5	3.7E-5	2.0E-5	5.7E-5	1.8E-6	2.0E-5	2.9E-6	2.2E-3	1.2E-3	3.4E-3

Notes: The errors are based on the errors in replicability of the measurements.

Plag=plagioclase, oliv=olivine, cpx=augite. t(min) =duration of the run in minutes

Table 4, continued: Results of dissolution experiment									
Dissolution rates (mm/s)				Dissolution rates mm/s					
Run #	Plag	Cpx	Total	Errors	Plag	Cpx	Total	Plag	Total
AK0018	1.5E-5	8.8E-6	2.4E-5	7.6E-7	8.8E-6	1.2E-6	5.3E-4	3.1E-4	8.3E-4
AK0024	4.6E-6	1.2E-5	1.7E-5	2.3E-7	1.2E-5	8.3E-7	5.5E-4	1.4E-3	2.0E-3
AK0101	4.1E-6	5.2E-6	9.4E-6	2.1E-7	5.2E-6	4.7E-7	2.5E-4	3.1E-4	5.6E-4
AK0102	2.1E-6	3.3E-6	5.4E-6	1.0E-7	3.3E-6	2.7E-7	1.8E-4	2.8E-4	4.6E-4
AK0103	8.8E-7	1.5E-6	2.3E-6	4.4E-8	1.5E-6	1.2E-7	2.0E-4	3.3E-4	5.3E-4
AK3K14	1.5E-5	4.0E-5	5.5E-5	7.5E-7	4.0E-5	2.8E-6	1.2E-3	3.2E-3	4.3E-3
AK3K15	1.7E-5	5.8E-5	7.5E-5	8.5E-7	5.8E-5	3.8E-6	7.2E-4	2.5E-3	3.2E-3
AK3K16	8.7E-6	4.1E-6	1.3E-5	4.3E-7	4.1E-6	6.4E-7	5.2E-4	2.5E-4	7.7E-4
AK3K17	4.0E-6	5.8E-6	9.9E-6	2.0E-7	5.8E-6	4.9E-7	4.2E-4	6.1E-4	1.0E-3
AK3K19	1.0E-6	2.4E-7	1.3E-6	5.1E-8	2.4E-7	6.3E-8	2.0E-4	4.8E-5	2.5E-4
AK3K21	3.5E-5	1.1E-4	1.5E-4	1.8E-6	1.1E-4	7.3E-6	1.8E-3	5.7E-3	7.6E-3
AK3K22	6.0E-5	7.9E-5	1.4E-4	3.0E-6	7.9E-5	6.9E-6	1.8E-3	2.4E-3	4.2E-3
AK3K23	1.2E-5	1.4E-4	1.5E-4	6.2E-7	1.4E-4	7.7E-6	5.5E-4	6.3E-3	6.9E-3
AK3K24	4.3E-6	4.1E-6	8.4E-6	2.2E-7	4.1E-6	4.2E-7	5.7E-4	5.4E-4	1.1E-3
AK3K26	2.1E-6	2.0E-6	4.0E-6	1.0E-7	2.0E-6	2.0E-7	4.4E-4	4.2E-4	8.7E-4
AK3K27	1.8E-6	1.2E-6	3.0E-6	9.1E-8	1.2E-6	1.5E-7	2.9E-4	1.9E-4	4.8E-4

Notes: The errors are based on the errors in replicability of the measurements.
 Plag=plagioclase, oliv=olivine, cpx=augite. t(min) =duration of the run in minutes

2.d. Attainment of equilibrium

Our phase equilibrium experiments were all made with synthetic compositions. Reversal experiments were not conducted and therefore equilibrium has not been demonstrated with respect to all exchange components. However, the Fe-Mg bearing crystalline phases show relatively consistent partitioning of magnesium and iron into the melt (Table 4-2B). The $Kd_{cpx/melt}^{Fe/Mg}$ is 0.27 ± 0.02 , the $Kd_{oliv/melt}^{Fe/Mg}$ is 0.27 ± 0.03 and $Kd_{plag/melt}^{Ca/Na}$ is 1.07 ± 0.2 measured in the AK3 experiments. For the Fo73 experiments $Kd_{cpx/melt}^{Fe/Mg}$ was found to be 0.21 ± 0.02 and $Kd_{plag/melt}^{Ca/Na}$ 1.11 ± 0.27 . The partition coefficients are close to the expected values from other phase-equilibrium experiments, especially at these refractory compositions (Grove and Bence, 1977; Ulmer, 1989; Grove et al., 1992). Secondly, at least for the experiments 1170°C and higher, the mineral and melt-compositions are homogeneous within the analytical uncertainty for each analyzed element. To achieve very homogeneous phases for all experiments, we would have liked to run the experiments for longer times. However, this was not practical because we wanted to minimize Na-loss in these experiments. In fact, the Fo73 experiments were run approximately 10 times longer than AK3 experiments, resulting in better exchange Kd's but at the expense of much higher Na-loss. For the purpose of comparing the equilibrium melting behavior of these mineral pairs with the dissolution behavior, however, we feel that our experiments have approached equilibrium to a sufficient extent.

3. Discussion

3.a. Experimental results

Phase Equilibrium Experiments: AK3 has olivine on the liquidus in the highest temperature experiment (1230°C), and is accompanied by plagioclase at 1210°C, and augite at 1196°C. Below the olivine-plagioclase-augite saturation boundary, at 1150°C, we produced a second set of solid compositions; augite + plagioclase followed by pigeonite. The minerals in these lower temperature experiments (<1150°C) coexist with a very silicic melt and olivine was not found at these temperatures. The Fo73

Evolution of Oceanic Gabbros: In-situ and Ancient Examples

composition was not run at temperatures higher than 1190°C, as it was obvious to us that the composition had a very low olivine component, and we therefore chose to pursue the composition with a higher olivine component (e.g. AK3). At the highest temperatures of Fo73, investigated plagioclase and clinopyroxene coexist with a melt with ~56 wt% SiO₂. The solidus was like in AK3 found at ~1150°C, although small fractions of unusually silicic melts were observed below this temperature. Biggar and Humphries (1981) showed that the temperature-difference between the olivine-clinopyroxene-plagioclase eutectic and the olivine-free clinopyroxene-plagioclase cotectic is only 4°C. We used a materials balance technique to assess whether the bulk composition of the experimental charged changed during the course of each experiments. In the case of the "Fo73" experiments the results of these calculations did not do a good job of recovering the starting compositions. Therefore, we also recalculated the modal proportions by excluding Na₂O, as shown in italics in Table 4-2a, improving the errors. This improved the materials balance results, and did not change the modes significantly, suggesting that the original modes are adequate. The compositions of the melts produced under equilibrium conditions are shown in Figure 4-1 in the Olivine – Clinopyroxene – Plagioclase pseudo-ternary projection scheme.

In these isothermal experiments, the saturation-boundary (~solidus) for the plagioclase-clinopyroxene-olivine-melt is 1150°C, and the saturation-boundary for augite-plagioclase-melt and olivine-plagioclase-melt is inferred to be ~5°C and ~40°C higher, respectively, based on comparison with previous studies (Biggar and Humphries, 1981) carried out in iron-free systems.

Melting Kinetics Experiments: In the earliest experiments (Fo₇₃-An₆₀ (AK00- and AK01-), Mg#~83(Cpx) - An₆₀ (AK3K-)), we placed the less dense mineral, plagioclase, on top of the mafic mineral to prevent convection in the melt following the method used in previous investigations (e.g. Tsuchiyama, 1985, 1986). However, experiments that melted to a significant extent, and exceeded the generation of a melt film between the two, developed a complex geometry of melt distribution and mineral shape in the plagioclase (Fig. 4-2 a). We found that if we placed the denser mineral on top of the

Evolution of Oceanic Gabbros: In-situ and Ancient Examples

assembly (used for the latter half of the experiments; Fo_{82} - An_{54} , and $\text{Mg}\# \sim 83(\text{Cpx})$ - An_{54}) the geometry of disintegration was easier to characterize (Fig. 4-2 b,c). With this geometry, the distance between the minerals stayed relatively constant and the melt was again pushed to the sides, but now it covered the minerals towards the top (Fig 4-2 d,e). Reaction only happened at the 2-phase interface with the melt. There was, however, excess melting towards the sides of each mineral slice, and along some phase-boundaries in the poly-crystals used for dissolution (Figure 4-3 a,e).

Olivine, the gabbroic mineral that has the fastest internal solid-state diffusion (Gaetani and Watson, 2000), developed only a very narrow (tens of μms) or no observable diffusion gradient along the actively melting interface (Fig. 4-3d, e, f), indicating that the melting rate is faster than solid-state diffusion for Fe/Mg in olivine. However, internally in olivine grains (Fig. 4-3f) melt-pockets originating around impurities that has melted completely re-equilibrate with the olivine. Some recrystallization occurred in the melt close to olivine, away from the most active melt interface (Fig. 4-3a, c). In addition, rare melt-pockets were found trapped inside olivine-grains away from the dissolving interface that have re-equilibrated with the host to form a lower Mg# melt (Fig. 4-3f and Table 4-5).

Plagioclase and clinopyroxene grains also melted without experiencing any internal diffusion of major elements. Plagioclase shows a very narrow ($\sim 10\mu\text{m}$) jagged reaction zone (Fig. 4-3b), but no significant anisotropy of melting is apparent at the melt-contact. There is no measurable chemical difference in plagioclase composition towards the melt-contact, within the resolution of the electron microprobe. The augite slab begins to melt internally in the highest temperature dissolution experiments (Fig. 4-3h), but does not show any sign of preferential melting of low-Ca pyroxene exsolution lamellae or preferential melting of different crystal faces (Fig. 4-3g-i) relative to the plagioclase interface.

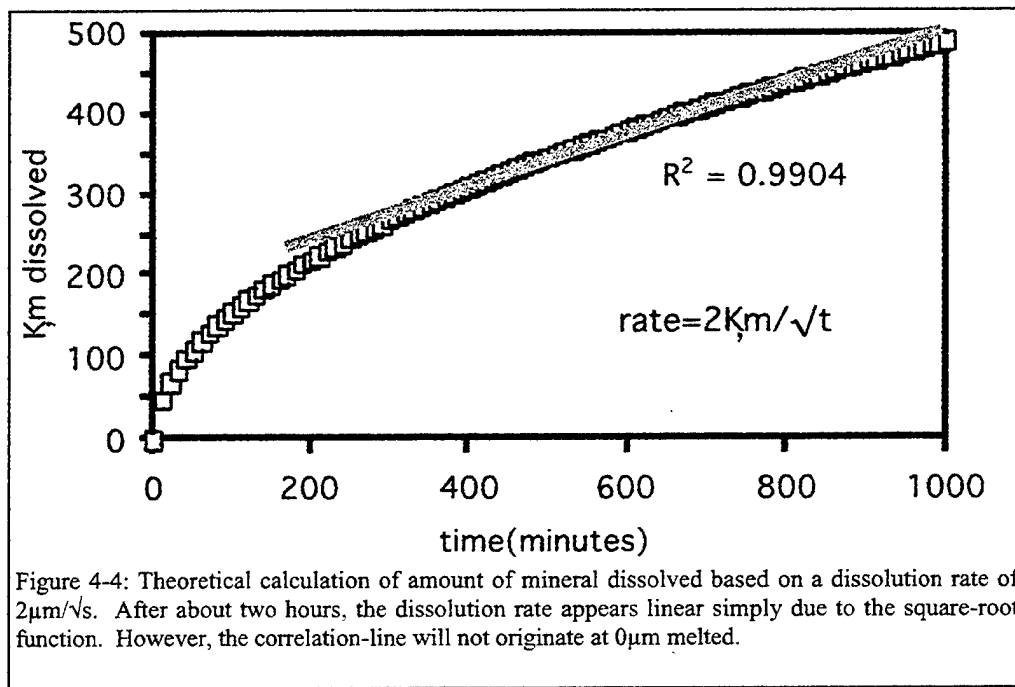
The traditional method of treating dissolution-experiments is to define a reaction function $\xi = f(\sqrt{t})$ or $\xi = f(t)$. These types of experiments are usually designed with one large mineral-grain dissolving into a large volume of melt, both of known and constant

Evolution of Oceanic Gabbros: In-situ and Ancient Examples

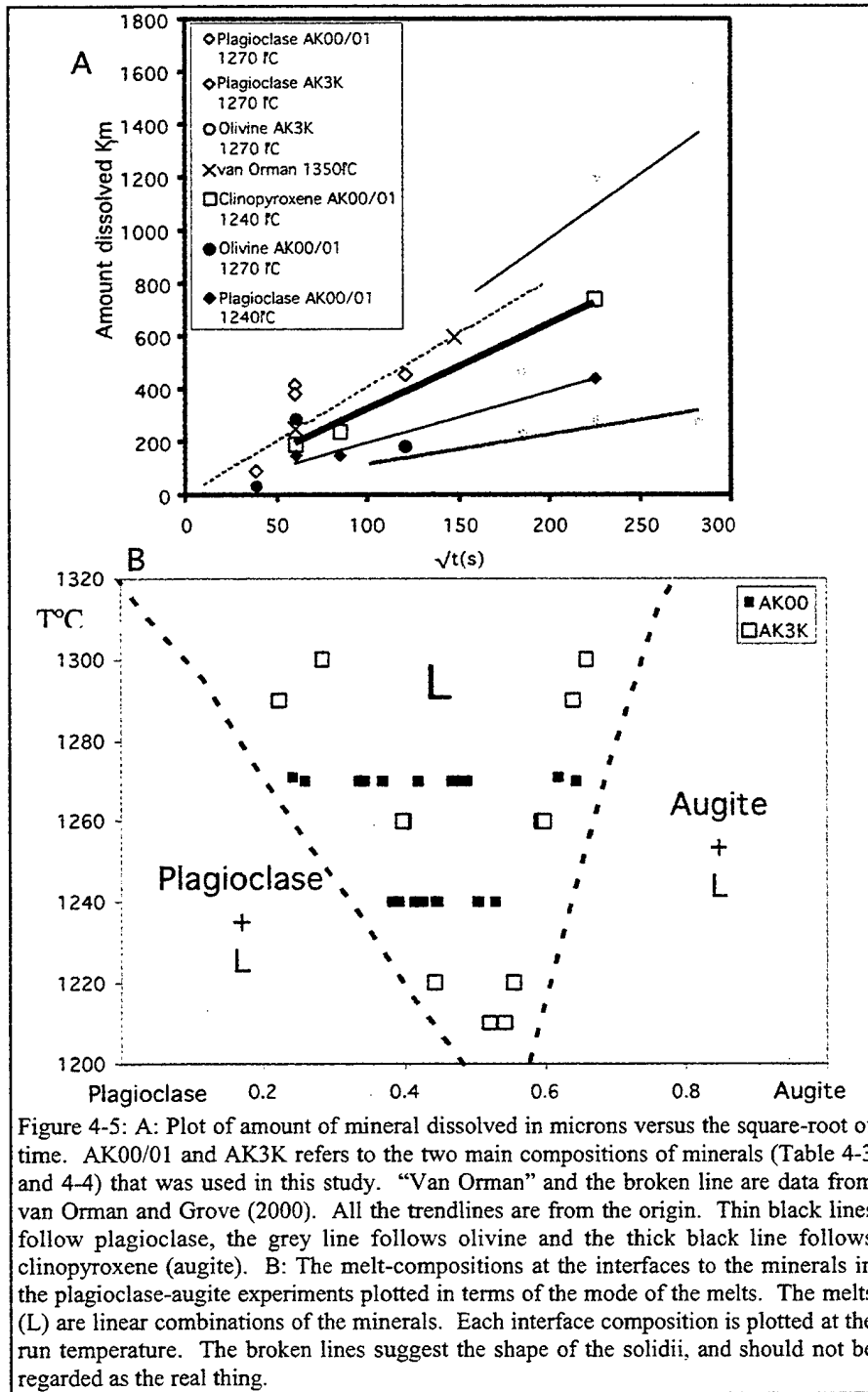
far-field compositions. The interface between the mineral and the melt is approximately fixed, thus the dissolution rate of the mineral into the melt and the resulting diffusion of components through the melt can readily be measured. Our experiments, however, are very different. At the start of each run, no melt is present between the two mineral-disks. As soon as the minerals are heated above the melting temperature, a melt-film forms between them. When minerals precipitate, interface-kinetics between the melts and crystals may control the rate at which the crystals grow. However, Zhang et al. (1989) used the interface-reaction rates from Kuo and Kirkpatrick (1985) and demonstrated that the interface-melts are saturated with the bounding crystals after ~ 1 second of dissolution, thus there is no interface-control of dissolution in our experiments. The melt-film has a near-constant thickness, as the weight of the overlying mineral squeezes the melt to the sides of the experiment. Each interface between the minerals and melt is therefore moving, and the center of the melt film experiences flow of melt from the minerals towards the center, in addition to flowing from the center of the run towards its sides. The reaction function cannot be solved analytically with these boundary conditions, and a thorough and extensive numerical model is beyond the scope of this paper. We found that the most meaningful way of approaching the reaction-function is to measure the linear loss of material from each mineral disk, in order to assess the rate of dissolution.

Our dissolution rates are summarized in Table 4-4. Marvin and Walker (1985) found that the melting rate at the onset of melting correlate with \sqrt{t} but as soon as a steady melt film is formed between the minerals (usually within 1-2 hrs), the newly formed melts are smeared out to the sides of the experiment, and the melting rate becomes linear with time. Unfortunately, they did not perform any experiments for longer than 200 minutes. We did perform experiments for as long as 24 hours, and these show good correlation with \sqrt{t} and linearly with time after a few hours. Thus, only the \sqrt{t} correlate with amount melted in a function that originates at the origin (Fig. 4-5a) as would be expected for diffusion-controlled dissolution. After a few hours, continued melting

Evolution of Oceanic Gabbros: In-situ and Ancient Examples



Evolution of Oceanic Gabbros: In-situ and Ancient Examples



Evolution of Oceanic Gabbros: In-situ and Ancient Examples

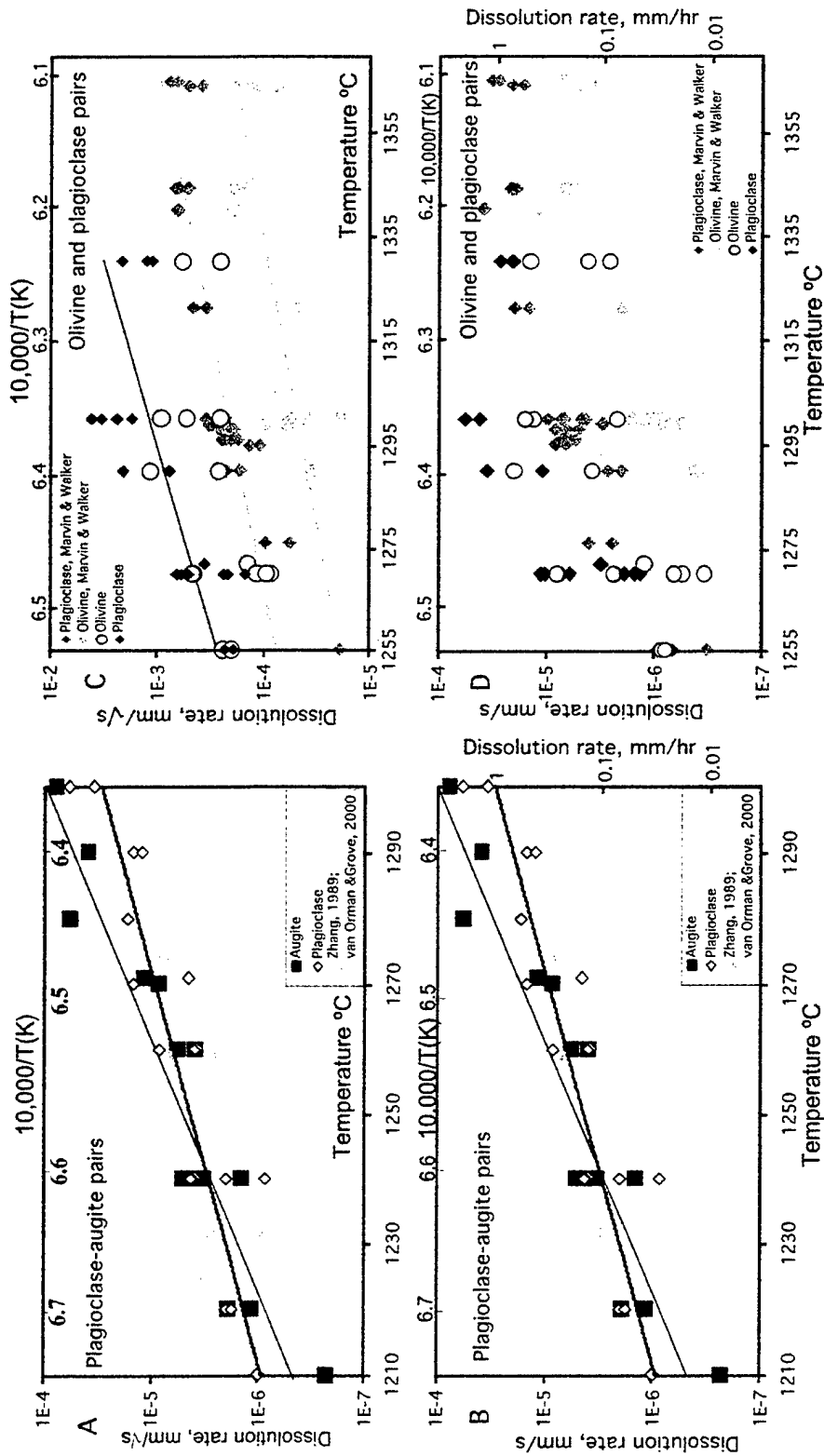


Figure 4-6: Dissolution rates for our experiments together with other studies (Zhang et al., 1989; van Orman and Grove, 2000).

Evolution of Oceanic Gabbros: In-situ and Ancient Examples

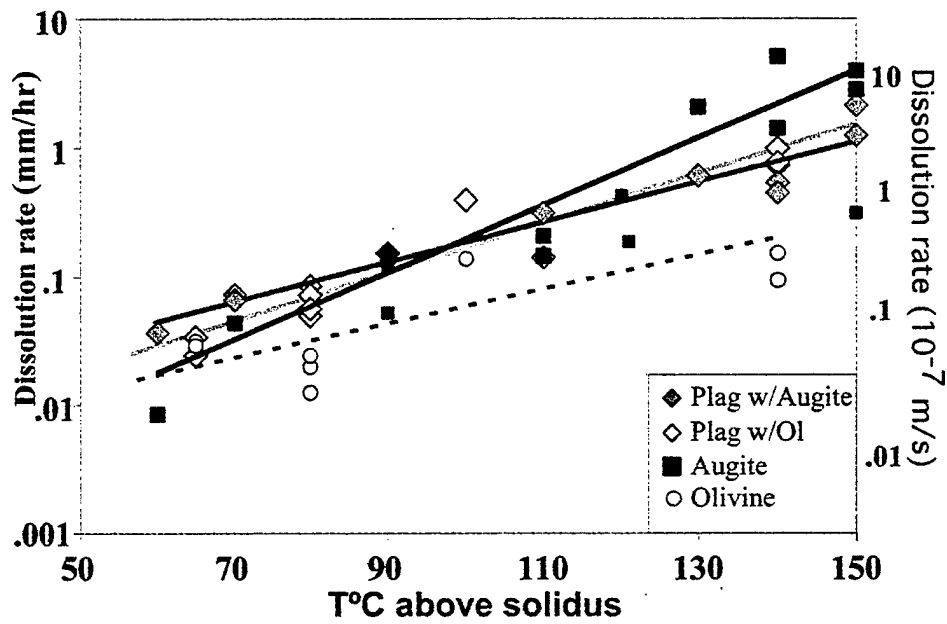


Figure 4-7: The dissolution rates for plagioclase dissolved with augite or olivine overlap when plotted vs. $\Delta T^\circ\text{C}$ above solidus.

Evolution of Oceanic Gabbros: In-situ and Ancient Examples

appears linear as a simple consequence of the \sqrt{t} relationship (Fig. 4-4). The reaction functions for dissolution may therefore be approximated as:

$$\xi = 2.43 * 10^{(-26)} * e^{.004\sqrt{T(^{\circ}\text{C})}} \text{ for augite melted with plagioclase;}$$

$$\xi = 3.47 * 10^{(-15)} * e^{.002\sqrt{T(^{\circ}\text{C})}} \text{ for plagioclase melted with augite;}$$

$$\xi = 1.79 * 10^{(-21)} * e^{.0032\sqrt{T(^{\circ}\text{C})}} \text{ for plagioclase melted with olivine}$$

The rates for olivine-dissolution have a poor correlation with \sqrt{t} (and t), and a reaction-function has not been calculated for olivine. For all these functions, the approximation with t is reasonable when working with 10's of mm's and times less than a week, and the dissolution-rates may be used in units of mm/hr.

Dissolution rates for the plagioclase – clinopyroxene and plagioclase - olivine pairs are plotted in Figure 4-6 along with other dissolution studies (Marvin and Walker, 1985; Zhang et al., 1989; Van Orman and Grove, 2000). Marvin and Walker (1985) investigated the melting rates of $\text{Fo}_{90}\text{-An}_{54}$ at 0.1MPa from 10 to 200 minutes, Zhang et al. (1989) dissolved diopside in an andesite, for 15 minutes to 23 hours at various pressures, whereas van Orman and Grove (2000) melted diopside with ilmenite at ~13GPa for 1-6 hours. Our rates for plagioclase and augite are very similar to each other, and the other authors' data agree well. Note that the temperatures of their experiments have been translated to 1 atm conditions (by subtracting 9°C/kbar, on the basis of the algorithms from Grove et al. (1992)). At a given temperature, plagioclase melts slower when in contact with an olivine than when in contact with an augite. For instance, An_{54} plagioclase at 1290°C melts 0.54-mm/hr when in contact with augite, but only 0.17-mm/hr in contact with olivine. The minerals of the augite-plagioclase pairs, however, melt at comparable rates to the plagioclase of the plagioclase-olivine pair, relative to their solidus temperature (Figure 4-7). Thus, the intermediate (relative to the spectrum of gabbros at Atlantis Bank) gabbro-composition that our experiments represent, would react very effectively with a melt of a temperature of 1230°C or higher. Neither of the individual minerals was held significantly above their individual solidi (An_{54} has a solidus of ~1320°C).

Evolution of Oceanic Gabbros: In-situ and Ancient Examples

Table 5: Range of melts from the dissolution experiments using gabbroic raw material.

Sample #	SiO ₂	TiO ₂	Al ₂ O ₃	Cr ₂ O ₃	FeO	MnO	MgO	CaO	Na ₂ O	K ₂ O	P ₂ O ₅	Mg#	Ca#	What
AK00 ol-pl														
AK19	49.1	.03	21.0		7.7	.12	10.9	8.8	3.21	.04	.09	71.6	60.3	Rim to olivine
AK19	50.6	.00	23.1		5.1	.12	7.3	10.0	3.64	.05	.10	71.8	60.4	Rim to plagioclase
AK19	50.6	.03	20.6		8.1	.12	9.5	8.4	3.17	.04	.08	67.5	59.4	Cotectic melt
AK21	49.3	.01	21.5		7.1	.13	10.3	9.0	3.71	.05	.06	72.1	57.2	Rim to olivine
AK21	50.8	.01	22.5		6.7	.09	9.8	8.8	4.03	.04	.15	72.4	54.8	Rim to plagioclase
AK21	48.4	.20	19.1	.006	7.8	.16	11.2	11.5	2.29	.04	.12	72.0	73.4	Cotectic melt
AK25	48.7	.18	20.9		8.3	.16	10.2	9.6	3.20	.06	.11	68.5	62.4	Rim to olivine
AK25	49.6	.13	23.2		6.0	.13	8.6	8.9	4.02	.07	.11	72.1	54.9	Rim to plagioclase
AK25	49.1	.11	21.5	.002	7.3	.11	10.2	9.2	3.29	.04	.08	71.5	60.6	Cotectic melt
AK25	45.8	.32	20.1	.008	13.6	.19	8.1	10.4	2.38	.05	.10	51.5	70.8	Pocket inside olivine
AK20	49.7	.31	15.0	.038	7.4	.12	10.9	12.5	2.25	.05	.13	72.4	75.4	Rim to olivine
AK20	50.8	.25	19.4	.019	4.8	.10	8.2	13.0	3.20	.07	.20	75.2	69.2	Rim to plagioclase
AK20	51.7	.30	17.9	.027	6.7	.14	8.7	10.7	2.62	.05	.13	70.0	69.3	Cotectic melt
AK00 cpx-pl														
AK22-1	53.6	.37	11.8	.080	5.1	.13	10.8	15.0	1.85	.03	.17	79.3	81.7	Rim to clinopyroxene
AK22-1	52.3	.17	20.6		2.9	.10	6.5	15.0	3.01	.02	.14	79.9	73.3	Rim to plagioclase
AK22-1	50.4	.50	15.8	.009	7.9	.15	10.5	12.6	2.19	.04	.16	70.3	76.1	Cotectic melt
AK22-2	55.3	.33	12.9	.057	4.2	.15	11.3	16.3	2.48	.02	.30	82.6	78.3	Rim to clinopyroxene
AK22-2	56.8	.26	17.9	.013	3.7	.11	9.0	15.1	2.65	.04	.81	81.3	75.9	Rim to plagioclase
AK18-1	53.1	.41	13.2	.033	4.2	.16	10.4	17.3	2.02	.03	.20	81.4	82.6	Rim to clinopyroxene
AK18-1	53.0	.34	14.3	.030	4.5	.11	9.7	15.8	2.22	.03	.16	79.3	79.7	Rim to plagioclase
AK18-1	50.8	.52	16.1	.014	5.1	.15	10.0	16.4	2.10	.03	.19	77.8	81.1	Cotectic melt
AK18-2	53.7	.77	10.1		5.7	.16	11.9	17.2	1.79	.03	.19	78.7	84.2	Rim to clinopyroxene
AK18-2	52.9	.13	25.3		1.8	.06	3.1	13.3	4.28	.05	.10	75.4	63.1	Rim to plagioclase
AK24	52.1	.52	9.9	.107	5.5	.21	13.4	17.6	1.61	.03	.24	81.3	85.8	Rim to clinopyroxene
AK24	49.2	.31	20.4	.057	3.7	.17	8.0	16.5	2.08	.04	.20	79.3	81.4	Rim to plagioclase
AK01 ol-pl														
ak0104-1	47.8	.08	19.5	.000	8.3	.10	12.4	9.3	3.01	.05	.06	72.6	63.0	Rim to olivine
ak0104-1	51.6	.07	24.5	.021	4.7	.07	6.9	8.8	4.76	.08	.04	72.2	50.6	Rim to plagioclase
ak0104-2	48.5	.13	19.5	.010	9.8	.20	11.8	8.6	3.03	.03	.11	68.1	61.1	Rim to olivine
ak0104-2	50.1	.13	23.6	.006	5.7	.13	7.8	8.7	4.13	.05	.01	70.8	53.7	Rim to plagioclase
ak0106-1	49.2	.07	19.7	.037	9.0	.10	12.9	8.7	2.63	.03	.15	71.8	64.7	Rim to olivine
ak0106-1	50.3	.05	25.9	.017	4.8	.09	7.3	8.0	4.40	.08	.14	73.0	50.1	Rim to plagioclase
ak0106-2	48.9	.06	20.4	.010	7.3	.11	11.9	8.9	3.18	.01	.06	74.4	60.7	Rim to olivine
ak0106-2	51.3	.11	24.0	.000	4.6	.06	7.7	7.6	4.76	.07	.06	74.9	46.8	Rim to plagioclase
AK01 cpx-pl														
ak0101	53.2	.36	15.1	.051	4.3	.03	9.7	15.5	2.48	.04	.17	80.1	77.5	Rim to clinopyroxene
ak0101	52.6	.32	16.5	.090	3.6	.04	8.2	16.0	2.60	.05	.19	80.3	77.3	Rim to plagioclase
ak0101	53.8	.45	15.4	.083	3.4	.11	9.8	15.3	2.34	.04	.16	83.5	78.3	Cotectic melt
ak0102	53.7	.40	14.5	.061	4.5	.11	9.8	15.1	2.52	.03	.13	79.6	76.8	Rim to clinopyroxene
ak0102	52.9	.30	17.0	.086	4.0	.13	9.1	15.3	2.74	.05	.15	80.3	75.4	Rim to plagioclase
ak0102	53.4	.73	13.9	.052	3.8	.14	10.8	15.8	2.00	.03	.33	83.5	81.3	Cotectic melt
ak0103	53.4	.52	13.5	.038	4.5	.11	10.6	15.7	2.11	.03	.14	81.0	80.5	Rim to clinopyroxene
ak0103	52.5	.44	17.9	.048	3.9	.10	8.9	15.5	2.55	.02	.11	80.4	77.1	Rim to plagioclase
ak0103	53.8	.61	14.5	.056	3.8	.13	10.2	15.8	2.24	.03	.15	82.5	79.5	Cotectic melt
AK3K ol-pl														
AK3K1	51.6	.01	21.7	.06	4.9	.06	11.1	8.6	3.16	.25	.00	80.2	60.1	Rim to plagioclase
AK3K1	53.3	.00	24.1	.05	3.3	.05	7.9	7.6	4.43	.36	.00	80.8	48.5	Rim to olivine
AK3K3	50.8	.09	22.2	.00	4.6	.07	9.6	8.9	3.87	.25	.00	78.6	55.9	Rim to plagioclase
AK3K3	52.6	.00	23.8	.00	3.2	.00	7.8	8.1	4.42	.40	.15	81.4	50.3	Rim to olivine
AK3K4	50.8	.09	21.6	.00	4.5	.05	10.8	8.3	3.05	.25	.00	81.0	60.1	Rim to plagioclase
AK3K4	52.4	.06	23.7	.02	3.5	.06	8.1	7.6	4.58	.40	.06	80.6	48.0	Rim to olivine

Evolution of Oceanic Gabbros: In-situ and Ancient Examples

Table 5: Range of melts from the dissolution experiments using gabbroic raw material.

Sample #	SiO ₂	TiO ₂	Al ₂ O ₃	Cr ₂ O ₃	FeO	MnO	MgO	CaO	Na ₂ O	K ₂ O	P ₂ O ₅	Mg#	Ca#	What
AK3K5	50.7	.00	20.5	.00	4.8	.04	12.2	8.6	3.06	.21	.00	81.8	60.9	Rim to plagioclase
AK3K5	53.0	.05	24.2	.02	2.7	.11	7.0	7.8	4.73	.40	.00	82.1	47.7	Rim to olivine
AK3K11	49.9	.00	19.4	.07	5.7	.01	14.5	8.3	3.14	.19	.00	82.0	59.2	Rim to plagioclase
AK3K11	53.3	.06	25.4	.00	2.1	.06	6.0	7.9	5.82	.41	.00	83.4	42.7	Rim to olivine
AK3K12	50.1	.05	19.3	.08	6.1	.02	14.8	8.4	3.23	.15	.00	81.2	59.0	Rim to plagioclase
AK3K12	53.6	.00	26.3	.04	2.0	.00	5.4	7.4	5.96	.44	.00	82.9	40.8	Rim to olivine
AK3K18	47.4	.00	16.7	.00	5.8	.06	19.3	6.4	3.39	.27	.00	85.6	50.9	Rim to plagioclase
AK3K18	52.2	.03	24.1	.00	2.4	.00	6.7	6.9	5.57	.63		82.9	40.7	Rim to olivine
AK3K cpx-pl														
AK3K16	52.2	.39	11.9	.08	4.2	.01	10.9	15.3	2.45	.18	.00	82.2	77.5	Rim to augite
AK3K16	52.5	.25	17.6	.00	2.7	.00	7.6	14.3	3.17	.21		83.5	71.4	Rim to plagioclase
AK3K17	52.3	.51	11.9	.09	3.8	.12	10.9	15.4	1.97	.17	.00	83.8	81.2	Rim to augite
AK3K17	51.8	.30	17.6	.11	2.5	.10	7.9	14.1	2.82	.26	.00	85.0	73.4	Rim to plagioclase
AK3K19	53.1	.27	15.3	.08	4.0	.13	8.5	14.3	2.95	.24		79.1	72.8	Rim to augite
AK3K19	53.0	.32	16.1	.00	3.7	.08	8.3	14.2	2.92	.19		80.2	72.9	Rim to plagioclase
AK3K22	52.6	.30	9.3	.10	4.5	.10	12.6	16.9	1.96	.12	.00	83.3	82.7	Rim to augite
AK3K22	52.1	.13	19.6	.03	2.2	.00	6.7	14.1	3.34	.29	.00	84.6	70.0	Rim to plagioclase
AK3K14	51.6	.56	7.2	.08	4.8	.10	14.1	16.8	1.42	.07	.00	83.9	86.7	Rim to augite
AK3K14	51.4	.19	18.4	.07	2.2	.07	7.0	13.9	3.24	.23	.00	85.0	70.3	Rim to plagioclase
AK3K26	53.6	.80	13.6	.15	5.8	.14	9.5	14.9	2.57	.17		74.6	76.2	Rim to augite
AK3K26	52.7	.59	16.7	.08	5.0	.19	8.0	14.3	2.92	.16	.17	73.8	73.0	Rim to plagioclase
Notes: Ol=olivine, cpx=augite, pl=plagioclase. Cotectic melt=melt compositions on sides of runs														
"Rim to"= compositions next to a mineral														

Evolution of Oceanic Gabbros: In-situ and Ancient Examples

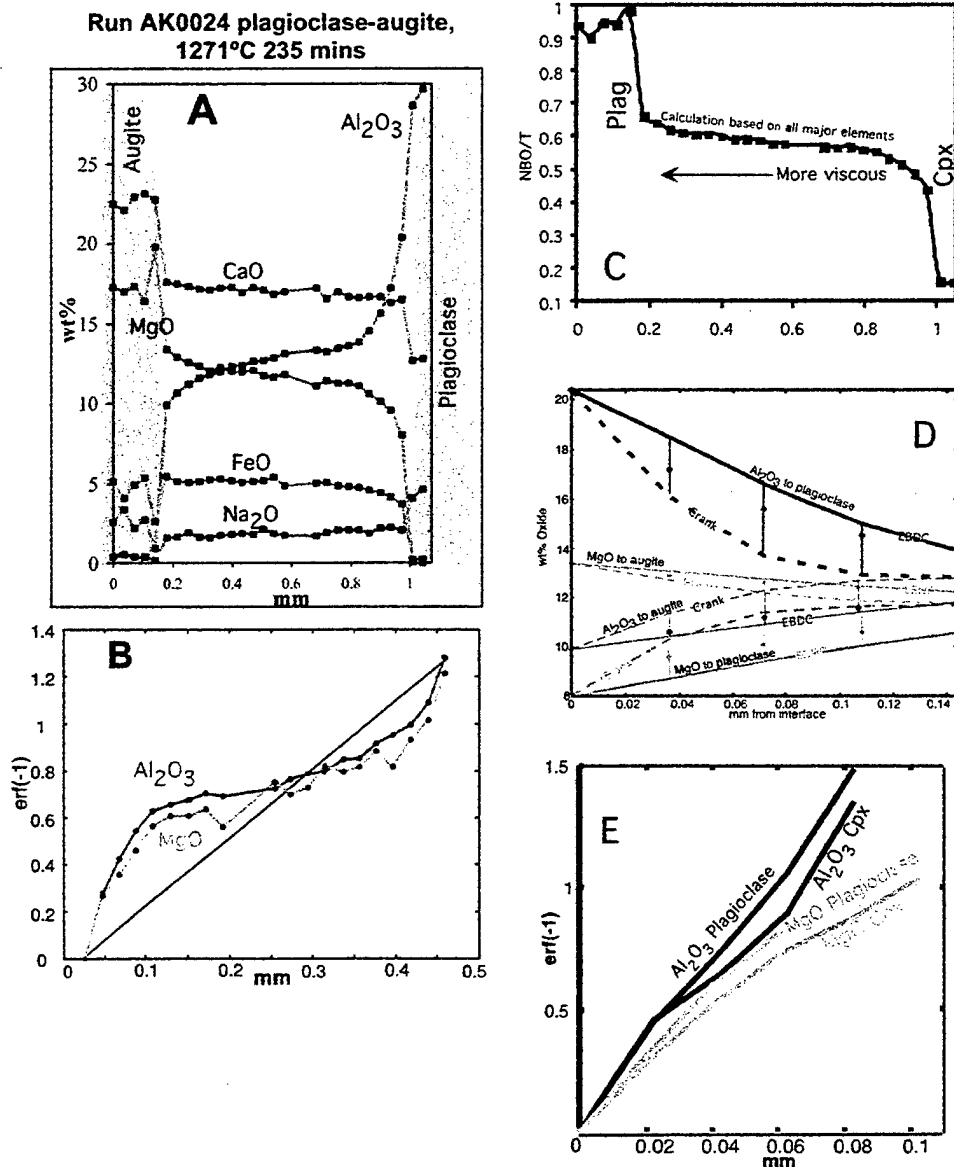


Figure 4-8: A: Chemical profiles across the augite-melt-plagioclase interface in sample AK0024. SiO_2 is not included as the concentrations are similar in both minerals. B: If the entire profile is diffusion controlled, $\text{erf}\left(\frac{x}{\sqrt{2Dt}}\right)$ should follow a straight line through the origin. C: The non-bridging oxygens per

tetrahedrally coordinated cation (NBO/T) (Mysen, 1988) are inversely related to the polymerization of the melt and melts to plagioclase are more viscous than those to augite. D: Fits to the data, using diffusion-coefficients calculated from only the melts closest to the interface. Broken lines are calculated using the classical method from Crank (1975), the full lines are using the effective binary diffusion coefficients (EBDC) from Zhang et al., (1989). Thick black lines are Al_2O_3 in the melt to plagioclase, thin black lines are Al_2O_3 in the melt to augite, thick grey lines are MgO in the melt towards plagioclase, thin grey lines are MgO to augite. The data are dots in the respective colors, connected to the corresponding diffusion-profiles by vertical lines. E: The melts close to the mineral interfaces follow a near straight line for erf^{-1} .

3.a.1. Melt compositions

We analyzed the melts in traverses perpendicular to the mineral surfaces (Fig. 4-8). The melt compositions are linear combinations of the mineral compositions (Figure 4-5b, the melt-compositions closest to the mineral-interfaces are recalculated as mineral-modes by simple inversion to the mineral compositions). In addition, in the experiments where we used the oceanic gabbros as starting material, we analyzed the melt that had been squeezed out on the sides of the minerals (labeled "Cotectic melt"). The results are listed in Table 4-5.

If the dissolution-rates are controlled by the rates of diffusion in the melt, the dissolution rates should be the same when we calculate them using the amount of material dissolved, similar to the above treatment, as if we calculate diffusion-coefficients for the melts near the mineral-melt interfaces to find the dissolution rates. In our crystal-pair dissolution-experiments, melt migration and convection during dissolution have modified the compositional profiles of the melt film. This approach will therefore be an approximation, at best. Due to the difficulties regarding the smeared melts, Tsuchiyama (1985) suggested a very different approach to calculating diffusion rates in the melt. However, we do not find our results using his techniques satisfactory.

The concentration profiles adjacent to the crystal interfaces for Al_2O_3 and MgO (Fig. 4-8A), do resemble diffusion profiles. As noted in other diffusion studies (Watson, 1982) some elements (e.g. Na_2O and CaO) undergo rapid initial diffusion and establish a steady state distribution. In addition, the chemical profile is strongly zoned in non-bridging oxygens per tetrahedrally coordinated cations (NBO/T, Fig. 4-8C) (Mysen, 1988) indicating that the melt is strongly polymerized near the plagioclase crystal making the melt more viscous. A quick analysis of the diffusion-profiles in sample AK0024 (clinopyroxene-plagioclase at 1271°C , ~4 hours) shows that if the diffusion-coefficient is modeled using the opposite mineral-melt-contact as the far-field composition, the profiles do not show diffusion behavior (Figure 4-8B). However, if only the profile next to the crystal is used (Figure 4-8E), and the composition at the middle of the melt film is used as the far-field melt, the diffusion coefficients may be calculated (Table 4-6).

Evolution of Oceanic Gabbros: In-situ and Ancient Examples

Table 4-6: Method of calculating the dissolution-coefficients using diffusion coefficients in the melt	
First: Calculate diffusion-coefficients in the melt-film at the interface to the minerals.	
A: Method from Crank (1975) for a semi-infinite volume:	
Calculation	Result
$\frac{C(x,t) - C_0}{C_\infty - C_0} = \operatorname{erf}\left(\frac{x}{2\sqrt{Dt}}\right),$ <p>C_0 = composition at the interface to the mineral, C_∞ = the far-field melt composition, and $C(x,t)$ = composition of the melt away from the interface</p>	<p>Diffusion-coefficients ("D") for the melt-interface to:</p> <p>Plagioclase: Al_2O_3: $5.9 \times 10^{-14} \text{ m}^2/\text{s}$ MgO: $7.6 \times 10^{-14} \text{ m}^2/\text{s}$</p> <p>Augite: Al_2O_3: $1.6 \times 10^{-13} \text{ m}^2/\text{s}$ MgO: $9.7 \times 10^{-14} \text{ m}^2/\text{s}$</p>
B: Method from Zhang et al. (1989) diffusion-controlled dissolution in a semi-infinite melt reservoir.	
<p>The effective binary diffusion coefficient (EBDC) is obtained by:</p> $\frac{C(x,t) - C_\infty}{C_0 - C_\infty} = \frac{\operatorname{erfc}\left(\frac{x}{2\sqrt{Dt}} - a\right)}{\operatorname{erfc}(-a)}$ <p>where a satisfies $\sqrt{\pi} a e^{a^2} \operatorname{erfc}(-a) = b$; $b = \frac{C_0 - C_\infty}{C_s - C_0}$,</p> <p>$a$ is found by a numerical fit, C_0 = composition at the interface to the mineral, C_∞ = the far-field melt composition, C_s = the composition of the solid, and $C(x,t)$ = composition of the melt away from the interface.</p>	<p>EBDC's ("D") for the melt-interface to:</p> <p>Plagioclase: Al_2O_3: $3.6 \times 10^{-13} \text{ m}^2/\text{s}$ MgO: $5.2 \times 10^{-13} \text{ m}^2/\text{s}$</p> <p>Augite: Al_2O_3: $6.5 \times 10^{-13} \text{ m}^2/\text{s}$ MgO: $5.9 \times 10^{-13} \text{ m}^2/\text{s}$</p>
Second: The diffusion coefficients can be used to determine the dissolution-rates:	
<p>$\text{rate} = \rho \sqrt{D}$</p> <p>$\rho$ = density of the minerals, a is the same as above: $\sqrt{\pi} a e^{a^2} \operatorname{erfc}(-a) = b$; $b = \frac{C_0 - C_\infty}{C_s - C_0}$,</p>	<p>Dissolution-rates using diffusion-coefficients from A: Plagioclase: $7.4 \text{ gm}^{-2}\text{s}^{-1/2}$ Augite: $23.5 \text{ gm}^{-2}\text{s}^{-1/2}$</p> <p>Dissolution-rates using EBDC from B: Plagioclase: $0.403 \text{ gm}^{-2}\text{s}^{-1/2}$ (Al_2O_3) $0.55 \text{ gm}^{-2}\text{s}^{-1/2}$ (MgO) Augite: $0.403 \text{ gm}^{-2}\text{s}^{-1/2}$ (Al_2O_3) $0.33 \text{ gm}^{-2}\text{s}^{-1/2}$ (MgO)</p> <p>Dissolution-rates using measured dissolution distance: Plagioclase: $\sim 1.4 \text{ gm}^{-2}\text{s}^{-1/2}$ Augite: $2.5 \text{ gm}^{-2}\text{s}^{-1/2}$</p>

Zhang et al. (1989) developed an approach for diffusion-controlled dissolution in a semi-infinite melt reservoir. This method has been used in other single crystal dissolution experiments (Van Orman and Grove, 2000) to quantify the dissolution process (Table 4-6). The fit to the chemical diffusion-profile using our calculated diffusion-coefficients is shown in figure 4-8D, and it is clear that the effective binary diffusion coefficient (EBDC) provide better fits than the traditional diffusion coefficients. Furthermore, the dissolution rates calculated from the diffusion-coefficients (Table 4-6) are smaller for Zhang et al. (1989) than the rates determined by volumetric dissolution (Table 4-6). This is probably because much of the melt has been pressed out of the interface to the sides of

Evolution of Oceanic Gabbros: In-situ and Ancient Examples

the experiment. The *measured* dissolution rate lies between the two determined from the method using the diffusion-coefficients. We therefore conclude that dissolution is controlled by the diffusion in the melt-disk between the minerals.

3.b. How efficient is dissolution?

In his classical paper on assimilation, Bowen (1928) identifies three general mechanisms by which rock/magma chemical reactions may occur. These are: a) reaction of the melt with minerals that are unstable in it to produce new stable minerals; b) direct solution of unstable minerals into the melt; and c) fusion or partial fusion of country-rock or xenoliths and subsequent mixing with the magma by diffusion in the molten stage. All these processes consume energy that must be accommodated by crystallization in the melt if the melt is near or below its liquidus.

Liang (1999) states that almost all dissolution in magmatic silicates is controlled by the diffusion of mass in the liquid, as the diffusion in the liquid is much faster than in the solid-solutions. The chemical disequilibrium between a solid phase (crystal) and a liquid causes dissolution below the solidus of the crystal and require simultaneous diffusion of heat and mass (Kerr, 1995; Tsuchiyama, 1986; Woods, 1993).

3.c. Dissolution of gabbro in the lower ocean crust

The lower ocean crust can interface with ascending magmas in several ways while it is conductively cooling. The efficacy of diffusion of heat into the country-rock depends on the geometry of the interface, and the size of the heat-reservoir. If the magma is a stagnant dike, the interface temperature between the dike and the wall-rock will never exceed half of the difference in temperature between them presuming that the heat diffusivity in the melt and solid are the same (Turcotte and Schubert, 1982). A flowing dike or convecting magma-chamber represents a more efficient heat-reservoir, since convection redistributes the heat, and the temperature of the wall-rock may rise towards that of the magma. In addition, new injection of magma will also increase the available heat. However, a xenolith stopping into a magma, completely encapsulated, would be the most efficient geometry to heat a wall rocks to magmatic temperatures.

Evolution of Oceanic Gabbros: In-situ and Ancient Examples

Table 7: The thermodynamic properties of the minerals at 1250°C						
	Diopside	An60	An54	Fo90	Fo73	Fo82
ΔH_f (J/mol)	133228	94254	91556	117594	112716	107969
Molecular weight (g/mol)	216.6	271.8	270.9	147.0	147.0	147.0
Cp solid (J/mol-K)	268	350	349	192	196	194
Cp liquid (J/mol-K)	345	399	395	265	260	263
Molecular volume (cm³)	68.5	103.5	103.6	46.1	46.5	46.3
T (K) of fusion	1664	1650	1624	2096	1981	2042
T (K) solidus	1573 (Augite82)	1613	1593		1773	1873
Density (g/cm³)	3.16	2.63	2.62	3.19	3.16	3.18

Note: Source of data given in text

Evolution of Oceanic Gabbros: In-situ and Ancient Examples

The lower crust at fast-spreading ridges is thought to contain a mush-zone with $\leq 20\%$ melt (Dunn et al., 2000); i.e. the system is above or close to the solidus. If a magma dissolves a xenolith of different isotopic and trace element signatures than itself, the effect on the hybrid magma composition will not be hidden by subsequent crystallization. Melts saturated with olivine only will show the effects of assimilation on its major-element compositions more than multiply-saturated melts. The addition of a primitive melt with only olivine as a liquidus phase into the lower mush-zone below the ridge may breakup previously generated networks of minerals (Philpotts and Dickinson, 2000; Jerram et al., 2003) and stope rocks into the magma. Bedard et al. (2000) reviewed the concept of syntexis (the processes, mechanical and chemical, by which magmas react with and assimilate their host rocks). They stated: "it seems self evident that host-rocks and xenocrysts will dissolve into an invading melt only if they are exposed to it" as an argument to support porous melt-flow through pre-existing cumulates. However, if enclosed in hot magma, xenoliths with two- and three-phase mineral boundaries ("triplejunctions") with solidii significantly below the magma-temperature, the xenolith melt along the internal mineral-boundaries when exposed to the heat of the magma. The thermal instability of the phase-boundary requires it to melt, as this is the only way to cool the interface-melt towards a thermally stable condition. We will show that the cumulates only need to be exposed to this heat from the ascending melts, and that if the melts do not escape from these cumulates, but crystallize *in-situ*, they still have a profound effect on the mineral-compositions.

Our melting-rates allow disintegration of a xenolith in hours to days. If a gabbro (i.e. ~50/50 augite/plagioclase) becomes heated above the solidus, the boundaries between the minerals will start to melt. Figure 4-9 demonstrates theoretically how fast a coarser-grained rock will likely melt. At 1240 °C, the slide in Figure 4-9A will look like 4-9B and at 1270°C like 4-9C, after only one hour. However, as we have repeatedly shown in our experiments, plagioclase is buoyant in this melt, whereas augite (and olivine) is denser. If a mineral melts on all sides, it will settle as high or low as possible (Figure 4-9D). Therefore, a close contact with efficient melting will be maintained along at least one interface at all times.

Evolution of Oceanic Gabbros: In-situ and Ancient Examples

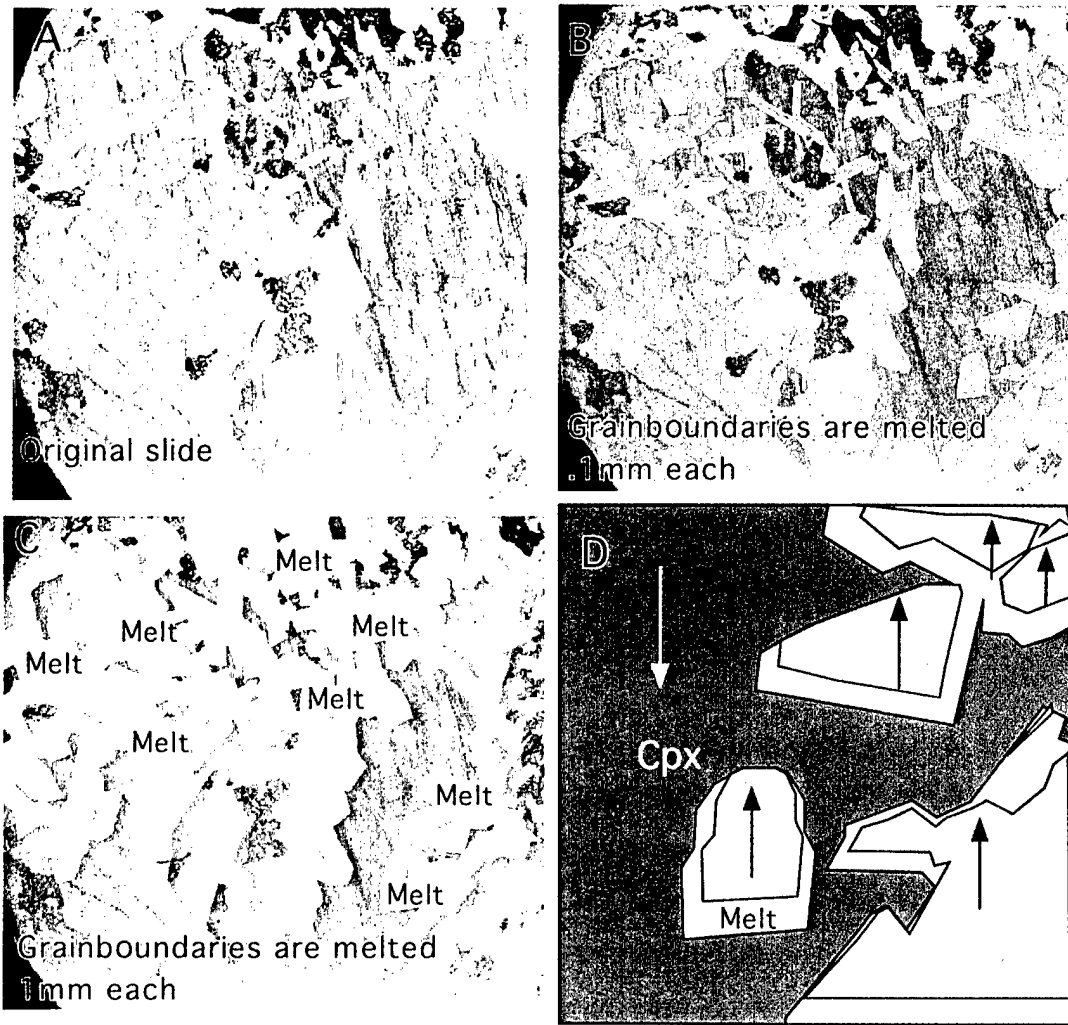


Figure 4-9: A: A thin-section in parallel light of olivine gabbro sample JR31-12-1 from Atlantis Bank. The ophitic minerals are augite, the long laths are plagioclase, and the other minerals are partially altered olivine. B: As a thought experiment, we draw the boundaries between plagioclase and augite and let the thickness of the lines represent amount dissolved on the mineral-boundary. Here, each mineral melted 0.1 mm each, as indicated in white. C: Each mineral has melted 1mm each. D: This sketch is of the lower right corner of the slide, with each grain melted 0.25mm. Here we let the minerals settle to their gravitationally stable level. Plagioclase will rise and clinopyroxene will sink relative to the melt. Thus, a tight connection is kept at least at one face of each mineral.

Evolution of Oceanic Gabbros: In-situ and Ancient Examples

Thermodynamic considerations

As melting and dissolution generally are endothermic processes, "inclusions pass into solution by precipitating their heat equivalent of the phase with which the liquid is saturated" (Bowen, 1928). However, Bowen also stated that the reaction between a melt and an assemblage higher up in the reaction series thus would be exothermic. Addition of rocks from lower in the reaction-series is endothermic and causes the system to cool gradually (e.g. addition of a gabbro to a primitive, mantle-derived melt). It is not clear, however, that the addition of gabbroic xenoliths with the accompanying fractionation of olivine causes the melt volume to reduce significantly.

Our results indicate that the phase-boundaries of lower crust from ocean ridges will melt efficiently and out of equilibrium at a temperature above the plagioclase-clinopyroxene-melt saturation boundary at $\sim 1150^{\circ}\text{C}$ (i.e. gabbro) and plagioclase-olivine-melt saturation boundary at $\sim 1195^{\circ}\text{C}$ (i.e. troctolite) or higher. The heat of fusion (ΔH_f) and conductive heat-loss to the surroundings controls how effective the melting will be in infusing the ascending magmas with lower crustal material. The ΔH_f 's of the minerals (calculated for 1250°C , Ghiorso and Carmichael, 1980) are listed in Table 4-7. The heat capacity (C_p) used for the system is $1.59 \text{ J/g}^{\circ}\text{C}$ (Robie et al., 1978). Stopping of xenoliths is the most efficient method of reheating wall-rock material by ascending melts. Other methods, including direct heating of the wall rock by a moving magma may be important, but will possibly not provide much new melt to the main magma-chamber as it will remain trapped in the wall rock where it is produced. We will consider two main scenarios: The stopping of gabbro-, or troctolite-xenoliths into a primitive magma (Table 4-8).

Evolution of Oceanic Gabbros: In-situ and Ancient Examples

Table 4-8: Stopping of gabbro or troctolite-xenoliths into a primitive magma
Thermal re-equilibration of a xenolith with ascending magma; the resulting temperature of the magma:
$\Delta T = \frac{(Cp_{Augite} * M_{Augite} + Cp_{Plag} * M_{Plag}) * (T_{magma} - T_{Xenolith})}{Cp_{System} * M_{System}}$ <p>T=temperature; Cp = heat capacity of the mineral, M=mass (grams) of mineral or magma. Therefore: If the initial magma is: 1250°C Add 10 wt% gabbro xenolith at 1150°C (i.e. solidus) ⇒ ~9°C drop in magma temperature Add 10 wt% troctolite xenolith at 1190°C (i.e. solidus) ⇒ ~3°C drop in magma temperature ⇒ (The subsequent heat of fusion due to new crystallization is ignored.)</p>
Thermal re-equilibration of a xenolith with ascending magma: how fast does it happen?
$X = \sqrt{Dt}, D = 0.008 \text{ cm}^2 / \text{s}; X=\text{distance, } t=\text{time in seconds}$ <p>5 cm cube: 16 minutes; 20 cm cube: 8 hours</p>
Need to compensate assimilation of the xenolith by crystallization in the magma to prevent heat-loss/ -gain
$\Delta H = M_a \Delta H_f^a - M_c \Delta H_f^c; \text{ Kelemen (1990)}$ <p>ΔH=heat of fusion, M=mass (grams) a=assimilated, f = "of fusion", c=crystallized.</p>

If 10 wt% xenoliths (relative to the magma) just below their solidus are emplaced into a primitive magma by stopping, assuming isenthalpic conditions, the temperature of the magma will only drop slightly (Table 4-8). If the magma is not above its liquidus, it will crystallize to compensate for the heat-loss. The rate of thermal re-equilibration is dependent on the size of the xenolith. When the temperature inside the xenolith oversteps the melting-temperature of the mineral-boundaries, the minerals starts to dissolve independently of the surrounding magma. The mono-mineralic phase-boundaries in contact with the surrounding melts have significantly higher temperature solidii, and will therefore dissolve more sluggishly. Assume the mineral-grains of our idealized xenolith are 1-cm cubes, and the xenolith is a 20-cm cube with the mineral-grains stacked randomly, almost all grains will touch a different mineral and start melting upon emplacement. The melting starts along the outer zone and progresses inward as the heat diffuses. Philpotts and Dickinson (2000) showed that plagioclase-frameworks produced during crystallization keep a rock coherent until 75% melting (by volume). Even still, our gabbro-xenolith will then completely disintegrate in less than 45 hours supplying the magma with a melt of similar viscosity and density as itself (Figure 4-10), together with 25 wt% xenocrysts of augite and plagioclase (relative to the initial

Evolution of Oceanic Gabbros: In-situ and Ancient Examples

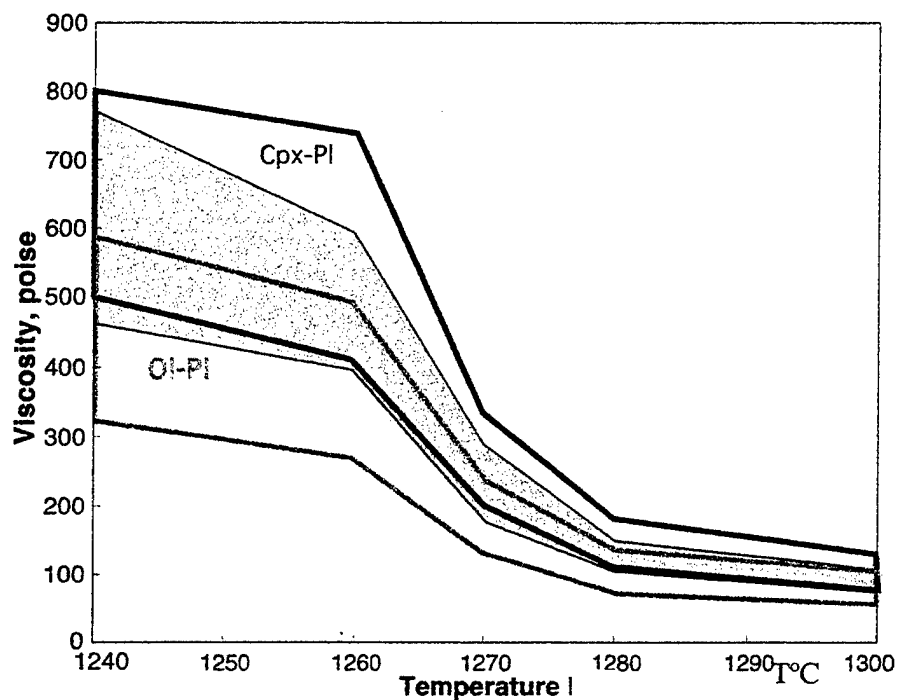


Figure 4-10: The viscosities of the melts produced in our dissolution experiments calculated using Bottinga and Weill (1972). The results are compared to viscosities calculated for lavas from the Southwest Indian Ridge.

Evolution of Oceanic Gabbros: In-situ and Ancient Examples

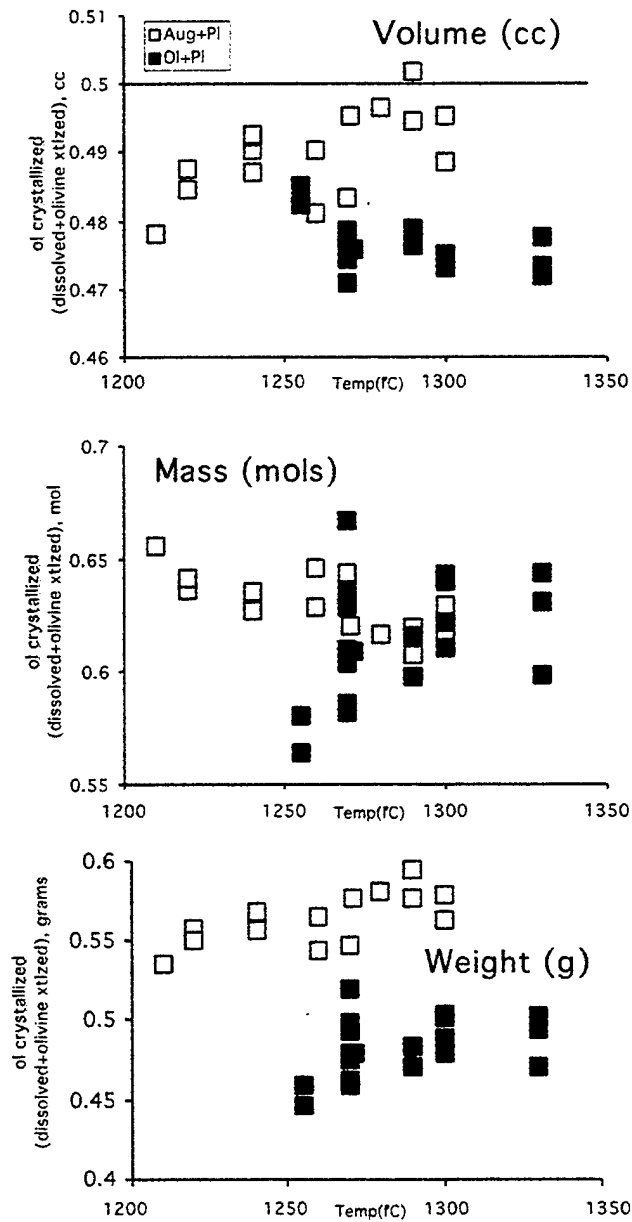


Figure 4-11: The relative fraction of olivine that must be crystallized in order to equal out the heat balance for dissolving gabbro or troctolite. Top: Volume; middle: molar; bottom: grams.

Evolution of Oceanic Gabbros: In-situ and Ancient Examples

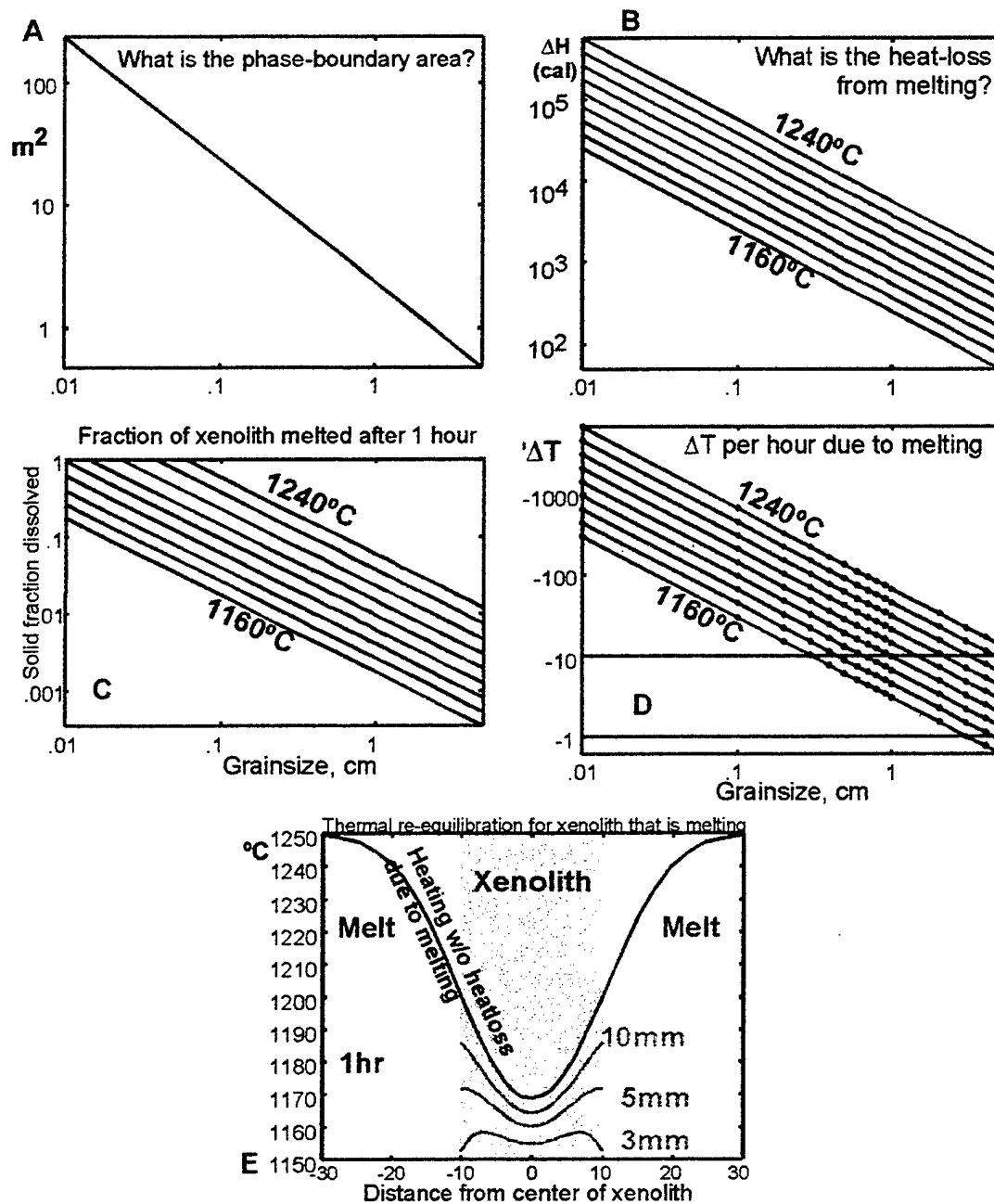


Figure 4-12: A: The geometric area of contact between the minerals of a 20cm biminerale (50:50) cube for varying grainsizes. B: The heat-loss from melting after one hour at different temperatures and grainsizes. C: The fraction of melting relative to the volume of the original xenolith after one hour. D: the temperature drop calculated per hour due to melting on the boundaries. E: The thermal re-equilibration of the xenolith calculated with and without the heat-loss due to dissolution for varying grain sizes in one hour. The results for grain-sizes less than 3mm yield heat-losses so large that they prevent the heat from penetrating the xenolith.

Evolution of Oceanic Gabbros: In-situ and Ancient Examples

xenolith), possibly chained or clustered. A 20 cm xenolith-cube of troctolite will disintegrate in 8 days.

During the melting of the xenolith, the magma itself must compensate for the heat-loss due to the reequilibration and heat of fusion of the minerals. The olivine-saturated melt surrounding the xenolith will therefore start precipitating olivine as the temperature drops in the xenolith's immediate vicinity. In order to be isenthalpic (~no heat lost or gained), ΔH has to be 0. The relative amount of olivine that has to be precipitated from the melt in order to accommodate the heat-loss due to the melting in our experiments is shown in Figure 4-11. Again, assuming isenthalpic conditions (i.e. no heat-loss to the surroundings), if the xenolith melts equal molar amounts of plagioclase and augite, the magma can compensate by crystallizing ~59% as many grams of Fo₈₅. This is both because the ΔH_f for refractory olivine is high, and because plagioclase has a much smaller density than olivine (Table 4-7). In fact, by volume, balancing the heat by crystallization of olivine causes the volume of the melt to increase by 1.2%. A 20 cm xenolith-cube of troctolite cause crystallization of ~58% as many grams of Fo₈₅ and the melt volume will increase by 0.4%. The volume-change depends mostly on the large density-difference between the mafic minerals and plagioclase.

3.d. The effect of grain-size

The previous calculations were performed as a simple two-step calculation, and thus ignored the effect of incipient melting upon the heating of the xenolith. It is clear that the grain-size of a given xenolith is important regarding the amount of heat that is lost due to melting on the phase-boundaries. During the melting-process, the solids must be super-heated relative to the solidus of the phase-boundaries (Wood, 1993). Once the minerals at the phase-boundaries are superheated, the phase-boundaries melt, as this is the more stable state. If the phase-boundaries are close to each other, the melting may cool the xenolith back down to the solidus-temperature. If the phase-boundaries are far enough apart, the heat-loss due to melting is not sufficient to bring them back to the saturation-boundary, and the coarser-grained xenolith-interior can be heated and melt. This provides a mechanism where xenoliths can provide super-solidus melts that are linear combinations of the mineral-phases, causing the entire xenolith to disintegrate.

Evolution of Oceanic Gabbros: In-situ and Ancient Examples

Figure 4-12A demonstrates the potential phase-boundary area for a 20cm xenolith-cube consisting of two phases (1:1) stacked randomly with varying grain-sizes. Since this resembles potential Hole 735B gabbro-xenoliths, we have used the thermodynamic data for typical Atlantis Bank plagioclase and diopside to model the melting. In basaltic systems, troctolite has more plagioclase than olivine, and therefore has a smaller area of two-phase boundaries. The possibility of superheating of the solids during melting of the phase-boundaries is therefore higher in troctolites than in the gabbros. Smaller grain-sizes provide more volume-loss on the phase-boundaries relative to the xenolith. Therefore, the heat supplied by the magma may not be able to penetrate the xenolith at a rate that is faster than the melting process can cool the rock.

A small amount of heating in a fine-grained rock would cause a large fraction of melting (Figure 4-12C), and quickly cause a substantial heat- and temperature-loss (Figure 4-12B, D). A fine-grained gabbro-xenolith would therefore be prevented from thermally re-equilibrating with the melt internally and would instead experience dissolution along its surface. However, if the grains are $\geq 0.3\text{cm}$, then the grain-boundary area is small enough, and the mineral-volume melted in one hour is less than 1% of the original xenolith. This results in less than 10°C temperature-drop due to the melting.

If we model our xenolith as infinite in Y and Z (i.e a one-dimensional model), this provides a simple calculation for the heating of the xenolith in the melt:

$$T(X,t) = T_c + \frac{1}{2} * (T_0 - T_c) * \left[\text{erf}\left(\frac{\xi + 1}{2\sqrt{\tau}}\right) - \text{erf}\left(\frac{\xi - 1}{2\sqrt{\tau}}\right) \right],$$

$$\xi \equiv \frac{X}{a}, \quad \tau \equiv \frac{\kappa * t}{a^2},$$

where κ is the thermal diffusivity ($= 0.008 \text{ cm}^2\text{sec}^{-1}$), T is the temperature at any given place in the X-direction, T_0 is the original temperature at the intrusion time in the xenolith, T_c is the temperature of the melt, a is the half-width of the xenolith, and t is the heating time in seconds. We can then subtract the heat due to melting. In our one-hour model, we found $\Delta T_{\text{melting}} = 9.495 * 10^{(-22)} * (1/\phi(m)) * e^{(3.87110^{02} * T(^{\circ}\text{C}))}$ (ϕ =grain-size) by an exponential fit. Therefore $T_{\text{total}} = T(X,t) - \Delta T_{\text{melting}}$. Figure 4-12E shows how this affects the heating of the xenolith. Cooling of the melt next to the xenolith, as shown in Figure 4-12, would cause it to crystallize, though the thermal effect of this on the melt and xenolith is

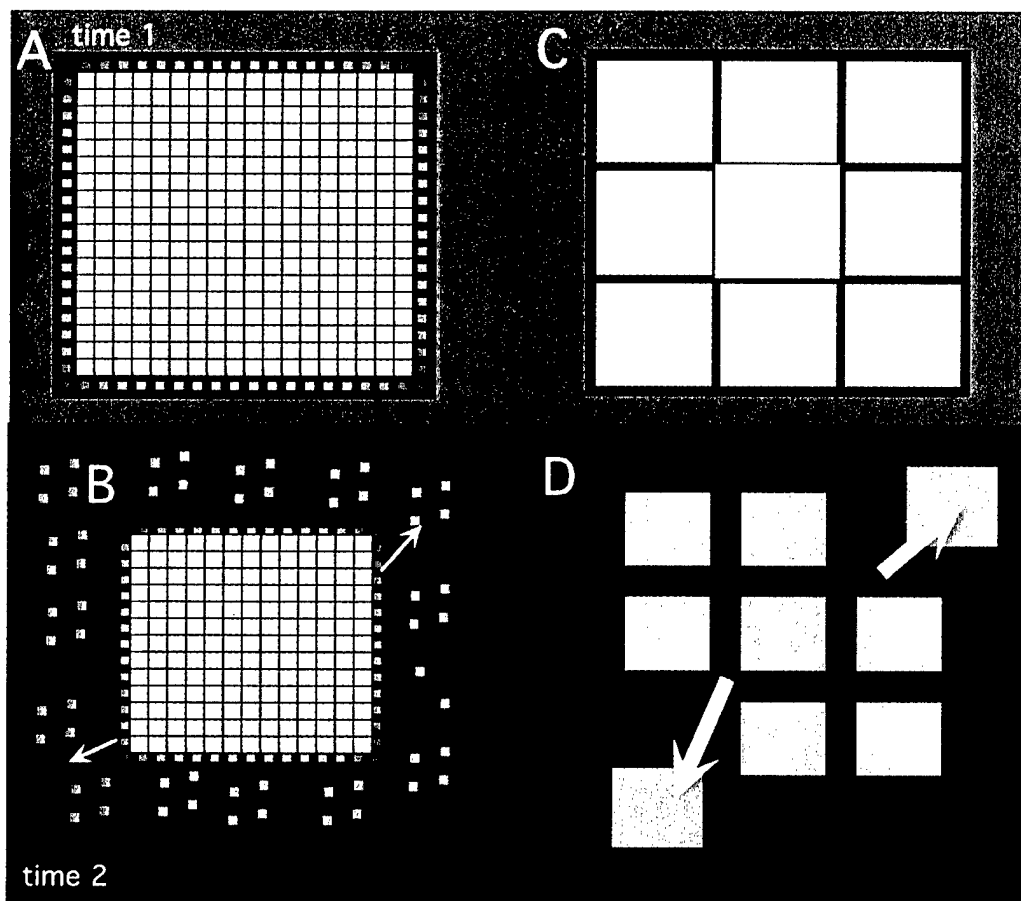


Figure 4-13: The mechanism of dissolution of a xenolith. A: Time 1: A fine-grained xenolith (gridded square) is penetrated by heat (orange) from the surrounding magma (black), causing the minerals to melt in the surroundings. Due to the volume of the melt produced, the dissolution consumes so much heat that none penetrates deep into the xenolith (white= $T < \text{solidus}$). B: Time 2: The same xenolith has generated a mush-zone (much like that described by McLeod and Sparks (1998)) around it, leaving the interior unheated. This creates xenocrysts smaller than in the initial xenolith. C: Time 1: A coarse-grained xenolith with the same amount of melting on the mineral-boundaries as in A has much less melt by volume. Thus, the heat of the magma is able to penetrate into the interior of the xenolith. D: Time 2: The outline of the xenolith is larger than that of B at the same amount of melting. The melt is released either by being compaction, or total disaggregation where (large) xenocrysts are released from the xenolith.

Evolution of Oceanic Gabbros: In-situ and Ancient Examples

not considered directly here. Again, only xenoliths with grain-sizes $\geq 3\text{mm}$ will the support superheat in the solids relative to the solidus of the phase-boundaries. Xenoliths with grain-sizes $< 3\text{mm}$ will be effectively insulated by melting of the outer layer of the xenolith, effectively preventing heat-transfer into the xenolith (Figure 4-13). In fact, if the xenolith has grain-sizes $\sim 0.1\text{mm}$, the melting overwhelms the surface layer in less than 1 minute. Therefore, fine-grained rocks will disintegrate by melting on the outer surface only, whereas larger-grained rock may melt internally and disintegrate after a large fraction of disequilibrium melting.

Our results may explain why fine-grained diabase is frequently found as unmelted xenoliths in lavas, and why layer 2B (the sheeted dikes) is thermally stable and is hard to melt even with a stable magma-chamber lying right beneath it (Sinton and Detrick, 1992). A seismic layer 2B, composed of typical fine-grained sheeted dikes, will be insulated due to preferential melting along its base in contact with a magma-chamber. This effectively prevents the heat transport upward and the rocks are not easily disaggregated and assimilated into the melt. Likewise, it has been observed that fast ridges have finer-grained gabbros compared to slow ridges (observed by Dick et al., 2002, and quantified using crystal-size distributions by Coogan et al., 2002 (EPR); Meyer and Sapp, 1994 (Hole 735B)). In fact, the slow spreading ridges often have ultraphyric lavas containing large grains ($> 3\text{mm}$) of plagioclase (Mével et al., 2002), suggested to be xenocrysts (Coettze, 2001).

3.e. The effect of mineral density

We found that the melting rate slowed down in our early experiments as the minerals floated apart, and the melting-rates are thus faster if the minerals are kept in close contact. Plagioclase is buoyant ($\rho \sim 2.7\text{g/cc}$) and clinopyroxene is dense ($\rho \sim 3.2\text{g/cc}$) relative to the melt produced within the xenolith, allowing the minerals to separate if there is no rotation of the xenolith. If the olivine precipitating from the melt uses the xenolith to nucleate on, it might become completely capped by the olivine, further accommodating the separation of the minerals, since the release of the minerals to the magma will not happen independently of the others. If the enclosure is complete, pressure might start rising inside the xenolith, and failure of the olivine-layer may cause

Evolution of Oceanic Gabbros: In-situ and Ancient Examples

catastrophic mixing with the surrounding magma. The now isolated plagioclase crystals will rise and the clinopyroxene and olivine will sink.

3.f. Geochemical consequences of syntexis

At least for major elements, xenoliths that melt out of equilibrium will not significantly equilibrate by solid-state diffusion with the magma until they are disaggregated into it as mono-mineralic clusters or are far enough away from other xenocrysts. The interstitial dissolution-derived melts formed within the xenoliths have similar viscosities as magma with the same temperature, and should therefore be able to readily mix with it following disaggregation (Figure 4-10).

If gabbro-xenoliths are assimilated into the ascending magma in this way, the liquid line of descent (LLD) will be disturbed (Figure 4-14, bottom). Normally, an olivine-saturated magma (a) will precipitate olivine along path 2 until the melt is of composition 'b' at the plagioclase-olivine-melt saturation-boundary and proceed towards the olivine-plagioclase-augite-melt saturation-boundary at 'e'. However, 'pl-ol' and 'cpx-pl' represent typical melts produced in our melting-experiments. If melt 'a' assimilates a gabbro xenolith-suite, 'cpx-pl', and accommodates the heat-loss by crystallization of olivine, the melt will start to follow the curved path 1. If the melt assimilates troctolitic xenoliths (pl-ol), it will start to follow curved path 3. 'e' is the olivine-plagioclase-augite-melt saturation-boundary at 1atm, and the boundary moves downwards with pressure (white squares representing 2, 4 and 8kbar, respectively). If gabbro-assimilation happens at lower crustal pressures (~2-3kbar), then less troctolite will be initially produced before augite starts crystallizing. The melt that forms the initial olivine-gabbro assemblages at the 4-phase saturation boundary will therefore have higher Mg#'s and Ca#'s than the melt following path 2. Assimilation of troctolite, however, brings the liquid onto the plagioclase-olivine-melt saturation boundary higher up towards "pl-ol", and causes more, high Mg#, troctolite to form. Since the mafic minerals dissolve without solid-state re-equilibration the Mg# of the consumed solid becomes the Mg# of the xenolith-derived melt causing elevated Mg#'s in the hybrid melts. Figure 4-14 (top) shows that gabbro-assimilation (the arrow with Cpx-pl) creates melts that have a larger clinopyroxene-component compared to the melt that only crystallized olivine ("Ol frac")

Evolution of Oceanic Gabbros: In-situ and Ancient Examples

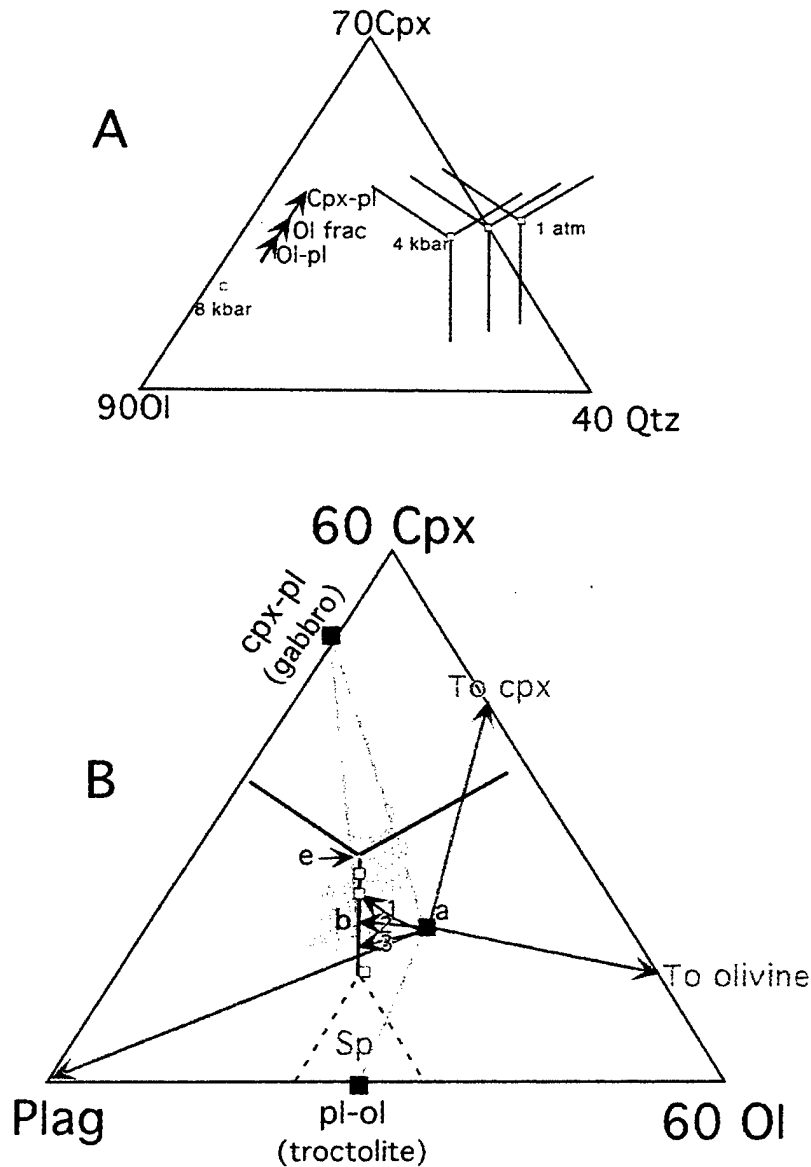


Figure 4-14: The pseudoternary projection (as in Figure 1) of the potential compositions of melts that have assimilated lower crustal material. A: The black arrow shows the LLD of a primary melt that has just crystallized olivine (Ol frac), has in addition assimilated gabbro (Cpx-pl) and has assimilated troctolite (Ol-pl). The experimentally determined saturation-boundaries are indicated (right to left) for 1atm, 2kbar, 4kbar and 8kbar. B: a=the mantle derived, primary melt (Kinzel and Grove, 1992); pl-ol=troctolite; cpx-pl=gabbro; e=4-phase saturation boundary; grey arrows point to mineral compositions; gray lines show the vectors from the melt to the lower crustal compositions; b=where 2 intersects the plagioclase-olivine cotectic; black lines=cotectics; broken black line is the projected field for spinel; Plag=100% plagioclase, gray squares are basalt glasses from the entire Southwest Indian Ridge. Curve 1 is fractionation of olivine only, curve 2 indicates gabbro-assimilation while fractionating olivine, and curve 3 indicates assimilation of troctolite while fractionating olivine. See text for additional explanation.

Evolution of Oceanic Gabbros: In-situ and Ancient Examples

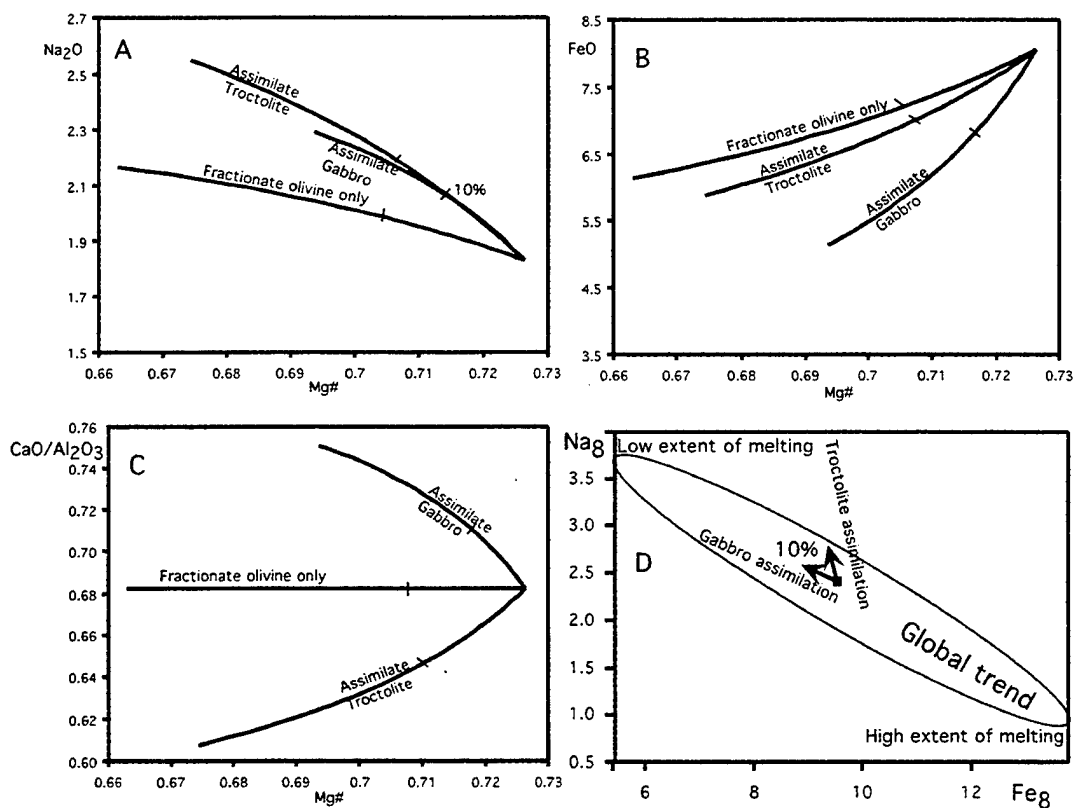


Figure 4-15: A-C: The chemical effect of assimilation of lower crustal material. The heat is balanced by fractionation of olivine. The tag on the lines indicates 10% assimilation or crystallization. Mg\# =molar $\text{Mg}/(\text{Mg}+\text{Fe})$. D: The effect of assimilation of 10wt% gabbros or troctolite on a primary melt composition. Klein and Langmuir (1987) suggested that the global trend of the basalt compositions emulate the potential temperature of the mantle. High temperatures cause higher extent of melting than lower temperature melting of identical sources.

Evolution of Oceanic Gabbros: In-situ and Ancient Examples

giving the appearance of originating at lower pressure. Troctolite-assimilation, on the other hand, makes the melts have less augite-component and more olivine component, causing them to appear as if they crystallized at a higher pressure, possibly causing the local trends described by Klein and Langmuir (1989).

In summary, melts produced by dissolution of cumulates will have higher Mg#’s than the liquids that originally precipitated the cumulate minerals. If these dissolution-produced liquids are added to a MORB melt, the resulting mixed melt would appear more primitive than the melt that was left from the initial crystallization of the cumulates. Mixing of xenolith-derived magmas into a mantle-derived magma as described above will increase the Na₂O content of the magma, and decrease the FeO-content (Figure 4-15). However, the CaO/Al₂O₃ ratio moves in opposite directions, gabbro assimilation increases the ratio, whereas troctolite assimilation decreases it. Therefore, with respect to the “Global trend” of Klein and Langmuir (1987), gabbro assimilation into primitive magma makes the hybrid melt appear as if was produced by a lower degree of melting, whereas assimilation of troctolite moves the melt along the local trend of Klein and Langmuir (1989).

4. Conclusions

We have shown that the lower ocean crust melts efficiently when exposed to ascending melts at ocean ridges. We find that average plagioclase-olivine and plagioclase-augite pairs from the lower crust at the Southwest Indian Ridge have solidii at 1195 and 1150°C, and melt fast and out of equilibrium at temperatures significantly above the solidii. Dissolution experiments performed using natural, average olivine – plagioclase and clinopyroxene - plagioclase mineral pairs, under conditions applicable to oceanic magmatism, show dissolution mechanisms similar to those found in other experimental studies that utilized endmember mineral compositions.

The experimental results indicate that melting of oceanic lower crust may produce disequilibrium melt compositions. However, lower crustal material can only be easily and pervasively superheated relative to the solidii of the phase-boundaries if the grain sizes are sufficiently large. Coarse-grained rocks (>3mm) will disintegrate internally upon reheating, whereas finer grained rocks will melt from the outside in. The resulting

Evolution of Oceanic Gabbros: In-situ and Ancient Examples

disequilibrium melts are linear mixes of the mineral-compositions. If these melts are allowed to mix into the ascending magma, the new magma will have higher Na_8 and lower Fe_8 than the original emulating the global trend of Klein and Langmuir (1987).

Assimilation of gabbro into magma with only olivine on the liquidus forces the liquid line of descent towards the olivine-plagioclase-augite-melt eutectic, effectively suppressing the formation of troctolite as it brings the liquid onto the plagioclase-olivine-melt saturation boundary closer to the olivine-plagioclase-augite-melt saturation boundary. Thus, crustal assimilation of gabbro will result in the less troctolites in the lower crust, and will lead to the early onset of high-Mg# olivine-gabbros. Troctolite assimilation, on the other hand, leads the liquid line of descent further up on the plagioclase-olivine saturation boundary, producing more, and more primitive-looking troctolites, causing the hybrid melts to define the local trends of Klein and Langmuir (1989).

Caution should be taken when using basalts and gabbros to deduce the extent and pressure of melting in the mantle and crystallization in the lower crust and estimating crustal thickness (e.g. Klein and Langmuir, 1987; McKenzie and Bickle, 1988). Instead, the entire crustal budget should be known, including lavas, dikes and gabbros, so that the effect of assimilation between the ascending magmas and the lower crust can be eliminated.

References cited

- Armstrong, JT, 1995: CITZAF: A package of correction programs for the quantitative electron microbeam x-ray analyses of thick polished materials, thin films, and particles. *Microbeam analysis*, 4: 177-200.
- Bédard JH, 1988: Magma chamber dynamics and recycling of crustal cumulates by the mantle: Evidence from the Bay of Islands Ophiolite (abs): *Eos* 69:1476.
- Bédard JH, 1991: Cumulate recycling and crustal evolution on the Bay of Islands ophiolite. *Journ Geol* 99: 225-249.
- Bédard JH, 1993: Oceanic crust as a reactive filter: Synkinematic intrusion, hybridization and assimilation in an ophiolitic magma chamber, Newfoundland. *Geology* 21: 77-80.
- Bédard JH, 2000: Syntexis and the genesis of lower ocean crust. In Dilek Y. Moores EM> Elthon D> Nicholas A (eds), *Ophiolites and Oceanic Crust: New insights from Field Studies and the Ocean Drilling Program: Boulder Colorado, Geological Soc America Spec Paper* 349: 105-119.
- Biggar GM. Humphries DJ, 1981: The plagioclase, forsterite, diopside liquid equilibrium in the system $\text{CaO-Na}_2\text{O-MgO-Al}_2\text{O}_3\text{-SiO}_2$. *Min Mag Vol* 44: 309-314.
- Bottinga Y. Weill DF, 1972. The viscosity of magmatic silicate liquids: a model for calculation. *Amer Journ Sci* 272: 438-475.
- Boudier F. Nicholas A. Ildefonse B, 1996: Magma chambers in the Oman ophiolite: Fed from the top and the bottom. *Earth Planet Sci Lett* 144, 239-250.

Evolution of Oceanic Gabbros: In-situ and Ancient Examples

- Bowen NL, 1928: The evolution of the igneous rocks. Princeton University Press (Reprinted by Dover Press 1956).
- Chen YJ and Lin J in press: High sensitivity of ocean ridge thermal structure to changes in magma supply: the Galápagos Spreading Center. *Earth Planet Sci Lett*, in press.
- Chen YJ, 2001: Thermal effects of gabbro accretion from a deeper second melt lens at the fast spreading East Pacific Rise. *Journ Geophys Res.* 106 (B5) 8581-8588.
- Coetzee, M, 2001: Petrography and Geochemistry of Plagioclase Phyric Basalts: Xenocrysts and melt inclusions as evidence of magma mixing. Honours Project, Department of Geological Sciences, University of Cape Town, South Africa.
- Coleman, 1977: Ophiolites. John Wiley and sons, 229pp.
- Coogan LA. Gillis KM. MacLeod CJ. Thompson GM. Hékinian R, 2002: Petrology and geochemistry of the lower ocean crust form at the East Pacific Rise and exposed at Hess Deep: A synthesis and new results. *Geochem. Geophys. Geosyst.*, 3(11) 8604, doi: 101029/2001GC000230.
- Crank, J 1975, The Mathematics of Diffusion. Oxford: Clarendon Press.
- Crawford WC. Webb SC, 2002: Variations in the distribution of magma in the lower crust and at the Moho beneath the East Pacific Rise at 9°-10°N. *Earth Planet Sci Lett* 203: 117-130.
- DePaolo DJ, 1981: Trace element and isotopic effects on combined wallrock assimilation and fractional crystallization. *Earth Planet Sci Lett* 53:189-202.
- Detrick RS. Buhl P. Vera E. Mutter J. Orcutt J. Madsen J. Brocher T, 1987: Multi-channel seismic imaging of a crustal magma chamber along the East Pacific Rise. *Nature* 326: 35-41.
- Dewey JF. Kidd WSF, 1977: Geometry of plate accretion. *Geol Soc Am. Bull* 88:960-968.
- Dick HJB. Natland JH. Alt JC. Bach W. Bideau D. Gee JS. Haggas S. Hertogen JGH. Hirth JG. Holm PM. Ildefonse B. Iturrino GJ. John BE. Kelley DS. Kikawa E. Kingdon A. LeRoux PJ. Maeda J. Meyer PS. Miller DJ. Naslund HR. Niu YL. Robinson PT. Snow J. Stephen RA. Trimby PW. Worm HU. Yoshinobu A (2000) A long in situ section of the lower ocean crust; results of ODP Leg 176 drilling at the Southwest Indian Ridge. *Earth Planet Sci Lett* 179 (1): 31-51.
- Dunn RA. Toomey DR. Solomon SC, 2000: Three-dimensional seismic structure and physical properties of the crust and shallow mantle beneath the East Pacific Rise at 9°30'N. *J. Geophys Res.* 105: 23,537-23,555.
- Fodor RV. Galar P, 1997: A View onto the Subsurface of Mauna Kea Volcano, Hawaii: Crystallization Processes Interpreted through the Petrology and Petrography of Gabbroic and Ultramafic Xenoliths. *Journ Petrol* 38 (5): 581-624.
- Gaetani GA. Watson EB, 2000: Open system behavior of olivine-hosted melt inclusions. *Earth Planet Sci Lett* 183: 27-41.
- Ghiorso MS. Carmichael ISE, 1980: A Regular Solution Model for Met-Aluminous Silicate Liquids: Applications to Geothermometry, Immiscibility, and the source regions of Basic Magmas. *Contrib Mineral Petrol* 71: 323-342.
- Green DH. Falloon TJ. Eggins SM. Yaxley GM, 2000: Primary magmas and mantle temperatures. *Eur Journ Mineral* 13: 437-451.
- Grove TL, 1981: Use of FePt alloys to eliminate the iron-loss problem in 1-atmosphere gas mixing experiments: theoretical and practical considerations. *Contrib Mineral Petrol* 78: 289-304.
- Grove TL. Bence AE, 1977: Experimental study of pyroxene-liquid interaction in quartz-normative basalt 15597. *Proc Lunar Sci Conf* 8th: 1549-1579.
- Grove, TL. Kinzler RJ, 1992: Fractionation of mid-ocean ridge basalts (MORB). In: J Sinton et al. (eds) *Mantle flow and melt generation at mid-ocean ridges*. *Geophys Monograph*, AGU, Wash DC: 281-310.
- Harding AJ. Orcutt JA. Kappus ME. Vera EE> Mutter JC. Buhl P. Detrick RS. Brocher TM, 1989: Structure of young oceanic crust at 13°N on the East Pacific Rise from expanding spread profiles. *Journ Geophys Res* 94: B12,163-12,196.
- Hawkesworth C. George R. Turner S. Zellmer G, 2004: Time scales for magmatic processes. *Earth Planet Sci Lett* 218: 1-16, doi:10.1016/S0012-821X(03)00634-4.
- Henstock TJ. Woods AW. White RS, 1993: The accretion of oceanic crust by episodic sill intrusion. *Journ Geophys Res* 98:B4,143-4,161.
- Huebner JS. Turnock AC, 1980: The melting relations at 1bar of pyroxenes composed largely of Ca-, Mg-, and Fe-bearing components. *Amer Mineral* 65 (3-4): 225-271.

Evolution of Oceanic Gabbros: In-situ and Ancient Examples

- Jerram DA, Cheadle MJ, Philpotts AR, 2003: Quantifying the Building Blocks of Igneous Rocks: Are Clustered Crystal Frameworks the Foundation? *Journ Petrol* 44 (11): 2033-2051. DOI: 10.1093/petrology/egg069.
- Kelemen PB, 1990: Reaction between Ultramafic Rock and Fractionating Basaltic Magma 1: Phase Relations, the Origin of Calc-alkaline Magma Series and the Formation of Discordant Dunite. *Journ Petrol* 31 (1): 51-98.
- Kelemen PB, Koga K., Shimizu N, 1997b: Geochemistry of gabbro sills in the crust-mantle transition zone of the Oman ophiolite: implications for the origin of the oceanic lower crust. *Earth Planet Sci Lett* 146: 475-488.
- Kerr RC, 1995: Convective crystal dissolution. *Contrib Mineral Petrol* 121: 237-246.
- Kinzler RJ. and Grove TL, 1992: Primary magmas of midocean ridge basalts: 1. Experiments and Methods. *Journ Geophys Res* 97: B6,885-6,906.
- Klein EM, Langmuir CH, 1989: Local versus global variations in ocean ridge basalt composition: A reply. *Journ Geophys Res*: 94 (B4): 4241-4252.
- Klein EM, Langmuir CH, 1987: Global correlations of ocean ridge basalt chemistry with axial depth and crustal thickness. *J. Geophys. Res.*, 92 (B8) 8089-8115.
- Korenaga J, Kelemen PB, 1997: Origin of gabbro sills in the Moho transition zone of the Oman ophiolite: Implications for magma transport in the oceanic lower crust. *J. Geophys. Res.*, 102 (B12): 27,729-27,749.
- Kuo LC, Kirkpatrick RJ, 1985: Kinetics of crystal dissolution in the system diopside-forsterite-silica. *Amer Journ Sci* 285: 51-90.
- Liang Y, 2000: Dissolution in molten silicates: effects of solid solution. *Geochim Cosmochim Acta* 64 (9): 1617-1627.
- MacLennan J, Hulme T, Singh SC, 2004: Thermal models of oceanic crustal accretion: Linking geophysical, geological and petrological observations. *Geochim Geophys Geosyst* 5 (2) doi 10.1029/2003/GC000605.
- Marvin UB, Walker D, 1985: A Transient Heating Event in the History of a Highlands Troctolite from Apollo 12 Soil 12033. *Proc 5th Lunar Planet Sci Conf* (2), *Journ Geophys Res* 90: C421-C429.
- McKenzie D, Bickle MJ, 1988: The volume and composition of melt generated by extension of the lithosphere. *Journ Petrol* 29: 625-679.
- McLeod P, Sparks RSJ, 1998: The dynamics of xenolith assimilation. *Contrib Mineral Petrol* 132:21-33.
- Mével C, Toplis MJ, Humpler E, Meyzen C, Ludden J, 2002: Major and Rare Earth Element Zoning of Plagioclase Phenocrysts in Basalts from the Southwest Indian Ridge (69-49°E). In: *Interridge Workshop on the Southwest Indian Ridge*, Southampton Oceanography Centre, UK, p 52.
- Meyer PS, Sapp K, 1994: Crystal Size Distribution, Mineral Chemistry, and Crystallization History of ODP Site 735B Gabbros. In: *EOS Suppl, Fall AGU*: 627.
- Mysen BO, 1988: Structure and properties of silicate melts. In: *Developments in Geochemistry* 4, Elsevier, Amsterdam, Netherlands, 354p.
- Pedersen RB, 1986: The nature and significance of magma chamber margins in ophiolites: examples from the Norwegian Caledonides. *Earth Planet Sci Lett* 77: 100-112.
- Presnall, DC, Gundfínsson GH, Walther MJ, 2002: Generation of mid-ocean ridge basalts at pressures from 1 to 7 GPa. *Geochim Cosmochim Acta* 66 (12): 2073-2090.
- Natland JH, Dick HJB, 2000: Stratigraphy and Composition of Gabbros Drilled in Ocean Drilling Program Hole 735B, Southwest Indian Ridge: A synthesis of Geochemical Data. In Natland JH, Dick HJB, Miller DJ, Von Herzen RP (eds) *Proceedings of the Ocean Drilling Program, Scientific Results Volume 176*. 1-69 (CD-ROM).
- Neumann ER, Sørensen VB, Simonsen SL, Johnsen K, 2000: Gabbro xenoliths from La Palma, Tenerife and Lanzarote, Canary Islands: evidence for reactions between mafic alkaline Canary Islands melts and old oceanic crust. *Journ Volcanol Geotherm Res* 103: 313-342.
- Philpotts AR, Dickinson LD, 2000: The formation of plagioclase chains during convective transfer in basaltic magma. *Nature* 406 (6791): 59-61.
- Phipps Morgan J. and Chen YJ, 1993: The genesis of oceanic crust, magma injection, hydrothermal circulation and crustal flow. *Journ Geophys Res* 98: B6,283-6,297.
- Phipps Morgan, J., and Y.J. Chen, 1993b: Dependence of ridge-axis morphology on magma supply and spreading rate, *Nature*, 364, 706-708,

Evolution of Oceanic Gabbros: In-situ and Ancient Examples

- Quick JE, Denlinger RP, 1993: Ductile deformation and the origin of layered gabbro in ophiolites. *Journ Geophys Res* 98: B14,015-14,027.
- Rivalenti G 1980: Guide to the excursion in the Balmuccia Zone, Sesia Valley, Ivrea-Verbano Complex. In: *Proceedings of the 2nd symposium Ivrea-Verbano, Memorie degli Istituti Geologia e Mineralogia dell' Università di Padova*, vol. 33, pp 3-9, 1979.
- Robie RA, Hemingway BS, Fisher JR, 1978: Thermodynamic properties of minerals and related substances at 298.15K and 1bar (105 pascals) pressure and higher temperatures. *US Geological Survey Bulletin Vol 1452*: 456pp.
- Sinton JM, Detrick RS, 1992: Mid-ocean ridge magma chambers. *J. Geophys. Res.*, 97 197-216.
- Sleep NH, 1975. Formation of oceanic crust: Some thermal constraints. *Journ Geophys Res* 80: B4,037-B4,042.
- Spear, FS, 1993: Metamorphic Phase Equilibria and Pressure-Temperature-Time Paths. *Mineral Soc Am Monograph* 799p.
- Tormey DR, Grove TL, Bryan WB, 1987: Experimental petrology of normal MORB near the Kane Fracture Zone: 22°-25°N, mid-Atlantic ridge. *Contrib Mineral Petrol* 96: 121-139.
- Tsuchiyama A, 1985: Partial melting kinetics of plagioclase-diopside pairs. *Contrib Mineral Petrol* 91:12-23.
- Tsuchiyama A, 1986: Melting and dissolution kinetics: Application to partial melting and dissolution of xenoliths. *Journ Geophys Res* 91 (B9): 9395-9406.
- Tucholke BE, Lin J, Kleinrock MC, 1998: Megamullions and mullion structure defining metamorphic core complexes on the Mid-Atlantic Ridge. *J. Geophys Res.* 103 (B5) 9857-9866.
- Turcotte DL, Schubert G, 1982: Geodynamics: Applications of Continuum Physics to Geological Problems. *John Wiley & Sons, Inc. New York*, pp450.
- Ulmer P, 1989: The dependence of the Fe²⁺-Mg cation partitioning between olivine and basaltic liquid on pressure, temperature and composition. *Contrib Mineral Petrol* 101: 261-273.
- Van Orman JA, Grove TL, 2000: Origin of lunar high-titanium ultramafic glass: Constraints from phase relations and dissolution kinetics of clinopyroxene-ilmenite cumulates. *Meteor Planet Sci* 35: 783-794.
- Vera EE, Mutter JC, Buhl P, Orcutt JA, Harding AJ, Kappus ME et al., 1990: The structure of 0- to 0.2 m.y. old oceanic crust at 9°N on the East Pacific Rise from expanded spread profiles. *Journ Geophys Res* 95: B15,529-B15,556.
- Watson EB, 1982: Basalt Contamination by Continental Crust: Some Experiments and Models. *Contrib Mineral Petrol* 80:73-87
- Watson S, McKenzie D, 1991: Melt generation by plumes; a study of Hawaiian volcanism. *Journ Petrol* 32 (3): 501-537.
- Woods AW, 1992: Melting and dissolving. *Journ Fluid Mech* 239: 429-448.
- Yang HJ, Frey FA, Clague DA, 2003: Constraints on the Source Components of Lavas Forming the Hawaiian North Arch and Honolulu Volcanics. *Journ Petrol* 44 (4): 603-627.
- Zhang Y, Walker D, Leshner CE, 1989: Diffusive crystal dissolution. *Contrib Mineral Petrol* 102:492-513.

Chapter 5

Mineral chemistry of gabbros from Atlantis Bank outside Hole 735B

Abstract

We have analyzed the major element compositions of the magmatic minerals of 99 gabbros from on and around Atlantis Bank, South West Indian Ridge, including the top carapace of the bank, the Western Wall, and the slopes to the north and the south, covering an area of almost 660-km². Samples from the northern area have the most primitive magmatic minerals, extending to ferrogabbros with evolved mineral-compositions. The southern rocks are all evolved, including layered olivine-gabbros sampled at gabbro-peridotite contacts. Gabbros from the Western Wall and the top of the bank have intermediate compositions. Despite the large variations in mineral chemistry in our samples, the primitive and evolved ends of the ODP Hole 735B spectrum are not present in our data. No plagioclase with anorthite contents higher than An_{71.5} has been recovered, anorthite higher than An₆₄ is rare, and no magmatic plagioclase has been found with anorthite below An₃₂. Likewise, augite compositions generally range from 60 to 86.3 molar Mg/(Fe+Mg)*100 or Mg#, where Hole 735B augite compositions range from 54 to 89. Although we have sampled the area extensively, we find that, like the gabbros from Hole 735B, the surface samples represent melts that have crystallized 50-90% relative to mantle-derived compositions. As discussed in Chapter 3, the overall variation of the gabbros is broadly consistent with control of the liquid-line of descent by fractional crystallization (modified by post-cumulus processes). If the lower crust was accreted by fractional crystallization, large amounts of troctolite should exist somewhere in the lowermost crust or intruded into residual mantle at depths below what is exposed on the sea-floor or drilled in Hole 735B.

As in Hole 735B, augite is more magnesian than expected for any coexisting plagioclase anorthite content, and plagioclase and augite are frequently reversely zoned. TiO₂ contents of augite vary inversely with Mg# at all levels of evolution, even after

Evolution of Oceanic Gabbros: In-situ and Ancient Examples

magnetite and ilmenite crystallized, suggesting extensive reaction, dissolution and reprecipitation within the cumulate pile. A simple fractional-crystallization model would therefore not be suitable. We propose an alternative model where some originally primitive cumulates may have been re-homogenized and transformed by later, interstitial melts.

1 Introduction

The nature of accretion of the lower crust at spreading-ridges has mainly been determined by the study of ophiolites as analogues. The origin of many ophiolites is unfortunately uncertain (e.g. Miyashiro, 1979), and the exact crystallization conditions and primary melt compositions may be different at modern ocean ridges.

Tectonic windows make the investigation of the lower ocean crust in the modern oceans possible, and current technology makes them accessible. Atlantis Bank is a well-known example of an paleo-inside corner high found at the ultraslow spreading Southwest Indian Ridge. It is located 11-Ma off axis, south of the present-day rift valleys on the eastern side of Atlantis II Fracture Zone (Dick *et al.*, 1987). Spreading rate is asymmetric, 8.5-mm/y to the South and 5.5-mm/y to the North. The 700-meter deep platform and its surrounding slopes represent the largest outcrop of gabbroic rocks known in the modern oceans. The lower crustal section is exposed along a low-angle detachment-fault surface that rooted in the dike/gabbro transition, or possibly in a shallow magma-chamber or crustal mush-zone (Dick *et al.*, 2001). The exhumation exposed lower crustal rocks for 4-My of seafloor spreading at the ridge, and we have mapped gabbroic outcrops over 660-km² (Figure 5-1) extending 39-km in the plate spreading direction (Dick *et al.*, 2001). ODP Hole 735B provides a 1500 meter deep vertical section, contributing to a 3D perspective of the platform. In addition, Hole 1105A was drilled about 1.3-km northeast of Hole 735B and penetrated 158-m (Shipboard Scientific Party, 1999).

The Western Wall of Atlantis Bank faces the Atlantis II Transform Valley. Altered mantle rocks are exposed on the trench wall, more than 2000-m below the bottom depth Hole 735B to the northwest and < 500-m to the southwest at all depths

Evolution of Oceanic Gabbros: In-situ and Ancient Examples

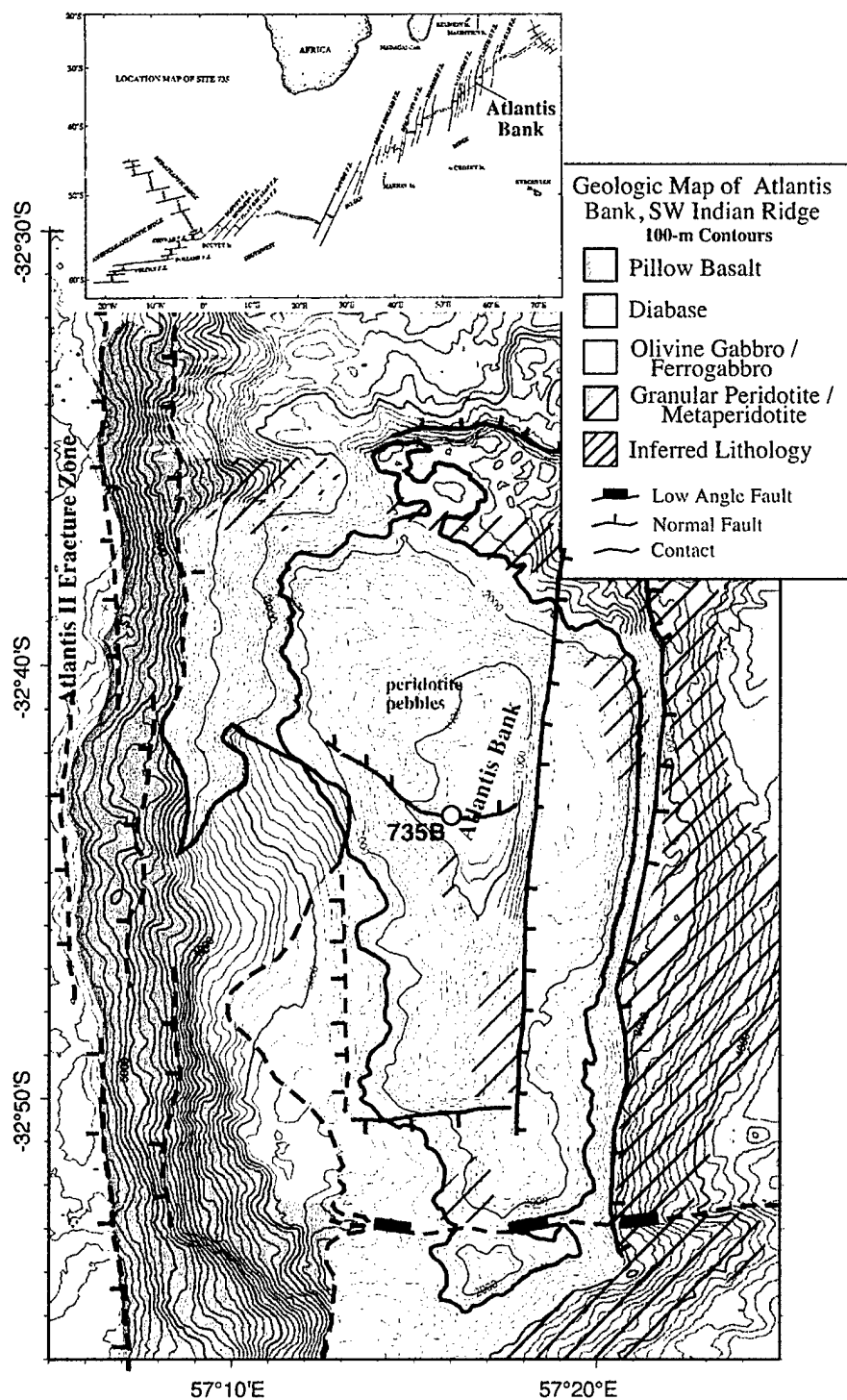


Figure 5-1: The geology of Atlantis Bank (Dick et al., in prep). A thick contour-line outlines the bottom of Hole 735B.

Evolution of Oceanic Gabbros: In-situ and Ancient Examples

shallower than the Hole along the transform wall to the west (Fig. 5-1). The Northern Wall faces the termination of the detachment with pillow basalts exposed to the north. The Eastern wall has two down-faulted blocks that terminate in a volcanic terrain to the east. The detachment break-away zone to the south has not yet been found, although it is inferred morphologically from apparent constructional volcanic edifices that replace the gabbro-dike terrain south of 32° 52' S.

Bloomer et al. (1991), Dick et al., (2000, 2001) and Coogan et al., (2001) observed that the expected primitive section of cumulates is missing in Hole 735B. Coogan et al (op. cit.) argued that Hole 735B was drilled closer to Atlantis II Fracture Zone than to the magmatic segment center (AN-1) and the authors therefore proposed that the missing cumulates were either deeper in the section towards the crust-mantle boundary, or towards the eastern wall of the bank if not in the mantle itself. They also suggested that the evolved nature of the lower crustal rock is due to incorporation of large amounts of trapped melt. Serpentinities west of Hole 735B represent gouge intruded laterally along the detachment fault, and show that these locally overlie the gabbro massifs west of Hole 735B (Fig. 5-1) (Dick pers. comm.). Dick et al (1987) and Hosford et al (2003) showed that Atlantis Bank is the center of a small sub ridge-segment and Muller *et al.*, (1997) found the seismic crustal thickness is 5 ± 1 -km close to Hole 735B, thinning towards the sides of the platform. An extensive sampling-survey was performed on and around Atlantis Bank to allow us to constrain the regional distribution of lithologies and the magmatic mineral-compositions in both time and space.

The results of major element mineral analysis of gabbro samples from James Clark Ross 31 ("JR-31") Bridge ("BR")- and British Geological Survey ("BGS")-cores and dredges, and SHINKAI 6500 dive samples from the MODE 98 and ABCDE expeditions to Atlantis Bank are reported here. The purpose of this paper is to describe the 3-D distribution of mineral-compositions on and around Atlantis Bank and to find the primitive, missing cumulates, or explain why they are missing.

Evolution of Oceanic Gabbros: In-situ and Ancient Examples

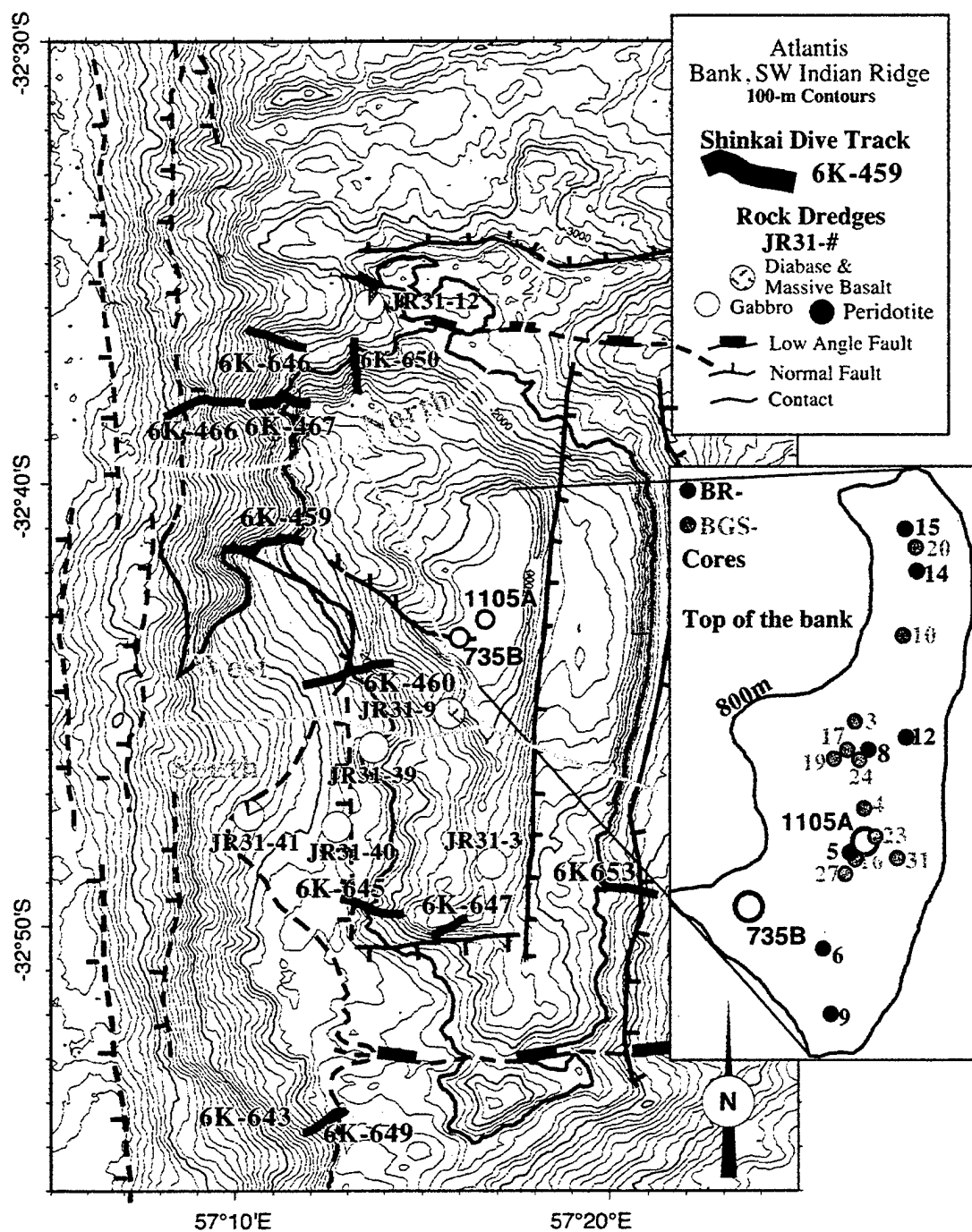


Figure 5-2: Sample locations for this study. The thick gray contour line indicates the termination of Hole 735B, and the thinner gray lines show the geographic sample divisions discussed in the text.

Evolution of Oceanic Gabbros: In-situ and Ancient Examples

2 Materials

The rocks from this study are sampled from the top and sides of Atlantis Bank. Site collections were chosen based on lack of alteration, number of useful samples in each collection and density of sampling in a given area. We attempted to analyze magmatic plagioclase and clinopyroxene (\pm olivine and orthopyroxene) for each sample, and if one of these two were completely altered to metamorphic minerals, the sample was not chosen for analysis. Some collections were picked even with a single sample, if it was the only one in the given area. Likewise, somewhat altered samples were not chosen in areas with a lot of coverage. The locations of the dives, dredges, and cores from which we chose samples are shown in Figure 5-2.

The JR-31 expedition sampled a number of shallow (1-2-m) rock drill-cores on the top of the bank, and 52 dredges around its sides. Six of these dredges (JR31-3, 9, -12, -39, -40, and -41) were chosen for this study as they contained several samples of fresh gabbro. Seven of the oriented BR-cores and 10 non-oriented BGS-cores from the 22-km² platform at the top of the bank were also selected for analysis.

The MODE 98 and ABCDE expeditions used SHINKAI 6500 to sample traverses up the sides of the bank. Mode 98 sampled the west wall of the bank, and dives 6K-459, 6K-460, 6K-466, and 6K-467 were selected for analysis. One sample, 6K-467-11, is a dike that contains plagioclase and clinopyroxene. Cruise ABCDE sampled all sides of the bank and seven dives were selected (6K-643, -645, -646, -647, -649, -650, and -653). The samples are listed in Table 5-1 and collection-locations are shown in Figure 5-2.

We have divided the bank into four study areas. The platform area ("Top of the bank") includes all the JR31-BR- and BGS-drill cores, and Hole 735B. The northern area ("North") includes JR31-12, 6K-466/467, 6K-646, and 6K-650, the western area ("West") JR31-9, and 6K-459 and 6K-460, and the southern area ("South") consists of JR31-3, -39, -40, and -41 and 6K-643, -645, -647, -649, and -653.

3 Methods

The magmatic minerals, olivine, clinopyroxene, orthopyroxene and plagioclase, were analyzed with the MIT 4 and 5-spectrometer JEOL 733 Superprobes, using 15kV accelerating voltage and 10nA beam current. When possible, continuous 10- μ m 10-spot traverses in the core and the rim of adjacent mineral-grains of plagioclase and clinopyroxene were analyzed. Continuous 10- μ m 6-spot traverses in the core and rim of orthopyroxene were analyzed, whereas olivines were analyzed in six spots throughout the crystal. A 10 nA beam current, 15 kV acceleration potential, and a 10- μ m beam were used for the analyses. Counting times were 10-40 seconds, depending on the elements. Standards used were DJ35, Marjalotti Olivine, Synthetic Fayalite, Alp7 orthopyroxene and Lake County Labradorite, and the major elements have a standard deviation of less than 2%. Data were reduced with the CITZAF correction package using the atomic number correction of Duncumb and Reed, the absorption coefficients of Heinrich and the fluorescence correction of Reed (Armstrong, 1995). The results of the mineral analyses from this study are listed in Table 5-2.

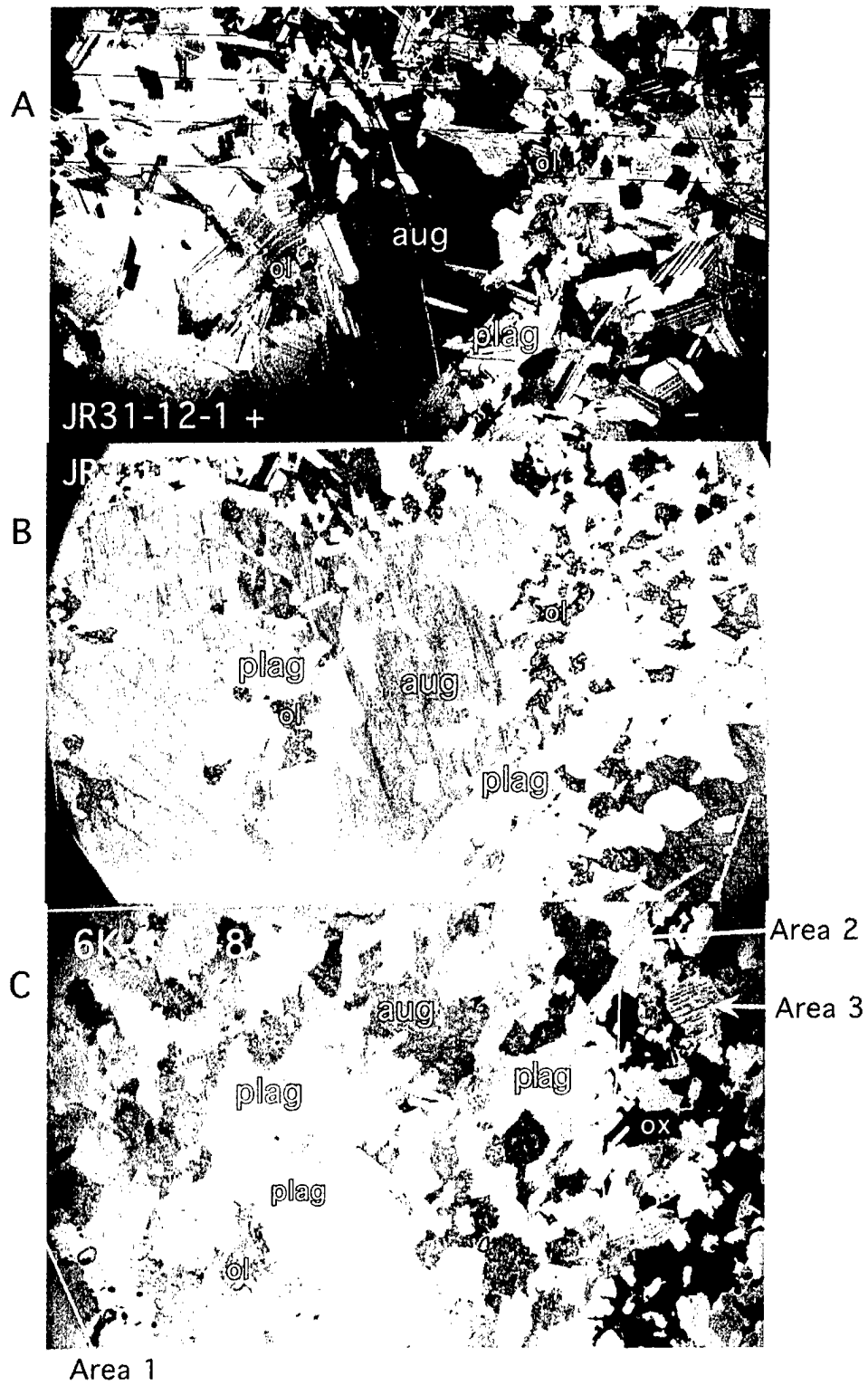
4 Results

4.1 *General mineral distribution and petrography*

Plagioclase and clinopyroxene are ubiquitous throughout the sample-suite. The grain-sizes range from medium grained to very coarse-grained, and fine-grained micro-gabbros are only rarely present. In undeformed samples, fresh plagioclase appears as randomly oriented euhedral laths, surrounded by subophitic clinopyroxene (Fig. 5-3a,b). Olivine appears as anhedral grains, with a characteristic cracking-pattern, whereas orthopyroxenes are granular, or appear as rims around olivine (Fig. 5-3e). Oxide-minerals are common, and are usually interstitial to the other minerals (Fig. 5-3c). Ilmenite and magnetite occur in individual grains or as trellis-twin exsolution-lamellae after ulvöspinel.

High temperature deformation has caused kink-bands in plagioclase with anhedral and granular augite and plagioclase (Fig. 5-3d). Some samples have saussuritized

Evolution of Oceanic Gabbros: In-situ and Ancient Examples



Evolution of Oceanic Gabbros: In-situ and Ancient Examples

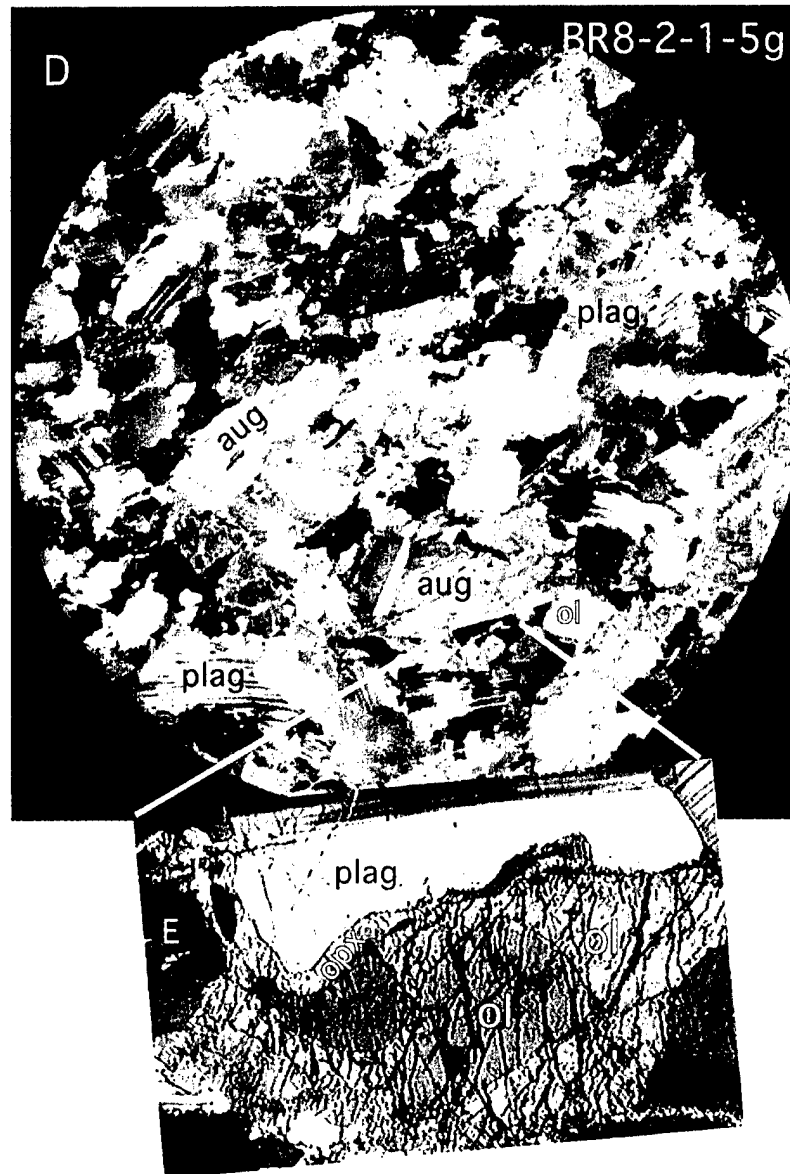


Figure 5-3: **A:** Sample # JR31-12-1: Sub-ophitic augite surrounds plagioclase-laths with interstitial olivine. Cross-polarized light. Plag=plagioclase, aug=augite, ol=olivine. Field of view is 3" from left to right. **B:** Same slide in parallel light. **C:** Sample 6K-466-8, field of view is 1" across. An olivine-gabbro-norite-oxide-gabbro-norite contact, as seen by the extensive interstitial oxide-crystals to the right. The boundaries between the lithologies are indicated by the white line. The picture is taken using a combination of reflected and parallel light to distinguish the different minerals. Three areas (indicated) have been analyzed. **D:** Sample # BR8-2-1-5g: The sample has been partially deformed at high temperatures, as seen in the kink-banded plagioclase and rounded augite. Cross-polarized light, the slide is 1" across. **E:** Detail of C; a thin orthopyroxene-grain lies between an olivine grain (with the characteristic cracking-pattern) and plagioclase

Evolution of Oceanic Gabbros: In-situ and Ancient Examples

plagioclase and clinopyroxene altered to green amphibole; these are signs of greenschist-facies alteration. These samples were therefore not chosen for mineral-analysis. Olivine is altered to iddingsite under the same conditions, and fresh material was not available representing most of the rocks that originally containing olivine, although we have found olivines from the entire compositional spectrum of gabbros. Orthopyroxene is also more susceptible to this low-grade alteration than augite, but small mineral-cores are often available for analysis.

Point-counting of thin-sections in order to obtain mineral norms has not been performed, as the rocks are generally so coarse-grained that even a large (2"x3") thin-sections does not adequately represent the mode of the rock (Fig. 5-3a). However, Coogan et al, 2000 analyzed the whole-rock compositions of the rocks around Atlantis Bank sampled during the JR-31 expedition. We have calculated norms based on the methods outlined in Grove et al. (1992) (Fig. 5-4), and compared them to MORB from the ridge to the north and transform walls, and to the average of Hole 735B (Dick, et al., 2000). If the gabbros were formed by pure fractional crystallization, the whole-rock compositional norms should start as pure olivine (dunite), continue along the plagioclase-olivine cotectic and end at the 4-phase saturation-boundaries outlined in Figure 5-4. The whole-rock compositions clearly span a wider range than this, with large excesses in plagioclase and augite, suggesting mechanical separation of the minerals or reactive modification of mineral proportions after cotectic crystallization. The presence of non-cotectic proportions of olivine, plagioclase and clinopyroxene is even more pronounced in the samples from Hole 735B. The Hole 735B samples are, however, very small in volume, so they may not be as representative for the bulk-rock composition as the grain-size is coarse.

Mineral analyses

4.1.1 Plagioclase

The average plagioclase has 49.5 % An, the median is 49.8%, and the highest is 71.5 % An. Only a few plagioclase grains have An below 32.3%, and those grains are possibly

Evolution of Oceanic Gabbros: In-situ and Ancient Examples

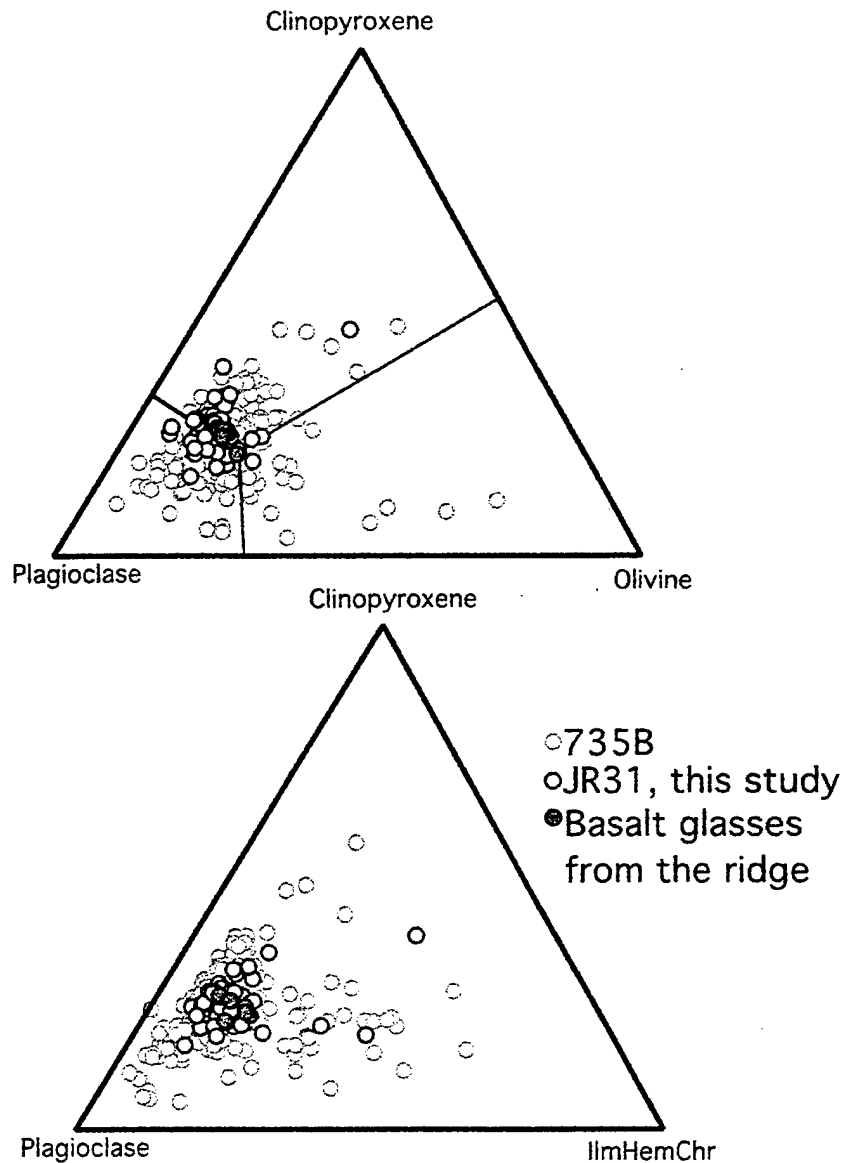


Figure 5-4: The mineral modes of Atlantis Bank gabbros and average Hole 735B compositions calculated from whole rock data using Grove *et al.*, (1992). The cotectic lines in the uppermost figure represents 1atm olivine-plagioclase-augite-melt saturation-boundary based on a basalt-glass from the spreading ridge, thus suggesting the cumulative nature of the gabbroic rocks.

Evolution of Oceanic Gabbros: In-situ and Ancient Examples

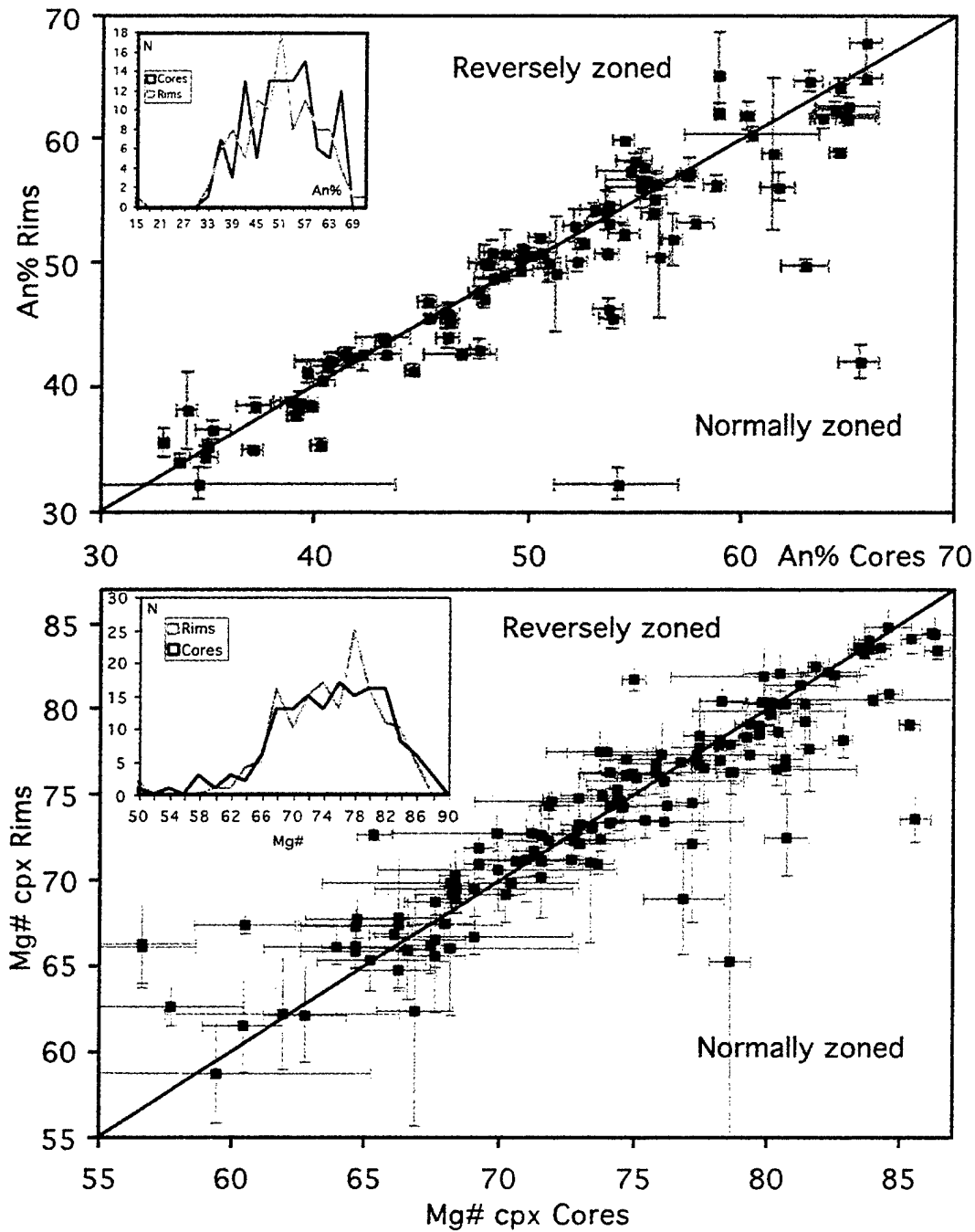


Figure 5-5A: Cores and rims of clinopyroxene and plagioclase from this study. Note how the distribution between cores and rims are indistinguishable (insert). Line indicate 1:1.

Evolution of Oceanic Gabbros: In-situ and Ancient Examples

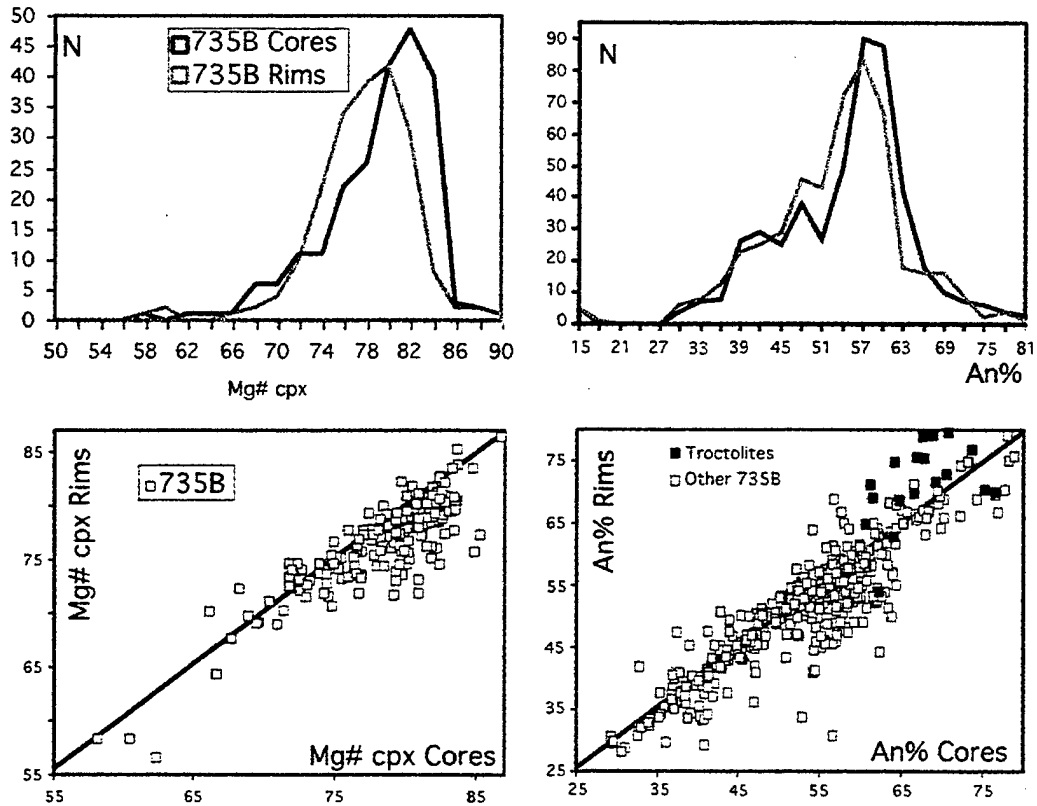


Figure 5-5B: The distribution of cores and rims of plagioclase and clinopyroxene from Hole 735B. The data are from Dick *et al.*, (2001) and Angeloni and Dick (1990) (troctolite-dikes from the upper 550m of the hole). The crossing line indicate 1:1. The core-rim information is not generally available for the upper 550 m of Hole 735B.

Evolution of Oceanic Gabbros: In-situ and Ancient Examples

altered. The orthoclase contents increase slightly as An decreases, although it rarely is higher than 1-mol%.

Zoning is common (Figure 5-5a). Plagioclase is reversely zoned in 50 out of 109 cases (i.e. rims are more An-rich than the cores), with respect to An. The core to rim difference in An contents is $>1\sigma$ for microprobe uncertainty (and mineral inhomogeneity) in 23 of the 50 reversely zoned samples. 59 plagioclase grains are normally zoned, and the core to rim change in An content is $>1\sigma$ in 37 of the 59 normally zoned samples. Low anorthite plagioclase cores are also often overgrown by higher anorthite plagioclase with a different crystal orientation, suggesting that the low An-core acted as a nucleation site for the larger crystal (Fig. 5-7).

4.1.2 Clinopyroxene

The augites analyzed in this study ranges from Mg# 48.1 to 86.3 %, with an average of 74.5 % and a median of 74.9 % (Figure 5-5A and 5-6). Rims of the clinopyroxene are defined as the contacts with other minerals, whereas the cores are the respective areas furthest away from this contact. Cores and rims were analyzed in 158 clinopyroxenes (Figure 5-5A). Of these, 78 have reverse zoning ($24 > 1\sigma$), whereas 80 are normally zoned ($27 > 1\sigma$).

The minor elements also vary significantly. Figure 5-7A shows two large clinopyroxene crystals enclosing many large plagioclase laths. The cores and rims of these grains show a wide range in compositions. Both Cr_2O_3 and TiO_2 show a range comparable with the range of clinopyroxene compositions analyzed in the entire lower half of Hole 735B (Dick et al., 2002). This large single-sample range for the minor elements is common throughout the suite (Figure 5-7B).

4.1.3 Orthopyroxene

Low-Ca pyroxene appears as orthopyroxene. The grains are susceptible to sea-floor alteration, and thus fewer have been analyzed than in the more protected and unaltered Hole 735B. Orthopyroxene compositions range from Mg# 56 to 78%, with an average of 67% (Figure 5-6). Chemical zoning is not pronounced in the orthopyroxenes.

Evolution of Oceanic Gabbros: In-situ and Ancient Examples

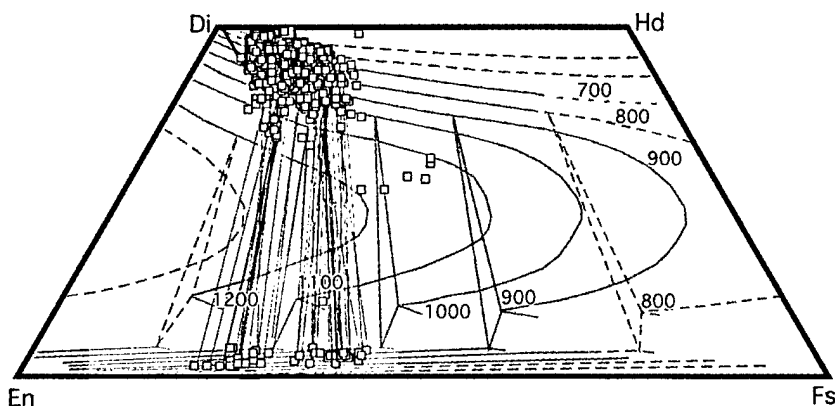


Figure 5-6: The tetrahedral components of the pyroxenes from this study calculated from Lindsley (1983). A thin black line connects coexisting minerals.

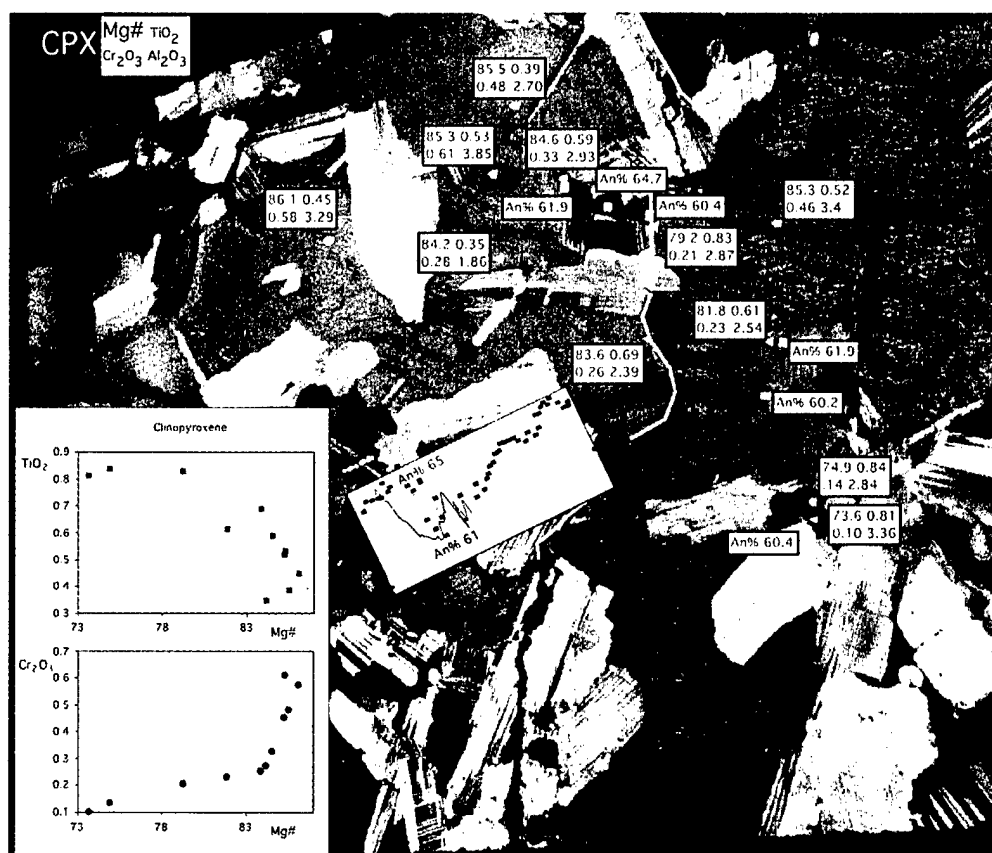


Figure 5-7: Sample #JR31-12-6. Each mineral analysis-point is shown with a white point and the analysis is shown with it. The key is to the upper left. The cross-sections through two large plagioclase crystals are shown. Two large augite-grains surround laths of plagioclase (their separation is marked by a yellow line). There is pronounced zoning in the minerals, and the Mg#, TiO₂ and Cr₂O₃ span almost the entire range in composition seen otherwise in the suite (insert). Notice how the plagioclase-grains have near constant compositions throughout the thin-section. Field of view is ~4cm from left to right.

Evolution of Oceanic Gabbros: In-situ and Ancient Examples

4.1.4 Olivine

Seafloor alteration has also reduced the number of magmatic olivines available to be analyzed in this study. The forsterite content ranges from 46 to 80 %, with an average of 67%, and a median of 69%. No zoning is observed, and grains within a sample are generally uniform in composition.

4.2 *Geographical Variability Around Atlantis Bank*

Four areas on and around Atlantis Bank appear to have distinctive distributions of magmatic minerals. Figure 5-8 (a,b,c) shows the anorthite content of plagioclase vs. the Mg# of coexisting augite, and orthopyroxene, and the forsterite content of olivine respectively. The northern area clearly has the widest range in compositions, although they never reach the high Mg#'s in clinopyroxene and An contents in plagioclase of the primitive cross-cutting troctolites in the upper levels of Hole 735B. In fact, one of the more primitive analyses among the surface samples is from a dike crosscutting the Dive 6K-647 section. Dive 6K-466, directly below 6K-467, sampled gabbros just above a contact with the residual peridotites, and these rocks have plagioclase as low as An₃₅. The samples from the top of the bank exhibit more intermediate compositions, where few plagioclases are higher than An₆₁ or lower than An₄₀. Some of the individual cores are unusual, as shown by BGS-24, which has a composition trend opposite to the other samples (Fig. 5-8a). The Western Wall of the bank has an even narrower trend, and resembles the distribution for the lower 500 meters of Hole 735B. This is interesting, as traverse 6K-460 was sampled close to Hole 735B, at a water depth just below the total depth from sea-surface to the bottom of the Hole. The southern part of the bank is also evolved geochemically. The layered olivine gabbros from the crust-mantle transition in this area (Dive 6K-649 and 653) are surprisingly fractionated as well with An₄₈₋₆₀ and augite Mg#'s from 70 to 82 mol%. The sample areas do follow the composition fields for Hole 735B. By contrast, the composition field for Hole 1105A gabbros (Thy, 2003) is offset to consistently more anorthitic plagioclase (or less Mg-rich augite) compositions than Hole 735B. A comparison of the whole-rock data from Hole 735B (Natland and

Evolution of Oceanic Gabbros: In-situ and Ancient Examples

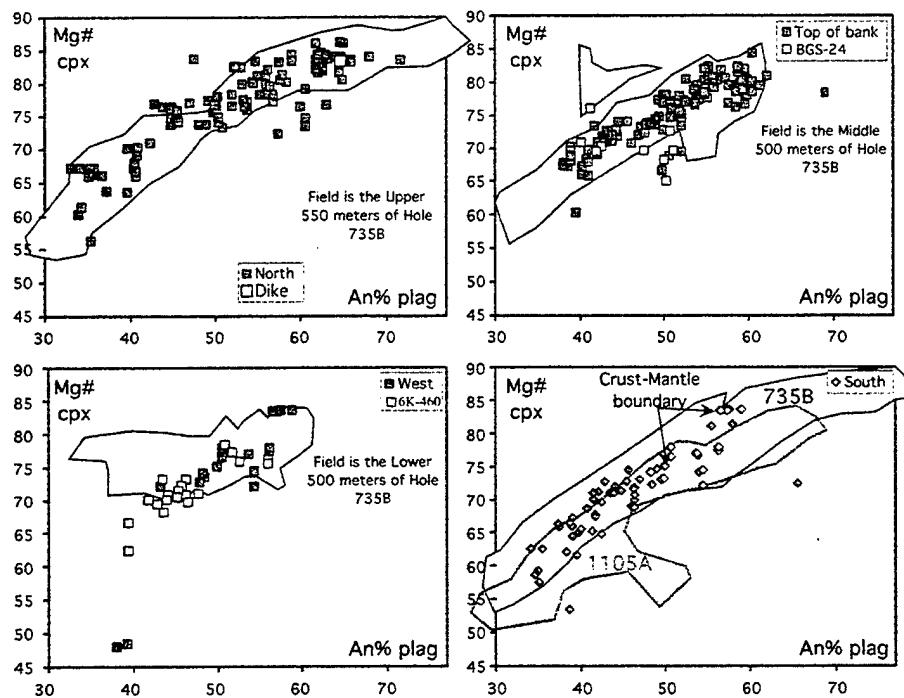


Figure 5-8: A: The composition of coexisting plagioclase (plag) and augite (cpx) for each of the areas from around Atlantis Bank. The fields represent the distribution of Hole 735B gabbros (Dick *et al.*, 2001) and the lower right diagram also shows Hole 1105A field (Thy *et al.*, 2003).

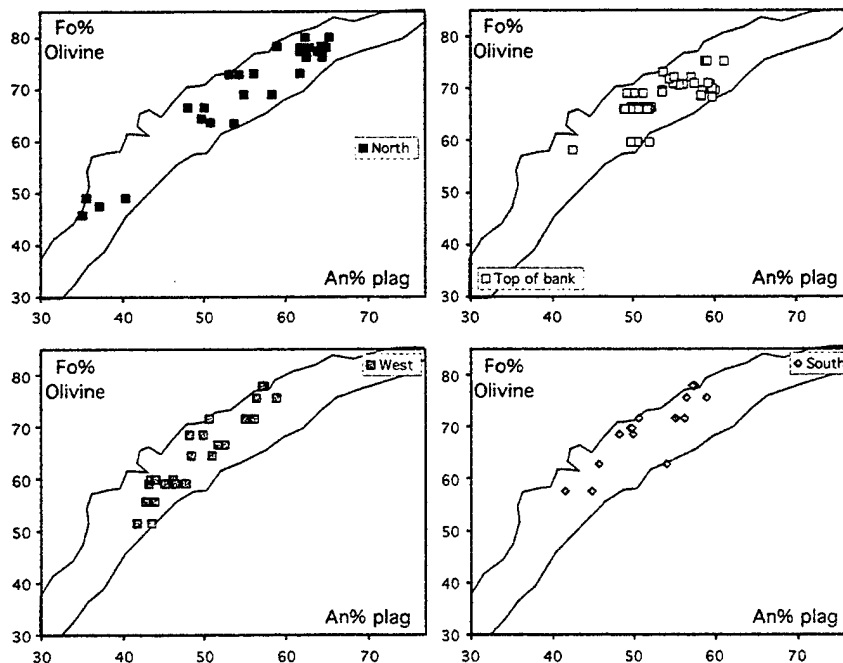


Figure 5-8: B: The composition of coexisting plagioclase (plag) and olivine (Fo%). The fields represent Hole 735B olivine-gabbros.

Evolution of Oceanic Gabbros: In-situ and Ancient Examples

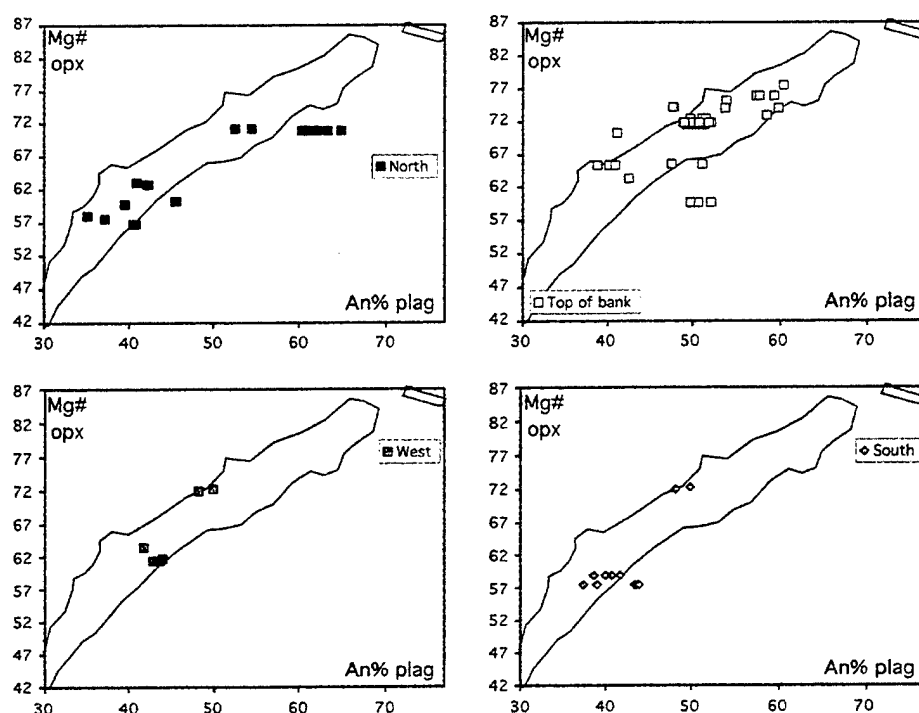


Figure 5-8: C: The composition of coexisting plagioclase (plag) and orthopyroxene (Mg#). The fields represent Hole 735B gabbro. The fields represent Hole 735B gabbro.

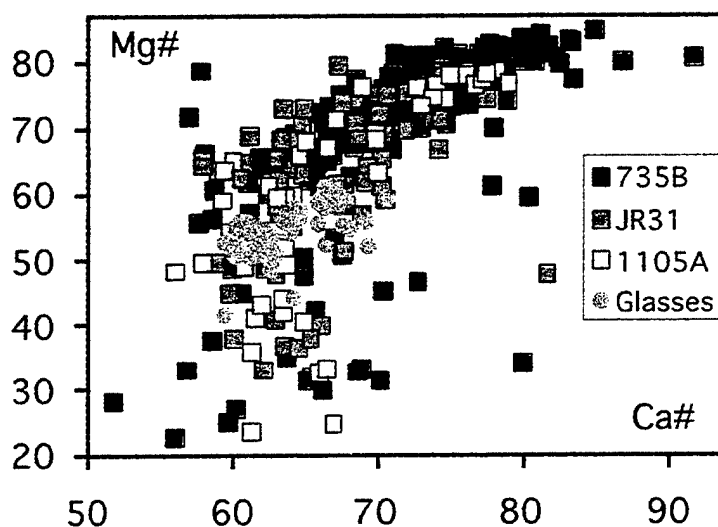


Figure 5-9: Whole-rock composition of gabbros from 735B (Dick et al., 2000), JR31 (Coogan et al. 2000), Hole 1105A (Casey et al., 2000) and unpublished glass-compositions from the fracture-zone and actively spreading ridge. It is clear that there is no distinctive difference in Mg#'s between 1105A and the rest of Atlantis Bank.

Evolution of Oceanic Gabbros: In-situ and Ancient Examples

Dick, 2002) to those obtained by JR-31 (Coogan et al., 2000) and Hole 1105A (Shipboard Scientific Party, 1999), however, show no discernable difference in Ca# vs. Mg#'s (Figure 5-9). Therefore, there may be analytical differences between the electron-probe methods used by Thy (2003) and the one in this study and by other investigators.

Olivine, as mentioned, is more rare than in Hole 735B due to iddingsite-alteration. The pause in olivine-crystallization, seen in many layered intrusions (Bowen and Schairer, 1935), is not expressed in these rocks or in Hole 735B, as olivine exists continuously from Fo₈₀ to Fo₄₅. Orthopyroxene is even scarcer, but is again found at all the areas, with an intermediate range of compositions compared to Hole 735B.

5 Discussion

The rocks sampled on and around Atlantis Bank likely represent crystallization-products formed during 50 to almost 90% fractionation of a primitive magma in equilibrium with the mantle based on modeling their composition using Melts (Ghiorso and Sack, 1995) and the "SWIR PMORB" composition discussed in Chapter 3 (Fig. 5-10A, see Chapter 3 for extensive explanation of the fractionation model). The northern sample-collection has the widest compositional range, whereas the top of the bank has a narrower range, from ~55 to 82% crystallization. The rocks from the south are surprisingly evolved, representing 65-90% crystallization, including a well exposed layered olivine-gabbro with An_{<60} and Fo_{<78} at the gabbro-peridotite contact. The samples from the western wall are also evolved, and the rocks include mylonitized ferro-gabbros from the crust-mantle boundary. The most primitive sample along the wall is in fact a dike cross-cutting the section. Thus, we have not found the "missing cumulates" exposed anywhere around Atlantis Bank (i.e. hypothetical troctolites that should have been produced by the initial stages of crystallization from melts extracted from the mantle and emplaced in the Hole 735B section).

It is clear that the troctolites do not exist at or near the gabbro-peridotite contacts exposed or inferred on the transform wall, where numerous samples of evolved olivine-gabbros and ferrogabbros were recovered. Although the exact origin of this contact between serpentinized peridotites and evolved gabbros is uncertain, it could be an

Evolution of Oceanic Gabbros: In-situ and Ancient Examples

intrusive contact between gabbroic rocks and residual peridotites, which was later altered and exhumed. Locally, it could be a faulted tectonic contact whose origin has been obscured by syn- and post-tectonic alteration, as believed to have been the case immediately to the west of Hole 735B. To the Southwest on that transform wall, it has been found in outcrop as a intrusive contact with gabbro overlying massive peridotite (Moroshita et al., in prep).

The northern suite has gabbros that are somewhat more primitive than found elsewhere over the bank, but they are not troctolites with primitive plagioclase and olivine. The most primitive troctolites found at Atlantis Bank are, in fact, the troctolite dikes that crosscut the upper 550-m of Hole 735B. The transform wall may be an unusual place to find primitive gabbros at very-slow spreading ridges if the mantle-derived magmas are emplaced at the segment centers and then intruded down-axis towards the transform (e.g. Whitehead et al., 1984; Dick, 1989). If we assume that melts in equilibrium with the mantle were indeed emplaced in the crust at the center of the segment, and that only evolved melts reached the transform-area (e.g. after more than 65% of crystallization), then it is possible to estimate a minimum crustal thickness below Hole 735B. Far to the southwest of Hole 735B the gabbro-peridotite contact is exposed 500 vertical meters below termination of the drill-hole. Vanko and Stakes (1991) found that Atlantis Bank has 1.65-km of missing (upper) crust based on fluid-inclusions. If the gabbro-peridotite boundary is that of the crust-mantle boundary, and it has no topography (unlikely), this would suggest an original crustal thickness on the order of 3.7-km at the ridge-transform intersection. Thus, as the crustal thickness suggested by fractional crystallization is 4.4-km (See Chapter 3), the center of the segment should be proportionally thicker. At the center of the segment, e.g. Hole 735B, the cross-cutting troctolites are the only cumulates in Fe-Mg and Ca-Na equilibrium with the spatially associated lavas. The latter are interpreted as liquids derived by 25-40% of crystallization from a primitive, mantle-derived parent (Fig. 5-10a and Chapter 3). In addition, troctolite dikes have sharp but somewhat irregular contacts with the coarse-grained olivine gabbros. This suggests that the troctolites in the upper part of Hole 735B

Evolution of Oceanic Gabbros: In-situ and Ancient Examples

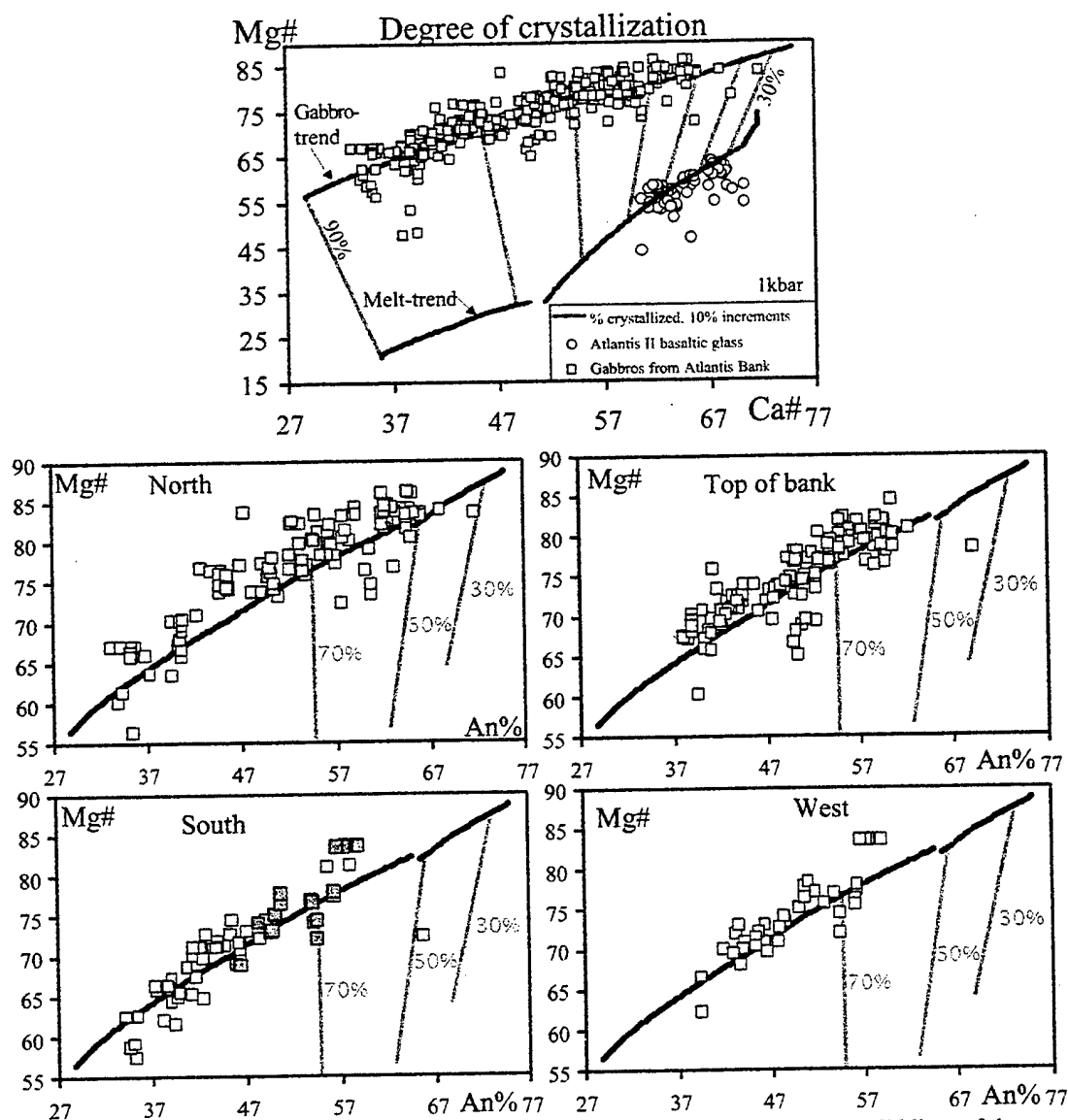


Figure 5-10: The distribution of mineral-compositions relative to modeled liquid and solid lines of descent. A: All the samples, compared to the 1kbar crystallization model presented in Chapter 2. The Gabbro-trend represents the anorthite of plagioclase with the Mg# of co-existing augite, whereas the Melt-trend represent the Mg# and Ca# of the evolving melt. The Atlantis II basaltic glasses are from Johnson et al. (1990). Each gray tie-line connects mineral-assemblage and a melt at the same stage of evolution in 10% increments. B: The Gabbro-trend compared to the area in the North. C: The Gabbro-trend compared to the top of Atlantis Bank. D: The Southern area. Note that the gray squares indicate the olivine-gabbros at the crust-mantle boundary. E: The Western area.

Evolution of Oceanic Gabbros: In-situ and Ancient Examples

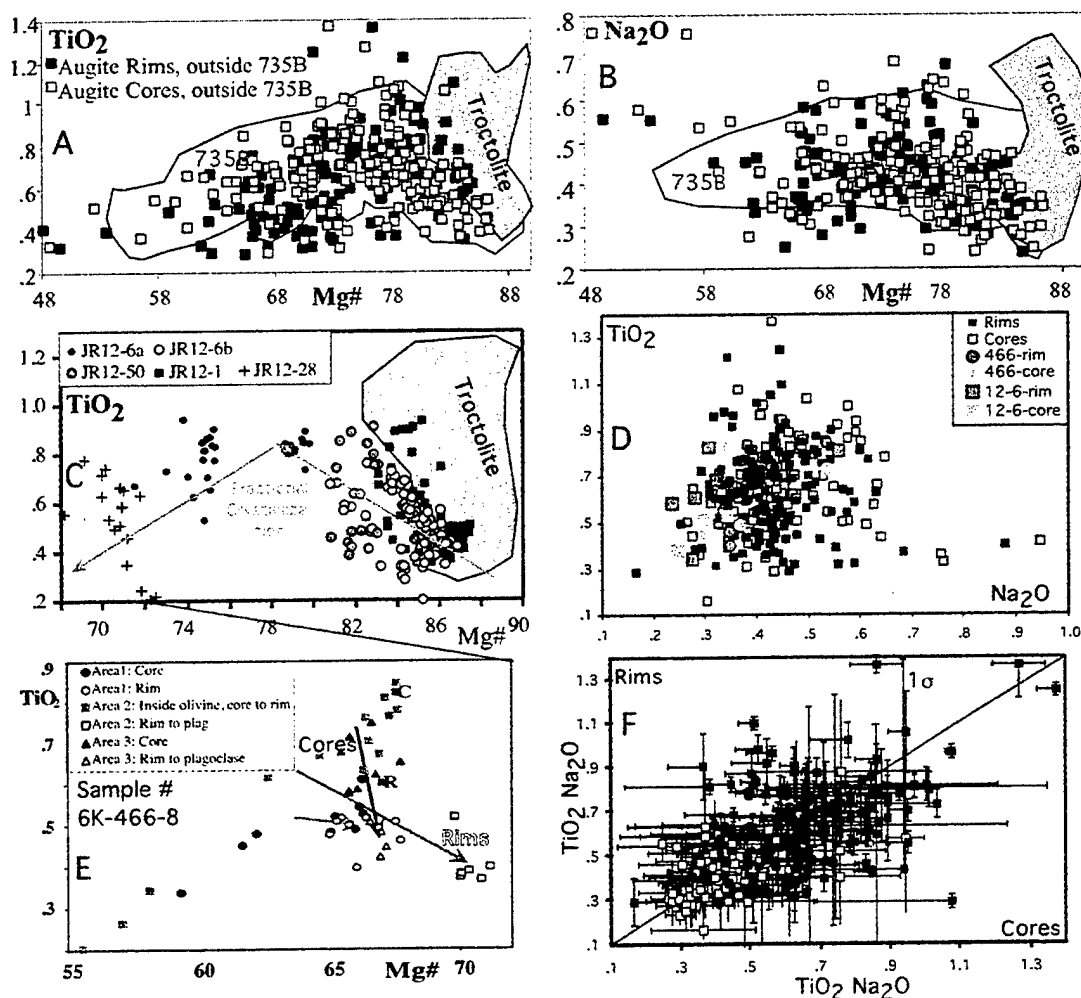


Figure 5-11: Minor element chemistry of augites analyzed in this study, compared to the upper 550-m of Hole 735B. A: Average Mg#-TiO₂ of augites from our study compared to the general outline of Hole 735B and the cross-cutting Hole 735B troctolites from the upper 550 meters of the core. B: Average Mg#'s vs. Na₂O for the same rocks. C: Rocks in a single dredge in the northern showing wide ranges of compositions in augite (individual analyses). In addition, single samples can have dramatically different augite compositions between grains (JR12-6a and 6b). The more evolved JR12-28 sample plot perpendicular to a normal fractionation trend. D: There is no direct linear relationship between Na₂O and TiO₂ in augite. E: Augites from a single, evolved oxide-olivine gabbro has more refractory cores than rims, plotting perpendicular to the fractional crystallization trend in C. F: There are as many reversely zoned augites as there are normally zoned ones: true both for Na₂O (open squares with bars indicating 1 σ variation) and for TiO₂ (closed squares with bars indicating 1 σ variation).

Evolution of Oceanic Gabbros: In-situ and Ancient Examples

have an intrusive/reactive relationship to the wall-rocks and represent melt-channels for magma potentially erupted through the lower crust.

Figure 5-11 shows the distribution of minor-elements for the surface samples (this study) and for Hole 735B. The high Ti-Na troctolites from Hole 735B are clearly different from the rest of the core. Meyer et al. (1989) and Bloomer et al. (1989) both noted the Mg/Fe ratios of the mafic minerals in Southwest Indian Ridge gabbros are high, compared to the anorthite content of the coexisting plagioclase. Sample JR31-12-6 (Fig 5-7, 5-11E) has a large chemical range, while the more evolved rock from the same dredge-haul (12-28) plots perpendicular to the fractionation-trend. Sample 6K-466-8 is an olivine-gabbro-norite – oxide-gabbro-norite contact (Fig. 5-3C and 5-11G) and has augite-rims with more primitive compositions than the respective cores. In addition, the oxide-rich part has higher Mg# augites than the olivine-rich ones in the same sample. Figure 5-11F shows how the minor-element distribution is indistinguishable between the primitive and evolved gabbros, thus and that there are as many reversely zoned as normal zoned augites (Fig. 5-11H).

Meyer et al., (1989) argued that the interstitial melts in 7°E Southwest Indian Ridge gabbros reacted and equilibrated Fe and Mg with olivine, causing interstitial melt to maintain a higher Mg# during fractionation. Therefore, the augite that precipitated from this melt appears refractory relative to the melt that produced it. Minor, incompatible oxides like TiO_2 increase in a fractionating melt, explaining why the high Mg# clinopyroxene has high incompatible element concentrations. If the melts that produced the entire crustal section reacted in this way with olivine, individual dredge suites or even individual samples would show a positive correlation between Mg# and TiO_2 and Mg# and Na_2O . Inspection of Figure 5-11 indicates that the opposite is the case. When the fine-grained troctolites are excluded from the upper 550-m of Hole 735B, it's hard to say that there are any systematics in the scatter at all. In our surface-sample data-set, individual samples and dredge-hauls have unusually large variability.

Meyer et al.'s (1989) plagioclase and clinopyroxene analyses also commonly showed reverse zoning. Angeloni and Dick (1990) demonstrated that the cross-cutting troctolites

Evolution of Oceanic Gabbros: In-situ and Ancient Examples

of Hole 735B consistently have reversely-zoned plagioclase, suggesting a process of melt percolation and overgrowth on plagioclase by later, more calcic melts with higher levels of incompatible elements. In addition, Bloomer et al. (1991) found that Unit V of Hole 735B characteristically has reversely zoned plagioclase. They argued that the high Mg# clinopyroxene and the plagioclase originated from separate magma sources, and that the crystallization happened in a mushy boundary layer. The interstitial melts are therefore a mix between main magma chamber and the interstitial equilibrium melt. Langmuir (1989) developed such a model for *in situ* crystallization in magma chambers. In this model, "melts from magma-chamber margins" mix with comparatively primitive melts within "magma-chamber melts", and magmas then evolve along a chemical path different from that of fractional crystallization. However, the in-situ crystallization model only returns the interstitial melts to the magma-chamber, it does not allow for fresh, primitive melts to enter the mush. Therefore, Langmuir's model would not make the intercumulus minerals of the most primitive cumulates appear more refractory.

Three processes may lower the TiO_2 -content of melt along a given liquid-line of descent: Mixing with a primitive melt; crystallization of ilmenite; and melting of, and reaction with, pre-existing cumulates by interstitial melts. Mixing of evolved and primitive melt will increase the melt Cr_2O_3 and decrease the Na_2O relative to the end-members. Cr_2O_3 is generally low in the more evolved rocks, thus extensive mixing with primitive melts are unlikely. Crystallization of ilmenite will not increase the Mg# of the melt significantly. It was shown in Chapter 4 that dissolution of gabbroic cumulates produce melts that are low in TiO_2 , high in Na_2O and have high Mg#'s and Ca#'s ($\text{Ca}/(\text{Ca}+\text{Na})$). In fact, if plagioclase-augite phase-boundaries melt, the new melt will have ~10-15 mol% higher Mg#'s and 10% of the TiO_2 relative to the melt that produced the gabbros in the first place. Reprecipitation consequently produce the reverse zoning seen in the evolved cumulates.

Our results from gabbroic surface samples from on and around Atlantis Bank suggest that, with respect to chemistry, the rocks are more like the lower 1000-m of Hole 735B than the upper 550-m. In terms of petrography, the presence of numerous massive

Evolution of Oceanic Gabbros: In-situ and Ancient Examples

ferrogabbros is more like the characteristics of the upper 500-m of Hole 735B. In Chapter 3, the olivine-gabbros from the lower 1000-m were shown to be out of equilibrium. It is therefore possible that reaction and dissolution with migrating melts has modified the entire section. This process evidently may have eradicated both the very primitive, and the highly evolved compositions around the Bank (except at the most extreme end of the spreading segment). There, termination of detachment fault, which is believed to have rooted in a shallow crystal mush zone below the sheeted dikes (Dick pers. comm.), may have halted the process of melt migration before the primitive character of the gabbros was lost. Thus, even more primitive cumulates could at some point have existed, but may have been largely modified by later ascending melts. This assimilation-model is explored further in the next chapter, using trace-element compositions for the gabbroic rocks on and around Atlantis Bank.

6 Conclusion

The gabbros on and around Atlantis Bank, Southwest Indian Ridge are likely the products of ~50-90% fractional crystallization from a mantle-derived magma, and do not represent a complete cumulate section. The area to the north of Hole 735B has the most primitive magmatic minerals, whereas the southern gabbros are all evolved, including layered olivine-gabbros sampled at gabbro-peridotite contacts. Gabbros from the Western Wall and the top of the bank have intermediate compositions. The primitive and evolved ends of the ODP Hole 735B spectrum are not recovered in our data.

Augite is more magnesian than expected for any coexisting plagioclase anorthite content, and plagioclase and augite are frequently reversely zoned. TiO_2 of augite varies inversely with Mg\# at all levels of evolution, even after magnetite and ilmenite crystallization. We propose an alternative model to simple fractional crystallization, as there is evidence for extensive melt-rock reaction, possibly with simultaneous reaction and dissolution in the cumulate pile. Assimilation of pre-existing cumulates during crystallization will change the magma-budget and make our interpretation of the amount of crystallization at Atlantis Bank very different. Thus, more primitive cumulates may

Evolution of Oceanic Gabbros: In-situ and Ancient Examples

have existed at an early magmatic stage, but have been completely reconstituted by later ascending melts. This alternative model will be investigated further in the next chapter.

References

- Angeloni LM, Dick HJB, 1990: Troctolitic Gabbros from Hole 735B, Atlantis II Fracture Zone, Southwest Indian Ridge. *EOS* 71(43): 1704.
- Armstrong, JT, 1995: CITZAF: A package of correction programs for the quantitative electron microbeam x-ray analyses of thick polished materials, thin films, and particles. *Microbeam analysis*, 4: 177-200.
- Bloomer SH, Meyer PS, Dick HJB, Ozawa K, Natland JH, 1991: Texture and mineralogic variations in gabbroic rocks from Hole 735B. In: *Proceeding of the Ocean Drilling Program, Scientific Results*, 118: 21-39.
- Bloomer SH, Natland JH, Fisher RL, 1989: Mineral relationships in gabbroic rocks from fracture zones of Indian Ocean ridges: evidence for extensive fractionation, parental diversity and boundary-layer recrystallization. In: Saunders AD, Norry MJ, (eds) *Magmatism in the Ocean Basins*, *Geol Soc Spec Publ* 42: 107-124.
- Coogan LA, MacLeod CJ, Dick HJB, Edwards SJ, Kvassnes A, Natland JH, Robinson PT, Thompson G, O'Hara MJ, 2001: Whole-rock geochemistry of gabbros from the Southwest Indian Ridge: constraint on geochemical fractionations between the upper and lower oceanic crust and magma chamber processes at (very) slow-spreading ridges. *Chem Geol* 178:1-22.
- Coogan LA, Kempton PD, Saunders AD, Norry MJ, 2000a: Melt aggregation within the crust beneath the Mid-Atlantic Ridge: evidence from plagioclase and clinopyroxene major and trace element compositions. *Earth Planet Sci Lett* 176:245-257.
- Dick HJB, 1989: Abyssal peridotites, very slow spreading ridges and ocean ridge magmatism. In: Saunders AD, Norry MJ, (eds): *Magmatism in the ocean basins*, *Geol Soc Spec Publ* 42: 71-105.
- Dick HJB, Meyer PS, Bloomer S, Kirby S, Stakes D, Mawer C, 1991a: Lithostratigraphic evolution of an in-situ section of oceanic layer 3. In: Von Herzen RP, Robinson PT, et al., *Proc ODP, Sci Res* 118: College Station, TX (Ocean Drilling Program): 439-538.
- Dick HJB, Natland JH, Alt JC, Bach W, Bideau D, Gee JS, Haggas S, Hertogen JGH, Hirth JG, Holm PM, Ildefonse B, Iturrino GJ, John BE, Kelley DS, Kikawa E, Kingdon A, LeRoux PJ, Maeda J, Meyer PS, Miller DJ, Naslund HR, Niu YL, Robinson PT, Snow J, Stephen RA, Trimby PW, Worm HU, Yoshinobu A, 2000: A long in situ section of the lower ocean crust; results of ODP Leg 176 drilling at the Southwest Indian Ridge. *Earth Planet Sci Lett* 179 (1): 31-51.
- Dick HJB, Ozawa K, Meyer PS, Niu Y, Robinson PT, Constantin M, Hébert R, Natland JH, Hirth JG, Mackie SM, 2002: 10. Primary silicate mineral chemistry of a 1.5-km section of very slow spreading lower ocean crust: ODP Hole 735B, Southwest Indian Ridge. In Natland JH, Dick HJB, Miller DJ, Von Herzen RP (eds) *Proceedings of the Ocean Drilling Program, Scientific Results Volume 176*. (CD-ROM).
- Dick HJB, Schouten H, Meyer PS, Gallo DG, Bergh H, Tyce R, Patriat P, Johnson KTM, Snow J, Fisher A, 1991b: Tectonic evolution of the Atlantis II Fracture Zone. In: Von Herzen RP, Robinson PT, et al., *Proc ODP, Sci Res* 118: College Station, TX (Ocean Drilling Program): 359-398.
- Grove TL, Kinzler RJ, Bryan WB, 1992: Fractionation of mid-ocean ridge basalts. In: *Mantle flow and melt generation at mid-ocean ridges*, *Geophys monogr* 71: 281-310.
- Hosford A, Tivey M, Matsumoto T, Dick HJB, Schouten H, Kinoshita H, 2003: Crystal magnetization and accretion at the Southwest Indian Ridge near the Atlantis II Fracture Zone, 0-25Ma. *Journ Geophys Res* 108 (B3):doi: 10.1029/2001JB000604.
- Jerram DA, Cheadle MJ, Philpotts AR, 2003: Quantifying the Building Blocks of Igneous Rocks: Are Clustered Crystal Frameworks the Foundation? *Journ Petrol* 44 (11): 2033-2051. DOI: 10.1093/petrology/egg069.
- Langmuir, CH, 1989: Geochemical consequences of in situ differentiation. *Nature*, 340, 199-205.

Evolution of Oceanic Gabbros: In-situ and Ancient Examples

- Lindsley DH. Andersen DJ, 1983: A two-pyroxene thermometer. *Proceeding 13th lunar planet sci conf 2*: Journ Geophys Res 88 (Suppl) A887-A906.
- Meyer PS. Dick HJB. Thompson G, 1989: Cumulate gabbros from the Southwest Indian Ridge, 54°S-7°16'E: implications for magmatic processes at a slow ridge. *Contrib Mineral Petrol* 103: 44-63.
- Miyashiro A, 1973: The Troodos Ophiolitic Complex was probably formed in an Island Arc. *Earth Planet Sci Letts* 19: 218-224.
- Muller MR. Robinson CJ. Minshull TA. White RS. Bickle MJ, 1997: Thin crust beneath Ocean Drilling Program Borehole 735B at the Southwest Indian Ridge? *Earth Planet Sci Lett* 148 (1-2): 93-107.
- Natland JH. Dick HJB, 2002: Stratigraphy and Composition of Gabbros Drilled in Ocean Drilling Program Hole 735B, Southwest Indian Ridge: A synthesis of Geochemical Data. In Natland JH. Dick HJB. Miller DJ. Von Herzen RP (eds) *Proceedings of the Ocean Drilling Program, Scientific Results Volume 176*. 1-69 (CD-ROM).
- Shipboard Scientific Party, 1999: Hammer Drill Sotes (1104 and 1106) and Site 1105. In: Pettigrew T. Casey J. Miller DJ. et al., *Proc ODP, Init Repts*, 179: College Station, TX (Ocean Drilling Program) CD Rom.
- Thy P, 2003: 2. Igneous Petrology of Gabbros from Hole 1105A: Oceanic Magma Chamber Processes. In: Casey JF. Miller DJ (eds): *Proceeding of the Ocean Drilling Program, Scientific Results, Vol 179*. Web publication.
- Tucholke BE. Lin J. Kleinrock MC, 1998: Megamullions and mullion structure defining metamorphic core complexes on the Mid-Atlantic Ridge. *J. Geophys Res.* 103 (B5) 9857-9866.
- Vanko DA. Stakes DS, 1991: Fluids in oceanic layer 3: Evidence from veined rocks, Hole 735B, Southwest Indian Ridge. *Proc Ocean Drill Prog Sci Res* 118: 181-215..
- Whitehead JM. Dick HJB. Schouten H, 1984: A mechanism for magmatic accretion under spreading centers. *Nature* 312: 146-148.

Evolution of Oceanic Gabbros: In-situ and Ancient Examples

Table 1: The samples analysed in this study

Table 1: The samples analysed in this study																					
Tool	Core	Piece	interval	Tool	Core	Piece	interval	Tool	Dive	Piece	Tool	Dive	Piece	Tool	Dredge	Piece					
BGS	2-1	7c	37-45	BGS	27-1	1a	3	SHINKAI	459	3	SHINKAI	643	8	JR31	3	51					
BGS	3-1	2a	0-5	BGS	27-1	1b	8.5	SHINKAI	459	9	SHINKAI	645	18	JR31	9	2					
BGS	4-1	4c	43-48	BGS	27-1	1b	19.5	SHINKAI	460	6	SHINKAI	645	17	JR31	9	4					
BGS	4-2	4d	0	BGS	27-1	1b	25.5-31	SHINKAI	460	11	SHINKAI	646	1	JR31	12	1					
BGS	4-2	4d	17	BGS	27-1	1d	56-62	SHINKAI	460	13	SHINKAI	646	4	JR31	12	6					
BGS	4-2	4d		BGS	31-1	1c	34.5-39.5	SHINKAI	460	14	SHINKAI	646	6	JR31	12	8					
BGS	10-1	1a	31-36	BGS	31-1	1a	0-5	SHINKAI	460	15	SHINKAI	647	1	JR31	12	10					
BGS	16-1	1	7-12	BR	5-1	1b	4.5-8.5	SHINKAI	460	16	SHINKAI	647	10	JR31	12	16					
BGS	17-1	1a		BR	5-1	1h	74	SHINKAI	466	4	SHINKAI	647	13	JR31	12	28					
BGS	17-1	1b	25-30	BR	5-1	5c	48-51.6	SHINKAI	466	6	SHINKAI	647	9	JR31	12	39					
BGS	17-1	1f	65-67	BR	6-1	1g	20.5-24.5	SHINKAI	466	7	SHINKAI	649	8	JR31	12	42					
BGS	19-2	12a	10-11.5	BR	8-1	5d	34-36	SHINKAI	466	9	SHINKAI	649	8	JR31	12	45					
BGS	19-2	12a	38.5	BR	8-1	5g	69-71.5	SHINKAI	466	11	SHINKAI	649	12	JR31	12	46					
BGS	20-1	3b	28.5-32	BR	8-2	5h	3	SHINKAI	467	1	SHINKAI	649	14	JR31	12	47					
BGS	20-1	6a	64-67	BR	8-2	5m	18.5-23	SHINKAI	467	2	SHINKAI	650	4	JR31	12	50					
BGS	20-2	6b	0-5.5	BR	9-1	1d	26-28.5	SHINKAI	467	3	SHINKAI	650	6	JR31	12	68					
BGS	20-2	6b		BR	12-1	3b	33-35.5	SHINKAI	467	4	SHINKAI	650	9	JR31	39	1					
BGS	23-1	2b	23-28	BR	14-1	7a	35-37.5	SHINKAI	467	6	SHINKAI	653	2	JR31	39	3					
BGS	23-1	2b	29-34	BR	15-1	3b	17.5-20	SHINKAI	467	8	ABCDE: 18 thinsections from 7 dives					4					
BGS	23-1	2c	44.5-48.5	BR=Oriented drill cores from the top of Atlantis Bank				SHINKAI	467	9						7					
BGS	23-1	2e		12 thinsections				SHINKAI	467	11						8					
BGS	24-1	3a	6-10					SHINKAI	467	12						10					
BGS	24-1	3c	21-24					SHINKAI	467	13						11					
BGS	24-1	3d	24	BGS=non-oriented drill cores				SHINKAI	467	15						13					
BGS	24-1	3h	47	from top of Atlantis Bank				SHINKAI	467	17	Mode 98: 25 thinsections from 4 dives					17					
BGS	24-1	3h	51.5	35 thinsections												40					
BGS	24-1	3i	60													41					
BGS	24-1	3k	77													41					
													Total: 99			JR: 27 thinsections from 7 dredges					

Evolution of Oceanic Gabbros: In-situ and Ancient Examples

Table 2A: The average composition of plagioclase from on and around Atlantis Bank.

Sample# and placement		Averages		Standard deviations																	
				C	R	SiO ₂	Al ₂ O ₃	FeO	MgO	CaO	Na ₂ O	K ₂ O	Total	An%	SiO ₂	Al ₂ O ₃	FeO	MgO	CaO	Na ₂ O	K ₂ O
6K-459-3 plc(6)		x		67.28	22.22	.02	.02	2.62	10.69	.03	102.9	11.9	.55	.13	.03	.03	.29	.18	.01	.40	1.32
6K-459-3 prf(6)		x	x	68.00	21.35	.15	.04	1.66	11.38	.03	102.6	7.5	.93	.72	.08	.03	.29	.18	.01	.94	3.36
6K-459-9 plc(6)		x		59.33	27.03	.11	.02	8.43	7.25	.11	102.3	39.1	.25	.13	.02	.06	.75	.44	.01	.94	3.36
6K-459-9 plr(5)		x	x	59.58	26.92	.16	.01	8.17	7.43	.09	102.4	37.8	.18	.08	.03	.00	.75	.11	.01	.25	.36
6K-460-6 pl c-r(8)		x	x	54.70	27.57	.65	.13	10.44	5.61	.07	99.2	50.7	1.07	.59	.02	.01	.07	.10	.04	.11	.48
6K-460-6 pl c-r(7)		x	x	53.50	28.45	.60	.19	11.44	4.99	.09	99.2	55.9	1.29	1.04	.27	.02	.66	.39	.02	.45	3.30
6K-460-11 pl(outside cpx)c(6)		x		56.82	27.31	.02	.00	8.94	6.48	.02	99.6	43.3	.44	.23	.01	.18	1.02	.53	.34	4.86	
6K-460-11 pl(outside cpx)r(6)		x	x	56.97	27.47	.12	.00	9.04	6.39	.02	100.0	43.9	.20	.26	.06	.00	.24	.17	.01	.39	1.27
6K-460-11 plr(6)		x	x	56.14	27.44	.19	.02	9.36	6.06	.09	99.3	46.0	.31	.11	.06	.00	.12	.09	.01	.41	.34
6K-460-13 plc(6)		x		56.73	27.67	.26	.02	9.43	6.13	.08	100.3	46.0	.49	.22	.07	.01	.05	.10	.01	.49	.36
6K-460-13 plr(6)		x	x	55.13	28.19	.10	.01	10.85	5.43	.09	99.8	52.5	.27	.13	.01	.01	.08	.09	.00	.65	.44
6K-460-14 pl1 c-r(5)		x	x	55.37	28.02	.26	.08	10.68	5.55	.08	100.0	51.5	.28	.17	.25	.01	.07	.01	.25	.29	.29
6K-460-14 pl2 c-r(3)		x	x	57.66	25.47	.19	.35	8.97	6.38	.08	99.1	43.7	.98	.57	1.42	.01	.06	.07	.01	.55	.29
6K-460-14 pl3 c(6)		x	x	56.88	25.29	.20	.00	9.09	6.56	.06	98.7	43.4	.33	.42	.02	.60	.22	.20	.05	.42	.37
6K-460-14 pl3 r(6)		x		57.10	25.88	.06	.00	8.90	6.61	.07	98.9	42.6	.41	.31	.03	.00	.14	.09	.00	.52	.69
6K-460-15 plc(12)		x		57.59	25.33	.14	.01	8.11	6.95	.15	99.7	39.2	.50	.36	.03	.02	.12	.07	.01	.56	.40
6K-460-16 pl1 c-r(6)		x	x	58.12	26.44	.12	.00	8.11	6.95	.15	99.5	47.5	.34	.28	.34	.01	.28	.15	.01	.76	1.24
6K-460-16 pl1 c-r(5)		x	x	56.23	25.71	.41	.15	9.85	6.01	.10	98.5	47.5	.22	.55	.19	.21	.13	.06	.01	.26	.16
6K-460-16 pl1 r(5)		x	x	56.81	25.48	.21	.01	9.65	6.19	.10	98.5	46.3	.22	.55	.19	.21	.13	.06	.01	.26	.16
6K-460-16 pl1 r2(6)		x	x	56.97	25.65	.14	.00	9.41	6.24	.10	98.5	45.4	.36	.48	.29	.00	.09	.07	.01	.23	.39
6K-460-16 pl2 c-r(5)		x	x	56.38	24.64	.47	.14	9.34	6.28	.10	97.4	45.1	.36	.48	.29	.00	.09	.07	.01	.50	.46
6K-460-16 pl2 c-r(5)		x	x	56.52	24.82	.15	.01	9.41	6.36	.10	97.4	45.0	.33	.55	.01	.19	.20	.09	.01	.33	.79
6K-466-4 plc(6)		x	x	56.21	27.85	.11	.01	9.71	6.10	.09	100.1	46.8	.42	.40	.04	.01	.21	.17	.01	.45	1.17
6K-466-4 prf(6)		x		57.06	27.16	.13	.01	8.88	6.60	.06	99.9	42.7	.33	.12	.02	.01	.35	.20	.03	.67	1.67
6K-466-4 plr(6)		x	x	56.64	27.50	.12	.01	9.30	6.35	.07	100.0	44.7	.37	.26	.03	.01	.05	.10	.03	.38	.33
6K-466-4 plc(6)		x	x	56.85	27.33	.13	.01	9.09	6.47	.07	99.9	43.7	.35	.19	.02	.01	.20	.15	.03	.52	1.00
6K-466-6 plr(6)		x	x	54.69	28.81	.18	.02	10.67	5.48	.05	99.9	51.8	.71	.54	.03	.01	.13	.12	.03	.45	.67
6K-466-6 plc(6)		x		53.38	29.46	.16	.01	11.63	4.91	.06	99.6	56.7	.26	.07	.02	.02	.41	.25	.01	.69	2.10
6K-466-7 plc(6)		x	x	58.02	26.88	.10	.01	8.37	6.86	.10	99.4	40.3	.33	.25	.02	.00	.14	.08	.00	.36	.51
6K-466-7 prf(6)		x	x	58.81	25.83	.13	.01	7.40	7.45	.05	99.7	35.4	.45	.16	.05	.01	.09	.07	.01	.58	.38
6K-466-8 a plc(6)		x		57.91	26.43	.19	.02	7.82	7.32	.13	99.8	37.1	.14	.09	.02	.01	.10	.10	.01	.40	.46
6K-466-8 a prf(6)		x	x	58.43	26.32	.23	.02	7.45	7.64	.14	100.2	35.0	.15	.16	.03	.00	.06	.12	.03	.14	.48
6K-466-8 a2 prf-c(9)		x	x	57.84	27.05	.20	.03	8.28	7.02	.12	100.5	39.5	.54	.16	.04	.00	.05	.07	.04	.20	.22
6K-466-8 a3 prf(10)		x	x	57.28	27.26	.25	.04	8.52	6.92	.09	100.4	40.5	.40	.31	.13	.01	.16	.18	.03	.47	.94
6K-466-9 plr(6)		x		55.56	27.61	.17	.02	10.42	5.61	.09	99.5	50.7	.27	.22	.01	.05	.29	.15	.04	.35	1.32
6K-466-9 plc(6)		x	x	54.49	28.32	.24	.02	10.97	5.25	.09	99.4	53.6	.46	.29	.14	.01	.05	.07	.01	.35	.30
6K-466-9 pl2-r(6)		x	x	55.62	27.32	.78	.16	10.01	5.63	.16	99.7	49.6	.65	.61	.75	.01	.06	.10	.01	.61	.57
6K-466-11 plc(6)		x	x	58.13	26.03	.12	.01	8.39	6.85	.13	99.6	40.4	.13	.24	.05	.18	.27	.18	.11	.66	.56
6K-466-11 prf(6)		x	x	58.46	26.20	.15	.02	8.43	6.81	.12	100.2	40.6	.45	.27	.05	.01	.04	.14	.01	.36	.59
6K-467-1 plc(6)		x		54.28	29.21	.11	.03	11.29	5.14	.04	100.1	54.9	.16	.11	.02	.03	.07	.09	.01	.65	.47
6K-467-1 prf(cpx)c(6)		x	x	53.53	29.83	.18	.04	11.88	4.72	.14	100.2	58.2	.28	.13	.04	.01	.10	.13	.01	.15	.84
6K-467-2 plc(6)		x	x	59.93	25.54	.14	.01	6.95	7.54	.14	100.2	33.7	.14	.15	.04	.04	.15	.07	.01	.23	.60
6K-467-2 prf(6)		x	x	59.78	25.62	.13	.00	6.99	7.46	.13	100.1	34.1	.23	.15	.03	.01	.05	.10	.01	.17	.26
6K-467-3 plc(6)		x		60.18	25.04	.20	.00	6.80	7.65	.12	100.0	32.9	.42	.12	.19	.00	.09	.11	.01	.37	.53
		x														.01	.05	.09	.01	.46	.20

and are accompanied by standard deviations.

Evolution of Oceanic Gabbros: In-situ and Ancient Examples

Sample# and placement	Averages										Standard deviations									
	C	R	SiO ₂	Al ₂ O ₃	FeO	MgO	CaO	Na ₂ O	K ₂ O	Total	An%	SiO ₂	Al ₂ O ₃	FeO	MgO	CaO	Na ₂ O	K ₂ O	Total	An%
6K-467-3 plr(6)	x	x	59.25	25.56	24	.04	7.33	7.33	.10	99.8	35.6	.27	.35	.25	.09	.24	.15	.07	.18	1.10
6K-467-3 pl2 c-r(12)	x	x	59.63	25.74	.24	.00	7.27	7.42	.10	100.4	35.1	.48	.12	.16	.00	.17	.15	.01	.34	.90
6K-467-3 pl3 c-r(10)	x	x	59.70	24.46	.16	.00	7.06	7.57	.17	99.1	34.0	.35	.20	.05	.01	.16	.08	.01	.49	.39
6K-467-4a plc(6)	x	x	59.74	25.63	.13	.02	7.27	7.45	.15	100.4	35.0	.46	.19	.05	.01	.16	.13	.02	.60	.73
6K-467-6 pl c-r(9)	x	x	57.15	26.76	.11	.01	8.87	6.06	.75	99.8	44.6	1.23	1.26	.04	.01	1.48	.63	1.39	.51	5.47
6K-467-9 plc(6)	x	x	55.76	28.00	.16	.05	10.01	5.80	.06	99.8	48.8	.19	.28	.09	.07	.11	.05	.03	.13	.36
6K-467-9 plr(3)	x	x	55.61	28.07	.58	.21	10.08	5.81	.03	100.4	49.0	.17	.13	.19	.17	.11	.09	.00	.13	.54
6K-467-9 pl2c-r(4)	x	x	55.66	28.62	.21	.04	10.48	5.75	.05	100.8	50.2	.35	.11	.07	.06	.14	.10	.00	.42	.52
6K-467-10 plc(6)	x	x	56.43	28.07	.09	.01	9.87	5.94	.07	100.5	47.9	.18	.18	.03	.01	.12	.12	.01	.21	.70
6K-467-10 plr(cpx)(6)	x	x	55.66	28.54	.17	.06	10.29	5.70	.06	100.5	50.0	.38	.21	.23	.12	.25	.20	.01	.18	1.36
6K-467-1 plr(4)	x	x	55.37	25.95	.21	1.00	9.01	5.82	.07	99.4	47.3	6.07	2.51	3.57	1.72	3.17	2.53	.05	2.01	18.19
6K-467-1 pl2c(6)	x	x	54.62	28.04	.15	.02	10.69	5.44	.07	99.0	52.0	1.56	1.07	.07	.02	.33	.08	.03	2.93	.51
6K-467-1 pl3r(12)	x	x	55.00	28.40	.29	.18	10.88	5.34	.07	100.2	52.9	.30	.52	.40	.40	.47	.08	.01	.31	1.26
6K-467-13 plc(5)	x	x	52.61	29.70	.59	.30	13.16	3.98	.04	100.4	64.6	.49	.34	.32	.23	.39	.14	.01	.38	1.37
6K-467-13 plr(6)	x	x	56.28	27.26	.16	.03	9.36	6.24	.08	99.4	45.3	.17	.10	.04	.01	.07	.04	.01	.25	.11
6K-467-13 pl(6)	x	x	56.62	27.44	.16	.03	9.41	6.23	.08	100.0	45.5	.45	.15	.02	.01	.07	.04	.01	.47	.23
6K-467-15 plc(5)	x	x	56.45	27.35	.16	.03	9.39	6.24	.08	99.7	45.4	.31	.13	.03	.01	.07	.04	.01	.36	.17
6K-467-15 plr(6)	x	x	54.24	29.16	.26	.03	11.49	5.02	.05	100.2	55.9	.37	.16	.03	.02	.04	.09	.01	.42	.37
6K-467-15 plr(6)	x	x	53.94	29.36	.26	.02	11.57	4.97	.05	100.2	56.3	.33	.06	.04	.02	.01	.17	.00	.24	.85
6K-467-17 plr(6)	x	x	55.00	28.95	.21	.01	11.02	5.26	.06	100.5	53.6	.34	.26	.02	.01	.19	.12	.01	.40	.97
6K-467-17 pl2 c-r(10)	x	x	54.94	28.77	.20	.01	10.96	5.34	.07	100.3	53.2	.28	.10	.03	.01	.09	.10	.01	.26	.56
6K-467-20 plc(6)	x	x	65.33	21.93	.02	.00	2.95	10.17	.00	100.4	13.8	.58	.23	.03	.00	.36	.27	.01	.49	1.77
6K-467-20 plr(6)	x	x	52.17	30.79	.22	.03	13.07	4.11	.02	100.4	63.7	.10	.17	.02	.01	.10	.08	.00	.20	.58
6K-467-20 plr(cpx)(6)	x	x	52.77	30.62	.20	.01	12.64	4.34	.02	100.6	61.7	.27	.22	.05	.01	.15	.11	.01	.37	.81
Leg. ABCDE																				
6K-645-r18 pl(10)	x	x	57.49	27.58	.00	.00	9.21	6.67	.10	101.0	43.3	.36	.14	.01	.01	.04	.15	.01	.47	.64
6K-645-r18 plc(6)	x	x	57.88	27.40	.14	.01	9.13	6.59	.10	101.3	43.3	.18	.19	.12	.01	.10	.10	.01	.38	.49
6K-645-r18 plr(6)	x	x	57.86	27.65	.07	.00	9.20	6.53	.07	101.4	43.8	.18	.11	.04	.01	.05	.06	.01	.24	.30
6K-645-r17 plr(5)	x	x	59.95	26.02	.23	.00	7.30	7.39	.05	101.0	35.3	.22	.18	.25	.00	.07	.10	.02	.24	.39
6K-645-r17 plc(5)	x	x	59.80	25.96	.09	.00	7.22	7.40	.18	100.7	35.0	.24	.28	.02	.00	.07	.03	.01	.12	.21
6K-647-1 plr(5)	x	x	56.30	27.95	.21	.00	9.62	6.03	.04	100.1	46.8	.14	.19	.02	.00	.06	.12	.02	.11	.46
6K-647-1 plc(5)	x	x	56.63	27.45	.41	.02	9.28	6.20	.08	100.1	45.3	.36	.18	.41	.01	.10	.06	.01	.20	.42
6K-647-r10 plr(5)	x	x	59.53	25.77	.27	.01	7.22	7.58	.05	100.4	34.5	.15	.18	.04	.02	.14	.16	.03	.25	.82
6K-647-r10 plc(5)	x	x	59.63	25.73	.17	.00	7.23	7.47	.11	100.3	34.9	.44	.07	.01	.00	.10	.13	.02	.40	.64
6K-647-r13 pl r-c(6)	x	x	55.98	28.27	.24	.00	10.01	5.93	.02	100.4	48.3	.32	.24	.16	.01	.33	.17	.03	.18	1.48
6K-647-r09 plr(5)	x	x	55.83	28.31	.24	.01	10.11	5.85	.04	100.4	48.8	.33	.19	.05	.01	.16	.08	.02	.56	.44
6K-647-r09 plc(5)	x	x	56.53	27.83	.23	.01	9.49	6.15	.05	100.3	46.0	.36	.23	.04	.01	.09	.16	.02	.19	.83
6K-646-r01 plc(6)	x	x	52.33	31.02	.19	.01	13.28	4.08	.02	100.9	64.3	.11	.12	.03	.01	.12	.13	.00	.17	.86
6K-646-r01 plr(6)	x	x	52.66	30.73	.16	.01	12.77	4.26	.03	100.6	62.4	.38	.49	.03	.00	.21	.09	.01	.16	.65
6K-646-r04 plc(6)	x	x	51.87	30.45	.25	.04	13.07	3.76	.08	99.5	65.7	.32	.31	.02	.02	.28	.09	.03	.57	.77
6K-646-r04 plr(6)	x	x	51.11	31.06	.24	.03	13.64	3.58	.08	99.7	67.8	.77	.57	.03	.01	.65	.39	.05	.38	3.35
6K-646-r04 plr(2)	x	x	50.50	31.27	.23	.04	14.19	3.13	.05	99.4	71.5	.33	.45	.04	.02	.13	.03	.04	.28	.38
6K-646-r04 plr(6)	x	x	51.87	30.45	.25	.04	13.07	3.76	.08	99.5	65.7	.32	.31	.02	.02	.28	.09	.03	.57	.77
6K-646-r04 plr(2)	x	x	51.79	30.40	.27	.04	13.06	3.90	.13	99.6	64.9	.21	.09	.01	.01	.13	.12	.05	.18	.50
6K-646-r06 plc(6)	x	x	52.67	30.93	.22	.02	12.85	4.19	.04	100.9	62.9	.87	.44	.01	.01	.17	.16	.01	.66	1.12
6K-646-r06 plr(6)	x	x	56.19	28.65	.19	.00	10.33	5.77	.03	101.2	49.7	.28	.15	.06	.00	.10	.08	.02	.18	.41

Each analysis is indexed with the mineral (ol) and core (c), rim (r) c-c (core to rim traverse) or particular notes, and the number of analyses (n) and are accompanied by standard deviations.

Evolution of Oceanic Gabbros: In-situ and Ancient Examples

Sample# and placement	Averages										Standard deviations									
	C	R	SiO ₂	Al ₂ O ₃	FeO	MgO	CaO	Na ₂ O	K ₂ O	Total	An%	SiO ₂	Al ₂ O ₃	FeO	MgO	CaO	Na ₂ O	K ₂ O	Total	An%
6k-649-r06 plc(6)	x		56.80	27.99	.26	.04	9.98	5.96	.08	101.1	48.1	.23	.21	.05	.00	.07	.10	.01	.44	.52
6k-649-r06 plir(6)	x		56.36	28.33	.22	.02	10.37	5.78	.07	101.1	49.8	.12	.17	.06	.01	.06	.10	.00	.22	.45
6k-643-r08 plir(6)	x		56.69	28.32	.13	.02	9.96	5.65	.34	101.1	49.3	.32	.15	.02	.01	.10	.11	.03	.43	.49
6k-643-r08 plc(6)	x		56.58	28.22	.19	.05	9.96	5.60	.19	100.8	49.6	.10	.21	.07	.03	.05	.13	.11	.28	.63
6k-649-r08 plc(6)	x		53.99	29.93	.11	.03	11.97	4.92	.07	101.0	57.3	.31	.26	.03	.01	.05	.09	.01	.43	.41
6k-649-r08 plir(6)	x		54.00	29.85	.19	.04	11.93	4.97	.07	101.0	57.0	.34	.13	.14	.03	.07	.08	.01	.57	.33
6k-649-r08 plir(ol)(5)	x		54.02	29.98	.33	.24	11.87	5.08	.06	101.3	58.7	.18	.07	.04	.01	.16	.08	.01	.30	.51
6k-649-r12 plc(6)	x		55.35	28.55	.25	.05	10.72	5.14	.29	100.4	53.5	.32	.13	.06	.01	.08	.11	.07	.19	.66
6k-649-r12 plir(6)	x		55.18	29.16	.20	.03	10.89	5.09	.08	100.6	54.2	.38	.28	.02	.02	.29	.21	.06	.48	1.59
6k-649-r14 plc(6)	x		54.50	29.37	.34	.02	11.60	5.03	.07	100.9	56.0	.48	.08	.13	.01	.11	.15	.01	.62	.54
6k-649-r14 plir(5)	x		56.07	28.96	.20	.01	10.62	5.79	.07	101.7	50.4	1.24	.75	.04	.01	.87	.72	.01	.32	4.98
6k-649-r14 plir-r(10)	x		54.87	29.65	.26	.01	11.50	5.20	.06	101.6	55.0	.44	.20	.10	.01	.19	.11	.01	.28	.83
6k-650-r04 plc(5)	x		53.22	30.99	.15	.01	13.11	4.25	.03	101.8	63.0	.18	.13	.02	.01	.03	.12	.01	.26	.65
6k-650-r04 plir(6)	x		52.19	31.70	.23	.02	13.25	3.99	.04	101.4	64.7	.16	.72	.24	.03	.14	.18	.05	.71	.85
6k-650-r06 plc(2)	x		53.70	29.99	.12	.00	12.03	4.65	.03	100.5	58.9	.71	.47	.04	.00	.37	.18	.00	1.75	1.18
6k-650-r06 plir(cpx)(6)	x		53.25	30.87	.19	.01	12.80	4.29	.00	101.4	62.2	.20	.15	.02	.01	.16	.08	.01	.12	.70
6k-650-r06 plir(ol)(6)	x		52.38	31.27	.25	.03	13.46	3.97	.01	101.4	65.2	.94	.68	.08	.05	.77	.39	.01	.23	3.51
6k-650-r09 plc(5)	x		55.12	29.16	.22	.19	11.21	5.50	.05	101.4	53.0	.55	.44	.24	.40	.22	.14	.01	.60	.66
6k-650-r09 plir(6)	x		54.97	29.59	.11	.00	11.48	5.35	.04	101.6	54.2	.22	.14	.01	.01	.12	.08	.01	.21	.56
6k-653-r2 plir(5)	x		51.36	27.36	2.23	2.18	8.45	5.40	.06	97.0	46.2	8.46	1.88	4.35	4.87	2.37	1.42	.03	4.92	.82
6k-653-r2 plc(5)	x		54.59	28.90	.21	.01	10.80	5.14	.08	99.7	53.7	.30	.24	.03	.01	.15	.08	.02	.35	.70
BGS-Cores																				
BGS-2-1-7c 37-41 plc(5)	x		58.00	26.41	.22	.05	8.08	6.91	.12	99.8	39.3	.17	.21	.05	.09	.07	.11	.02	.25	.40
BGS-2-1-7c 37-41 plir(5)	x		58.04	26.16	.20	.06	7.85	6.99	.11	99.4	38.3	.25	.11	.08	.13	.19	.10	.02	.24	.29
BGS-3-1-2a 0-5 plc(6)	x		53.62	29.45	.06	.00	11.55	5.13	.04	99.8	55.4	.14	.26	.02	.00	.10	.07	.04	.31	.44
BGS-3-1-2a 0-5 plir(4)	x		53.46	29.74	.07	.00	11.85	5.02	.02	100.2	56.6	.14	.27	.03	.00	.07	.11	.01	.26	.69
BGS-4-1-4c 43-48 plc(6)	x		53.42	30.03	.17	.01	12.19	4.61	.07	100.5	59.4	.71	.52	.06	.01	.45	.29	.02	.42	2.41
BGS-4-2 0-4 plir(6)	x		52.85	30.02	.14	.03	12.48	4.56	.15	100.2	60.2	1.89	.97	.06	.01	1.16	.68	.04	.61	5.75
BGS-4-2 0-4 plir(6)	x		52.52	30.66	.09	.06	12.94	4.39	.07	100.7	62.0	.54	.28	.04	.04	.16	.15	.03	.51	1.06
BGS-4-2 17-44plir(6)	x		53.62	29.66	.14	.03	12.09	4.75	.15	100.4	58.4	1.24	.87	.04	.02	.97	.51	.03	.35	4.54
BGS-4-2 17-44plir(6)	x		54.35	29.56	.15	.09	11.44	4.95	.05	100.6	56.1	.41	.44	.12	.20	.38	.13	.02	.59	1.31
BGS-4-2 4d a1 plir(ol) r-r (8)	x		54.72	29.35	.19	.03	11.34	5.11	.06	100.8	55.1	.33	.17	.04	.01	.08	.12	.02	.46	.60
BGS-4-2 4d a1 plir(ol) r-r (8)	x		54.79	29.44	.11	.03	11.43	5.04	.04	100.9	55.6	.53	.26	.05	.03	.31	.20	.02	.32	1.54
BGS-10-1-1a 31-36 plc(6)	x		55.22	28.25	.20	.00	10.28	5.76	.08	99.8	49.7	.27	.13	.01	.00	.10	.08	.00	.19	.20
BGS-10-1-1a 31-36 plir(6)	x		55.16	28.47	.20	.00	10.48	5.57	.04	99.9	51.0	.10	.13	.02	.00	.07	.08	.02	.25	.37
BGS-16-1-1 7-12 plc(6)	x		55.13	28.53	.06	.00	10.38	5.63	.08	99.8	50.5	.16	.21	.02	.00	.06	.10	.00	.21	.47
BGS-16-1-1 7-12 plir(6)	x		54.77	28.74	.07	.00	10.72	5.48	.08	99.9	52.0	.15	.25	.01	.00	.07	.05	.01	.28	.29
BGS-16-1-1 7-12 plir(ol)(12)	x		55.26	28.31	.13	.00	10.20	5.72	.08	99.7	49.6	.27	.26	.03	.00	.14	.11	.01	.23	.73
BGS-17-1-1A 12 plir(10)	x		55.55	30.36	.28	.00	11.97	4.91	.05	103.1	57.4	.90	.54	.10	.01	.65	.35	.02	.41	3.07
BGS-17-1b 25-30 plc(5)	x		54.90	29.41	.06	.01	11.46	5.37	.01	101.2	54.1	.94	.45	.02	.01	.56	.37	.01	.55	2.93
BGS-17-1b 25-30 plir(3)	x		60.20	25.48	.13	.00	6.82	7.89	.04	100.6	32.3	.88	.42	.06	.00	.22	.19	.04	1.21	1.24
BGS-17-1f-65-67 plc(4)	x		58.80	25.34	.38	.06	7.08	7.33	.03	99.0	34.7	2.58	1.75	.41	.05	1.99	.87	.02	.21	9.23
BGS-17-1f-65-67 plir(4)	x		53.44	28.99	.26	.04	12.28	4.75	.06	99.8	58.8	.46	.21	.10	.10	.12	.12	.01	.73	.78
BGS-19-2 10-11.5 plir(10)	x		54.25	30.12	.15	.01	12.33	4.82	.04	101.7	58.6	.21	.29	.03	.01	.15	.06	.01	.36	.42

Each analysis is indexed with the mineral (ol) and core (c), rim (r) r-c (core to rim traverse) or particular notes, and the number of analyses (#) and are accompanied by standard deviations.

Evolution of Oceanic Gabbros: In-situ and Ancient Examples

Sample# and placement	Averages										Standard deviations									
	C	R	SiO ₂	Al ₂ O ₃	FeO	MgO	CaO	Na ₂ O	K ₂ O	Total	An%	SiO ₂	Al ₂ O ₃	FeO	MgO	CaO	Na ₂ O	K ₂ O	Total	An%
BGS-19-2-12a 38.5 pl2(15)	x	x	54.07	29.68	28	.05	12.42	4.72	.06	101.3	59.2	.55	.41	.28	.14	.38	.24	.01	.55	1.82
BGS-20-1-3B 28.5-32 plc(9)	x	x	55.24	27.62	36	.24	10.10	5.65	.05	99.3	49.7	.39	.73	.33	.37	.45	.35	.04	.84	2.31
BGS-20-1-6a pl inside cpx(5)	x	x	55.52	28.81	38	.04	10.72	5.72	.05	101.2	50.9	.30	.13	.05	.01	.11	.08	.01	.24	.52
BGS-20-1-6a pl (ol)-c(10)	x	x	55.76	29.09	23	.03	10.92	5.76	.06	101.8	51.1	.20	.18	.03	.01	.27	.14	.01	.31	1.12
BGS-20-1-6a pl r(cpx)-c(10)	x	x	55.96	28.86	26	.11	10.40	5.75	.04	101.4	50.0	.77	.27	.27	.24	.35	.23	.01	.68	1.58
BGS-20-1-6a 64-67	x	x	55.34	28.59	27	.17	10.58	5.37	100.3	52.1										
BGS-20-1-6a 64-67 plc(16)	x	x	55.85	27.59	19	.11	10.19	5.74	99.7	49.5		.47	.64	.10	.15	.34	.16		.72	1.43
BGS-20-1-6a 64-67 plr(9)	x	x	55.52	27.65	21	.08	10.40	5.72	99.6	50.1		.57	.32	.10	.16	.22	.11		.45	.78
BGS-20-1-6a 64-67 plc2(6)	x	x	55.40	27.78	30	.13	10.50	5.52	99.6	51.2		.72	.36	.13	.21	.10	.13		.91	.53
BGS-20-1-6a 64-67 plr(cpx)(10)	x	x	55.83	27.33	25	.14	10.07	5.85	99.5	49.1		1.10	1.07	.16	.24	1.07	.44		.57	4.63
BGS-20-2-6b al pl(undeformed) r-r(10)	x	x	55.96	28.05	14	.04	9.67	5.63	.04	99.5	48.7	.24	.24	.05	.05	.11	.09	.02	.42	.36
BGS-20-2-6b al pl r(cpx)-c(10)	x	x	55.71	28.24	09	.00	9.90	5.64	.03	99.6	49.2	.28	.23	.04	.00	.16	.12	.03	.41	.78
BGS-20-2-6b a2 pl r-c(10)	x	x	55.53	28.75	22	.01	10.48	5.35	.01	100.4	52.0	.65	.33	.05	.01	.45	.28	.01	.42	.32
BGS-20-2-6b a2 pl r-c(10)	x	x	56.12	28.31	11	.01	10.08	5.60	.04	100.3	49.9	.45	.18	.04	.01	.17	.11	.01	.42	.78
BGS-20-2-6B 0-5.8 plc(6)	x	x	55.27	28.27	19	.00	10.14	5.87	.02	99.8	48.8	.35	.23	.02	.00	.09	.10	.01	.34	.45
BGS-20-2-6B 0-5.8 plr(7)	x	x	54.55	27.46	89	.36	10.40	5.39	.04	99.1	51.6	1.11	.96	1.52	.63	.42	.65	.02	.64	1.15
BGS-20-2-6B 0-5.8 pl(6)	x	x	57.91	27.22	33	.04	8.72	6.52	.08	100.8	42.5	.39	.33	.12	.07	.17	.17	.01	.57	1.00
BGS-23-1-2b 23-28 al pl(inside cpx) r-r(10)	x	x	58.23	27.31	14	.01	8.60	6.59	.08	101.0	41.9	.43	.24	.05	.01	.23	.17	.02	.35	1.06
BGS-23-1-2b 23-28 al pl(inside cpx) r-r(10)	x	x	58.22	27.44	27	.06	8.77	6.45	.11	101.3	42.9	.28	.29	.13	.11	.12	.14	.01	.54	.35
BGS-23-1-2b 23-28 a2 pl r-c(2)	x	x	58.23	26.71	52	.28	8.89	6.51	.10	101.2	43.0	.23	.99	.26	.35	.25	.02	.00	.36	.79
BGS-23-1-2b 23-28 a2 pl(inside) r-c(5)	x	x	57.51	27.54	65	.13	9.01	6.28	.05	101.2	43.1	.42	.17	.05	.00	.17	.19	.02	.41	1.10
BGS-23-1-2b 23-28 a3 pl r-r(9)	x	x	57.84	27.76	17	.00	8.96	6.54	.05	101.3	43.1	.66	.14	.32	.18	.11	.19	.02	.49	.84
BGS-23-1-2b 23-28 a3 pl-c(6)	x	x	59.57	26.66	29	.10	8.91	6.36	.06	101.0	43.6	.29	.13	.13	.11	.09	.07	.02	.26	.23
BGS-23-1-2b 23-28 a4 pl r-c(10)	x	x	56.61	27.67	34	.03	7.78	7.08	.11	101.4	45.9	.64	.48	.09	.03	.49	.31	.02	.50	2.45
BGS-23-1-2b 29-34 al pl r-r(4)	x	x	57.37	27.31	19	.07	8.97	6.57	.09	100.6	43.0	.20	.20	.09	.11	.11	.08	.01	.33	.43
BGS-23-1-2b 29-34 al pl2 r-c(10)	x	x	57.72	26.99	14	.00	8.63	6.74	.10	100.3	41.5	.43	.20	.02	.00	.06	.11	.00	.53	.29
BGS-23-1-2b 29-34 a2 plc(6)	x	x	57.31	27.27	16	.01	8.86	6.60	.09	100.3	42.6	.22	.17	.03	.01	.39	.09	.00	.25	.51
BGS-23-1-2b 29-34 a3 pl r-r(9)	x	x	56.42	27.69	56	.17	9.22	6.45	.07	98.8	44.3	.89	.39	.82	.46	.33	.24	.01	.83	.61
BGS-23-1-2b 29-34 a4 pl(inside cpx) r-r(5)	x	x	56.14	27.02	21	.04	9.02	6.28	.07	98.8	44.3	.67	.24	.06	.04	.09	.11	.01	.83	.61
BGS-23-1-2b 29-34 a4 pl2 r-r(8)	x	x	56.53	27.65	28	.06	9.30	6.17	.10	100.1	45.4	.83	.25	.30	.14	.42	.23	.02	.62	1.93
BGS-23-1-2b 29-34 a5 pl r-r(8)	x	x	56.52	26.93	65	.21	8.94	6.40	.10	99.7	43.6	1.14	.60	.96	.37	.20	.26	.03	.73	.85
BGS-23-1-2b 44.5-48.5 pl r-r(9)	x	x	56.14	25.57	126	.94	9.60	6.04	.14	99.7	46.7	.81	2.70	1.15	1.71	1.36	.62	.03	.71	6.01
BGS-23-1-2e al pl(10)	x	x	57.63	26.44	18	.01	8.27	6.83	.11	99.5	40.1	.48	.22	.02	.01	.28	.22	.01	.32	1.52
BGS-23-1-2e a2 pl r-c(10)	x	x	58.34	27.01	18	.03	8.28	6.72	.13	100.7	40.5	.60	.27	.12	.05	.36	.22	.03	.14	1.85
BGS-23-1-2e a3 pl r-c(10)	x	x	58.19	26.82	16	.02	8.19	6.77	.12	100.3	40.1	.44	.14	.08	.03	.15	.11	.02	.39	.71
BGS-23-1-2e a4 pl r-c(10)	x	x	58.25	26.92	19	.03	8.43	6.77	.11	100.7	40.8	.41	.23	.07	.14	.11	.10	.03	.51	.58
BGS-24-1-3a 6-10 plc(6)	x	x	55.65	28.50	17	.02	10.34	5.71	.09	100.5	50.0	.37	.08	.02	.01	.11	.13	.01	.45	.70
BGS-24-1-3a 6-10 plr(6)	x	x	55.18	28.27	22	.04	10.36	5.59	.09	99.8	50.6	.25	.14	.10	.07	.08	.10	.01	.25	.57
BGS-24-1-3a 21-24 pl r-c(6)	x	x	57.61	27.20	20	.01	8.80	6.63	.08	100.5	42.3	.45	.27	.05	.01	.25	.19	.04	.57	1.18
BGS-24-1-3d 24 pl(10)	x	x	60.48	27.19	64	.22	8.19	6.82	.30	103.8	39.9	.74	1.11	1.28	.70	.60	.34	.27	.71	1.33
BGS-24-1-3h 47 pl(6)	x	x	58.04	26.46	20	.02	8.78	6.78	.15	100.4	41.7	.16	.49	.03	.04	.20	.27	.03	.71	1.33
BGS-24-1-3h 51.5 pl(13)	x	x	57.35	28.02	19	.00	9.88	6.07	.09	101.6	47.4	.36	.24	.03	.00	.09	.07	.01	.30	.15
BGS-24-1-3h 51.5 pl2(6)	x	x	56.52	28.40	20	.00	10.59	5.65	.10	101.5	50.9	.52	.36	.02	.01	.51	.30	.01	.39	2.49

Each analysis is indexed with the mineral (ol) and core (c), rim (r) r-c (core to rim traverse) or particular notes, and the number of analyses (#) and are accompanied by standard deviations.

Evolution of Oceanic Gabbros: In-situ and Ancient Examples

Sample# and placement	Averages										Standard deviations									
	C	R	SiO ₂	Al ₂ O ₃	FeO	MgO	CaO	Na ₂ O	K ₂ O	Total	An#	SiO ₂	Al ₂ O ₃	FeO	MgO	CaO	Na ₂ O	K ₂ O	Total	An#
BGS-24-1-31-60 pl(6)	x	x	56.16	27.89	.18	.00	10.39	5.78	.09	100.5	49.8	1.01	.36	.03	.00	.64	.36	.01	.41	3.08
BGS-24-1-31-77 pl(9)	x	x	59.88	27.53	.26	.09	8.48	6.74	.12	103.1	41.0	.66	.41	.25	.27	.24	.05	.02	.68	.72
BGS-27-1-1A 3 pl(9)	x	x	56.37	29.73	.18	.00	10.89	5.21	.04	102.4	53.6	.31	.15	.03	.01	.14	.08	.02	.30	.59
BGS-27-1-1B 8.5 pl(6)	x	x	55.63	29.29	.18	.00	11.30	5.14	.04	101.6	54.8	.24	.25	.03	.00	.16	.16	.01	.33	.93
BGS-27-1-1B 8.5 pl(28)	x	x	55.02	29.37	.22	.05	11.26	5.22	.02	101.2	54.4	.28	.29	.09	.13	.18	.21	.01	.34	1.39
BGS-27-1-1B 19.5 pl(15)	x	x	54.19	29.05	.44	.18	11.39	5.15	.04	100.4	55.0	.63	.56	.93	.54	.68	.21	.02	.76	1.92
BGS-27-1-1B 25.5-31 pl(5)	x	x	53.56	28.98	.13	.00	11.17	5.14	.05	99.0	54.6	.18	.11	.05	.00	.17	.09	.01	.21	.52
BGS-27-1-1d 56-62 pl-c(10)	x	x	51.09	31.72	.40	.33	13.56	3.37	.03	100.5	69.0	.88	.79	.75	1.02	1.09	.22	.02	.99	1.53
BGS-31-1-1c 34.5-39.5 plc(6)	x	x	55.95	27.83	.19	.01	9.88	5.95	.10	99.9	47.8	.24	.25	.07	.00	.04	.04	.01	.35	.26
BGS-31-1-1c 34.5-39.5 plr(6)	x	x	56.33	27.93	.14	.01	9.73	6.05	.05	100.2	47.0	.28	.15	.03	.01	.09	.12	.02	.41	.69
BGS-31-1a 0-5 plc(12)	x	x	54.83	28.73	.20	.02	10.77	5.51	.08	100.1	52.0	.31	.22	.03	.01	.10	.13	.01	.51	.70
BR-Drills																				
BR-5-1-1B 4.5-8.5 plc(6)	x	x	54.16	29.42	.12	.01	11.40	5.01	.05	100.2	55.7	.19	.09	.04	.01	.06	.09	.00	.20	.48
BR-5-1-1B 4.5-8.5 plr(6)	x	x	54.57	29.09	.11	.08	11.09	5.22	.05	100.2	54.0	.43	.20	.11	.15	.14	.10	.00	.25	.57
BR-5-1-1H 74-78 plc(6)	x	x	54.62	28.55	.21	.11	11.07	5.27	.09	99.9	53.7	.36	.18	.11	.18	.07	.12	.01	.34	.53
BR-5-1-1H 74-78 plr(6)	x	x	54.35	28.88	.11	.01	11.26	5.16	.07	99.8	54.7	.28	.19	.01	.01	.21	.13	.01	.25	1.02
BR-5-1-1H 74-78 plc-r(12)	x	x	54.60	28.65	.16	.03	11.04	5.33	.07	99.9	53.4	.26	.18	.07	.04	.09	.08	.01	.31	.49
BR-5-1-5c 48-51.5 plc	x	x	53.73	29.00	.20	.01	10.85	5.46	.05	99.3	52.4	.28	.20	.01	.02	.07	.08	.01	.31	.47
BR-6-1-1g 20.5-24.5 plc(6)	x	x	55.74	27.87	.13	.03	10.01	6.08	.11	100.0	47.6	.39	.09	.05	.01	.03	.11	.01	.45	.44
BR-6-1-1g 20.5-24.5 plr(6)	x	x	55.90	27.92	.13	.01	10.00	6.10	.09	100.2	47.5	.38	.39	.09	.04	.19	.09	.01	.55	.67
BR-8-1-SD 34-36 pl r-r(11)	x	x	54.42	27.00	.22	.03	10.95	5.26	.07	98.0	53.5	.29	.38	.08	.08	.23	.07	.01	.39	.76
BR-8-1-SD 34-36 plc c-r(8)	x	x	52.96	28.17	.23	.05	12.10	4.52	.04	98.1	59.6	.65	.21	.02	.01	.28	.17	.02	.51	1.47
BR-8-1-5G 69-71.5 plr-r(15)	x	x	53.02	27.78	.25	.02	11.86	4.69	.07	97.7	58.3	.81	.50	.04	.09	.49	.26	.02	.57	2.28
BR-8-2-5h 3 pl(10)	x	x	53.40	28.73	.26	.05	11.81	4.92	.07	99.2	57.0	.59	.54	.04	.04	.00	.28	.08	.01	.76
BR-8-2-5h 3 pl(26)	x	x	53.83	29.37	.20	.00	11.99	4.92	.04	100.3	57.4	.62	.47	.18	.01	.26	.14	.05	.99	1.25
BR-8-2-5h 3 pl(34)	x	x	52.89	29.25	.31	.01	12.29	4.69	.07	99.5	59.1	.56	.31	.27	.26	.21	.10	.02	.19	.56
BR-8-2-5m 18.5-23 pl c-r(8)	x	x	52.17	29.19	.45	.20	11.80	4.30	.04	98.2	60.3	.89	.36	1.41	.02	.24	.12	.01	.37	.82
BR-9-1-1D 26-28.5 plc(5)	x	x	55.13	27.59	.76	.03	9.80	5.80	.05	99.2	48.3	.41	.17	.05	.01	.05	.16	.07	.56	.62
BR-9-1-1D 26-28.5 plr(6)	x	x	55.06	27.93	.15	.01	9.99	5.81	.06	99.0	48.8	.41	.17	.05	.01	.05	.16	.07	.56	.62
BR-14-1-7a 35-37.5 pl(10)	x	x	54.47	28.12	.16	.01	10.73	5.55	.09	99.1	51.7	.22	.19	.06	.04	.11	.07	.01	.30	.37
BR-14-1-7a 35-37.5 plc(6)	x	x	54.68	28.19	.25	.12	10.40	5.63	.04	99.3	50.5	.35	.25	.19	.24	.23	.09	.01	.24	.78
BR-14-1-7a 35-37.5 plr(6)	x	x	54.55	28.13	.33	.20	10.37	5.57	.04	99.2	50.7	.47	.39	.25	.19	.24	.23	.09	.01	.42
BR-15-3B 17.5-20 plc-r(10)	x	x	52.68	30.00	.23	.04	12.70	4.46	.05	100.2	61.1	.31	.21	.06	.01	.13	.07	.01	.39	.48
BR-15-3B 17.5-20 plr c-r(10)	x	x	53.54	29.67	.17	.05	12.20	4.68	.03	100.4	59.0	.39	.24	.07	.09	.10	.09	.01	.45	.51
JCR31-Dredges																				
JR31-3-51 plc(6)	x	x	52.33	30.99	.56	.17	13.70	3.99	.03	101.8	65.5	.07	.35	.03	.02	.15	.13	.01	.38	.94
JR31-3-51 plr(6)	x	x	57.98	26.67	.81	.11	8.98	6.86	.09	101.5	42.0	.38	.32	.07	.04	.31	.16	.01	.37	1.33
JR31-9-2 plc(6)	x	x	56.69	28.69	.23	.03	10.13	6.01	.07	101.8	48.2	.12	.15	.03	.01	.16	.08	.01	.26	.58
JR31-9-2 plr(6)	x	x	56.16	29.10	.27	.02	10.77	5.76	.06	102.1	50.8	.30	.09	.05	.01	.14	.14	.01	.24	.90
JR31-9-4 plc(6)	x	x	57.05	28.35	.26	.06	10.13	6.14	.09	102.1	47.7	.24	.15	.03	.01	.08	.08	.00	.30	.44
JR31-9-4 plr(5)	x	x	58.53	27.32	.31	.16	8.95	6.55	.10	101.9	43.0	.23	.30	.12	.17	.14	.13	.01	.25	.80
JR31-12-1 al pl r(cpx)(6)	x	x	52.89	30.53	.20	.03	12.67	4.35	.03	100.7	61.7	.34	.23	.03	.01	.13	.07	.01	.22	.51
JR31-12-1 al pl c(6)	x	x	51.94	31.00	.20	.05	13.05	3.91	.03	100.2	64.9	.09	.09	.04	.02	.94	.09	.01	1.00	1.51
JR31-12-1 al pl r(ol)(6)	x	x	52.75	30.65	.27	.05	12.93	4.24	.03	100.9	62.7	.24	.24	.02	.02	.22	.07	.01	.41	.64
JR31-12-1 a2 pl r(cpx)(6)	x	x	53.09	29.81	.29	.24	12.06	4.65	.04	100.2	58.9	.21	.32	.05	.42	.16	.11	.02	.28	.33
JR31-12-1 a2 pl c(6)	x	x	52.46	30.92	.23	.06	13.16	4.01	.05	100.9	64.4	.29	.13	.01	.04	.19	.07	.02	.54	.40

Each analysis is indexed with the mineral (ol) and core (c), rim (r) c (core to rim traverse) or particular notes, and the number of analyses (#) and are accompanied by standard deviations.

Evolution of Oceanic Gabbros: In-situ and Ancient Examples

Sample# and placement	Averages										Standard deviations									
	C	R	SiO ₂	Al ₂ O ₃	FeO	MgO	CaO	Na ₂ O	K ₂ O	Total	An%	SiO ₂	Al ₂ O ₃	FeO	MgO	CaO	Na ₂ O	K ₂ O	Total	An%
JR31-12-1 a2 pl r(ol)(6)	x		52.39	30.97	.20	.04	13.16	4.06	.04	100.8	64.2	.24	.17	.03	.01	.16	.09	.02	.16	.73
JR31-12-6 plr-c4(6)	x		52.79	30.16	.19	.03	12.30	4.45	.04	100.0	60.4	.90	.61	.05	.02	.79	.31	.01	.37	3.17
JR31-12-6 plr-r8(6)	x		53.12	30.44	.23	.03	12.70	4.31	.03	100.9	61.9	.11	.29	.02	.01	.29	.11	.01	.44	1.12
JR31-12-6 plr(2)(6)	x		52.95	30.06	.13	.00	12.38	4.49	.03	100.0	60.4	.32	.20	.03	.01	.08	.09	.01	.53	.59
JR31-12-6 plr(1)(6)	x		52.20	30.24	.16	.04	12.77	4.34	.04	99.8	61.9	.08	.13	.02	.02	.23	.06	.01	.31	.55
JR31-12-6 plr c3(6)		x	51.65	30.84	.19	.03	13.25	3.99	.03	100.0	64.7	.39	.29	.03	.01	.30	.18	.01	.19	1.49
JR31-12-6 plr c7(6)	x		53.31	30.04	.38	.06	12.36	4.52	.06	100.7	60.2	.45	.38	.45	.03	.09	.04	.02	.46	.31
JR31-12-6 plr r(30)	x		53.21	30.17	.20	.02	12.64	4.46	.04	100.7	61.0	.48	.35	.05	.02	.40	.23	.02	.43	1.84
JR31-12-6 plr r(50)	x		52.35	30.54	.22	.03	12.84	4.14	.04	100.1	63.2	.56	.39	.07	.02	.44	.24	.02	.34	2.06
JR31-12-8 plr(6)	x		54.76	29.42	.11	.13	11.42	5.24	.02	101.1	54.7	.46	.38	.04	.17	.38	.16	.01	.19	1.52
JR31-12-8 plr(4)	x		54.11	30.14	.20	.03	11.98	4.92	.01	101.4	57.4	.36	.15	.03	.01	.16	.12	.01	.22	.75
JR31-12-8 plr(outside ol)(4)	x		53.45	30.20	.27	.18	12.30	4.76	.02	101.2	58.8	1.30	1.26	.16	.26	1.29	.72	.01	.42	6.21
JR31-12-8 plr(outside ol)(4)	x		52.98	30.57	.14	.03	12.77	4.44	.03	100.9	61.4	.22	.15	.07	.01	.07	.09	.01	.32	.46
JR31-12-8 plr(inside ol) c-r(4)	x		53.25	30.48	.11	.03	12.58	4.53	.03	101.0	60.5	.44	.16	.01	.02	.30	.21	.01	.19	1.69
JR31-12-10 plr(6)	x		54.13	29.35	.27	.04	11.67	4.77	.05	100.3	57.5	.18	.19	.08	.02	.13	.09	.01	.36	.43
JR31-12-10 plr(cpx)(3)	x		53.79	29.67	.17	.03	11.62	4.80	.04	100.1	57.3	.42	.05	.02	.05	.07	.23	.04	.50	1.22
JR31-12-16 plr(cpx)(5)	x		54.23	29.47	.14	.00	11.66	5.06	.06	100.6	56.1	.25	.20	.04	.00	.00	.21	.12	.60	.69
JR31-12-16 plr(cpx)(2)	x		54.77	29.52	.15	.03	11.97	5.07	.02	101.5	56.6	.52	.02	.03	.02	.16	.40	.01	.78	2.26
JR31-12-16 plr(4)	x		54.62	29.02	.26	.19	11.27	5.06	.05	100.5	55.2	.58	.45	.14	.28	.38	.19	.01	1.01	1.64
JR31-12-28 plr(6)	x		58.16	26.84	.18	.08	8.46	6.81	.06	100.6	40.7	.63	.44	.18	.18	.30	.26	.09	.48	1.60
JR31-12-28 plr(cpx)(6)	x		58.23	27.13	.19	.00	8.82	6.72	.07	101.2	42.0	.14	.08	.07	.00	.08	.16	.03	.29	.74
JR31-12-39 plr(6)	x		57.99	26.89	.31	.10	7.16	7.26	.05	100.6	35.3	.36	.21	.10	.10	.06	.17	.04	.65	.50
JR31-12-39 plr(cpx)(5)	x		59.67	26.46	.20	.00	7.67	7.34	.02	101.4	36.6	.21	.18	.04	.00	.08	.14	.01	.59	.81
JR31-12-42 plr(6)	x		55.69	29.13	.15	.04	10.92	5.53	.05	101.5	52.2	.34	.20	.02	.01	.09	.08	.01	.49	.48
JR31-12-42 plr(6)	x		55.70	28.79	.22	.03	10.57	5.82	.02	101.2	50.1	.30	.19	.15	.01	.08	.17	.02	.25	.88
JR31-12-45 plr(6)	x		54.85	29.63	.15	.02	11.46	5.31	.01	101.4	54.4	.14	.17	.02	.01	.14	.14	.00	.35	.75
JR31-12-45 plr(6)	x		55.06	29.35	.16	.04	11.09	5.58	.02	101.3	52.3	.18	.26	.03	.01	.11	.09	.01	.29	.57
JR31-12-46 plr(5)	x		54.63	29.00	.28	.16	11.24	5.20	.05	100.6	54.4	.97	.75	.29	.25	.08	.07	.06	1.16	.47
JR31-12-46 plr(cpx)(1)	x		54.27	27.98	.11	.00	11.80	4.37	.02	98.6	59.9	.14	.09	.02	.01	.12	.11	.01	.24	.64
JR31-12-47 plr(6)	x		54.29	29.66	.18	.01	11.68	5.12	.07	101.0	55.8	.18	.20	.02	.01	.08	.11	.02	.31	.68
JR31-12-47 plr(6)	x		54.41	29.62	.16	.01	11.62	5.23	.05	101.1	55.1	.48	.30	.14	.01	.18	.11	.01	.84	.79
JR31-12-50 plr(6)	x		51.83	29.90	.28	.06	12.69	4.36	.04	99.2	61.6	.31	.30	.03	.02	.10	.18	.01	.41	1.10
JR31-12-50 plr(5)	x		53.19	29.05	.19	.05	11.47	4.96	.04	99.0	56.1	.33	.17	.25	.01	.30	.11	.01	.46	.89
JR31-12-68 plr(cpx)(6)	x		53.91	29.85	.36	.05	11.85	4.79	.07	100.9	57.8	.21	.11	.03	.03	.14	.07	.01	.39	.49
JR31-39-1 plr(6)	x		55.13	29.33	.21	.05	10.89	5.30	.03	100.9	53.2	.18	.18	.19	.02	.11	.12	.02	.16	.62
JR31-39-1 plr(cpx)(6)	x		54.09	28.99	.27	.06	11.04	5.23	.05	99.7	53.9	.25	.15	.01	.01	.20	.11	.02	.46	.81
JR31-39-1 plr(6)	x		56.52	27.55	.23	.05	9.26	6.14	.08	99.8	45.4	.25	.15	.01	.01	.20	.11	.02	.46	.81
JR31-39-3 plr(6)	x		57.05	27.67	.16	.01	9.21	6.32	.08	100.5	44.6	.14	.23	.13	.01	.18	.06	.01	.35	.34
JR31-39-3 plr(6)	x		57.90	27.18	.33	.01	8.50	6.67	.11	100.7	41.3	.15	.14	.05	.01	.14	.10	.02	.30	.40
JR31-39-4 plr(6)	x		58.86	26.77	.19	.03	8.20	7.11	.12	101.3	38.9	.23	.06	.02	.01	.10	.15	.00	.29	.79
JR31-39-4 plr(inclusion)(4)	x		59.22	26.44	.28	.03	7.88	7.32	.11	101.3	37.3	.27	.36	.05	.00	.38	.31	.01	.30	2.14
JR31-39-4 plr(6)	x		59.03	26.73	.20	.03	8.24	7.14	.09	101.5	38.9	.25	.15	.01	.01	.04	.08	.02	.29	.18
JR31-39-7 plr(6)	x		60.38	26.11	.13	.01	7.27	7.79	.14	101.8	34.1	.30	.17	.04	.01	.03	.15	.02	.53	.48
JR31-39-7 plr(6)	x		58.77	26.34	.47	.10	7.82	7.00	.32	100.8	38.1	.95	1.10	.42	.16	.88	.53	.52	1.73	3.03
JR31-39-8 plr(6)	x		56.70	27.82	.25	.00	9.40	6.04	.09	100.3	46.2	.11	.15	.06	.01	.13	.10	.01	.31	.50

Each analysis is indexed with the mineral (ol) and core (c), rim (r) c-c (core to rim traverse) or particular notes, and the number of analyses (#) and are accompanied by standard deviations.

Evolution of Oceanic Gabbros: In-situ and Ancient Examples

Sample# and placement	Averages											Standard deviations										
	C	R	SiO ₂	Al ₂ O ₃	FeO	MgO	CaO	Na ₂ O	K ₂ O	Total	An%	SiO ₂	Al ₂ O ₃	FeO	MgO	CaO	Na ₂ O	K ₂ O	Total	An%		
JR31-39-8 p1r2(6)		x	56.68	27.81	.26	.00	9.30	6.06	.08	100.3	45.9	.22	.11	.03	.01	.29	.09	.01	.27	.79		
JR31-39-8 p1r1(6)		x	56.94	27.68	.27	.01	8.96	6.32	.08	100.3	43.9	.31	.27	.03	.02	.29	.10	.02	.71	.75		
JR31-39-10 p2c(6)		x	58.45	26.68	.18	.00	8.13	6.94	.09	100.5	39.3	.19	.13	.07	.01	.17	.16	.01	.34	.83		
JR31-39-10 p2r(6)		x	58.41	26.60	.37	.01	8.06	7.04	.08	100.6	38.7	.31	.28	.08	.01	.24	.07	.03	.23	.86		
JR31-39-10 p1c(6)		x	57.37	26.85	.28	.01	8.59	6.66	.07	99.8	41.6	.24	.18	.03	.01	.15	.06	.04	.33	.47		
JR31-39-10 p1r(6)		x	57.36	27.03	.34	.02	8.73	6.59	.07	100.1	42.3	.24	.20	.05	.01	.18	.10	.02	.44	.78		
JR31-39-11 p1c(6)		x	59.10	26.69	.18	.00	8.14	6.85	.12	101.1	39.7	.19	.16	.03	.01	.05	.06	.01	.16	.15		
JR31-39-11 p1r(6)		x	58.69	27.19	.24	.00	8.58	6.77	.07	101.5	41.2	.25	.27	.03	.01	.23	.11	.03	.48	.84		
JR31-39-13 p1c(6)		x	59.59	26.51	.23	.03	7.91	7.38	.14	101.8	37.2	.19	.12	.02	.01	.12	.15	.02	.16	.81		
JR31-39-13 p1r(6)		x	59.13	26.95	.29	.03	8.26	7.28	.13	102.1	38.5	.30	.23	.02	.01	.10	.11	.02	.34	.59		
JR31-39-17 p1c(6)		x	58.03	26.77	.17	.03	8.24	6.87	.10	100.2	39.8	.27	.18	.02	.01	.14	.06	.02	.26	.38		
JR31-39-17 p1r(6)		x	58.24	26.57	.18	.02	8.03	7.08	.10	100.2	38.5	.14	.22	.03	.01	.11	.10	.03	.37	.41		
JR31-39-17 p2r(6)		x	57.66	27.18	.36	.04	8.63	6.70	.10	100.7	41.6	.27	.14	.03	.03	.10	.07	.02	.17	.40		
JR31-39-17 p2c(5)		x	57.88	27.00	.22	.08	8.30	6.71	.10	100.3	40.6	.40	.29	.10	.10	.25	.09	.02	.59	.71		
JR31-40-1 p1c(6)		x	54.86	29.87	.21	.02	11.81	5.27	.04	102.1	55.3	.84	.35	.04	.01	.04	.08	.01	1.07	.38		
JR31-40-1 p1r(6)		x	54.79	30.45	.28	.02	12.33	4.98	.04	102.9	57.8	.34	.36	.05	.01	.37	.15	.01	.44	1.45		
JR31-41-4 p1c(6)		x	58.69	27.94	.07	.01	9.09	6.86	.07	102.7	42.3	.28	.12	.02	.00	.15	.06	.02	.26	.57		
JR31-41-4 p1r(6)		x	58.67	27.97	.20	.04	9.15	6.80	.04	102.9	42.6	.42	.45	.12	.06	.31	.15	.02	.24	1.33		

Each analysis is indexed with the mineral (ol) and core (c), rim (r) r-c (core to rim traverse) or particular notes, and the number of analyses (#) and are accompanied by standard deviations.

Evolution of Oceanic Gabbros: In-situ and Ancient Examples

Table 2B: The average composition of augite from on and around Atlantis Bank.

Sample # and placement	Averages				Standard deviations																			
	C	R	SiO ₂	TiO ₂	FeO	MnO	MgO	CaO	Na ₂ O	Total	Mg#	SiO ₂	TiO ₂	Al ₂ O ₃	Cr ₂ O ₃	FeO	MnO	MgO	CaO	Na ₂ O	Total	Mg#		
Mode 98																								
6K-459-3 cpxc(8)	x		51.61	.51	3.58	.01	18.67	.21	11.59	12.37	.58	99.1	52.5	.49	.13	.49	.01	1.09	.05	.51	.17	.15	.55	2.44
6K-459-3 cpxr(1)	x	x	51.14	.32	4.13	.03	19.96	.16	11.01	12.23	.56	99.5	49.6	1.61	.13	1.60	.02	.92	.04	.60	1.59	.32	.58	2.01
6K-459-9 cpxc(7)	x		50.22	.33	3.88	.03	20.13	.21	10.71	13.37	.76	99.6	48.7	1.20	.11	1.35	.01	1.84	.04	.35	2.69	.25	.70	3.08
6K-459-9 cpxr(7)	x	x	49.41	.41	4.75	.03	19.89	.18	10.31	13.43	.88	99.3	48.1	.35	.04	.16	.02	.18	.01	.13	.20	.00	.73	.50
6K-460-6 cpxc(6)	x		51.81	.86	2.14	.16	8.10	.25	16.67	18.96	.00	99.0	78.6	.25	.07	.37	.10	.48	.01	.28	.25	.00	.41	1.34
6K-460-6 cpxr(6)	x	x	49.76	1.37	3.72	.22	8.18	.21	14.90	20.13	.00	98.5	76.4	.56	.15	.10	.06	.41	.02	.56	.27	.00	.53	1.53
6K-460-6 cpx2c(6)	x		50.77	1.27	3.13	.16	8.65	.21	15.15	20.28	.00	99.6	75.7	.39	.06	.21	.01	.15	.03	.16	.25	.05	.57	.28
6K-460-11 cpxc(8)	x	x	52.10	.49	2.19	.00	9.03	.28	13.91	21.57	.44	100.0	73.3	.39	.06	.21	.01	1.85	.01	.47	1.65	.32	.56	4.65
6K-460-11 cpxr(2)	x	x	51.50	.33	1.84	.01	9.70	.31	13.33	21.07	.59	98.7	71.1	.74	.08	1.14	.01	1.85	.01	.47	1.65	.32	.56	4.65
6K-460-13 cpxc(10)	x		52.39	.72	2.59	.02	10.18	.24	17.48	16.37	.41	100.4	76.0	.79	.23	.62	.01	3.78	.06	3.39	7.31	.21	.37	2.95
6K-460-13 cpxr(10)	x	x	52.43	.70	2.41	.02	8.17	.22	15.56	20.45	.38	100.3	77.4	.50	.12	.18	.01	1.60	.04	1.20	2.80	.06	.55	1.84
6K-460-14 cpxc(6)	x	x	52.33	.68	1.85	.00	10.43	.30	13.86	20.33	.42	100.2	70.3	.28	.07	.07	.01	.34	.03	.17	.41	.03	.30	.63
6K-460-14 cpx2r(6)	x	x	51.94	.61	1.80	.01	12.11	.32	14.45	18.65	.37	100.3	68.3	.30	.07	.24	.01	2.53	.07	1.18	3.56	.07	.44	2.50
6K-460-14 cpx2c(10)	x		52.21	.66	1.82	.01	11.03	.30	14.17	20.02	.39	100.6	69.6	.40	.08	.14	.01	.94	.05	.28	1.24	.02	.75	1.51
6K-460-15 cpxc(6)	x		52.30	.17	.95	.00	12.23	.30	13.82	17.97	.30	98.1	66.8	1.39	.11	.60	.00	1.42	.04	1.46	4.86	.13	1.19	1.40
6K-460-15 cpxr(2)	x	x	51.90	.29	1.82	.00	13.82	.26	12.72	16.92	.46	98.2	62.5	1.77	.29	1.84	.00	3.95	.03	.01	7.18	.28	2.61	6.74
6K-460-16 cpxc(8)			52.00	.68	2.02	.01	11.08	.30	15.00	18.94	.40	100.4	71.2	.44	.15	.36	.01	2.77	.06	1.60	4.19	.12	.47	2.40
6K-460-16 cpxr(10)	x		52.22	.67	2.00	.01	10.08	.27	14.73	20.22	.41	100.6	72.4	.34	.08	.12	.01	1.35	.03	.84	2.26	.05	.45	1.34
6K-460-16 cpxc(8)	x		51.89	.66	1.99	.00	13.05	.32	16.13	15.70	.36	100.1	69.9	.48	.26	.74	.01	5.85	.14	3.28	8.55	.23	.20	4.43
6K-460-16 cpxc(6)	x	x	51.79	.75	2.17	.00	10.21	.28	14.46	20.20	.46	100.3	71.7	.57	.13	.33	.00	1.51	.02	1.00	2.37	.14	.73	1.50
6K-460-16 cpxr(10)	x	x	52.10	.65	1.91	.01	10.98	.31	14.68	19.63	.38	100.7	70.7	.36	.13	.23	.01	2.35	.05	1.29	3.58	.07	.49	2.31
6K-466-4 cpxc(9)	x		51.67	.78	2.82	.01	7.54	.21	14.36	21.69	.65	99.7	77.2	.28	.04	.15	.01	.24	.02	.14	.29	.10	.40	.54
6K-466-4 cpxr(10)	x	x	52.35	.55	2.11	.01	7.67	.24	14.46	21.91	.54	99.9	77.1	.38	.05	.15	.01	.21	.01	.15	.24	.07	.59	.66
6K-466-4 cpxr-(f5)	x	x	52.22	.63	2.28	.01	7.92	.26	14.55	21.63	.48	100.0	76.6	.51	.14	.43	.01	.39	.02	.28	.25	.11	.30	1.20
6K-466-6 cpxr(10)	x	x	51.39	.81	2.97	.06	7.59	.27	14.16	21.35	.60	99.2	76.8	.55	.24	.58	.02	1.15	.13	.91	.44	.20	.58	3.84
6K-466-6 cpxc(9)	x	x	51.19	.97	2.96	.06	7.51	.22	14.44	21.87	.41	99.5	77.4	.26	.05	.11	.01	.26	.03	.14	.18	.05	.50	.60
6K-466-6 cpxr2(10)	x	x	51.72	.81	2.71	.07	7.47	.22	15.31	20.27	.44	99.0	78.5	.44	.38	.44	.01	.55	.03	.46	.96	.10	.57	1.50
6K-466-7 cpxc(7)	x	x	51.56	.70	2.16	.03	11.16	.32	12.93	20.91	.44	100.2	67.4	.43	.04	.15	.02	.43	.01	.12	.22	.02	.19	.93
6K-466-7 cpxr(7)	x	x	51.82	.63	2.30	.01	12.24	.33	13.57	17.87	.58	99.4	66.3	1.88	.53	.78	.01	.77	.03	1.35	3.10	.19	.99	1.67
6K-466-8 a1 cpxc(8)	x		52.17	.49	1.62	.00	14.12	.43	14.00	18.36	.37	101.6	63.9	.28	.08	.23	.00	2.86	.08	1.07	3.54	.10	.36	2.70
6K-466-8 a1 cpxr(10)	x	x	52.01	.50	1.68	.00	11.76	.40	12.95	20.83	.37	100.5	66.2	.56	.02	.04	.01	.49	.03	.12	.42	.03	.69	1.04
6K-466-8 a2 cpx(inside ol) c-r(15)	x	x	51.81	.63	1.79	.01	14.48	.44	14.32	16.87	.34	100.7	63.8	.23	.20	.51	.01	4.94	.12	1.71	6.13	.14	.45	4.19
6K-466-8 a2 cpxr(pl)(6)	x	x	52.66	.40	1.62	.00	10.30	.33	13.72	21.87	.35	101.3	70.4	.29	.06	.07	.01	.22	.04	.08	.27	.04	.47	.52
6K-466-8 a3 cpxc(9)	x		51.69	.74	2.42	.01	12.11	.39	13.20	20.26	.53	101.3	66.0	.80	.28	.77	.01	.61	.04	.36	.95	.24	.60	.93
6K-466-8 a3 cpxr(pl)(4)	x	x	52.09	.46	1.90	.01	11.62	.36	13.19	21.27	.35	101.3	66.9	.36	.04	.04	.01	.23	.03	.12	.39	.03	.58	.26
6K-466-9 cpxr(10)	x	x	51.78	.70	2.61	.04	9.73	.26	15.14	19.52	.41	100.2	73.5	.21	.03	.07	.02	.40	.02	.31	.59	.04	.42	.47
6K-466-9 cpxc(9)	x		51.91	.66	2.54	.03	9.56	.25	16.42	17.98	.37	99.7	76.1	.60	.18	.58	.02	4.18	.06	3.69	7.64	.17	.48	2.96
6K-466-9 cpxr3(10)	x	x	51.52	.71	2.46	.03	8.24	.22	14.56	21.54	.40	99.7	75.9	.46	.09	.23	.01	.33	.02	.20	.40	.03	.55	.93
6K-466-11 cpx2c(10)	x		51.63	.67	2.04	.05	11.66	.32	14.00	19.15	.42	99.9	68.2	.67	.05	.02	.01	.69	.03	.20	.82	.04	1.05	1.38
6K-466-11 cpx2r(10)	x	x	52.43	.48	1.82	.04	10.80	.32	13.65	20.42	.43	100.4	69.3	.27	.06	.18	.01	.35	.02	.10	.81	.04	.50	.78
6K-466-11 cpxc(10)	x	x	52.01	.56	2.01	.05	10.12	.31	13.50	21.33	.44	100.3	70.4	.40	.08	.23	.01	.18	.04	.12	.33	.04	.30	.53
6K-466-11 cpxr(10)	x	x	52.33	.48	1.66	.03	10.31	.30	13.44	21.45	.37	100.4	69.9	.33	.06	.17	.02	.40	.04	.09	.46	.02	.33	.77
6K-466-11 cpxr(10)	x		52.57	.51	2.76	.11	6.70	.19	16.34	20.67	.26	100.1	81.3	.27	.06	.29	.01	.56	.02	.41	1.08	.06	.33	.94
6K-467-1 cpxc(9)	x	x	52.20	.63	2.53	.10	6.60	.22	15.15	22.30	.31	100.0	80.4	.55	.08	.28	.01	.24	.03	.27	.33	.05	.48	.60
6K-467-1 cpxr(pl)(9)																								

Each analysis is indexed with the mineral (ol) and core (c), rim (r) c-r (core to rim traverse) or particular notes, and the number of analyses (#) and are accompanied by standard deviations.

Evolution of Oceanic Gabbros: In-situ and Ancient Examples

Sample # and placement	Averages													Standard deviations												
	C	R	SiO ₂	TiO ₂	Al ₂ O ₃	Cr ₂ O ₃	FeO	MnO	MgO	CaO	Na ₂ O	Total	Mg#	SiO ₂	TiO ₂	Al ₂ O ₃	Cr ₂ O ₃	FeO	MnO	MgO	CaO	Na ₂ O	Total	Mg#		
6K-467-2 cpxc(9)	x		49.76	.66	2.45	.00	13.83	.40	11.81	19.48	.55	98.9	60.4	.40	.03	.19	.01	.68	.05	.19	.54	.02	.41	1.50		
6K-467-2 cpxr(3)	x	x	50.74	.33	1.79	.00	13.70	.36	12.30	18.96	.45	98.6	61.6	.82	.06	.45	.00	1.29	.04	.24	1.81	.06	.77	2.70		
6K-467-3 cpxc(10)	x		52.04	.29	1.25	.02	11.20	.33	12.95	20.97	.43	99.5	67.3	.83	.11	.27	.01	.40	.04	.28	.38	.10	.80	1.02		
6K-467-4 cpxc(9)	x		51.55	.51	1.90	.03	11.50	.36	12.83	20.80	.48	99.9	66.5	.43	.04	.18	.01	.37	.03	.11	.15	.04	.50	.84		
6K-467-4 cpxr(10)	x	x	51.82	.37	1.59	.03	11.96	.32	13.03	20.49	.44	100.1	66.1	1.05	.03	.17	.01	1.32	.03	.34	.80	.04	.73	2.92		
6K-467-6 cpxc-r(16)	x	x	51.42	1.02	2.84	.03	8.84	.26	14.02	21.12	.69	100.2	73.9	1.14	.64	.97	.01	.79	.02	.19	1.34	.26	.62	1.87		
6K-467-8 cpxc(10)	x	x	50.93	.94	3.25	.03	8.93	.25	14.92	19.72	.59	99.5	74.9	.85	.95	.74	.01	.78	.05	.46	1.24	.12	.59	1.84		
6K-467-8 cpxr(9)	x	x	52.79	.43	1.82	.03	8.00	.26	14.46	22.11	.46	100.4	76.3	.77	.26	.90	.01	.47	.07	.15	1.18	.22	.40	1.22		
6K-467-9 cpxl(10)	x		52.14	.83	2.60	.03	9.76	.31	15.44	18.91	.42	100.4	73.9	.76	.49	.08	.22	.01	.49	.05	1.13	2.56	.06	.32	1.50	
6K-467-9 cpxl-r(10)	x	x	52.23	.70	2.44	.04	7.50	.24	14.55	21.88	.43	100.0	77.6	.44	.11	.29	.02	.97	.02	.70	1.57	.09	.48	1.07		
6K-467-9 cpx2c(10)	x		51.68	.86	2.80	.04	9.19	.26	14.86	20.12	.53	100.3	74.3	.44	.11	.29	.02	.97	.02	.70	1.57	.09	.48	1.07		
6K-467-9 cpx2r(10)	x	x	51.81	.80	2.51	.04	8.88	.25	14.94	20.46	.49	100.2	75.0	.23	.16	.34	.01	.90	.03	.44	1.63	.06	.48	1.40		
6K-467-10 cpxc(8)	x		51.99	.84	2.61	.03	9.70	.28	15.45	18.98	.44	100.3	74.0	.20	.05	.12	.01	.98	.02	.71	1.48	.05	.28	1.08		
6K-467-10 cpxr(9)	x	x	52.39	.61	2.23	.03	8.02	.23	14.52	21.83	.41	100.3	76.4	.21	.08	.18	.01	.49	.03	.21	.71	.03	.23	.93		
6K-467-11 cpxl-r-r(12)	x	x	51.75	.66	3.37	1.11	6.05	.15	17.61	18.81	.00	99.5	83.8	.96	.17	.95	.22	.58	.02	1.01	.74	.00	.36	1.51		
6K-467-11 cpx2r-r-r(11)	x	x	50.36	1.06	4.57	1.03	6.15	.14	16.29	19.68	.00	99.3	82.5	.85	.24	.19	.35	.03	.38	.61	.00	.44	.85			
6K-467-11 cpx3r-r-r(8)	x	x	52.21	.66	2.95	.78	5.87	.16	17.63	19.24	.00	99.5	84.2	.39	.17	.24	.19	.61	.02	.73	.55	.00	.33	1.60		
6K-467-12 cpxl(10)	x	x	51.07	.85	2.58	.03	10.10	.27	15.02	18.89	.48	99.3	72.7	.98	.07	.15	.01	1.17	.03	.84	2.05	.05	1.26	1.90		
6K-467-12 cpxl-r(10)	x	x	51.77	.85	2.54	.03	10.51	.29	15.40	18.27	.48	100.1	72.4	.31	.07	.17	.01	1.17	.04	.81	1.93	.07	.45	1.28		
6K-467-12 cpx2c(10)	x		51.63	.89	2.64	.03	10.67	.28	15.18	18.50	.46	100.3	71.7	.40	.07	.13	.02	.70	.03	.56	1.13	.04	.28	.71		
6K-467-12 cpx2r(10)	x	x	51.95	.75	2.46	.03	8.92	.24	14.56	20.87	.46	100.3	74.4	.48	.06	.16	.01	.53	.03	.48	.91	.04	.51	.78		
6K-467-13 cpxc(10)	x		52.06	.63	2.38	.02	7.96	.26	14.27	21.96	.48	100.0	76.2	.54	.11	.31	.01	.36	.03	.22	.38	.04	.44	1.04		
6K-467-13 cpxr(9)	x	x	51.35	.88	2.80	.01	8.72	.24	14.25	21.04	.51	99.8	74.5	.53	.13	.19	.01	.44	.02	.21	.52	.02	.55	1.01		
6K-467-13 cpxc(10)	x		51.26	1.01	2.86	.01	8.48	.22	13.93	21.40	.58	99.7	74.5	.28	.08	.05	.01	.27	.02	.12	.24	.06	.44	.48		
6K-467-13 cpxr(1)	x	x	51.94	.79	2.41	.02	8.63	.31	14.33	21.59	.50	100.5	74.7	.50	.13	.39	.01	.50	.03	.65	.75	.06	.72	1.91		
6K-467-13 cpxr(9)	x	x	51.42	.82	2.65	.03	8.65	.24	14.05	21.33	.51	99.7	74.3	.36	.12	.23	.01	.72	.02	.11	.61	.04	.69	1.67		
6K-467-13 cpxc-r(cpx)(10)	x	x	51.62	.70	2.50	.01	8.64	.26	14.15	21.35	.45	99.7	74.5	.87	.03	.44	.01	.26	.04	.68	.69	.06	.66	.97		
6K-467-15 cpxc(7)	x	x	51.18	.62	4.00	.08	6.60	.19	14.90	20.74	.51	99.8	80.1	.79	.07	.42	.01	.62	.02	.16	.97	.03	.90	1.37		
6K-467-15 cpxr(10)	x		51.42	.80	2.95	.06	7.04	.21	15.19	21.28	.46	99.4	79.4	.90	.06	.30	.01	.22	.02	.21	.40	.08	.97	.44		
6K-467-15 cpxc(10)	x	x	50.58	.59	3.52	.07	6.56	.16	16.02	20.75	.45	98.7	81.3	1.02	.04	.50	.01	.19	.02	.128	2.36	.05	.57	1.03		
6K-467-15 cpxr(10)	x		50.96	.66	3.55	.07	6.96	.18	15.41	20.75	.49	99.0	79.8	1.04	.36	.05	.11	.01	.19	.02	.128	2.36	.05	.57	1.03	
6K-467-17 cpxc(10)	x	x	52.09	.60	2.71	.05	8.55	.20	16.37	18.95	.44	100.0	77.4	.36	.05	.11	.01	.19	.02	.128	2.36	.05	.57	1.03		
6K-467-17 cpxr(10)	x		51.88	.80	2.65	.06	7.62	.19	14.97	21.02	.52	99.7	77.8	.38	.04	.16	.02	.40	.02	.37	.74	.04	.47	.62		
6K-467-17 cpxl(10)	x	x	51.99	.70	2.68	.05	8.09	.19	15.67	19.99	.48	99.8	77.6	.37	.05	.14	.01	.80	.02	.82	1.55	.04	.52	.83		
6K-467-17 cpxl-r(10)	x		52.37	.50	3.43	.51	5.66	.15	16.91	20.39	.33	100.2	84.2	.14	.02	.05	.02	.22	.02	.30	.40	.03	.08	.37		
6K-467-20 cpxc(9)	x	x	52.03	.78	3.03	.29	5.52	.18	15.91	21.91	.38	100.0	83.7	.58	.04	.55	.02	.26	.01	.14	.59	.10	.37	.71		
6K-467-20 cpxr(p)(9)	x		52.03	.78	3.03	.29	5.52	.18	15.91	21.91	.38	100.0	83.7	.58	.04	.55	.02	.26	.01	.14	.59	.10	.37	.71		
Leg ABCDE																										
6K-645-r18 cpxr(8)	x	x	51.78	.83	2.56	.01	10.35	.10	14.16	20.87	.54	101.2	71.2	2.14	.13	.40	.01	3.00	.10	.56	1.18	.11	.61	6.02		
6K-647-r17 cpxr(p)(9)	x	x	51.68	.52	1.89	.01	13.14	.40	12.41	20.15	.43	100.6	62.8	.46	.05	.64	.01	.85	.04	.34	1.49	.05	.56	1.10		
6K-647-r17 cpxc(9)	x		48.94	.55	1.90	.02	15.44	.43	11.78	19.86	.54	99.5	57.7	1.17	.06	.13	.02	1.37	.07	.24	.41	.02	.47	2.74		
6K-647-r01 cpxr(p)(10)	x	x	51.68	.65	2.70	.01	9.01	.24	13.86	21.10	.57	99.8	73.3	.64	.17	.89	.01	.41	.02	.18	1.47	.17	.59	.76		
6K-647-r01 cpxc(10)	x		51.63	.87	2.74	.01	9.31	.26	14.04	20.74	.57	100.2	72.9	.09	.02	.04	.01	.38	.01	.16	.41	.05	.17	.71		
6K-647-r10 cpxr(p)(5)	x	x	49.48	.49	2.24	.03	14.65	.42	11.74	19.81	.45	99.3	58.9	1.09	.04	.78	.02	1.24	.04	.45	.87	.03	.75	2.90		
6K-647-r10 cpxc(6)	x		49.80	.54	2.05	.03	14.64	.43	11.83	20.02	.43	99.8	59.4	2.77	.12	1.01	.01	3.30	.04	.57	1.45	.03	1.08	5.85		
6K-647-r13 cpx c-r(14)	x	x	52.35	.43	1.96	.15	9.56	.26	14.07	21.18	.38	100.3	72.4	.29	.08	.20	.03	.38	.03	.17	.44	.05	.39	.86		
6K-647-r13 cpx c-r(14)	x	x	52.19	.79	2.75	.01	8.97	.24	14.90	19.40	.46	99.7	74.7	.76	.21	.15	.01	.60	.03	1.08	2.86	.06	.78	.54		
6K-647-r09 cpxr(p)(7)	x		51.26	1.01	2.89	.02	10.66	.28	15.19	18.65	.41	100.4	71.9	.59	.08	.20	.01	1.74	.03	.44	1.25	.04	.37	2.88		

Each analysis is indexed with the mineral (c) and core (c), rim (r) c-c (core to rim traverse) or particular notes, and the number of analyses (n) and are accompanied by standard deviations.

Evolution of Oceanic Gabbros: In-situ and Ancient Examples

Sample # and placement	Averages												Standard deviations											
	C	R	SiO ₂	TiO ₂	Al ₂ O ₃	Cr ₂ O ₃	FeO	MnO	MgO	CaO	Na ₂ O	Total	Mg#	SiO ₂	TiO ₂	Al ₂ O ₃	Cr ₂ O ₃	FeO	MnO	MgO	CaO	Na ₂ O	Total	Mg#
6K-646-r01 cpxc(5)	x		51.15	.54	3.75	.63	6.60	.13	17.24	18.91	.39	99.3	82.4	.32	.05	.18	.02	1.22	.03	1.65	2.78	.09	.36	1.22
6K-646-r01 cpxr(pl)(5)		x	50.36	.78	3.23	.61	5.91	.14	15.17	22.23	.42	98.8	82.1	.68	.05	.34	.03	.35	.03	.28	.49	.03	.51	.66
6K-646-r01-cpx2c(4)	x		50.10	.63	3.58	.67	6.27	.14	15.77	20.71	.47	98.3	81.7	.37	.03	.12	.02	.12	.02	.47	.81	.03	.23	.29
6K-646-r01-cpx2r(4)		x	50.28	.91	3.71	.59	5.62	.12	14.98	21.70	.44	98.3	82.6	.21	.04	.38	.02	.34	.04	.25	.42	.03	.65	.64
6K-646-R04 cpxc(5)	x		50.98	.41	3.41	.37	5.73	.16	16.51	21.09	.38	99.0	83.7	.61	.03	.32	.01	.35	.01	.62	1.04	.03	.58	.53
6K-646-R04 cpxr(7)		x	51.91	.58	2.57	.29	5.40	.16	16.05	22.62	.34	99.9	84.1	.10	.04	.08	.02	.12	.02	.24	.44	.04	.33	.33
6K-646-R04 cpxr2(7)	x		51.59	.52	2.55	.32	5.58	.17	16.08	22.52	.33	99.7	83.7	.48	.05	.25	.02	.19	.03	.28	.43	.04	.49	.46
6K-646-R04 cpxc2(6)		x	51.04	.56	3.73	.46	5.47	.18	15.35	22.76	.41	99.9	83.4	.33	.03	.12	.02	.07	.03	.25	.22	.06	.51	.19
6K-646-r06 cpxc(2)	x		51.40	.58	3.41	.11	8.99	.21	16.97	16.10	.63	98.4	76.9	1.04	.28	.55	.04	.28	.05	2.36	5.01	.13	1.48	3.02
6K-649-r06 cpxc(8)		x	50.83	.86	3.12	.07	9.80	.29	15.86	18.37	.49	99.7	74.3	.67	.07	.22	.01	1.13	.03	.95	2.04	.06	.79	1.11
6K-649-r06 cpxr(8)		x	50.64	.93	3.25	.07	8.96	.29	15.29	19.64	.46	99.5	75.3	.50	.06	.38	.02	1.29	.04	1.30	2.66	.09	.57	1.06
6K-649-r08 a2 cpxc(9)	x		53.33	.71	2.83	.20	5.78	.00	16.69	21.45	.47	101.5	83.7	.26	.05	.06	.02	.47	.00	.39	.79	.09	.33	.26
6K-649-r08 a2 cpxr(10)		x	53.47	.69	2.73	.19	5.85	.00	16.75	21.40	.47	101.5	83.6	.22	.03	.07	.02	.63	.00	.60	.84	.04	.33	1.06
6K-649-r12 cpxc(8)	x		51.78	.69	2.65	.02	8.15	.25	15.42	20.59	.46	100.0	77.1	.55	.06	.13	.01	.36	.02	.83	1.66	.06	.73	.61
6K-649-r12 cpxr(6)		x	51.43	.71	3.63	.01	10.41	.28	15.11	16.96	.50	99.0	72.3	.129	.12	1.01	.01	2.16	.02	.59	2.73	.12	1.05	4.62
6K-649-r12 cpxr2(8)	x		51.22	.87	2.72	.02	8.96	.25	14.76	20.91	.43	100.2	74.6	.56	.04	.19	.01	1.00	.04	.24	1.06	.07	.70	2.15
6K-649-r14 cpxc(9)		x	50.19	1.04	3.68	.02	7.68	.23	14.89	21.21	.49	99.4	77.6	.43	.06	1.00	.01	.24	.04	.28	.30	.02	.32	.47
6K-649-r14 cpxr(4)	x		50.71	.73	3.54	.02	9.83	.30	17.31	16.67	.29	99.4	76.6	.48	.30	.45	.02	4.99	.09	5.01	10.12	.20	2.7	3.28
6K-649-r14 cpx2c(10)		x	51.15	.66	3.01	.07	7.95	.24	15.92	20.04	.45	99.5	78.1	.33	.07	.22	.01	.69	.04	.71	1.16	.06	.54	.93
6K-649-r14 cpx2r(3)	x		51.07	.75	2.89	.01	7.53	.23	15.00	21.56	.39	99.4	78.0	.94	.04	.64	.01	.32	.01	.38	.43	.05	.60	.47
6K-650-r04 cpxc(5)		x	52.54	.37	1.93	.24	5.56	.12	16.18	22.39	.29	99.6	83.9	.120	.15	.54	.11	1.27	.03	.40	.50	.05	.30	3.24
6K-650-r04 cpxr(pl)(3)	x		51.14	.90	3.44	.12	6.37	.14	14.90	21.55	.54	99.1	80.7	.67	.10	.68	.00	.12	.03	.27	.66	.17	.85	.37
6K-650-r06 cpxc(8)		x	51.70	.63	3.48	.17	5.47	.12	16.62	20.79	.39	99.4	84.4	.43	.03	.44	.02	.50	.03	.65	1.19	.03	.54	.90
6K-650-r06 cpxr(pl)(6)	x		51.29	.62	3.05	.19	4.95	.13	15.58	22.85	.35	99.0	84.9	1.21	.16	1.48	.02	.44	.02	.55	1.01	.10	.62	.98
6K-650-r09 cpxc(8)		x	53.22	.82	2.50	.03	7.18	.10	16.16	21.34	.48	101.8	80.1	.35	.03	.04	.01	.47	.11	.36	.52	.03	.41	.86
6K-650-r09 cpxr(7)	x		53.14	.83	2.45	.02	6.86	.07	15.84	22.12	.43	101.8	80.5	.33	.07	.18	.01	.44	.04	.13	.46	.02	.39	1.02
6K-653-r2 cpxr(pl)(7)		x	51.25	.51	3.02	.01	10.68	.29	13.28	19.71	.46	99.2	69.0	.72	.15	1.40	.00	1.74	.05	.33	2.93	.18	.75	3.21
6K-653-r2 cpxc(7)	x		51.87	.67	3.29	.02	9.25	.24	17.06	17.06	.35	99.8	76.8	.67	.11	.82	.01	1.68	.04	1.66	3.17	.08	.22	1.51
BGS-Cores																								
BGS-2-1-7c-37-41 cpx1c(5)	x		50.77	.42	3.68	.05	16.14	.28	13.86	11.63	.95	97.8	60.5	1.68	.14	1.28	.01	.61	.01	.60	.34	.33	.54	1.89
BGS-2-1-7c-37-41 cpx2r(4)		x	49.09	.55	2.10	.03	10.84	.35	12.60	20.24	.57	96.4	67.5	1.75	.02	.10	.01	.36	.02	.21	.37	.06	2.31	.50
BGS-3-1-2a 0-5 cpxc(5)	x		51.54	.49	2.74	.16	7.24	.20	15.94	20.40	.61	99.3	79.8	1.16	.18	1.09	.04	1.57	.02	1.06	3.34	.30	.68	3.49
BGS-3-1-2a 0-5 cpxr(7)		x	52.15	.46	2.43	.20	6.18	.19	15.73	22.02	.44	99.8	82.0	.56	.10	.42	.03	.69	.03	.21	.73	.10	.28	1.71
BGS-4-1-4c 43-48 cpx2(4)			51.03	.98	3.16	.11	6.90	.18	15.06	21.00	.47	98.9	79.5	.26	.07	.16	.01	.14	.01	.06	.38	.11	.36	.32
BGS-4-1-4c 43-48 cpx3(5)			51.66	.51	3.22	.17	6.33	.18	16.12	21.01	.33	99.5	81.9	.50	.02	.04	.02	.22	.02	.12	.21	.02	.68	.47
BGS-4-1-4c 43-48 cpx(4)			50.71	.81	2.71	.11	7.89	.22	16.51	17.04	.33	96.3	78.9	.24	.05	.07	.02	.20	.01	.39	.88	.03	.56	.26
BGS-4-1-4c 43-48 cpx(5)			52.45	1.07	2.96	.11	8.01	.24	16.14	19.56	.31	100.8	78.2	.45	.03	.09	.02	.78	.01	.61	1.25	.04	.59	1.06
BGS-4-1-4c 43-48 cpx(5)			51.44	1.10	2.85	.10	8.36	.25	15.58	19.56	.24	99.5	76.9	.18	.04	.04	.01	.13	.04	.16	.29	.05	.26	.20
BGS-4-1-4 -43-48 cpxr(5)			51.77	1.22	3.18	.11	7.27	.23	15.40	21.10	.34	100.6	79.0	.30	.05	.06	.01	.17	.03	.12	.33	.04	.11	.41
BGS-4-2-0-4d cpx1c(10)	x		52.11	.45	2.99	.16	5.74	.17	17.59	20.16	.27	99.7	84.5	.41	.02	.08	.01	.33	.02	.51	.84	.03	.32	.49
BGS-4-2-0-4d cpxr(8)		x	52.51	.52	2.20	.17	6.50	.19	15.53	21.72	.30	99.6	81.0	.30	.05	.13	.01	.18	.03	.16	.36	.08	.46	.52
BGS-4-2-17-4d cpx1c(10)		x	51.67	.56	3.13	.27	7.42	.19	16.23	19.53	.34	99.3	79.6	.30	.03	.07	.02	.51	.02	.54	1.07	.05	.32	.59
BGS-4-2-17-4d cpxr(8)		x	51.43	.96	2.97	.12	7.13	.22	15.18	20.98	.32	99.3	79.1	.29	.07	.09	.02	.36	.04	.22	.49	.06	.46	.70
BGS-4-2-4d a1 cpxc(9)		x	52.86	.53	2.57	.17	7.14	.19	16.63	20.79	.34	101.2	80.6	.44	.06	.13	.02	1.16	.02	1.12	2.20	.04	.61	1.37
BGS-4-2-4d a1 cpx c-r(pl)(15)	x		52.72	.66	2.54	.17	6.71	.19	16.12	21.53	.34	101.0	81.1	.39	.14	.23	.02	.54	.03	.51	.98	.06	.47	1.06
BGS-4-2-4d cpxr(ol)(6)		x	51.90	.98	2.84	.16	6.80	.19	15.62	22.33	.34	101.1	80.4	.35	.06	.09	.02	.21	.03	.06	.27	.04	.44	.48
BGS-4-2-4d a1 cpx r(ol)-r(pl)	x	x	52.72	.71	2.45	.14	6.04	.21	15.88	23.34	.32	101.8	82.4	.77	.05	.13	.03	.11	.04	.23	.18	.05	.84	.47

Each analysis is indexed with the mineral (ol) and core (c), rim (r) c (core to rim traverse) or particular notes, and the number of analyses (#) and are accompanied by standard deviations.

Evolution of Oceanic Gabbros: In-situ and Ancient Examples

Sample # and placement	Averages											Standard deviations											Total	Mg#
	C	R	SiO ₂	TiO ₂	Al ₂ O ₃	Cr ₂ O ₃	FeO	MnO	CaO	Na ₂ O	Total	Mg#	SiO ₂	TiO ₂	Al ₂ O ₃	Cr ₂ O ₃	FeO	MnO	MgO	CaO	Na ₂ O	Total		
BGS-4-2-4d al cpx (xtp)(r)(intp)	x	x	52.18	.62	2.83	.19	6.52	.19	15.47	22.50	37	100.9	80.9	.81	.20	.58	.03	.34	.02	.33	1.10	.09	.77	.79
BGS-4-2-4d a2 cpxc(8)	x	x	52.44	.55	2.72	.14	7.05	.18	15.87	21.66	33	100.9	80.0	.23	.11	.42	.03	1.52	.02	.39	2.48	.08	1.17	2.86
BGS-4-2-4d a2-cpxr(p)(5)	x	x	52.00	.92	2.76	.12	6.71	.19	15.02	22.16	35	100.2	80.0	.45	.10	.27	.01	.11	.01	.18	1.12	.05	1.19	.42
BGS-10-1-1a 31-36 cpxc(5)	x	x	49.61	.86	3.46	.06	9.48	.22	14.27	20.09	60	98.7	72.9	.57	.02	.12	.01	.50	.02	.23	.32	.02	.50	1.34
BGS-10-1-1a 31-36 cpxr(6)	x	x	51.58	.78	2.67	.05	8.90	.26	14.88	20.04	54	99.7	74.9	.71	.11	.43	.01	.69	.02	.50	1.29	.05	.42	1.48
BGS-16-1-1 7-12 cpxc(10)	x	x	50.78	.89	3.10	.06	12.07	.35	14.66	17.13	59	99.6	69.0	.77	.19	.56	.02	3.72	.06	1.71	5.74	.17	3.9	3.66
BGS-16-1-1 7-12 cpxr(9)	x	x	51.56	.73	2.25	.05	10.88	.35	13.91	19.66	50	99.7	66.8	.46	.06	.17	.01	1.28	.05	.62	1.70	.03	.52	1.62
BGS-16-1-1 7-12 cpxr(8)	x	x	51.42	.66	1.98	.04	11.78	.37	13.31	19.66	50	99.7	66.8	.46	.06	.17	.01	.67	.02	.33	3.64	.06	.50	1.06
BGS-17-1-1A 12-cpx(19)	x	x	53.56	.44	2.39	.03	8.35	.20	15.41	20.05	32	100.8	77.0	.125	.25	1.24	.02	2.34	.03	.50	3.70	.17	1.66	4.64
BGS-19-2 10-11.5-cpx(15)	x	x	51.79	.94	2.74	.11	6.80	.17	15.27	22.32	29	100.4	80.0	.64	.10	.08	.01	.16	.03	.09	.24	.04	.55	.43
BGS-19-2 10-11.5-cpx(16)	x	x	52.96	.53	2.95	.12	6.67	.18	16.46	21.03	28	101.2	81.5	.54	.04	.05	.01	.59	.02	.77	1.26	.07	.72	.75
BGS-19-2-12a 38.5-cpx(14)	x	x	54.21	.58	2.18	.13	6.32	.19	15.76	22.36	30	102.0	81.6	.26	.12	.35	.02	.16	.03	.11	.24	.06	.56	.46
BGS-19-2-12a 38.5-cpx(16)	x	x	52.36	.53	2.48	.17	6.10	.18	15.69	22.61	33	100.4	82.1	.69	.09	.22	.02	.10	.02	.10	.39	.05	.62	.26
BGS-19-2-12a 38.5-cpx(25)	x	x	52.81	.65	2.79	.15	6.01	.17	15.54	22.60	34	101.0	82.2	.54	.08	.18	.02	.13	.01	.16	.21	.02	.32	.40
BGS-19-2-12a 38.5-cpx(36)	x	x	53.18	.70	3.44	.12	5.92	.16	15.57	21.87	46	101.4	82.4	.54	.15	.95	.05	.11	.03	.12	.81	.26	.27	.32
BGS-19-2-12a 38.5-cpx(36)	x	x	52.95	.38	1.66	.01	7.81	.21	14.71	22.21	64	96.6	78.2	.161	.06	.16	.01	.11	.02	.32	.10	.06	1.66	.65
BGS-20-1-3B-28.5-32 cpxr(7)	x	x	51.31	.44	1.76	.08	6.96	.25	13.99	21.17	64	96.6	78.2	.161	.06	.16	.01	.11	.02	.32	.10	.06	1.66	.65
BGS-20-1-3B-28.5-32 cpx(2)	x	x	50.22	.37	1.43	.06	7.37	.25	14.92	20.98	68	96.3	78.3	.08	.02	.04	.01	.37	.02	.16	.28	.05	.64	.67
BGS-20-1-3B-28.5-32 cpx(1r(2)	x	x	52.47	.84	2.51	.04	9.43	.28	15.89	19.07	38	100.9	75.0	.43	.08	.16	.02	.91	.02	.80	1.50	.10	.60	.82
BGS-20-1-6a al cpxc(7)	x	x	52.47	.84	2.51	.04	9.43	.28	15.89	19.07	38	100.9	75.0	.43	.08	.16	.02	.91	.02	.80	1.50	.10	.60	.82
BGS-20-1-6a al cpxr(6)	x	x	51.53	.71	2.50	.03	8.33	.24	14.85	21.00	43	99.6	76.1	.88	.07	.47	.02	.64	.04	.31	.79	.11	.61	1.01
BGS-20-1-6a al r-cpx(20)	x	x	52.06	.87	2.53	.04	9.16	.28	15.53	19.80	41	100.7	75.2	.39	.07	.14	.02	.84	.04	.70	1.28	.08	.66	1.07
BGS-20-1-6a a3 cpxc(14)	x	x	52.20	.72	2.30	.03	7.87	.27	15.02	22.23	43	101.1	77.3	.27	.07	.10	.02	.22	.01	.07	.33	.08	.36	.50
BGS-20-1-6a a3 cpxc(14)	x	x	52.36	.94	2.50	.10	7.95	.27	15.26	20.48	40	99.9	77.4	.36	.04	.20	.01	.57	.03	.53	1.06	.00	.54	.67
BGS-20-1-6a-64-67 cpx(1c-r(15)	x	x	52.74	.46	2.17	.02	7.30	.20	14.67	21.91	41	99.9	78.2	.28	.11	.12	.01	.14	.07	.09	.18	.02	.31	.33
BGS-20-1-6a-64-67 cpx(2r(5)	x	x	52.07	.70	2.29	.03	7.83	.25	15.07	21.94	40	100.6	77.4	.49	.09	.22	.01	.27	.04	.13	.26	.06	.65	.55
BGS-20-1-6a a3 cpxr(9)	x	x	51.32	.88	2.48	.00	9.41	.21	14.83	20.20	48	99.8	73.8	.81	.21	.27	.01	.19	.04	.56	2.53	.05	.69	1.59
BGS-20-2-6b al cpxc(10)	x	x	50.87	.77	2.41	.00	8.43	.21	14.21	21.67	49	99.1	75.0	.110	.07	.20	.01	.30	.02	.57	.42	.11	1.94	.58
BGS-20-2-6b al cpxr(10)	x	x	51.38	.95	2.38	.00	9.33	.21	15.40	20.09	44	100.2	74.6	.28	.05	.13	.00	.87	.04	.66	1.43	.04	.28	.97
BGS-20-2-6b a2 cpxc(10)	x	x	52.10	.55	2.00	.01	7.94	.18	15.05	22.62	40	100.9	77.2	.24	.10	.17	.01	.39	.02	.20	.53	.04	.35	.72
BGS-20-2-6b a2 cpxr(p)(18)	x	x	52.06	.70	2.23	.00	8.26	.19	14.82	22.49	44	101.2	76.2	.29	.05	.07	.01	.22	.03	.17	.60	.02	.20	.34
BGS-20-2-6b a2 cpx r(p)(1)-(ol)(5)	x	x	52.38	.41	1.75	.02	7.89	.22	15.31	22.33	47	100.8	77.6	.48	.13	.29	.01	.40	.01	.22	.56	.05	.47	1.05
BGS-20-2-6b a2 cpx r(p)(1)-(ol)(5)	x	x	52.38	.41	1.75	.02	7.89	.22	15.31	22.33	47	100.8	77.6	.48	.13	.29	.01	.40	.01	.22	.56	.05	.47	1.05
BGS-20-2-6B 0-5 cpxc(8)	x	x	51.37	.93	2.45	.03	9.03	.24	14.72	19.53	55	98.8	74.4	.53	.03	.14	.01	.42	.02	.46	.66	.03	.68	.49
BGS-20-2-6B 0-5 cpxr(8)	x	x	51.29	.78	2.43	.03	8.55	.23	14.18	21.31	61	99.4	74.7	.61	.11	.25	.01	.35	.03	.40	.43	.10	.63	1.17
BGS-23-2b 23-28 al cpxr(18)	x	x	52.44	.46	1.74	.00	10.07	.32	14.49	20.38	40	100.3	71.9	.23	.03	.11	.00	.60	.02	.40	.90	.04	.31	.68
BGS-23-2b 23-28 al cpxc(7)	x	x	51.69	.83	2.43	.00	11.83	.35	14.86	18.09	46	100.6	69.1	.29	.04	.09	.00	.43	.02	.16	.61	.05	.32	.55
BGS-23-2b 23-28 al cpxr(2)(p)(5)	x	x	52.22	.61	2.03	.00	10.44	.34	14.35	19.71	44	100.1	71.0	.42	.08	.14	.00	.56	.03	.21	.94	.05	.78	.82
BGS-23-2b 23-28 al cpxc(8)	x	x	52.16	.61	2.02	.01	10.41	.32	14.37	20.64	43	101.0	71.1	.54	.07	.09	.01	.81	.02	.35	1.17	.03	.54	1.10
BGS-23-12b a2 cpxc(8)	x	x	52.62	.37	1.54	.02	9.70	.32	14.55	21.52	42	101.5	72.8	.16	.06	.10	.01	.28	.02	.08	.19	.03	.34	.49
BGS-23-12b a2 cpxr(6)	x	x	53.08	.49	1.78	.02	10.05	.32	14.46	21.08	42	101.2	72.0	.35	.06	.10	.01	.54	.02	.22	.68	.03	.44	.80
BGS-23-12b a2 cpx	x	x	52.62	.49	1.78	.02	10.05	.32	14.46	21.08	42	101.2	72.0	.35	.06	.10	.01	.54	.02	.22	.68	.03	.44	.80
BGS-23-1-2b 23-28 a3 cpxr(p)(6)	x	x	51.95	.73	2.38	.00	10.31	.26	14.39	20.36	41	100.8	71.3	.45	.06	.26	.01	.26	.03	.11	.36	.04	.29	.38
BGS-23-1-2b 23-28 a3 cpxc(9)	x	x	52.28	.65	2.28	.00	10.08	.26	14.17	20.70	41	100.8	71.5	.59	.09	.33	.01	.47	.03	.21	.69	.03	.56	.76
BGS-23-1-2b 23-28 a3 cpxr(ol)(6)	x	x	52.69	.52	2.05	.01	9.42	.24	14.10	21.42	38	100.8	72.7	.53	.08	.25	.01	.32	.02	.21	.89	.04	.88	.56
BGS-23-1-2b 23-28 a3 cpx c-r(10)	x	x	52.08	.67	2.34	.00	10.36	.26	14.37	20.35	40	100.8	71.2	.43	.10	.21	.01	.32	.02	.21	.89	.04	.88	.56
BGS-23-1-2b 23-28 a4 cpxc(12)	x	x	51.61	.70	2.07	.02	11.26	.35	13.35	19.92	53	99.8	67.9	.67	.06	.08	.02	.37	.02	.43	.74	.06	.64	1.32
BGS-23-1-2b 23-28 a4 cpxr(p)(8)	x	x	51.27	.60	2.23	.02	11.44	.36	13.33	20.07	47	99.8	67.6	.131	.08	.55	.01	.14	.03	.22	1.13	.03	.87	2.20
BGS-23-1-2b 23-28 a4 cpxr(p)(8)	x	x	51.33	.73	2.26	.02	10.37	.31	14.10	20.37	43	99.9	70.8	.76	.06	.14	.01	.79	.02	.36	.40	.04	.84	1.78
BGS-23-1-2b 29-34 al cpx(18)	x	x	51.36	.63	2.41	.02	10.26	.30	14.20	20.53	42	100.1	71.2	1.20	.17	.71	.01	1.03	.03	.41	.93	.04	1.12	2.55

Each analysis is indexed with the mineral (ol) and core (c), rim (r) c-c (core to rim traverse) or particular notes, and the number of analyses (n) and are accompanied by standard deviations.

Evolution of Oceanic Gabbros: In-situ and Ancient Examples

Sample # and placement	Averages												Standard deviations											
	C	R	SiO ₂	TiO ₂	Al ₂ O ₃	Cr ₂ O ₃	FeO	MnO	MgO	CaO	NaO	Total	Mg#	SiO ₂	TiO ₂	Al ₂ O ₃	Cr ₂ O ₃	FeO	MnO	MgO	CaO	NaO	Total	Mg#
BGS-23-1-2b 29-34 a2 cpxc(10)	x		53.06	.31	1.33	.01	9.15	.28	14.29	21.69	.38	100.5	73.6	.40	.05	.16	.01	.27	.02	.17	.25	.04	.67	.64
BGS-23-1-2b 29-34 a2 cpxr(10)		x	52.07	.53	1.87	.00	10.14	.32	13.96	21.02	.44	100.3	71.1	.59	.06	.21	.00	.31	.03	.19	.34	.04	.78	.65
BGS-23-1-2b 29-34 a3 cpxc(10)	x		52.76	.48	1.51	.02	9.56	.30	14.36	21.46	.36	100.8	72.8	.51	.27	.14	.01	.24	.04	.15	.24	.02	.66	.52
BGS-23-1-2b 29-34 a3 cpxr(10)		x	52.76	.35	1.50	.01	9.47	.28	14.34	21.19	.36	100.3	73.0	.43	.07	.22	.01	.24	.03	.11	.38	.04	.47	.57
BGS-23-1-2b 29-34 a4 cpxr(pl)-c	x		51.17	.39	1.57	.01	8.69	.24	13.97	20.89	.56	97.5	74.1	.65	.07	.25	.01	.36	.04	.17	.45	.07	1.26	.61
BGS-23-1-2b 29-34 a5 cpxc-r(10)		x	52.15	.54	1.97	.02	9.67	.31	14.04	21.22	.41	100.3	72.1	.41	.10	.20	.01	.39	.02	.13	.26	.04	.74	.89
BGS-23-1-2e cpx al r(oxide)-r(pl)	x		52.27	.50	1.73	.00	11.10	.35	13.57	20.79	.44	100.8	68.5	.64	.06	.16	.00	.42	.03	.21	.21	.02	.50	1.10
BGS-23-1-2e a2 cpx cpxc(7)	x		51.81	.63	2.23	.00	11.03	.34	13.30	20.48	.47	100.3	68.2	.62	.12	.14	.00	.45	.03	.43	.137	.05	.83	.52
BGS-23-1-2e a2 cpx cpxr(pl)(8)		x	52.78	.32	1.24	.00	10.19	.32	13.59	21.93	.32	100.7	70.4	.57	.22	.71	.00	.63	.02	.20	1.11	.14	.51	1.48
BGS-23-1-2e a2 cpx cpxr(plm)(3)	x		52.99	.37	1.46	.00	10.68	.33	13.86	21.23	.37	101.3	69.8	.63	.04	.10	.00	.64	.01	.26	.31	.02	.43	1.65
BGS-23-1-2e a2 cpx cpxr(mt)(5)	x		52.60	.44	1.52	.00	10.96	.33	13.70	20.72	.43	100.7	69.0	.26	.03	.08	.00	.27	.04	.22	.27	.04	.42	.79
BGS-23-1-2e a3 cpxr(pl)(8)		x	51.56	.55	1.73	.00	11.40	.34	13.32	21.06	.42	100.4	67.5	2.10	.07	.20	.00	1.91	.04	.31	.77	.04	.86	3.87
BGS-23-1-2e a3 cpxc(8)	x		51.68	.61	2.41	.00	11.96	.31	13.17	19.49	.47	100.1	66.2	.68	.17	.29	.00	2.09	.04	.20	2.46	.07	.94	3.79
BGS-23-1-2e a4 cpxr(pl)(8)		x	51.19	.76	2.13	.00	12.02	.36	13.18	20.49	.52	100.6	66.1	1.69	.06	.14	.00	1.83	.03	.40	.68	.03	.86	3.87
BGS-23-1-2e a4 cpxc(9)	x		51.45	.67	2.38	.00	10.90	.31	13.07	21.32	.63	100.7	68.1	1.86	.41	1.46	.00	1.68	.01	.89	1.94	.49	.93	4.77
BGS-23-1-2e a4 cpxc(pl)(10)		x	49.04	.85	2.75	.01	10.59	.34	13.81	21.20	.41	101.1	69.9	.43	.02	.14	.00	.45	.02	.21	.38	.04	.37	1.13
BGS-24-1-3a 6-10 cpxc(3)	x		52.60	.51	1.68	.00	12.28	.37	12.94	19.78	.53	98.6	65.3	.32	.02	.07	.01	.39	.04	.17	.02	.52	.66	.66
BGS-24-1-3a 6-10 cpxr(10)		x	52.54	.42	1.66	.00	9.44	.28	14.13	21.16	.40	100.0	72.7	.47	.05	.16	.00	.15	.01	.13	.28	.02	.75	.32
BGS-24-1-3e21-24 cpxc(3)	x		52.11	.62	2.07	.00	10.21	.28	13.63	20.71	.45	100.1	70.4	.89	.02	.13	.00	.30	.03	.23	.51	.04	1.53	.62
BGS-24-1-3d 21-24 cpxc(9)			52.76	.78	2.72	.01	10.72	.28	14.55	19.31	.46	101.6	71.0	1.04	.25	.63	.01	2.74	.05	.196	4.66	.10	.98	2.68
BGS-24-1-3h 47 cpx(4)			52.50	.72	2.50	.01	10.53	.30	13.52	21.10	.50	101.7	69.6	.36	.04	.10	.01	.12	.04	.13	.10	.03	.36	.27
BGS-24-1-3h 47.5 cpx(14)			53.35	.65	2.66	.02	11.46	.30	14.80	19.03	.40	102.7	69.8	1.15	.19	.42	.01	1.05	.05	.77	2.10	.08	1.78	1.18
BGS-24-1-3i 60 cpx(6)			53.31	.61	2.46	.01	11.03	.32	13.37	21.21	.47	102.8	68.4	1.00	.05	.08	.01	.89	.09	.30	.62	.04	.93	2.19
BGS-24-1-3k 77 cpx(4)			51.75	.71	2.74	.01	8.10	.24	14.49	20.45	.36	98.8	76.2	.50	.16	.57	.01	.91	.03	.14	1.23	.14	.67	2.12
BGS-27-1-1A 3 cpx(16)			54.16	.70	2.86	.03	7.04	.23	15.36	21.50	.36	102.2	79.5	.31	.03	.12	.01	.17	.03	.32	.31	.04	.56	.38
BGS-27-1-1A 3 cpx(26)			54.02	.76	2.50	.03	9.22	.23	18.02	17.08	.31	102.2	77.9	.49	.08	.30	.02	2.09	.06	2.44	4.74	.08	.57	1.88
BGS-27-1-1A 3 cpx(36)			53.67	.81	2.69	.05	8.59	.23	17.47	17.00	.32	100.8	78.6	1.47	.13	.27	.01	2.24	.05	.232	3.16	.21	3.06	2.36
BGS-27-1-1B 8.5 cpx(9)			53.01	.69	2.57	.04	6.89	.19	15.33	22.00	.29	101.0	79.9	.60	.05	.18	.01	.25	.02	.10	.36	.02	.55	.60
BGS-27-1-1B 19.5 cpx(7)			52.55	.90	2.77	.06	7.89	.22	15.48	20.57	.35	100.8	77.8	.44	.13	.26	.01	.59	.02	.40	1.29	.05	.94	1.02
BGS-27-1-1b 25.5-31 a1 cpxr(ploutsid)	x		51.58	.67	2.21	.08	6.62	.18	15.24	21.73	.31	98.6	80.4	1.62	.12	.62	.02	.66	.05	.51	1.10	.03	1.97	1.96
BGS-27-1-1b 25.5-31 a1 cpxc(10)	x		52.20	.59	2.66	.13	7.64	.19	17.57	18.69	.31	100.0	80.4	.42	.09	.20	.02	1.66	.05	2.07	3.89	.07	.34	1.39
BGS-27-1-1b 25.5-31 a1 cpxr(pl interr)		x	51.48	.68	2.51	.10	6.13	.15	15.85	21.60	.35	98.8	82.2	1.06	.08	.58	.02	.48	.02	.23	.83	.06	.92	1.06
BGS-27-1-1b 25.5-31 a2 cpxc(10)	x		52.28	.60	2.50	.10	7.96	.25	17.10	18.54	.38	99.7	79.3	.30	.03	.08	.01	.52	.03	.54	.95	.04	.31	.59
BGS-27-1-1b 25.5-31 a2 cpxr(9)		x	51.96	.78	2.66	.10	7.70	.23	16.46	19.35	.42	99.7	79.2	.25	.02	.07	.01	.29	.03	.28	.54	.03	.35	.45
BGS-27-1-1b 25.5-31 a3 cpxc(2)	x		50.87	.95	2.34	.10	7.13	.22	15.21	21.58	.45	98.8	79.2	1.03	.19	.28	.03	.06	.02	.14	.25	.04	1.65	.31
BGS-27-1-1b 25.5-31 a3 cpxr(6)	x		51.44	1.06	2.78	.09	7.22	.25	14.74	21.50	.43	99.5	78.5	.32	.05	.06	.01	.30	.03	.24	.42	.03	.62	.65
BGS-27-1-1d 56-62 cpxc(8)	x		51.92	1.08	2.67	.10	7.33	.17	15.07	22.84	.36	101.5	78.6	.29	.03	.04	.02	.33	.03	.11	.48	.04	.77	.76
BGS-27-1-1d 56-62 cpxr(pl)	x		51.87	.97	2.38	.08	7.29	.18	14.50	23.41	.36	101.0	78.0	.55	.02	.08	.02	.17	.02	.17	.19	.04	.71	.44
BGS-27-1-1d 56-62 cpxc(differen)(3)	x		53.20	.29	.84	.06	10.88	1.1	11.64	23.60	.16	101.8	65.4	.37	.40	.84	.01	3.27	.81	2.33	.94	.15	.26	11.2
BGS-31-1-1c 34.5-39 cpxc(10)	x		51.97	.63	2.32	.01	8.88	.25	14.18	21.31	.44	100.0	74.0	.82	.08	.41	.01	.24	.03	.23	.92	.06	1.05	.60
BGS-31-1-1c 34.5-39 cpxr(9)		x	52.40	.44	1.89	.00	8.96	.27	13.85	22.08	.38	100.3	73.4	.58	.09	.36	.01	.20	.03	.16	.39	.04	.40	.55
BGS-31-1a 0-5 cpxc(10)	x		52.22	.65	2.30	.02	8.27	.26	14.19	22.07	.38	100.3	75.4	.46	.16	.42	.02	.31	.04	.17	.44	.07	.30	.70
BGS-31-1a 0-5 cpxr(9)		x	51.96	.57	2.31	.00	9.06	.26	14.14	20.94	.49	99.7	73.6	.75	.22	.58	.01	.41	.04	.24	1.29	.08	1.09	1.03
BR-Cores																								
BR-5-1-1B 4.5-8.5 cpxc(10)	x		52.66	.67	2.29	.05	7.00	.24	15.02	22.37	.40	100.7	79.3	.83	.26	.86	.01	.37	.02	.20	1.02	.23	.39	.98
BR-5-1-1B 4.5-8.5 cpxr(10)	x		52.43	.68	2.26	.05	7.69	.25	14.78	21.65	.51	100.3	77.4	1.27	.28	1.03	.01	.41	.02	.25	1.07	.19	.73	1.12
BR-5-1-1H 74-78 cpxc(10)	x		51.85	.75	3.07	.02	6.89	.20	15.10	21.43	.43	99.7	79.6	.27	.02	.14	.01	.25	.03	.19	.53	.03	.58	.65

Each analysis is indexed with the mineral (ol) and core (c), rim (r) c-c (core to rim traverse) or particular notes, and the number of analyses (#) and are accompanied by standard deviations.

Evolution of Oceanic Gabbros: In-situ and Ancient Examples

Sample # and placement	Averages										Standard deviations										Total	Mg#	
	C	R	SiO ₂	TiO ₂	Al ₂ O ₃	Cr ₂ O ₃	FeO	MnO	CaO	Na ₂ O	Total	Mg#	SiO ₂	TiO ₂	Al ₂ O ₃	Cr ₂ O ₃	FeO	MnO	CaO	Na ₂ O	Total	Mg#	
BR-5-1-1H 74-78 cpxr(10)	x	x	51.79	.78	2.72	.03	7.21	.19	14.82	21.75	.41	99.7	78.6	.41	.13	.30	.01	.22	.02	.14	.38	.05	.57
BR-5-1-1H 74-78 cpx			51.82	.76	2.90	.02	7.05	.20	14.96	21.59	.42	99.7	79.1	.34	.08	.22	.01	.24	.02	.17	.45	.04	.58
BR-5-1-5e 48-51.5 a cpxc(10)	x		51.74	.71	2.82	.03	6.46	.16	15.08	22.30	.37	99.7	80.6	.73	.20	.62	.01	.30	.03	1.28	.25	.61	.63
BR-5-1-5e 48-51.5 b cpxr(10)			51.44	.63	2.54	.03	7.95	.20	14.71	20.47	.63	98.6	76.7	.87	.26	.99	.01	.63	.02	.37	.16	.22	.55
BR-5-1-5e 48-51.5 cpx c-r(8)	x	x	51.87	.84	2.74	.05	7.06	.23	14.55	22.04	.41	99.8	80.6	.34	.02	.09	.01	.25	.02	.14	.21	.03	.26
BR-5-1-5e 48-51.5 cpxc	x		51.74	.71	2.82	.03	6.46	.16	15.08	22.30	.37	99.7	80.6	.73	.20	.62	.01	.30	.03	1.28	.25	.61	.63
BR-5-1-5e 48-51.5 cpxr	x		51.66	.59	2.34	.03	7.82	.20	14.79	20.70	.59	98.7	77.1	.55	.24	.80	.01	.50	.02	.26	.15	.19	.43
BR-6-1-1g 20.5-24.5 cpxc(10)	x		52.35	.71	2.43	.00	9.52	.22	14.98	19.02	.47	99.7	73.7	1.00	.21	.40	.01	.52	.03	1.16	.27	.05	1.08
BR-6-1-1g 20.5-24.5 cpxr(10)	x		51.73	.80	2.55	.01	9.68	.25	14.27	20.42	.50	100.2	72.4	.32	.11	.28	.01	.29	.05	.24	.69	.07	.39
BR-8-1-5D 34-36 cpxc(10)	x		51.71	.72	2.50	.06	8.31	.20	15.32	19.90	.40	99.1	76.7	.50	.03	.11	.02	.59	.02	.61	1.24	.04	.60
BR-8-1-5D 34-36 cpxc(10)	x		51.73	.71	2.39	.06	8.31	.19	15.59	19.73	.38	99.1	77.0	.49	.04	.09	.01	.89	.03	1.04	1.87	.04	.57
BR-8-1-5D 34-36 cpxc(10)	x		52.26	.63	2.51	.07	8.00	.19	16.09	19.28	.36	99.4	78.2	.47	.05	.09	.01	.77	.04	.77	1.61	.04	.55
BR-8-1-5D 34-36 cpxc(10)	x		52.06	.58	2.13	.07	6.45	.16	15.01	21.95	.41	98.8	80.6	.66	.14	.55	.02	.29	.01	.15	.84	.16	.44
BR-8-1-5G 69-71.5 cpxc(10)	x		52.13	.50	2.85	.10	7.70	.17	15.92	19.59	.39	99.4	78.7	.30	.04	.15	.01	.57	.02	.84	1.33	.05	.30
BR-8-1-5G 69-71.5 cpxr(10)	x		51.58	.79	2.72	.06	8.27	.18	15.02	20.40	.42	99.5	76.4	.23	.04	.20	.01	.62	.02	.63	1.32	.07	.32
BR-8-2-5h 3 cpxc(10)			54.62	.39	1.87	.04	6.72	.17	15.86	22.49	.24	102.4	80.8	1.06	.20	.71	.02	.85	.02	.70	1.77	.27	.63
BR-8-2-5h 3 cpxc(10)			51.98	.57	2.92	.10	7.49	.20	16.35	20.27	.50	100.4	79.6	.77	.13	.54	.02	.78	.02	.91	1.43	.18	.42
BR-8-2-5h 3 cpxc(10)			52.44	.66	2.98	.09	7.75	.19	16.33	20.19	.43	101.0	79.0	.59	.08	.23	.01	.16	.02	.20	.25	.03	.68
BR-8-2-5m 18.5-23 cpxc(10)	x		51.40	.78	2.57	.06	6.59	.16	15.10	21.82	.41	98.9	80.3	.31	.11	.14	.01	.59	.04	.47	1.09	.05	.43
BR-8-2-5m 18.5-23 cpxr(10)	x		51.26	1.02	2.83	.06	7.58	.18	15.77	19.92	.40	99.0	78.8	.128	.50	.87	.01	1.26	.03	.16	1.91	.20	.64
BR-9-1-1D 26-28.5 cpxc(10)	x		51.07	.86	2.29	.01	8.87	.23	14.12	19.88	.49	98.5	74.0	.31	.05	.14	.01	.26	.03	.14	.43	.02	.52
BR-9-1-1D 26-28.5 cpxr(10)	x		51.59	.60	2.29	.01	8.42	.24	13.79	21.35	.38	98.7	74.5	.61	.04	.11	.01	.73	.03	.27	.24	.03	1.04
BR-12-1-3B 33-35.5 cpxc(10)	x		51.19	.54	1.53	.04	9.65	.24	13.78	21.68	.45	99.1	71.8	.75	.05	.10	.01	.29	.02	.57	.33	.07	.41
BR-12-1-3B 33-35.5 cpxc(9)	x		51.55	.63	1.64	.05	9.84	.24	13.64	21.65	.45	99.7	71.2	.68	.04	.04	.01	.29	.02	.19	1.10	.04	1.03
BR-12-1-3B 33-35.5 cpxc(5)	x		52.25	.35	.75	.02	10.36	.19	13.86	22.02	.42	100.2	70.5	.54	.09	.24	.01	1.56	.03	1.52	3.20	.07	.59
BR-14-1-7a 35-37.5 cpxc(10)	x		51.72	.76	2.63	.02	9.10	.24	15.82	19.27	.43	100.0	75.7	.54	.09	.24	.01	.75	.03	.78	2.36	.06	2.30
BR-14-1-7a 35-37.5 cpxr(10)	x		51.57	.74	2.22	.03	8.12	.21	15.12	20.49	.41	98.9	76.9	1.26	.09	.19	.02	.75	.03	.54	1.75	.06	.98
BR-14-1-7a 35-37.5 cpxc(10)	x		51.64	.70	2.21	.03	8.45	.24	15.10	20.93	.40	99.7	76.2	.76	.09	.19	.01	.93	.03	.54	1.75	.06	.98
BR-15-3B 17.5-20 cpxc(7)	x		50.82	.74	1.68	.21	7.21	.14	15.87	20.86	.44	98.0	79.7	.80	.51	.10	.02	.67	.02	.39	.72	.03	.64
BR-15-3B 17.5-20 cpxr(1)	x		52.06	.72	1.25	.16	6.70	.11	15.50	22.41	.38	99.3	80.5										
JR31-1-Dredges			50.72	1.37	2.96	.02	10.41	.20	15.48	19.25	.43	100.8	72.6	.14	.03	.03	.02	.45	.03	.20	.65	.04	.25
JR31-3-51 cpxc(10)	x		50.85	1.25	2.85	.02	11.24	.23	15.64	18.36	.45	100.9	71.3	.21	.05	.05	.01	.17	.02	.18	.16	.03	.34
JR31-3-51 cpxr(10)	x		52.04	.79	2.62	.00	10.27	.24	15.87	19.67	.45	102.0	73.6	.39	.11	.25	.01	.25	.05	1.99	3.53	.09	2.64
JR31-9-2 cpxc(10)	x		52.17	.66	2.52	.01	7.73	.17	15.00	22.24	.39	100.9	77.6	.29	.04	.16	.01	.55	.01	.27	.59	.03	.65
JR31-9-2 cpxr(10)	x		51.74	.80	2.60	.01	9.46	.28	14.28	21.70	.51	101.4	72.9	.28	.06	.17	.01	.64	.03	.22	.63	.05	.42
JR31-9-4 cpxc(11)	x		51.88	.56	2.36	.00	9.69	.30	14.15	21.48	.44	100.9	72.2	.52	.09	.59	.00	.39	.04	.17	.56	.06	.65
JR31-9-4 cpxr(10)	x		52.55	.54	3.36	.50	4.70	.12	16.46	22.36	.36	100.9	86.2	.28	.13	.15	.08	.35	.03	.52	.80	.03	.49
JR31-12-1 a1 cpx r-(20)	x		52.86	.45	3.23	.41	4.90	.11	17.24	21.10	.35	100.7	86.2	.48	.03	.14	.03	.82	.02	1.37	2.20	.04	.42
JR31-12-1 a1 cpxc(12)	x		52.20	.69	3.24	.45	5.42	.13	16.52	21.74	.35	100.7	84.5	.44	.14	.13	.03	.71	.02	.93	1.81	.04	1.00
JR31-12-1 a2 cpxr(10)	x		52.77	.40	3.25	.50	5.93	.14	16.85	21.16	.36	101.2	83.5	.24	.15	.10	.04	.47	.02	.74	1.18	.05	.32
JR31-12-1 a2 cpxc(10)	x		52.57	.59	2.93	.33	5.44	.12	16.70	21.78	.23	100.7	84.6	.18	.02	.08	.03	.40	.02	.79	1.29	.03	.46
JR31-12-6 cpxc(10)	x		51.85	.53	3.15	.74	4.91	.12	17.37	21.19	.34	101.1	86.3	.28	.02	.08	.03	.40	.02	.20	.30	.04	.30
JR31-12-6 cpxc(10)	x		51.85	.53	3.15	.74	4.91	.12	17.37	21.19	.34	101.1	86.3	.28	.02	.08	.03	.40	.02	.20	.30	.04	.30
JR31-12-6 cpxc(10)	x		51.85	.53	3.15	.74	4.91	.12	17.37	21.19	.34	101.1	86.3	.28	.02	.08	.03	.40	.02	.20	.30	.04	.30
JR31-12-6 cpxc(10)	x		51.85	.53	3.15	.74	4.91	.12	17.37	21.19	.34	101.1	86.3	.28	.02	.08	.03	.40	.02	.20	.30	.04	.30
JR31-12-6 cpxc(10)	x		51.85	.53	3.15	.74	4.91	.12	17.37	21.19	.34	101.1	86.3	.28	.02	.08	.03	.40	.02	.20	.30	.04	.30
JR31-12-6 cpxc(10)	x		51.85	.53	3.15	.74	4.91	.12	17.37	21.19	.34	101.1	86.3	.28	.02	.08	.03	.40	.02	.20	.30	.04	.30
JR31-12-6 cpxc(10)	x		51.85	.53	3.15	.74	4.91	.12	17.37	21.19	.34	101.1	86.3	.28	.02	.08	.03	.40	.02	.20	.30	.04	.30
JR31-12-6 cpxc(10)	x		51.85	.53	3.15	.74	4.91	.12	17.37	21.19	.34	101.1	86.3	.28	.02	.08	.03	.40	.02	.20	.30	.04	.30
JR31-12-6 cpxc(10)	x		51.85	.53	3.15	.74	4.91	.12	17.37	21.19	.34	101.1	86.3	.28	.02	.08	.03	.40	.02	.20	.30	.04	.30
JR31-12-6 cpxc(10)	x		51.85	.53	3.15	.74	4.91	.12	17.37	21.19	.34	101.1	86.3	.28	.02	.08	.03	.40	.02	.20	.30	.04	.30
JR31-12-6 cpxc(10)	x		51.85	.53	3.15	.74	4.91	.12	17.37	21.19	.34	101.1	86.3	.28	.02	.08	.03	.40	.02	.20	.30	.04	.30
JR31-12-6 cpxc(10)	x		51.85	.53	3.15	.74	4.91	.12	17.37	21.19	.34	101.1	86.3	.28	.02	.08	.03	.40	.02	.20	.30	.04	.30
JR31-12-6 cpxc(10)	x		51.85	.53	3.15	.74	4.91	.12	17.37	21.19	.34	101.1	86.3	.28	.02	.08	.03	.40	.02	.20	.30	.04	.30
JR31-12-6 cpxc(10)	x		51.85	.53	3.15	.74	4.91	.12	17.37	21.19	.34	101.1	86.3	.28	.02	.08	.03	.40	.02	.20	.30	.04	.30
JR31-12-6 cpxc(10)	x		51.85	.53	3.15	.74	4.91	.12	17.37	21.19	.34	101.1	86.3	.28	.02	.08	.03	.40	.02	.20	.30	.04	.30
JR31-12-6 cpxc(10)	x		51.85	.53	3.15	.74	4.91	.12	17.37	21.19	.34	101.1	86.3	.28	.02	.08	.03	.40	.02	.20	.30	.04	.30
JR31-12-6 cpxc(10)	x		51.85	.53	3.15	.74	4.91	.12	17.37	21.19	.34	101.1	86.3	.28	.02	.08	.03	.40	.02	.20	.30	.04	.30
JR31-12-6 cpxc(10)	x		51.85	.53</																			

Evolution of Oceanic Gabbros: In-situ and Ancient Examples

Sample # and placement	Averages										Standard deviations																	
	C	R	SiO ₂	TiO ₂	Al ₂ O ₃	Cr ₂ O ₃	FeO	MnO	MgO	CaO	Na ₂ O	Total	Mg#	SiO ₂	TiO ₂	Al ₂ O ₃	Cr ₂ O ₃	FeO	MnO	MgO	CaO	Na ₂ O	Total	Mg#				
JR31-12-6 cpx6r(10)		x	52.35	.61	2.54	.23	6.24	.13	15.78	22.55	.28	100.7	81.8	.36	.09	.41	.02	.25	.01	.17	.44	.07	.30	.69	.30			
JR31-12-6 cpx7c(10)		x	51.33	.84	2.84	.14	8.65	.21	14.48	21.88	.33	100.7	74.9	.68	.08	.41	.02	.21	.03	.19	.82	.10	.91	.45	.30			
JR31-12-6 cpx8r(10)		x	51.07	.81	3.36	.10	9.10	.20	14.23	21.20	.56	100.6	73.6	.78	.25	1.00	.01	.64	.05	.26	1.39	.23	.58	1.28	.30			
JR31-12-6 cpx9c(9)		x	53.76	.39	2.70	.48	5.36	.15	17.73	20.44	.25	101.3	85.5	.19	.03	.10	.03	.54	.02	.94	1.44	.08	.59	.60	.30			
JR31-12-6 cpx9r(10)		x	52.49	.69	2.93	.26	5.61	.13	16.33	22.04	.32	100.8	83.8	.28	.03	.11	.01	.19	.02	.30	.69	.06	.50	.29	.30			
JR31-12-6 cpx10c(10)		x	53.10	.45	3.29	.58	4.93	.13	17.13	21.34	.30	101.2	86.1	.18	.02	.07	.02	.20	.02	.29	.68	.04	.44	.37	.30			
JR31-12-8 cpxc(8)		x	52.15	.51	3.24	.44	5.87	.09	16.76	20.94	.39	100.4	83.6	.22	.03	.05	.02	.27	.04	.34	.61	.03	.30	.49	.30			
JR31-12-8 cpxr(pl)(10)		x	51.42	1.10	3.29	.23	5.70	.11	16.04	21.74	.45	100.1	80.7	.27	.04	.11	.02	.14	.04	.34	.61	.03	.30	.49	.30			
JR31-12-10 cpxc(10)		x	52.08	.53	2.79	.04	6.86	.17	16.19	20.04	.38	99.1	83.4	.33	.02	.10	.02	.53	.03	.54	.95	.08	.45	.83	.30			
JR31-12-10 cpxr(pl)(8)		x	52.55	.45	2.64	.01	10.41	.19	15.40	15.41	.48	97.5	72.6	1.44	.20	.75	.01	1.51	.02	.90	3.82	.15	1.18	2.25	.30			
JR31-12-16 cpxc(8)		x	52.44	.66	2.58	.05	7.32	.19	14.97	22.65	.41	101.3	78.5	.63	.07	.20	.01	.26	.02	.24	.27	.06	.12	.51	.30			
JR31-12-28 cpxc(10)		x	51.63	.65	2.22	.00	10.23	.28	13.59	20.73	.44	99.8	70.5	.32	.09	.29	.00	.60	.02	.20	1.45	.09	.77	1.07	.30			
JR31-12-28 cpxr(pl)(8)		x	52.46	.40	1.37	.00	9.98	.30	13.82	20.76	.29	99.4	71.2	.58	.16	.40	.00	.42	.02	.11	.80	.07	.50	.90	.30			
JR31-12-39 cpxr(ilm)(7)		x	52.04	.40	1.46	.00	11.93	.32	13.18	19.77	.40	99.5	66.4	.62	.15	.61	.01	1.11	.02	.48	2.31	.17	.85	2.26	.30			
JR31-12-39 cpxc(8)		x	51.35	.36	3.01	.00	17.54	.24	12.82	11.61	.76	97.7	56.6	1.04	.05	.95	.00	.66	.05	.64	.57	.21	.58	2.04	.30			
JR31-12-39 cpxr(pl)(7)		x	51.46	.43	1.77	.00	11.78	.32	12.93	19.54	.52	98.7	66.2	.50	.10	.43	.00	1.23	.06	.34	1.73	.13	.70	2.39	.30			
JR31-12-42 cpxc(10)		x	52.24	.50	2.65	.04	6.37	.13	17.16	18.97	.33	98.4	82.8	.31	.02	.04	.01	.28	.02	.42	.61	.03	.43	.39	.30			
JR31-12-42 cpxr(pl)(10)		x	51.88	.63	2.36	.03	8.10	.20	16.30	18.58	.35	98.4	78.3	.42	.05	.13	.02	1.04	.04	1.16	2.30	.07	.48	.99	.30			
JR31-12-46 cpxc(5)		x	51.47	.51	2.68	.03	7.58	.16	17.37	17.74	.56	98.1	80.3	.71	.10	.63	.02	1.09	.05	1.00	1.41	.17	1.45	3.01	.30			
JR31-12-46 cpxr(pl)(7)		x	51.26	.87	2.78	.02	8.01	.19	14.73	20.19	.43	98.5	76.6	.67	.08	.19	.02	.25	.03	.85	.94	.14	1.26	1.00	.30			
JR31-12-47 cpx1(10)		x	51.48	.73	2.48	.21	7.22	.17	14.81	21.90	.44	99.4	78.5	.37	.05	.09	.02	.25	.02	.19	.45	.06	.50	.66	.30			
JR31-12-50 cpxc(10)		x	51.62	.45	2.85	.27	6.42	.17	16.63	19.75	.42	98.6	82.2	.36	.03	.26	.01	.65	.02	.75	1.15	.13	.62	1.14	.30			
JR31-12-50 cpxr(pl)(8)		x	51.16	.82	2.84	.10	6.19	.16	16.09	21.04	.39	98.8	82.3	.40	.06	.18	.03	.44	.03	.47	.84	.07	.40	.79	.30			
JR31-12-68-cpx(cpx)(10)		x	52.14	.52	2.87	.15	6.78	.16	16.73	19.96	.40	99.7	81.5	.34	.03	.18	.02	.27	.02	.22	.69	.03	.62	.57	.30			
JR31-12-68-cpx(small)c(10)		x	51.18	.83	2.99	.03	8.03	.19	14.56	21.31	.48	99.6	76.6	.22	.08	.09	.01	.27	.02	.17	.35	.05	.35	.42	.30			
JR31-12-68 cpxr(pl)(10)		x	51.86	.60	2.90	.08	7.90	.17	15.25	20.23	.51	99.5	77.8	.98	.20	.79	.01	1.21	.04	.55	2.74	.10	.90	2.46	.30			
JR31-39-1 cpxc(8)		x	52.24	.71	2.59	.08	9.36	.24	15.19	20.63	.40	101.4	74.3	.35	.05	.07	.02	.45	.03	.45	.83	.05	.40	.61	.30			
JR31-39-1 cpxr(8)		x	52.23	.77	2.29	.05	9.13	.23	15.02	20.88	.36	101.0	74.7	.53	.15	.28	.01	1.61	.05	1.09	2.42	.08	.57	1.71	.30			
JR31-39-3 cpx1c(10)		x	52.31	.79	2.31	.02	10.05	.28	14.13	21.56	.41	101.9	71.5	.24	.04	.10	.01	.58	.03	.26	.77	.06	.24	.81	.30			
JR31-39-3 cpx1r(8)		x	52.32	.74	2.03	.01	10.61	.30	14.10	20.99	.33	101.4	70.3	.17	.05	.14	.01	.27	.03	.32	.56	.07	.30	.40	.30			
JR31-39-3 cpx1r2(9)		x	52.20	.77	2.13	.01	10.50	.27	14.62	20.17	.39	101.1	71.3	1.07	.30	.90	.01	1.21	.04	.81	.89	.25	.55	3.33	.30			
JR31-39-4 cpx1c(10)		x	51.68	.55	1.67	.00	13.38	.34	13.61	18.49	.36	100.1	64.6	.22	.07	.15	.01	1.95	.03	.79	2.57	.07	.27	2.08	.30			
JR31-39-4 cpxr(cpx)(10)		x	51.87	.48	1.58	.00	12.34	.31	13.42	19.84	.36	100.2	66.0	.33	.09	.13	.00	.72	.03	.18	.93	.03	.31	1.06	.30			
JR31-39-4 cpxr(ilm)(6)		x	51.88	.50	1.72	.00	12.06	.34	13.24	19.87	.35	100.0	66.2	.23	.06	.13	.00	.54	.04	.13	.80	.03	.55	1.14	.30			
JR31-39-4 cpxr(pl)(6)		x	51.92	.32	2.03	.00	11.07	.31	12.88	20.59	.47	99.6	67.4	.13	.04	.18	.00	.27	.03	.73	.82	.37	.25	.89	.30			
JR31-39-7 cpxc(10)		x	51.45	.57	1.92	.00	13.43	.32	12.66	20.50	.43	101.3	62.7	.71	.08	.37	.00	.91	.02	.39	.77	.06	.48	1.55	.30			
JR31-39-7 cpxr(9)		x	51.96	.45	1.42	.00	14.68	.33	13.45	18.51	.35	101.2	62.3	.21	.06	.12	.00	.255	.05	.67	2.89	.06	.55	2.74	.30			
JR31-39-8-2 cpxc(7)		x	52.27	.77	2.23	.00	10.96	.32	14.41	19.99	.37	101.3	70.1	.22	.05	.07	.00	.79	.02	.44	1.06	.09	.23	.89	.30			
JR31-39-8-2 cpxr(10)		x	52.20	.82	2.20	.01	12.01	.34	15.09	18.57	.31	101.6	69.2	.42	.17	.14	.01	1.40	.04	.73	2.11	.04	.91	1.56	.30			
JR31-39-8 cpx3b(6)		x	52.04	.90	2.26	.03	10.10	.31	14.64	20.50	.41	101.2	72.1	.23	.03	.05	.01	.16	.01	.16	.43	.07	.37	.28	.30			
JR31-39-8 cpx3b(6)		x	52.18	.91	2.35	.02	10.11	.28	14.50	20.24	.41	101.0	71.9	.26	.09	.24	.01	.43	.04	.14	.63	.03	.45	.86	.30			
JR31-39-8 cpxc(10)		x	52.06	.82	2.29	.02	11.24	.31	15.18	18.79	.39	101.1	70.9	.45	.13	.31	.01	2.63	.05	1.91	4.33	.14	.52	1.94	.30			
JR31-39-8 cpxr(14)		x	52.42	.69	2.07	.02	11.49	.34	15.59	18.15	.41	101.2	71.3	.39	.11	.32	.01	4.32	.08	3.24	7.11	.13	.59	2.46	.30			
JR31-39-10 cpxc2(10)		x	51.16	.65	1.86	.01	15.43	.38	13.55	17.53	.28	100.9	61.9	.55	.17	.47	.01	5.56	.08	1.72	6.37	.15	.72	4.41	.30			
JR31-39-10 cpxc(10)		x	51.62	.63	2.06	.05	12.40	.34	13.57	19.76	.31	100.7	66.9	.18	.06	.15	.01	1.33	.04	.52	1.40	.08	.47	1.41	.30			
JR31-39-10 cpxr(10)		x	52.22	.39	1.63	.04	11.53	.31	13.66	21.12	.28	101.2	67.2	.38	.05	.25	.01	.49	.02	.16	.37	.05	.24	1.14	.30			
JR31-39-10 cpxr(10)		x	51.34	.67	1.88	.00	14.53	.35	13.36	18.53	.23	101.0	62.3	1.06	.08	.26	.00	2.70	.05	.92	3.10	.10	.96	3.22	.30			
JR31-39-10 cpxr(ilm)(10)		x	51.34	.67	1.88	.00	14.53	.35	13.36	18.53	.23	101.0	62.3	1.06	.08	.26	.00	2.70	.05	.92	3.10	.10	.96	3.22	.30			

Evolution of Oceanic Gabbros: In-situ and Ancient Examples

Sample # and placement	Averages													Standard deviations												
	C	R	SiO ₂	TiO ₂	Al ₂ O ₃	Cr ₂ O ₃	FeO	MnO	MgO	CaO	Na ₂ O	Total	Mg#	SiO ₂	TiO ₂	Al ₂ O ₃	Cr ₂ O ₃	FeO	MnO	MgO	CaO	Na ₂ O	Total	Mg#		
JR31-39-10 cpxr(pl)(6)	x		51.96	.50	1.64	.00	12.84	.35	13.28	20.28	.25	101.1	64.9	.15	.04	.04	.00	1.08	.03	.44	1.29	.04	.43	1.08		
JR31-39-11 cpxc(10)	x		51.17	.71	1.96	.02	14.13	.38	13.85	17.68	.33	100.2	65.2	.67	.12	.20	.01	4.25	.07	1.12	4.85	.14	.57	2.01		
JR31-39-11 cpxr(10)	x		51.85	.61	1.79	.00	12.92	.35	13.69	19.35	.32	100.9	65.4	.26	.05	.11	.01	1.29	.03	.53	1.63	.04	.39	1.82		
JR31-39-11 cpx(inside mt)r(10)	x		51.90	.45	1.74	.00	12.20	.34	13.81	19.71	.36	100.5	67.8	.42	.10	.14	.00	2.05	.04	.49	3.58	.06	.76	1.10		
JR31-39-11 cpx(inside mt)c(10)	x		51.50	.64	1.97	.00	13.49	.38	13.89	18.23	.40	100.5	64.7	.20	.05	.19	.00	1.80	.04	.71	2.29	.05	.27	1.96		
JR31-39-13 cpxc(10)	x		51.61	.71	2.01	.03	12.03	.31	13.40	20.39	.45	100.9	66.5	.08	.06	.10	.00	.82	.02	.31	.57	.01	.50	.99		
JR31-39-13 cpxr(10)	x		50.56	.40	3.47	.03	18.55	.22	12.01	12.87	.55	98.7	53.6	.16	.10	.16	.00	1.11	.00	.56	1.64	.13	.76	2.65		
JR31-39-17 cpx1(inside mt)r(15)	x		52.20	.63	1.79	.00	13.25	.39	13.94	18.91	.37	101.5	65.7	.27	.13	.32	.01	3.86	.09	1.28	4.92	.10	.45	3.36		
JR31-39-17 cpx2(outside mt)r(pl)(10)	x		51.92	.61	2.00	.01	12.23	.36	13.65	20.19	.34	101.3	66.6	.39	.05	.11	.01	1.21	.03	.36	1.54	.05	.47	1.62		
JR31-39-17 cpx3c(8)	x		52.47	.43	1.58	.01	11.64	.35	13.58	21.05	.35	101.5	67.5	.22	.04	.05	.01	.46	.04	.17	.69	.06	.47	1.11		
JR31-39-17 cpx3r(9)	x		52.48	.41	1.46	.00	11.00	.33	13.61	20.84	.43	100.6	68.8	.41	.05	.11	.01	.44	.02	.13	.48	.08	1.05	.76		
JR31-40-1 cpxc(10)	x		53.11	.58	2.96	.04	7.57	.14	18.17	19.08	.41	102.1	81.2	.37	.06	.21	.01	1.58	.03	2.07	3.67	.10	.31	1.34		
JR31-40-1 cpxr(10)	x		53.19	.64	2.38	.04	6.66	.14	16.41	21.99	.42	101.9	81.5	.20	.04	.07	.01	.44	.04	.30	.75	.04	.31	.73		
JR31-41-4 cpxc(10)	x		52.39	.58	2.25	.01	12.36	.27	15.44	18.29	.46	102.0	69.8	.62	.20	.66	.01	5.07	.12	2.83	7.84	.20	.41	3.86		
JR31-41-4 cpxr(10)	x		52.24	.54	2.26	.00	9.48	.23	14.26	22.34	.46	101.8	72.8	.57	.01	.06	.00	.45	.01	.26	.43	.03	.37	1.02		

Each analysis is indexed with the mineral (ol) and core (c), rim (r) c-c (core to rim traverse) or particular notes, and the number of analyses (#) and are accompanied by standard deviations.

Evolution of Oceanic Gabbros: In-situ and Ancient Examples

Table 2C: The average composition of low-Ca pyroxene from on and around Atlantis Bank.

The average composition of 100-µm Biotine from oil and around returning bank.																							
Sample # and placement		Averages										Standard deviations											
		SiO ₂	TiO ₂	Al ₂ O ₃	Cr ₂ O ₃	FeO	MnO	MgO	CaO	Na ₂ O	Total	Mg#	SiO ₂	TiO ₂	Al ₂ O ₃	Cr ₂ O ₃	FeO	MnO	MgO	CaO	Na ₂ O	Total	Mg#
Mode 98																							
6K-460-14 opxc(10) 6K-460-14 opx c-r(8) 6K-460-14 opxr(10) 6K-466-8 a1 opx(2) 6K-466-8 a1 opx c-r(8) 6K-466-8 a2 opx (inside cpx) c-r(7) 6K-466-11 opx(4) 6K-466-11 opxc(6) 6K-466-11 opxr(6) 6K-467-12 opx r-c-r(pl)	52.20	.42	1.08	.02	20.88	.50	19.75	5.24	.10	100.2	63.6	.77	.12	.40	.01	5.93	.13	3.01	8.42	.19	.66	4.64	
	52.80	.31	.84	.01	23.17	.55	21.19	1.49	.02	100.4	62.0	.57	.06	.04	.01	.36	.02	.40	.11	.03	.88	.66	
	52.89	.36	.84	.02	23.31	.54	21.01	1.55	.01	100.5	61.6	.44	.03	.04	.01	.18	.02	.17	.08	.01	.63	.23	
	51.40	.32	.83	.00	25.34	.67	19.47	1.12	.01	99.2	57.8	.17	.11	.02	.00	.11	.04	.30	.12	.01	.21	.47	
	51.65	.35	.78	.02	25.14	.64	19.66	1.41	.17	99.8	58.2	.17	.03	.07	.01	.37	.04	.18	.20	.06	.40	.44	
	52.59	.22	.73	.01	24.89	.66	20.86	1.04	.01	101.0	59.9	.49	.04	.02	.02	.23	.03	.22	.11	.02	.60	.12	
	51.19	.30	1.67	.03	24.86	.60	18.51	1.85	.18	99.2	57.0	.148	.08	1.32	.01	1.04	.06	1.54	1.37	.27	1.66	1.13	
	52.54	.35	.89	.02	23.33	.58	20.65	1.57	.00	99.9	61.2	.29	.02	.03	.01	.47	.02	.20	.39	.00	.72	.28	
	52.14	.32	.82	.02	23.88	.60	20.37	1.31	.00	99.5	60.3	.18	.03	.03	.01	.54	.02	.16	.12	.00	.77	.38	
	53.23	.45	1.35	.00	18.72	.42	23.86	1.84	.04	99.9	69.4	.36	.09	.07	.01	.25	.03	.26	.39	.02	.47	.25	
Leg ABCDE																							
6K-645-R18 opx(5) 6K-649-R06-2 opxr(4) 6K-643-r08 opxr(7) 6K-643-r08 opxc(9)	52.44	.43	.78	.02	25.77	.40	19.73	1.81	.01	101.4	57.7												
	52.58	.44	2.41	.03	16.95	.34	24.98	1.08	.01	98.8	72.4												
	53.82	.47	1.69	.00	16.73	.35	25.62	2.26	.05	101.0	73.2	.64	.04	.04	.01	.17	.02	.43	.12	.05	1.08	.36	
	54.00	.43	1.70	.00	16.73	.39	25.85	2.13	.03	101.3	73.4	.22	.03	.05	.00	.30	.04	.34	.58	.03	.42	.21	
BGS Cores																							
BGS-16-1-1 7-12 opxc BGS-16-1-1 7-12 opxr BGS-16-1-1 7-12 opx c-r(10) BGS-20-1-6a a2 opx r(cpx)-r(pl)(6) BGS-20-1-6a a3 opx r(ol)-r(pl)(12) BGS-20-2-6b a2 opx (inside ol)(6) BGS-23-1-2e opx(9) BGS-24-1-3c 21-24 opx(11) BGS-24-1-3c 21-24 opxr(7) BGS-24-1-3h 51.5 opx(6) BGS-24-1-3k 77 opx(6) BGS-27-1-1A 3 opx(6)	52.37	.36	1.02	.01	23.79	.59	20.36	1.61	.05	100.2	60.4	.36	.08	.08	.01	.45	.03	.18	.40	.01	.75	.42	
	52.39	.34	.92	.02	23.76	.61	20.36	1.66	.04	100.1	60.4	.30	.04	.05	.01	.36	.06	.13	.19	.01	.49	.41	
	52.30	.33	.75	.00	24.08	.67	20.10	1.63	.00	99.9	59.8	.24	.03	.05	.00	.34	.02	.16	.18	.01	.39	.39	
	54.26	.36	1.15	.03	17.68	.42	26.35	1.24	.00	101.5	72.7	.22	.11	.08	.01	.17	.04	.34	.26	.00	.30	.32	
	53.94	.40	1.24	.03	18.23	.45	25.76	1.40	.01	101.5	71.6	.22	.07	.04	.01	.30	.03	.14	.24	.02	.44	.31	
	53.94	.13	1.02	.03	18.03	.37	25.91	.80	.09	100.3	71.9	.28	.02	.06	.02	.14	.03	.11	.07	.04	.21	.16	
	52.85	.19	.77	.00	21.25	.49	22.65	1.28	.03	99.5	65.5	.39	.03	.05	.00	.39	.04	.15	.07	.03	.53	.40	
	52.79	.26	.88	.00	22.67	.56	22.08	.98	.03	100.2	63.4	.20	.02	.02	.00	.21	.05	.06	.01	.02	.25	.23	
	52.77	.26	.86	.00	22.67	.55	22.10	.98	.02	100.2	63.5	.99	.04	.11	.00	.28	.05	.11	.07	.02	.92	.38	
	52.69	.39	1.12	.00	20.73	.52	22.27	1.58	.00	99.3	65.7	.32	.03	.03	.01	.40	.03	.20	.30	.01	.50	.34	
55.17	.29	.94	.00	18.92	.45	25.14	1.12	.00	102.0	70.3	.47	.10	.11	.01	.36	.03	.19	.44	.00	.96	.48		
56.67	.28	1.13	.01	16.12	.37	27.55	.88	.00	103.0	75.3	.54	.06	.11	.01	.25	.01	.35	.11	.00	.75	.37		
BR Cores																							
BR-6-1-1g 20.5-24.5 opx c-r(7) BR-8-1-5d 34-36 opx c-r BR-8-1-5g 69-71.5 opx r-r BR-8-2-5h opx(2) BR-8-2-5m 18.5-23 opx c-r(8)	51.80	.29	1.52	.00	9.18	.20	14.85	21.67	.02	99.5	74.3	1.04	.05	.13	.00	1.47	.03	.17	.50	.01	.48	3.00	
	54.68	.16	.97	.00	16.33	.37	26.25	.83	.01	99.6	74.1	.42	.03	.12	.00	.30	.02	.21	.04	.01	.16	.44	
	53.66	.29	1.27	.00	16.74	.37	25.49	1.07	.04	98.9	73.1												
	54.50	.22	1.14	.00	15.51	.32	27.58	.95	.00	100.2	76.0	.11	.02	.01	.00	.58	.02	.08	.01	.00	.33	.74	
JR31 Dredges																							
JR31-12-6 opx c-r(10) JR31-12-28 opxc(10) JR31-12-28 opxr(pl)(9) JR31-12-28 opx(5) JR31-12-45 opx(6) JR31-39-4 opx(6) JR31-39-17 opx c-r(6)	53.93	.51	1.47	.05	18.01	.39	24.88	1.96	.00	101.2	71.1	.31	.13	.06	.02	.43	.03	.38	.32	.0	.43	.74	
	52.39	.39	.94	.00	22.25	.51	21.51	2.05	.05	100.1	63.3	.19	.12	.08	.0	.37	.04	.31	.58	.04	.37	.4	
	52.23	.39	1.00	.00	22.50	.52	21.37	1.67	.06	99.8	62.9	.41	.03	.05	.01	.62	.03	.26	.33	.04	.76	.71	
	52.45	.38	.93	.00	22.43	.50	21.31	1.70	.04	99.7	62.9	.37	.05	.07	.0	.55	.03	.26	.3	.04	.79	.48	
	53.51	.35	1.33	.00	17.35	.37	24.41	1.78	.04	99.1	71.5	.48	.08	.01	.0	.6	.05	.33	.34	.03	.2	.83	
	51.88	.32	.81	.01	25.39	.63	19.42	1.54	.00	100.0	57.7	.13	.04	.03	.01	.12	.03	.01	.15	.0	.17	.18	
51.28	.33	.74	.01	24.48	.61	19.79	1.68	.02	98.9	59.0	.19	.05	.04	.01	.46	.03	.14	.19	.01	.44	.49		

Each analysis is indexed with the mineral (ol) and core (c), rim (r) or (core to rim traverse) or particular notes, and the number of analyses (n) and are accompanied by standard deviations.

Evolution of Oceanic Gabbros: In-situ and Ancient Examples

Table 2D: The average composition of olivine from on and around Atlantis Bank.

Table 2D: The average composition of olivine from on and around Atlantis Bank.																						
Label	Averages											Standard deviations										
	SiO ₂	TiO ₂	Al ₂ O ₃	Cr ₂ O ₃	FeO	MnO	MgO	CaO	NiO	Total	Fo	SiO ₂	TiO ₂	Al ₂ O ₃	Cr ₂ O ₃	FeO	MnO	MgO	CaO	NiO	Total	Fo
Mode 98																						
6K-460-R11 ol r-r(4)	36.04	.00	.01	.00	34.55	.64	29.10	.02	.06	100.4	60.0	.21	.00	.01	.00	.66	.03	.57	.02	.03	1.07	.64
6K-460-R13 olc(6)	37.17	.04	.00	.02	29.60	.44	33.27	.05	.00	100.6	66.7	.08	.01	.00	.00	.42	.03	.15	.01	.00	.54	.26
6K-460-R13 olr(6)	37.14	.03	.00	.02	29.50	.45	33.26	.04	.00	100.4	66.8	.19	.01	.00	.01	.39	.04	.44	.01	.00	.85	.23
6K-460-R14 ol c-r(5)	34.87	.00	.02	.02	40.36	.60	24.11	.03	.00	100.0	51.6	.11	.00	.02	.00	.42	.01	.16	.01	.00	.37	.35
6K-460-R14 olc c-r(9)	35.65	.00	.01	.00	37.33	.60	26.59	.01	.00	100.2	55.9	.22	.00	.00	.00	.31	.03	.18	.01	.00	.37	.26
6K-460-R16 olc(7)	35.77	.00	.00	.00	34.80	.56	28.58	.03	.00	99.7	59.4	.12	.00	.00	.01	.57	.03	.23	.00	.00	.68	.31
6K-460-R16 olr(7)	35.95	.00	.00	.00	35.13	.56	28.83	.04	.00	100.5	59.4	.37	.00	.00	.00	.38	.04	.09	.01	.00	.47	.27
6K-466-R7 olr(4)	34.44	.00	.02	.00	41.79	.83	22.68	.06	.11	99.9	49.2	.08	.01	.01	.01	.39	.05	.16	.01	.07	.30	.36
6K-466-R8 a2 olr-r(10)	33.99	.05	.00	.07	42.86	.75	21.89	.09	.18	99.9	47.6	.30	.01	.01	.02	.29	.04	.31	.02	.04	.60	.37
6K-466-R8 a2 r(pl)-r(mt)(10)	34.03	.07	.00	.07	44.38	.74	21.18	.06	.21	100.7	46.0	.42	.05	.00	.01	.27	.03	.43	.02	.03	.73	.59
6K-466-R9 olc(6)	36.57	.05	.00	.03	31.69	.51	31.36	.06	.00	100.3	63.8	.17	.01	.00	.01	.28	.04	.26	.00	.00	.36	.19
6K-466-R9 olr(4)	36.72	.04	.00	.03	31.68	.47	31.16	.06	.00	100.2	63.7	.16	.02	.00	.01	.16	.04	.46	.01	.00	.52	.37
6K-467-R9 olc-r(10)	36.72	.00	.00	.00	31.01	.48	31.79	.04	.02	100.1	64.6	.48	.00	.00	.00	.78	.03	.71	.01	.02	.64	1.05
6K-467-R1 ol(6)	37.46	.01	.01	.00	27.63	.42	34.79	.04	.07	100.4	69.2	.18	.02	.01	.01	.20	.04	.12	.01	.01	.10	.19
6K-467-R10 ol(6)	36.56	.00	.00	.00	29.54	.41	33.35	.05	.05	100.0	66.8	.64	.00	.00	.00	.39	.01	.20	.01	.02	.95	.27
6K-467-R20 ol(6)	38.64	.02	.01	.00	20.82	.30	40.44	.05	.08	100.4	77.6	.07	.00	.01	.01	.19	.02	.62	.01	.04	.48	.20
Leg ABCDE																						
6K-646-R01 ol(16)	37.62	.01	.38	.01	21.74	.36	39.44	.02	.11	99.7	76.4	.15	.01	.45	.01	.34	.04	.38	.01	.02	.44	.27
6K-646-R01 ol2 c-r(6)	37.49	.01	.07	.00	21.59	.33	39.70	.05	.03	99.3	76.6	.30	.01	.07	.00	.47	.02	.21	.01	.03	.76	.35
6K-649-R06 ol(12)	36.61	.00	.63	.00	27.48	.42	33.87	.07	.04	99.1	68.7	.04	.00	.72	.00	.44	.06	.59	.03	.02	.71	.72
6K-643-R08 ol r-c(6)	37.33	.02	.00	.01	27.69	.43	35.95	.04	.16	101.6	69.8	.13	.02	.00	.01	.41	.07	.15	.03	.03	.55	.28
6K-649-R08 ol2(6)	38.59	.01	.03	.00	20.47	.42	40.89	.03	.01	100.4	78.1	.52	.01	.01	.00	.24	.03	.62	.01	.02	.67	.28
6K-649-R14 ol(6)	36.75	.01	.28	.00	25.48	.37	36.19	.04	.04	99.2	71.7	.35	.01	.45	.01	.33	.04	.27	.03	.02	.49	.33
6K-650-R06 ol c-r(7)	38.20	.00	.49	.00	18.25	.31	41.63	.03	.04	99.0	80.3	.57	.00	.40	.01	.30	.03	.63	.01	.03	.74	.42
6K-650-R09 ol(9)	37.80	.01	.00	.02	25.22	.56	38.56	.03	.00	102.2	73.2	.34	.01	.01	.02	.33	.04	.24	.01	.00	.27	.24
BGS Cores																						
BGS-4-1-4c 43-48 ol(6)	37.26	.03	.01	.02	26.54	.36	36.44	.02	.10	100.8	71.0	.25	.01	.01	.01	.12	.03	.18	.02	.02	.21	.18
BGS-4-2-17 ol(6)	37.26	.01	.02	.00	27.18	.42	35.37	.05	.12	100.4	69.9	.17	.01	.01	.00	.31	.02	.26	.01	.02	.48	.16
BGS-4-2-4d a1 ol r(pl in0)-r(pl ext)(10)	37.47	.00	.00	.00	26.29	.35	35.97	.03	.02	100.1	70.9	.28	.00	.00	.00	.94	.06	.18	.01	.02	1.00	
BGS-4-2-4d a2 ol r(pl)-r(ilm)(10)	37.33	.00	.00	.00	26.39	.36	35.96	.04	.01	100.1	70.8	.13	.00	.00	.00	.33	.04	.17	.01	.01	.30	.30
BGS-16-1-1 7-12 ol	52.30	.33	.75	.00	24.08	.67	20.10	1.63	.00	99.9	59.8	.24	.03	.05	.00	.34	.02	.16	.18	.01	.39	.39
BGS-19-2 10-11.5-ol(6)	38.38	.00	.00	.00	22.47	.31	38.67	.02	.07	99.9	75.4	.24	.00	.01	.00	.36	.03	.32	.01	.02	.73	.22
BGS-20-1-6a a3 ol r-r(6)	36.82	.00	.00	.03	29.88	.44	33.47	.02	.09	100.8	66.6	.20	.00	.00	.02	.19	.04	.31	.01	.08	.42	.13
BGS-20-1-6a 64-67 ol2 c-r(7)	38.23	.09	.08	.10	27.42	.45	34.60	.08	.00	101.0	69.2	.26	.00	.01	.01	.32	.02	.18	.01	.00	.46	.27
BGS-20-2-6b a2 ol r-c(10)	36.69	.00	.00	.00	29.84	.46	32.72	.03	.06	99.8	66.1	.19	.01	.00	.00	.40	.05	.37	.02	.03	.48	.49
BGS-24-1-3c 21 ol c-r(6)	35.71	.04	.00	.07	35.94	.59	28.22	.07	.00	100.6	58.3	.19	.01	.00	.01	.19	.02	.14	.01	.00	.31	.14
BGS-27-1-1a 3 ol(2)	36.71	.01	.00	.03	24.21	.34	37.26	.00	.00	98.5	73.3	.18	.01	.00	.01	.37	.01	.15	.00	.00	.37	.38
BGS-27-1-1b 8.5 ol(4)	36.86	.02	.01	.03	25.60	.39	35.58	.03	.00	98.5	71.2	.30	.01	.01	.02	.28	.03	.25	.01	.00	.33	.35
BGS-27-1-1b 8.5 ol2(10)	37.32	.01	.00	.02	25.23	.38	36.44	.04	.00	99.4	72.0	.46	.01	.00	.01	.25	.03	.31	.01	.00	.57	.25
BGS-27-1-1b 19.5 ol(6)	37.51	.01	.01	.03	25.14	.38	36.85	.02	.00	99.9	72.3	.30	.01	.01	.02	.27	.02	.63	.01	.00	.78	.46
BR Cores																						
BR-8-1-5D 34-36 ol1c(5)	37.51	.00	.00	.00	26.64	.35	34.57	.03	.00	99.1	69.8	.06	.00	.00	.00	.13	.02	.14	.01	.00	.23	.12
BR-8-1-5D 34-36 ol1r(6)	37.51	.00	.00	.00	26.97	.36	34.47	.03	.00	99.3	69.5	.42	.00	.00	.00	.69	.02	.23	.01	.00	.63	.58
BR-8-1-5D 34-36 6ol2(3)	37.13	.00	.00	.00	27.56	.40	33.71	.00	.00	98.8	68.6	.17	.00	.00	.00	.08	.04	.19	.00	.00	.32	.10
BR-8-1-5D 34-36 ol2c(5)	37.36	.00	.00	.00	26.25	.36	34.72	.03	.00	98.7	70.2	.08	.00	.00	.00	.40	.01	.13	.01	.00	.43	.29

Each analysis is indexed with the mineral (ol) and core (c), rim (r) r-c (core to rim traverse) or particular notes, and the number of analyses (#) and are accompanied by standard deviations.

Evolution of Oceanic Gabbros: In-situ and Ancient Examples

Label	Averages											Standard deviations										
	SiO ₂	TiO ₂	Al ₂ O ₃	Cr ₂ O ₃	FeO	MnO	MgO	CaO	NiO	Total	Fo	SiO ₂	TiO ₂	Al ₂ O ₃	Cr ₂ O ₃	FeO	MnO	MgO	CaO	NiO	Total	Fo
BR-8-1-5g 69-71.5 olc(5)	37.13	.00	.00	.00	27.65	.37	34.15	.03	.00	99.3	68.8	.26	.00	.00	.00	.41	.03	.13	.03	.00	.62	.33
BR-8-1-5g 69-71.5 olr(5)	36.88	.00	.00	.00	27.44	.39	34.05	.01	.00	98.8	68.9	.24	.00	.00	.00	.43	.04	.39	.01	.00	.40	.56
BR-8-2-5h ol1(3)	36.23	.00	.01	.01	24.97	.35	36.78	.03	.06	98.4	72.4	.11	.00	.01	.00	.25	.05	.39	.01	.01	.14	.42
BR-8-2-5h ol2(4)	36.75	.02	.01	.00	25.83	.43	35.97	.02	.06	99.1	71.3	.24	.02	.01	.00	.17	.05	.28	.01	.01	.33	.29
BR-15-3b 17.5-20 ol c-r(7)	38.79	.07	.22	.09	22.16	.36	38.15	.06	.00	99.9	75.4	.14	.00	.39	.01	.64	.02	.93	.01	.00	1.09	.42
JR31 Dredges																						
JR31-9-2 olc-r(6)	36.52	.01	.00	.01	31.48	.41	32.32	.07	.09	100.9	64.7	.34	.01	.00	.00	.66	.04	.79	.02	.02	.82	.98
JR31-9-4 olcr(5)	35.76	.01	.01	.00	35.33	.46	28.97	.06	.02	100.6	59.4	.15	.01	.00	.01	.65	.05	.20	.01	.01	.70	.44
JR31-12-1 a1 ol(10)	38.41	.02	.00	.00	20.11	.25	40.43	.05	.07	99.3	78.2	.24	.01	.00	.00	.41	.03	.22	.04	.02	.71	.30
JR31-12-1 a2 ol2(10)	38.83	.02	.00	.00	20.05	.25	40.78	.02	.07	100.0	78.4	.22	.02	.00	.00	.30	.02	.34	.01	.02	.57	.25
JR31-12-50 ol c-r(10)	37.59	.00	.00	.02	24.27	.37	37.24	.06	.08	99.6	73.2	.15	.00	.00	.01	.63	.02	.26	.02	.03	.68	.51
JR31-39-1 ol(6)	36.10	.02	.00	.00	32.55	.48	31.02	.07	.04	100.3	62.9	.11	.02	.00	.00	.34	.02	.21	.02	.02	.28	.34
JR31-39-3 ol(8)	35.99	.00	.00	.01	36.33	.53	27.91	.07	.00	100.9	57.8	.11	.01	.00	.01	.48	.04	.49	.01	.00	.74	.54

Each analysis is indexed with the mineral (ol) and core (c), rim (r) r-c (core to rim traverse) or particular notes, and the number of analyses (#) and are accompanied by standard deviations.

Chapter 6

Trace element mineral-chemistry of gabbros from Atlantis Bank: Evidence for melt-rock interaction

Abstract

Trace elements in augite from gabbros on and around Atlantis Bank reflect melts that crystallized 50-95% relative to a parental magma in equilibrium with the mantle. This agrees well with our previous results using major-elements in Chapter 3. The gabbros cannot have formed by simple fractional crystallization alone, as the rocks have increasing LREE/HREE ratios with fractionation. The gabbros may instead have crystallized by in-situ crystallization, or by significant assimilation of pre-existing olivine gabbros. Even if the magmas have assimilated host-rocks upon ascent, they still must have crystallized ~50% elsewhere before emplacement in the crust. Our previous estimate for the original crustal thickness at Atlantis Bank of 4.4-km is therefore valid.

Augites from a diabase-dike represent much more depleted melts than the melts that produced the gabbros. No known mineral-fractionation can produce the refractory pattern seen in this rock and we suggest that this dike represents depleted melts that did not mix with the melts found on and around Hole 735B.

1 Introduction

Lower ocean crust gabbros are believed to form from the same basaltic melts that are parental to the upper crust. Trace- and rare-earth element analyses are frequently used to interpret the origin and evolution of such oceanic lavas. The lower crust, however, is more rarely analyzed for REE and trace element variability due both to limited accessibility and because it consists of cumulus and inter-cumulus minerals with potentially very TE- and REE-rich accessory-minerals. For the Atlantis Bank gabbros, an extensive major and trace element data-set now exists in compilations of whole-rock analyses from Hole 735B and Atlantis Bank area (Hart et al., 1999; Natland and Dick, 2002; and Coogan et al., 2001).

Evolution of Oceanic Gabbros: In-situ and Ancient Examples

The method of accretion of the lower ocean-ridge crust has long been debated, though fractional crystallization is considered the main process for the evolution of the upper crust. *In-situ* crystallization (Langmuir, 1989), assimilation-fractionation-crystallization (AFC, e.g. DePaolo 1981 and discussion in Chapter 3 and 4), and magma-mixing may also be important in the evolution of the lower crust. *In-situ* mineral-analyses of oceanic gabbros may help in interpreting the origin and evolution of the melts that formed lower crustal rocks. Coogan et al. (2000) showed that very primitive Mid-Atlantic Ridge olivine gabbros have plagioclase-grains with cores that have a different origin than that of the overgrowing plagioclase rims and interstitial clinopyroxene, and interpreted this as the result of magma mixing within the lower crust. Dixon et al. (1986) investigated an unusual aphyric ferrobalt containing evolved gabbro-xenoliths from the Juan de Fuca Ridge, and concluded that the basalt represents hybrid magma formed by highly evolved magma, mixed with more primitive melts. The evolved melt-component produced the oxide-gabbros by filter pressing along a partially crystallized mush boundary. Coogan et al. (2002) demonstrated that East Pacific Rise gabbros exposed at Hess Deep represent a complex mixture of melts, some of which are mixed in the mantle, some of which are not. They suggested that all the melts added to the crust do not mix within a central axial magma chamber, and some partially crystallize in isolation within the lower crust. The homogeneity within the upper ocean crust is therefore surprising, as the existing knowledge of accretion of lower ocean-crust suggests a very heterogeneous process of accretion.

We have analyzed augites in eight Atlantis Bank gabbros for trace- and rare-earth elements. The sample set includes the entire compositional range of gabbros recovered from Atlantis Bank, from very primitive troctolites in Hole 735B to ferrogabbros recovered along the side of the platform, and one coarser-grained diabase sample from the northern wall (see Chapter 5). This data-set allows us to re-evaluate the magma-budget for Atlantis Bank when assimilation is taken into account.

2 Analytical methods

Unaltered cores and rims of clinopyroxene from eight samples were analyzed on the CAMECA IMS 3f ion probe at Woods Hole Oceanographic Institution using the

Table 6-1: REE and Trace-elements content of augites in ppm

	Ti	V	Cr	Sr	Y	Zr	La	Ce	Nd	Sm	Eu	Dy	Er	Yb
ODP-735B-83-7-139 rim to plagioclase	4282	370	3000	7.7	21.7	39.3	.45	3.27	4.80	2.94	.69	4.36	2.57	2.71
ODP-735B-83-7-139 core	1590	230	3764	4.7	6.5	3.5	.23	1.10	1.53	1.09	.41	1.90	1.14	1.24
ODP-735B-83-7-139 rim to olivine							.57	3.29	4.54	2.70	.55	4.53	2.58	2.65
JR31-12-6 grain 1 rim	2593	340	939	10	11.9	7.8	.29	1.48	2.32	1.59	.61	3.07	1.53	1.62
JR31-12-6 grain 1 core	2424	315	1739	12.3	13.9	10.2	.24	1.25	2.21	1.34	.46	2.33	1.35	1.24
JR31-12-6 grain 1 in between	2212	301	1476	10.6	12	8.3	.44	1.88	2.30	1.53	.64	2.77	1.70	1.62
JR31-12-6 grain 2 rim	3056	338	1776	12.2	19.1	22.1	.24	1.09	1.58	.96	.45	1.81	1.03	.93
JR31-12-6 grain 2 core	1686	264	787	6.4	7.5	4.6	.023	.128	.292	.222	.072	.540	.675	.945
JR31-12-28 rim	2547	198	112	0.9	5.7	4.6	.036	.234	.507	.423	.134	1.025	.811	1.150
JR31-12-28 core	4187	200	109	1.9	5.4	5.3	.030	.171	.387	.274	.072	.635	.632	.844
JR31-12-28 repeat							.30	1.65	2.86	1.86	.51	3.41	1.99	1.98
JR31-12-1 rim	3207	323	1227	7.7	20.7	44	.19	1.06	1.67	1.26	.41	1.90	1.13	1.21
JR31-12-1 core	1876	267	1848	8.3	9.1	7.1	1.90	9.20	12.38	5.82	1.28	9.82	5.71	5.89
6K-466-R11 rim	2732	369	175	8.9	61.5	107.4	1.84	10.46	13.56	6.32	1.31	11.29	6.42	6.75
6K-466-R11 core	3307	452	253	9.5	76.3	135.1	.40	2.52	3.76	1.85	.65	3.37	2.00	2.10
6K-467-R09 rim	4196	429	147	10.1	28.4	25.9	.43	2.79	4.72	2.37	.83	4.57	2.62	2.51
6K-467-R09 core	3027	395	145	9.5	26	28.8	1.79	9.83	12.59	5.98	1.65	11.03	6.65	6.56
6K-466-R08 rim1	3086	477	98	9.6	58.1	52.9	1.78	8.48	11.06	5.43	1.66	9.81	5.54	5.99
6K-466-R08 core	5009	560	133	12.2	68.1	54.1	1.43	7.33	9.73	4.85	1.36	8.59	5.42	5.44
6K-466-R08 rim2	3820	525	112	10.5	61.9	58	1.52	7.74	10.99	5.92	1.49	10.92	6.77	6.42
6K-466-R08 rim3	3208	428	82	10.5	69.5	65	1.62	7.85	9.79	4.88	1.26	8.37	4.64	4.66
JR31-39-8 rim	4246	398	99	9.9	54.3	94.7	1.85	8.27	10.40	5.55	1.41	8.40	4.71	5.09
JR31-39-8 core	3430	389	80	10.3	52.9	113.9	.78	3.96	5.23	2.71	.67	4.46	2.55	2.85
6K-460-R13 rim	3706	396	138	9.4	34.9	52.4	.52	2.27	2.65	1.61	.46	2.31	1.51	1.20
6K-460-R13 core1							.88	4.16	4.73	2.45	.71	4.50	2.69	2.40
6K-460-R13 core2	2705	303	116	8.2	23.9	31.2								

Evolution of Oceanic Gabbros: In-situ and Ancient Examples

methods of Shimizu and Hart (1982). A primary beam of O^+ ions was focused to $\sim 20\mu\text{m}$ for REE (La, Ce, Nd, Sm, Eu, Dy, Er, Yb) and $\sim 10\mu\text{m}$ for other trace elements (Ti, V, Cr, Sr, Y, Zr). Molecular interferences were eliminated by energy-filtering and a secondary voltage offset of -30 to -60V for the REE, and -90 for the other trace elements. Uncertainties based on counting statistics were 5-10% (1σ) for REE and 1-5% (1σ) for the other trace elements. The data is presented in Table 6-1.

3 Results

The spider-diagrams and REE-plots for the augites are shown in Figure 6-1 and 6-2 respectively. It is clear that there are several populations. The diabase (JR31-12-28) has a very steep, refractory pattern, different from the rest. Almost all of the augites have negative Eu-anomalies, indicating that the augite crystallized after substantial volume of plagioclase had been fractionated. The REE-concentrations have been inverted using the partition-coefficients from Table 6-2 in order to present the data as the hypothetical equilibrium melts for the augites (Bédard, 1984)(Figure 6-4B).

4 Discussion

Except for the refractory diabase pattern, melt produced by 5.5 % by batch equilibrium melting in the spinel facies of depleted upper mantle (DMM) provides an adequate, sub-parallel, fit to the melts compositions calculated from the most primitive gabbroic augites (Figure 6-2B and Table 6-2). We used the DMM-composition and the partition-coefficients of Workman (in prep). Robinson et al. (2001) showed that basalts representing the upper crust formed contemporaneously to Atlantis Bank likely formed by fractional melting of a mantle with a potential temperature as high as that of the Mid-Atlantic Ridge at 23°N or Juan de Fuca Ridge at 45°N . They found that the difference in trace-element compositions and melt-production is due to a 20-km conductive lid on the mantle in this region, causing a larger fraction of melting to occur in the garnet stability-field below the dry solidus. Thus, the melts that are produced have slightly higher La/Sm-values than normal MORB even if the isotopes are those of a normal MORB (Robinson et al., 2001; Snow, 1993). The calculated crustal thickness as inverted from trace-elements corresponds to $3\pm 1\text{km}$ of crust (Robinson et al., 2001), shallower than

Evolution of Oceanic Gabbros: In-situ and Ancient Examples

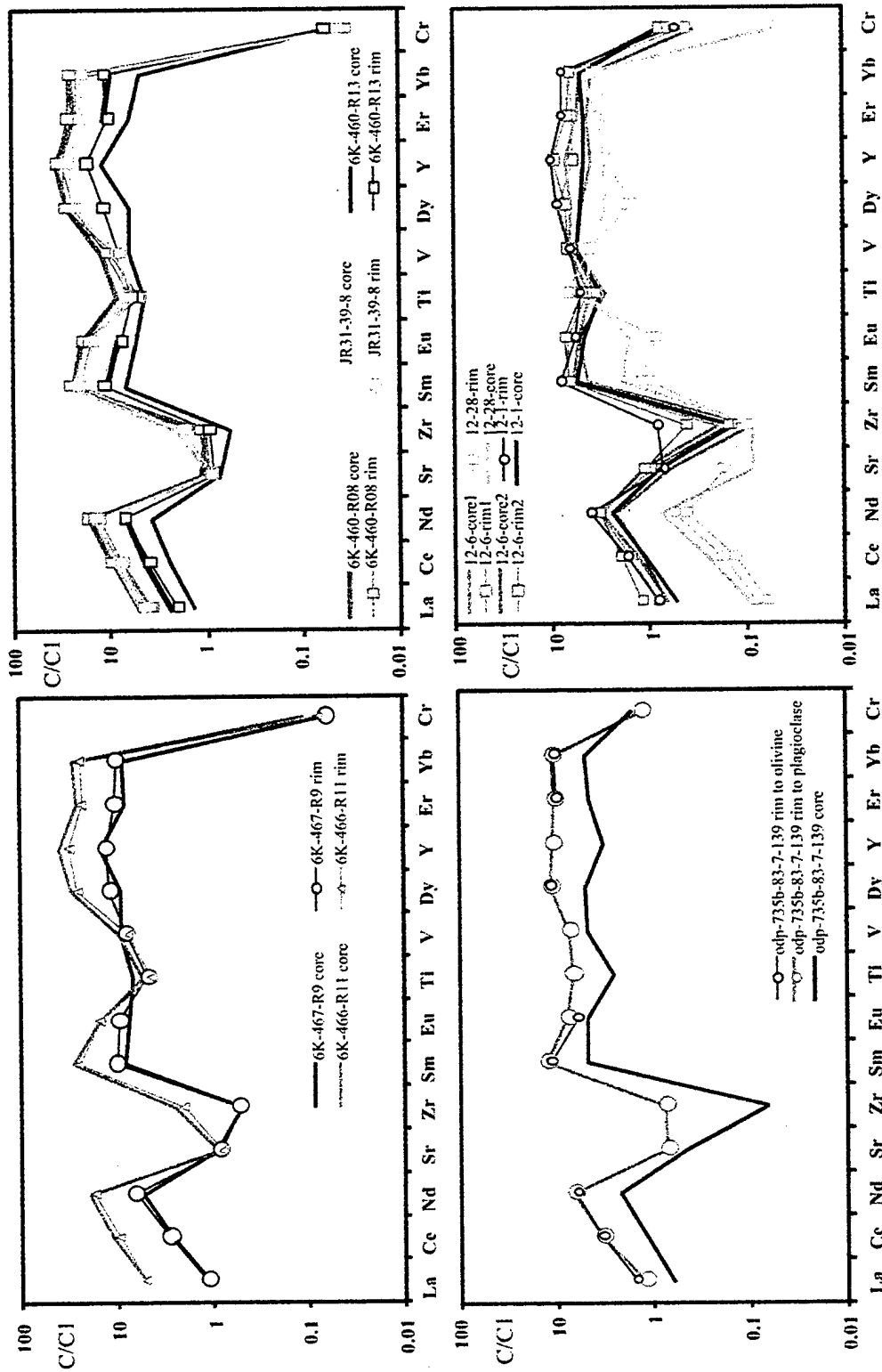


Figure 6-1: Spider diagrams for the augites in this study. Concentrations are normalized to that of C1 chondrite (Taylor and MacLennan, 1985). The sample-areas are described in Chapter 5.

Evolution of Oceanic Gabbros: In-situ and Ancient Examples

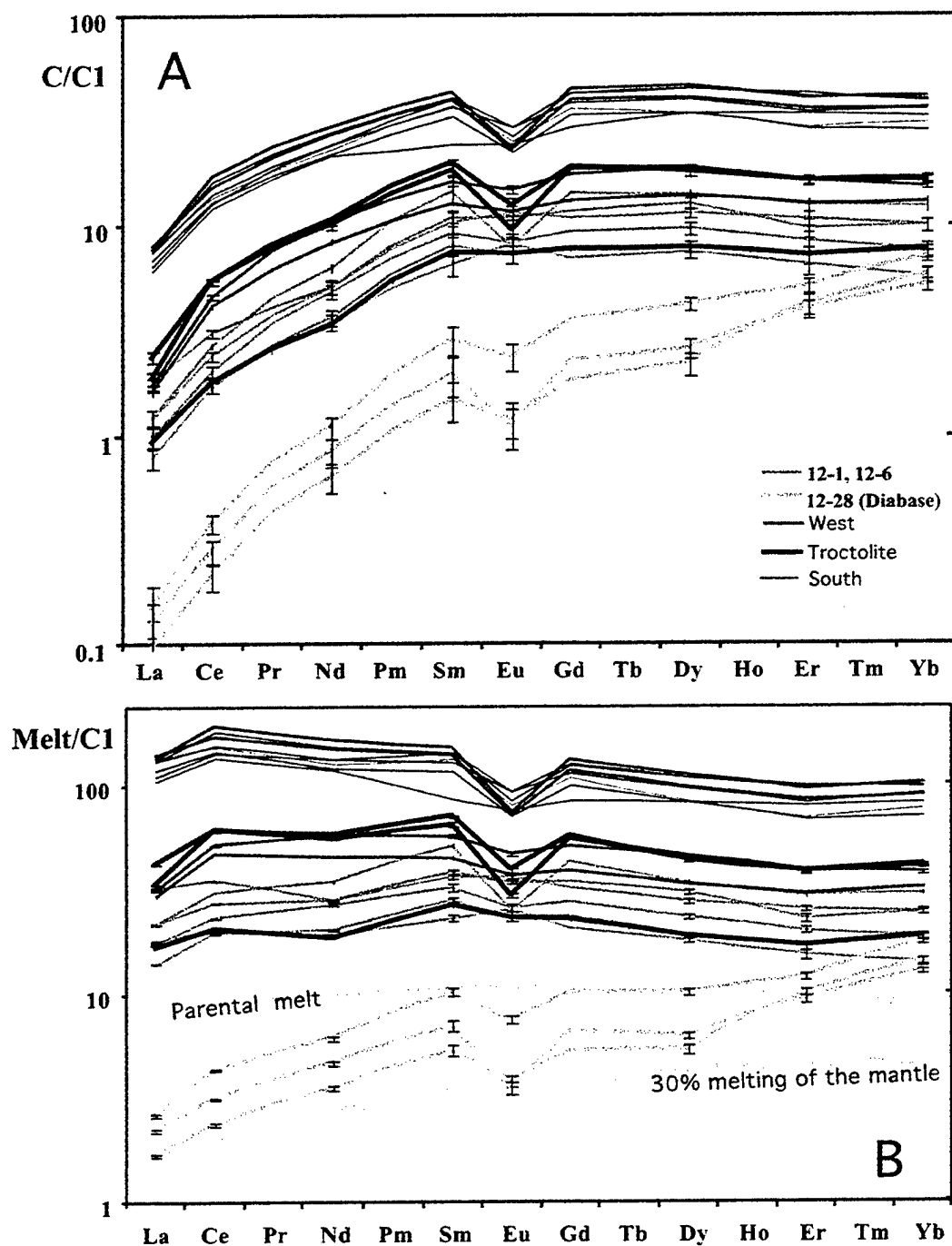


Figure 6-2: A: REE-plots for the augites in this study. The error-bars indicate 1σ . B: The hypothetical melts in equilibrium with the gabbro augite-crystals. Two parental melts, made from 5.5 and 30% batch equilibrium melting of the depleted upper mantle (Workman, in prep) are also shown. The partition coefficients used are from Bédard (1994).

Evolution of Oceanic Gabbros: In-situ and Ancient Examples

what was found by Muller et al. (1997) by seismic surveying, if one assumes that the seismic Moho represents the crust-mantle boundary.

Inspection of Figure 6-2A shows three main groups of augite-crystals: the JR31-12-28, diabase with very low concentrations; the primitive and intermediate gabbros, which show equilibrium melt REE-patterns nearly parallel to the parental melt; and the very evolved rocks with a more LREE-enriched pattern. Figure 6-3 shows the evolution of the liquid-lines of descent for magmas calculated for 1) fractional crystallization (i.e. Rayleigh fractionation); 2) In-situ crystallization (Langmuir, 1989) where magmas crystallize and create a mush along the walls of the magma-chamber, and varying fractions of the interstitial melt (f) returns to the main magma body; and 3) Assimilation-Fractionation-Crystallization (AFC; DePaolo, 1981) by assimilation of a typical Atlantis Bank olivine-gabbro (Table 7-2). The liquid-lines of descent represent 0-90% crystallization relative to the primitive MORB calculated from DMM. The bulk-partition coefficients are calculated assuming fractionation of 35% augite, 15% olivine and 50% plagioclase for all stages of crystallization. Figure 6-3A shows that in-situ crystallization where a small fraction of the interstitial melt is returned to the magma-body, or AFC, where the mass assimilated is similar to the mass crystallized, describe the evolution of the augites better than simple fractional crystallization. Figure 6-3B suggests that none of these models work very well, and that the gabbros have complex, multi-stage evolutions than can be modeled for these processes. The best fitting AFC and In-situ-model are further investigated in Figure 6-4. If AFC or in-situ fractionation controlled the melt evolution, then the range of trace-elements concentrations formed in the gabbros represents >50% - 95% crystallization. This is consistent with the model result developed in Chapter 3, and the melt budget of more than 4.4-km crust produced at Atlantis Bank, in contrast to the conclusions of Robinson et al. (2001).

The very refractory-looking diabase augite is not explained by any of the fractionation models, even though the augites are fairly evolved with Mg#s as low as 75 (see Figure 5-11C). In fact, it is almost impossible to produce such a primitive, depleted composition by accumulated melt of a MORB-source mantle. Figure 6-2B shows a melt produced by 30% melting of primitive upper mantle, and although the composition has as low concentration as JR31-12-28, it is nowhere near as depleted in LREE relative to.

Evolution of Oceanic Gabbros: In-situ and Ancient Examples

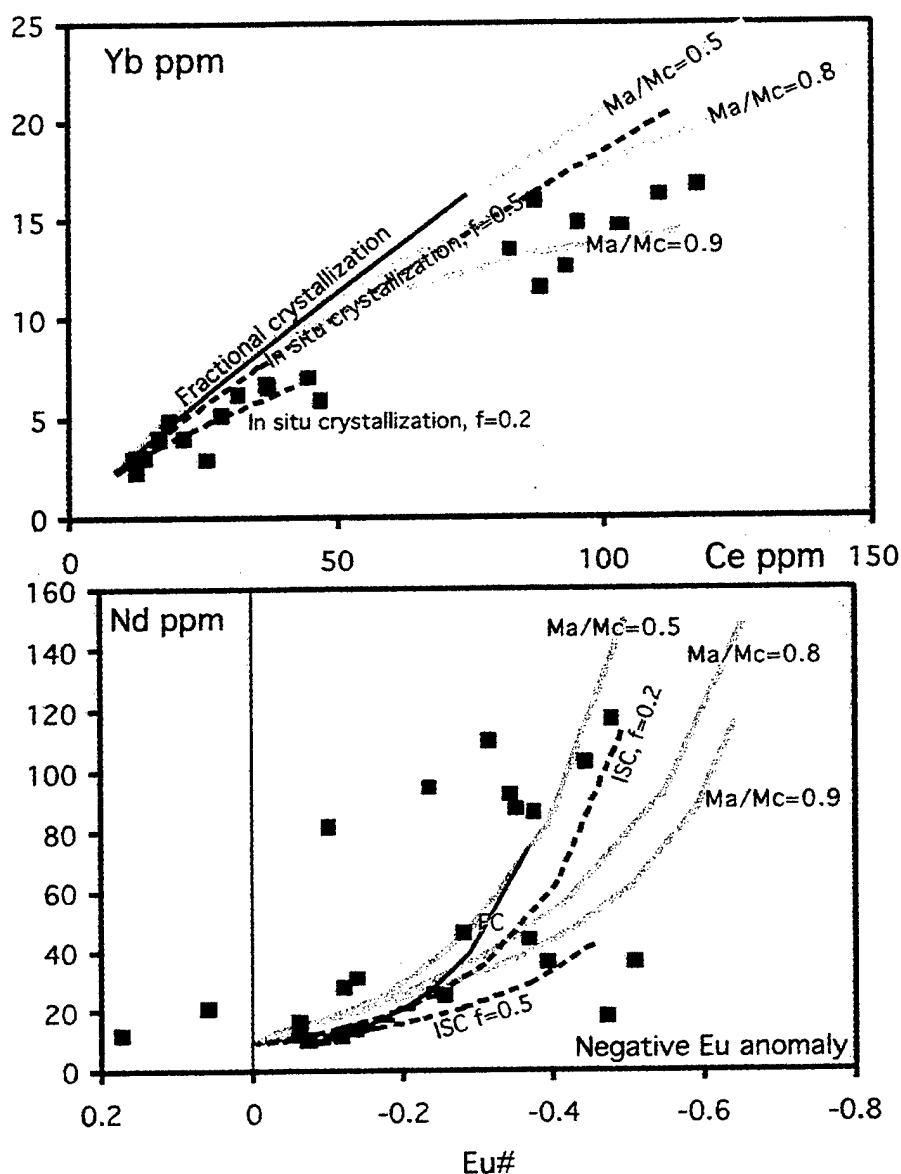


Figure 6-3: Crystallization models for our samples compared to the hypothetical melts in equilibrium with the augites. A: It appears that the AFC-models and in-situ fractionation fit the augite-melts better than a pure fractional crystallization model. "Ma"=Mass assimilated; "Mc"=Mass crystallized; "f" = fraction of melt returned from the mush-zone to the magma chamber; $Eu\# = (Eu^* - ([Sm^* + Gd^*] \times 0.5) - 1)$, where Eu^* , Sm^* and Gd^* represent chondrite-normalized values. Negative $Eu\#$'s are negative Eu-anomalies, indicating fractionation of plagioclase from the melt.

Evolution of Oceanic Gabbros: In-situ and Ancient Examples

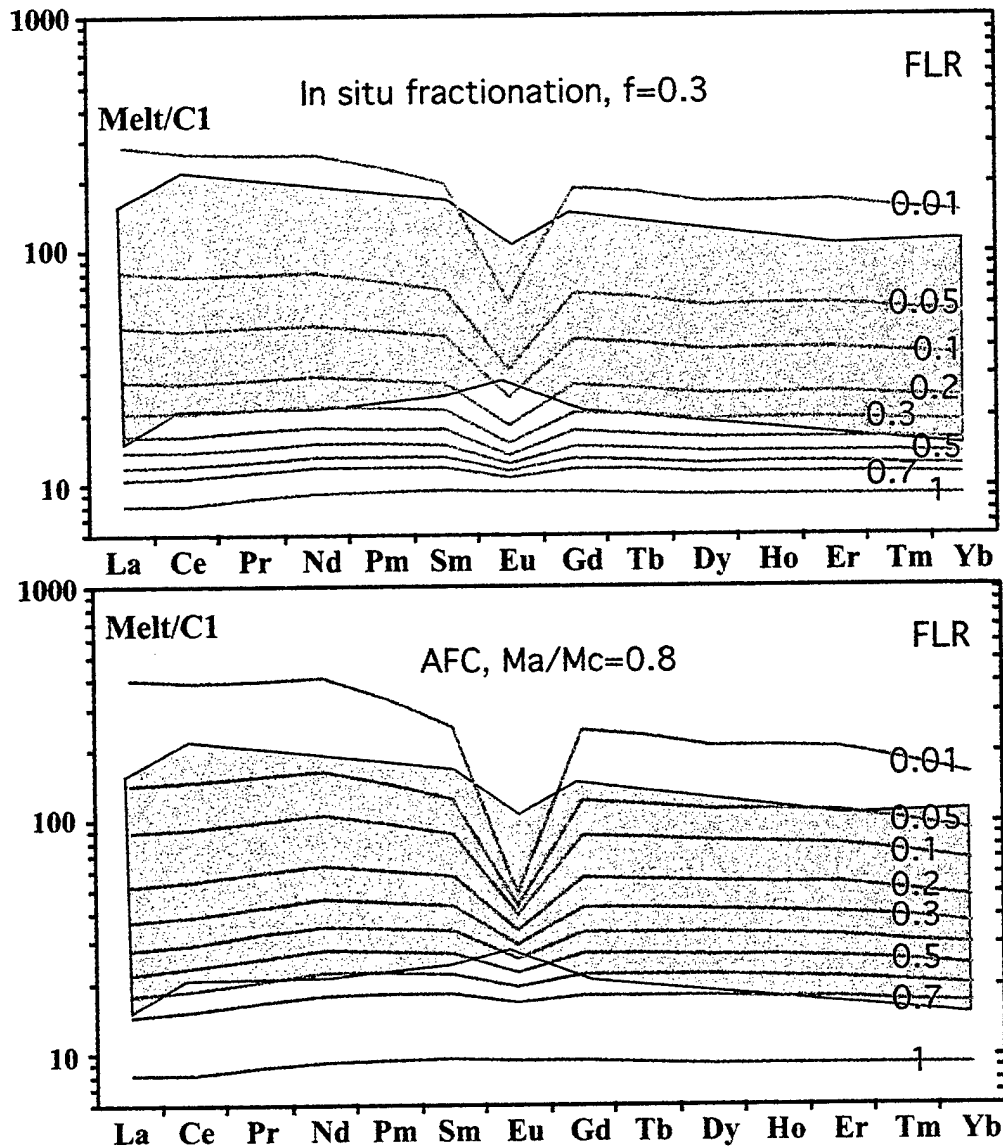


Figure 6-4: REE-element plots for crystallization models (normalized to the C1 chondrite of Taylor and MacLennan (1995)). FLR=Fraction of liquid remaining, the gray lines describe degree of fractionation. FLR(0.05) = 95% crystallized relative to the original melt. The gray field outlines the theoretical melt compositions based on the composition of augite in the gabbros (note that the diabase-data are excluded). A: In-situ fractionation, where only 30% of the interstitial melt is returned from the mush-zone to the central magma. B: The fractionation and crystallization of the DMM-derived melt happens during bulk-assimilation of the average olivine gabbro from Hole 735B (Natland and Dick, 1992). The diagram demonstrates that even if the melt experienced assimilation of pre-existing olivine-gabbros, the gabbros represent melts that first fractionated 50% elsewhere, but then crystallized to near completion.

Evolution of Oceanic Gabbros: In-situ and Ancient Examples

HREE. This is not the first diabase augite analyzed with such refractory compositions. Dick and Johnson (1995) found similarly depleted diopside and augite minerals from dikes in Hole 504B near the East Pacific Rise. They suggested that the strongly depleted patterns were due crystal-growth phenomena and heterogeneous nucleation in the early stages of melt crystallization prior to intrusion of the dikes as explored by Shimizu (1983, 1990). In the case examined by Dick and Johnson (1995), however, their augite phenocrysts were strongly sector zoned with respect to trace-elements. This is not the case here. In addition, as stated by Shimizu (1990) the kinetic effects mostly affect the M1 site of clinopyroxene, where the high field-strength elements reside (e.g. Ti, V, Sr, Cr). The M2-site is the host-site for the REE, and is not affected by kinetics of crystallization in the same way. It is likely that the theoretical melt composition derived from the diabase augite-composition are similar to the actual melt composition that produced it, representing a very depleted melt that did not mix with the other mantle-derived melts on ascent. The theoretical melt composition determined from the augite-composition is not as depleted as the "ultra-depleted melt" from Sobolev and Shimizu (1993). However, in this thesis, we have explored the effects of melts interacting with ascending magmas from the viewpoint of the gabbros. We find extreme variations in the magmatic evolution of gabbros, and it is not surprising that dikes, which are melt conduits from the lower to the upper crust, show diverse compositions too.

It can be rightfully argued that Chapter 3 to 5 of this thesis have shown that gabbroic augites are not the ideal candidates for deduction of the evolution of the melts in lower ocean crust environments, as they appear to be out of equilibrium with the rest of the cumulate. This is also evident from Figure 6-3B. The whole-rock trace-element contents of the gabbros represent the cumulate-minerals together with interstitial residual melt-fractions, and may also not directly demonstrate the evolution of the system. Ideally, we would like to support this type of calculation with analyses of all the minerals in each studied sample. Coogan et al. (2000) did show that the melt that produced the plagioclase was different from the one that produced the augite. In addition, the trace-element composition of high-valent ions in primitive olivine (potentially experiencing slower solid-state diffusion than Fe and Mg) can provide information on the evolution of these gabbroic rocks. If detailed geochemical studies are performed in gabbroic samples,

Evolution of Oceanic Gabbros: In-situ and Ancient Examples

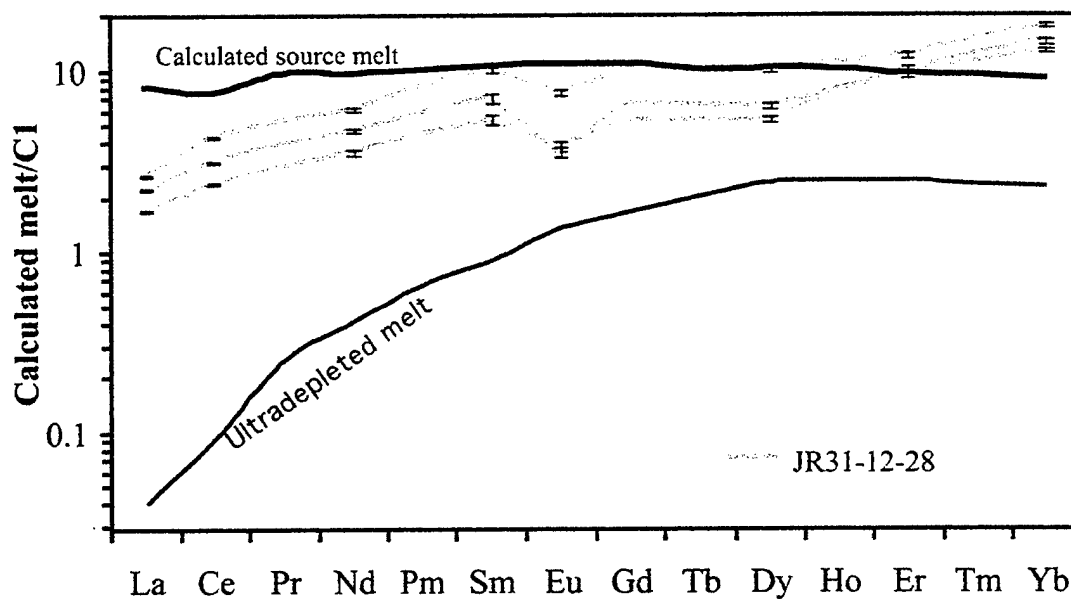


Figure 6-5: The augites-compositions from the diabase-dike represent melt-compositions much more depleted than the gabbroic rocks, and the assumed parental melt. However, the melt-compositions are not as refractive as the Ultra-depleted melt of Sobolev and Shimizu (1993).

Evolution of Oceanic Gabbros: In-situ and Ancient Examples

the entire accretion-history, including early precipitation of the initial gabbro, the assimilation of the lower crust into ascending magmas and subsequent crystallization of the hybrid magma might be deconvolved. However, it is clear that the cores and rims of the gabbro augites in this study do show complex evolution that must involve more than a simple fractional crystallization accretion model.

5 Conclusion

The trace element compositions of augites in Atlantis Bank gabbros show that they cannot have formed by fractional crystallization of olivine, plagioclase and clinopyroxene alone, as the rocks have increasing LREE/HREE ratios with fractionation. The gabbros may have crystallized by in-situ crystallization, or by significant assimilation of olivine gabbros. Even if the magmas have assimilated host-rocks upon ascent, they still must have crystallized >50% elsewhere before emplacement. The trace-element and REE-compositions show that the gabbros therefore represent melts that had crystallized > 50% -95% relative to a parental magma in equilibrium with the mantle. This agrees well with our previous results using major-elements in Chapter 3, and our estimate for the crustal thickness at Atlantis Bank is still valid.

One diabase-dike has augite-crystals representing a much more depleted melt-composition than the melts that produced gabbros. No known mineral-fractionation can produce the very depleted and refractory REE-pattern seen in this rock and we suggest that this dike represents depleted melts that did not mix with the melts that formed the gabbros sampled on and around Hole 735B.

Evolution of Oceanic Gabbros: In-situ and Ancient Examples

Table 2: Partition Coefficients and starting compositions used in this study					
	Augite	Plagioclase	Olivine	Parental melt composition	Assimilated olivine gabbro
La	0.0536	0.124	0.003	2.97	1.06
Ce	0.0858	0.117	0.004	7.26	3.21
Sr	0.06	1.8	0.008	97	164
P	0.13	0.08	0.008	742	99
Nd	0.187	0.068	0.01	6.90	3.19
Sm	0.291	0.058	0.02	2.45	1.12
Zr	0.26	0.01	0.02	59.0	24.7
Ti	0.34	0.04	0.02	6523	2420
Eu	0.33	0.37	0.02	0.94	0.59
Gd	0.37	0.04	0.03	3.32	1.66
Tb	0.40	0.03	0.035	0.59	0.30
Dy	0.38	0.03	0.034	3.90	2.02
Y	0.41	0.03	0.033	24.1	11.63
Er	0.39	0.01	0.04	2.37	1.24
Yb	0.43	0.01	0.05	2.23	1.16
Cr	3.8	0.02	1.25	389	224
Ni	2	0.04	10	97	108
V	3.1	0.03	0.03	273	153
Sc	3.9	0	0.16	36.9	36.5

Evolution of Oceanic Gabbros: In-situ and Ancient Examples

References:

- Coogan LA, Gillis KM, MacLeod CJ, Thompson GM, Hékinian R, 2002: Petrology and geochemistry of the lower ocean crust form at the East Pacific Rise and exposed at Hess Deep: A synthesis and new results. *Geochem. Geophys. Geosyst.*, 3(11) 8604, doi: 101029/2001GC000230.
- Coogan LA, Kempton PD, Saunders AD, Norry MJ, 2000: Melt aggregation within the crust beneath the Mid-Atlantic Ridge: evidence from plagioclase and clinopyroxene major and trace element compositions. *Earth Planet Sci Lett* 176:245-257.
- Coogan LA, MacLeod CJ, Dick HJB, Edwards SJ, Kvassnes A, Natland JH, Robinson PT, Thompson G, O'Hara MJ, 2001: Whole-rock geochemistry of gabbros from the Southwest Indian Ridge: constraint on geochemical fractionations between the upper and lower oceanic crust and magma chamber processes at (very) slow-spreading ridges. *Chem Geol* 178:1-22.
- DePaolo DJ, 1981: Trace element and isotopic effects on combined wallrock assimilation and fractional crystallization. *Earth Planet Sci Lett* 53:189-202.
- Dick HJB, Johnson KTM, 1995: 11. REE and trace-element composition of clinopyroxene megacrysts, xenocrysts, and phenocrysts in two diabase dikes from Leg 140, Hole 504B. In: Erzinger J, Becker K, Dick HJB, and Stokking LB (eds). *Proc Ocean Drilling Progr* 137/140: 121-130.
- Dixon JE, Clague DA, 1986: Gabbroic xenoliths and host ferrobasalts from the southern Juan de Fuca Ridge. *Journ Geophys Res* 91 (B3): 3795-3820.
- Langmuir, CH, 1989: Geochemical consequences of in situ differentiation. *Nature*, 340, 199-205.
- Muller MR, Robinson CJ, Minshull TA, White RS, Bickle MJ, 1997: Thin crust beneath Ocean Drilling Program Borehole 735B at the Southwest Indian Ridge? *Earth Planet Sci Lett* 148 (1-2): 93-107.
- Natland JH, Dick HJB, 2002: Stratigraphy and Composition of Gabbros Drilled in Ocean Drilling Program Hole 735B, Southwest Indian Ridge: A synthesis of Geochemical Data. In Natland JH, Dick HJB, Miller DJ, Von Herzen RP (eds) *Proceedings of the Ocean Drilling Program, Scientific Results Volume 176*. 1-69 (CD-ROM).
- Robinson CJ, Bickle MJ, Minshull TA, White RS, Nichols ARL, 2001: Low degree melting under the Southwest Indian Ridge: the roles of mantle temperature, conductive cooling and wet melting. *Earth Planet Sci Lett* 188: 383-398.
- Sobolev AV, Shimizu N, 1993: Ultra-depleted primary melt included in an olivine from the Mid-Atlantic Ridge. *Nature* 363: 151-154.
- Shimizu N, 1983: Interface kinetics and trace-element distribution between phenocrysts and magma. In: Augustithis SS (ed): *The significance of trace elements in solving petrogenetic problems and controversies*: Athens (Theophrastus Publ) 175-195.
- Shimizu N, 1990: The oscillatory trace element zoning of augite phenocrysts. *Earth Sci Rev* 29: 27-37.
- Shimizu N, Hart SR, 1982: Applications of the ion microprobe to geochemistry and cosmochemistry. *Ann Rev Earth Planet Sci* 10: 483-526.
- Snow JE, 1993: The isotope geochemistry of abyssal peridotites and related rocks. Doctoral dissertation, Woods Hole Oceanographic Institution.
- Taylor RS, MacLennan SM, 1985: *The continental crust: its composition and evolution*. Blackwell, Oxford.

Chapter 7

Residual melt porosities in gabbros from Atlantis Bank

Abstract

We have developed a method for calculation of trapped melt-fractions in gabbros from the Southwest Indian Ridge from whole-rock analyses. We use published data for basaltic rocks to define the liquid-line of descent for REE, Ti and P, and major-elements. The model is calibrated with the use of in-situ mineral analyses mass-balanced with whole-rock compositions. We find that the trapped melt-fraction of ODP Hole 735B is ~15%. Eu-anomalies are inversely related to the trapped melt-fraction. This suggests that the whole-rock positive Eu-anomalies in Hole 735B, the signature of cumulate plagioclase, are masked by other REE's.

1 Introduction

Lower crustal magmatic rocks are thought to consist of cumulus minerals that precipitated from magma and accumulated along the roof, walls and floors of intrusions. Depending on the closeness of packing of the crystals, melts become trapped in the pore-spaces and may not be able to escape. This "trapped melt"-fraction, or residual melt porosity contributes to the whole-rock composition, possibly modifying pre-existing cumulate minerals, and crystallize interstitially to form the inter-cumulus minerals. Methods to identify and calculate the residual melt-fractions are complicated, poorly constrained, and frequently criticized (Natland et al, 1991; Coogan et al., 2001; Bédard, 1994).

We have directly estimated the amount of trapped melt gabbroic rocks using major-and trace-element mineral and whole-rock compositions of the gabbros and basaltic glasses from the area. We have then used our results to develop a more accurate and internally consistent method for calculating trapped melts at Atlantis Bank simply from whole-rock compositions, using the first method to calibrate it.

Evolution of Oceanic Gabbros: In-situ and Ancient Examples

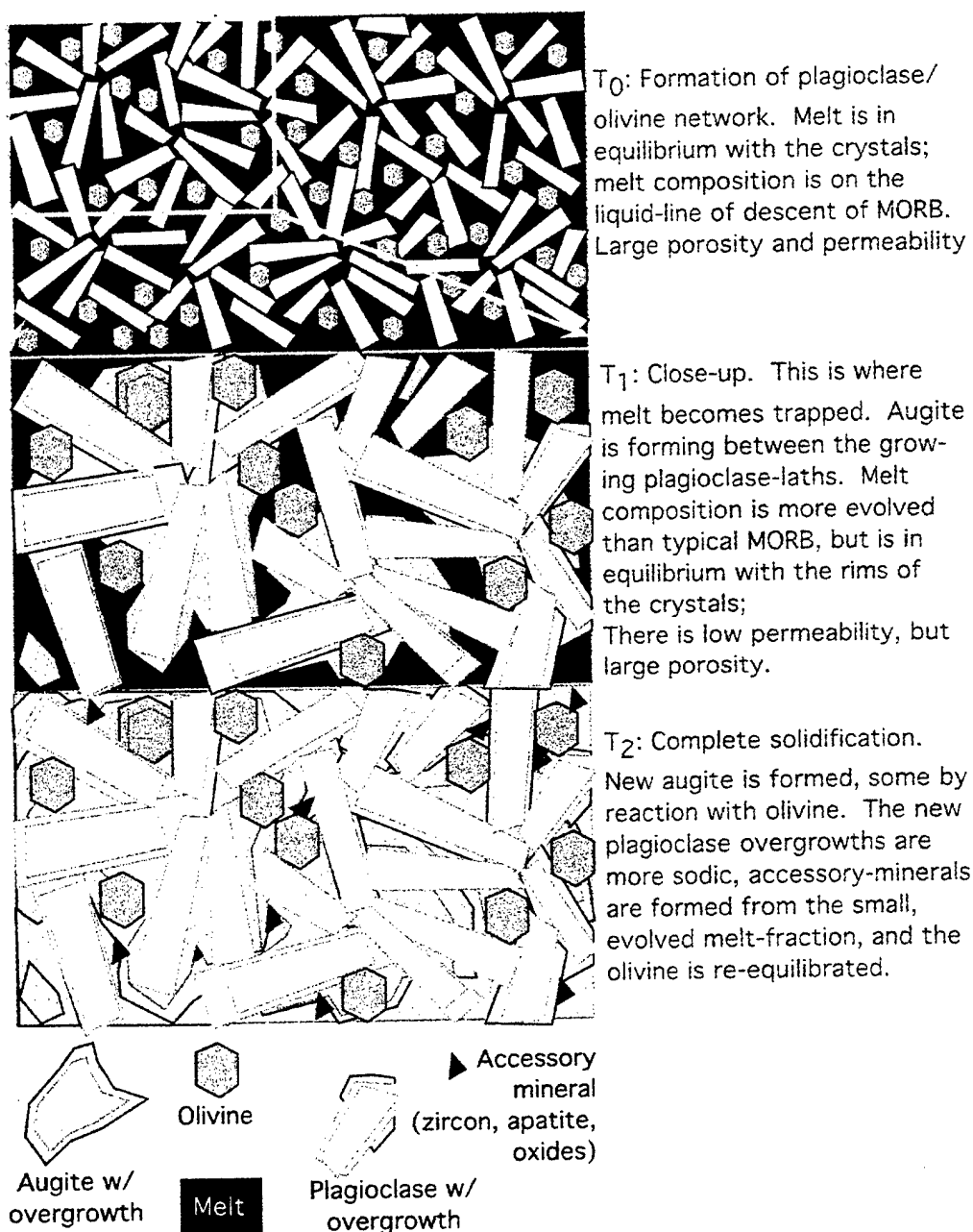


Figure 7-1: The formation of trapped melts. The figure is based on Wager et al. (1960).

2 Results

Our method for estimating the amount of trapped melt in oceanic gabbros is based on the approach by Natland et al. (1991). The theoretical accretion of an olivine-gabbro is outlined in Figure 7-1. At T_0 , plagioclase glomerocrysts form plagioclase-chains in a semi-rigid network. At this stage, the minerals are in equilibrium with the melt, and the network is permeable enough for the melts to flow through it and react with it. At T_1 , permeability is reduced due to overgrowth on the cumulate minerals and increased viscosity of the melt, and the interstitial melt is effectively trapped. The melts in between the minerals at this stage are what is calculated as the "residual melt porosities". This melt continues to form minerals in-situ, and will re-equilibrate with olivine. As nucleation of mineral-grains requires substantial under-cooling, the melt preferentially crystallizes on pre-existing grains. Therefore, the minerals develop evolved overgrowths, and the melt-pockets become smaller while the melt becomes more enriched in incompatible elements. At T_2 , solidification is complete. The remnants of the small, fractionated melt pockets are observed as the location of the most evolved plagioclase and augite, together with accessory minerals like zircon, magnetite, ilmenite and apatite. These accessory minerals contain most of the magma-budget for elements like Ti, P and REE's. Of the cumulus minerals (olivine, plagioclase and some of the augite), augite has the largest partition-coefficients for these elements. As it is difficult to discern how an augite grew without making very detailed maps of the elemental distribution, we have tried to estimate the composition at the time of melt-entrapment by analyzing both core and rim compositions for augite to get the potential range of the residual melt porosity. Ideally, we would like to have the trace-element compositions of plagioclase also, in order to estimate the internally consistent composition of the melt that fractionated the cumulates.

Natland et al. (1991) used glass-compositions from the Southwest Indian Ridge to estimate liquid-lines of descent for each element (TiO_2 , P_2O_5 and Zr) with respect to MgO. They related the bulk Mg# ($\text{Mg}/(\text{Mg}+\text{Fe}^{2+})$) of a given gabbro to the melt that crystallized it. TiO_2 in the rock vs. the theoretical amount in the liquid was used to get the fractional dilution of augite by plagioclase and olivine, in order to calculate excess Zr in the rock and thereby the amount of trapped melt in that cumulate.

Evolution of Oceanic Gabbros: In-situ and Ancient Examples

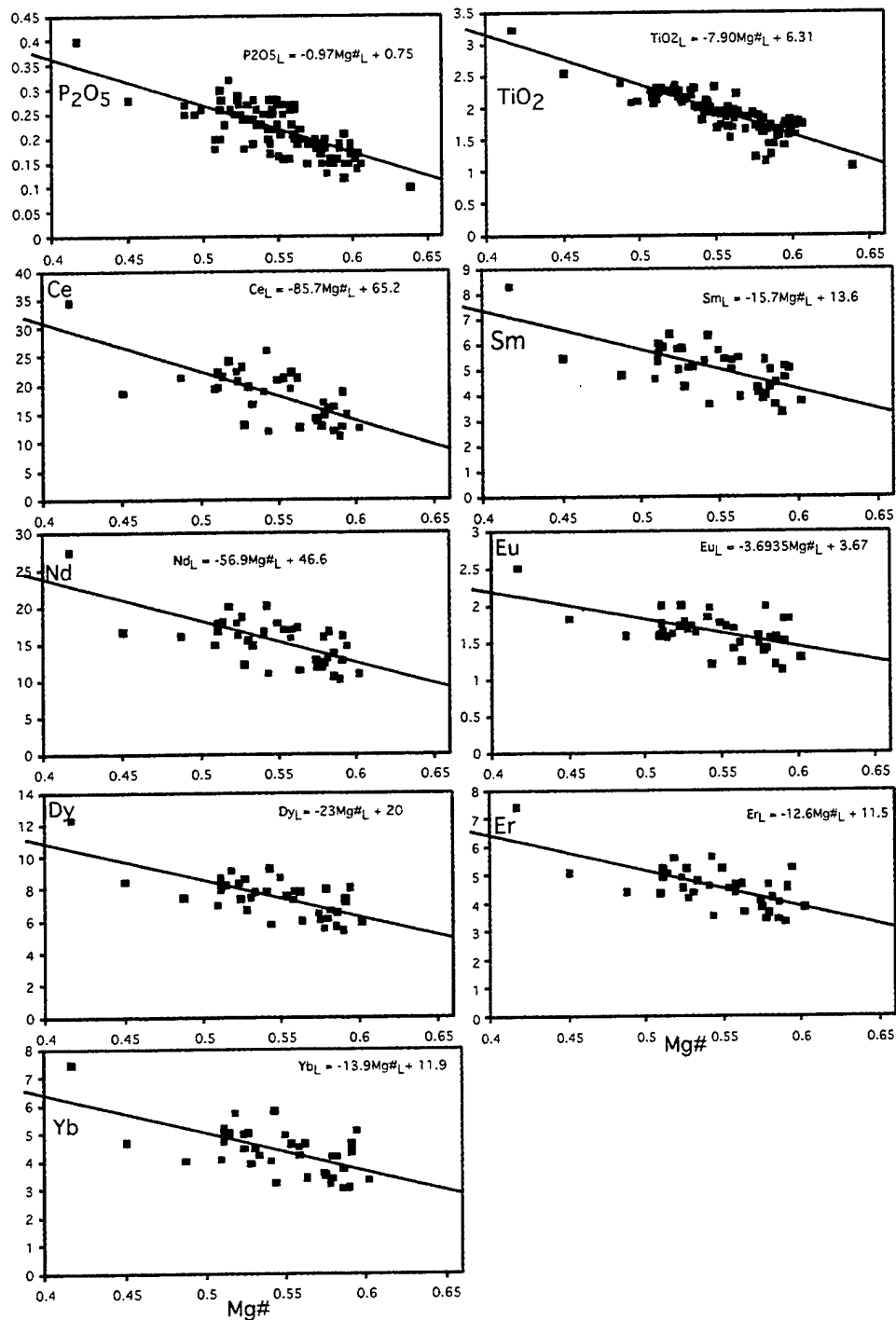


Figure 7-2: Liquid lines of descent for P₂O₅, TiO₂ and REE for basalts from Southwest Indian Ridge lavas from 25°-60°E (Mahoney et al., 1992; Le Roex et al., 1989; David et al., 2000). A least-squares fit is made for each element, and the equations are listed on each figure.

Evolution of Oceanic Gabbros: In-situ and Ancient Examples

Our model involves four steps:

- 1) It is necessary to find the composition of the interstitial melt at time of entrapment. We determined the liquid line of descent for the regional lavas with respect to P_2O_5 , TiO_2 and REE (Fig. 7-2; data from PetDB), just like Natland (op. cit) did. Therefore, if we know the Mg# of the melt, we can estimate the incompatible element content of that melt. Note that the trace-element composition at a given Mg# has a large variation and *visa versa*, thus any errors in the Mg#-estimate for the melt may not matter.
- 2) We found the Mg# of the interstitial melt by using the composition of augite in the gabbro, assuming $Kd_{augite/melt}^{Fe/Mg}$ of 0.23. With respect to the discussions of Chapter 3 and 5, a lower partition-coefficient will give us a higher Mg# of the melt, and will therefore give us slightly larger residual melt fractions. This partition-coefficient therefore provides minimum values. We have performed complete major-, and trace-element mineral composition analyses for all the samples in this study, while Coogan, et al. (2001) provide whole-rock compositions for three of these. We were therefore able to calibrate this well-constrained model to one for the whole-rock compositions. Thus, if the Mg# of the augite is not known, we find that a $Kd_{rock/melt}^{Fe/Mg}=0.32$ can be used to calculate the Mg# of the melt. This partition-coefficient was found by comparing the Mg#'s of the whole-rocks to those of augite, and fitting a $Kd_{rock/melt}^{Fe/Mg}$ to what would correspond to $Kd_{augite/melt}^{Fe/Mg}=0.23$. The whole-rock calculation will, of course, include the interstitial minerals, but again the range of REE along the liquid-lines of descent is large enough that a $Mg\#\pm 5$ is accurate enough to give a satisfying model result.
- 3) We calculated the modes of the rocks where we had complete analyses by mass-balance of the major-element mineral-compositions to the whole-rock composition. We found that the whole-rock norm-algorithm equations from Grove et al. (1992) provide adequate modes for our gabbros.
- 4) The residual melt porosities can therefore be calculated for each element using:

$$\text{Residual porosity} = 100 * \frac{C_{Rock} - C_{Mineral} * Mode_{Mineral}}{C_{Melt}}$$

Evolution of Oceanic Gabbros: In-situ and Ancient Examples

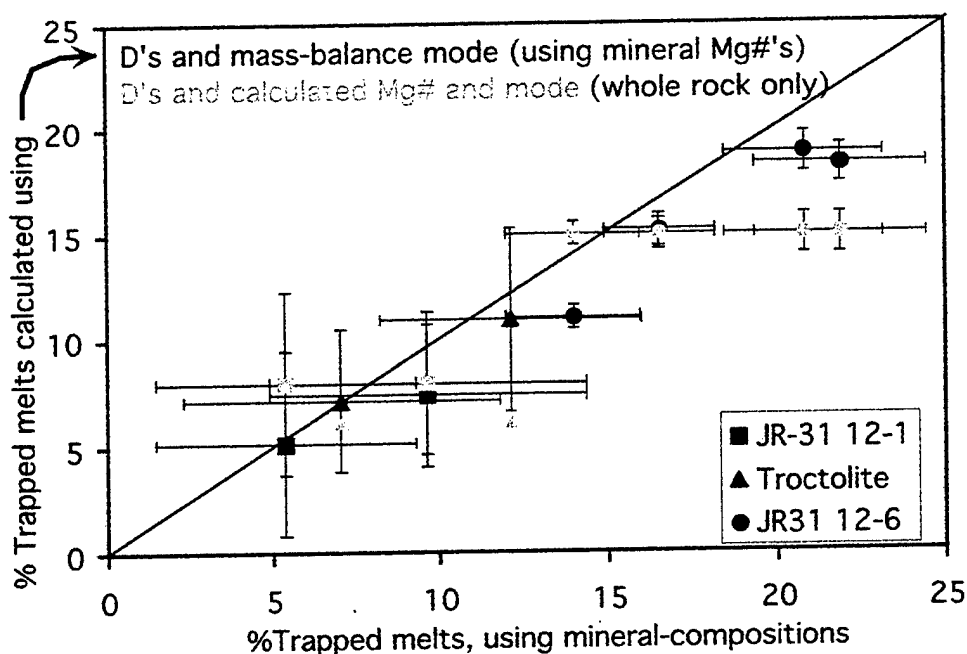


Figure 7-3: A comparison of the calculations for the residual melt porosity ("trapped melts") using the well-constrained method with mineral-compositions and the modes determined by mass-balance, to the whole-rock method (black symbols) and a method using the mass-balance mode and Mg#'s of the minerals and partition-coefficients with the LLD's to get the trace-element mineral-compositions (gray symbols). The mass-balance method gives negative residual-melt porosities for sample JR31 39-8. For each of the other samples (ODP-87-3, JR31 12-1, -6) the porosities are calculated for the cores and rims analyzed in each rock. For ODP-87-3, we used only Ti and P to find the residual melt porosity.

Evolution of Oceanic Gabbros: In-situ and Ancient Examples

$\text{Mode}_{\text{Mineral}}$ is the calculated mode of augite, and C_{rock} , C_{Mineral} and C_{Melt} are the concentration in the whole-rock, minerals (olivine, plagioclase and augite), and melt, respectively. For our calculations, it was assumed that olivine and plagioclase contain insignificant amounts of these incompatible trace elements (except for Eu in plagioclase). If the concentration in the augite and plagioclase is not known, it was calculated from the theoretical melts using the partition-coefficients in Table 7-2, Chapter 6 and the Mg# of the whole-rock. The results from the calculations for the rocks from which we had complete mineral-analyses are shown as basalt regressions in Figure 7-2 and Table 7-1 and an example of the calculations is shown in Table 7-2.

3 Discussion

We tested our whole-rock procedure for calculating residual melt porosities (using partition-coefficients, calculated modes (Grove et al., 1992) and Mg#'s) by comparing it to the more exact method involving the actual mineral-compositions, and find that the results generally agree for all the trace-elements (Fig. 7-3). The 1σ for the average residual melt-porosities using 7 different REE's is generally less than 5%. Unfortunately, our technique is not valid for the evolved oxide gabbros (e.g. JR31 39-8) as the oxides change the Mg# of the whole-rock, and increases the TiO_2 content dramatically. The technique seems valid for the more primitive olivine-gabbros, however, and the results for the cores and rims using the mineral-composition method bracket the results from the whole-rock method. Our results are in agreement with the technique developed by Bédard (1994).

We have applied our technique to the large whole-rock data-sets from Atlantis Bank. We have, obviously, excluded ilmenite and apatite cumulates, and the felsic veins from these calculations. The results are presented in Figure 7-4. We find that for Hole 735B (excluding the most evolved gabbros) the average trapped melt-fraction is 15%, and the average standard deviation of 7 REE's for each measurement is 3%. We also find an exponential inverse correlation between the amount of trapped melts and Eu-anomalies ($\text{Eu\#} = (\text{Eu}^* - ([\text{Sm}^* + \text{Gd}^*] \times 0.5) - 1$; Pedersen et al. (1996)), where Eu^* , Sm^* and Gd^* represent chondrite-normalized values (Taylor and MacLennan, 1985). Positive

Table 7-1: Residual melt fractions calculated by whole-rock compositions, and by the well-constrained method involving the major and trace-element concentrations of the minerals and whole-rock

	Well-							
	Whole-rock method	JR31 12-6 method	JR31 12-6 grain1 rim1 core	JR31 12-6 rim1 core	JR31 12-6 core1 rim1 core	JR31 12-6 rim2 core2	JR31 12-6 rim core	JR31 12-6 rim core
	Mineral composition:							
P ₂ O ₅	0.02	0.03	0.02	0.02	0.02	0.02	0.02	0.02
TiO ₂	0.24	0.34	0.59	0.59	0.59	0.59	0.59	0.59
Ce	1.74	3.36	3.02	3.02	3.02	3.02	3.02	3.02
Nd	1.69	3.26	3.43	3.43	3.43	3.43	3.43	3.43
Sm	0.64	1.24	1.44	1.44	1.44	1.44	1.44	1.44
Eu	0.43	0.72	0.85	0.85	0.85	0.85	0.85	0.85
Dy	1.10	2.24	2.68	2.68	2.68	2.68	2.68	2.68
Er	0.71	1.38	1.69	1.69	1.69	1.69	1.69	1.69
Yb	0.65	1.25	1.56	1.56	1.56	1.56	1.56	1.56
Mg#	79.5	75.6	64.2	64.2	64.2	64.2	64.2	64.2
Mg#, melt	55.4	49.8	36.5	36.5	36.5	36.5	36.5	36.5
Mode augite	0.16	0.22	0.19	0.19	0.19	0.19	0.19	0.19
Theoretical melt composition:								
P ₂ O ₅	0.21	0.40	0.27	0.27	0.27	0.27	0.27	0.27
TiO ₂	1.9	3.4	2.4	2.4	2.4	2.4	2.4	2.4
Ce	18	34	23	23	23	23	23	23
Nd	4.9	7.9	5.8	5.8	5.8	5.8	5.8	5.8
Sm	1.5	2.6	1.8	1.8	1.8	1.8	1.8	1.8
Eu	1.6	2.3	1.8	1.8	1.8	1.8	1.8	1.8
Dy	7.4	11.6	8.6	8.6	8.6	8.6	8.6	8.6
Er	4.5	6.8	5.2	5.2	5.2	5.2	5.2	5.2
Yb	4.3	6.8	5.0	5.0	5.0	5.0	5.0	5.0
% Residual trapped melts, on the basis of:								
P ₂ O ₅	8	4	10	10	10	10	10	10
TiO ₂	7	13	15	15	15	15	15	15
Ce	5	6	10	10	10	10	10	10
Nd	8	10	14	14	14	14	14	14
Sm	9	13	15	15	15	15	15	15
Eu	3	11	11	11	11	11	11	11
Dy	9	15	17	17	17	17	17	17
Er	9	17	17	17	17	17	17	17
Yb	9	15	16	16	16	16	16	16
Average	7	12	14	14	14	14	14	14
σ	2	4	3	3	3	3	3	3

Evolution of Oceanic Gabbros: In-situ and Ancient Examples

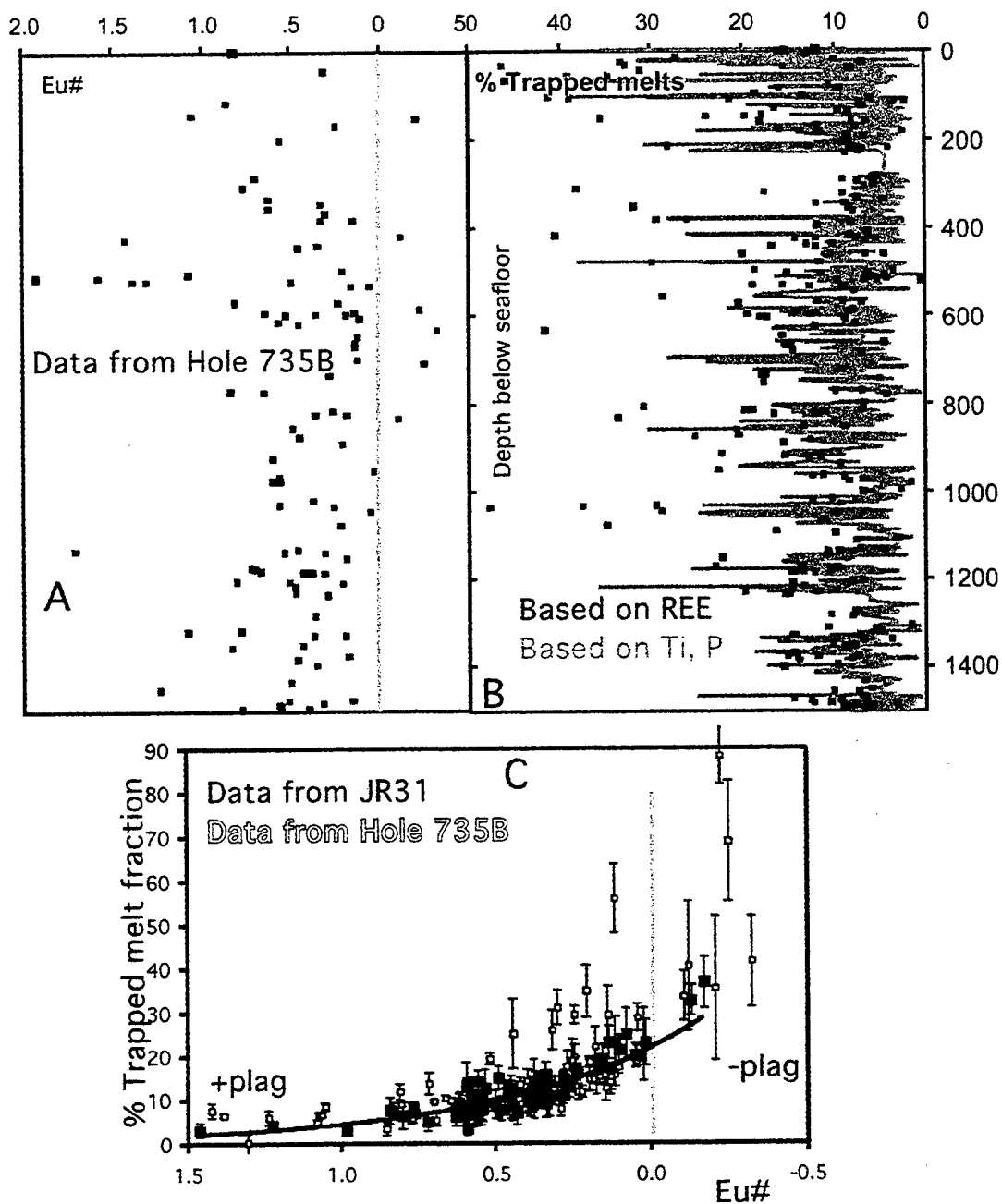


Figure 7-4: Trapped melt fractions from ODP Hole 735B. A: Eu# anomalies for Hole 735B gabbros based on whole rock analyses (Natland and Dick, 2002). B: Residual-melt porosities calculated from whole-rock composition for Hole 735B gabbros based on the average results for REE, and for Ti and P. C: The correlation between Eu# and the residual melt porosity in Hole 735B and in the gabbros around Atlantis Bank.

Evolution of Oceanic Gabbros: In-situ and Ancient Examples

and negative Eu-anomalies are thought to indicate accumulated or removed plagioclase in a rock, respectively. In Hole 735B, however, it seems that the Eu#'s are more a function of the extent of trapped melt than they are of plagioclase accumulation, and can therefore act as a proxy for residual melt porosity.

4 Conclusion

We have developed a technique for calculating residual melt porosity for oceanic gabbros at the Southwest Indian Ridge from whole-rock analyses of major-elements with rare-earth elements, Ti and P. The model is calibrated with the use of in-situ mineral analyses. We find that the trapped melt-fraction of Hole 735B is ~15%. The Eu-anomalies are inversely related to the trapped melt-fraction, possibly indicating that the Eu# in Hole 735B is masked by the abundance of other REE's in the whole-rock compositions, as is often seen in diabase-dikes.

Evolution of Oceanic Gabbros: In-situ and Ancient Examples

References:

- Bedard JH, 1994: A procedure for calculating the equilibrium distribution of trace-elements among the minerals of cumulate rocks, and the concentration of trace-elements in the coexisting liquids. *Chemical Geology* 118: 143-153.
- Coogan LA, MacLeod CJ, Dick HJB, Edwards SJ, Kvassnes A, Natland JH, Robinson PT, Thompson G, O'Hara MJ, 2001: Whole-rock geochemistry of gabbros from the Southwest Indian Ridge: constraint on geochemical fractionations between the upper and lower oceanic crust and magma chamber processes at (very) slow-spreading ridges. *Chem Geol* 178:1-22.
- David K, Schiano P, Allegre CJ, 2000: Assessment of the Zr/Hf fractionation in oceanic basalts and continental materials during petrogenetic processes. *Earth Planet Sci Lett* 178: 285-301.
- Grove TL, Kinzler RJ, Bryan WB, 1992: Fractionation of mid-ocean ridge basalts. In: *Mantle flow and melt generation at mid-ocean ridges*, *Geophys monogr* 71: 281-310.
- Le Roex AP, Dick HJB, Erlank AJ, Reid AM, Frey FA, Hart SR, 1989: Geochemistry, mineralogy and petrogenesis of lavas erupted along the Southwest Indian Ridge between the Bouvet Triple Junction and 11°E. *Journ Petrol* 24: 267-318.
- Mahoney JJ, Le Roex AP, Peng Z, Fisher RL, Natland JH, 1992: Southwestern limits of Indian Ocean Ridge mantle and the origin of low 206Pb/204Pb mid-ocean ridge basalt: Isotope systematics of the central Southwest Indian Ridge (17°-50°E). *Journ Geophys Res* 97: 19771- 19790.
- Natland JH, Dick HJB, 2002: Stratigraphy and Composition of Gabbros Drilled in Ocean Drilling Program Hole 735B, Southwest Indian Ridge: A synthesis of Geochemical Data. In Natland JH, Dick HJB, Miller DJ, Von Herzen RP (eds) *Proceedings of the Ocean Drilling Program, Scientific Results Volume 176*. 1-69 (CD-ROM).
- Natland JH, Meyer PS, Dick HJB, Bloomer SH, 1991: Magmatic oxides and sulfides in gabbroic rocks from Hole 735B and the later development of the liquid line of descent. In: Von Herzen RP, Robinson PT et al., *Proc ODP, Sci Res*, 118: College station, TX (Ocean Drilling Program): 75-111.
- Pedersen RBS, Malpas J, Falloon, T, 1996:1. Petrology and geochemistry of gabbroic and related rocks from site 894, Hess Deep. In: Mével C, Gillis KM, Allan JF, Meyer PS (eds) *Proceedings of the Ocean Drilling Program, Scientific Results*, 147: 3-19.
- Taylor RS, MacLennan SM, 1985: *The continental crust: its composition and evolution*. Blackwell, Oxford.
- Wager LR, Brown GM, Wadsworth WJ, 1960: Types of igneous cumulates. *Journ Petrol* 1: 73-85.

Evolution of Oceanic Gabbros: In-situ and Ancient Examples

Table 7-2: An example of the residual melt fraction calculation for JR31-12-1 calculated for Dy.	
Method of calculation when the mineral-compositions are available	
Calculation	Result
Determine the Mg# of the melt on the basis of augite compositions: $Mg\#_{melt} = \frac{Mg\#_{augite} * 0.23}{1 - Mg\#_{augite} + Mg\#_{augite} * 0.23}$	For the augite: Mg# core 0.86 => Mg# melt = 0.59 Mg# rim 0.84 => Mg# melt = 0.55
Determine the Dy-content for the melt on the basis of the Mg# $Dy_{melt} = -23 * Mg\#_{melt} + 20$	Dy in the melt (core) = 7ppm Dy in the melt (rim) = 8ppm
Need to know: Augite norm based on mass-balance = 0.24 Measured Dy in core 1.9 ppm Measured Dy in rim 3.4 ppm Whole-rock content of Dy = 1.1 ppm	
$\text{Residual porosity} = 100 * \frac{C_{Rock} - C_{Mineral} * Mode_{Mineral}}{C_{Melt}}$	Residual porosity for the Core = $100 * (1.1 - (1.9 * 0.24)) / 7 = 9.2\%$ Rim = $100 * (1.1 - (3.4 * 0.24)) / 8 = 4.1\%$
Method of calculation when only the whole-rock compositions are available	
$Mg\#_{melt} = \frac{Mg\#_{rock} * 0.32}{1 - Mg\#_{rock} + Mg\#_{rock} * 0.32}$	Mg# (rock) = 0.795, => Mg# melt = 0.55
From Grove et al. (1992): Recalculate whole - rock composition from weight % oxides to mol %, and Al, Fe ³⁺ , K, Na and P as : $AlO_{1.5}$, $K_{0.5}O$, $Na_{0.5}O$ and $PO_{2.5}$. Then combine molar MgO and FeO to FMO and $K_{0.5}O$, $Na_{0.5}O$ to Alk. $Sum = SiO_2 - CaO - 2 * Alk + Cr_2O_3 + TiO_2 + 2 * PO_{2.5} + FeO_{1.5}$ $Quartz = [SiO_2 - 0.5 * FMO - 1.5 * CaO - 0.25 * AlO_{1.5} - 2.75 * Alk + 0.5 * Cr_2O_3 + 0.5 * TiO_2 + 2.5 * PO_{2.5}] / Sum$ $Plagioclase = 4 * [AlO_{1.5} + NaO_{0.5} - KO_{0.5}] / [2 * Sum]$ $Olivine = 2 * [FMO + 0.5 * (AlO_{1.5} - Alk) - CaO - TiO_2 - Cr_2O_3 + 1.667 * PO_{2.5}] / [2 * Sum]$ $Augite = 3 * [CaO - 0.5 * AlO_{1.5} + 0.5 * Alk - 1.667 * PO_{2.5}] / Sum$ $IlmeniteHematiteChromite = 1.5 * [Cr_2O_3 + TiO_2 + FeO_{1.5}] / Sum$ $Orthoclase = 4 * [KO_{0.5}] / Sum$ $Apatite = 6 * PO_{2.5} / Sum$ Normalize all the minerals to 1 to get the mode of the rock.	
Calculated mode of augite based on whole-rock = 0.16	
Theoretical Dy of melt (as calculated above): 7.36	Mineral Dy composition using partition-coefficient from Table 6-2: $Dy_{Augite} = 0.4 * Dy_{melt} = 3$
Residual trapped melt (as calculated above): $100 * (1.1 - (3 * 0.16)) / 7.36 = 8.2\%$	

REPORT DOCUMENTATION PAGE	1. REPORT NO. MIT/WHOI 2004-06	2.	3. Recipient's Accession No.
4. Title and Subtitle The Evolution of Oceanic Gabbros: <i>In-situ</i> and Ancient Examples			5. Report Date June 2004
7. Author(s) Astri Jæger Sweetman Kvassnes			6.
9. Performing Organization Name and Address MIT/WHOI Joint Program in Oceanography/Applied Ocean Science & Engineering			8. Performing Organization Rept. No.
12. Sponsoring Organization Name and Address National Science Foundation Charles D. Hollister Endowed Fund			10. Project/Task/Work Unit No. MIT/WHOI 2004-06
			11. Contract(C) or Grant(G) No. (C) OCE-9618442; (G) OCE-9907630
			13. Type of Report & Period Covered Ph.D. Thesis
15. Supplementary Notes This thesis should be cited as: Astri Jæger Sweetman Kvassnes, 2004. The Evolution of Oceanic Gabbros: <i>In-situ</i> and Ancient Examples. Ph.D. Thesis. MIT/WHOI, 2004-06.			14.
6. Abstract (Limit: 200 words) This study is a geochemical investigation into the accretion of lower oceanic crust and processes of shallow melt-rock reaction at mid-ocean ridges. Geochemical signatures from the 480-My Lyngen Gabbro indicate the complex formed from hydrous supra-subduction zone magmas. Minerals in gabbros from Atlantis Bank, Southwest Indian Ridge, an <i>in-situ</i> example of lower ocean-crust, formed by near-fractional crystallization at mid-crustal pressures, modeled by the MELTS algorithm. The lower crust is more evolved than the lavas, representing mantle-derived melts fractionated 50-95%. >770-m of additional primitive cumulates remains below the 1500-m deep Hole 735B or within the underlying mantle. The Atlantis Bank gabbros minerals have internal disequilibrium. Melt-rock interaction may have caused this. Dissolution-experiments for plagioclase-olivine and plagioclase-augite pairs were performed at 1180°-1330°C and 20-min-24hrs. Dissolution occurs rapidly and out of equilibrium, the dissolution rates dependent on ΔT above the solidus. Coarse-grained rocks will heat internally when enclosed in hot magma, melt and disaggregate. The hybrid magma crystallizes more refractory-looking minerals than the melts that precipitated the original gabbroic rocks. Assimilation increases the Na content and decreases the Fe content of the melt that digests gabbro, thus hybrid basaltic glasses will falsely reflect a lower degree and pressure of mantle melting.			
17. Document Analysis a. Descriptors Gabbro mid-ocean ridge Southwest Indian Ridge b. Identifiers/Open-Ended Terms c. COSATI Field/Group			
18. Availability Statement Approved for publication; distribution unlimited.		19. Security Class (This Report) UNCLASSIFIED	21. No. of Pages 264
		20. Security Class (This Page)	22. Price